ISOTOPIC RESETTING OF ZIRCON: INFLUENCE OF AGE, TEMPERATURE AND CHEMICAL ENVIRONMENT.

By

BONISWA NOLWAZI MAGWAZA

Dissertation

Submitted in fulfilment of the requirements for the degree of

MAGISTER SCIENTIAE

in

GEOLOGY

Faculty of Science

UNIVERSITY OF JOHANNESBURG

August 2019

SUPERVISOR: PROF. M. A. ELBURG

Declaration of authorship

This serves to confirm that I, Miss B.N. Magwaza (student number: 200911369) have submitted the dissertation for the degree of Magister Scientiae in Geology to the University of Johannesburg. The dissertation was conducted under the supervision of Prof. M.A. Elburg. This is my original work and has not been presented for examination elsewhere. I am aware of the university's plagiarism policy and where other people's work has been used, a proper acknowledgement has been made according to the university's requirements.

SIGNATURE…… ……. DATE……13-08-2019……..

Acknowledgements

I would first like to thank my sponsors, Council for Geoscience and CIMERA for funding my studies.

I would like to express my special thanks of gratitude to my supervisor Professor Marlina Elburg for her continuous guidance, support and time dedication throughout this MSc research. I have learnt a lot about the subject, and it was a great privilege working under her guidance.

I would also like to thank UJ laboratory specialists and technicians for assisting with sample preparations and laboratory analyses.

I am also grateful to my family and friends for their encouragement and continuous support throughout my research.

Above all I would like to thank God for making it all possible even through difficult times.

Abstract

To assess the causes and extent of isotopic resetting of zircon, U-Pb and Lu-Hf analyses have been performed on zircons from Archean and Bushveld granites as well as Transvaal sediments which have been intruded by magmas of the Bushveld Complex, Pilanesberg Complex, Spitskop Complex, Goudini Complex, and Karoo dolerites in the vicinity of Bushveld Complex using laser ablation multi-collector inductively coupled plasma source mass spectrometry (LA-MC-ICPMS). U-Pb results for zircon analyses from both Archean granites and Transvaal sedimentary rocks indicate that they have undergone partial Pb loss and age resetting. Pb loss was influenced by radiation damage in zircons and metamorphism. Contributions from the Bushveld Complex thermal overprint cannot be excluded, based on evidence from concordia diagrams and $^{207}Pb/^{206}Pb$ ages; two samples of Magaliesberg sandstones (MEMG 3, 4), closest to the contact with the Marginal Zone, are affected the most. The presence of common Pb and its correction also contributed in shifting the data towards younger $^{207}Pb/^{206}Pb$ ages. Younger alkaline intrusions as well as Karoo dolerites did not have much influence on zircon signatures. There are only small differences in initial Hf ratios of analyses within the same sample, indicating that the Lu-Hf isotope system remained undisturbed. There are no appreciable effects on trace element concentrations to support that disturbance in U-Pb signatures of zircons is accompanied by their modifications. The cathodoluminescence (CL) images can provide some guidance on U-Pb isotopic disturbance but correlations are imperfect.

Table of Contents

List of Figures

List of Tables

Chapter 1

1. Introduction

1.1. Overview

A number of characteristics of the mineral zircon, including its wide occurrence in various types of crustal rocks, very stable physical and chemical properties, robustness under a wide range of geological processes, and the fact that it also accommodates significant amounts of temperature- and/or process-sensitive trace elements (e.g. Williams, 1992; Bruguier et al., 1997; Zheng et al., 2005; Harley and Kelly, 2007; Chen et al., 2015) makes it extremely useful for geochronological purposes. Zircon contains U and Th, which, through radioactive decay, produce radiogenic Pb (Belousova et al., 2002). The U-Th-Pb isotopic system provides valuable information about the age of rocks provided that zircon remains a closed system for both radioactive parent and radiogenic daughter isotopes (Schoene et al., 2013). The ages can be presented in a concordia diagram that was first introduced by Wetherill (1956). The concordia diagram plots $^{206}Pb^*/^{238}U$ versus $^{207}Pb^*/^{235}U$ from the same analyses, and analyses with $^{207}Pb^*/^{235}U$ and $^{206}Pb^*/^{238}U$ both corresponding to the same age will lie on the concordia curve represented by a blue line in figure 1.1, these analyses are referred to as 'concordant' (Dickin, 2005).

In addition to U-Th-Pb isotopic system, hafnium being very similar in its chemical behaviour to zirconium, forms an essential part in zircon lattice, which is very resistant to Hf mobility and contamination (Dickin, 2005). So, Hf isotope analysis, based on the radioactive decay of ^{176}Lu to ^{176}Hf, can be used to determine the source environment where zircon crystallized, and can also be used to track the isotopic distinction of mantle and crustal reservoirs because Lu fractionates from Hf during magma generation (Kinny and Maas, 2003; Roberts and Spencer, 2014). A combination of U-Pb and Lu-Hf isotopic studies are certainly important in geochronology as well as for petrogenetic information of the rocks (Gerdes and Zeh, 2010).

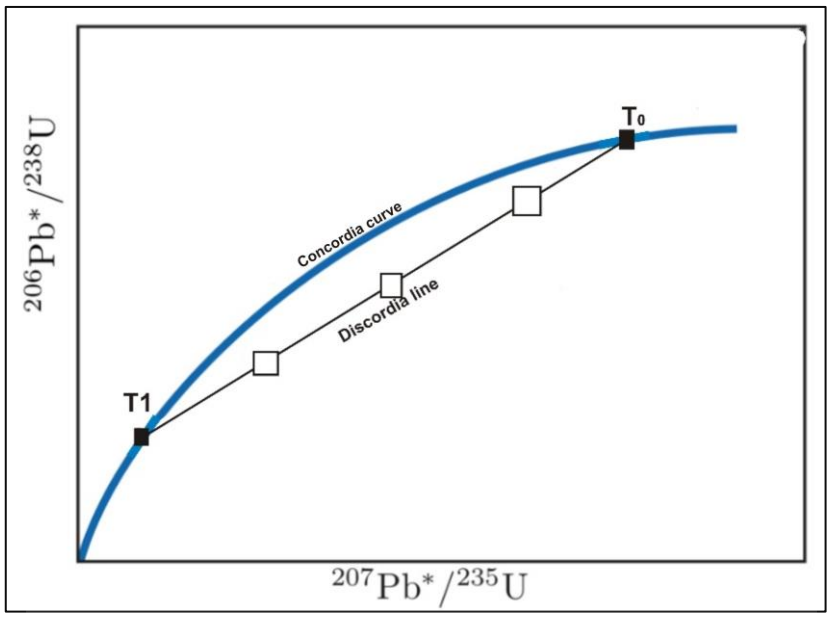

Figure 1.1: A schematic concordia diagram showing concordant (filled squares) and discordant analyses (empty squares) affected by degrees of Pb loss.

After zircon formation, zircon may behave as an open-system. This can result in the change in composition of Pb, which often results in partial resetting of the ages (Holmes, 1954; Mezger and Krogstad, 1997). The process of isotopic zircon age resetting involves transport of U and/or Pb within and out of zircon crystals, which may result in isotopic systems in zircons to be partially or totally disturbed. Pb loss in zircon can be visualised in concordia diagrams. The analyses that have lost Pb (or gained U) lie on a discordia line below the concordia curve and they are referred to as 'discordant' (Fig. 1.1). Pb loss can result from a number of processes including metamorphism (Grauert and Hall, 1974; Gebauer et al., 1981; Gulson and Krogh, 1975; Johnston et al., 2008), sub-solidus recrystallization under hydrous conditions, dissolution-reprecipitation processes under high-grade conditions (Williams, 1992; Harlov and Dunkley, 2010; Bindeman and Melnik, 2016). It is also possible that Pb loss result from radioactive decay of trace amounts of U and Th which substitute for Zr causing accumulated radiation damage to zircon structure, this process is called metamictization (Mezger & Krogstad, 1997).

Like the U-Pb isotope system, Hf isotopic compositions may be affected by post-crystallization disturbances like metamorphism (Patchett, 1983). However, because zircons contain high concentrations of Hf, and have very low Lu/Hf ratios, thereby reducing the importance of age corrections on the initial $^{176}Hf/^{177}Hf$ ratio 21l48events, or any other geological processes that may results in Pb loss in zircons.

1.2. Aims and objectives

The present study aims to answer the following questions: under which circumstances are zircons reset, and to what extent? Does the age and chemical environment of the zircon affect their susceptibility to be reset? Is evidence for isotopic disturbance obvious from the techniques traditionally used to image zircons prior to analysis?

This was accomplished by the interpretation of isotopic data of zircon from sedimentary (Transvaal Supergroup) and igneous rocks (Archean intrusives) that have been affected by later igneous events (intrusion of the magmas of the Bushveld Complex, Pilanesberg Complex, Goudini Complex, Spitskop Complex, and Karoo dolerites). Laser ablation multi-collector inductively coupled plasma source mass spectrometry (LA-MC-ICPMS) is the microanalytical technique that was used for U-Pb and Lu-Hf analyses, and zircon imaging was done using the cathodoluminescence (CL) detector on a scanning electron microscope (SEM). Additionally, trace element analysis was performed on selected reset samples using LA-Q (quadrupole)-ICPMS to constrain the effects on the elemental composition of the zircon. All analyses were done at the University of Johannesburg.

Chapter 2

2. Literature Review

2.1. Zircon structure, occurrence and stability

Zircon ($ZrSiO_4$) is a tetragonal orthosilicate mineral in which isolated SiO_4^{4-} tetrahedra are connected to ZrO_8 dodecahedra through sharing edges and corners (Finch and Hanchar, 2003). It occurs as an accessory mineral in igneous and metamorphic rocks, and as detrital zircon in sedimentary rocks. Apart from Zr, Si and O, zircon also incorporates up to thousands of ppm in trace elements and about 3% of minor elements (Hoskin and Schaltegger, 2003). Zircon does not contain much lead at the time of its formation and has very high ratios of U/Pb. The radioactive decay of uranium to lead with time makes it a valuable geochronometer (Belousova et al., 2002). Zircons are also known to have very stable physical and chemical properties making them robust under a variety of geological processes such as weathering, transportation and high temperature metamorphic events. Zircon age information is contained within their U-Pb system; zircons with disturbed crystal structures are vulnerable to alteration and/or partial to complete destruction or loss of their U-Pb isotope signatures during low-temperature metamorphic or hydrothermal events (e.g. Kramers et al., 2009).

2.2.

2.2.1. U-Pb system principles and application to zircon studies

The U-Pb method is the most widely used technique for determining the age of igneous and metamorphic rocks. The U-Th-Pb method is based on the radioactive decay of U and Th to stable isotopes of Pb (Faure, 1977). Uranium naturally occurs as radioactive isotopes ^{238}U, ^{235}U and ^{234}U, and Th occurs as radioactive ^{232}Th. Pb occurs as radiogenic isotopes ^{206}Pb, ^{207}Pb, ^{208}Pb and non-radiogenic isotope ^{204}Pb (Faure, 1977). The parent isotopes decay to different stable isotopes of Pb with different half-lives, but none of the parent isotopes decays directly to Pb, instead they follow a sequence of alpha (α) and beta (β) decays that generate a sequence of intermediate daughter isotopes, and always lead to the stable isotopes of Pb (Dickin, 2005). ^{238}U decays to ^{206}Pb, ^{235}U to ^{207}Pb and ^{232}Th to ^{208}Pb (Faure, 1977). The equations for these decay schemes are:

$$^{207}Pb^{*} = {}^{235}U\,(e^{\lambda 235 t}-1) \text{ ----- (1)} \qquad \lambda^{235} = 9.85\times10^{-10}\ yr^{-1}$$

$$^{206}Pb^{*} = {}^{238}U\,(e^{\lambda 238 t}-1) \text{ ----- (2)} \quad \lambda^{238} = 1.55\times10^{-10}\ yr^{-1}$$

$$^{208}Pb^{*} = {}^{232}Th\,(e^{\lambda 232 t}-1) \text{ ----- (3)} \quad \lambda^{232} = 4.95\times10^{-11}\ yr^{-1}$$

The stars (*) are to indicate that the Pb isotopes are radiogenic. λ^{238}, λ^{235}, and λ^{232} are the decay constants for ^{238}U, ^{235}U and ^{232}Th (Schoene et al., 2013). ^{235}U and ^{238}U decay to ^{207}Pb and ^{206}Pb at different rates, so the Pb isotope ratios change with time, therefore the age may be acquired by measuring Pb ratios alone which eliminates the necessity to measure the abundances of U and Pb because the age is independent of the parent/daughter ratio. So, when you divide equation one by equation two, you can get the $(^{207}Pb/^{206}Pb)^{*}$ ratio which can be used to determine the $^{207}Pb/^{206}Pb$ age.

Measurements of the U and Pb concentrations and Pb isotopic composition of zircon result in two independent ages namely the $^{206}Pb/^{238}U$ and $^{207}Pb/^{235}U$ age which can be plotted in a $^{207}Pb/^{235}U$ vs. $^{206}Pb/^{238}U$ diagram (

), which was first introduced by Wetherill (1956). The analyses with the same $^{207}Pb/^{235}U$ and $^{206}Pb/^{238}U$ ages will plot on the concordia curve and they are referred to as concordant, whereas they are referred to as discordant if these ages disagree (Wetherill, 1956). The concordia diagram does not only allow interpretations of geological histories. Discordance is attributed to loss of Pb or gain of U in the zircon lattice (Holmes, 1954; Mezger and Krogstad, 1997). Discordance in age data may be caused by many factors including temperature, fluid flow events, and metamorphism. Recoiling nuclei produced in the α-emission process causes structural damages in zircon (Dickin, 2005). A variety of structural

damage within the zircon crystals from one rock means that the response of the zircon U-Pb system to events causing isotopic disturbance differs from grain to grain (Silver, 1963). This feature was recognised and has been exploited by numerous studies in the history of zircon U-Pb geochronology. Within the population of zircon crystals from a single rock there tends to be a correlation between mean radioactivity and U-Pb discordance (Silver, 1963).

Zircon is commonly used for dating studies because of its abundance in most igneous and metamorphic rocks and because it incorporates U and Th but allows very little or no Pb in its lattice at the time of crystallisation (Mezger & Krogstad, 1997).

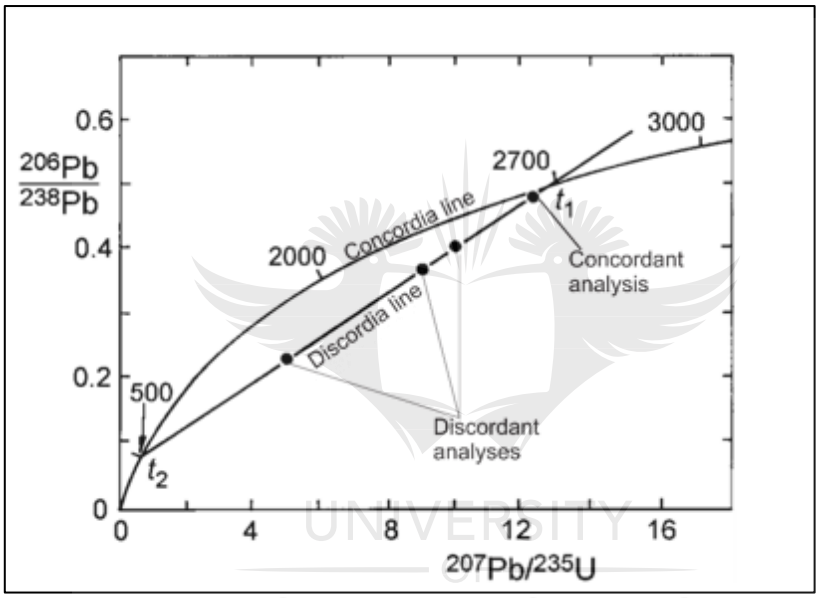

Figure 2.1: U-Pb concordia diagram illustrating the concordia line with ages given in Ma, and a discordia line generated by variable Pb loss at 500 Ma from a 2700 Ma old sample (Dickin, 2005).

2.2.2. Metamictization

Zircons can differ significantly in their trace element contents, including the radioactive element uranium. Zircon can contain U contents of up to 3000 ppm (Slama et al., 2008). Metamictization is a process resulting from accumulated radiation damage to the crystal structure caused by radioactive decay of trace amounts of uranium and thorium substituting for zirconium in the zircon crystal lattice (Nasdala et al., 1995). The damage is a result of recoiling nuclei produced in the α-emission decay (Nasdala et al., 1995). This radiation damage results in the physical and structural modification of zircon and it increases with uranium content (Dickin, 2005). It is well known that accumulation of radiation damage in a zircon structure enhances the susceptibility of zircon to alteration and age resetting (e.g.

Mezger & Krogstad, 1997; Geisler et al., 2001); therefore it is important to understand how zircons become metamict. Metamict zircons most often show reduced chemical stability, which often leads to radiogenic lead loss (Gentry et al., 1982). Such zircons are found in rocks enriched in volatiles such as water, fluorine, CO_2, and elements such as U, Th and REE, and they are formed at low temperatures usually towards the end of crystallization or in hydrothermal veins (Speer, 1980). Previous studies have shown that metamictization is a major variable controlling zircon susceptibility to alteration (e.g. Pidgeon et al., 1966; Tole, 1985). Högdahl et al. (2001) also looked at the role of radiation damage and fluid-influenced recrystallization in resetting of the U-Pb system in zircons under low-temperature conditions. Their conclusion was that the original variations in U and Th contents occurred during igneous crystallization and resulted in different degrees of radiation damage within individual grains, and that the observed discordance was produced by Pb loss from the most radiation-damaged domains. There has been a lot of debate on whether water has a strong effect on metamictization and annealing of zircon; for example Frondel and Collette (1957) found that water lowers the temperature and increases the rate of recrystallization of metamict zircon in annealing experiments; on the other hand Pidgeon et al. (1966) found that in hydrothermal experiments, distilled water had little effect on the rate of recrystallization. At low temperatures associated with weathering, diagenesis and low-grade metamorphism, radiogenic Pb can be much more readily lost from damaged crystals than from non-metamict crystals, resulting in significant age discordance in the U-Pb system (e.g. Geisler et al., 2007; Kramers et al., 2009).

2.2.3. Lu-Hf system principles and application to zircon studies

The Lu-Hf isotope system was first investigated in the early 1980s (Patchett and Tatsumoto, 1980; Patchett, 1983) following the successful application of the Rb-Sr and Sm-Nd isotope systems to geological problems, such as age dating and isotopic fingerprinting a couple of years earlier (Patchett and Tatsumoto, 1980). The Lu-Hf isotope method involves the spontaneous β^- decay of an unstable radionuclide, ^{176}Lu, to stable ^{176}Hf, with a half-life of approximately 35 billion years (Tatsumoto et al., 1981; Patchett, 1983). This half-life was later revised by Scherer et al. (2001) to 37.3 billion years. In the case of the Lu-Hf isotope system, the parent is the heaviest of the rare earth elements (REE) and it has geochemical similarities with all other +3 valence REEs. The daughter element Hf, however, is not an REE, but a high-field-strength element with a +4 valence similar to Zr, so it will behave similar to Zr and differently from the REEs. Hence zircons have high Hf/Lu ratios.

The Lu-Hf system in zircon can be used for fingerprinting purposes and to also to track the isotopic distinctions of mantle and crustal reservoirs because Lu fractionates from Hf during magma generation (Roberts and Spencer, 2014). The two main geochemical reservoirs within bulk silicate earth (BSE) are depleted mantle (DM) and continental crust (CC). The abundances of Lu and Hf in bulk Earth can be approximated by chondritic meteorites, also known as the chondritic uniform reservoir (CHUR). The crust, which is enriched in incompatible elements, was created from silicate melts that were removed from the mantle, and this creation of the crust is what formed the depleted mantle (Hofmann, 2014). Continental crust has lower Lu/Hf ratios than the bulk Earth, hence its $^{176}Hf/^{177}Hf$ increases more slowly than bulk earth whereas the depleted mantle has a higher Lu/Hf ratio and its $^{176}Hf/^{177}Hf$ increases more rapidly than bulk Earth (Fisher et al., 2014). Therefore, the epsilon value (εHf- is basically an expression of $^{176}Hf/^{177}Hf$ ratio of a sample with respect to $^{176}Hf/^{177}Hf$ ratio of CHUR, and is expressed as $\varepsilon Hf = [(^{176}Hf/^{177}Hf)_t / (^{176}Hf/^{177}Hf)_{CHUR} - 1)*10^4)$ for depleted mantle constituents will advance towards positive values, whereas the components of enriched crust will advance towards the negative epsilon values as illustrated in **Error! Reference source not found.** (Kinny and Maas, 2003; Fisher et al., 2014). Zircon is an excellent mineral for Hf isotope analysis for several reasons. Firstly, Hf forms an essential part of the zircon lattice, which is therefore extremely resistant to Hf mobility and

contamination, and secondly there are high concentrations of Hf in zircons which yield very low Lu/Hf ratios and therefore reduce age corrections (Dickin, 2005), hence this system is less susceptible to be reset than U-Pb system. A good example is the study conducted by Guitreau *et al.* (2012) where zircons were analyzed by both solution chemistry and laser ablation. U-Pb data indicated that the zircon grains have suffered intense lead loss, whereas their Hf isotopes remained unaffected.

Initial $^{176}Hf/^{177}Hf$ ratio preserved in zircons provides a record of the Hf isotopic composition of their source environment at the time of crystallization. This ratio can then be used either to determine a Hf model age (with respect to primitive or depleted mantle), contribute to a Lu–Hf isochron, or, if the crystallization age of the zircon is known separately from U–Pb dating, to determine an initial εHf value with respect to the Hf isotope evolution reference curve for the bulk Earth (Kinny and Maas, 2003).

Patchett et al. (1981) produced a schematic Hf isotope evolution diagram (

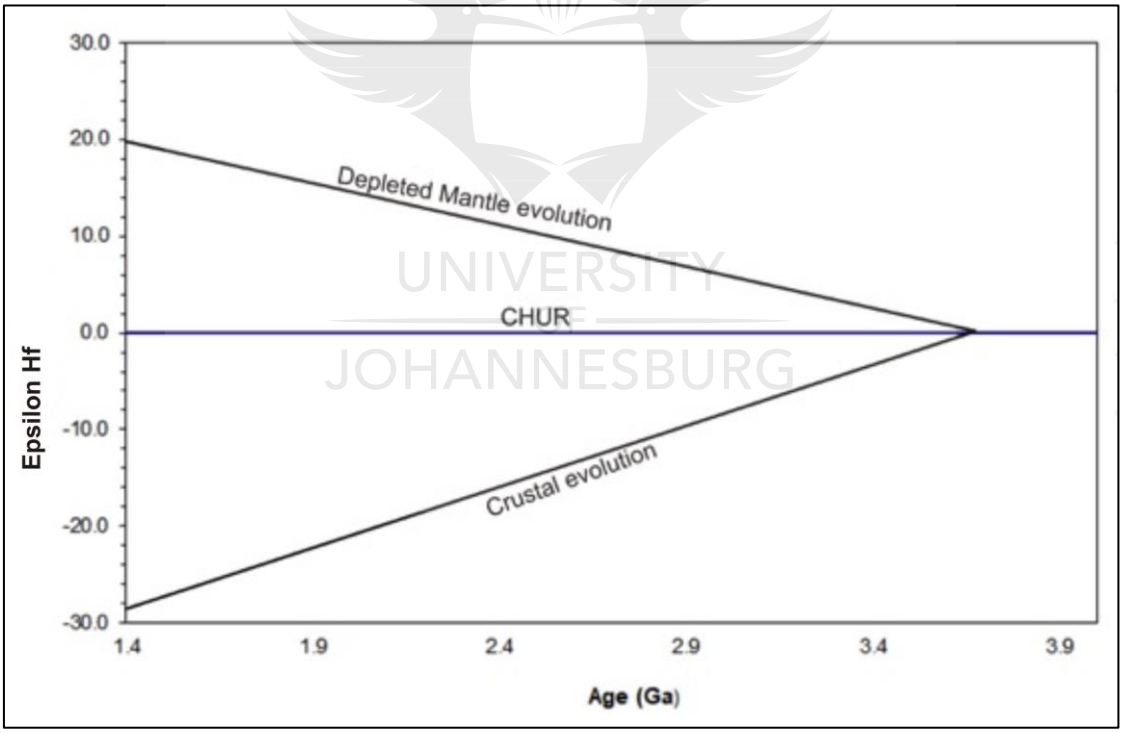

Figure 2.2: Schematic diagram showing the hypothetical Hf isotope evolution of different geochemical reservoirs (after Vervoort, 2014).

) which shows how an episode of partial melting in Earth's mantle at time t_1 results in divergent Hf isotope evolution paths for the newly generated crust (low Lu/Hf) and the residual mantle (high Lu/Hf). Having extremely low Lu/Hf, any zircons formed within that crust will preserve its initial $^{176}Hf/^{177}Hf$ ratio, and hence over time deviate in composition from the remainder of the host rock (Kinny and Maas, 2003). At time t_2 a variety of possible sources may contribute to newly formed crust. Any inherited zircon cores at t_2 would be expected to have lower εHf than the newly crystallized host rock (Kinny and Maas, 2003).

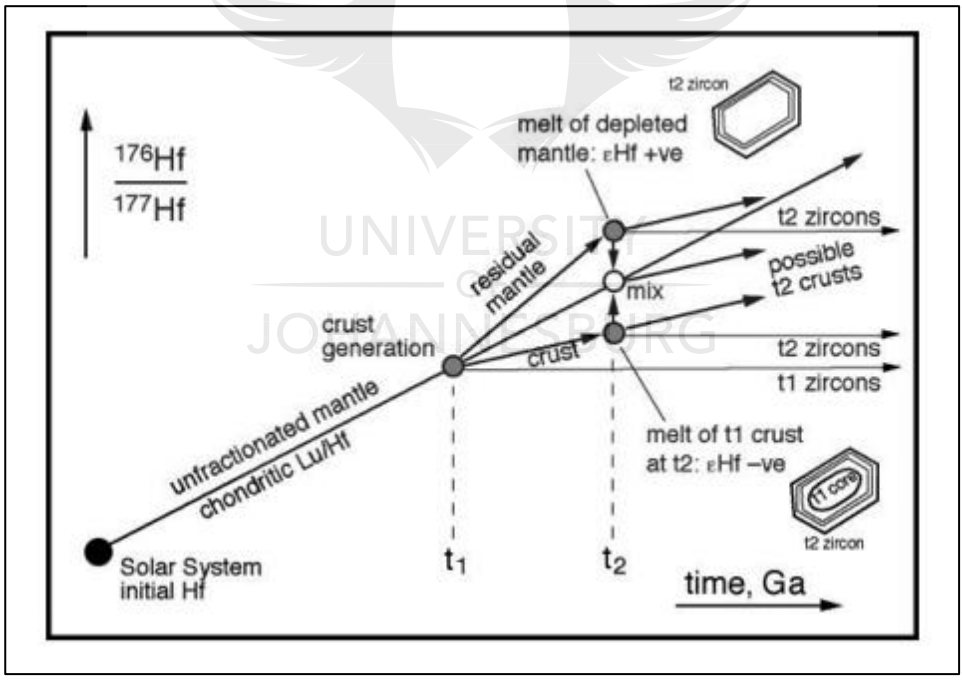

Figure 2.3: A schematic Hf isotope evolution diagram produced by Patchett et al. (1981) and modified by Kinny and Maas (2003).

Combination of U-Pb and Lu-Hf data

Studies combining the U–Pb and Lu–Hf isotope information are unquestionably the most powerful, as the age of the zircon must be determined accurately using U-Pb isotopic measurements if the petrogenetic information contained within the Hf initial ratio is to be

disclosed (Gerdes and Zeh, 2009). A study by Laurent and Zeh (2015) used U-Pb and Lu-Hf isotope data of zircon grains from the granitoid rocks of the Pietersburg block, northern Kaapvaal Craton, to obtain a better understanding of Hf isotope-age arrays with respect to the granitoid petrogenesis and geodynamics during Archaean terrane formation. Zircon textures together with U-Pb isotope analyses showed that zircon populations in the studied granitoids suffered Pb loss. Their results also indicated that the $^{207}Pb/^{206}Pb$ ages obtained from the cores were different to those obtained from the rims. U-Pb data showed that the ages from the zircon rims were younger and dated the age of intrusion due to the presence of magmatic zoning and high Th/U ratios, whereas the ages obtained on the cores were older and were interpreted to be xenocrysts inherited from the magma source. The results from their study also showed that linear Hf age arrays are a result to crustal reworking, and can involve granitoids that vary compositionally, derived from different sources within the crust, and formed in different tectonic setting.

2.2.4. Trace element analyses

Besides U and Th, zircon can also incorporate elements such as P, Sc, Nb, Hf, Ti and REE in minor and trace amounts. Zircon trace element data is of increasing importance in geosciences as zircon is not only used for geochronology using its U-Th-Pb isotopic system, but as a trace element monitor as well (Piazolo *et al.,* 2017). Many studies have looked at how chemical alteration resulting from different processes e.g. metamorphism and metasomatism can affect zircon geochemistry (e.g. Vavra et al., 1999; Hoskin and Black, 2000; Poitrasson et al., 2002; Hoskin and Schaltegger, 2003; Bell et al., 2016). Bell et al. (2016) looked at the geochemistry of zircons to assess if chemical alteration can affect zircon's geochemistry. There are many ways in which these assessments can be done, the most common being looking at the zircon REE patterns. In a normal magmatic zircon, the LREE concentrations are lower than HREE concentrations and therefore they will fit to smaller Zr sites (Hoskin and Schaltegger, 2003). According to Hoskin and Schaltegger (2003), fluid-induced alteration normally results in flat high LREE; in fact any change in LREE content in zircons is the first sign that isotopic composition of zircon has changed. In their study, Bell et al. (2016) proposed the so-called LREE index (LREE-I), which is defined by (Dy/Nd) + (Dy/Sm), and thus tracks the enrichment in middle relative to light rare earth elements. LREE-I decreases with increasing hydrothermal alteration (Bell et al., 2016). Based on their study of detrital zircons from Jack Hills (Australia), they suggested that LREE-I < 30

indicates alteration and LREE-I < 10 indicates that zircons are metamict, whereas pristine zircons have LREE-I > 30.

2.3. Cathodoluminescence principles and application to zircon studies

It is difficult to determine whether discordance is the result of Pb-loss from damaged domains of zircon or from other processes such as partial or complete recrystallization of zircon at high metamorphic grades (Vavra et al., 1996) based on the U-Pb data only. Cathodoluminescence (CL) imaging of zircon crystals represent a powerful tool to analyze the complex internal structure of zircon grains (Vavra et al., 1996; Rubatto and Hermann, 2007).

One way to generate a CL image is by SEM. When a zircon surface is bombarded by energetic electrons, the photons of particular wavelengths are emitted; this process is referred to as cathodoluminescence (Boggs and Krinsley, 2006). The trace elements present within a mineral at identical valence states within particular portion within the crystal initiate the cathodoluminescence (Pagel et al., 2000). This method yields high-resolution images of internal structures that often cannot be detected using other techniques (

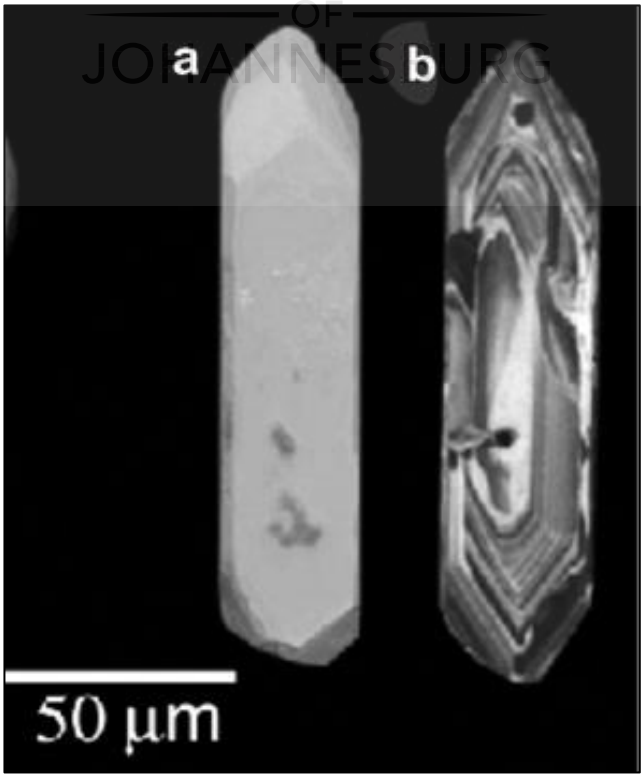

), and it can show growth structures, dissolution surfaces, metamict domains, etc. (Boggs and Krinsely, 2006). The

cathodoluminescence image obtained by SEM is a greyscale image. The luminescence of different parts in zircon grains can range from very weak (dark areas) to very strong (bright areas) (Figure 2.5 a).

Figure 2.4: Images of different zircon crystals obtained by (a) secondary electron (SE) (b) cathodoluminescence (CL) detector.

The dominant signature in zircon is oscillatory zoning, reflecting variations in the abundances of uranium (U) and yttrium (Y) within the zircons. Bands that are rich in U and Y are dark in CL images, where as bright areas are relatively poor in these elements (Rubatto and Gebauer, 2000), so this means that the emission in zircon is inversely proportional to their content of U and Y. Therefore, the emission of CL must be caused by elements other than U and Y because these act as cathodoluminescence quenchers resulting in CL dark bands (Boggs and Krinsely, 2006).

CL images from different zircon grains may show a variety of internal structures with different luminescence intensities that may provide clues about its modification through different stages of their growth. Rubatto and Gebauer (2000) showed that magmatic zircons commonly display oscillatory zoning, as well as sector zoning superimposed on the oscillatory zoning (Figure 2.5 b, c). Metamorphic zoning can be recognized by external CL zones, which are normally irregular in shape and can form rims around an older core. Metamorphic rims tend to show patchy and/or cloudy zoning, and the cores of such grains

may be very complex (Figure 2.5 d). The rims are referred to as overgrowths (e.g. Kempe et al., 2000), and these overgrowths may differ depending on whether they are growths from hydrothermal fluid, melt or solid-state crystallization. Kempe et al. (2000) stated that in their study, the overgrowth resulted from solid-state crystallization. Rubatto and Gebauer (2000) suggested that hydrothermal zircons are characterized by euhedral, elongated shapes, and narrow growth zones, which may display a weak luminescence signal; therefore it is possible to differentiate between magmatic zircons and the ones crystalized from hydrothermal fluids.

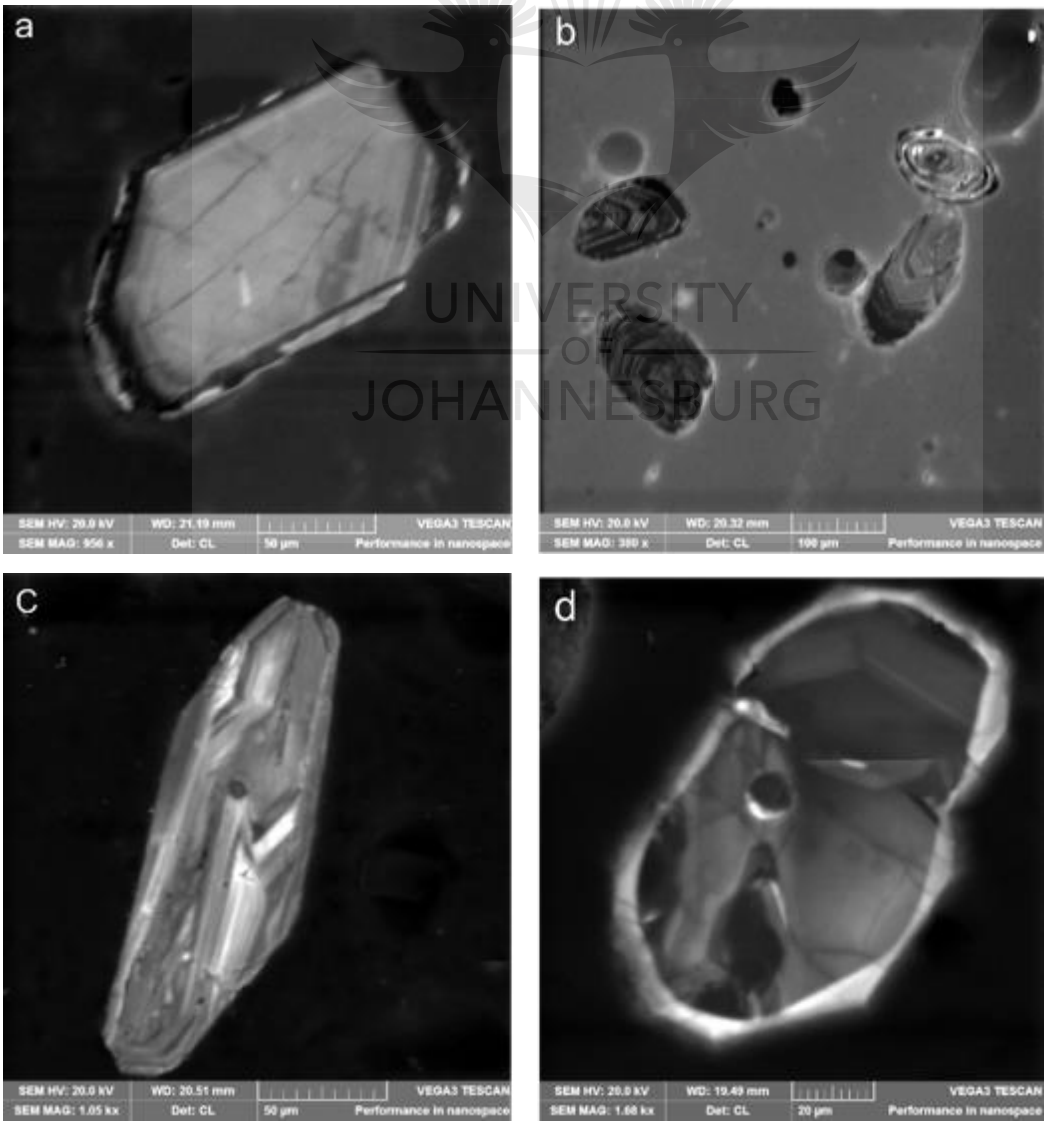

Figure 2.5: Cathodoluminescence images of magmatic (b,c) and metamict zircon (a,d) showing (a) different luminescence intensities (b) characteristic oscillatory zoning (c) convoluted zoning superimposed on the oscillatory zoning and (d) zircons showing a younger rim and complex structures in the core.

2.4. Measurement techniques

Different analytical techniques have been adopted and utilized in zircon studies to measure the isotopic ratios of elements like U-Pb and Lu-Hf used in geochronological and other isotopic studies.

2.4.1. Thermal ionisation mass spectrometry (TIMS)

TIMS instruments advanced in the mid-20th century and have been used for analysing isotopic data for a variety of elements (Schoene and Braxter, 2017). This technique involves heating of a chemically purified sample by applying a current through the metal filament so that atoms in the sample are ionized (Dickin, 2005). Variants of this technique are isotope dilution-TIMS (ID-TIMS), chemical abrasion-TIMS (CA-TIMS) as well as zircon evaporation technique. ID-TIMS is considered one of the most precise among the isotopic techniques available for U-Th-Pb geochronology because it is insensitive to chemical yields or mass spectrometric sensitivity (Parrish and Noble, 2003), and because of the isotopic tracer it does not require any calibration on external standards, which themselves need to be characterized isotopically (Tessalina et al., 2015). This method involves addition of an isotope tracer to a dissolved sample to make a homogeneous mixture, and the measurements of isotopic ratios of the mineral are done using a thermal ionization mass spectrometer (Parrish and Noble, 2003). When applied to zircon studies, this method needs zircon to be dissolved and the U and Pb separated from the other elements before the analysis (Schoene et al., 2010).

There have been a lot of studies where ID-TIMS was shown to be a powerful method in zircon studies. This technique can be used for high precision dating of igneous zircon across the range of geological time (e.g. Schmitz and Bowring, 2001). In spite of the virtual absence of zircon in basaltic rocks, zircon can occur in similar compositions of broadly gabbroic composition, so this method can also be used to date mafic rocks (e.g. Parrish 1989; Kamo et al., 1996). While the above examples show the power of the technique, the main

disadvantage is that because the sample is dissolved, some important information in the crystal may not be obtained (Guitreau et al., 2016).

CA-TIMS is an improved method that has an ability to completely remove zircon domains that have lost Pb, and then analysing remaining, perfectly closed-system zircon (Mattinson, 2005). The chemical abrasion treatment of selected zircon crystals before their dissolution involves annealing at 850-900°C, followed by partial dissolution in HF or HF-HNO_3 mixtures (Mattinson, 2005). This technique results in the most precise and accurate U-Pb dates when applied to magmatic zircons. When dealing with multi-domain zircons, chemical abrasion increases precision and reproducibility, but it removes uranium-rich zones which might also give valuable information.

The zircon evaporation technique was developed by Kober (1986), and it does not require any pre-treatment of zircon after its separation from the rock. The Kober method involves covering a zircon crystal with folded evaporation filament made from Re ribbon with a central cavity for holding zircon within a thermal ionization mass spectrometer (Parrish and Noble, 2003). Zircon is converted to baddeleyite (ZrO_2) by heating to release SiO_2 (Parrish and Noble, 2003). This release of SiO_2 acts as ionization activator (Davis et al., 2003). Pb is evaporated then analysed for its Pb isotopic composition by TIMS (Parrish and Noble, 2003). However, the disadvantage of this technique is that there is no information obtained on uranium, therefore there is no information on whether or not the zircon is concordant.

Secondary Ion Mass Spectrometry (SIMS)

SIMS is a highly sensitive microanalytic technique, which is able to measure small-scale (down to roughly 10 microns) elemental and isotopic composition in minerals (Black et al., 2003). A finely focussed ion beam is applied to the targeted crystal site and the ionised portion of the crystal is transferred directly to the mass spectrometer for determination of its chemical and isotopic composition (Stern, 1997). Ions generated by this process form the secondary beam and are subsequently transmitted within a continuous high vacuum environment to a mass spectrometer (Stern, 1997). This analytical method only works for solid materials and polishing of the crystal is required prior to analysis (Williams, 1992).

The SIMS analyses are perfomed under Ultra High Vacuum to avoid primary and secondary species scattering and also adsorption of gases onto mineral surfaces under investigation. SIMS instruments are able to analyse a variety of element/isotope systems from hydrogen (H) up to uranium (U), including oxygen-isotopes (e.g Kita et al., 2011).

SIMS instrument has different designs which include CAMECA 1280, 7F, and NanoSIMS, ASI's SHRIMP and SHRIMP RG, EAG's ToF SIMS and CAMECA 1300 HR. Most of SIMS instruments are characterized by a source region with controlled intensity, energy, and orientation of the primary beam, relative to the sample (Benninghoven et al., 1987).

The mass spectrum produced by an ion probe is a complex mixture of atomic and molecular species. Some of the early ion probe studies (e.g. Lovering et al., 1981) suffered from the low mass resolution of the probes that were used back then, which involved large difficult corrections for the interferences between species that could not be separated by mass (Black et al., 2003). SIMS uses a high mass resolution to reduce interferences to levels, hence reducing the corrections required, but when using SIMS reference material is used for calibration, therefore the precision of the results is also determined by the external standards as well (Black et al., 2003). Another limitation of SIMS instrumentation is that they tend to be expensive for both purchasing and running costs.

2.4.2. Laser ablation-multi collector-inductively coupled plasma mass spectrometry (LA-MC-ICPMS)

The first studies to show the potential of LA-ICPMS to perform *in situ* isotopic ratio determinations on zircon with high precision took place in the early 1990s (Fryer et al., 1993; Feng et al., 1993). This method eliminates previous laborious sample preparation, dissolution and element separation required by the traditional ID-TIMS (Bühn et al., 2008), and gives isotopic ratios and age data with a high spatial resolution (Guitreau et al., 2012).

An ICPMS consists of an ICP source where the ionization takes place, a number of focusing lenses, an energy filter, a mass analyser, and a detector array (Kylander-Clark, 2017). The ICPMS can be either single- or multi-collector (MC) ICPMS. A MC-ICPMS uses a series of collectors where isotopes of interest are measured simultaneously, and this is an advantage over a single-collector instrument because the sensitivity is increased by measuring each isotope in a different collector e.g. for U–Pb measurements, six different isotopes ^{238}U, ^{232}Th, ^{208}Pb, ^{207}Pb, ^{206}Pb, and ^{204}Pb are measured simultaneously on an MC-ICPMS, whereas each has to be measured sequentially on single collector ICPMS (Kylander-Clark, 2017). The primary advantage of the LA-MC-ICPMS is its ability to simultaneously analyse isotopes of a wide range of elements, including those with high ionization potential, which are difficult

to analyse by TIMS. This method in addition results in accurate and precise determination of isotope ratios, comparable to those obtained with TIMS (Albarède et al., 2004). However, there are also many disadvantages of LA-MC-ICPMS that restrict the accuracy and precision of the results. These include sensitivity drift, elemental fractionation, matrix effects, and calibration by using an external reference material (Lin et al., 2016).

Comparisons between the measurement techniques

In situ techniques such as SIMS and LA-MC-ICPMS have high spatial resolution and more flexibility in terms of the elements that can be precisely and accurately measured, where as with TIMS the spatial information is lost (Schoene and Baxter, 2017). These *in situ* methods are most useful when there is a need for quick analysis of many grains, and when crystals need to be reused for other geochemical analyses. TIMS produces more precise age data, but completely destroys the sample, requires clean lab and laborious chemical procedures, hence it is expensive (Tessalina et al., 2015). However, there will always be situations for which SHRIMP or LA-MC-ICPMS is more appropriate or advantageous than TIMS and vice-versa.

2.5. Different causes of zircon resetting

2.5.1. Influence of temperature

Elevated temperatures and the presence of aqueous phases play a role in enhancing dissolution of zircon and will also be important in controlling the annealing of radiation-damaged areas (Hay and Dempster, 2009). But this does not imply that zircon will only dissolve at high temperatures. Dissolution can occur during both recrystallization and metamorphism, and is enhanced by radiation damage. Dissolution-reprecipitation in zircon involves the breaking of bonds and release of elements in a crystal structure, followed by nucleation and growth of new zircon (Geisler et al., 2007), causing partial or complete modification of pre-existing zircons. Geisler et al. (2007) also noted that the zircon formed after a coupled dissolution-reprecipitation process will be poorer in trace elements than the original zircon and this is due to the fact that a zircon rich in trace elements has a higher solubility in the fluid than a pure zircon. This sub-solidus mechanism requires the presence of fluids and melts to actually transport components from one reaction site to another within a mineral (Tomaschek et al., 2003).

Previous studies have shown that elevated temperatures can also result in annealing of damaged zircons, and that it is a two-step process (e.g. Nasdala et al., 2001). First is the formation of zirconia then recrystallization to the original zircon structure. Healing radiation-

damaged zircon includes re-ordering of atoms to rehabilitate the disrupted bonds (Nasdala et al., 2001). Results of the annealing process are not a direct reverse of metamictization because domains of a crystal that are damaged may have allowed for the migration of radiogenic Pb, U and Th within the zircon lattice (Nasdala et al., 2001). Temperatures at which annealing occurs are dependent on the zircon's state of metamictization as well as how the annealing process takes place (Pidgeon et al., 2017). Murakamai et al. (1991) suggested that damaged zircons have a slower annealing rate than moderate to low damaged crystals and may then require high temperatures for recovery. This suggestion is in agreement with temperatures of more than 1000 ºC established by Weber (1990) for annealing a fully damaged zircon.

2.5.2. Influence of metamorphism

2.5.2.1. Metamorphism and anatexis

Zircon formation through igneous crystallization is influenced by the solubility of Zr in the melt (Watson and Harrison, 1983). During metamorphism the behaviour of zircon is more complex and depends on several factors. Zircon may precipitate from anatectic melts (e.g. Vavra et al., 1996), but it can also grow from the release of Zr from other mineral phases (Bingen et al., 2001), or it can recrystallize and change its isotopic composition in the presence of fluids (e.g. Hoskin and Black, 2000; Rubatto and Hermann, 2007).

During metamorphism it is possible for zircon textures and isotopic signatures to be modified. This could happen at any stage during metamorphism. There are several ways in which zircon can be reset during metamorphic events. It is important to note that metamorphic zircons can result from a number of processes. They can be a result of pseudomorphic alteration of magmatic zircon (e.g. Geisler et al., 2007) or form from new zircon growth (e.g. Möller et al., 2003; Rubatto and Hermann, 2007). Formation by new zircon growth can be by precipitation from a liquid phase (e.g. Rubatto and Hermann, 2007), or during a solid-state mineral reaction (e.g. Möller et al., 2003). Geisler et al. (2007) suggested that metamorphic zircon that formed by a pseudomorphic alteration process will maintain its original Hf isotopic composition even if the U–Th–Pb information and zoning is totally disturbed, and Zeh et al. (2010) suggested that metamorphic zircon that precipitates from a melt will have modified Hf isotopic composition because there may be sources supplying radiogenic Hf to the growing zircon. The Lu/Hf ratios from migmatites and associated granites in the Sulu orogeny and Cathaysian terrane studied by Chen et al. (2015) also showed that the Hf bearing minerals were involved in the reactions during anataxis, and

remarkable Hf isotope differences in some anatectic and primary zircon domains suggest source heterogeneity as well as variable non-zircon Hf contributions.

2.5.2.2. Subsolidus reactions involving other minerals, leading to zircon new growth

During metamorphism the behaviour of zircon gets more complex and depends on several factors. Not only does zircon precipitate during anatexis (e.g., Vavra et al. 1996; Möller et al., 2003), but it can also be released during the breakdown of minerals under sub-solidus conditions (Fraser et al., 1997; Pan, 1997). New growth of zircon can result from net transfer reactions that involve the breakdown of a phase bearing zirconium (Fraser et al., 1997). Zr is concentrated in certain minerals under metamorphic conditions; hence metamorphic reactions involving these minerals may have a considerable effect on the growth and modal percentage of zircon (Fraser et al., 1997). After looking at zirconium abundance in granulite-facies minerals in pelitic and metabasitc rocks, Fraser et al. (1997) established that breakdown of either garnet or hornblende may release Zr which is enough to result in a distinct episode of zircon growth. With increasing temperatures, hornblende will be replaced by pyroxene, so zircon grown during breakdown of hornblende will give age information of that specific prograde P-T history (Fraser et al., 1997). On the other hand, garnet breakdown in granulites is more often associated with decompression following peak metamorphic conditions (Fraser et al., 1997). Therefore before doing any zircon analyses it is important to first do petrographic analysis on rock samples and identify the alteration behaviours of minerals and even the amount of metamorphism that have affected the rock, which will then make it easier to correlate zircon textures, ages and even isotopic compositions.

2.5.3. Fluid flow events

It is most likely that Pb removal from zircon is accomplished by an aqueous phase (Goldich and Mudrey, 1975). Fluid flow plays an essential role in heat and mass transport in the crust (Cui et al., 2001). Fluids are often the main drivers of recrystallization because they act as dissolution and re-precipitation agents. Morris et al. (2015) argued that fluid flow events such as orogenic fluid flow associated with Caledonian orogenesis resulted in altered and discordant zircons. The results obtained from their study gave a remarkable number of discordant U-Pb zircon dates, and the discordance pattern marked partial or total radiogenic Pb loss during the Middle Devonian, possibly promoted by post-depositional fluid activity. Proposed fluid sources include a combination of orogenic uplift–driven meteoric groundwater, tectonic-driven dewatering, and mineral dehydration metamorphic reactions.

2.5.4. Fluids from nearby intrusions

Igneous intrusions are another important source of migrating fluids. These fluids, rich in dissolved ions, move into the surrounding rock as it is metamorphosed in response to heating from the intrusion. These fluids transport water as well as the heat from the magma (Harlov and Austrheim, 2013). Effects of fluids from nearby igneous intrusions on rocks, whether they have undergone any metamorphism or not after emplacement, can result in modifications in their zircon signatures hence discordant U-Pb ages (Mezger and Krogstad, 1997). Evidence of Pb loss caused by fluids from nearby intrusions was recently presented by Dowman et al. (2017). Their study showed that multiple fluid phases penetrated the surrounding country rocks resulting to their fenitization during metasomatism. Their results also showed that zircons in fenitized rocks, when compared to those in the original country rocks, exhibit different characteristics in terms of their textures and shape. In terms of their U-Pb isotope data, they suspect that Pb loss in zircon crystals was only due to fluid interactions during metasomatism, and they based this on crystal defects and variation in grain size. Effects of carbonatite intrusion on Pb loss in zircon were excluded because zircons actually predated the age of the carbonatite intrusion. This implies that caution is needed when dating rocks near the intrusions.

2.5.5. Fluids from mineral dehydration reactions

Fluids that are released from dehydration reactions during metamorphism can cause change of fluids from zircon undersaturation to zircon supersaturation (Hay and Dempster, 2009). Metamict zircons are always easily targeted because increased porosity in zircon allows for easy access of fluid to radiation-damaged zircon (Hay and Dempster, 2009). A study by Stahle et al. (1987) on granulite-facies rocks showed that depletion of Zr took place after depletions in elements such as U, Th and Pb, which are very mobile. These chemical changes are related to biotite and amphibole breakdown and the production of pyroxenes and feldspars (e.g. Janardhan et al. 1982) and Stahle et al. (1987) postulated these changes to have involved some dissolution of zircon.

Another study that indicated zircon dissolution driven by fluids from dehydration reactions was documented by Liermann et al. (2002). Evidence of zircon dissolution and overgrowth, which was driven by pore fluids of low salinity, produced during metamorphic dehydration reactions of biotite and zoisite to form garnet, was observed. Precipitation of zircon overgrowths was interpreted to have formed as a result of the water-consuming reaction of

phengite formation from garnet. Lack of evidence for pervasive fluid-rock interactions resulted in the authors' conclusion that fluids originated from mineral dehydration reactions.

There are however cases where fluids from dehydration reactions do not affect U-Pb systematics. Friend and Nutman (1992) used the ion-microprobe SHRIMP on zircons separated from the arrested amphibolite - granulite transition. Their study was attempting to see if the formation of granulite-facies assemblages by the influx of dehydrating fluids can result in resetting of U-Pb ages. The results showed that despite the zircon corrosion and bulk-Zr loss from the granulite-facies domain, there was no absolute effect on the U-Pb systematics of the zircons.

2.5.6. Meteoric fluids

Chemical and structural changes in zircon can result from interaction between zircon and meteoric fluids during weathering processes (Geisler et al., 2007). Significant work has been done on the mechanisms by which zircons lose their U-Pb information due to meteoric water-rock interactions. A study conducted by Black (1987) indicated a loss of Pb in zircon from the granite and pegmatite from the Rayner Complex in Antarctica due to interaction with meteoric fluids. According to Black (1987), the weathering solutions affect radiation-damaged zircons more as these fluids act as a transport medium responsible for migration of Pb within the grain, resulting in geologically meaningless age data. Remarkable changes in the oxygen isotopic composition of metamict zircon resulting from the interaction of amorphous zircon interaction with low-temperature weathering solutions were also described by Pidgeon et al. (2013).

2.5.7. Influence of crystal structure on resetting

As robust as zircon is during a wide range of geological processes, this mineral may deform at any time after crystallization. Zircons may deform by brittle fracture (Wayne and Sinha, 1988; Steyrer and Sturm, 2002); this is a process that will change the grain size and surface area of the zircon and therefore may result in diffusion and chemical reaction under different conditions in the crust. However, zircon may also undergo plastic deformation (Reddy et al., 2007). The presence of microfractures in zircons (which can be observed in CL images) can crucially affect the bulk diffusion properties of the crystal (Reddy et al., 2007). These microstructures act as fluid migration paths and elements diffusion paths, resulting in elements mobility in the crystalline zircon. The fluid migrating through these structures can

change chemical and isotopic composition of certain parts of the grain (Reddy and Timms, 2010) and therefore lead to isotopic resetting in the mineral domains.

2.6. Dealing with discordance

2.6.1. By correcting for common lead

The presence of common lead in zircons is a serious source of inaccuracy when it comes to U-Pb geochronology. There are many factors contributing to common-lead in a zircon crystal, these include geological processes that occur after its crystallization e.g. sub-solidus recrystallization under hydrous conditions and weathering processes, but besides such processes, the measured ^{204}Pb signal can also be affected by ^{204}Hg acquired from argon and helium gases that are used in ICP and ablation methods (Andersen, 2002). So, the calculation of on-mass background is done before each analysis to remove the signal of ^{204}Hg originating from the plasma. The laser energy that is used during ablation of a sample must also be low to ensure that ionization of ^{204}Hg does not occur. Analyses that have high background ratios above detection limit need to be corrected for common lead (Rosa et al., 2009). Correcting for common lead in a system allows the discordance and the history of Pb loss within zircon crystal domains to be understood (Horstwood et al., 2003).

There are many ways in which common-lead correction is done. The usual method is based on the non-radiogenic Pb isotope with a mass number 204; basically the amount of ^{204}Pb is measured in a sample of interest, and then the ^{206}Pb/^{204}Pb, ^{207}Pb/^{204}Pb and ^{208}Pb/^{204}Pb ratios of common-lead are estimated based on the measured ^{206}Pb/^{204}Pb ratio of zircon so that radiogenic ^{206}Pb, ^{207}Pb and ^{208}Pb can be calculated (Williams, 1998). There are other methods that can be used which assume that the only source of discordance in a zircon is the presence of common lead (e.g. Williams, 1998). This method is monitored by measuring ^{207}Pb/^{206}Pb ratios, and then the zircon ages are calculated by extrapolating data onto the concordia along the line extending from the composition of the common lead (Williams, 1998). The problem with this correction method is that should a zircon contain a discordant component caused by lead loss, there will be overcorrection, leading to meaningless age data.

There is another correction method that was designed by Andersen (2002) that does not use ^{204}Pb or assume concordance. This method uses equations that involve numerical solutions relating the radiogenic lead content in a zircon to its total Pb content, the amount of common lead present, the age of initial crystallization, the age of lead loss and the amount of lead lost in that process (see Andersen, 2002, for further details).

2.6.2. Novel models

Morris et al. (2015) considered in some detail discordant as well as concordant age data in detrital zircons from northernmost Greenland, with implications for post-depositional fluid-rock interaction. In their study they presented a novel modelling method to identify the time of radiogenic Pb-loss. They modelled the age of the discordant population assuming that Pb was lost at different times. Knowing the position of the discordant data in concordia space, they assumed a time of Pb loss, and then they calculated the upper intercept, which, assuming time of Pb loss, shows a model age that can be compared statistically with the model age of the concordant population. This process was repeated for every possible time of Pb loss, producing a variety of upper-intercept ages. Each modelled discordant population was then compared to the concordant population to see which modelled population is most similar to the concordant population. The greatest similarity between modelled population and concordant population is considered to reflect the most likely time of Pb loss. This modelling assumes that the discordant population is obtained from a similar geological province with a similar zircon age structure to the concordant zircon population. The Kolmogorov-Smirnov (K-S) statistic is used as a tool to examine the best similarity between model ages for the discordant population, compared to the concordant population (Press et al., 1986; Morris et al., 2015). The K-S statistic is mostly utilised to test the null hypothesis that two distributions come from the same population (Morris et al., 2015).

Principles for another novel model that is similar to that of Morris et al. (2015) were developed by Reimink et al. (2016). This model enables analysis of probabilistic relationships within U–Pb datasets to describe the age information present within discordant analyses by checking the relative likelihood of potential discordia lines. The model has been implemented in a program in the R coding language (Andersen et al.,2017) based on Reimink's principles, and it allows for extraction of the age information from discordant zircons which shows discordant analyses caused by Pb loss. This procedure defines a network of chords in a Wetherhill concordia plot (Figure 2.6) with pre-defined upper and lower intercepts (Reimink et al., 2016). These chords represent discordia lines that might occur within any zircon suite, either magmatic, metamorphic zircons or detrital zircons. The summed probability density related to zircon analyses along each of these lines can then be assessed, and this probability density can be used to estimate the likelihood of each line to represents a true discordia line (Reimink et al. 2016).

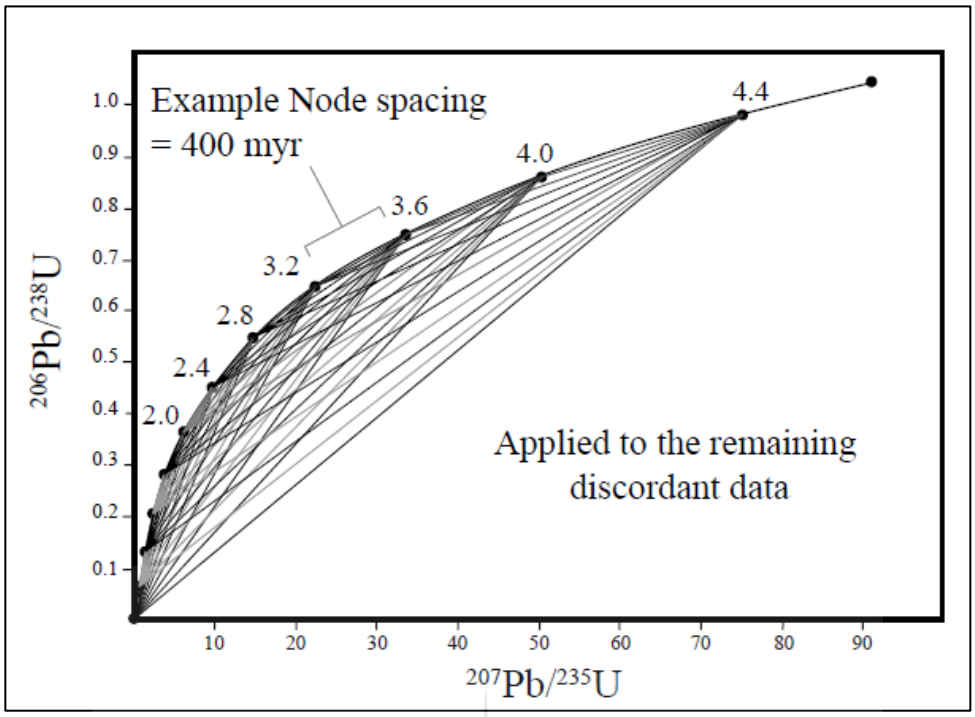

Figure 2.6: The network of chords representing possible discordia lines for a zircon suite, with upper and lower intercepts in a U-Pb concordia plot connected by a straight line (Reimink et al., 2016).

The output for this model is a data file with lower and upper intercept ages of each chord as well as likelihood along it. The lower and upper intercept have many lines associated with them, so the likelihood assigned to either lower or upper intercept age is abstracted from the line most likely to represent a true discordia chord at that age (Reimink et al., 2016). These two series may then be plotted on the same graph, showing likelihood as a function of age, as shown in Figure 2.7 (Reimink et al., 2016). Peaks shown in these diagrams represent upper and lower intercept ages, marking zircon crystallization and resetting events, respectively. It is important to verify this model with other geological evidence before important conclusions can be made because this model has an ability to create discordia lines which have no geological meaning (Reimink et al., 2016).

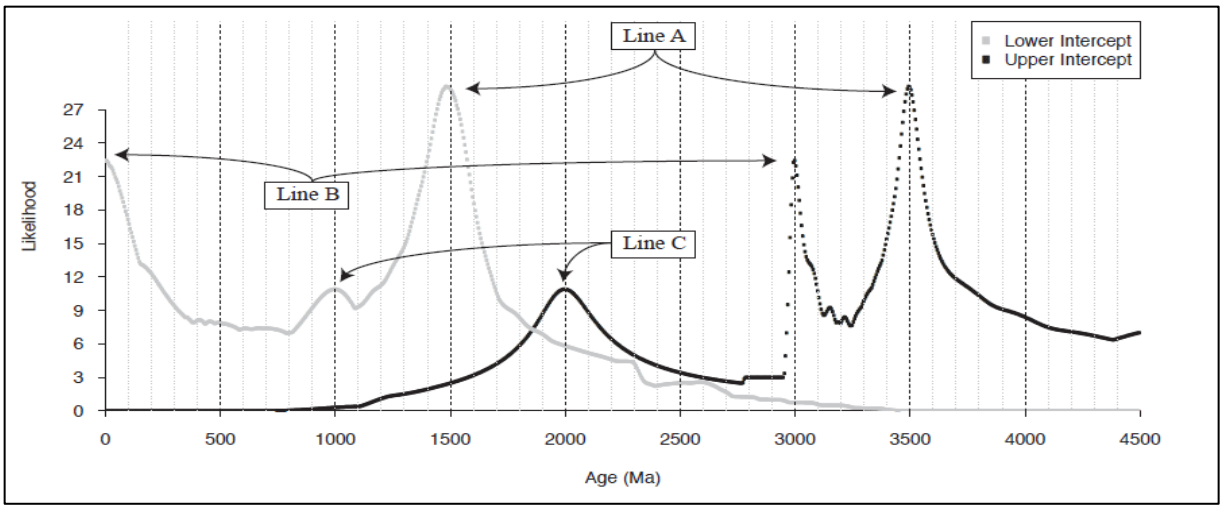

Figure 2.7: The output from R code run using artificial discordia lines. The output peaks in the spectra represent new upper and lower intercepts (Reimink et al., 2016).

2.7. Regional Geology (for sample locations)

2.7.1. The Kaapvaal Craton

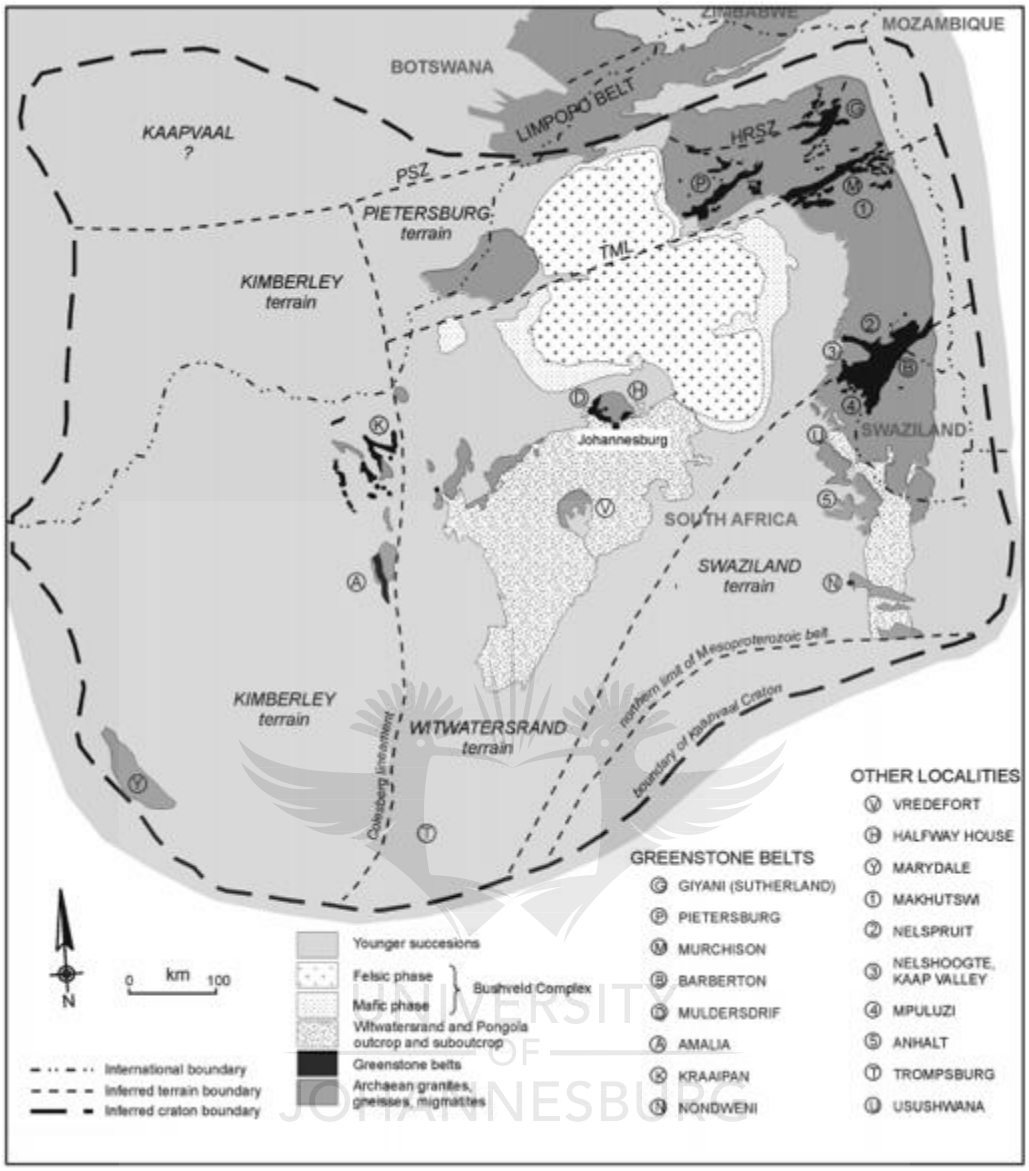

Figure 2.8: Figure showing the Kaapvaal Craton (Eglington and Armstrong, 2004).

The Palaeo- to Neoarchean Kaapvaal Craton (Figure 2.8) of ~ 1.2×10^6 km^2 is one of the most ancient and best-preserved Archean continental fragments on Earth (Poujol et al., 2002; Robb et al., 2006). A nearly continuous Archaean geological record from 3.6 to 2.6 Ga (e.g. De Wit et al., 1992) is preserved within this craton. It consists of an eastern, central, northern and western domain, with the oldest rocks occurring in the eastern part and the youngest rocks in the western terrane (James et al., 2003). These terranes of various geological histories were assembled from ca. 3.6 Ga to the late Archaean (James et al., 2003). The development of new crust that later became the Limpopo Belt, and which developed contemporarily with the first granitoid intrusions, occurred at ca. 3.25 Ga and 3.1 Ga. This was followed by igneous

activity near the major cratonic lineaments (Colesberg and Thabazimbi-Muchison) from ca. 3.1 to ca. 2.8 Ga. By ca. 3 Ga the lithosphere became firm enough to allow the development of Dominion, Witwatersrand and Pongola sedimentary basins, and that was followed by extensive volcanism during the late Archean Ventersdorp event throughout the craton (de Wit et al., 1992; Eglington and Armstrong, 2004). The Transvaal Supergroup unconformably overlies the Ventersdorp Supergroup and transgressed onto the older basement rocks at ca. 2.6 Ga (Eglington and Armstrong, 2004).

2.7.2. Archean Granites

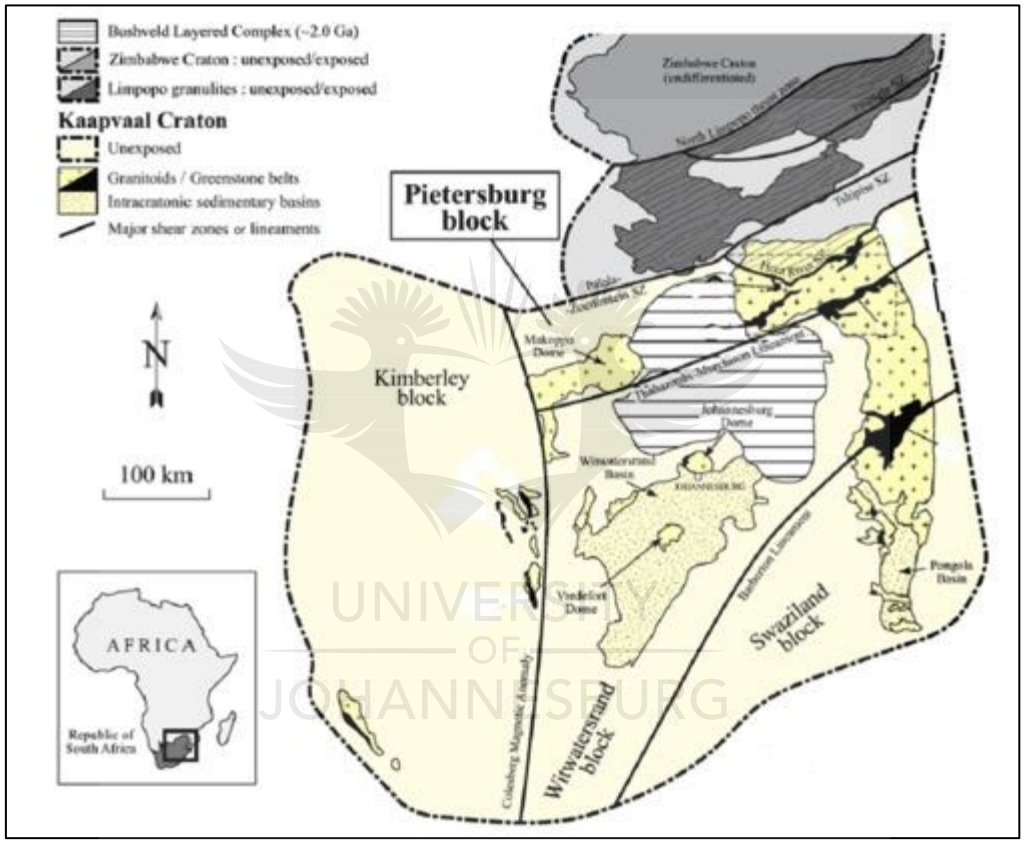

Figure 2.9: Sketch geological map showing the different positions for granitoid rocks of the Kaapvaal craton (after Laurent et al., 2013).

The Archean crystalline basement rocks are part of the lithologies of interest in the current study. The Archean granitoid rocks are exposed throughout the Kaapvaal Craton (Figure 2.9). The initial emplacement of Archean granitoids dates back to the Eoarchean (>3600 Ma) (Compston and Kröner, 1988) and the youngest granitoid intrusions date to Neoarchean times (2800 to 2500 Ma) (Kröner et al., 2000). The latter are mostly found in the northern terrane in the Kaapvaal Cratons (Figure 2.10)

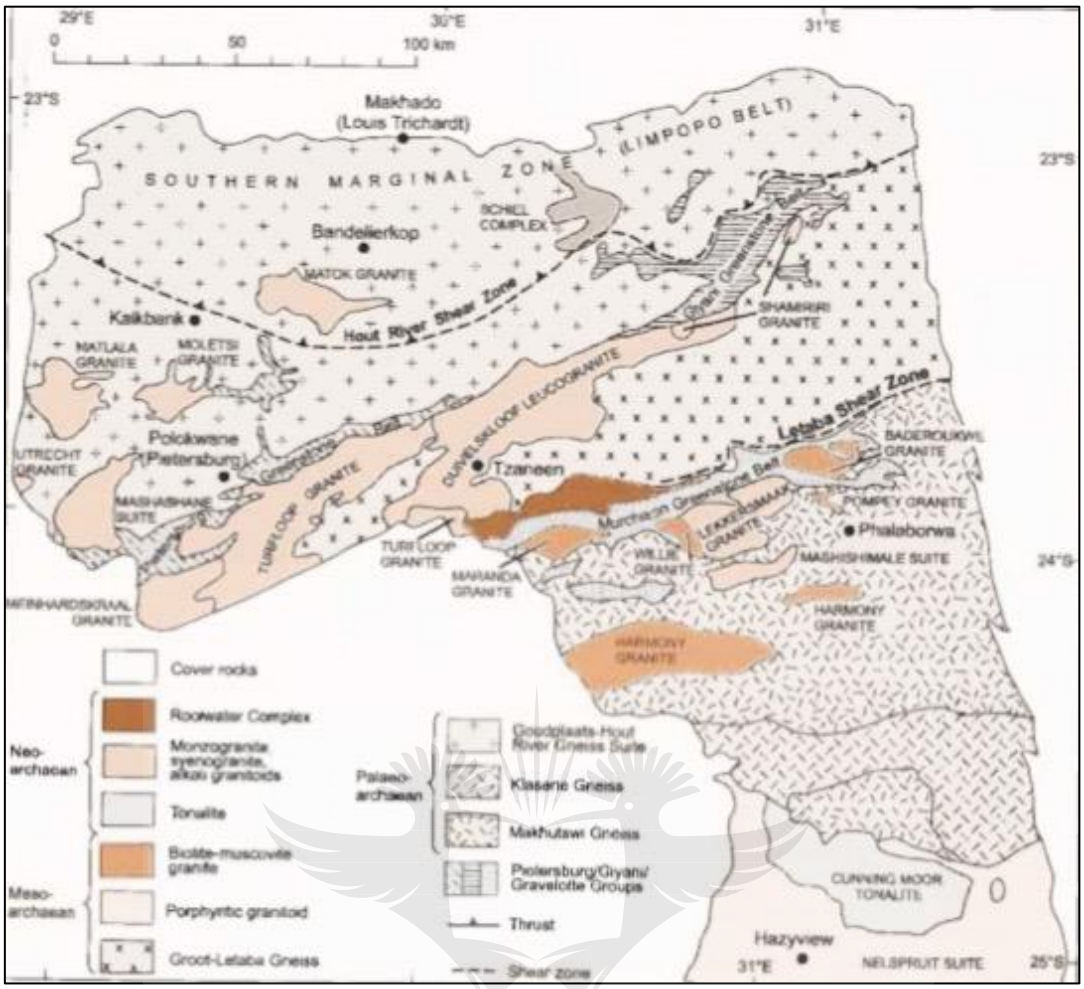

Figure 2.10 Map showing granitoid rocks occurring in the northern and northeastern terranes of the Kaapvaal Craton (Robb et al., 2006).

The Turfloop Granite is one of the members of Neoarchean granites. It occurs as an elongate north east trending batholith (Figure 2.10). This batholith is dominated by light grey to pinkish grey, medium to coarse-grained granites (Kröner et al., 2000). The mineralogy comprises plagioclase, quartz, and microcline with subordinate biotite and muscovite. Henderson et al. (2000) dated these granitoids using various methods and obtained ages of 2777±10 and 2674±16 Ma. Laurent and Zeh (2015) obtained U-Pb age of 2757±9 Ma using laser ablation sector field ICPMS (LA-SF-ICPMS). Along the south-western boundary of the Turfloop Granite is Meinhardskraal Granite whose age is unknown. According to Robb et al. (2000) the dominant mineralogy for these granites includes alkali feldspar, quartz and biotite. There is also Mashashane Granite Suite, which intrudes to the Goudplaats-Hout River Gneiss. The Mashashane comprises three phases namely, Uitvlugt Granite, Lunskip Granite and Uitloop Granite (Brandl, 1986). Laurent et al. (2013) obtained U-Pb ages of 2681±10 and 2678±10 Ma using LA-SF-ICPMS as a dating method. The Utrecht is also one of the

Neoarchean granites found in the northern terrane. It is medium to fine-grained and it has similar mineralogy to other granites in the northern Kaapvaal but it also includes garnet in its mineralogy (Brandl, 1986). There is not age information on this granite.

To the north of Mashashane suite is the Matlala Granite (Figure 2.10). This circular batholith has two main varieties, fine-grained and pophyritic pink granites (Brandl, 1986). The U-Pb ages obtained using LA-SF-ICPMS are 2677±5 and 2693±8 Ma (Laurent et al., 2013). East of Matlala batholith is the Moletsi Granite (Figure 2.10). This body is made up of three phases. From the core to the margin of the batholith is coarse-grained pinkish rock, coarse-grained grey to pinkish grey pophyritic rock and medium to fine dark grey tonalitic granite at the margin. Ages obtained for Moletsi granites are 2688±10 and 2685±7 Ma (Laurent et al., 2013).

There is also a unique body amongst other granite bodies in the northern part of Kaapvaal Craton, the Matok Granite (Brandl, 1986). This batholith was emplaced north of Hout River Shear Zone (Figure 2.10) and it contains charnockitic rocks which occur in equal propotions to granitic rocks (Brandl, 1986). Laurent et al. (2013) dated 3 samples from this igneous complex and obtained ages of 2688±8, 2679±9 and 2686±7 Ma. Other Neoarchean granite occurrences that are found in the northeastern terrene of the Kaapvaal (Figure 2.10) include the Shamiriri Granite, Baderoukwe Granite, Mashishimale Suite, Lekkersmaak Granite, Willie Granite, Harmony Granite, Maranda Granite and Pompey Granite (Robb et al., 2006).

2.7.3. The Transvaal Sequence

The Transvaal Supergroup is the earliest Proterozoic succession, of approximately 15 000 m thickness, that developed on the Kaapvaal Craton. It is dated between ~ 2.65 and 2.05 Ga (Zeh et al., 2016). It unconformably overlies the Ventersdorp Supergroup and its uppermost formations are intruded and overlain by mafic to felsic volcanic rocks of the Bushveld Complex and Rooiberg Group (Zeh et al., 2016). The stratigraphic column of the Transvaal Supergroup is shown in Figure 2.11. The Chuniespoort–Ghaap–Taupone Group forms the lower sequence of the Transvaal Supergroup and it is mostly made up of chemical sediments. The middle sequence of the Transvaal, the Pretoria Group, consists of clastic sediments and volcanics. The sedimentary rocks of the Timeball Hill Formation were deposited during the post-rift thermal subsidence at approximately 2.3 Ga (Catuneanu and Eriksson, 2002). The Timeball Hill Formation consists of three members, the upper and lower shale units which are separated by the Nooigedacht sandstone unit (from which sample MEMG5 was taken).

The Magaliesberg Quartzite (samples MEMG1-4) is a formation with an average thickness of 500 meters and consists of medium-grained pure arenites (Button, 1976). It was deposited in a complex environment of a shallow marine shelf and it is dated at ca. 2200 Ma (Eriksson et al., 2006). The Magaliesberg Formation grades upward to the Vermont Formation through a suite of impure sandstones (Button, 1976; Eriksson *et al.*, 2006).

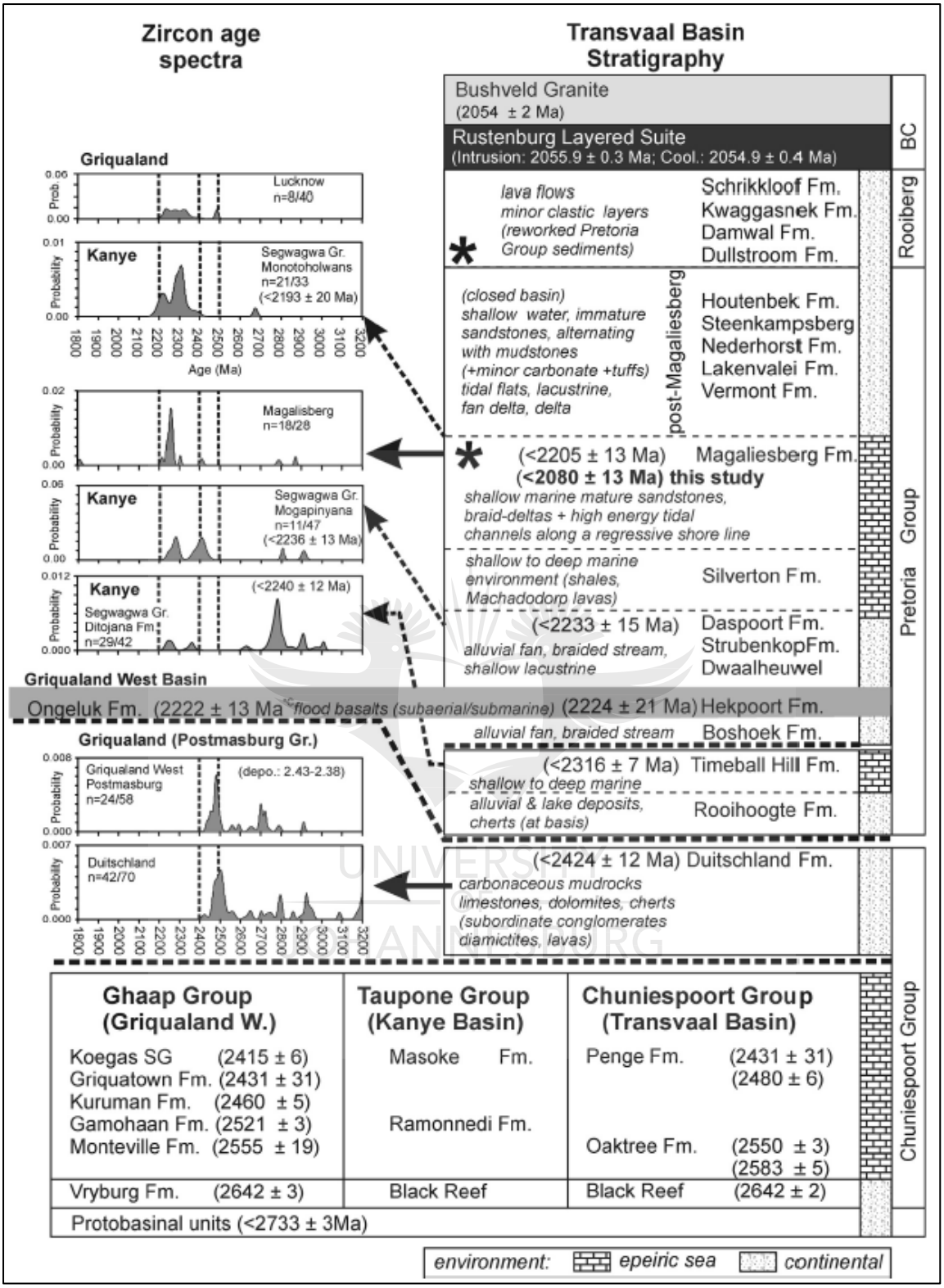

Figure 2.11: Diagram showing stratigraphic units, depositional ages, and age spectra of Transvaal Supergroup sediments and of overlying Rooiberg Group, and Bushveld Complex (Zeh et al., 2016). Note that this diagram does not take the new age determination of the Ongeluk Formation at 2426 ± 3 Ma into account (Gumsley et al., 2017).

2.7.4. Bushveld Complex (BC)

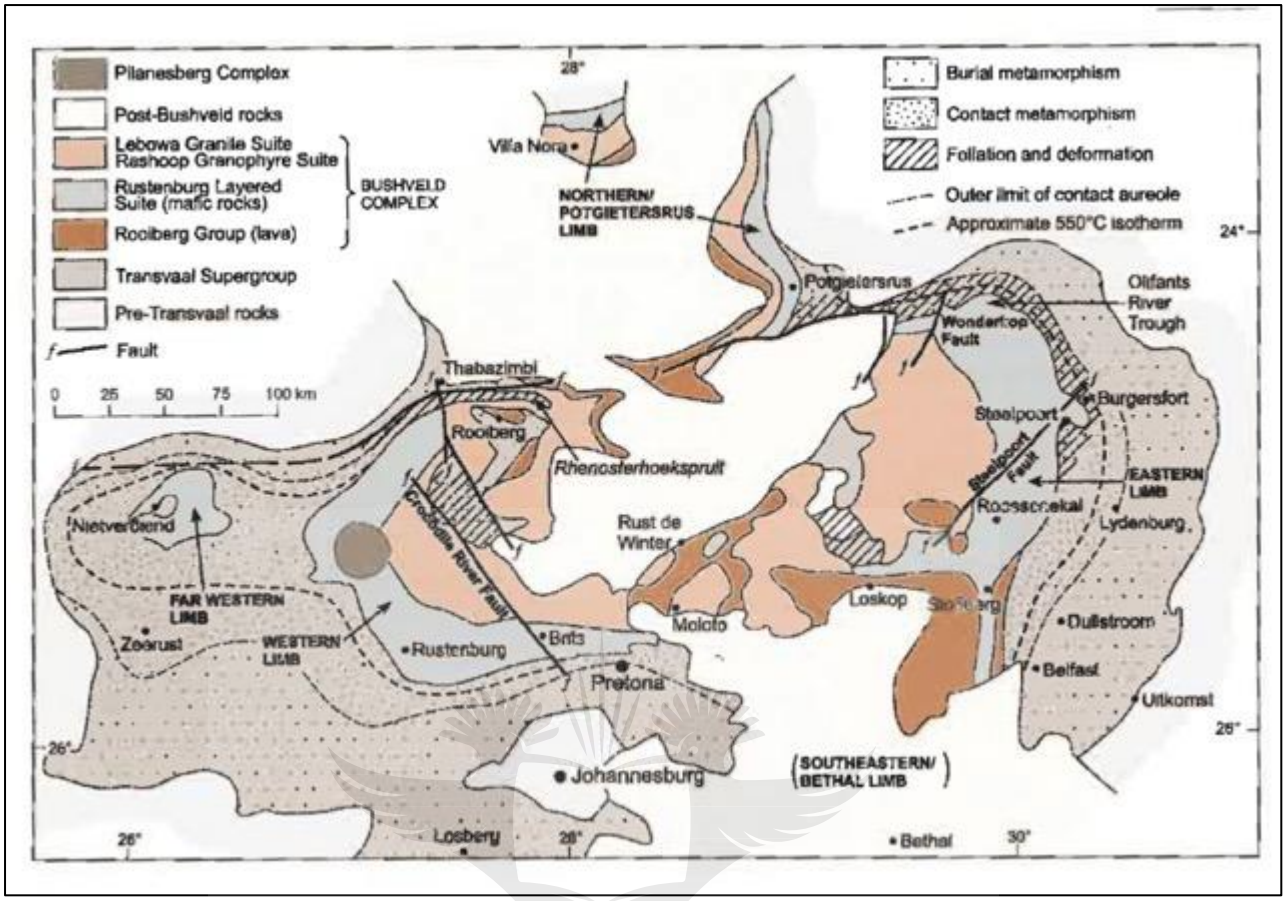

Figure 2.12: Map of the Bushveld Complex showing its different limbs as well as the metamorphic aureole (Cawthorn et al., 2006).

The Bushveld Complex is the geologically most complex igneous intrusion that intruded into the Transvaal and Archean supergroups at approximately 2055 Ma (Zeh *et al.*, 2015). This layered intrusion has an estimated total area of 66 000 km^2 (Hunter, 1976) and it consists of the eastern, western and northern or Potgietersrus limbs and southeastern/Bethal limb (Figure 2.12). The Bushveld Complex consists of voluminous layered mafic rocks, which constitute the Rooiberg Group, Rustenburg Layered Suite, and the successive felsic components, comprising the Lebowa Granite Suite (Harmer & Armstrong, 2000; Robb *et al*., 2000). The Rustenburg Layered Suite is subdivided into four stratigraphic units, the Lower Zone (pyroxenite-harzburgite-dunite), the Critical Zone (pyroxenite-anorthosite-norite), the Main Zone (norite-anorthosite-gabbronorite), and the Upper Zone (gabbronorite-magnetite gabbro-olivine diorite). The Rustenburg Layered Suite is overlain and intruded by the Lebowa Granite Suite, which occupies the central part of the complex, and it underlies the Rooiberg Group and the sills of Rashoop Granophyre (Robb *et al*., 2000).

The great extent and relative absence of deformation make this complex one of the best natural laboratories for studying the essential processes of metamorphism (Cawthorn and Walraven, 1998). Initial temperatures of around 1300 ºC for Bushveld injection were estimated by Cawthorn and Walraven (1998), and they estimated that the entire intrusion had cooled to 900ºC after 180 000 Ma. These temperatures and duration are sufficient to cause partial melting of the host rocks and probably result to partial resetting of zircon depending on compositional parameters of the melt. Maximum temperatures of 750ºC (first stage is related to the intrusion of the lower zone magma) and 900ºC (second stage is related to the intrusion of voluminous gabbroic liquids that gave rise to the upper critical, main, and upper zones) were determined in the metamorphic aureole of the Bushveld Complex in the Potgietersrus area (Nell, 1985).

2.7.5. The alkaline and carbonatite complexes

2.7.5.1. Pilanesberg Complex

The Pilanesberg Complex is the largest of all members of the Pilanesberg Alkaline Province with a diameter of ca. 30 km (Elburg and Cawthorn, 2017). This circular complex that lies on the western limb of the Bushveld Complex was emplaced around 1395 Ma (Elburg and Cawthorn, 2017). The geology of the Pilanesberg Complex comprises syenite, nepheline syenite as well as equivalent volcanic rocks.

Fluids released by alkaline magmas emplaced in the crust react with their surroundings and produce various metasomatic rocks including fenites. The term fenite first came up in the 1920's for a group of metasomatically altered rocks by Brögger (1921); this term is now widely used for metasomatised rocks normally associated with carbonatite complexes, metasomatism basically changes the composition of the rocks due to introduction or removal of chemicals which dissolve in fluids that migrate through the rock (Harlov and Austrheim, 2013). The alkaline fluids that were released by crystallising intrusive bodies of the Pilanesberg Complex caused metasomatism in rocks within the Pilanesberg Complex, but it is also possible that they penetrated the overlying rocks of the Bushveld Complex (Elburg and Cawthorn, 2017). The fluids from intrusions do not only deliver water, but also the heat from the magma (e.g. Harlov and Austrheim, 2013).

2.7.5.2. The Spitskop Complex

The Spitskop complex is found in the east of the Pilanesberg Alkaline Province (Harmer and Gittins, 1997). It is ca. 1341 Ma in age (Harmer, 1999), and it intruded into the Lebowa Granite Suite of the Bushveld Complex. The Spitskop complex is circular in shape and it covers a surface area of about 50 km^2 (Harmer, 1999). Its formation stages include the intrusion of a pyroxenite pipe which was then intruded by ijolite sheets, nepheline syenite bodies and composite carbonatites (Gose et al., 2013). The carbonatites in the Spitskop Complex are mostly dolomite carbonatite, but they also include calcite carbonatites. The carbonatite plug consists of an early discontinuous outer zone of calcite carbonatite that surrounds an intermediate zone of dolomite and calcite carbonatite and a centre of dolomite carbonatite. Fenitization of country rocks is dominant in the Spitskop Complex (Verwoerd, 1967).

2.7.5.3. The Goudini Complex

The Goudini carbonatite complex is Mesoproterozoic, with an age of ca. 1193 Ma (Harmer, 1992). It is almost oval in shape, and has a size of about 27 km^2 (Verwoerd, 1967). This complex is surrounded by the mafic rocks of the Bushveld Complex showing signs of fenitization at the contact (Verwoerd, 1967). The geology of this complex comprises a volcanic breccia which forms the rim of the complex and consists mostly of country rock fragments (Verwoerd, 1967). Overlying the volcanic breccia are volcanoclastic rocks (mainly tuffs) that appear to be washed into the "maar". The volcanoclastic rocks show varve-like layering in places and they have chemical compositions similar to that of fenitized norite (Verwoerd, 1967). These are then overlain by the calcite-rich carbonatites that have a medium-grained texture. The carbonatites cut across the volcanoclastic beds and contain some fluorite, barite, monazite and biotite (Verwoerd, 1967).

2.7.6. Karoo dolerites

The Karoo dolerites are mafic intrusions that extensively developed in the main Karoo basin (Duncan et al., 1997). They are dated at ca. 180 Ma and their formation is associated with Karoo magmatism (Svensen et al., 2012). They are also found intruding other sequences throughout the Kaapvaal Craton, such as the Bushveld Granites (sample MEMG12).

Chapter 3

3. Sampling and analytical techniques

3.1. Sample locations

The basement rocks analysed consist of granitic rocks from the Pietersburg block in the northern Kaapvaal Craton. Overlying the Archean granites are quartzite rocks from the Timeball Hill and Magaliesberg formations of the Pretoria Group (Transvaal Supergroup) on the eastern and western margins of the Bushveld complex, and these rocks from the Transvaal basin are intruded the Bushveld Complex. Intruding the Bushveld Complex are the Pilanesberg Complex, Spitskop Complex and the Goudini Complex, and Karoo-age dolerite dykes.

For the purpose of this study, a total of fourteen samples was collected in numerous locations where there was thought to be possibility of zircon age resetting by thermal or chemical effects of nearby intrusions in the vicinity of the Bushveld Complex. The rock samples include the sedimentary (Transvaal Supergroup) and igneous host rocks (Archean intrusives). Other targets were rocks that could be affected by chemical effects from Pilanesberg Alkaline Complex as well as Spitskop and Goudini complexes. Finally, one sample of Bushveld granite intruded by Karoo dolerite was also analyzed (Figure 3.1). Additional fenite samples were collected by Anıl Öztürk at the Spitskop Complex in the central Kaapvaal Craton of South Africa (Figure 3.2). A simplified stratigraphic column for the sample locations is presented in Figure 3.3 and sample descriptions are given in Table 3-1.

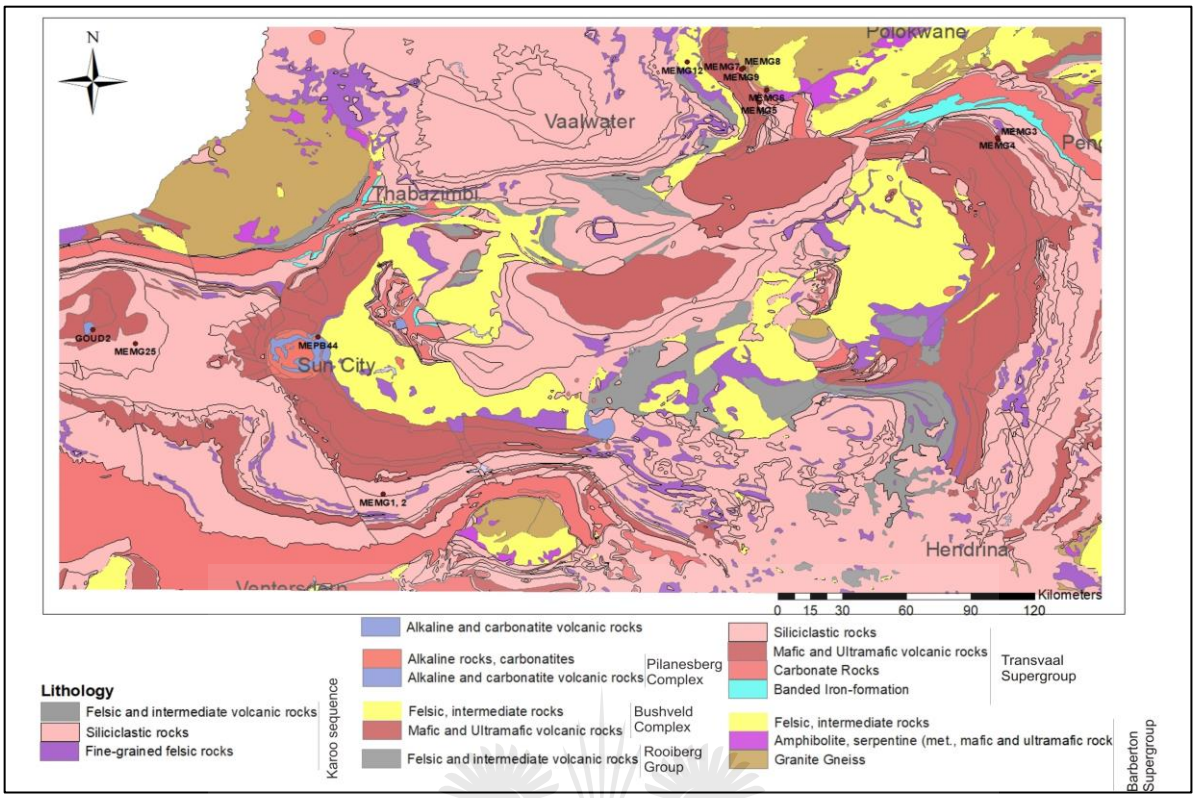

Figure 3.1: Geological map showing sample locations.

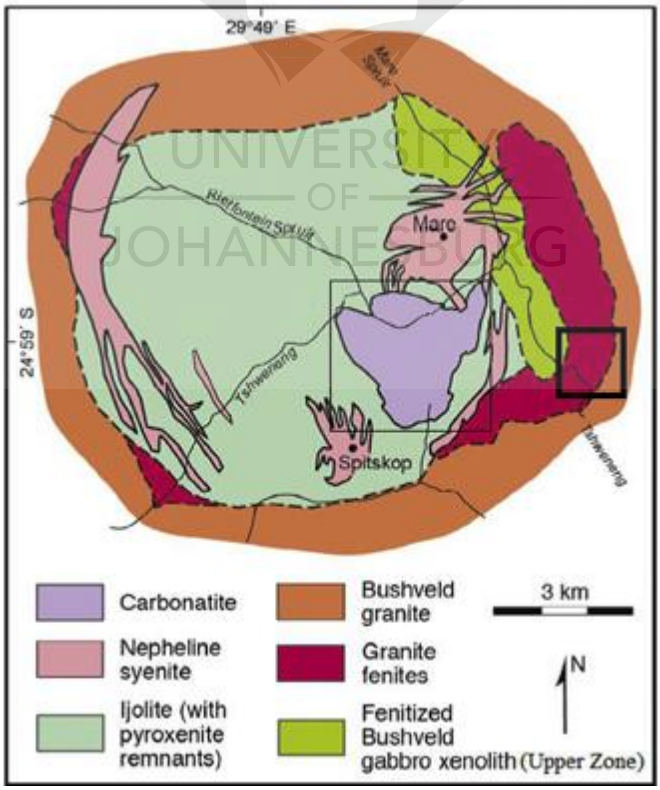

Figure 3.2: Geological map of Spitskop Complex showing sample locations for fenites inside the small thick black rectangle (Öztürk, 2017).

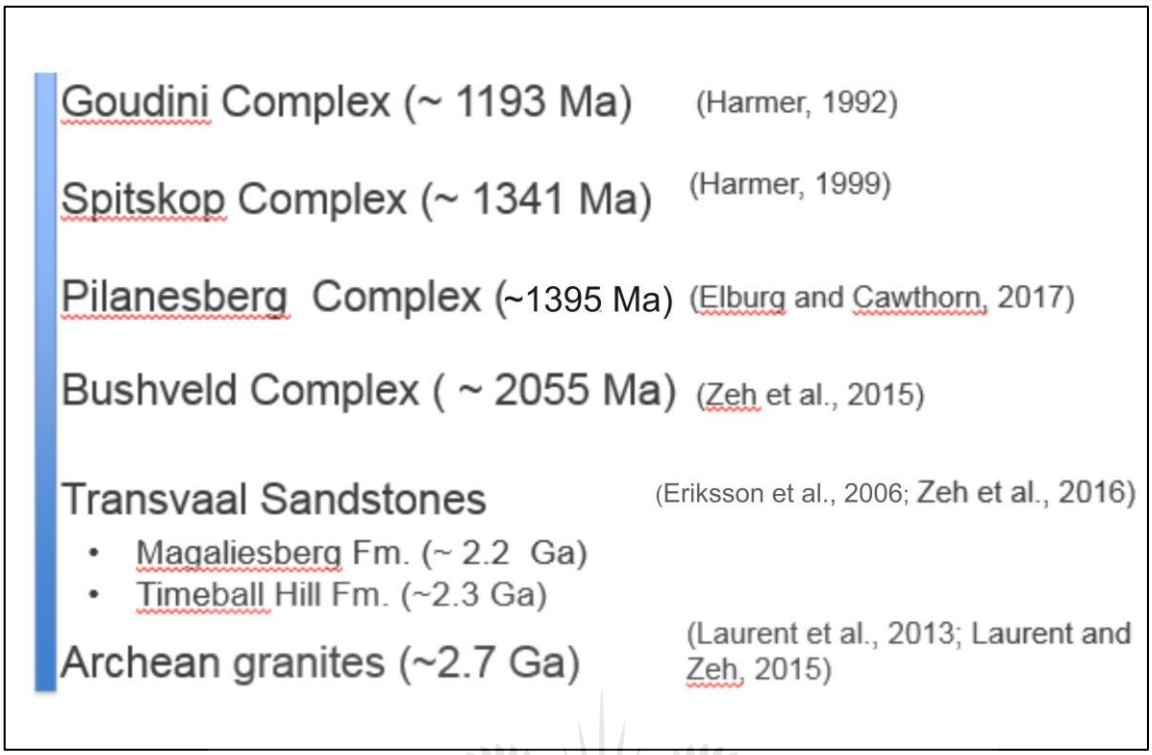

Figure 3.3: Simplified stratigraphic column for sample locations.

Sample name	Rock description	Latitude	Longitude	Height (masl)
MEMG6	Archean granite, taken a bit further from Rustenburg Layered Suite than MEMG7,8, but potentially affected by Bushveld intrusion	-24.0978	29.0549	1216
MEMG7	Archean granite removed ca. 1 km from Anglo American's Mogalakwena Platinum Mine, potentially affected by Bushveld intrusion	-24.0036	28.9584	1176
MEMG8	Archean granite, removed ca. 1 km from Anglo American's Mogalakwena Platinum Mine potentially affected by Bushveld intrusion	-24.0096	28.94997	1148
MEMG9	Aplite dyke within MEMG8	-24.0096	28.94997	1148
MEMG1, 2	Magaliesberg metasandstones, taken <1 km south of the Rustenburg Layered Suite in the western limb of the Bushveld Complex, potentially affected by Bushveld intrusion	-25.8602	27.44313	
MEMG3	Magaliesberg metasandstone, obtained at 0.5 meters from the contact with the Marginal Zone in the eastern limb of the Bushveld Complex	-24.3142	30.02871	
MEMG4	Magaliesberg metasandstone, obtained 230 meters from the contact with the Marginal Zone in the eastern limb of the Bushveld Complex	-24.3061	30.00475	936
MEMG5	Nooitgedacht quartzite member of Timeball Hill Formation, collected ca. 1 km from the Rustenburg Layered Suite, potentially affected by Bushveld intrusion	-24.1537	29.02508	1160
MEMG25	Magaliesberg metasandstone in contact aureole of Bushveld, south of the Goudini Complex	-25.2029	26.40063	1030
MEPB44	Bushveld Granite just north of Pilanesberg, potentially affected by Pilanesberg intrusion	-25.1758	27.16798	1103
MEMG12	Bushveld Granite intruded by Karoo dolerite	-23.9792	28.72187	1028
GOUD2	Loose block of silicate material within Goudini Complex, potentially affected by Goudini carbonatitic complex	-25.1448	26.22198	979
52.2	Feldspar fenite sample within Spitskop Complex, which could be potentially be affected by Spitskop Complex			1311

Table 3-1: Sample descriptions and coordinates.

3.2. Sample preparation

Weathered parts of the selected samples were removed with a diamond-blade saw. Then they were washed with a scrubbing brush to remove the impurities and oven-dried for about 30 minutes, then were left to further air-dry overnight. Samples were crushed with a hammer into smaller pieces, after which they were coarsely milled using C-steel pot. Then finally the samples were sieved to <250µm using a sieving mesh. Equipment was properly washed after preparing each sample to avoid contamination of samples. Zircons were separated from the

sample using a handheld magnet and the heavy liquids sodium polytungstate (NaPT) and lithium heteropolytungstate (LST) with a density of ~2.9 g/ml. A second separation was done on selected samples using methylene iodide (MI) with a density of 3.3 g/ml. Zircon grains were then handpicked from the heavy mineral fraction under the binocular microscope, which is preferred over magnetic separation to avoid bias and losing zircon grains (Andersen et al., 2011). Hand-picked zircons of different sizes and shapes were set in epoxy resin, polished and examined under binocular microscope to ensure that the zircon grains were exposed for imaging.

3.3. Analytical techniques

3.3.1. Cathodoluminescence Imaging

After carbon-coating, imaging of the zircons was done on a scanning electron microscope (SEM) equipped with a cathodoluminescence detector. Zircon grains were imaged prior to the isotopic analysis to examine the internal structure, and to precisely select the locations for further analyses. The equipment is available at the analytical facility of the University of Johannesburg, SPECTRUM.

Instrument and settings:

A VEGA TESCAN Scanning Electron Microscope equipped with a Centaurus detector was used to examine the internal structure of the zircon grains using the cathodoluminescence (CL) imaging. Imaging was done at a voltage (HV) of 20 kV, using a working distance (WD) of approximately 23 mm with variable magnification depending on the zircon grain size, at a scanning speed of seven.

3.3.2. LA-MC-ICPMS

Isotopic zircon analyses were carried out at the University of Johannesburg using laser ablation - multi collector - inductively coupled plasma source mass spectrometry (LA-MC-ICPMS) (Figure 3.4). LA-MC-CPMS was used for U-Pb dating and Lu-Hf analysis of zircon.

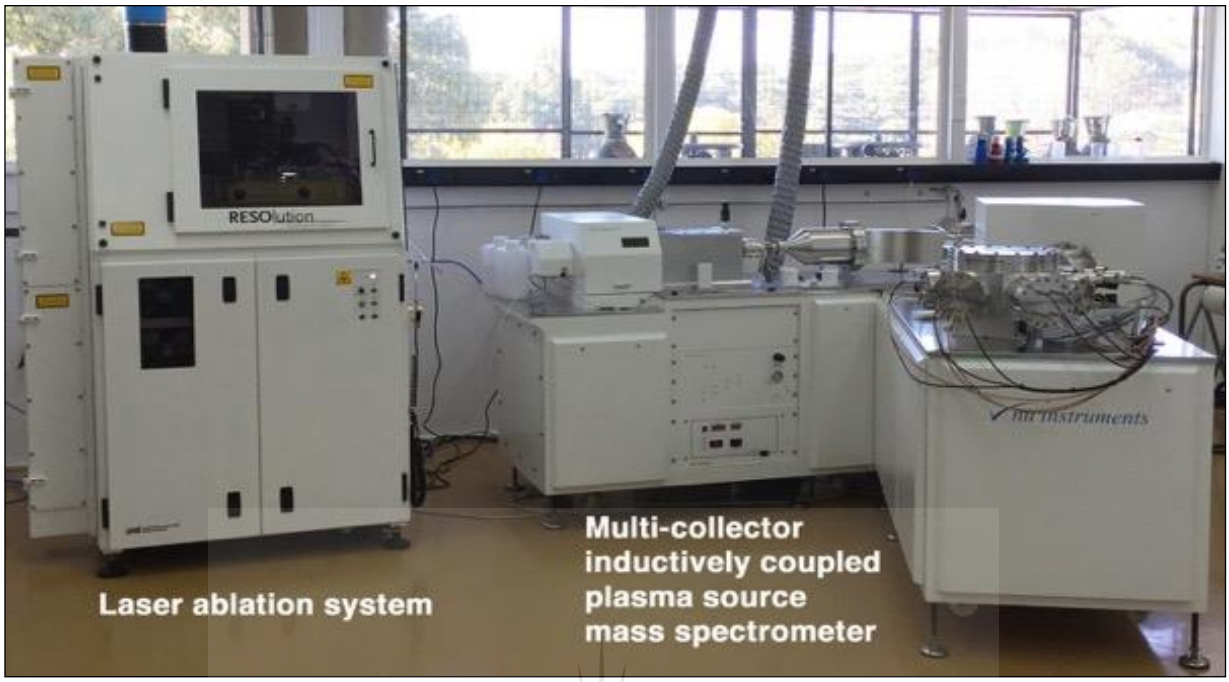

Figure 3.4 The laser ablation- multi collector- induced coupled plasma source mass spectrometry (LA-MC-ICPMS) used for determination of the U-Pb and Lu-Hf ages and ratios.

Instrument and settings:

The laser ablation multi-collector inductively coupled plasma source mass spectrometer used for determination of the U-Pb and Lu-Hf ages and ratios consists of a Nu Instruments Plasma II with sixteen Faraday detectors and 5 ion counting detectors, coupled to a 193 nm ArF Resolution SE excimer laser ablation system.

The instrument parameters that were set up prior to analysis include:

- RF Power of 1300 W to maintain the plasma
- Coolant gas flow of 13.0 L/min
- An auxiliary gas flow of 0.88 L/min to mix the gas with a sample
- Nebuliser gas flow of 0.8 L/min
- Laser He gas flow 0.25 L/min

U-Pb measurements:

Using a 25 µm spot size, beam energy of 3 mJ and a beam attenuation of 12.5%, zircon grains were ablated using a 193nm deep ArF RESOlution SE excimer laser at repetition rate of 3 Hz using 1.2 J/cm^2 ablation intensity (fluence). The analysis of a single sample takes 95 seconds, 25 seconds of blank signal then 70 seconds of ablation signal.

Detector configuration used is as follows: H8 = ^{238}U; H7 = ^{232}Th; IC0 = ^{208}Pb; IC1 = ^{207}Pb; IC2 = ^{206}Pb; IC3 = ^{204}Pb; IC4 = ^{202}Hg.

The primary reference materials used to correct for instrumental mass bias and elemental fractionation were zircons OGC1, A1772, A382 and GJ1. Although GJ1 and 91500 are known to contain negligible amounts of common lead (Wiedenbeck *et al*., 1995; Jackson *et al*., 2004), these two standards were not used for calibration for most of the samples because they are much younger than samples analyzed in this study. The reference material used to evaluate accuracy was zircon from the Cape Donnington Quartz Gabbro Norite Gneiss (CDQGNG). The accepted ages for these zircons are presented in the table below (Table 3-2). The average $^{207}Pb/^{206}Pb$ age obtained after analyzing 163 grains of CDQGNG during the present study is 1856 Ma with a standard deviation of 22 Ma.

Reference Sample	**Accepted $^{207}Pb/^{206}Pb$ age**
OGC1	3465±0.6 Ma (Stern et al., 2009)
A1772	2711±3 Ma (Huhma et al., 2012)
A382	1877 ±2 Ma (Huhma et al., 2012)
GJ1	609.7±1.3 Ma (Jackson et al., 2004)
CDQGNG	ca. 1850 Ma (Black et al., 2003)

Table 3-2: Table presenting the references materials used for this study and their accepted ages.

For the raw data, the background correction was done to remove the background signal that was collected prior to ablation. Then the reduction of data to U-Pb isotope ratios was done by calibration to reference zircons of known ages using protocols from Andersen et al. (2004) and Jackson et al. (2004). Ion counter counts were converted and reported as volts by the Nu Plasma time-resolved analysis software. The on-mass background measurement was used to eliminate ^{204}Hg before each analysis. The calculations were performed using an off-line interactive spreadsheet program written in Microsoft Excel by T. Andersen (Figure 3.5; see Rosa et al., 2009 for more details on the program). This program basically summarises and groups background-corrected signals for mass numbers 202, 204, 206, 207, 232 and 238, and the ^{207}Pb/^{206}Pb, ^{206}Pb/^{238}U and ^{207}Pb/^{235}U isotope ratios (with the ^{235}U signal calculated using the a present-day ^{238}U/^{235}U ratio of 138.77), then calculates the ages of the zircon grains from these ratios with 'central' and 'rim' discordance percentages. 'Central' discordance reflects the distance of the analytical point from the concordia, whereas 'rim' discordance takes the undertainty of the analysis into account. Therefore, 'rim' discordance is always less than 'central' discordance. This program also allows for ^{204}Pb correction for samples yielding common lead contents above the detection limit, assuming a composition of common Pb based on the Stacey and Kramers (1976) crustal growth curve. From the ratios it then calculates the ages.

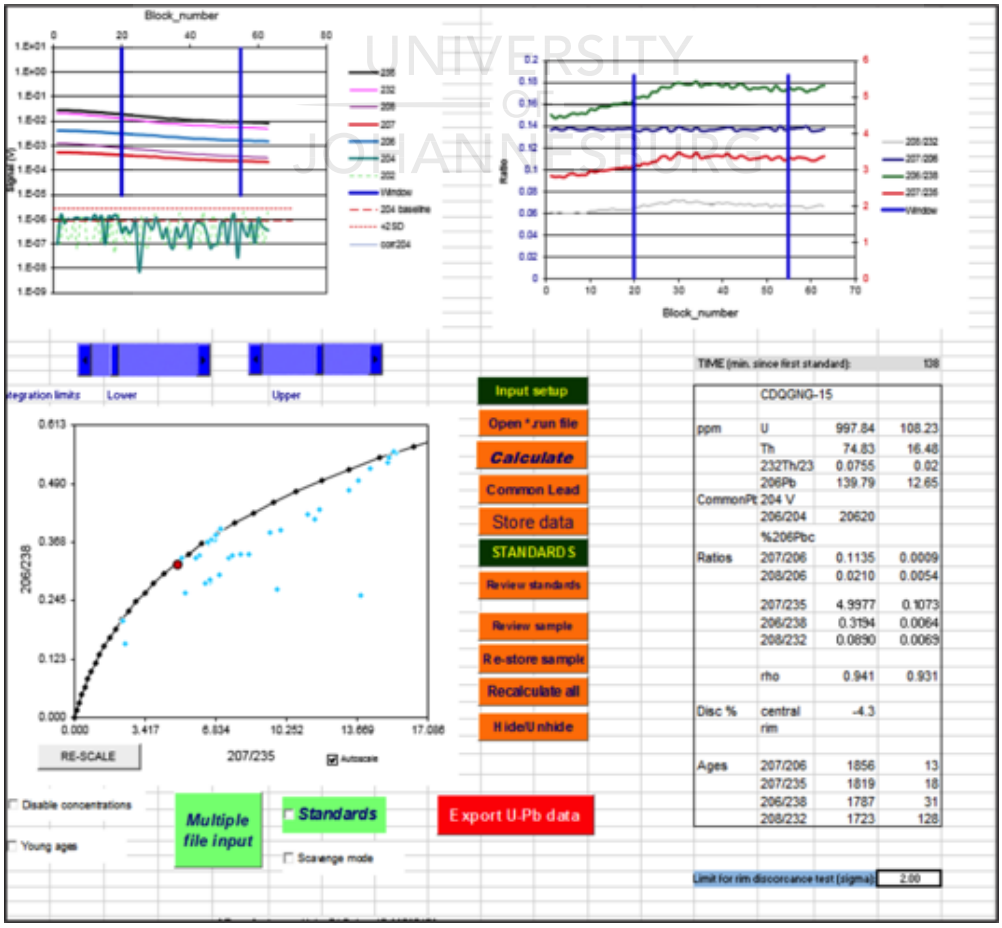

Figure 3.5 NuAge2 program used to calculate corrected isotopic ratios and ages.

U–Pb ages were calculated using ISOPLOT version 3 (Ludwig, 2003) with errors reported at 95% (±2σ) confidence level and plotted on concordia diagrams.

Lu-Hf measurements:

Using a 35-50 µm spot size, a beam energy of 4 mJ and a beam attenuation of 50%, the zircon grains were ablated at a repetition rate of 7 Hz using 4 J/cm^2 ablation intensity (fluence). The analysis of a single sample took 95 seconds, 25 seconds of blank signal then 70 seconds of ablation signal. The background correction was done by measuring background signal on mass prior to ablation and subtracting from signal.

Detector configuration used is as follows: H4 = ^{180}Hf; H3 = ^{179}Hf; H2 = ^{178}Hf; H1 = ^{177}Hf; Ax = ^{176}Hf + ^{176}Yb + ^{176}Lu; L1 = ^{175}Lu; L2 = ^{174}Hf + ^{174}Yb; L3 = ^{173}Yb; L4 = ^{172}Yb; L5 = ^{171}Yb.

For mass bias correction, the ^{171}Yb/^{173}Yb ratio was used to calculate Yb mass fractionation following the Russell equation (e.g. Smet et al., 2010) and Lu was assumed to have the same fractionation exponent; ^{179}Hf and ^{177}Hf were used to calculate Hf mass fractionation.

For interference corrections, ^{171}Yb was used to calculate and correct ^{174}Yb interference on ^{174}Hf and the ^{176}Yb interference on ^{176}Hf; ^{175}Lu was used to correct the ^{176}Lu interference on ^{176}Hf.

Secondary standards measured as unknowns to evaluate the accuracy were zircon standards Mud Tank, Temora2 and LV11. The accepted ages for these zircons are presented in Table 3-3 and values obtained from the study are presented in Table 3-4.

Accepted values

Reference Sample	Age	$^{176}Hf/^{177}Hf$ solution
LV11	~290 Ma	0.282830±28
Temora2	~418 Ma	0.282686±8
Mud Tank	~732 Ma	0.282507±6

Table 3-3: The accepted values for reference zircons used for Lu-Hf isotopic analyses (Woodhead and Hergt, 2005; Heinonen *et al.*, 2010).

Values obtained from current study

Analyzed sample	n	$^{176}Hf/^{177}Hf$	2SD
LV11	60	0.28284	0.00004
Temora2	49	0.28267	0.00002
Mud Tank	32	0.282495	0.00002

Table 3-4: The values for secondary reference zircons obtained from the current study.

3.3.3. LA-Quadrupole-ICPMS

Trace element analysis was performed on zircons from selected samples using LA-Q-ICPMS to constrain the effects on the elemental composition of the zircon.

Instrument and settings:

Zircon trace element concentrations were measured using the Thermo Electron X-Series II Quadrupole-based ICP-MS with dual mode detection system. The parameters were chosen to ensure optimal sensitivity for trace element analysis including light rare earth elements.

Parameters were as follows:

Using a 50 µm spot size, a beam energy of 6 mJ and a beam attenuation of 50%, the zircon grains were ablated at a repetition rate of 15 Hz using 3.5 J/cm^2 ablation intensity (fluence). The analysis of a single sample takes a total of 85 seconds, 25 seconds of blank signal then 60 seconds of spot ablation signal. The results obtained for the trace elements reported in this study were calibrated using NIST 612 glass as a calibration standard and GJ1 as a secondary

standard. Two NIST 612 standards and one GJ1 were analyzed before and after each analysis series, which had around ten unknown samples (samples used for this study).

Data reduction

The data collected was then reduced using GLITTER (Gemoc Laser ICPMS Total Trace Element Reduction) V4.4 (Van Achterbergh et al. 2001). This is an online interactive computer program that allows for inspection and evaluation of data in real time and to identify trace element analyses with linked graphic and analysis table. The secondary reference material used was GJ1, and accepted values for this material from previous studies are listed in a table below (Table 3-5); the values obtained from a total of nineteen analyzed GJ1 standards during current study are presented in (Table 3-6).

Analysis	**P**	**Ti**	**Y**	**Nb**	**La**	**Ce**	**Pr**	**Nd**	**Sm**	**Eu**	**Gd**	
Average	30.2	3.35	238	2.01	0.003	14.9	0.030	0.63	1.44	0.96	6.6	
1 SD	6.4	0.18	5.4	0.21	0.001	1.16	0.003	0.03	0.09	0.08	0.20	
Analysis	**Tb**	**Dy**	**Ho**	**Er**	**Tm**	**Yb**	**Lu**	**Hf**	**Ta**	**Pb**	**Th**	**U**
Average	1.88	20.0	6.7	28.7	6.4	64.8	11.52	6681	0.40	25.3	9.7	14
1SD	0.11	0.65	0.25	0.84	0.10	1.9	0.45	57	0.05	2.1	0.3	9.5

Table 3-5: LA-ICPMS data (ppm). Average and standard deviation for the GJ-1/81 zircon standard used as accepted values, 1 sigma was calculated using GLITTER (Piazolo et al., 2017).

Analysis	**P**	**Ti**	**Y**	**Nb**	**La**	**Ce**	**Pr**	**Nd**	**Sm**	**Eu**	**Gd**	**Tb**
Average	612	8.34	226	9.19	BDL	14.20	0.12	0.63	1.27	0.86	6.00	1.66
1 SD	1127	2.85	7.59	0.46	BDL	0.07	0.18	0.20	0.14	0.34	0.23	
Analysis	**Dy**	**Ho**	**Er**	**Tm**	**Yb**	**Lu**	**Hf**	**Ta**	**Pb**	**Th**	**U**	
Average	17.20	5.75	25.99	5.39	52.42	10.96	6252	0.40	26.05	8.45	257	
1SD	0.73	0.32	1.65	0.33	2.23	0.45	145	0.10	0.14	0.24	4.92	

Table 3-6: LA-ICPMS data (ppm). Average and standard deviation for the GJ-1 zircon standard obtained in the current study.

3.3.4. R coding program

Section 2.6 describes the principles behind this program. It basically allows for the analysis of predicted relationships within U-Pb datasets to try and analyze the information present within discordant analysis.

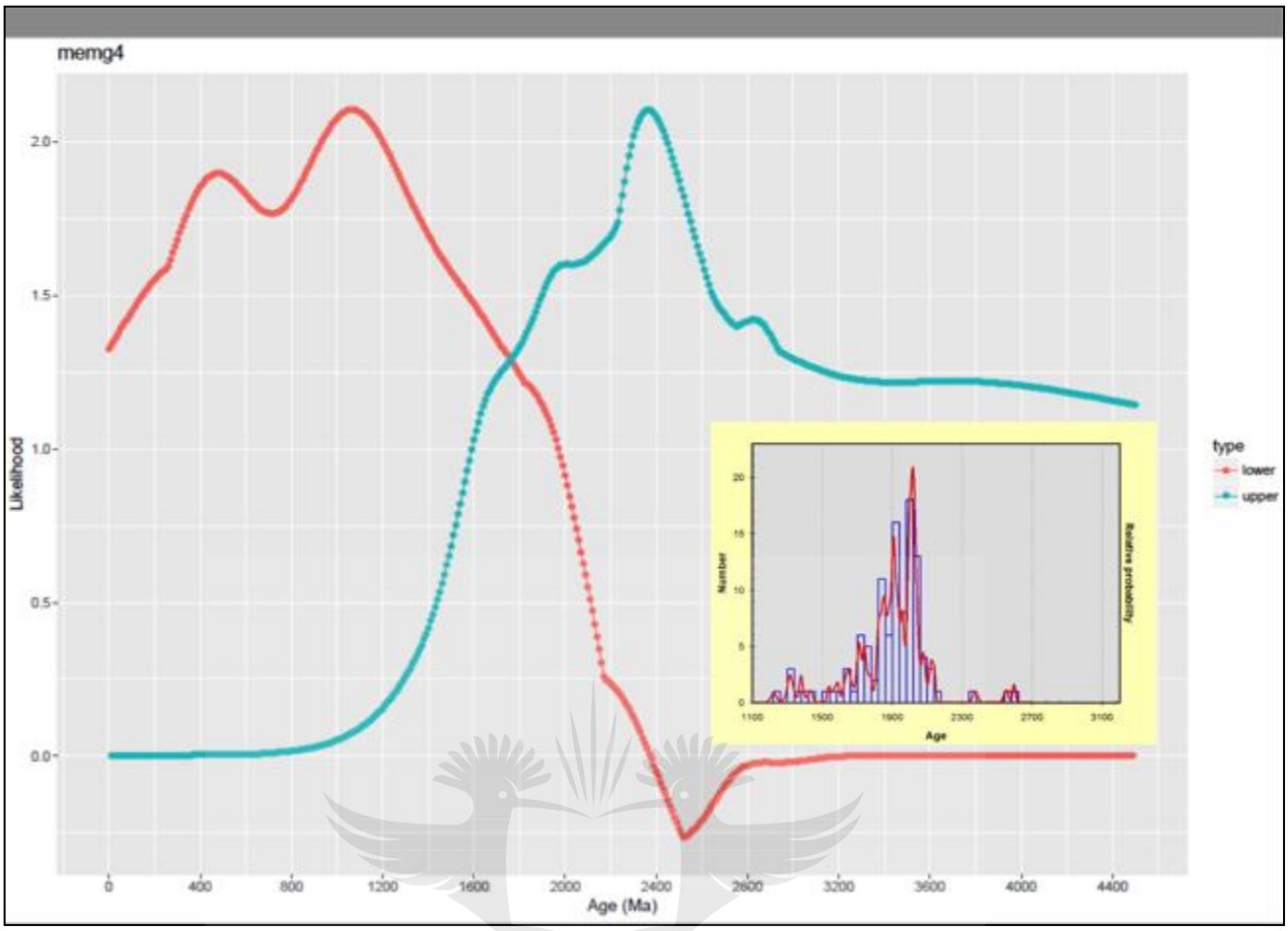

Figure 3.6: Example of output from the R program implementing the protocols of Reimink et al. (2016), showing peaks of events at different ages in both upper and lower intercepts.

This is a statistical programming written in the R coding language by Magnus Kristoffersen (University of Oslo) following the principles defined by Reimink et al. (2016). It inputs CSV files with the following information: $^{207}Pb/^{235}U$ ratio, 1 sigma 7/35, $^{206}Pb/^{238}U$ ratio, 1 sigma 6/38, rho, $^{207}Pb/^{206}Pb$ age (in Ma) in the exact order, together with *remink_plot.R*. Using the protocols defined by Reimink et al. (2016) this program then produces a data file containing upper intercept, lower intercept, summed probability density, and normalised likelihood (peaks) at different ages (e.g. Figure 3.6), and this can be used for plotting diagrams that relative likelihood for example probability density plots (e.g. insert in Figure 3.6).

3.4. Introduction to results chapters

3.4.1. U-Pb results

To aid discussion of the data presented in the results chapters, idealized diagrams are shown below to discuss the behavior of concordant and discordant analyses for a single population

of zircons in a U-Pb isotopic system. According to Tilton (1960), a group of zircons that suffered on single lead loss event would fit on the same discordia line in U-Pb isotope space, if this is the only time at which Pb was lost. Different possibilities are presented for zircon from a granite with an igneous crystallization age of 2700 Ma (Figure 3.7 a-f). Figure 3.7a shows a 2700 Ma old granite that partially lost Pb at 500 Ma (Dickin, 2005). Figure 3.7b shows a granite of which the zircons are concordant at 2700 Ma, without any Pb loss. Figure 3.7c shows a granite that has partially lost Pb at 2055 Ma. Figure 3.7d shows a granite that has completely lost Pb at 2055 Ma. Figure 3.7e shows a granite that has partially lost Pb at 0 Ma, with analyses falling on a straight line towards the origin of a diagram. Figure 3.7f shows granite that has partially lost Pb at 2055 Ma and 0 Ma; in this case the analyses fall within a triangle between the crystallization age, 2055 and 0 Ma.

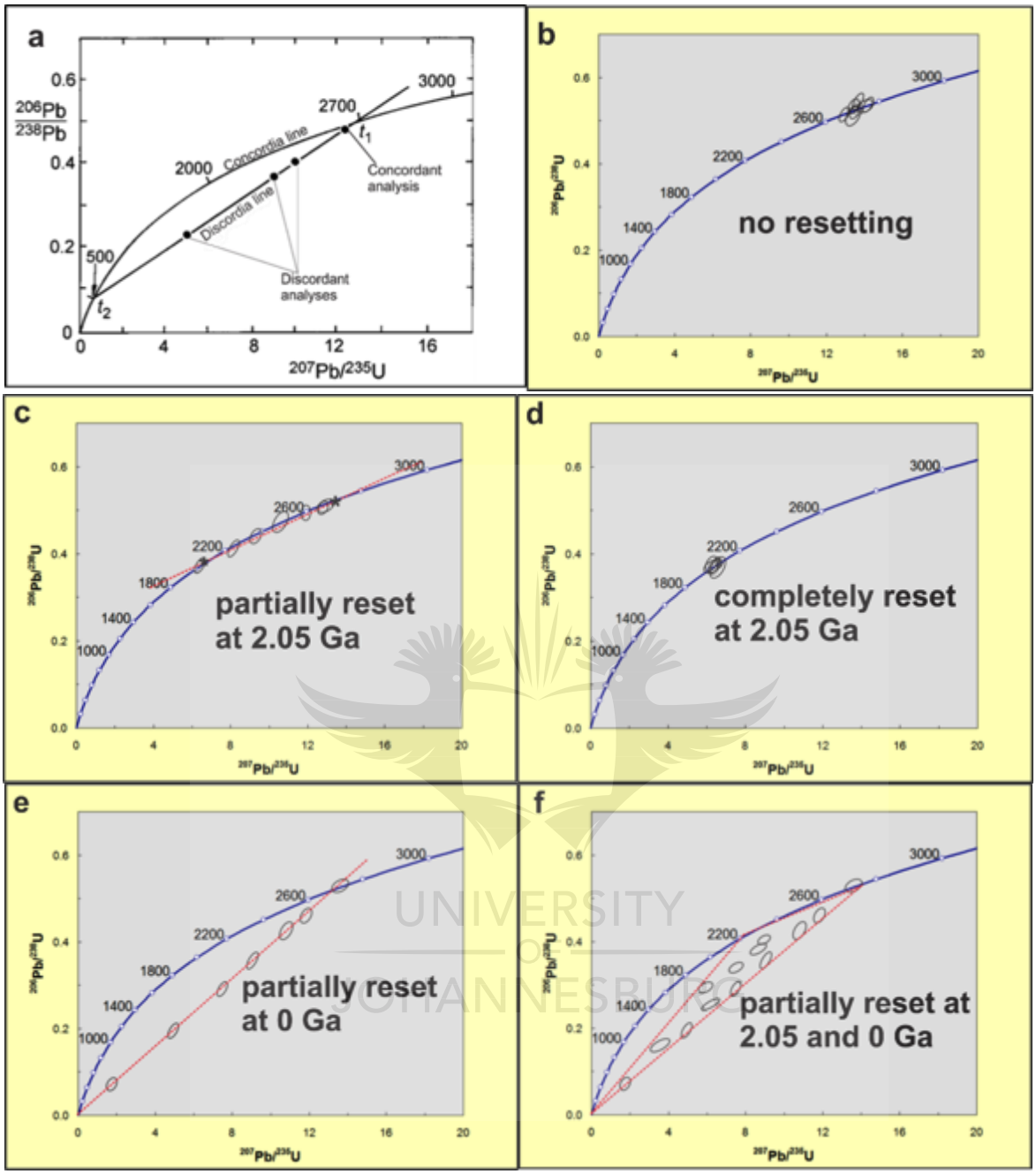

Figure 3.7 Hypothetical concordia diagrams for zircons from a 2700 Ma Archean granite that (a) partially lost Pb at 500 Ma (Dickin, 2005) (b) suffered no resetting (c) partially lost Pb at 2.05 Ga (d) were completely reset at 2.05 Ga (e) partially lost Pb at 0 Ga (f) partially lost Pb at 2.05 and 0 Ga.

Please note that in most diagrams there are analyses labelled “original” and “CPb”, whereby the former is used for analyses that contained negligible common Pb contents, based on the measured counts for ^{204}Pb, and were thus not corrected for common Pb; the latter is used for analyses that are corrected for common Pb. Also note that the data on uranium contents were obtained by comparison to the reference zircons analysed during isotopic analysis, and, as the uranium contents of reference zircon A382 is only know to within 50%, the reported concentrations will be less accurate than if trace elements are determined by comparison to NIST glasses. Comparison with data for reference materials analysed as unknowns indicates that U contents are likely to have been overestimated; however, the relative concentrations would still be correct.

3.4.2. Lu-Hf data

According to Laurent and Zeh (2015), zircons from a granite that have partially lost Pb will show a horizontal array of points from its time of crystallization in a ^{176}Hf/^{177}Hf versus ^{207}Pb/^{206}Pb age diagram. The constancy of the zircons’ Hf isotopic compositions, even if they have suffered Pb loss, stems from the very low Lu/Hf ratios of the zircon, and the fact that Hf, unlike Pb, substitutes for Zr, one of the major elements in the zircon structure. Idealized examples for possibilities in Hf ratio versus age diagram in Lu-Hf system are shown in Figure 3.8 (g-i). Figure 3.8g illustrates a case where zircons from a 0.42 Ga granite have not suffered any Pb loss. In this case, the vertical nature of the array reflects both the variability of the Hf isotopic composition of the zircons, as well as the uncertainty related to the LA-MC-ICPMS analyses of the isotopic composition. Figure 3.8h shows two granites with different ages, one ca. 2700 Ma and one ca. 2055 Ma that have not suffered any Pb loss, and Figure 3.8i illustrate a situation for a 2700 Ma granite that has suffered partial Pb loss.

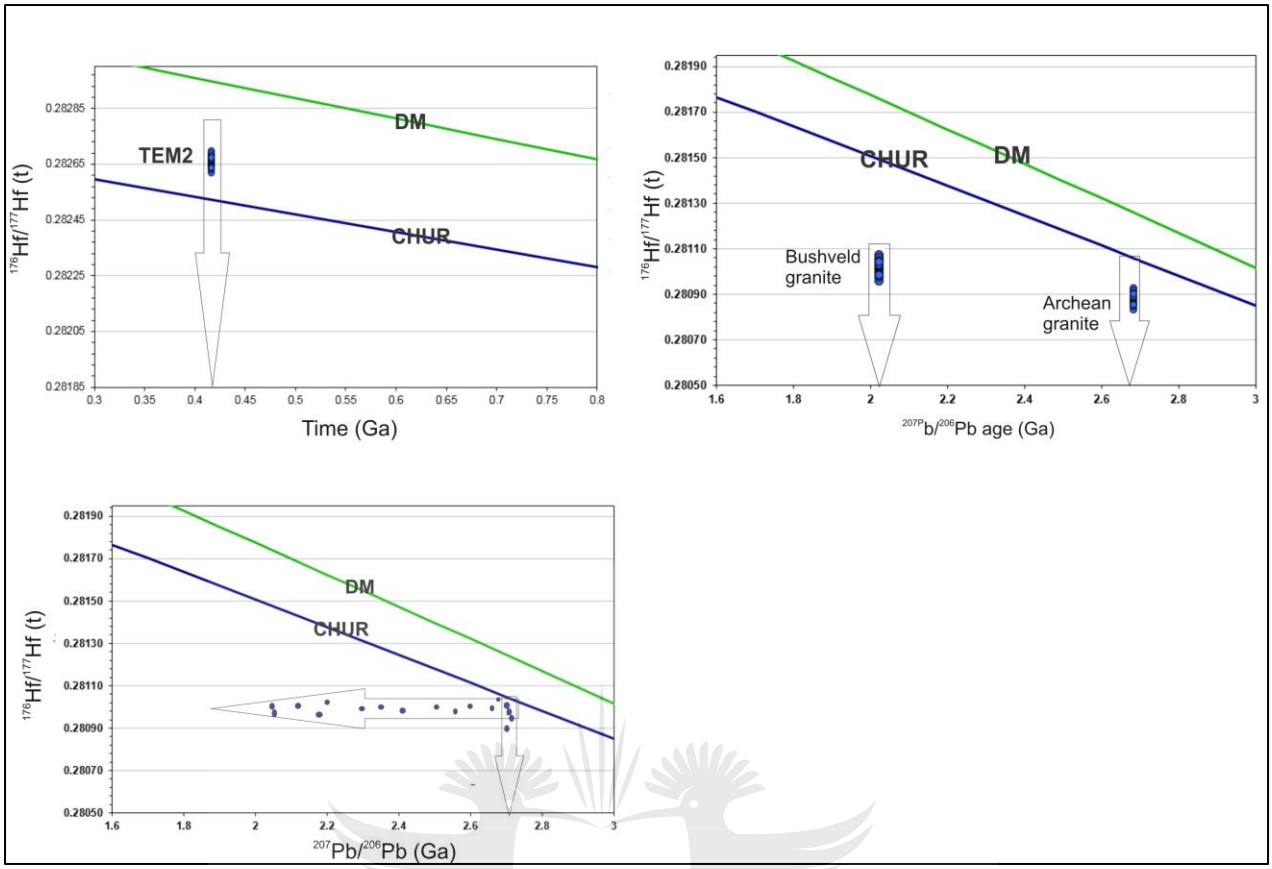

Figure 3.8: Example of initial Hf isotope ratio versus age diagram for (g) zircons from a granite that of which the U-Pb ages have not been reset (h) zircons from two granites of different ages that have not suffered Pb-loss (i) zircons from a granite that suffered partial Pb loss from after crystallization.

Chapter 4

4. Results: Archean Granites

The five Archean granite samples for which the results are presented below were taken at various distances from the Rustenburg Layered Suite, with sample MEMG6 at the greatest distance, and MEMG7 and 8 closest, ca. 1 km removed from Anglo American's Mogalakwena Platinum Mine (Figure 4.1). The zircon grains obtained from these samples were analyzed for their U-Pb characteristics, and a subset for their Lu-Hf isotopic ratios using the LA-MC-ICPMS. A minimum of 34, but about 100 grains were analyzed for each sample.

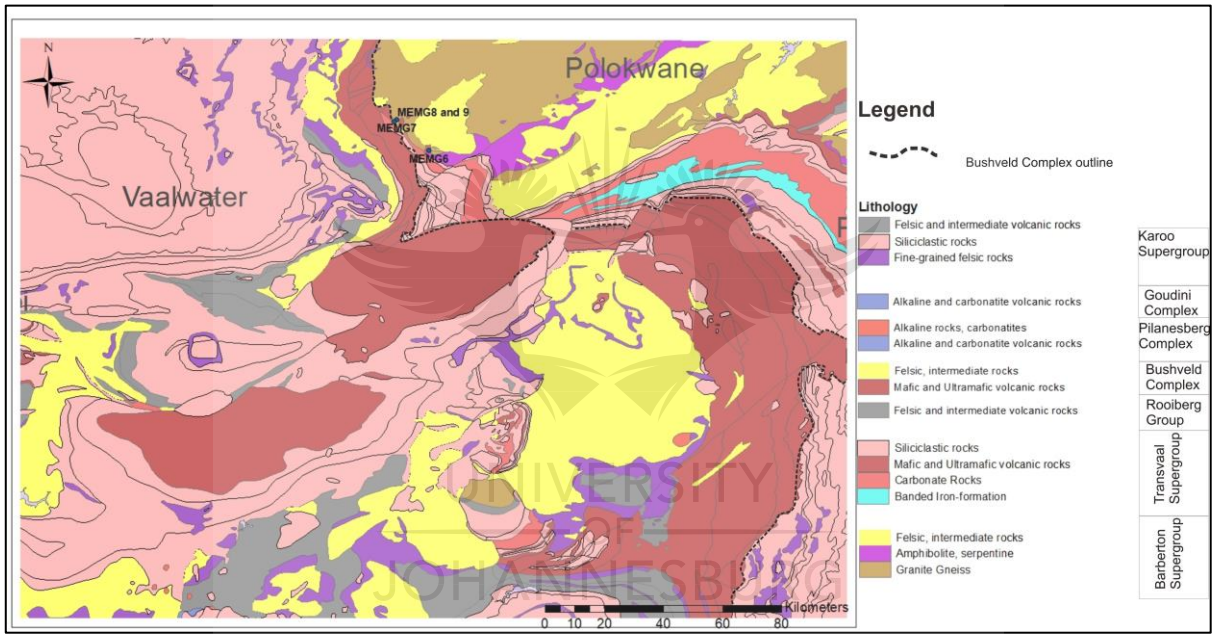

Figure 4.1: Geological map showing sample locations for Archean granites in the vicinity of the northern limb of Bushveld Complex.

The U-Pb data presented in this section provide information on the crystallization ages for these granites and the episodes of Pb-loss using concordia diagrams. The Lu-Hf isotopic data are presented to further investigate the isotopic changes associated with age resetting. Trace element analyses were also done on these samples to constrain the effects on the elemental composition of the zircon. Not many zircon analyses were discarded, and also the zircon grains that are more than 10% discordant were retained. This is done because, unlike conventional geochronological studies, this study actually focuses on the discordance more than dating these rocks, so the information carried by a discordant grain is as important as the information carried by a concordant grain. Due to small zircon sizes, the U-Pb analyses often

required ablation of the entire grain, hence the information on CL images was used to judge whether any mixed ages were obtained.

4.1. Sample MEMG6

This coarse-grained granitoid sample was taken from a boulder near the road between the Percy Fyfe and Witvinger conservancies (Figure 4.1). At the time of sampling, it was interpreted to be part of the Hout River Gneiss, close to the intrusion of the Mashashane Pluton.

4.1.1. Petrographic description

This granite is medium- to coarse-grained, with an average grain size ranging from about 1 mm up to 5 mm. It has an inequigranular texture, with large euhedral to subhedral crystals of plagioclase (Figure 4.2 d-f) enclosed within a groundmass of microcline and quartz. Hornblende occurs as a minor phase (Figure 4.2a). Microcline crystals show perthitic exsolution and can contain quartz inclusions (Figure 4.2b). The accessory minerals include zircon, apatite, as well as secondary titanite which is observed overgrowing the opaque mineral (Figure 4.2 c, d). Alteration of hornblende to a low-birefringence green mineral, interpreted to be chlorite, is observed in Figure 4.2 e, f.

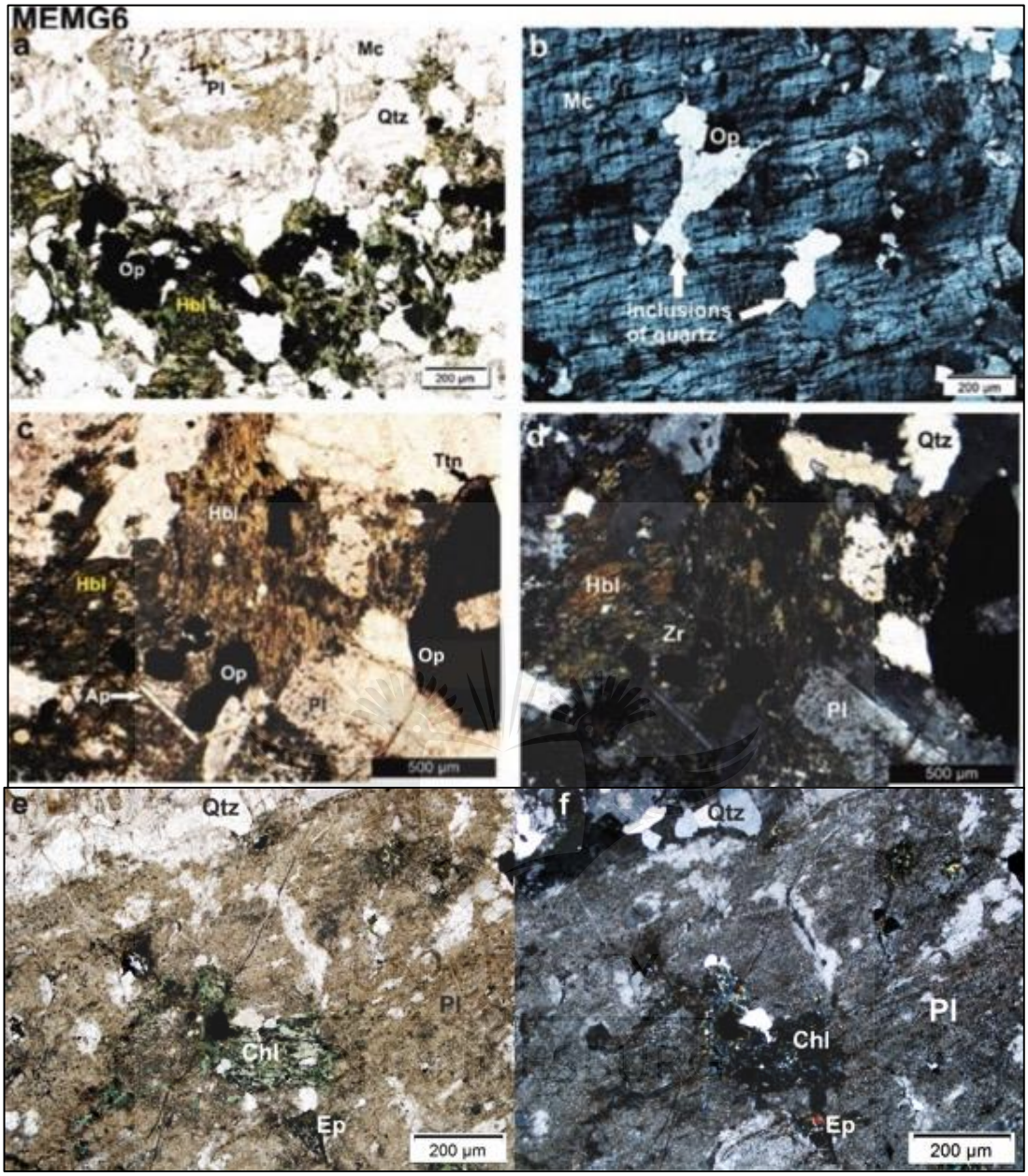

Figure 4.2: (a) Large crystals of altered plagioclase enclosed by microcline, quartz, hornblende and opaque minerals (PPL) (b) perthitic exsolution in microcline, with quartz inclusions (XPL) (c-d) occurrence of accessory mineral phases apatite, zircon and titanite (PPL and XPL resp.) (e-f) alteration of hornblende to chlorite (PPL and XPL respectively).

4.1.2. Zircon characteristics

Zircon crystals in this sample are typically euhedral, varying from prismatic to almost equidimensional in shape (Figure 4.3). They range in length between 500 and 50 µm. They exhibit oscillatory zoning, although zones are not clearly defined in some grains (e.g. Figure 4.3 d, f, k), and some crystals show patchy complex patterns (e.g. Figure 4.3 c, m). The zircons contain variable amounts of apatite (enhanced signal intensity on CL images, see Figure 4.3 b, c, m) and other inclusions (Figure 4.3 a, f, j, m). Most of the zircon crystals have cracks, which are mostly associated with inclusions (e.g. Figure 4.3 b, m).

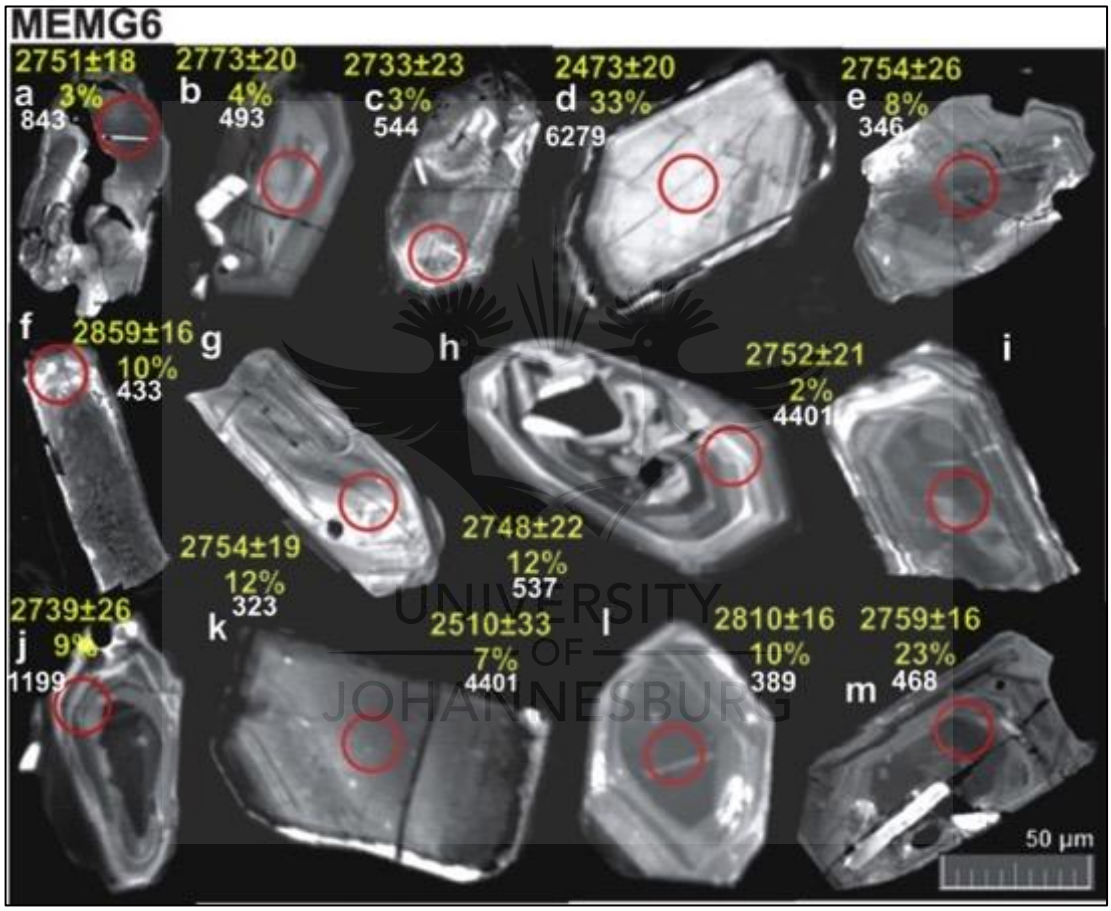

Figure 4.3: Cathodoluminescence images of selected zircon crystals of MEMG6 with the circles representing the U-Pb ablation spot, and the numbers displayed are $^{207}Pb/^{206}Pb$ ages in Ma with 2 sigma errors and the numbers in percentages represent the amount of discordance. Numbers below discordance percentages are uranium contents (ppm).

4.1.3. U-Pb isotope results

U-Pb results for this sample are given in Appendix A, Table 1. A concordia diagram for CPb-free analyses is shown in Figure 4.4a. These analyses show quite a spread in $^{207}Pb/^{206}Pb$ ages of concordant to near-concordant analyses between 2675±20 and 2776±15 Ma. The upper and lower intercepts ages are 2795±37 and 538±380 Ma respectively. Some of the CPb-free analyses are discordant, with the youngest discordant grain at a $^{207}Pb/^{206}Pb$ age of 2547±19 Ma.

A concordia diagram for all ninety-seven analyzed zircons is shown in Figure 4.4b. The upper and lower intercept ages determined by Isoplot are 2772±27 and 372±160 Ma, respectively. The upper intercept age is well defined whereas the lower intercept age is poorly defined. Only 12% of zircon grains are concordant and they give a weighted average $^{207}Pb/^{206}Pb$ age of 2709±31 Ma with MSWD of 24, and this high MSWD reflects the range in concordant ages. The weighted average age for concordant analyses is within error of the upper intercept age; analyses that are corrected for common Pb are mostly highly discordant. Most of the analyses lie within the triangle between the upper intercept age, 2.05 Ga and the 0 Ga, however, a few analyses lie outside this triangle on the older side.

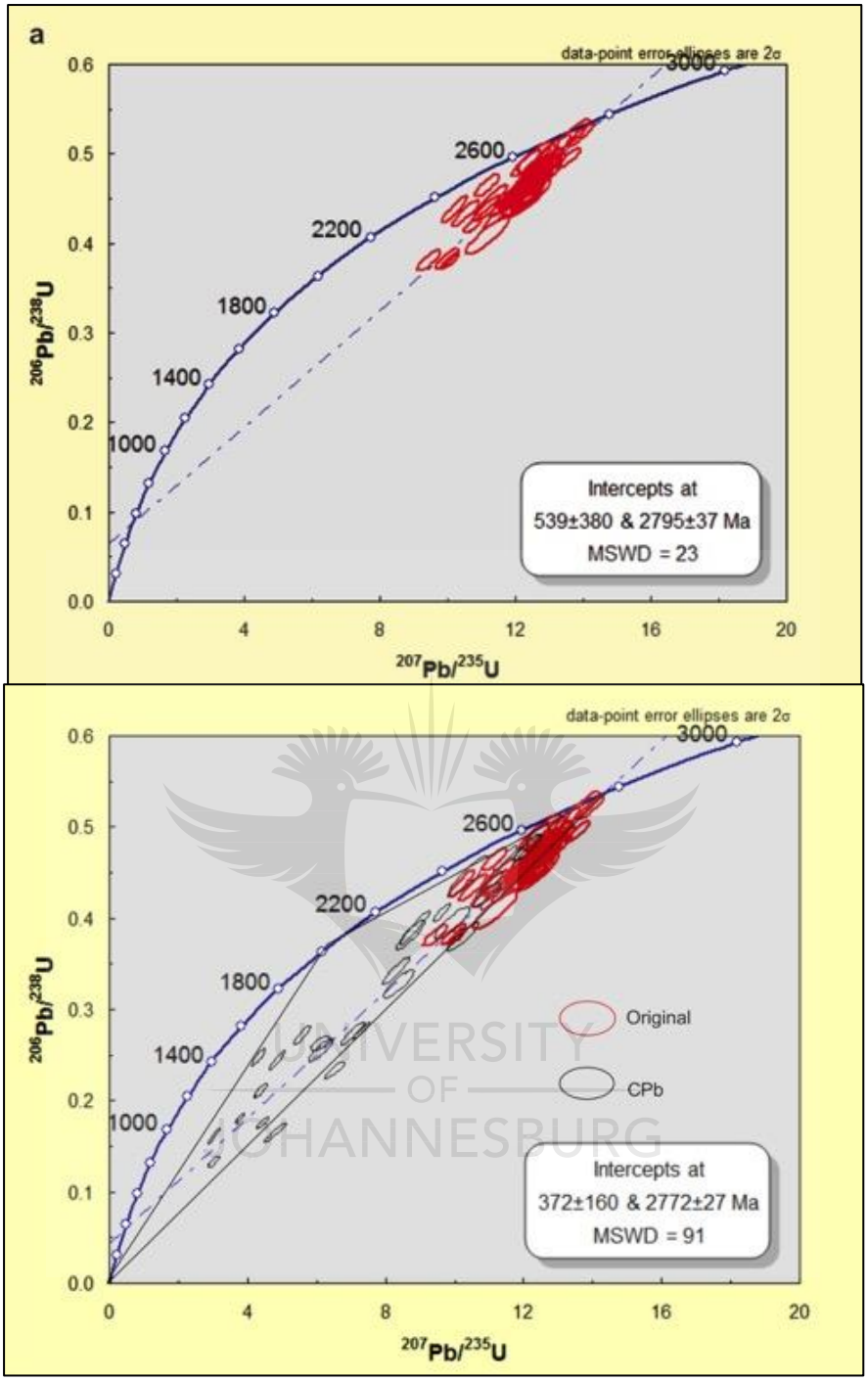

Figure 4.4: (a) A U-Pb concordia diagram for analyses that did not need CPb correction, showing quite a spread in concordant to near-concordant analyses (b) A concordia diagram for all zircon analyses for sample MEMG6. The zircons from this sample are dominantly highly discordant, with a poorly defined lower intercept age. More than 80% of the analyses lie within a triangle between crystallization age, 2.05 Ga and 0 Ma.

The values for the uranium content of zircons in this sample range between 222 and 7267 ppm, but, as noted before, the absolute values are likely to be an overestimate; the relative concentrations would still hold. Zircon crystals with higher uranium content show a higher degree of discordance (Figure 4.5 a, b). A correlation is also observed in the diagrams of $^{206}Pb/^{204}Pb$ versus uranium content and discordance (Figure 4.6 a, b); in these diagrams the $^{206}Pb/^{204}Pb$ ratios are inversely proportional to both uranium content and discordance.

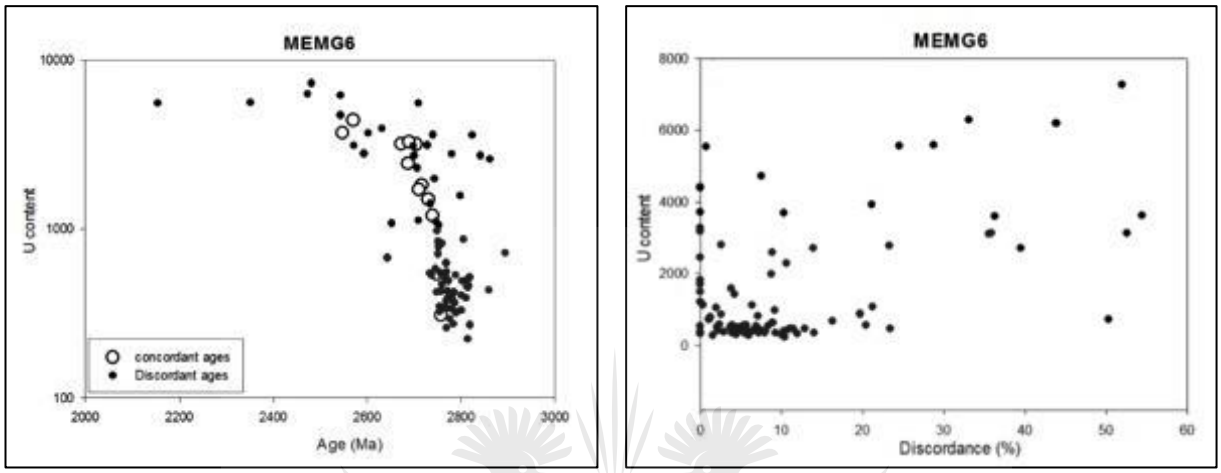

Figure 4.5: (a) Uranium content versus $^{207}Pb/^{206}Pb$ age diagram for MEMG6, showing a correlation between the two variables (b) uranium content versus discordance. The correlation is more pronounced for figure (a).

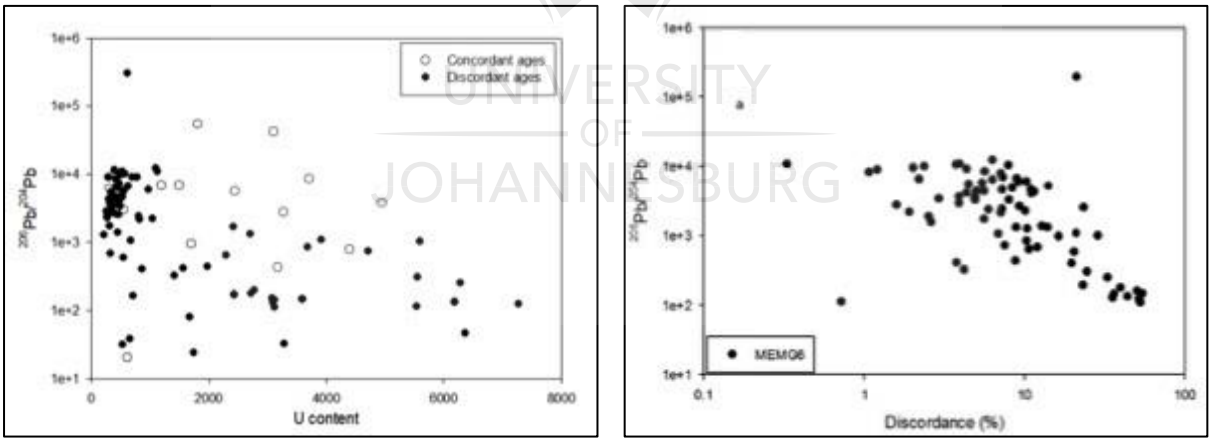

Figure 4.6: (a, b) Diagram of $^{206}Pb/^{204}Pb$ versus uranium content and discordance, respectively. A scattered negative correlation can be seen in both diagrams.

The likeliness of upper and lower intercept ages can be calculated using an R coding program (Andersen et al., 2017) based on the approach by Reimink et al (2016), of which the output shows an upper intercept peak at 2800 Ma and a lower intercept peak at around 400 Ma (Figure 4.7). These intercept ages are similar to ages observed in concordia diagram (Figure 4.4 b).

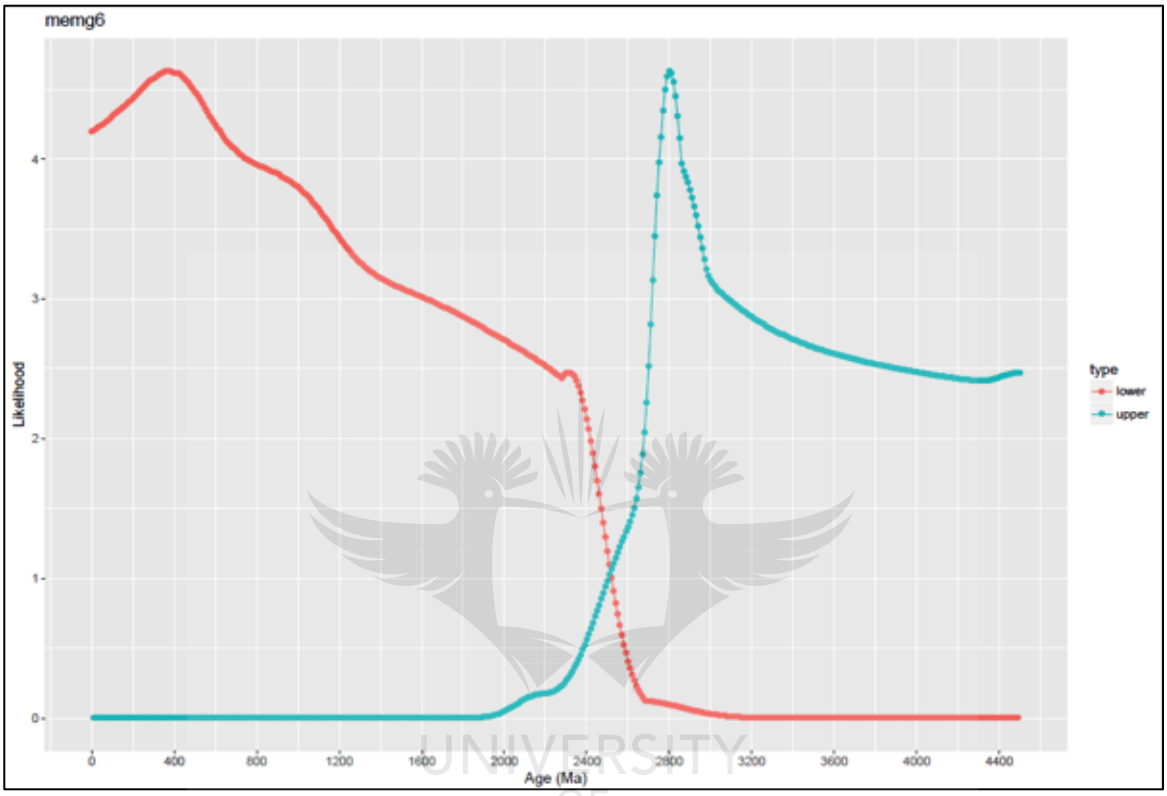

Figure 4.7: An output from R coding program showing peaks of events at different ages in both upper and lower intercept. Note that the ages presented in this output are the similar to ages shown in a concordia diagram.

4.2. Sample MEMG7

Sample MEMG7 is course-grained light-coloured granitoid that was obtained ca. 1 km from Anglo American's Mogalakwena Platinum Mine (Figure 4.1), potentially affected by Bushveld intrusion.

4.2.1. Petrographic description

This rock consists mainly of equigranular crystals of plagioclase (with quartz inclusions; Figure 4.8 b), quartz and microcline. Hornblende and biotite occur as interstitial phases (Figure 4.8 a, b). Zircon and apatite occur as accessory minerals (Figure 4.8 d). Myrmekitic texture is observed in Figure 4.8 c.

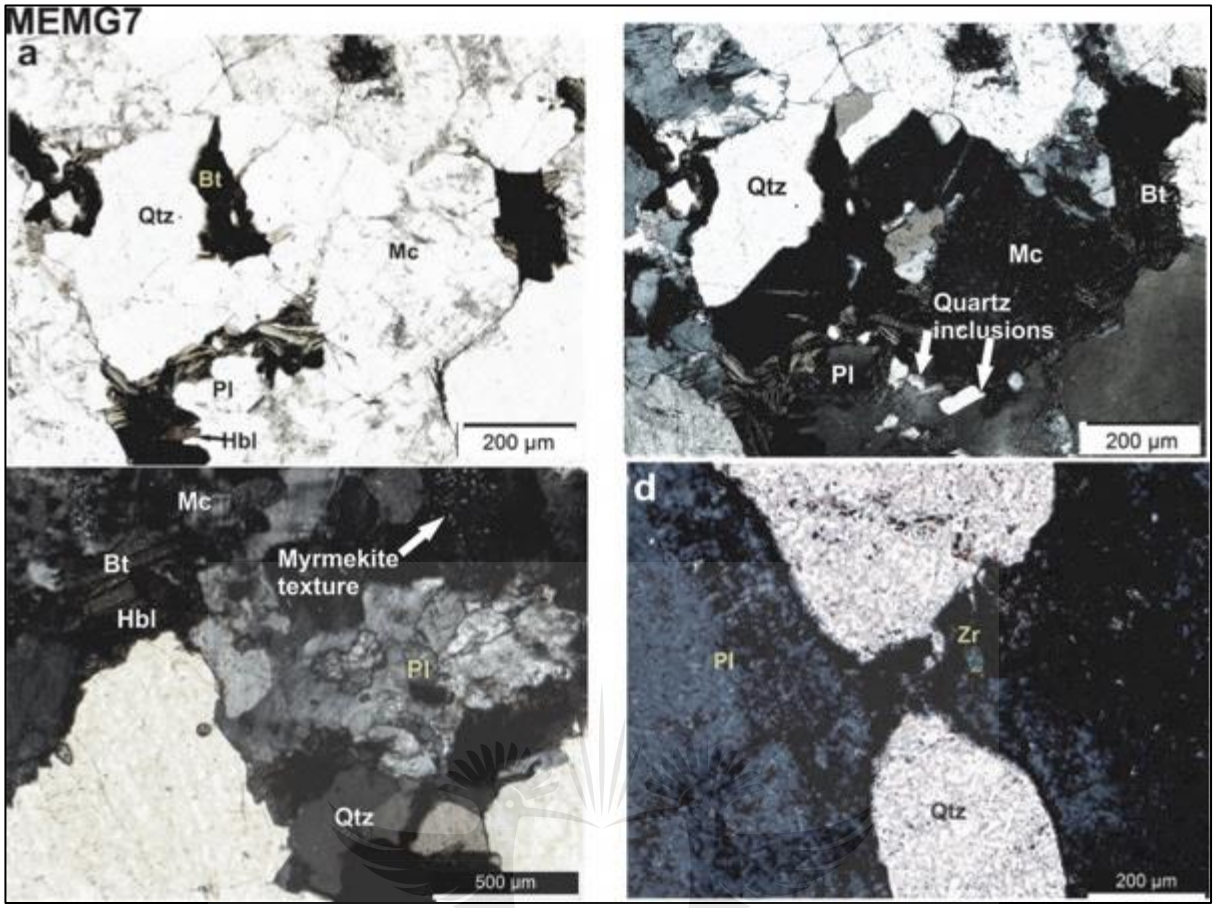

Figure 4.8: (a, b) Equigranular granite with interstitial biotite (XPL, PPL) (c) intergrowths of quartz in plagioclase (myrmekite; XPL) (d) occurrence of zircon between plagioclase and opaque minerals (XPL).

4.2.2. Zircon characteristics

Zircons in this sample are mostly prismatic, ranging from approximately 300 to 20 µm in length. They generally show oscillatory zoning typical for zircon from igneous rocks (Figure 4.9 e, g, d, h, i), superimposed by sector zoning in cases (e.g. Figure 4.9 a, h), and some grains are only weakly zoned (e.g. Figure 4.9 e, j, i). Some of the zircon crystals contain inclusions (e.g. Figure 4.9 b, k) and cracks (e.g Figure 4.9 f, l).

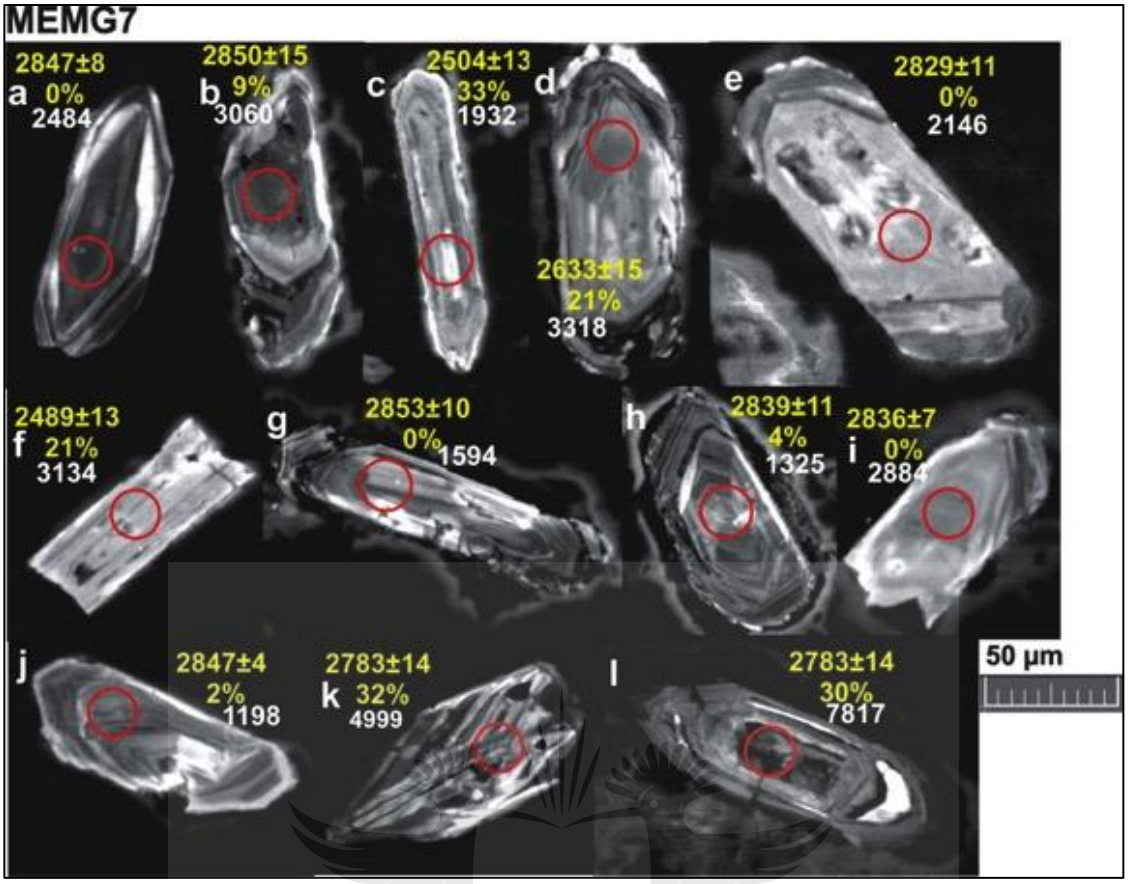

Figure 4.9 Cathodoluminescence images of selected zircon grains of sample MEMG7, with the circles representing U-Pb ablation spots; the numbers displayed are $^{207}Pb/^{206}Pb$ ages with 2 sigma error and the percentages represent the amount of discordance. Numbers below discordance percentages are uranium contents in ppm.

4.2.3. U-Pb results

U-Pb results for this sample are given in Appendix A, Table 2. A concordia diagram for CPb-free zircons is presented in Fig. 4.10. The concordant $^{207}Pb/^{206}Pb$ ages range between 2872±9 and 2813±10 Ma; discordant ages are in range of 2850±10 and 2181±12 Ma, and Isoplot calculates an upper and lower intercept ages of 2855±15 and 472±110 Ma respectively. A concordia diagram including the analyses corrected for common lead (indicated in black) is shown in figure 4.10b. Thirty-two percent of the grains are concordant with a well-defined upper intercept of 2850±12 Ma, a poorly defined lower intercept at 343±130 Ma, and a MSWD of 18. The majority of the analyses lie on the discordia towards ca. 0 Ma. The concordant analyses yield a weighted average $^{207}Pb/^{206}Pb$ age of 2841±11 Ma (MSWD = 26). The discordant analyses give a range of $^{207}Pb/^{206}Pb$ ages from 2850±10 to 1800±8 Ma with the youngest ages mainly represented by analyses that were corrected for CPb. To further

investigate the meaning of the range of ages observed, diagrams of U content versus age and discordance percentage are shown on Figure 4.11 (a, b), showing a rough negative correlation between age and U content, but no correlation is observed between discordance and U content. There is a scattered negative correlation between $^{206}Pb/^{204}Pb$ and uranium content, as well as discordance (Figure 4.12 a, b).

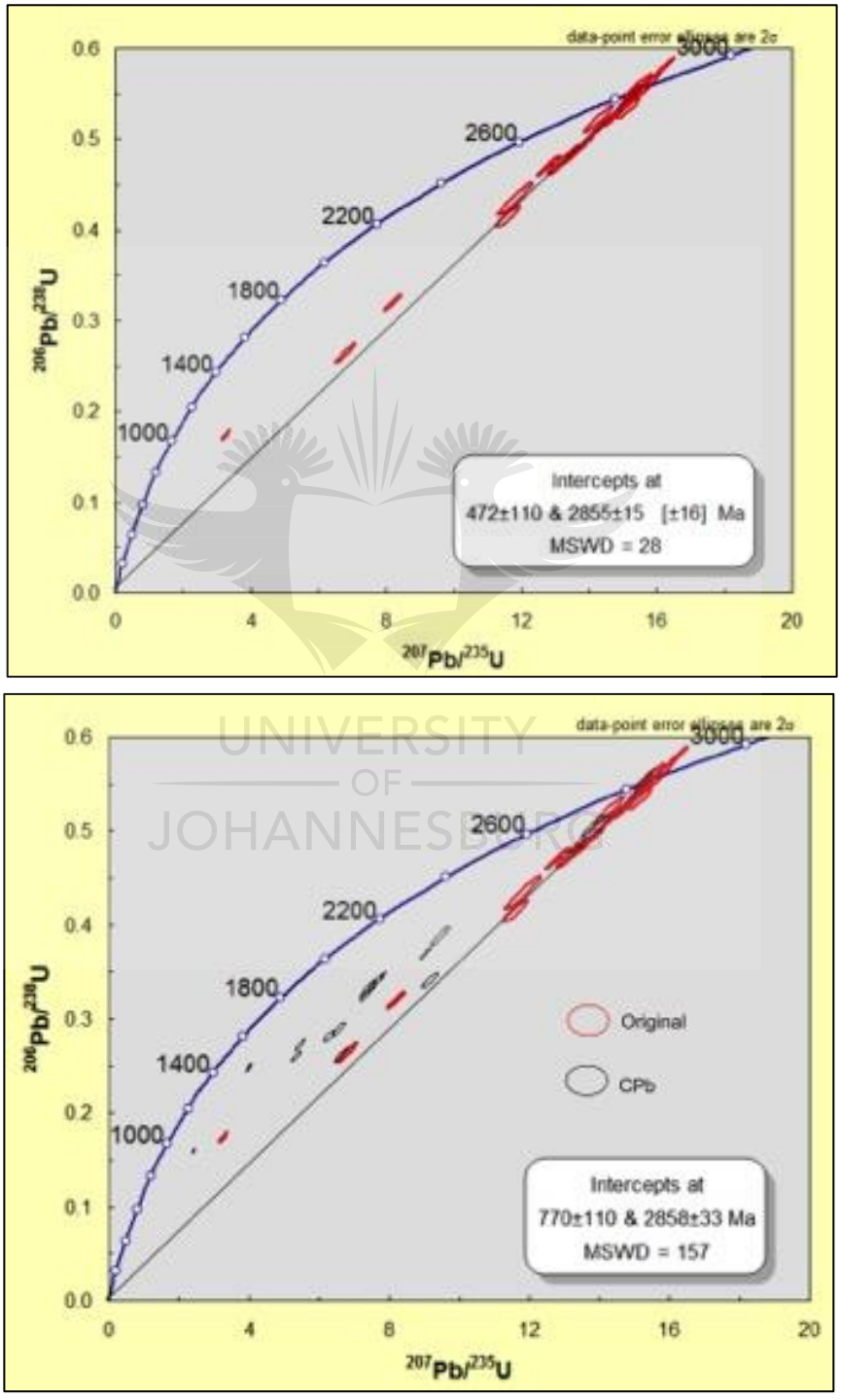

Figure 4.10: Wetherill concordia diagram for sample MEMG7 (a) CPb-free analyses fall on a discordia line towards ca. 0 Ma (b) all analyses, including the ones corrected for common lead.

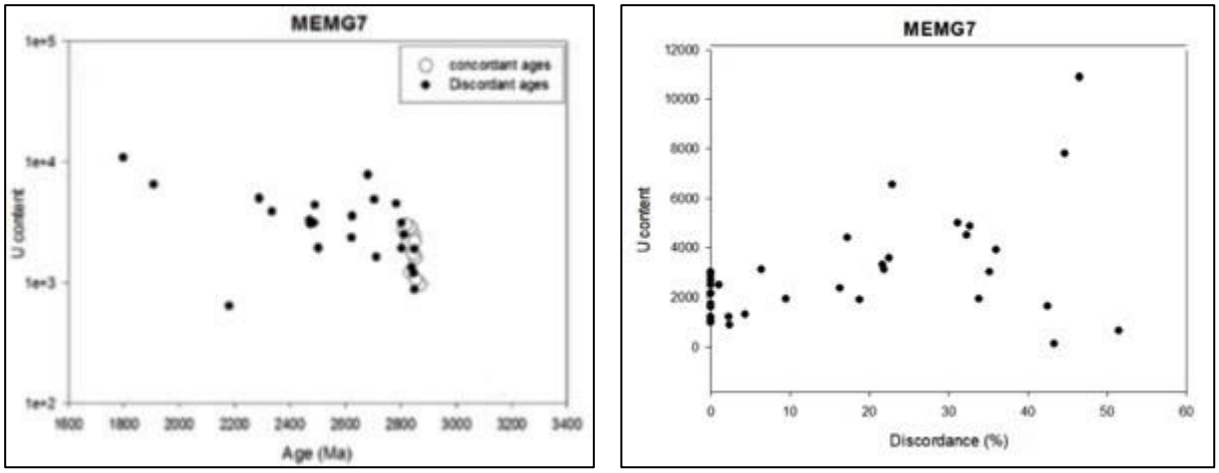

Figure 4.11: (a) Uranium content versus age diagram for MEMG7 (b) uranium content versus discordance for MEMG7. A scattered correlation is seen in both diagrams.

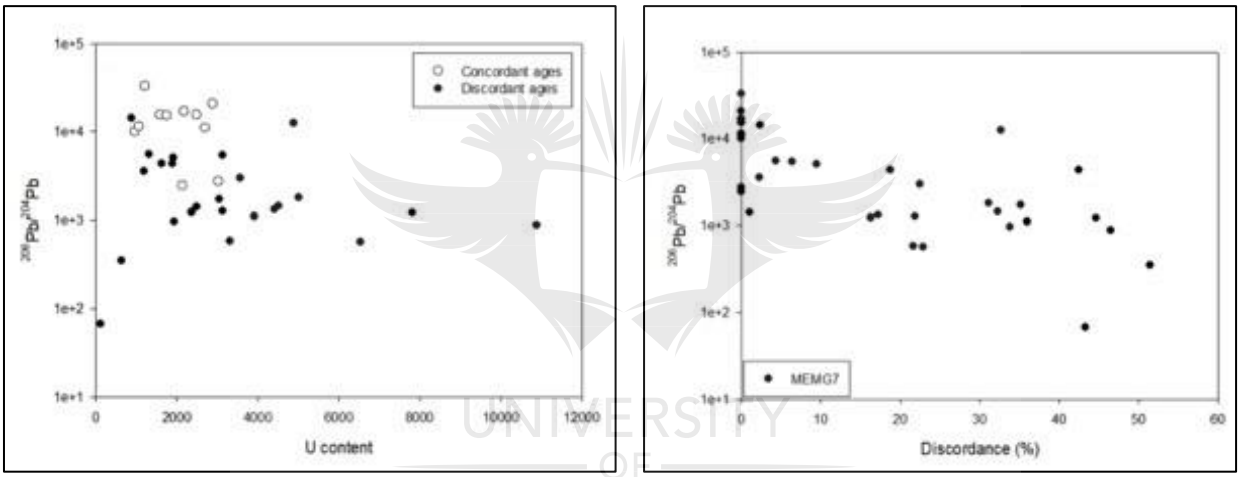

Figure 4.12: (a) $^{206}Pb/^{204}Pb$ versus uranium content (b) $^{206}Pb/^{204}Pb$ versus discordance. Again, both diagrams show a scattered correlation.

4.3. Sample MEMG8

Sample MEMG8 is a medium-grained light coloured granitoid obtained just north of MEMG7, ca. 1 km from Anglo American's Mogalakwena Platinum Mine (Figure 4.1).

4.3.1. Petrographic description

This granite has large crystals of microcline and plagioclase set in a matrix of quartz. The quartz crystals are small and have serrated boundaries which may be related to dynamic recrystallization (Figure 4.13 a). Minor biotite and hornblende occur as interstitial phases between feldspar and quartz. Zircon crystals occur as an accessory phase between plagioclase, quartz and hornblende (Figure 4.13 b). Microcline shows perthitic exsolution and

plagioclase cores are altered to sericite (Figure 4.13 a, b). The occurrence of muscovite and a green, low birefringent mineral, likely representing chlorite alteration of hornblende and biotite is observed in Figure 4.13 c, d.

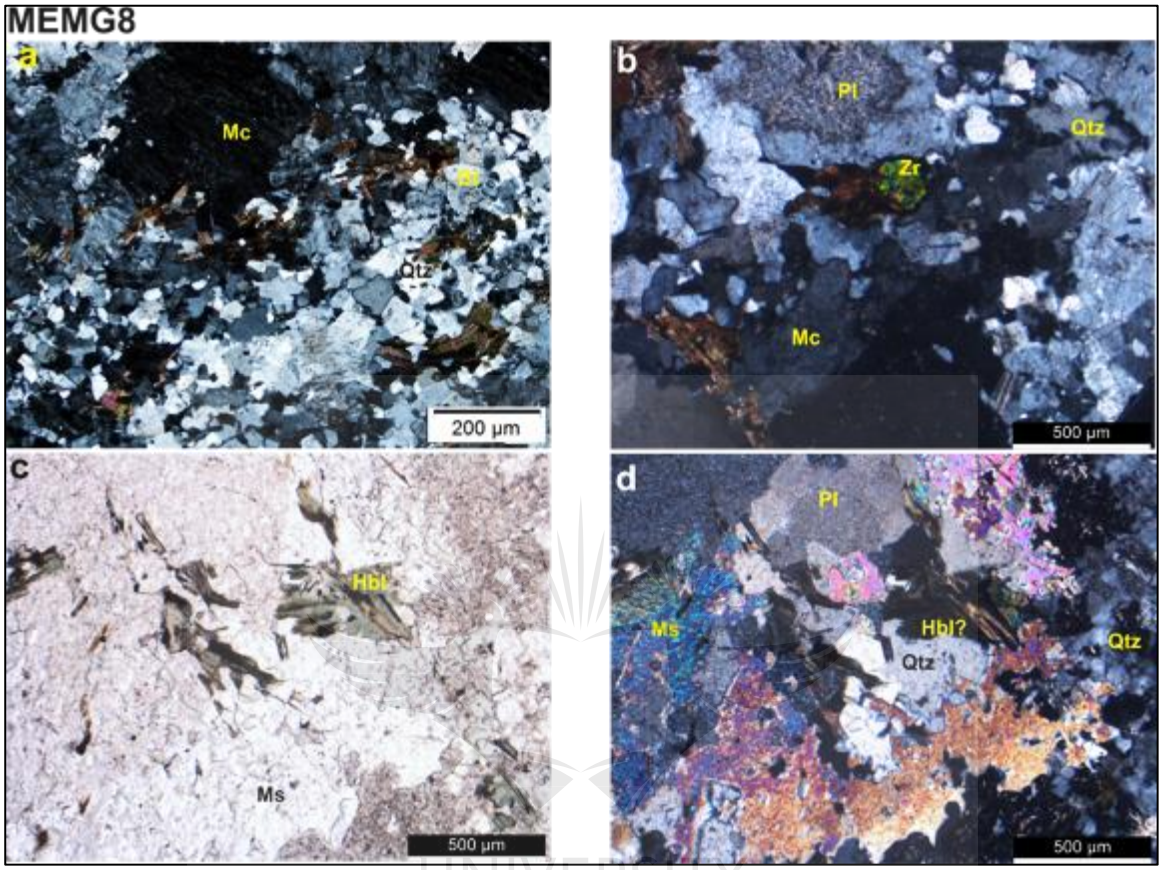

Figure 4.13: (a) Large altered crystal of microcline surrounded by small quartz crystals (XPL) (b) equidimensional zircon is observed between plagioclase, quartz and biotite (XPL). Also note alteration in plagioclase cores. (c, d) muscovite and green low-birefringent mineral, likely chlorite after hornblende (PPL and XPL, respectively).

4.3.2. Zircon characteristics

Zircon grains in this sample are all short to long prismatic, their length ranging from 300 to 30 µm (Figure 4.14). They show a wide spectrum of internal textures, the dominant one being oscillatory zoning. The oscillatory zoning either includes the entire zircon texture (Figure 4.14 i, j) or occurs in rims around unzoned cores (Figure 4.14 c) or more complexly zoned cores (Figure 4.14 a); convoluted zones are observed superimposing the oscillatory zoning in cases (Figure 4.14 d). The zircons shown in Figure 4.14 b, d still maintain their magmatic textures when compared to grains that are characterized by inclusions (Figure 4.14 a, f) as well as fractures (Figure 4.14 e).

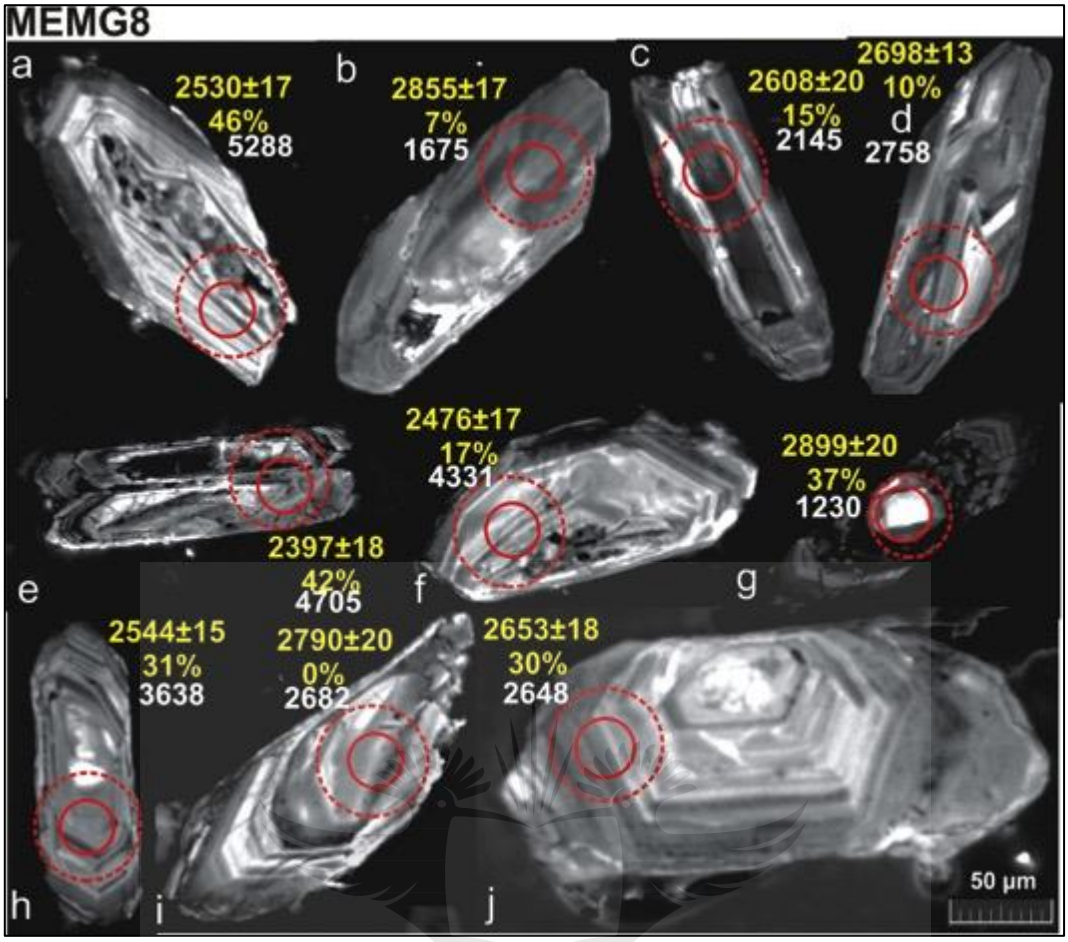

Figure 4.14: Cathodoluminescence images of selected zircon grains; the solid and dashed circles represent U-Pb ablation spots and Lu-Hf ablation sites respectively. The numbers displayed are $^{207}Pb/^{206}Pb$ ages with 2 sigma error and discordance percentages below ages at 1 sigma error. Numbers below discordance percentages are uranium contents measured in ppm.

4.3.3. U-Pb results

U-Pb results for this sample are given in Appendix A, Table 3. The concordant zircon grains show a spread in $^{207}Pb/^{206}Pb$ ages from ca. 2740 to 2830 Ma (Figure 4.15 a). The nominally concordant zircon grains define a weighted average $^{207}Pb/^{206}Pb$ age of 2821±38 Ma, with a high MSWD of 29. A concordia diagrams for analysed zircon grains that were not corrected for common Pb is presented in Figure 4.15 b: these zircon analyses lie on a discordia towards a poorly defined lower intercept age of 731±180 Ma. A concordia diagram of all analysed zircon grains, including the ones that needed common Pb correction, for sample MEMG8 is shown in Figure 4.15 c; these analyses fall in a triangle between the age defined by the two oldest near-concordant analyses at ca. 2.84 Ga, 2.05 Ga and 0 Ga. There is also one crystal that falls outside this triangle, which, after correction for common Pb, gives a $^{207}Pb/^{206}Pb$ age of 2925±16, and which might be a xenocryst. The analyses yield poorly defined upper and lower intercept ages of 2808±39 Ma and 725±94 Ma respectively; these intercepts are indistinguishable from those for the CPb-free zircons only.

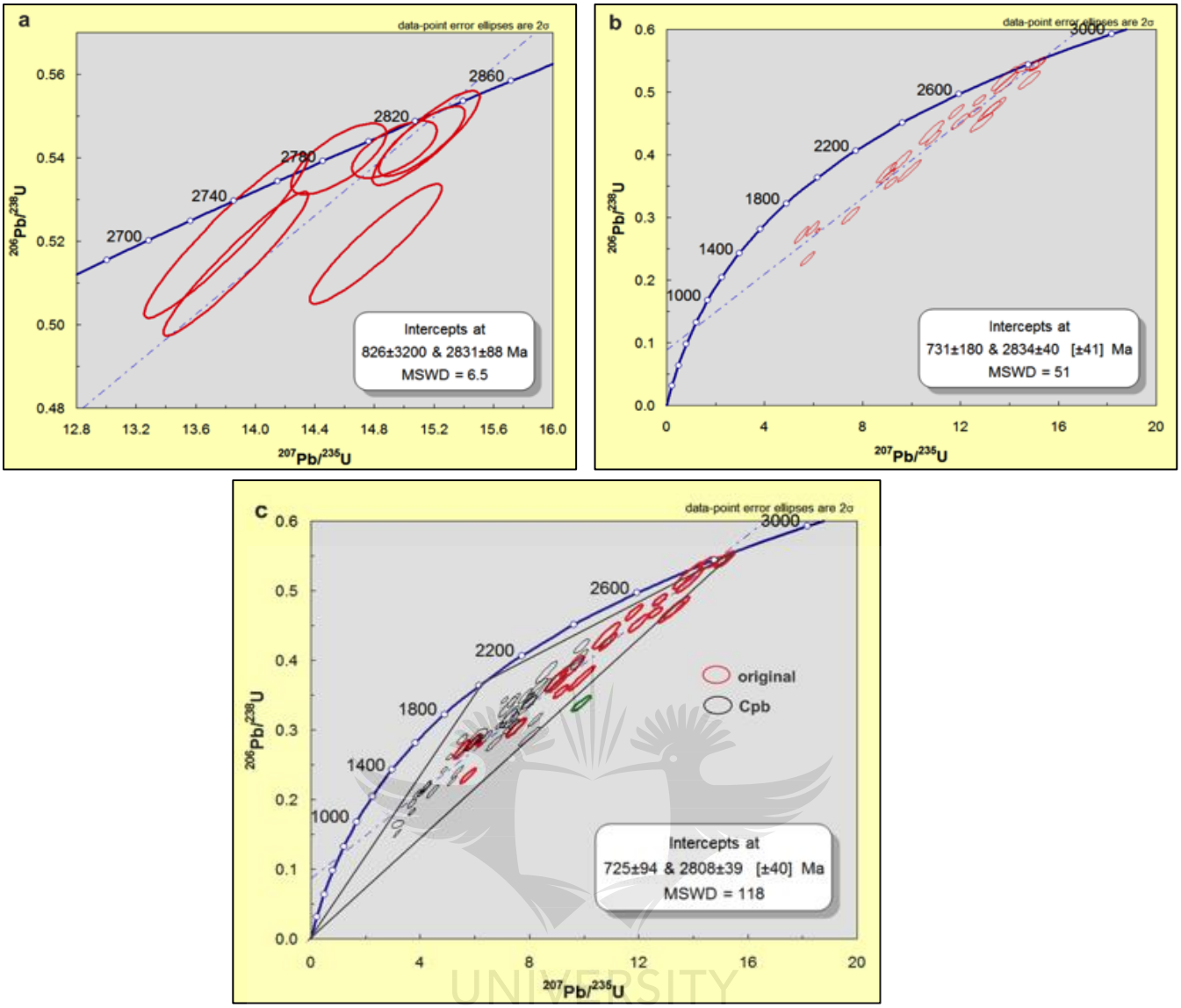

Figure 4.15: Wetherill concordia diagrams for sample MEMG8 (a) a close-up for analyses less than 10% discordant (b) zircon grains that have not been corrected for CPb (c) for all analyses including the ones corrected for CPb; the analysis outlined in green is interpreted as a xenocryst.

Diagrams of uranium content versus age and discordance (Figure 4.16 a, b) show a positive correlation between uranium content and discordance, and a negative correlation for U content and age. Correlations between $^{206}Pb/^{204}Pb$ ratio and uranium content and discordance are not as well defined, but zircon grains with high uranium content and discordance percentages tend to have lower $^{206}Pb/^{204}Pb$ ratios (Figure 4.16 c, d).

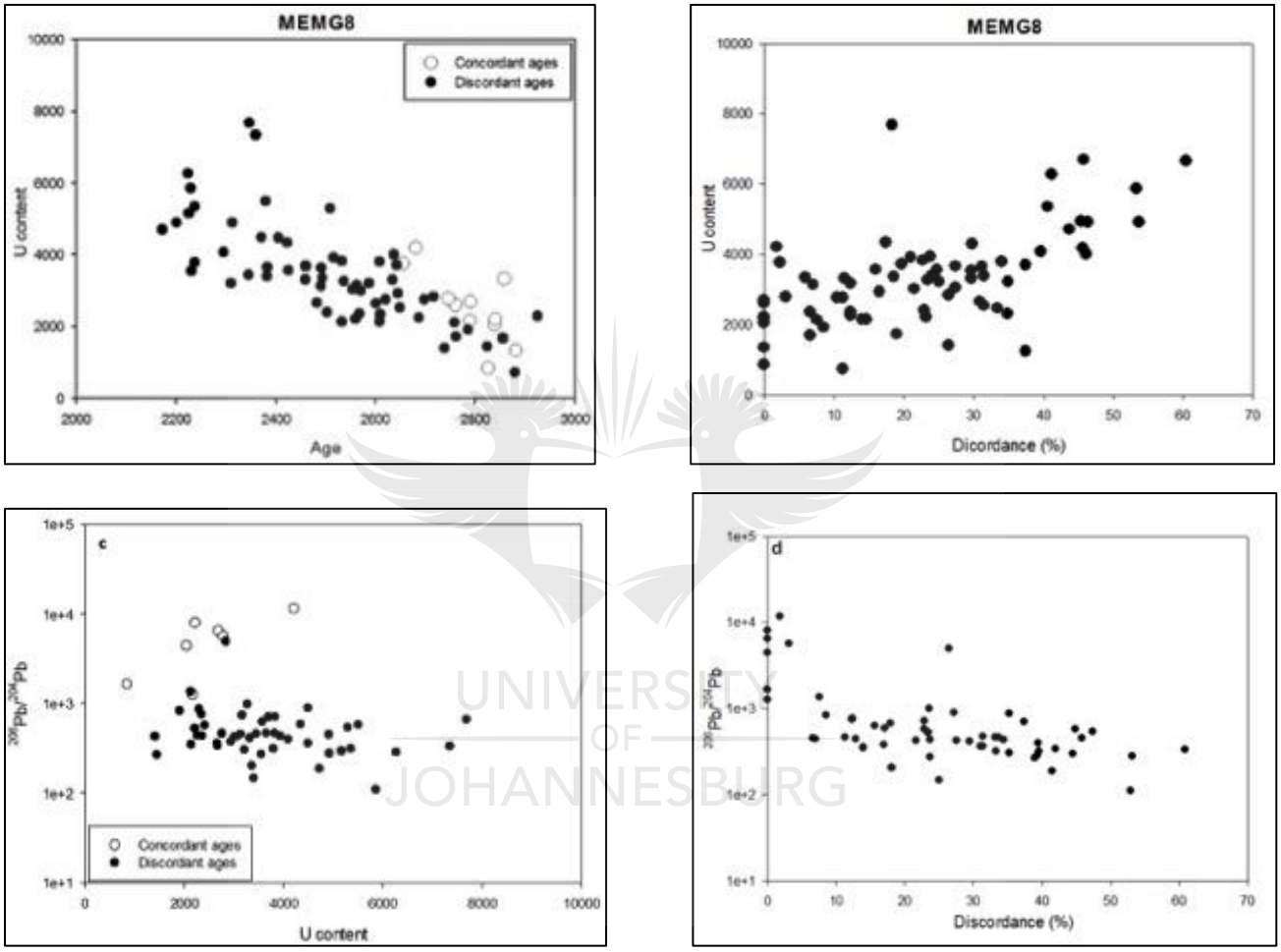

Figure 4.16: (a) Uranium content versus age diagram for MEMG8 (b) uranium content versus discordance for MEMG8. These diagrams show a strong correlation between discordance and uranium content. (c) $^{206}Pb/^{204}Pb$ versus uranium content (d) $^{206}Pb/^{204}Pb$ versus discordance. Both diagrams show a correlation between variables.

After using R coding program created by M. Kristoffersen (pers. comm.) to try and analyze the information present within discordant analyses for sample MEMG8, an output show peaks of events at an upper intercept age of ~ 2780 Ma and at a lower intercept age of ca. 700 Ma (Figure 4.17), which, again, are similar to the ones calculated by IsoPlot (Figure 4.15).

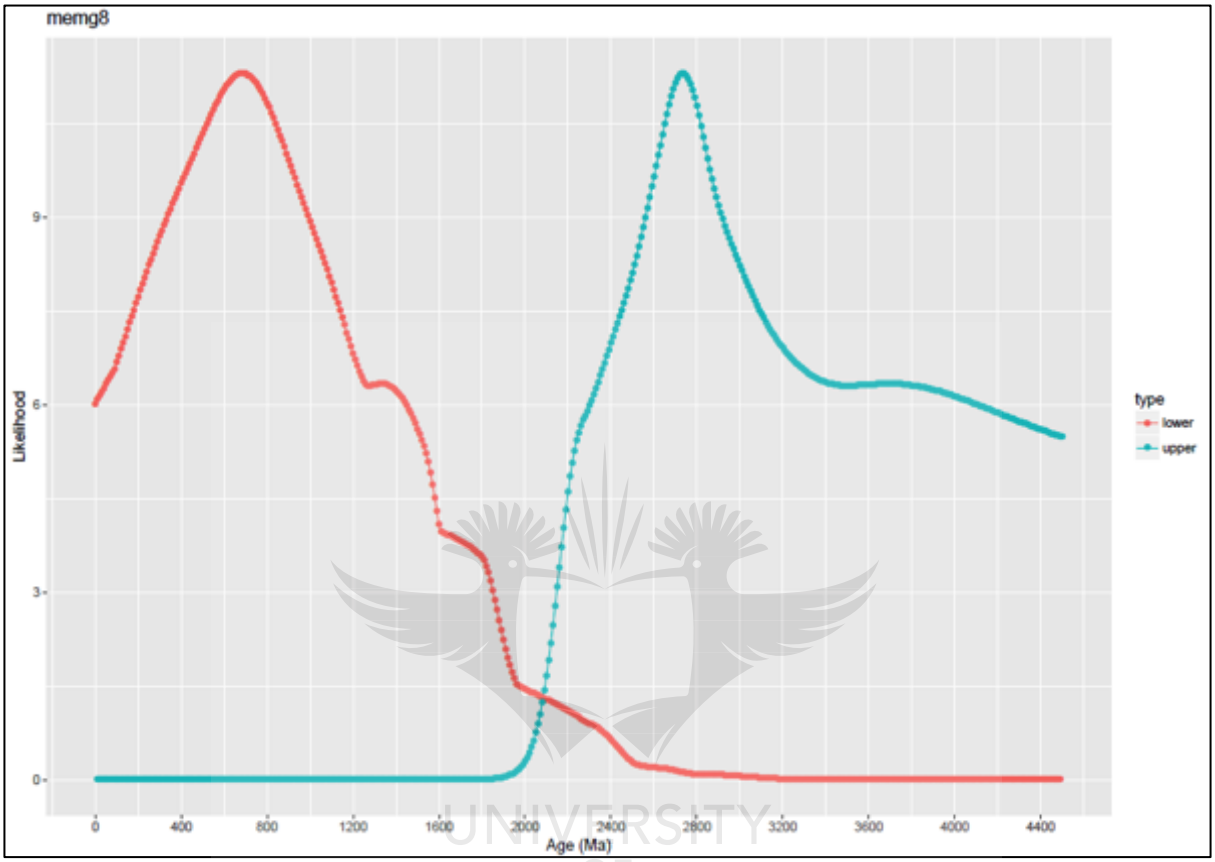

Figure 4.17: An output from R coding program showing peaks of events at upper and lower intercept ages.

4.3.4. Lu-Hf isotope results

The initial Hf isotope ratio against age diagram (Figure 4.18) shows a sub-horizontal array of points from the inferred crystallization age, apart from the older xenocryst with a lower $^{176}Hf/^{177}Hf$ ratio at 2925±16 Ma. The data for these analyses is presented in Appendix B, Table 1. The epsilon Hf values at the zircons' $^{207}Pb/^{206}Pb$ age range from +0.7 to -16.4. The $^{176}Yb/^{177}Hf$ ratios are low, ranging from ca. 0.03 to 0.06; they give an average of 0.044.

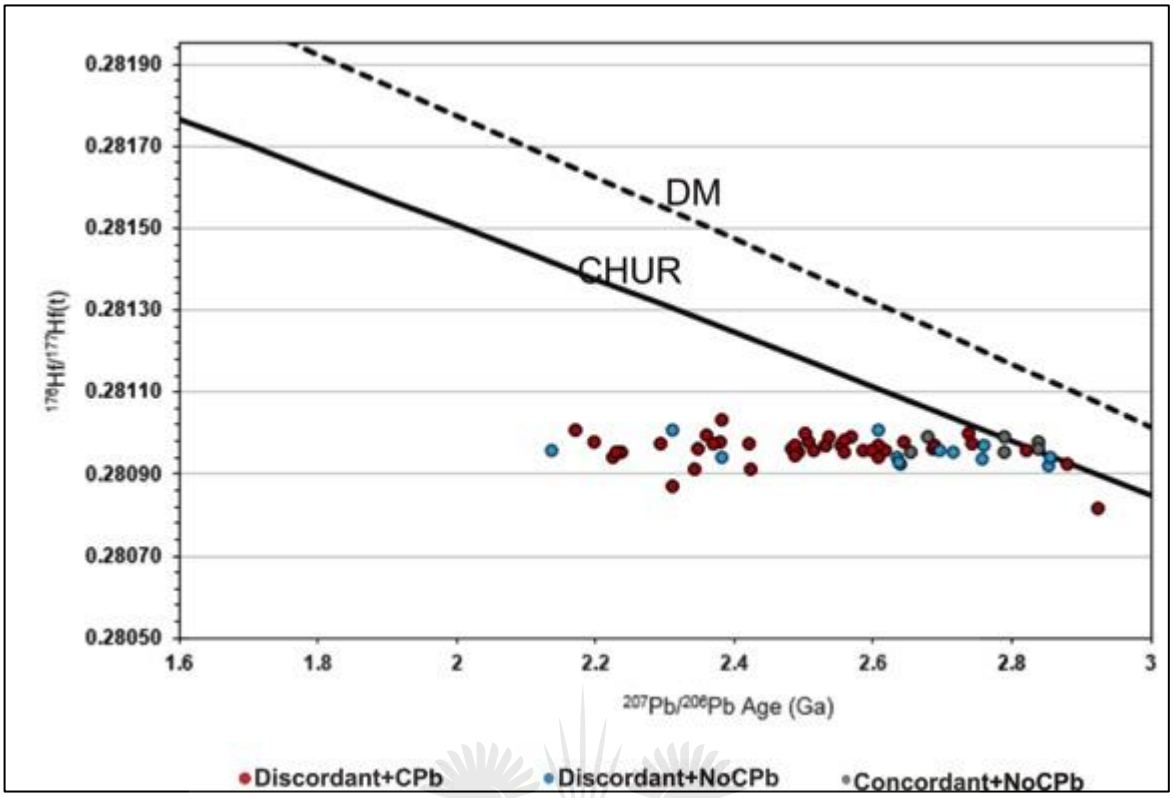

Figure 4.18 : Initial Hf ratios vs age diagram for sample MEMG8 showing a horizontal array of points from its crystallization age of ~ 2800 Ma.

4.3.5. Trace element chemistry

A range of trace elements, mainly rare earth elements (REE), were measured on concordant and discordant zircons grains that were analysed for both U-Pb and Lu-Hf to relate the trace element concentrations to the different textural and age domains. Representative trace element compositions are given in Appendix C, Table 1. It needs to be stressed that the ablation site for the trace elements was different from that of the original U-Pb analyses, and may therefore represent poorer quality material than the U-Pb ablation site. The zircons in this sample are characterized by flat light rare earth element (LREE) patterns with slightly positive Ce and well-defined negative Eu anomalies (Figure 4.19). Interestingly, a near-concordant grain (only 7 % discordant) at 2855±17 Ma has a very high LREE content (see CL image in Figure 4.14 b); although it is possible that this represents an inclusion, it cannot have been a phosphate such as monazite, as phosphorus contents are not elevated. No correlation is observed in cerium anomaly versus discordance diagram, and a slight correlation is observed in $(La/Sm)_N$ versus age diagram (Figure 4.20 a, b). These zircons have uranium concentrations between 168 and 949 ppm, and this shows that the U contents based on the U-Pb runs have been severely overestimated, however a positive correlation

correlation is observed between U contents based on U-Pb runs and U contents based on trace element analyses, although correlation coefficient is less than 1 (Figure 4.21). Ti concentrations range from 7 to 1241 ppm, and P concentrations range between 4 and 6985 ppm. Ti and P concentrations are not detectable in some grains. The Th/U ratios range from 0.08 to 0.85. Only 3 out of 29 zircon grains have a LREE index (which basically tracks the enrichment in middle relative to light rare earth elements and is defined by (Dy/Nd) + (Dy/Sm)) more than 10, and according to Bell et al. (2016) metamict zircons have LREE index less than 10. Diagrams of LREE index versus uranium (Figure 4.22 a) and discordance (Figure 4.22 b) were plotted to see if there is any correlation between these variables, no clear correlation is observed.

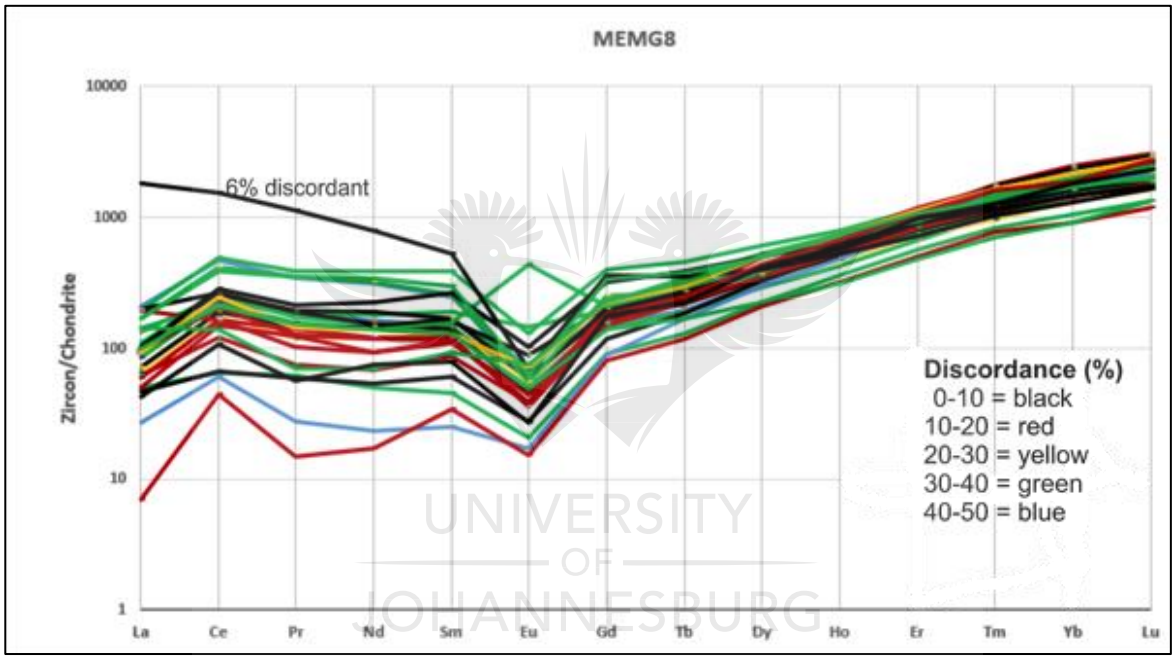

Figure 4.19: Chondrite-normalized REE patterns for zircons from the Archean granite sample MEMG8 (normalising values from Sun and McDonough, 1989).

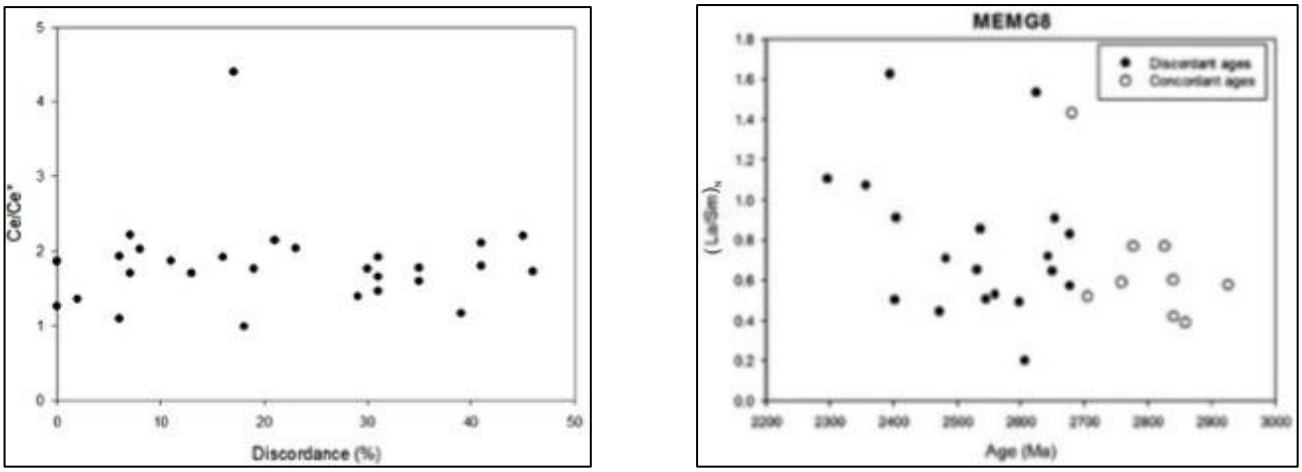

Figure 4.20: (a) Ce/Ce* versus discordance diagram showing no correlation between discordance and cerium anomalies, (b) $(La/Sm)_N$ ratio versus age diagram showing a slight negative correlation between these variables.

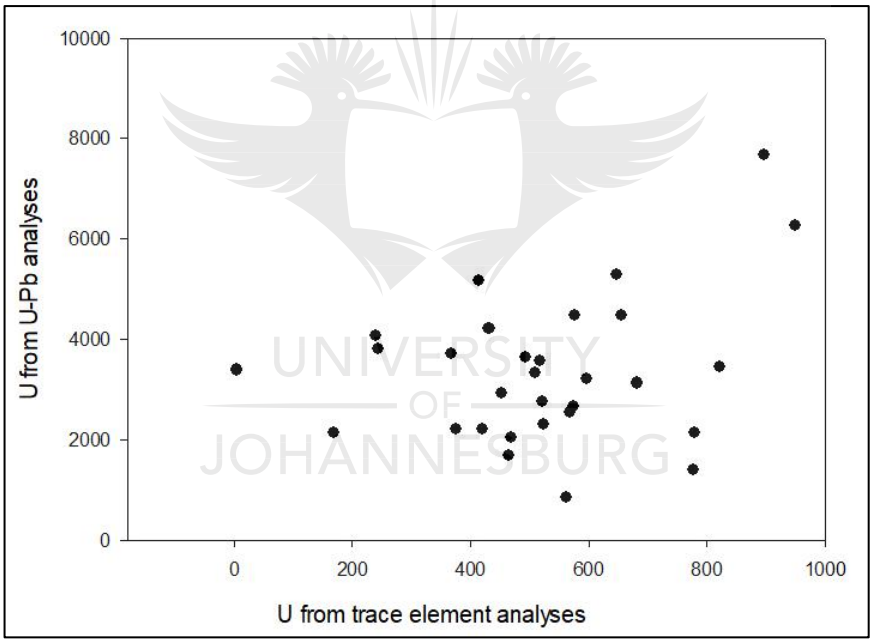

Figure 4.21: U contents based on U-Pb runs versus U contents obtained from trace element analyses. Most analyses are showing a positive correlation.

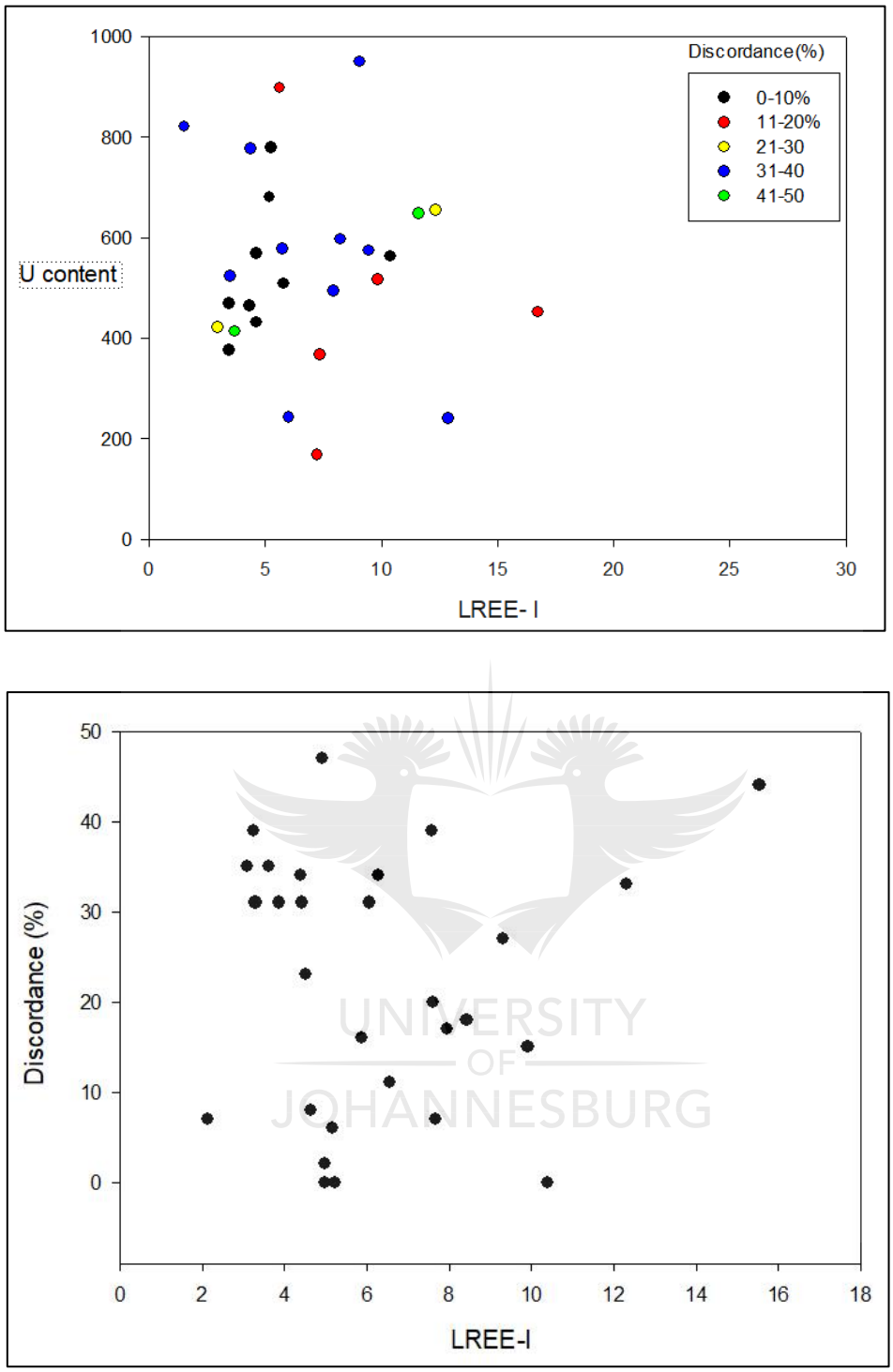

Figure 4.22: (a) LREE index versus uranium content in ppm (b) LREE index versus discordance. Both diagrams show a scattered correlation.

4.4. Sample MEMG9

Sample MEMG9 is an aplite dyke intruding into MEMG8, with the sample taken at the same distance to the Bushveld Complex as MEMG8.

4.4.1. Petrographic description

This dyke is mainly composed of medium-grained anhedral quartz crystals, plagioclase and microcline. There are also minor occurrences of garnet and green amphibole. Zircon and opaque minerals occur as accessory phases in the sample. Alkali feldspar and small crystals of quartz are also observed in Figure 4.23 c. Feldspar also appears as interstitial phase in Figure 4.23 c and d.

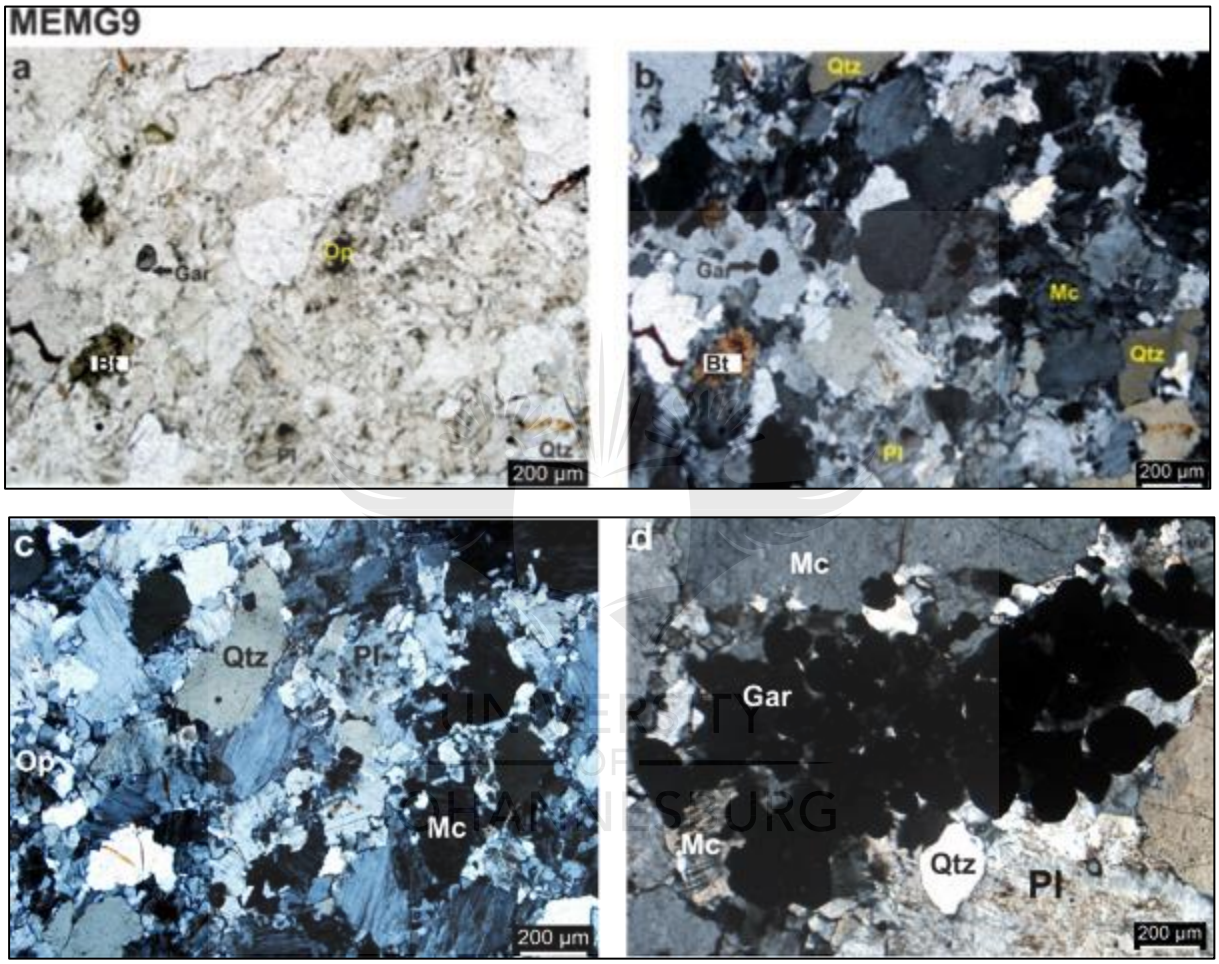

Figure 4.23: (a-b) Anhedral crystals of felsic minerals and minor occurrence of biotite and garnet (PPL and XPL respectively) (c-d) serrated grain boundaries in felsic minerals, surrounding garnet in (d), XPL.

4.4.2. Zircon characteristics

Zircon grains in this aplite dyke are elongate prismatic, ranging in length from 200 to 20 µm (Figure 4.24). Most grains are characterized by complex internal structures; oscillatory zoning is observed in cases but is more often interrupted by several resorption surfaces (Figure 4.24 a, b, i, l). Mineral and fluid inclusions are observed in most grains.

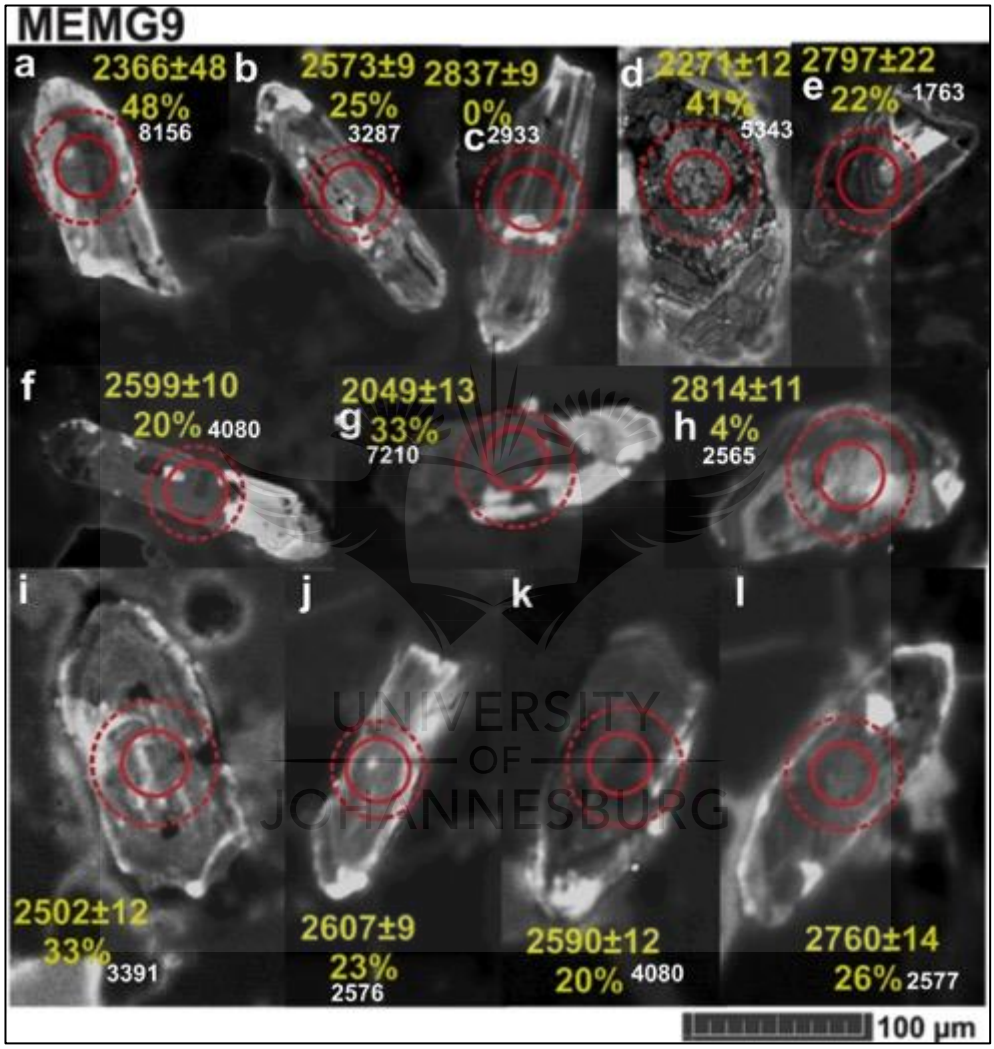

Figure 4.24: Cathodoluminescence images of representative zircon grains of MEMG9. The solid and dashed circles represent U-Pb and Lu-Hf ablation spots, respectively. The numbers displayed are $^{207}Pb/^{206}Pb$ ages at 2 sigma error and discordance percentages at 1 sigma errors. The numbers in white below percentages are U content (ppm), as obtained from the U-Pb runs, and therefore likely an overestimate.

4.4.3. U-Pb results

U-Pb results for this sample are given in Appendix A, Table 4. A Wetherill concordia diagram for eleven analyses that did not show any detectable common Pb is presented in Figure 4.25 a. The $^{207}Pb/^{206}Pb$ ages for these analyses range from 2814±11 to 2271±12 Ma and yield poorly defined upper and lower intercept ages of 2857±87 and 804±260 Ma respectively. The youngest ($^{207}Pb/^{206}Pb$ age of 2547±13 Ma) discordant crystal is characterized by the lowest $^{206}Pb/^{204}Pb$ ratio (1963 ppm) when compared to other CPb-free analyses within the sample. A concordia diagram for all fourty-six analysed grains is shown in Figure 4.25 b, including the zircons corrected for common Pb, which show $^{207}Pb/^{206}Pb$ ages down to 1593±15 Ma. Four zircon grains that are near concordant (<10% discordant) give a clearly meaningless weighted $^{207}Pb/^{206}Pb$ age of 2807±59 Ma, considering its high MSWD of 45. An upper intercept age of 2795±51 Ma and a poorly defined lower intercept age of 498±130Ma is calculated by IsoPlot (Fig 4.4.3.1b), but again with an extreme MSWD (342).

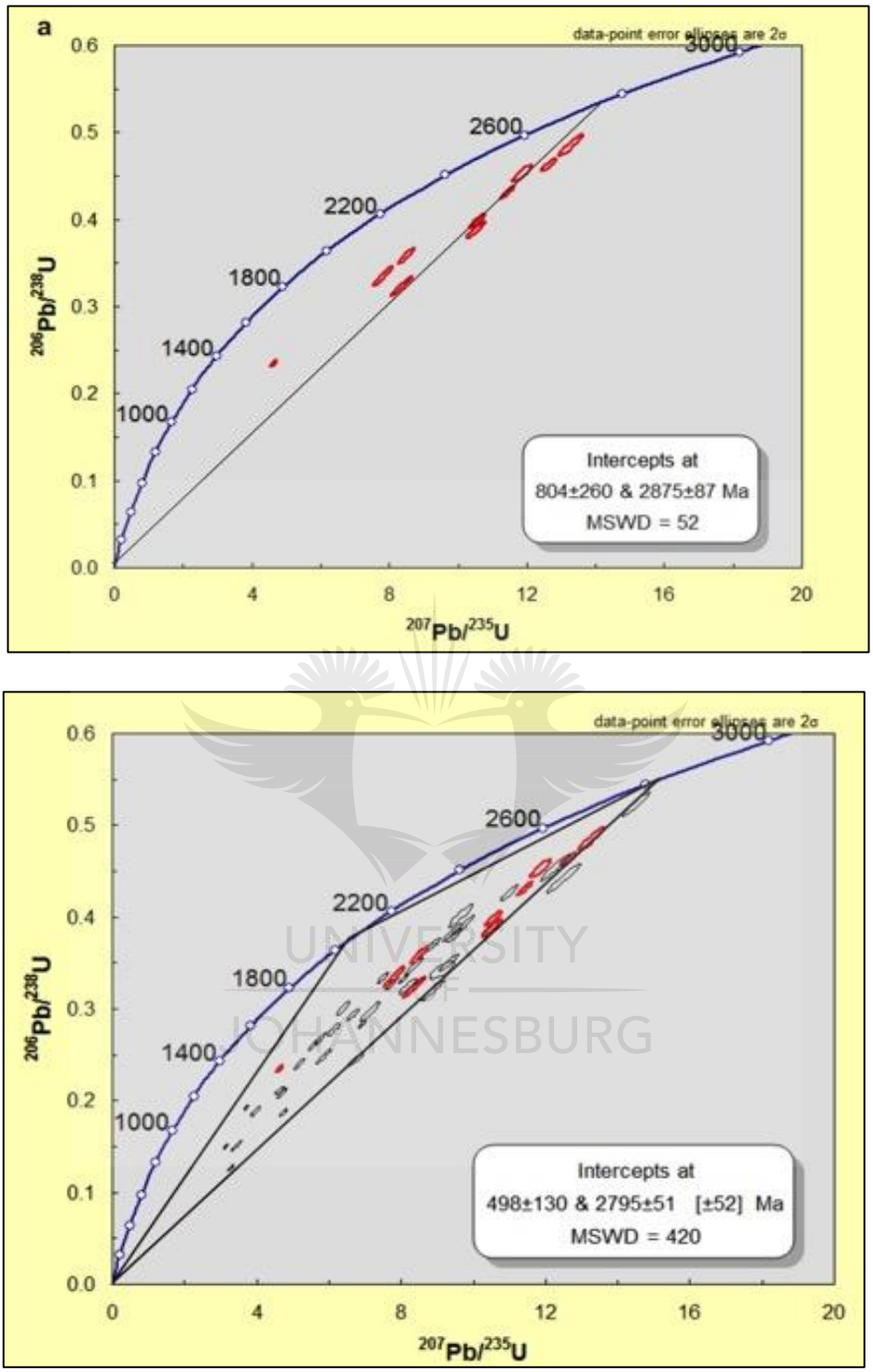

Figure 4.25: Wetherill concordia diagram for sample MEMG9 (a) for uncorrected analyses (b) for both corrected and uncorrected analyses. Analyses fall within a triangle between 2800, 2050 and 0 Ma.

Strong correlations are observed between uranium content, age (negative) and discordance (positive; Figure 4.26 c): zircon grains with high uranium contents are more discordant than those with lower uranium contents. Negative correlations are also observed between $^{206}Pb/^{204}Pb$ ratio versus uranium content and discordance respectively (Figure 4.26 e, f).

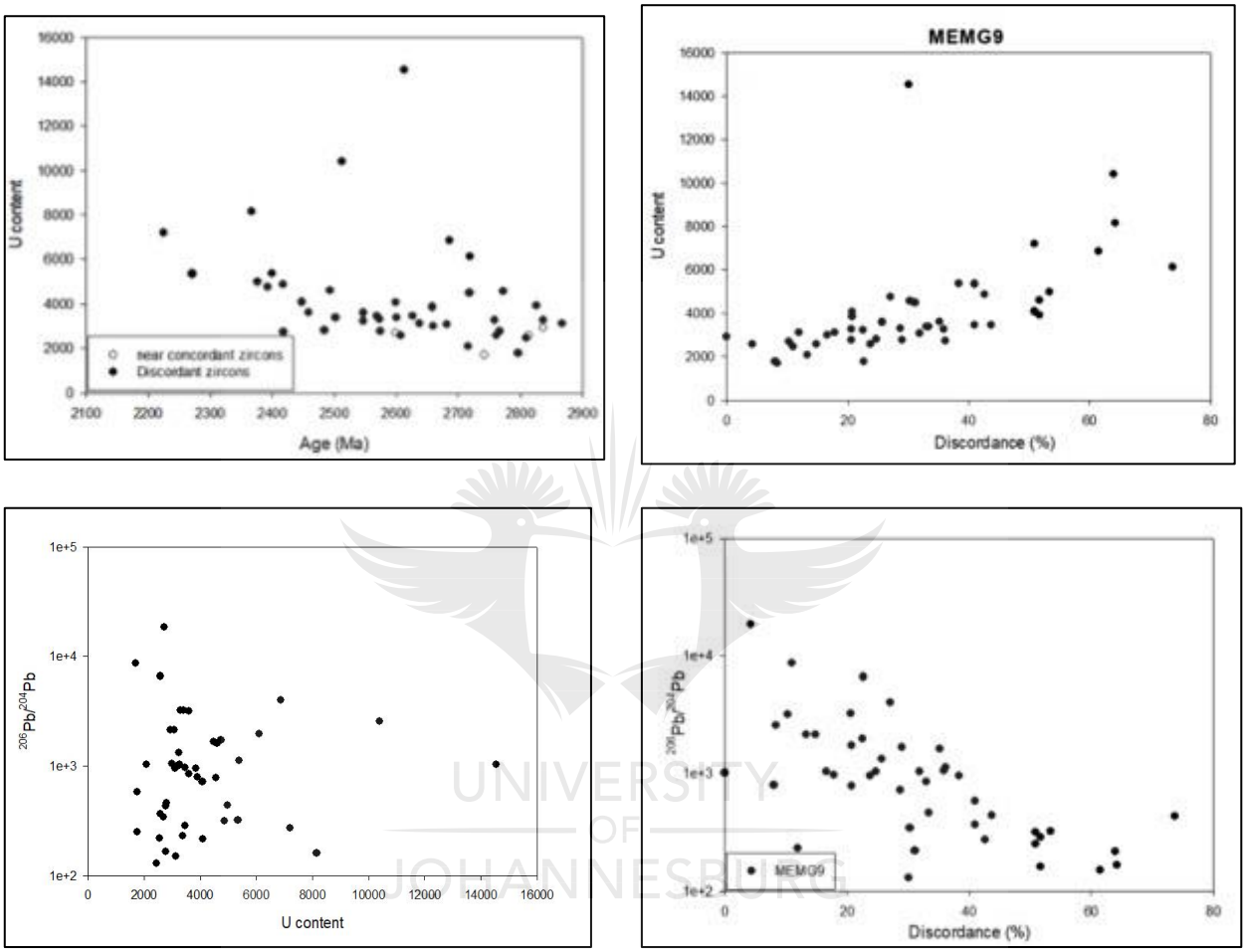

Figure 4.26: Diagrams of (a) uranium content versus age for MEMG9 (b) uranium content versus discordance for MEMG9, showing a distinct correlation between uranium content and discordance. A correlation is also observed between $^{206}Pb/^{204}Pb$ versus (c) uranium content and (d) discordance.

Output from from the program implementing the Reimink algorithm shows peaks for an upper intercept age of ca. 2700 Ma and at a lower intercept age of ca. 600 Ma (Figure 4.27). These ages are slightly younger but within error of the discordia intercepts.

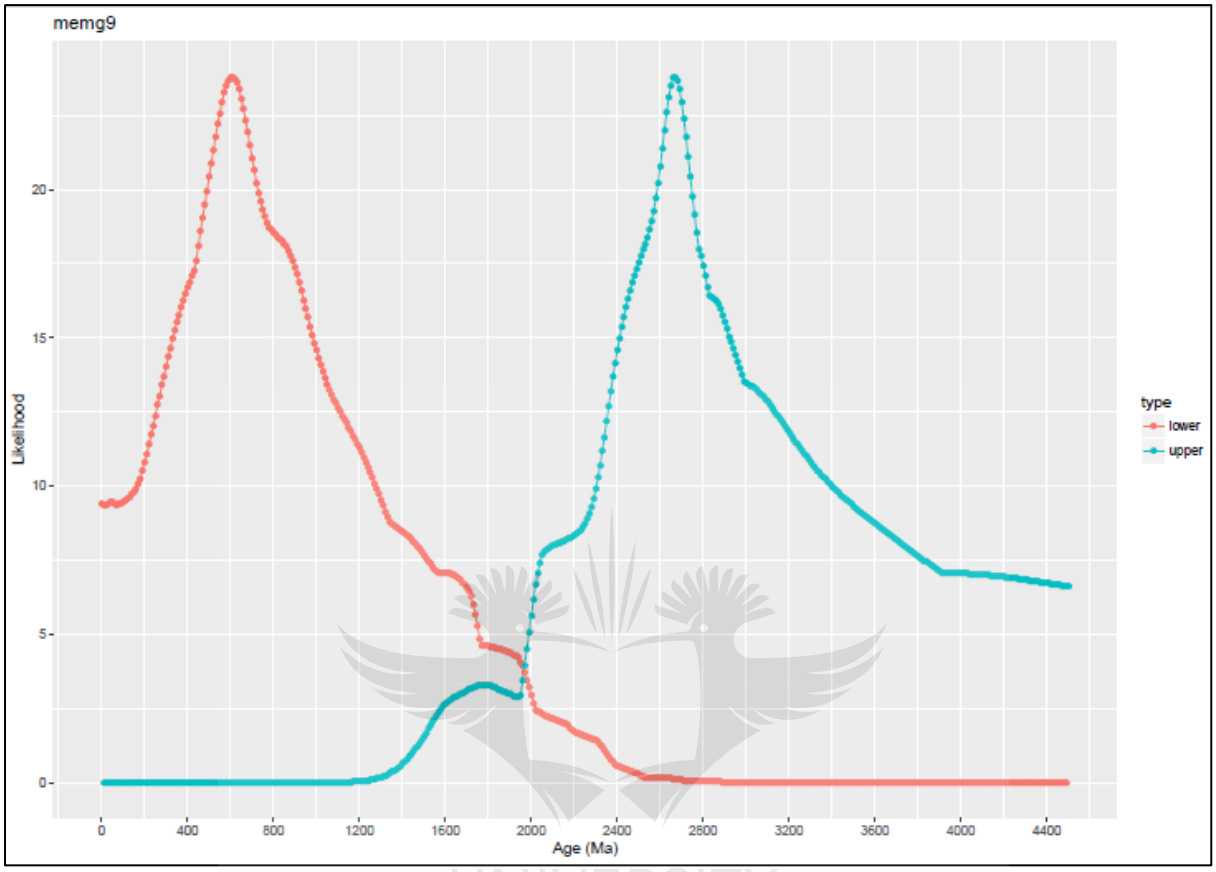

Figure 4.27: An output from Reimink-inspired program for sample MEMG9 showing peak an upper intercept age of ca. 2700 Ma and at a lower intercept age of ca. 600 Ma.

4.4.4. Lu-Hf isotope results

The Lu-Hf results for forty-five zircon grains are provided in Appendix B, Table 2. Like MEMG8, these zircon grains are mostly characterized by negative epsilon Hf values at their $^{207}Pb/^{206}Pb$ age, from values close to zero at the inferred crystallisation age of ca. 2.8 Ga, down to ca. -27 for the youngest ages. The average $^{176}Yb/^{177}Hf$ ratio is 0.041. An overall horizontal array is again observed in the $^{176}Hf/^{177}Hf$ ratio versus age diagram (Figure 4.28).

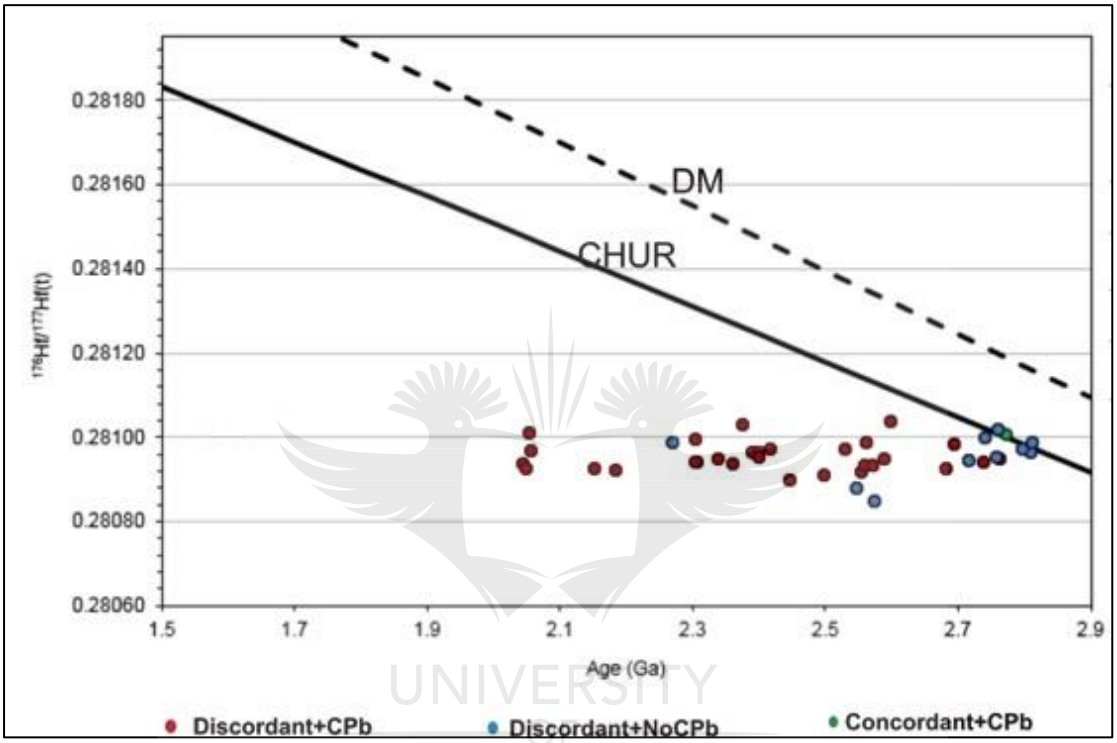

Figure 4.28: Initial $^{176}Hf/^{177}Hf$ ratio versus age diagram for zircons from MEMG9 showing a horizontal array of points from the crystallization age.

4.5. Discussion

4.5.1. Comparison to previous data

4.5.1.1. U-Pb results

From U-Pb isotope analyses in the current study, the ages in Table 4-1 were obtained as estimated crystallization ages for the analyzed Archean granites in proximity to the Bushveld Complex. The crystallization ages for the current study were obtained by calculating a weighted average $^{207}Pb/^{206}Pb$ ages for concordant analyses. The crystallization age for MEMG6 is slightly younger than others probably due to influence of younger granite intrusions.

Sample name	Inferred crystallization age (Ma)
MEMG6	2713±25
MEMG7	2841±11
MEMG8	2821±38
MEMG9	2837±9
MAS-05	2681±10
MAS-10	2678±7
HRG-1	2953±13
HRG2	2833±5

Table 4-1: Table showing inferred crystallization ages for analyzed samples from current study and a previous study by Laurent et al., 2013.

Please note that only CPb-free analyses are plotted in this section.

A Wetherill concordia diagram for analyses that are within 2 sigma error of being concordant for all four Archean granites is shown in Figure 4.29. Concordant ages for MEMG7 range from 2872±9 to 2813±10 Ma. Concordant ages for MEMG8, which shows the lowest number of formally concordant analyses, range from 2881±14 to 2760±17 Ma, excluding one xenocryst with an age of 2925±16 Ma; the one concordant analysis in MEMG9 has a $^{207}Pb/^{206}Pb$ age of 2837±9 Ma. The concordant ages for MEMG6 range from 2776±15 to 2547±19 Ma. The youngest two MEMG6 analyses with the ages of 2570±33 and 2547±19 Ma have a remarkably high uranium content (4401 and 3710 ppm) when compared to all concordant zircons within the sample. MEMG6 was collected about 20 km and 30 km from MAS-05 and -10 respectively, and was interpreted to be a part of the Hout River Gneiss, but very close to the contact with the Mashashane pluton. A concordia diagram for these samples indicates that MEMG6 has a spread in $^{207}Pb/^{206}Pb$ ages and a significant fraction of zircons

that are older than MAS-05 and -10 analyzed by Laurent et al. (2013) as shown in Figure 4.29 b, and the pattern of their Pb loss is not the same probably due to that the previous study eliminated analyses containing common Pb and characterized by more than 5-15% discordance (depending on the sample), whereas all analyses were included in the current study. When compared to the granitoid rocks previously studied by Laurent et al. (2013), MEMG-7, -8 and -9 can be correlated with HRG-1 and -2 in terms of map units shown in figure 2 of Laurent et al. (2013) (see Figure 4.30), again in terms of age HRG-1 is older than MEMG7-9. A concordia diagram for these samples shows that in terms of $^{207}Pb/^{206}Pb$ ages, HRG2 correlates more with MEMG7-9.

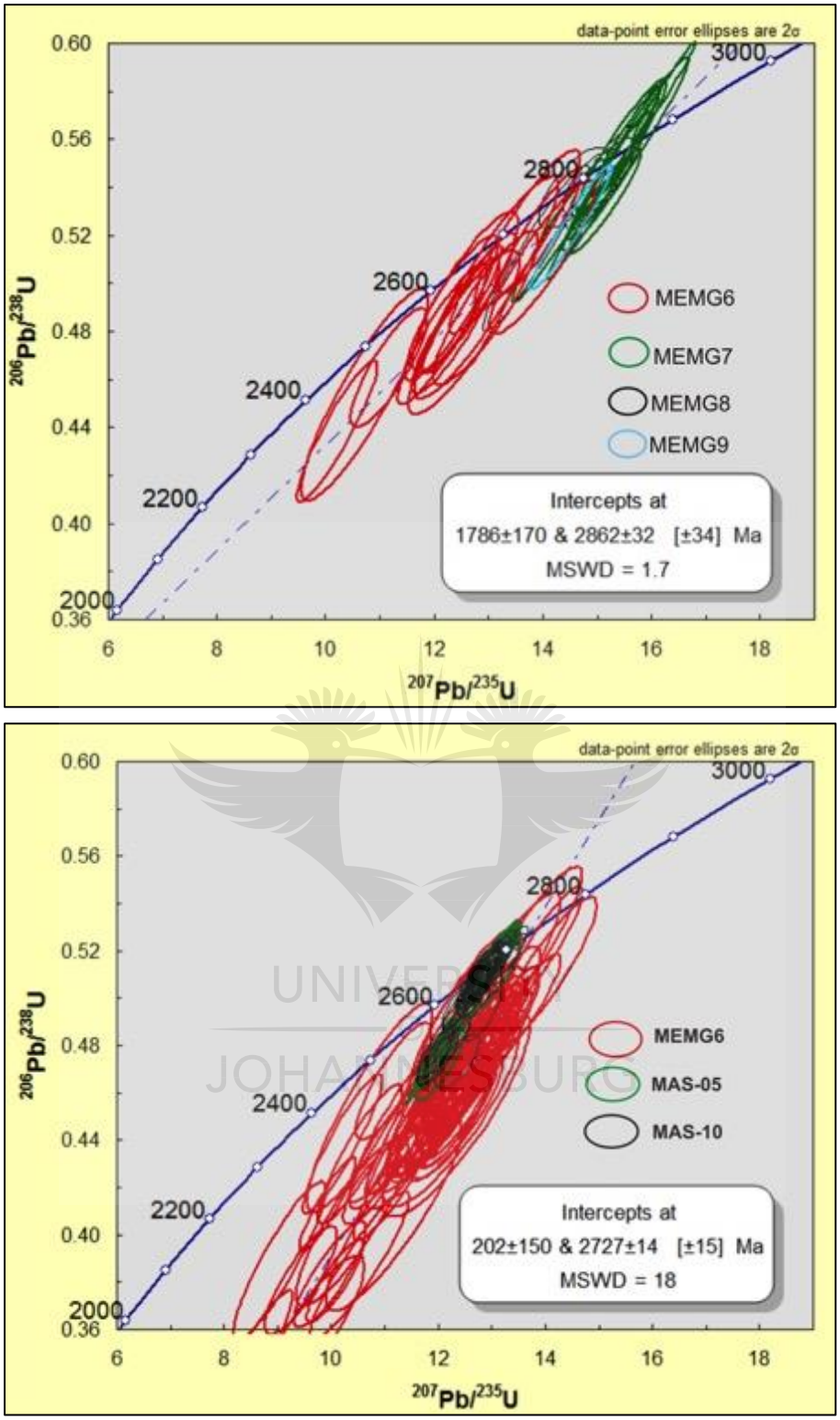

Figure 4.29:(a) A close-up concordia diagram for all concordant analyzed zircons for the Archean granites from current study (b) a close-up concordia diagram for MEMG6, MAS-5 and -6.

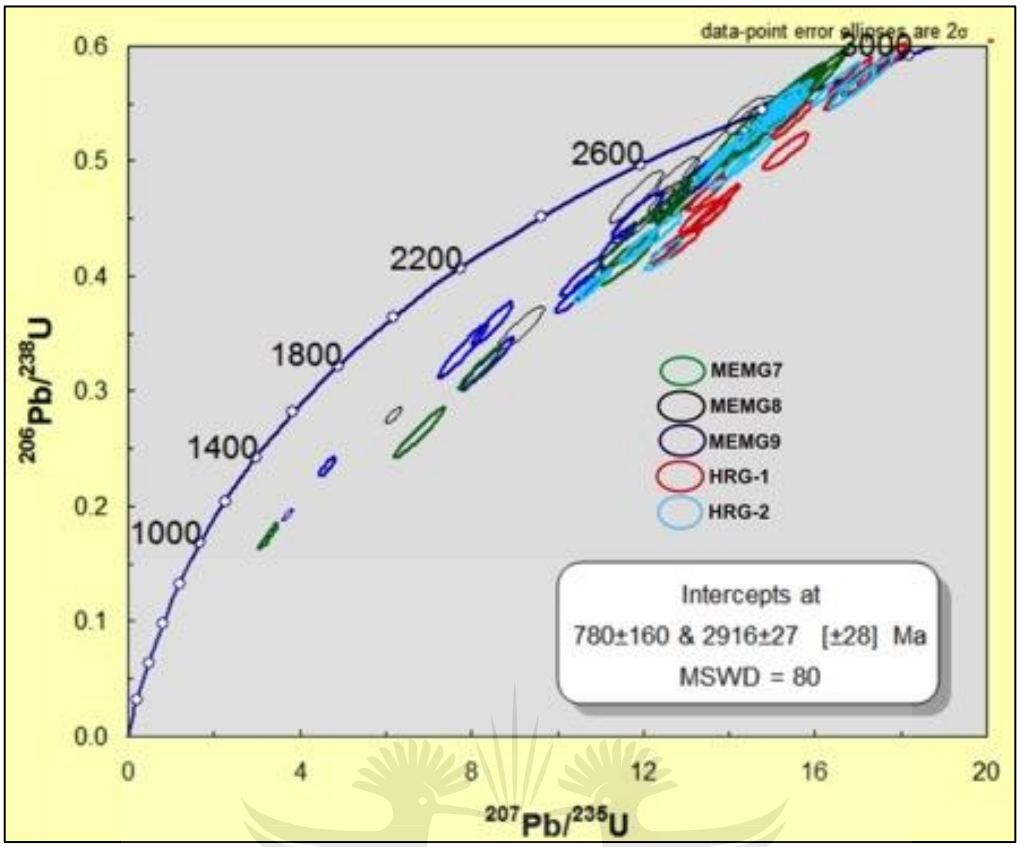

Figure 4.30: A concordia diagram for MEMG7-9, and HRG-1, -2. Data for HRG-1 and -2 is from that publication by Laurent et al. (2013).

4.5.1.2. Lu-Hf isotope results

The zircons from MEMG8 and MEMG9 were analyzed for their Lu-Hf isotopic characteristics. A diagram combining Lu-Hf data for MEMG8, MEMG9 as well as Hout Rivier Gneisses (after Laurent and Zeh, 2015) is shown in Figure 4.31. An overall sub-horizontal array of points is observed in granites from the current study, and HRG-1 and -2 show a cluster of points at their inferred crystallization ages. It is also observed that granite samples analyzed by Laurent and Zeh, 2015 (HRG-1 and -2) lie above the CHUR whereas over 90% of the analyses from samples MEMG8 and 9 lie below the CHUR. The epsilon values for MEMG8 and 9 vary significantly from HRG-1 and 2. MEMG8 and 9 from current study are characterized by negative epsilon values giving averages of -0.5±1.1 and -0.3±2.1, respectively. HRG-1 and 2 from Laurent and Zeh (2015) are characterized by positive epsilon Hf values giving averages of 2.5±1.8 and 2.5±1.5, respectively.

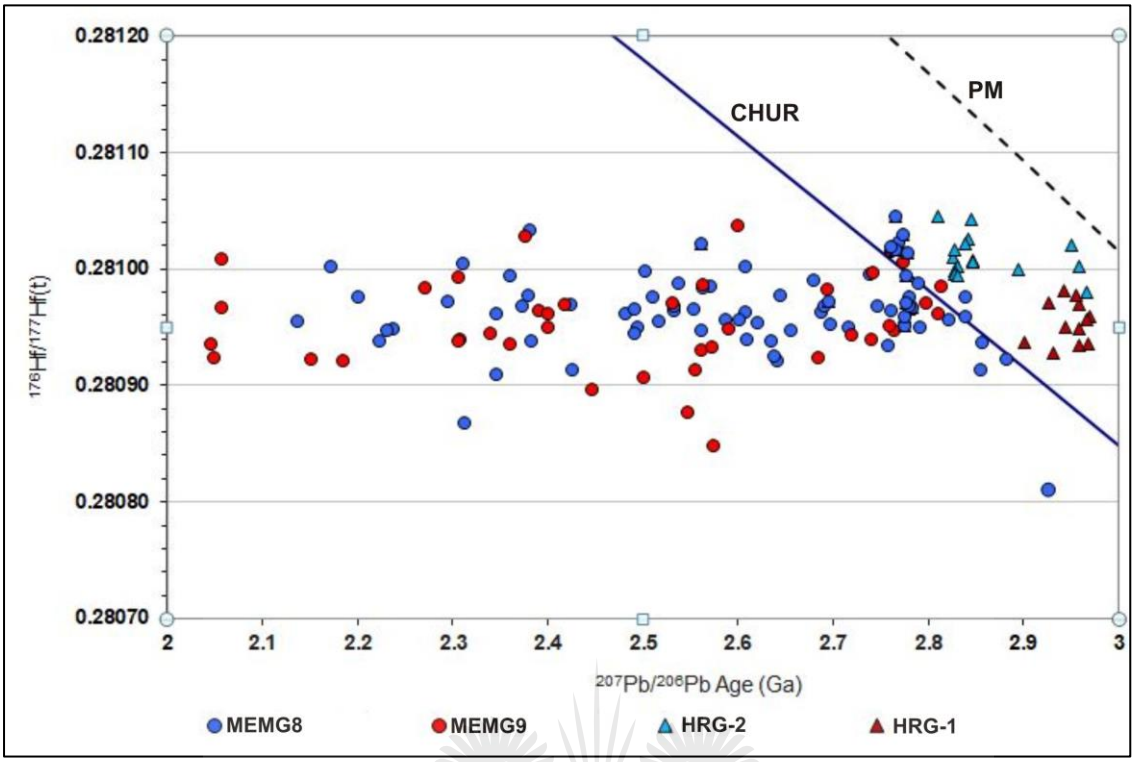

Figure 4.31: Initial $^{176}Hf/^{177}Hf$ ratio versus $^{207}Pb/^{206}Pb$ age diagram for MEMG8 and 9, as well as Hout River Gneiss samples HRG-1 and -2 (data from Laurent and Zeh, 2015).

4.5.2. Petrography

Zircon crystals mostly occur between major mineral phases e.g. quartz, feldspar, biotite and hornblende in these granites; however, there are instances where they are wholly enclosed within a crystal of one of the major minerals. The petrographic observations show that these granites are not pristine; most of the minerals are altered. Amongst them, biotite and/or hornblende are altered to chlorite in samples closest to Bushveld intrusion (MEMG6, MEMG8), but this chloritization is not pronounced in either sample, so, if this alteration is related to the Bushveld intrusion, the intrusion appears to have limited influence, based on the samples' petrographic characteristics. MEMG6 is deformed, which is shown by the size and shape of quartz grains that may be related to dynamic recrystallization, which could potentially be an effect of the intrusion of the BC, but could also be related to the location of the sample close to the Pietersburg-Lwaji shear zone, for which the main period of metamorphism and deformation has been proposed to be around 2840-2870 Ma (Kramers et al, 2014). MEMG8 and MEMG9 also show recrystallization of quartz. The myrmekite texture observed in sample MEMG7 may be an indication that these rocks have also been metasomatised, and this may be attributed to the hydrothermal and/or other fluid flow events

probably associated with Bushveld Complex, because, according to Rasmussen et al. (2007), hydrothermal effects associated with the Bushveld Complex extend more than 100 kilometres outward from the margins of the Complex. This myrmekite texture is, however, not observed in samples closest to the intrusion. There is no obvious evidence for partial melting in these rocks.

4.5.3. Zircon characteristics

Zircon crystals in all four granites show a variety of textures, the dominant one being oscillatory zoning. It can be noted in some cases that the oscillatory zoning is fading away and is replaced by weakly zoned to complex patchy textures. There is no consistency in correlation between uranium content and zircon textures in CL images as it can be observed in all granite samples that some may have patchy complex zircon textures while their uranium content is low and vice versa. However, zircon grains that have patchy complex textures show significant discordance; hence more evidence would be needed to show whether or not the crystals that were damaged by radiation from alpha decay of U and Th are the first ones to lose their primary igneous textures. The fractures seen in cathodoluminescence images of the zircons from these granites have often developed preferentially around the inclusions, probably because the thermal expansion coefficient of the inclusion and the zircon are different. These fractures may also have resulted from cooling of the pluton, or during expansion of the zircon crystal during metamictisation. There is a correlation between zircon internal textures (such as inclusions, fractures) and the degree of discordance of their U-Pb ages, as well as zircon growth zonation and discordance of their U-Pb ages. For example, in Figure 4.3a (sample MEMG6) a grain with a high discordance percentage of 33% and a young (2473±20 Ma) $^{207}Pb/^{206}Pb$ age is characterised by fractures and mineral inclusions.

4.5.4. U-Pb data

U-Pb results show that all the Archean granites have suffered lead loss after their time of crystallization. The spread in $^{207}Pb/^{206}Pb$ ages for zircons from samples MEMG6 and MEMG8 indicate that, in addition to zero-age Pb loss, an earlier event must have contributed to Pb loss; in these two samples ca. 90% of zircon grains fall within a triangle between the inferred crystallization ages, 2.05 Ga and 0 Ga. The fact that the analyses for MEMG7 also do not give a zero-age lower intercept indicates that the $^{207}Pb/^{206}Pb$ ages are variable. This could be interpreted as reflecting a ca. 300 Ma Pb-loss event, or an earlier one, similar to the model calculations shown in Figure 4.32 below. This then indicates that as much as the

dominant episode of partial Pb loss might have occurred recently, there may have been an earlier episode of Pb loss in view of the youngest $^{207}Pb/^{206}Pb$ ages, which could potentially be related to the intrusion of Bushveld Complex. However, the petrography show little evidence for effects of the intrusion of the Bushveld Complex, and the U-Pb data do not show a convincing trend towards its intrusive age of 2.05 Ga. Laurent et al. (2013) analysed granite samples that were collected further from the Bushveld complex but in the same geological unit as granite samples from current study, but it is also hard to compare results from Laurent et al. 2013 and current study because of different data screening used in both these studies.

The large variations in concordant $^{207}Pb/^{206}Pb$ ages in MEMG6 and MEMG8 indicate that even though these zircon grains might have formed at the same time most likely during magma crystallization (with MEMG6 being affected perhaps by the intrusion of the slightly later granites, hence slightly younger intrusive age), several zircon domains were later affected by Pb loss. MEMG7 has a well-defined upper intercept age; however lower intercept ages appear to be spurious in all granitoid rocks because they represent ages at which nothing is known to have happened in South Africa's geological history. In this case, one interpretation that could be valid for these spurious lower intercept ages is that lower intercept ages do not present any realistic geological event but recrystallization of metamict zircons caused by a continuous radiation damage of zircon lattice which is a result of radiation flux that occurs over time. This then decreases stability of zircon; hence it become more susceptible to be altered (e.g. Tilton, 1960; Mezger & Krogstad, 1997; Geisler et al., 2001). This interpretation is also supported by correlation observed in Figure 4.5, Figure 4.11 and Figure 4.16 where the uranium content is plotted against age as well as discordance. The results of a simulation of Pb-loss using an MS Excel spread sheet (Elburg, pers. comm.) are shown in Figure 4.32. The simulation assumes a population of zircons with a single crystallisation age, but variable U contents. The zircons can be set to lose Pb (up to a specified percentage) at two different events, and in each case, the amount of Pb loss is positively correlated with the amount of U in the zircon. This simulates the observation that zircons with a high U content are often most discordant. The results of these simulations show that the correlation between Pb loss and U contents during two events can lead to spurious upper and lower intercept ages.

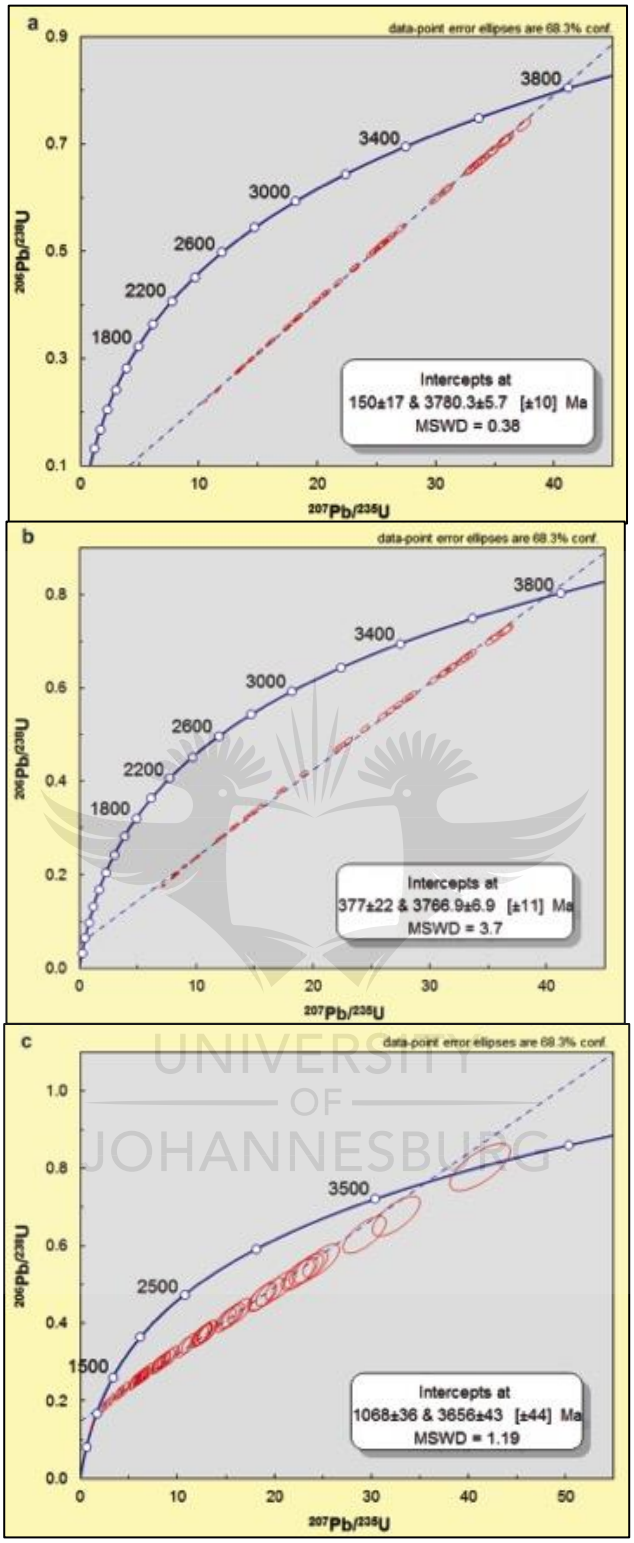

Figure 4.32: Concordia diagrams for model runs showing different episodes of Pb loss for 3800 Ma granite, with the amount of Pb loss correlated with U content: (a) loss of up to 20% of Pb during first episode at 2050 Ma and loss up to 100% of Pb at 0 Ma (b) loss of up to 50% of lead at 2050 Ma and loss of up to 100% of Pb at 0 Ma (c) loss of up to 100% of lead at 2050 and loss of up to 100% of Pb at 800 Ma. Note the shift in lower intercept ages; even upper intercept ages become more poorly defined for the scenario where the earlier Pb-loss event has caused significant resetting.

4.5.5. Lu-Hf data

The sub-horizontal arrays observed in the $^{176}Hf/^{177}Hf$ versus age diagram for zircons from MEMG8 and 9 indicate that the discordance observed on U-Pb concordia diagrams is indeed due to partial lead loss in zircon grains. Limited variations observed in initial Hf ratios indicate that Lu-Hf system remained undisturbed (e.g. Bomparola et al., 2006), so there is no correlation between textural differences in zircons and $^{176}Hf/^{177}Hf$ ratios. Again, with regards to the pattern observed in the $^{176}Hf/^{177}Hf$ versus age diagram (Figure 4.31) comparing MEMG8 and 9 with sample HRG-1 and-2 from Laurent and Zeh (2015), zircon analyses have similar initial Hf ratios.

4.5.6. Trace element chemistry

Trace element analyses were done on sample MEMG8, and partial Pb loss shown in U-Pb concordia diagrams is not reflected in the REE patterns. A diagram of Ce/Ce* vs discordance shows no clear correlation between the two parameters. However, a slight correlation between age and La/Sm ratio is observed, with concordant ages having lower La/Sm ratios than younger discordant ages, showing that there is a slight enrichment in light rare earth elements in discordant zircon grains. An LREE index of less than 10 in over 90% of zircon grains in MEMG8 indicate that zircon grains in this granite are metamict (e.g. Bell et al., 2016), however, the ablation spots used for trace elements were last left-over bits, hence the material may have been of poor quality.

4.6. Conclusion

Zircon grains from all Archean granite samples analyzed here have indeed undergone partial Pb loss, causing resetting of their $^{207}Pb/^{206}Pb$ ages. Although recent Pb-loss has obscured any contribution from the Bushveld Complex, the range in concordant $^{207}Pb/^{206}Pb$ ages that are CPb-free points towards an earlier Pb-loss event. Correlations between uranium and discordance show that the main cause of Pb loss from these zircons is likely radiation damage in zircon lattice which led to metamict zircon grains being more susceptible to be reset during various geological processes. The petrographic characteristics show little effect of the Bushveld intrusion, but U-Pb concordia diagrams for MEMG6, 7 and 8 indicate that most analyses plot in a triangle between crystallization age, Bushveld age and 0 Ma, so the conclusion is that if there are any effects from the Bushveld intrusion that caused Pb loss for these Archean zircons they are minor. The results from this study have also shown that complete zircon resetting is a rare case, as none of our analyses, nor analyses from previous studies on the same granite (e.g. Laurent and Zeh, 2013) have shown a complete zircon age

resetting, but rather a partial Pb loss in zircon grains. Limited variations in initial Hf ratios indicate that the Lu-Hf isotopic system was not affected during partial age resetting of these zircon grains, but horizontal arrays in Hf isotope versus age diagrams support the idea that discordance seen in concordia diagrams is indeed caused by partial Pb loss in zircon and partial resetting of $^{207}Pb/^{206}Pb$ ages. The results from CL images have demonstrated that discordance may be correlated with results shown by techniques traditionally used to image zircons, but that is not always the case. Lastly, the modifications in zircon grains are not always reflected in their trace element characteristics.

Chapter 5

5. Results: Transvaal Supergroup

Magaliesberg Sandstones

Five sandstone samples from the Magaliesberg Formation were collected at different distances to the Bushveld Complex to assess if there is any influence from the thermal effects of the Bushveld Complex on the isotopic characteristics of zircon. MEMG1 and MEMG2 were taken <1 km south of the Rustenburg Layered Suite in the western limb of the Bushveld Complex. MEMG3 and MEMG4 were obtained at distances of 0.5 and 230 meters from the contact with the Marginal Zone in the eastern limb of the Bushveld Complex (Figure 5.1). The detrital zircons obtained from these samples were analyzed for their U-Pb and in some cases Lu-Hf isotopic ratios using the LA-MC-ICPMS. A minimum of 50, but most often about 100 grains were analyzed for each sample. Again, due to small zircon sizes the U-Pb analyses often required ablation of the entire grain.

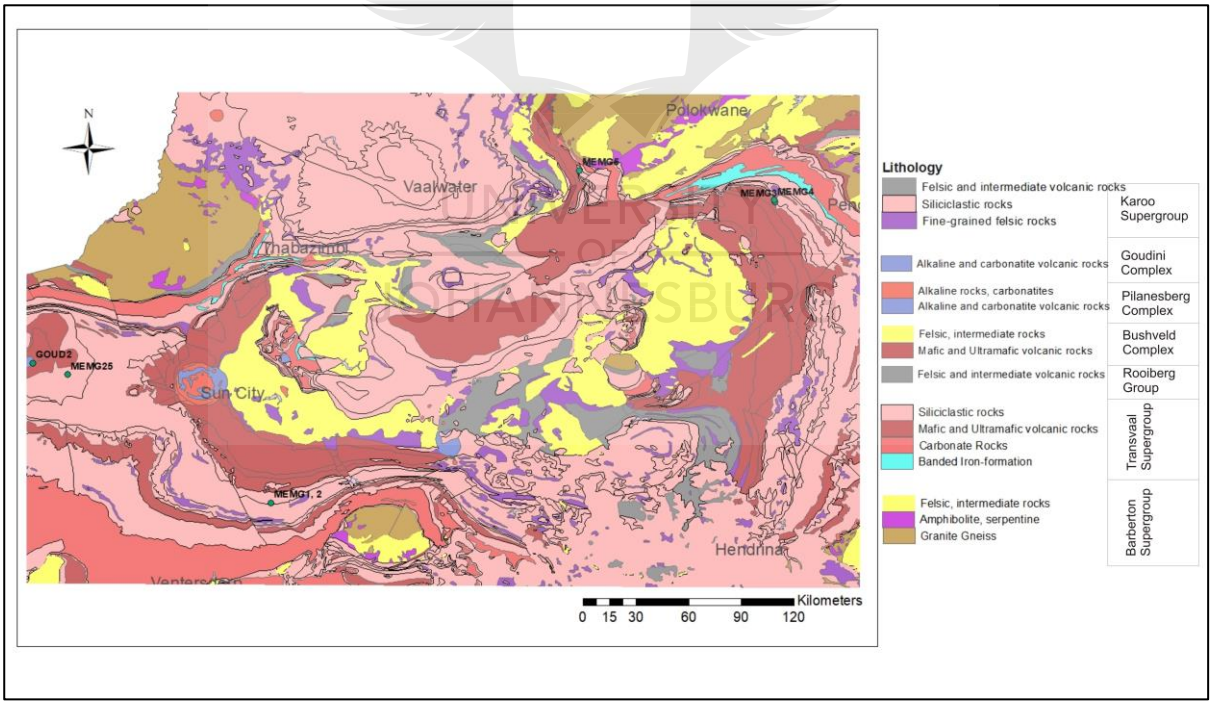

Figure 5.1: Map showing sample locations for Transvaal metasandstones.

5.1. Sample MEMG1

Sample MEMG1 was collected <1 km south of the Rustenburg Layered Suite in the western limb of the Bushveld Complex (Figure 5.1).

5.1.1. Petrographic description

Sample MEMG1 is a coarse-grained metasandstone, consisting mainly of angular recrystallized quartz grains, which occur with slightly altered alkali feldspar (Figure 5.2 a). Biotite and muscovite occur as minor mineral phases between quartz and alkali feldspar (Figure 5.2 b). Zircon occurs as an accessory phase within quartz (Figure 5.2 c) and alkali feldspar (Figure 5.2 d).

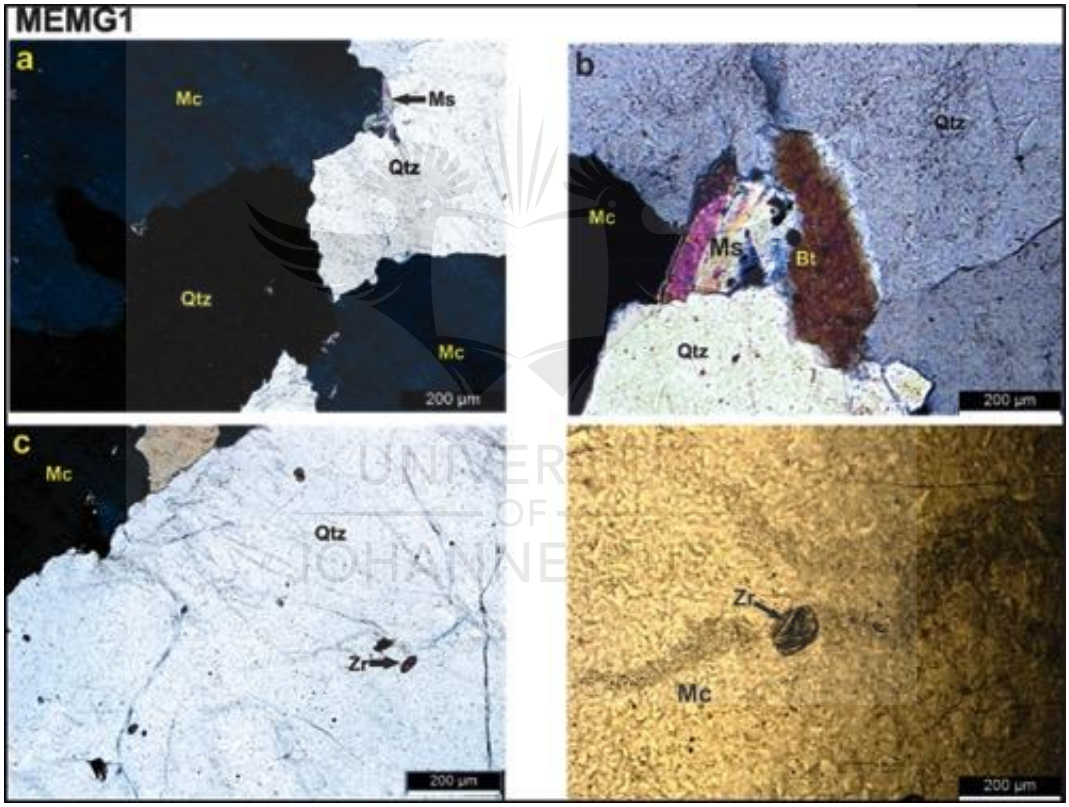

Figure 5.2: (a) Angular quartz occurring with microcline (XPL) (b) biotite and muscovite occurring interstitial to quartz and feldspar (XPL) (c) occurrence of zircon within quartz (XPL) (d) occurrence of zircon within microcline (PPL).

5.1.2. Zircon characteristics

Zircons in this sample are well-rounded to sub-rounded, and their length ranges from 200 to 80 µm (Figure 5.3). They have a variety of textures, most commonly oscillatory zoning (e.g. Figure 5.3 c, h, l, n, s). There are variations in cathodoluminescence intensities in these crystals, ranging from CL-dark (e.g. Figure 5.3 c, e, h, l, r) to CL-bright (e.g. Figure 5.3 a, b, g, k, o). In some grains zones with enhanced CL brightness are observed overprinting oscillatory zoning. Crystals that lack oscillatory zoning are characterized by CL dark areas at the margins. Fractures occur occasionally.

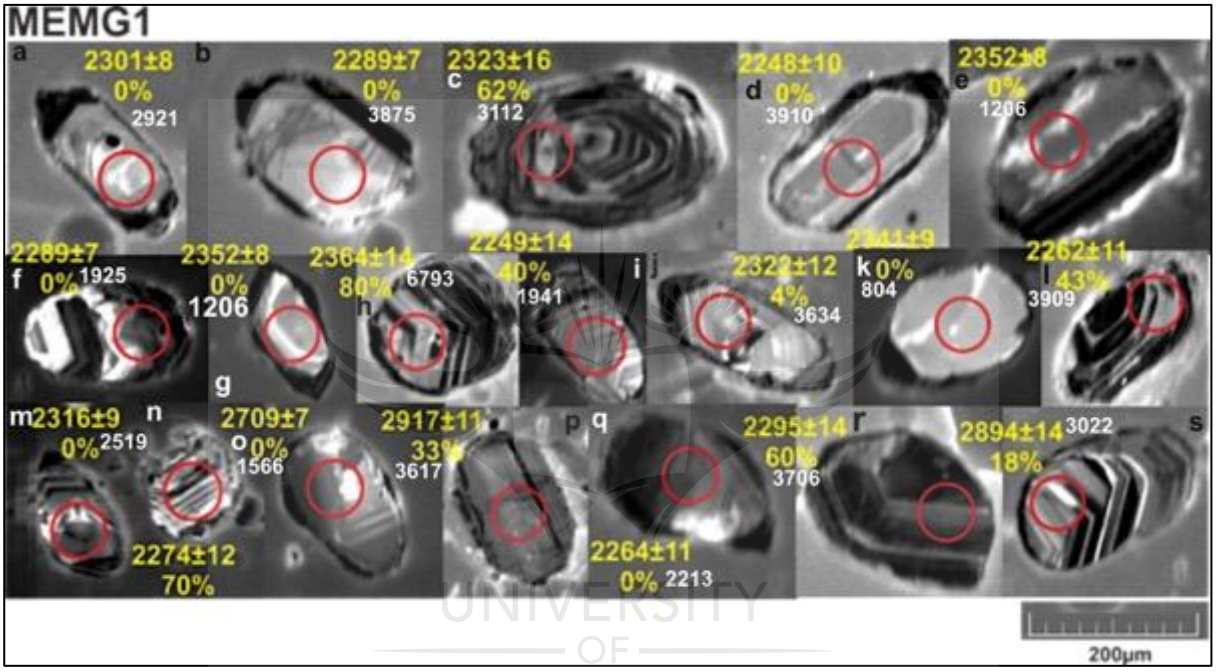

Figure 5.3: Cathodoluminescence images of selected zircon grains of MEMG1 with the circles representing U-Pb ablation sites and the numbers displayed are $^{207}Pb/^{206}Pb$ ages with 2 sigma errors. The discordance (in percent) is given below the age and numbers in white are uranium contents in ppm.

5.1.3. U-Pb results

U-Pb results for seventy-four analysed grains for MEMG1 are given in Appendix A, Table 5, and the analyses are displayed in a concordia diagram (Figure 5.4). Twenty-seven grains were concordant, and range in $^{207}Pb/^{206}Pb$ ages between 2752±10 and 2224±13 Ma. The remaining forty-eight were discordant, and the majority of Proterozoic zircons lie on a straight line towards the origin of the diagram. The youngest discordant grain has a $^{207}Pb/^{206}Pb$ age of 1759±18 Ma, but this grain is highly discordant and has been corrected for common Pb (23%), so its validity is doubtful. Zircon grains with Archean ages also show partial lead loss, and their $^{207}Pb/^{206}Pb$ ages range between 2649±8 and 2917±11 Ma. Figure

5.5 a, b show a clear positive correlation between uranium content and discordance, and a poor correlation between $^{206}Pb/^{204}Pb$ ratios and $^{207}Pb/^{206}Pb$ ages, but this is of course related to the detrital nature of the zircons analysed. It is clear that concordant zircons have higher $^{206}Pb/^{204}Pb$ ratios than discordant grains.

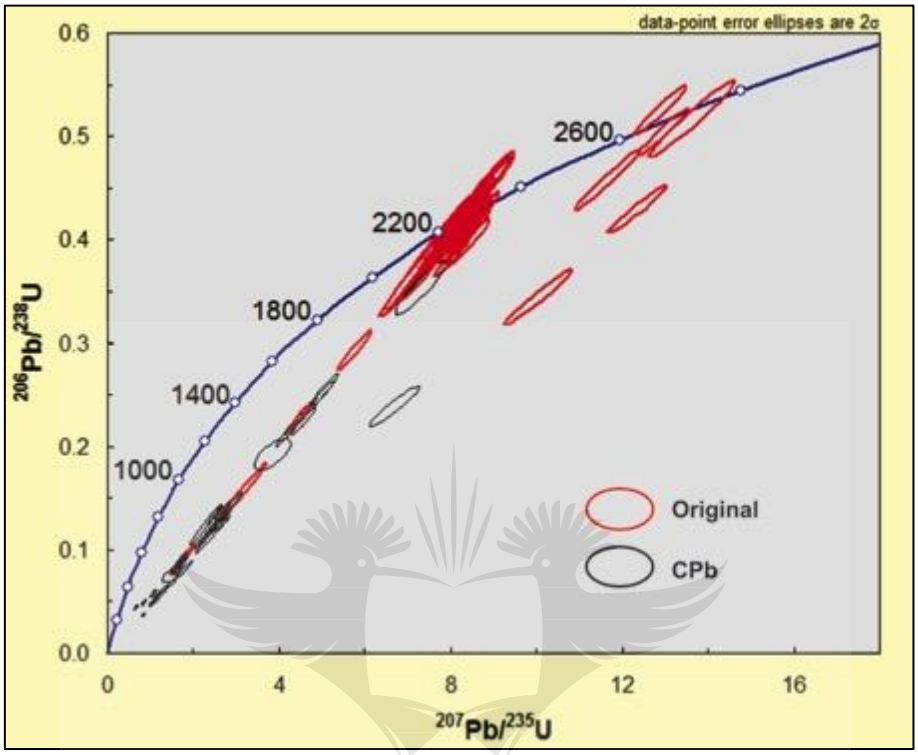

Figure 5.4: Wetherill concordia diagram for sample MEMG1. Zircon suffered partial Pb loss at 0 Ma.

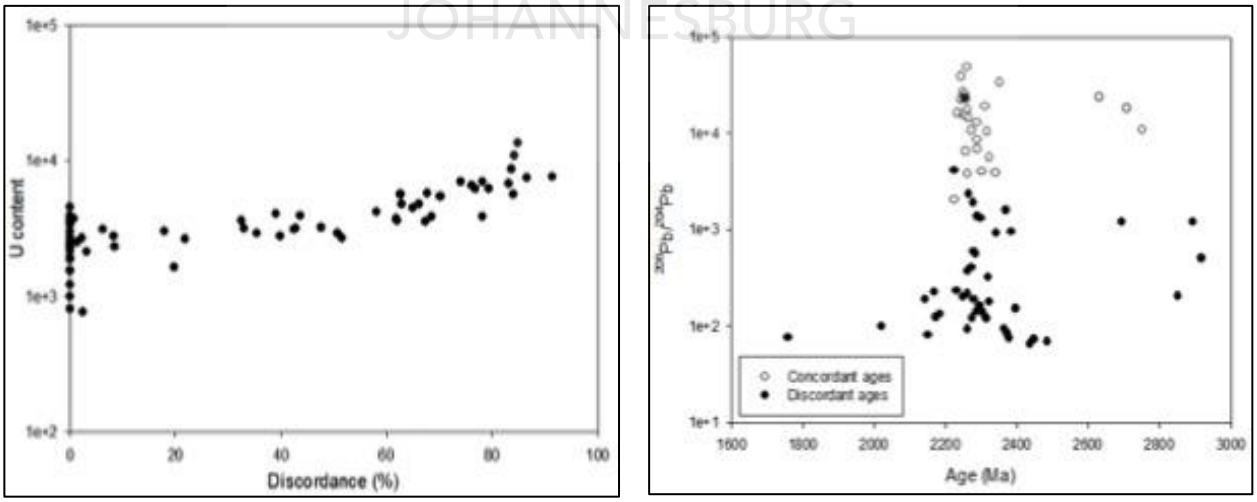

Figure 5.5: (a) Uranium content (in ppm; note log scale) versus discordance for MEMG1 showing a clear correlation between discordance and uranium content (b) $^{206}Pb/^{204}Pb$ ratio versus age diagram showing that concordant ages have higher $^{206}Pb/^{204}Pb$ ratios and vice versa.

5.2. Sample MEMG2

Sample MEMG2 is a coarse-grained metasandstone that was collected at the same location as sample MEMG1 (Figure 5.1)

5.2.1. Petrographic characteristics

This sample has similar mineralogy and grainsize to MEMG1, but it also contains cordierite as a minor phase and tourmaline as an accessory phase (Figure 5.6).

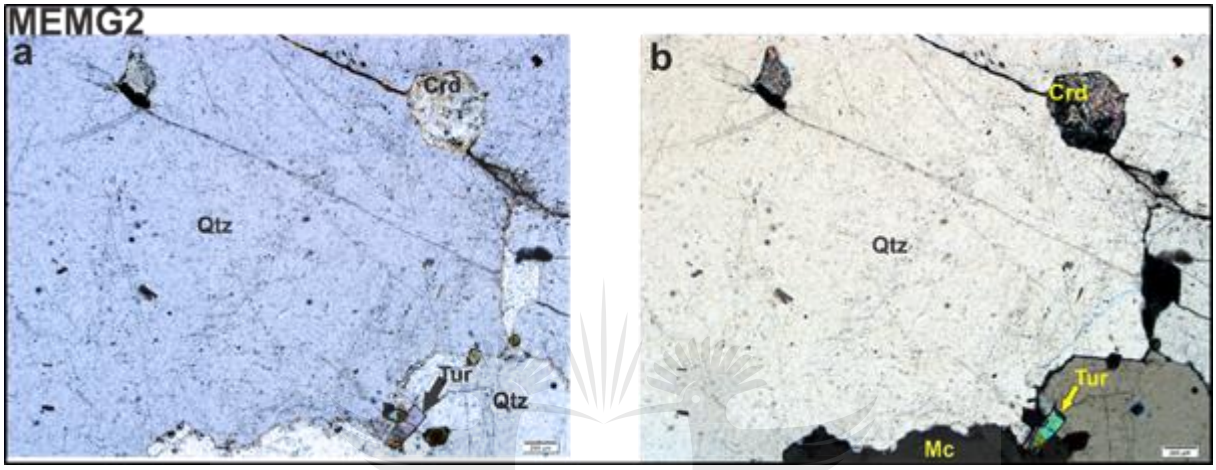

Figure 5.6: Occurrence of cordierite and tourmaline within quartz grains (a) PPL (b) XPL. The scale bar is 200µm.

5.2.2. Zircon characteristics

Detrital zircons in MEMG2 are rounded to sub-rounded, with lengths ranging from 100 to 20 µm. They are characterised by a variety of textures, including oscillatory zoning, sector zoning superimposed on oscillatory zoning (e.g. Figure 5.7 a, g), and some grains have complex zoning patterns (e.g. Figure 5.7 c). Most of the grains have fractures and mineral inclusions (Figure 5.7 a, b, e, g, n). Zircon grains in this sample often have domains of enhanced CL brightness overprinting zoning patterns.

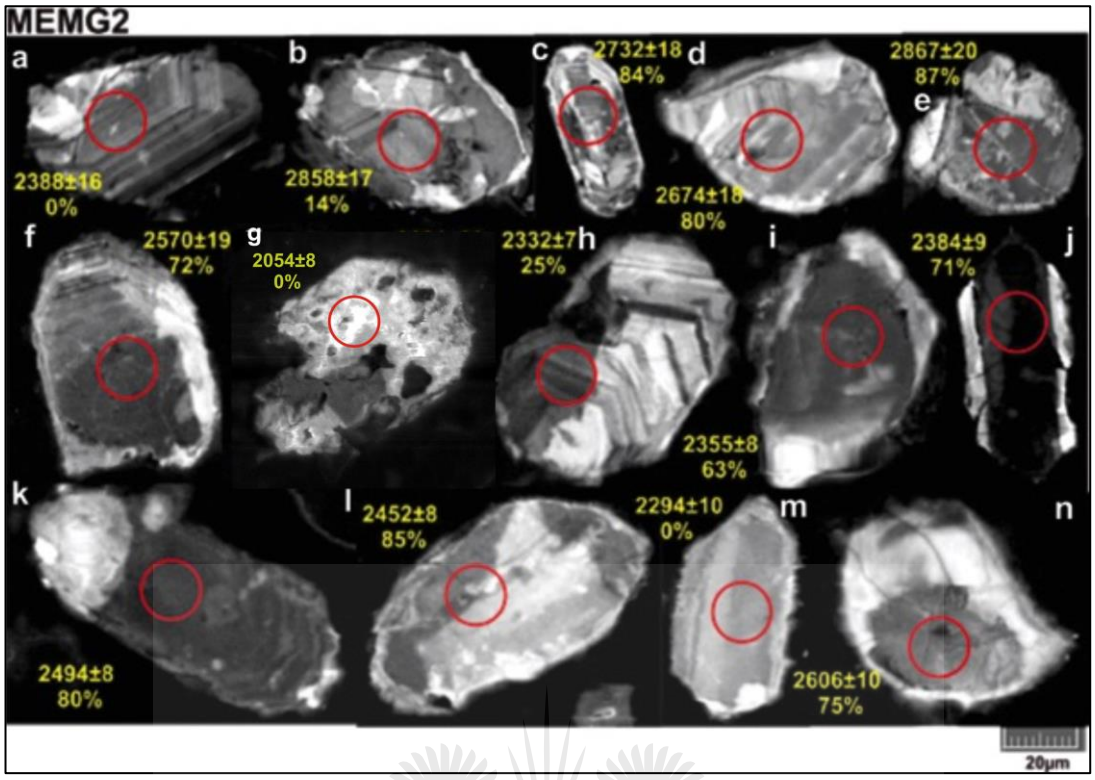

Figure 5.7: Cathodoluminescence images of selected zircon grains of MEMG2 with the circles representing U-Pb ablation spots and the numbers displayed are $^{207}Pb/^{206}Pb$ ages with 2 sigma errors and discordance percentage below the age.

5.2.3. U-Pb results

U-Pb results for eighty-six analysed detrital grains for sample MEMG2 are given in Appendix A, Table 6. Thirty-six grains have concordant ages and within the concordant analyses, five have Archean $^{207}Pb/^{206}Pb$ ages. There are two groups of concordant analyses, one group with $^{207}Pb/^{206}Pb$ ages ranging between 2896±10 and 2809±6 Ma, and another group shows $^{207}Pb/^{206}Pb$ ages between 2492±9 and 2211±7 Ma, with a single CPb-corrected (0.25%) zircon at 2054±8 Ma. Discordant zircon analyses show a similar trend of Pb loss as sample MEMG1 (Figure 5.8). Figure 5.9 a, b show that there is a positive correlation between uranium content and discordance as well as between $^{206}Pb/^{204}Pb$ ratio and $^{207}Pb/^{206}Pb$ ages.

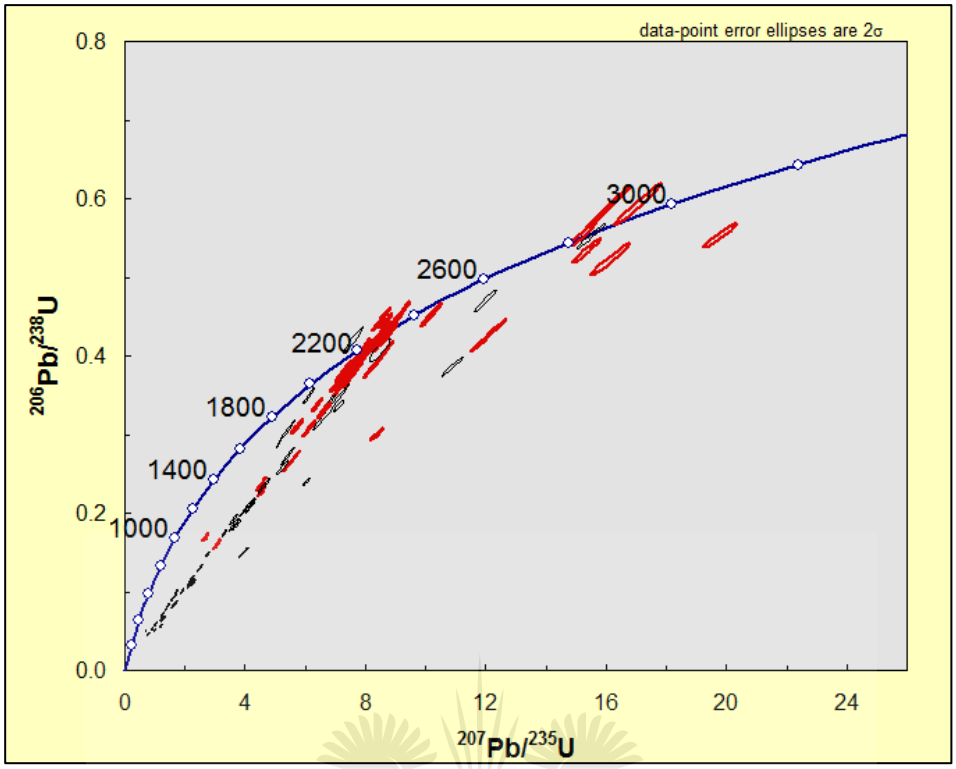

Figure 5.8: Wetherill concordia diagram for sample MEMG2, distinguishing between CPb-corrected analyses (black symbols), and analyses for which CPb was below detection limits (red symbols).

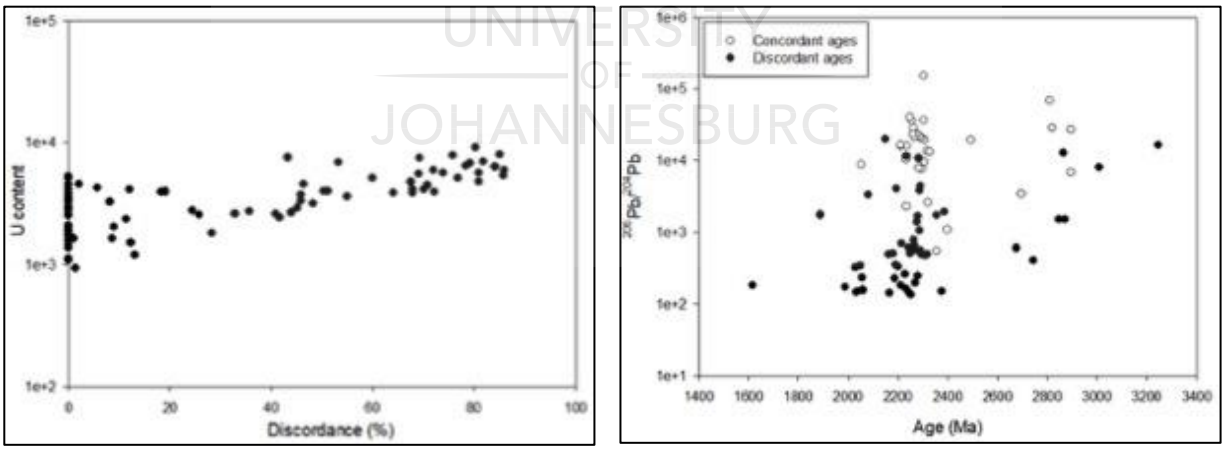

Figure 5.9: (a) Uranium content versus discordance for MEMG2 (b) $^{206}Pb/^{204}Pb$ ratio versus $^{207}Pb/^{206}Pb$ age.

5.3. Sample MEMG3

Sample MEMG3 is a coarse-grained metasandstone that was taken at 0.5 meters from the contact with the Marginal Zone in the eastern limb of the Bushveld Complex (Figure 5.1).

5.3.1. Petrographic characteristics

This metasandstone mainly consists of coarse-grained recrystallized quartz and microcline. Biotite and muscovite occur as minor mineral phases interstitial to quartz and feldspar (Figure 5.10 a, b). Andalusite also occurs as inclusions within quartz grains (Figure 5.10. c, d). Zircon occurs as an accessory phase within quartz.

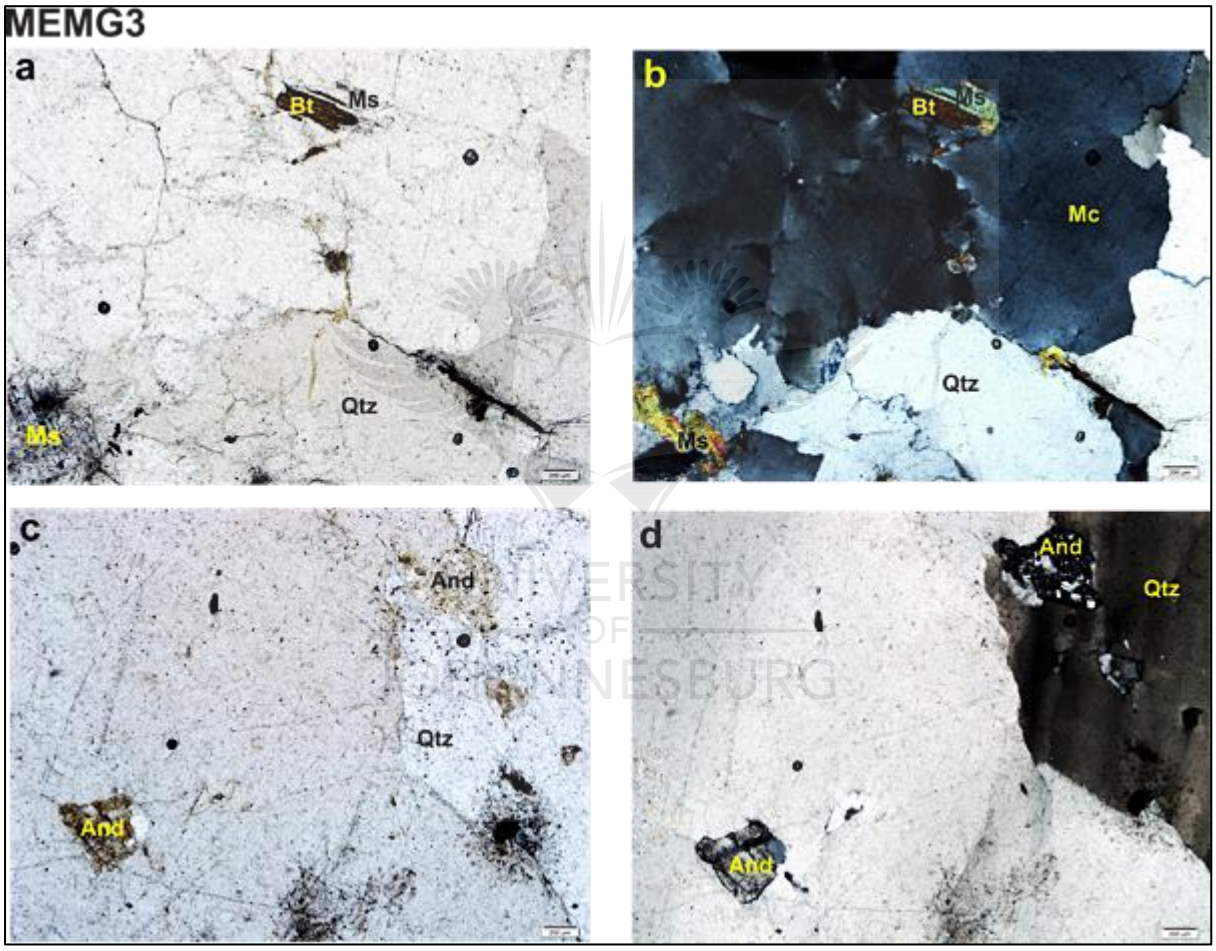

Figure 5.10: (a. b) Quartz and microcline as main mineral phases with micas as minor interstitial phases (PPL and XPL, respectively) (c, d) occurrence of andalusite within quartz grains. The scale bar is 200 µm (PPL and XPL, respectively).

5.3.2. Zircon characteristics

Detrital zircons in MEMG3 are rounded to prismatic. Their length ranges from 100 to 30 µm. The dominant texture is oscillatory zoning, but some grains are characterized by complex patchy zoning (e.g. Figure 5.11 h, i, k). Mineral and fluid inclusions are also observed, and some grains contain fractures (Figure 5.11 a, b). Similar to the two previously discussed samples there are variations in cathodoluminescence intensities in these crystals, but CL bright domains dominate in this sample.

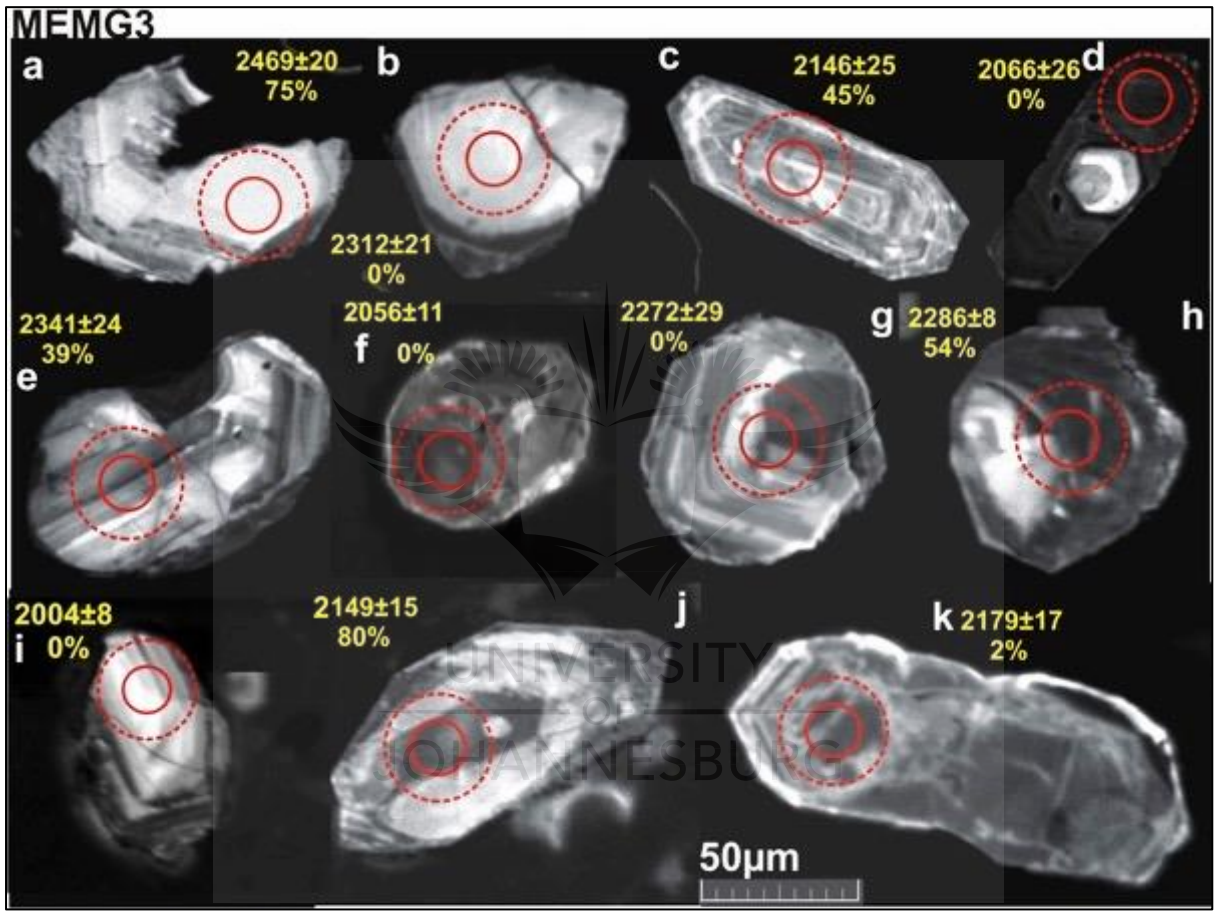

Figure 5.11: Cathodoluminescence images of selected zircon grains of MEMG3 with the solid circles representing U-Pb ablation site and dashed circles representing Lu-Hf ablation sites. The numbers displayed are $^{207}Pb/^{206}Pb$ ages with 2 sigma errors and discordance percentage below the age.

5.3.3. U-Pb results

U-Pb results for sixty-nine analysed zircon grains for sample MEMG3 are given in Appendix A, Table 7. The older zircons have Archean $^{207}Pb/^{206}Pb$ ages between 3047±13 and 2742±13 Ma, and younger zircons have Proterozoic $^{207}Pb/^{206}Pb$ ages between 2375±7 and 2004±8 Ma. Twenty-seven zircon grains are concordant, and within the concordant population there are two grains that are concordant around the Bushveld age and they have $^{207}Pb/^{206}Pb$ ages of 2056±11 (MEMG3-59; Figure 5.11f) and 2066±24 Ma (MEMG3-5; Figure 5.11 d); neither of them needed correction for common Pb. MEMG3-59 and MEMG3-5 have similar characteristics to older and younger zircon grains, for example, they have uranium contents of 1545 and 4261 ppm, and $^{206}Pb/^{204}Pb$ ratios of 1563 and 14572, respectively. The discordant grains lie on a partial Pb loss line towards ca. 450 Ma (Figure 5.12). After plotting U content and discordance (Figure 5.13 a) and $^{207}Pb/^{206}Pb$ ages versus $^{206}Pb/^{204}Pb$ ratios (Figure 5.13 b), the results show no real correlation between uranium and discordance, but a slight correlation is observed between $^{206}Pb/^{204}Pb$ ratio and $^{207}Pb/^{206}Pb$ ages.

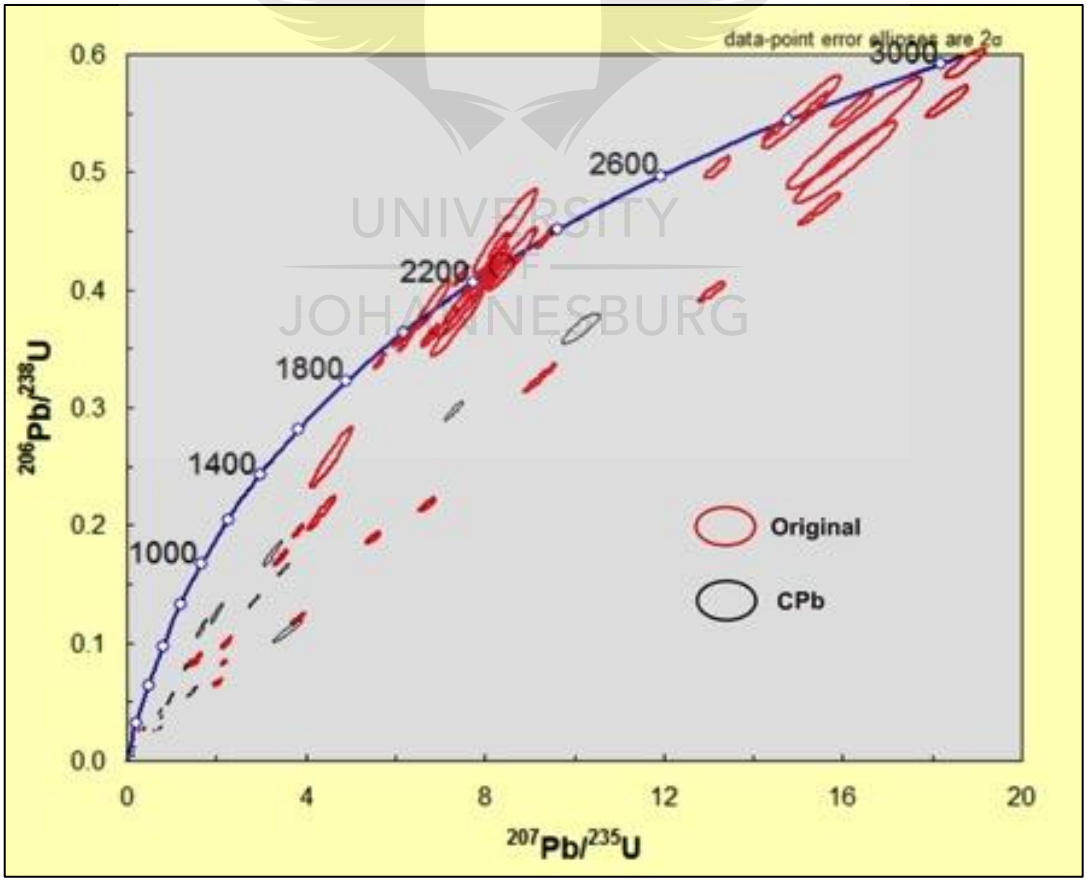

Figure 5.12: Wetherill concordia diagram for sample MEMG3.

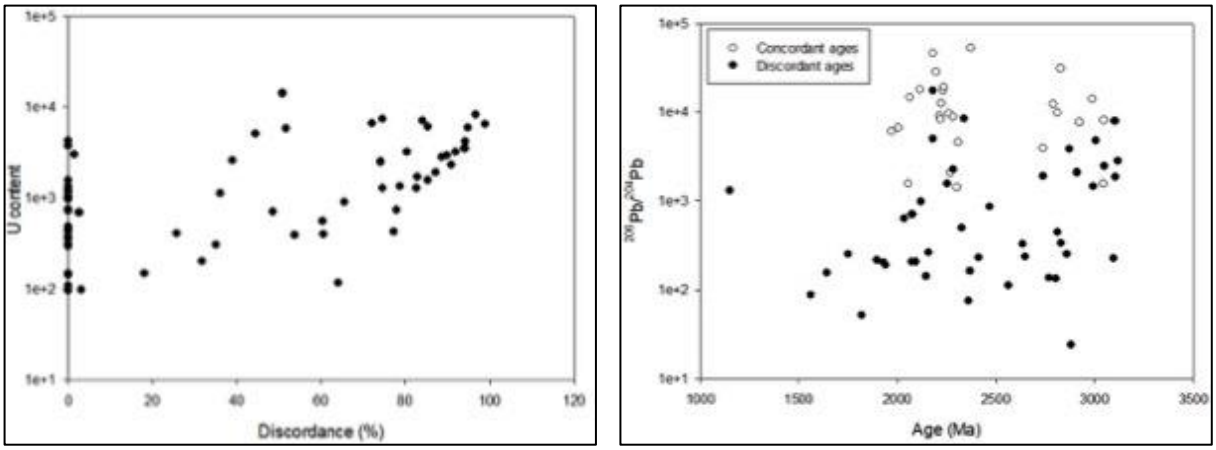

Figure 5.13: There is no correlation observed between variables in (a) Uranium content versus discordance and (b) $^{207}Pb/^{206}Pb$ age versus $^{206}Pb/^{204}Pb$ ratio.

5.3.4. Lu-Hf results

Lu-Hf results for MEMG3 are given in Appendix 2, Table 3. The initial Hf ratio against age diagram shows that zircon grains with Archean ages have lower $^{176}Hf/^{177}Hf$ ratios when compared with zircon grains with younger ages (Figure 5.14). Discordant grains and the ones that have been corrected for common Pb show a slight horizontal array of points. Epsilon Hf values at the zircons' $^{207}Pb/^{206}Pb$ age range from -21.72 to 7.3. MEMG3-59 and MEMG3-5 have initial $^{176}Hf/^{177}Hf$ values of 0.2814 and 0.2812 respectively and they seem to overlap with values for grains with older $^{207}Pb/^{206}Pb$ ages.

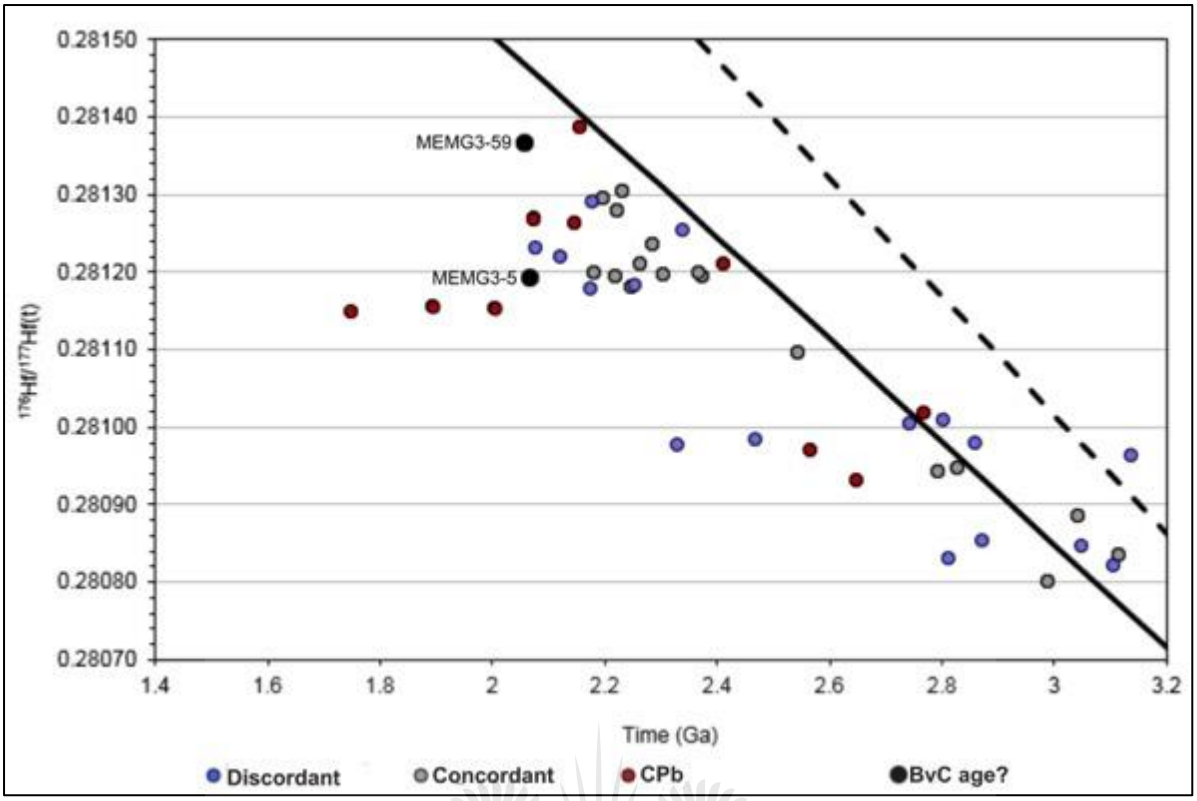

Figure 5.14: Initial Hf isotope ratios vs age diagram for sample MEMG3, with the concordant CPb-free grains that give ages around 2056 Ma indicated.

5.4. Sample MEMG 4

Sample MEMG4 is a medium-grained metasandstone collected 230 meters from the contact with the Marginal Zone in the eastern limb of the Bushveld Complex (Figure 5.1).

5.4.1. Petrographic characteristics

This is an inequigranular rock with large grains of plagioclase and recrystallized quartz set within a medium-grained matrix. Microcline and biotite occur as interstitial phases between quartz and plagioclase (Figure 5.15 a, b). The minor mineral phases in this metasandstone consist of low-pressure metamorphic minerals which include andalusite and low relief pseudomorphs, probably after cordierite (Figure 5.15 c, d). Zircon occurs as an accessory phase within quartz.

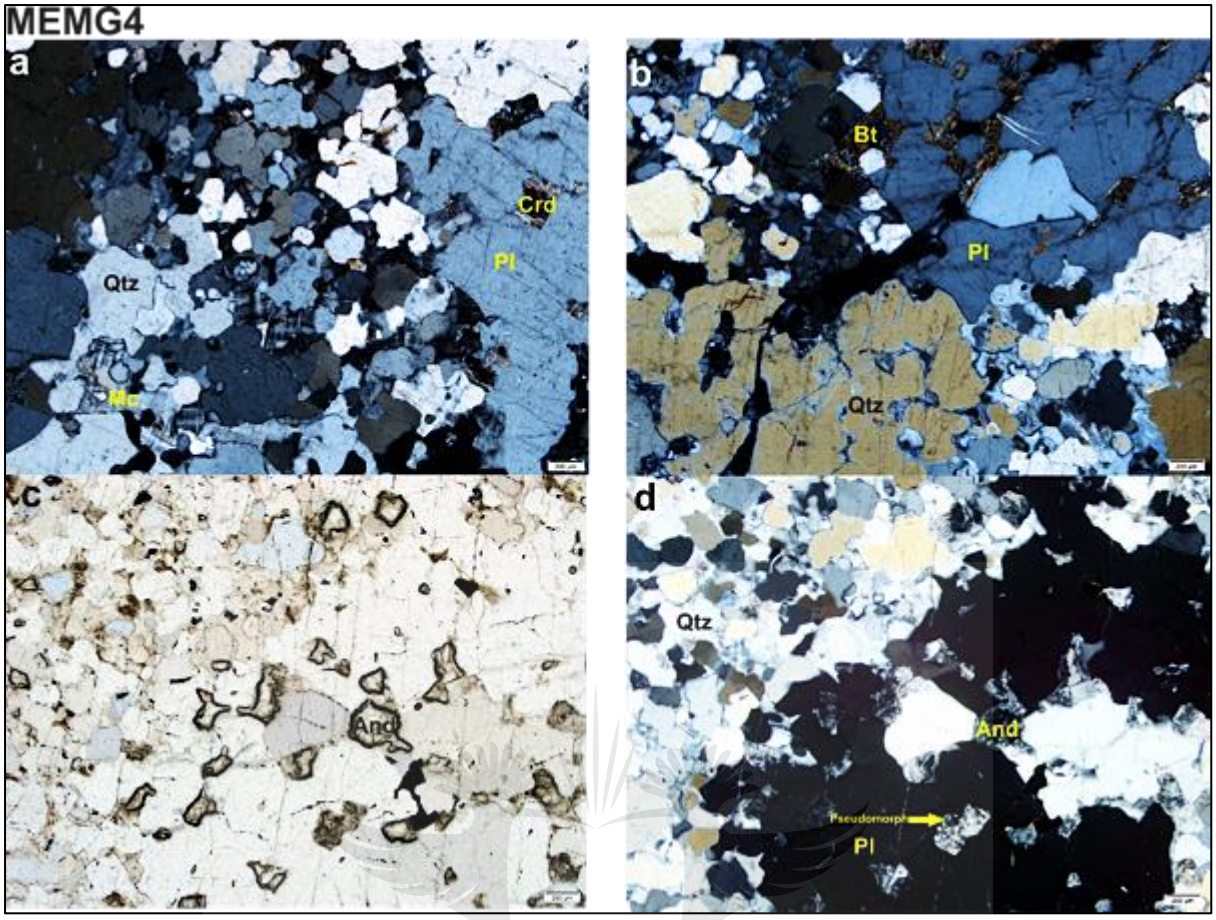

Figure 5.15: (a) Interstitial occurrence of microcline and occurrence of cordierite (XPL) (b) interstitial occurrence of biotite (XPL) (c) occurrence of andalusite (PPL) (d) occurrence of andalusite (XPL). The scale bar is 200µm.

5.4.2. Zircon characteristics

Zircon grains in MEMG4 are rounded to sub-rounded. They range in length from 300 to 20 µm. Textures include oscillatory zoning (e.g. Figure 5.16 b, i, k, l), patchy complex zoning (e.g. Figure 5.16 a, d, j), whereas some grains are unzoned (e.g. Figure 5.16 f). Most grains are characterised by overgrowths (e.g. Figure 5.16 c, d, h, i), and rims are most often cracked and have increased cathodoluminescence brightness. Inclusions are also observed (e.g. Figure 5.16 a, b, c, j, k).

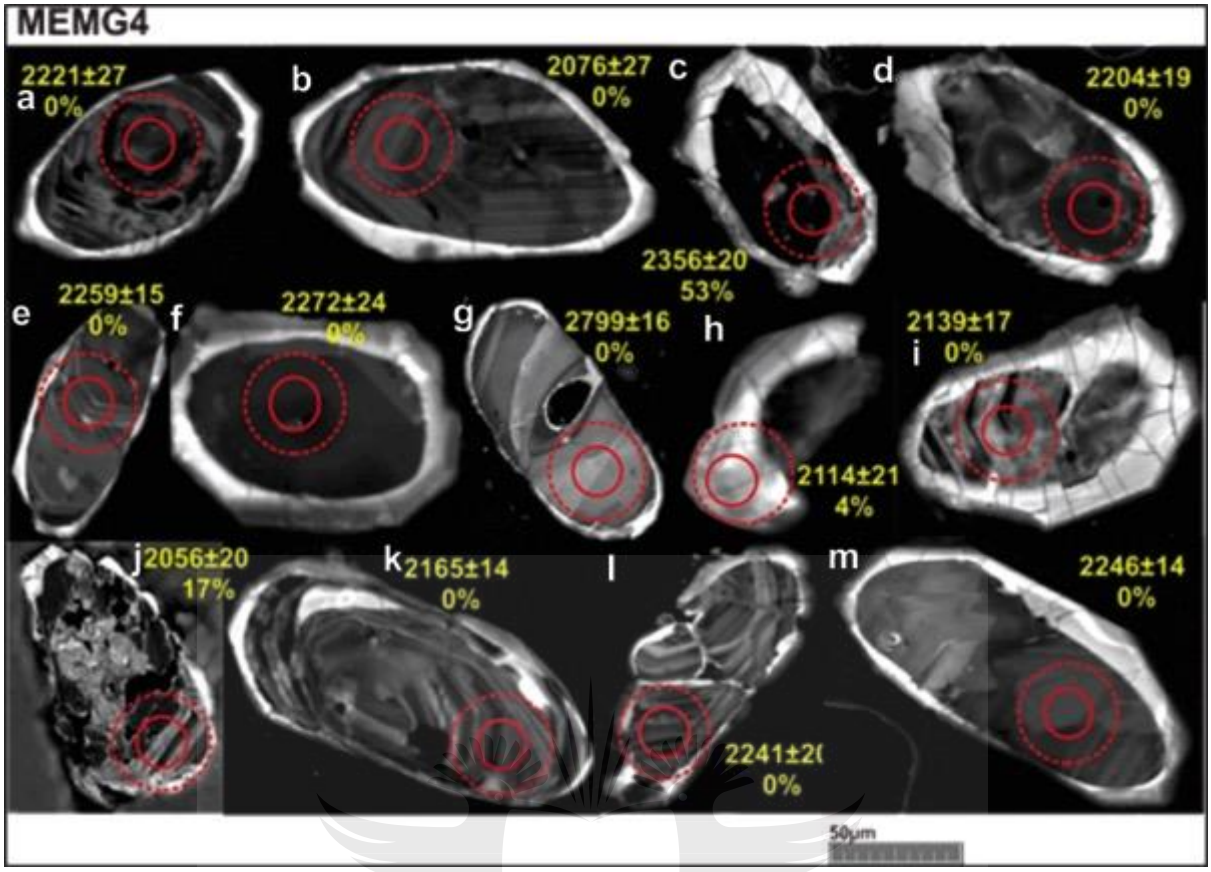

Figure 5.16: Cathodoluminescence images of selected zircon grains of MEMG4 with the solid and dashed circles representing U-Pb and Lu-Hf ablation sites, respectively. The numbers displayed are $^{207}Pb/^{206}Pb$ ages with 2 sigma errors and discordance percentage below the age.

5.4.3. U-Pb results

U-Pb results for ninety-eight analysed detrital grains for sample MEMG4 are given in Appendix A, Table 8. The concordia diagram for these analyses is shown in Figure 5.17. About 75% of these zircon grains are concordant within two sigma uncertainty. Among the concordant analyses, there is one grain with an Archean $^{207}Pb/^{206}Pb$ age of 2799±16 Ma, and the other analyses show $^{207}Pb/^{206}Pb$ ages ranging between 2379±12 and 2034±64 Ma. Within the concordant analyses there are two grains that are concordant at $^{207}Pb/^{206}Pb$ ages 2061±30 (MEMG4-7) and 2076±27 Ma (MEMG4-3), and therefore are the same age as the Bushveld Complex, taking the uncertainties into account. They did not need common Pb corrections; their uranium contents are 8172 and 3913 ppm, respectively, and their $^{206}Pb/^{204}Pb$ ratios are 2268 and 4237. The remaining 15% of MEMG4 zircon analyses are discordant and about 90% of these discordant grains have been corrected for common Pb. The youngest discordant CPb-corrected grain has a $^{207}Pb/^{206}Pb$ age of 1644±20 Ma. The diagrams of uranium content

versus discordance and $^{206}Pb/^{204}Pb$ versus $^{207}Pb/^{206}Pb$ age show a scattered correlation between variables (Figure 5.18 a, b).

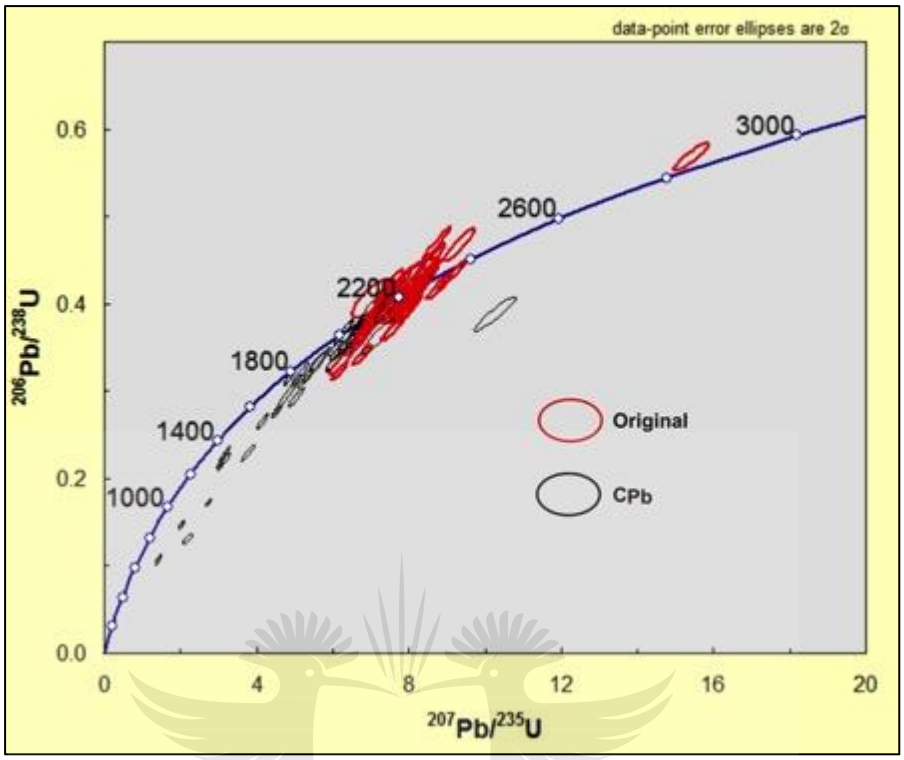

Figure 5.17 Wetherill concordia diagram for sample MEMG4. Zircon analyses show partial Pb loss towards the origin of the diagram.

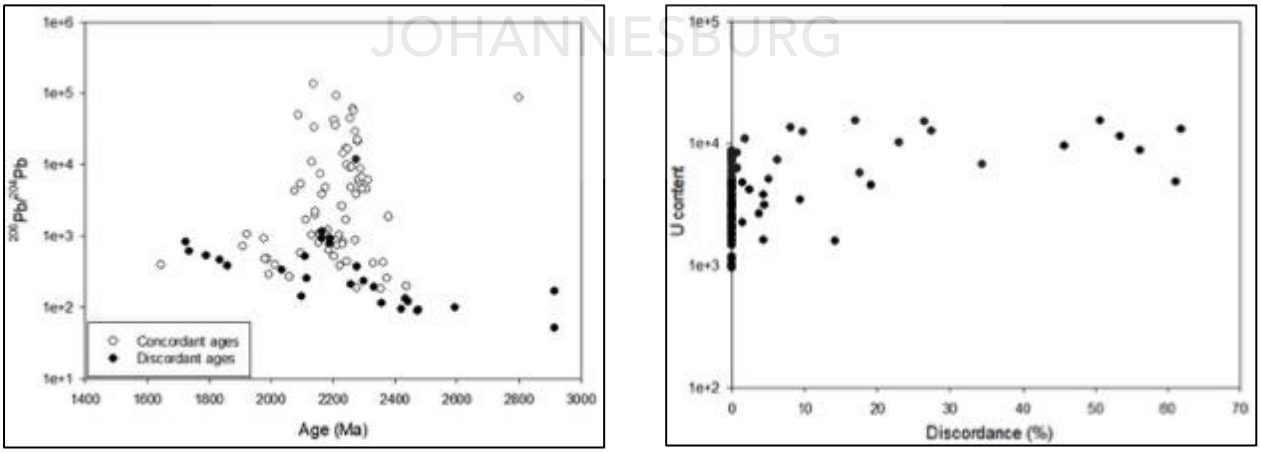

Figure 5.18: Diagrams showing a scattered correlation between variables (a) Uranium content versus discordance (b) $^{206}Pb/^{204}Pb$ versus $^{207}Pb/^{206}Pb$ ages.

5.4.4. Lu-Hf results

Lu-Hf results for sample MEMG4 are given in Appendix B, Table 4. The initial Hf isotope ratio against age diagram (Figure 5.19) shows an overall sub-horizontal array, albeit with a wide dispersion in the initial ratios, as can be expected from a detrital population. The two grains concordant at 2061±30 and 2076±27 Ma have initial Hf isotope values of 0.281323 and 0.281286 respectively. The two analyses that lie above the depleted mantle line are both discordant and have very low $^{206}Pb/^{204}Pb$ ratios. One zircon grain whose $^{207}Pb/^{206}Pb$ age is concordant around 2.8 Ga age has a lower initial Hf isotope ratio. The two analyses that lie above the depleted mantle line may have suffered from the fact that the Hf ablation spot encompasses a bigger area than the U-Pb ablation spot; therefore, the Hf ablation may have incorporated some younger material.

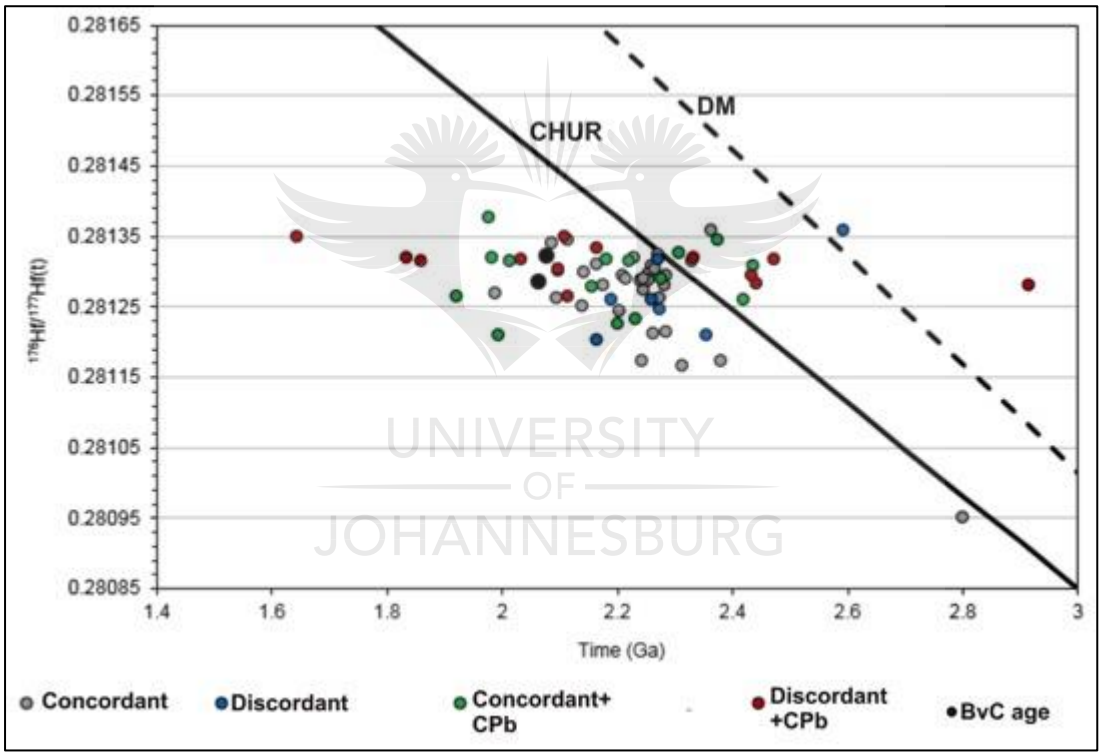

Figure 5.19 Initial Hf ratios vs age diagram for sample MEMG4 showing a sub-horizontal array of points.

5.4.5. Trace element chemistry results

Representative trace-element compositions for selected zircon grains are shown in Appendix C, Table 2. Zircons from this sample are characterized by mainly flat LREE patterns, although some grains have a positive slope. Most of analyses with high LREE concentrations are characterised by higher discordance percentages, however, there are concordant analyses with high LREE concentrations. Only one zircon (MEMG4-3) from the two that have $^{207}Pb/^{206}Pb$ Bushveld Complex ages was analysed for trace elements, and it shows a similar REE pattern as concordant zircon grains with older ages (Figure 5.20). A majority of analyses have positive Ce anomalies and negative Eu anomalies. Diagrams of cerium anomalies versus discordance and La/Sm ratios versus age (Figure 5.21 a, b) do not show any correlations between variables. Analyses that are concordant at younger ages also show a similar trend to the rest of the concordant analyses. A diagram of uranium content versus LREE-I (Figure 5.22) does not show any correlation between the variables, but the diagram of discodance versus LREE-I (Figure 5.23) show a bit of correlation because analyses that are more than 40% discordant are all plotting at LREE-I less than 10, however some of concordant analyses also plot at LREE-I less than 10.

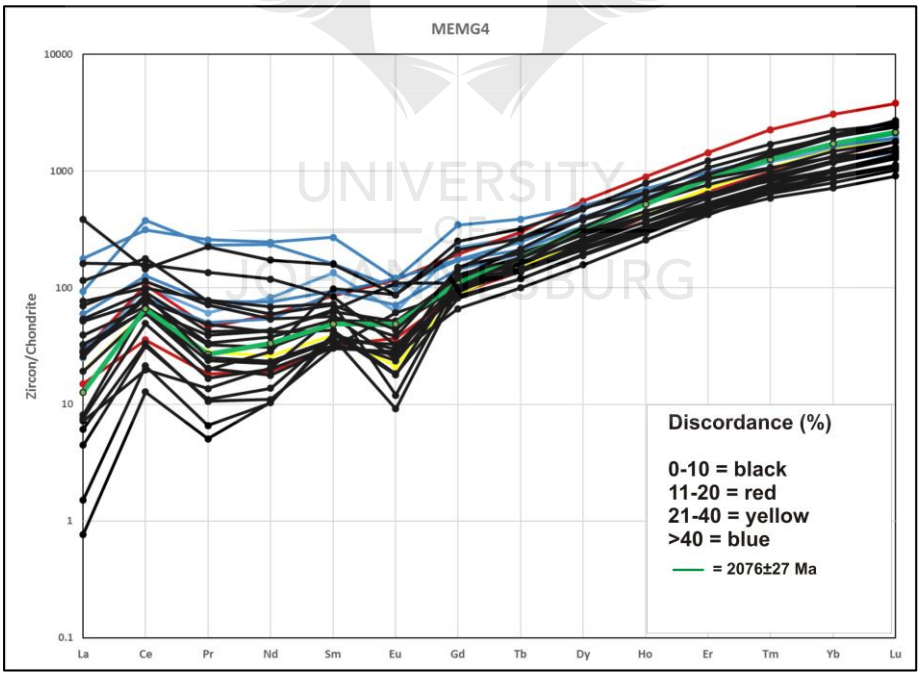

Figure 5.20: Chondrite-normalized REE patterns for zircons from Magaliesberg Formation, sample MEMG4 (normalising factors from Sun and McDonough, 1989).

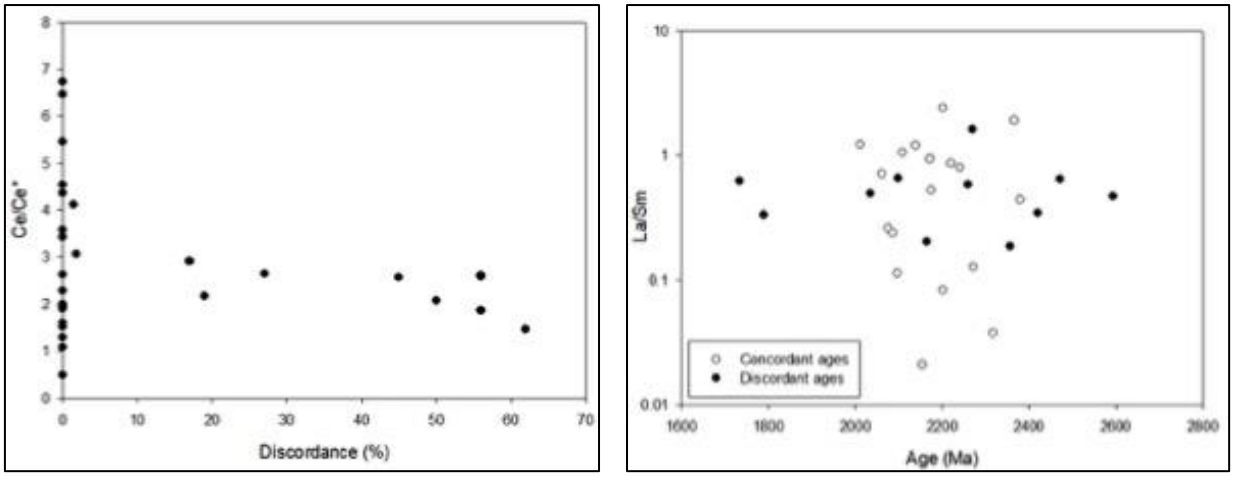

Figure 5.21: There is no correlation between variables in (a) Ce/Ce* vs discordance diagram (b) La/Sm ratio vs age diagram.

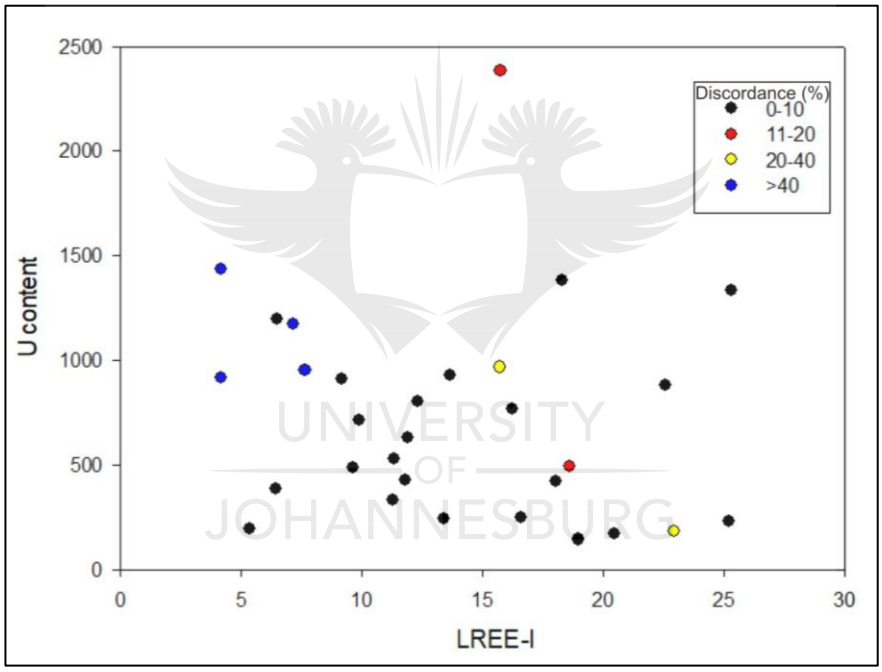

Figure 5.22: Diagram of U content versus LREE-I (after Bell et al., 2016).

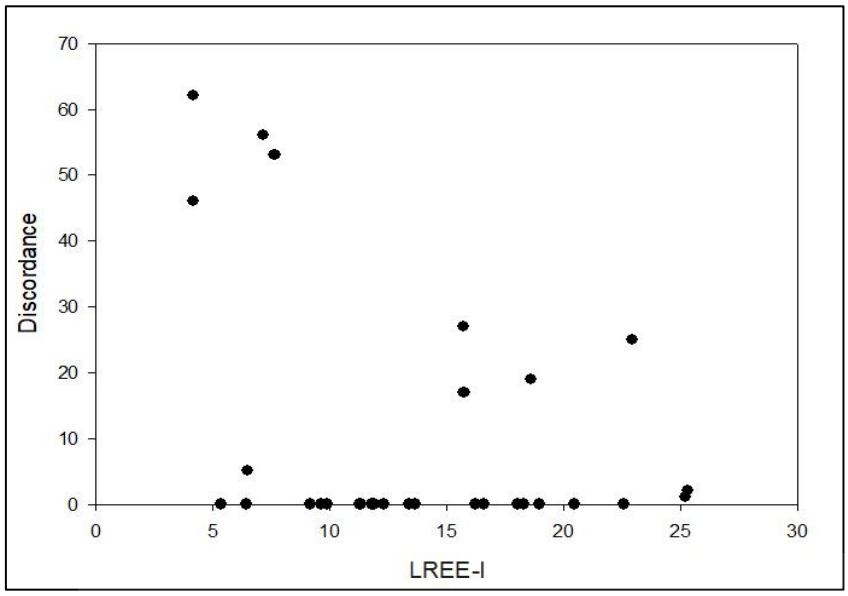

Figure 5.23: Diagram of discordance (%) versus LREE-I.

5.4.6. R coding results

An output from the R coding program created by M. Kristoffersen shows peaks of events for lower intercept age of about 450 Ma (Figure 5.24). This falls within the range of what is observed in the concordia diagram for MEMG4.

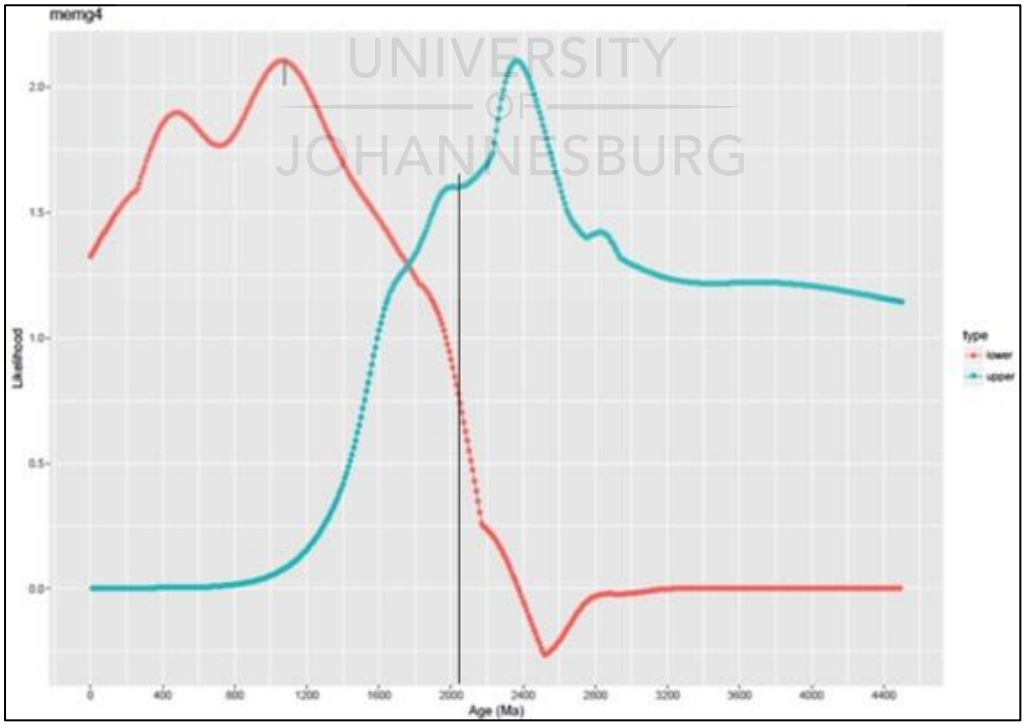

Figure 5.24: An output from R coding program showing peaks in ages similar to the illustrated in a concordia diagram.

5.5. Sample MEMG25

This quartzite is in contact aureole of Bushveld, south of the Goudini Complex. It forms part of Magaliesberg Formation (Figure 5.1).

5.5.1. Petrographic characteristics

This quartzite sample is medium-grained. Quartz dominates its mineralogy, with minor plagioclase occurring interstitial to quartz (Figure 5.25). Clinopyroxene and pseudomorphs after cordierite occur as minor mineral phases. Zircon and apatite occur as accessory phase within recrystallized quartz grains.

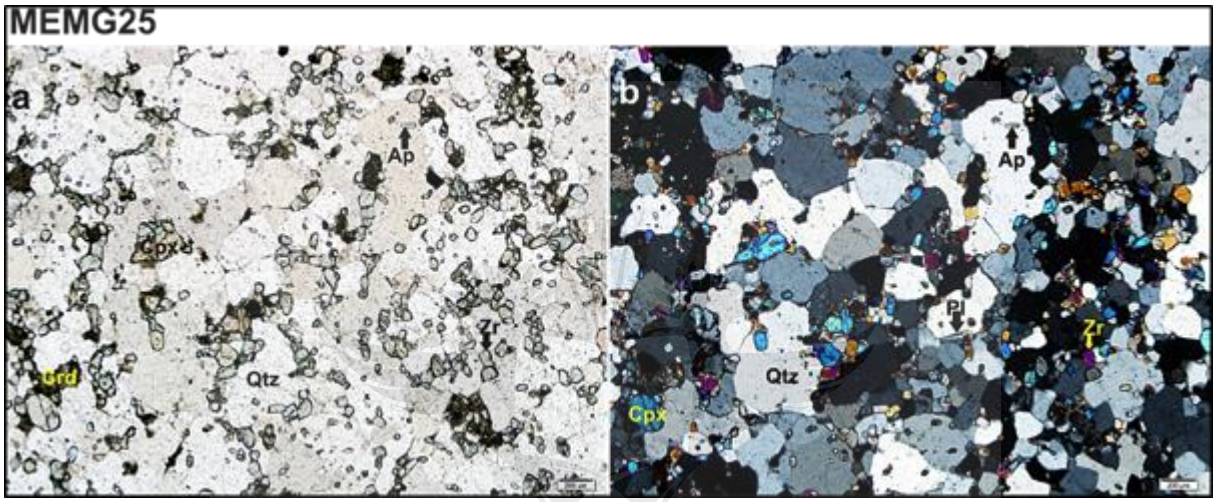

Figure 5.25: Quartzite sample with cpx and pseudomorphs after cordierite occurring as minor phases (a) PPL (b) XPL.

5.5.2. Zircon characteristics

The detrital zircons are euhedral, prismatic to sub-rounded (Figure 5.26). They range in length from 250 to 20 µm. They are characterized by a variety of textures, most commonly oscillatory zoning (e.g. Figure 5.26 b, g, h) and complex patchy textures (e.g. Figure 5.26 a, d, i).

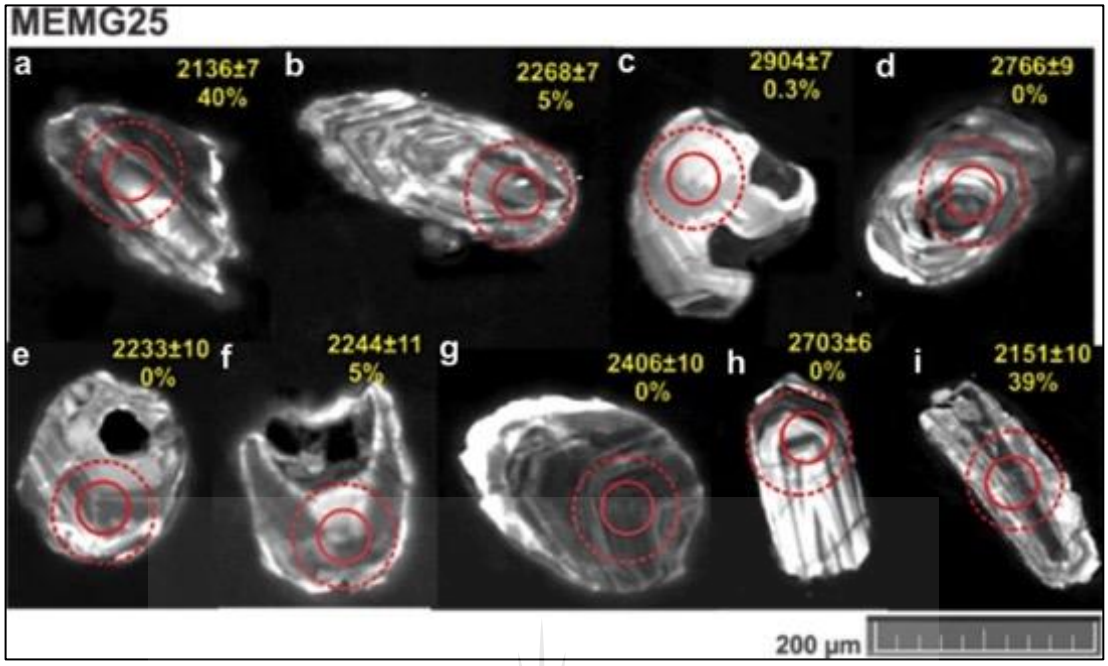

Figure 5.26: Cathodoluminescence images of selected zircon grains from MEMG25 with the solid and dashed circles representing U-Pb and Lu-Hf ablation sites respectively. The numbers displayed are $^{207}Pb/^{206}Pb$ ages with 2 sigma errors and discordance percentage below the age.

5.5.3. U-Pb results

U-Pb results for thirty-two analysed zircon grains for MEMG25 are given in Appendix A, Table 9. Most analyses are highly discordant (Figure 5.27). Only 28% of the analysed zircon grains are concordant within two sigma uncertainty and their $^{207}Pb/^{206}Pb$ ages range from 2561±6 to 2230±10 Ma. However, even these grains fall slightly below the concordia line. Most discordant grains also contained CPb. $^{207}Pb/^{206}Pb$ ages for the discordant grains vary from 1667±40 to 2625±12 Ma. Diagrams of uranium content versus discordance and $^{206}Pb/^{204}Pb$ ratio versus $^{207}Pb/^{206}Pb$ age (Figure 5.28) show a scattered correlation between variables.

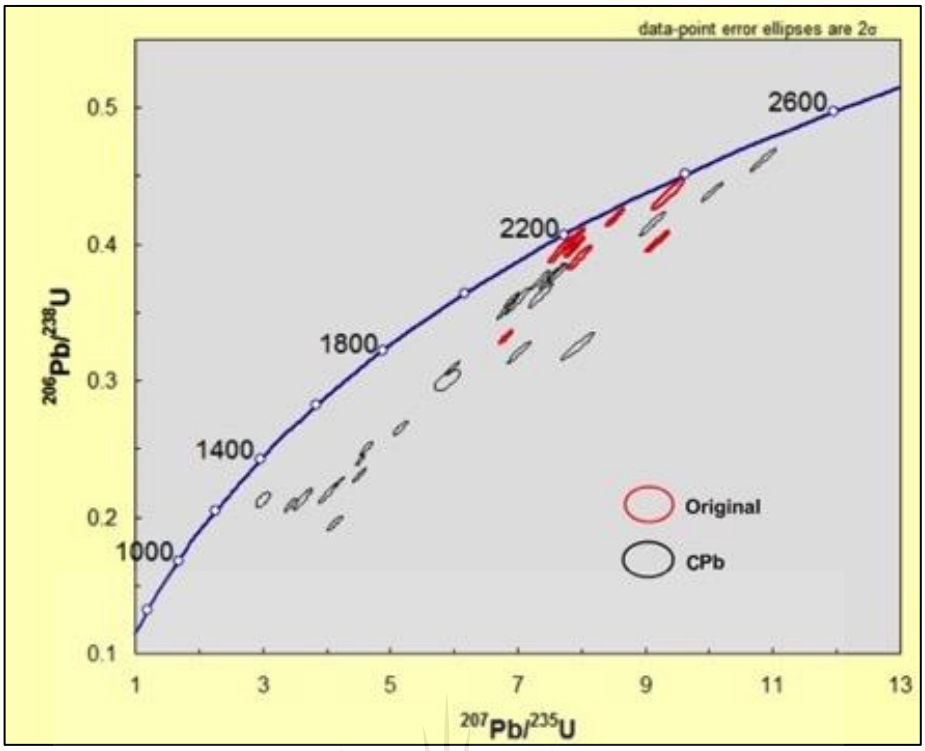

Figure 5.27: Wetherill concordia diagrams for sample MEMG25. Analyses are highly discordant.

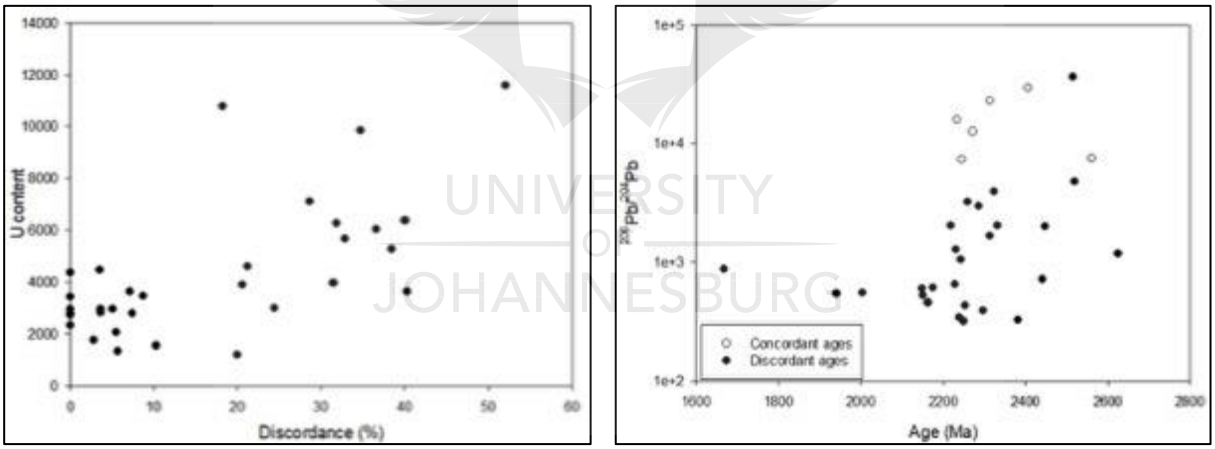

Figure 5.28: (a) Uranium content versus discordance (b) $^{206}Pb/^{204}Pb$ versus $^{207}Pb/^{206}Pb$ age. A scattered correlation is observed in both diagrams.

5.5.4. Lu-Hf results

Lu-Hf results for sample MEMG25 are given in Appendix B, Table 6. A scatter of points is observed (Figure 5.29). The concordant grains plot near the CHUR, whereas most discordant grains with CPb plot below the CHUR. Two grains with Archean ages have a lower $^{176}Hf/^{177}Hf$ ratio of 0.28096. There is also one grain which has a lower $^{176}Hf/^{177}Hf$ ratio of 0.28090 is discordant with CPb with a $^{207}Pb/^{206}Pb$ age of 2244±11, this grain has an epsilon Hf value of -16.1. The variation in epsilon Hf values at the zircons' $^{207}Pb/^{206}Pb$ age range between -17.8 and 5.4, apart from one highly discordant grain with a $^{207}Pb/^{206}Pb$ age of ca. 2.9 Ga, which yields an unrealistically high epsilon Hf value of 13.8.

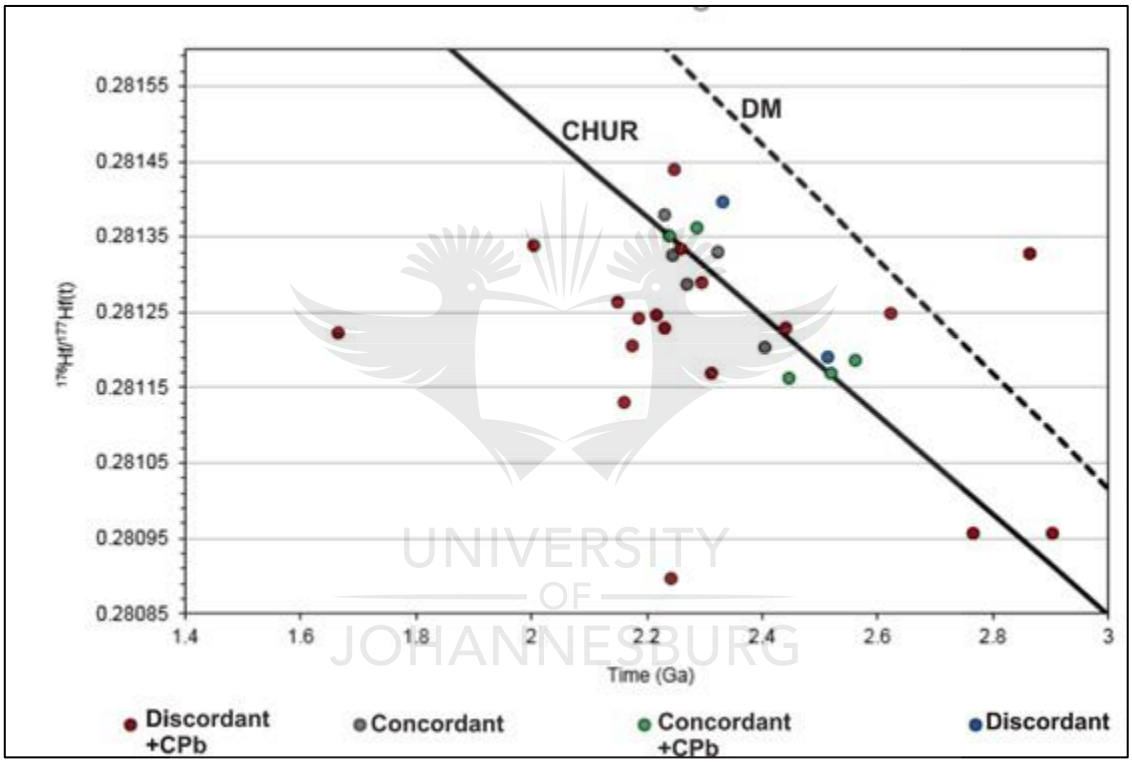

Figure 5.29: Initial Hf isotope ratios versus age diagram for sample MEMG25.

(Meta)sandstone from the Nooitgedacht Member of the Timeball Hill Formation

5.6. Sample MEMG5

Sample MEMG5 was collected northwest of Mokopane, ca. 1 km from the Rustenburg Layered Suite (Figure 5.1), a few kilometers south of where granitoid samples MEMG7 and 8 were taken.

5.6.1. Petrographic characteristics

This sandstone is medium-grained. It comprises quartz (with embayed outline) as a dominant mineral phase with subordinate microcline and biotite occurring as interstitial phases (Figure 5.30 a. b). Andalusite is also observed as a minor mineral phase within quartz grains (Figure 5.30c, d). Zircon occurs as an accessory phase within quartz and felspar.

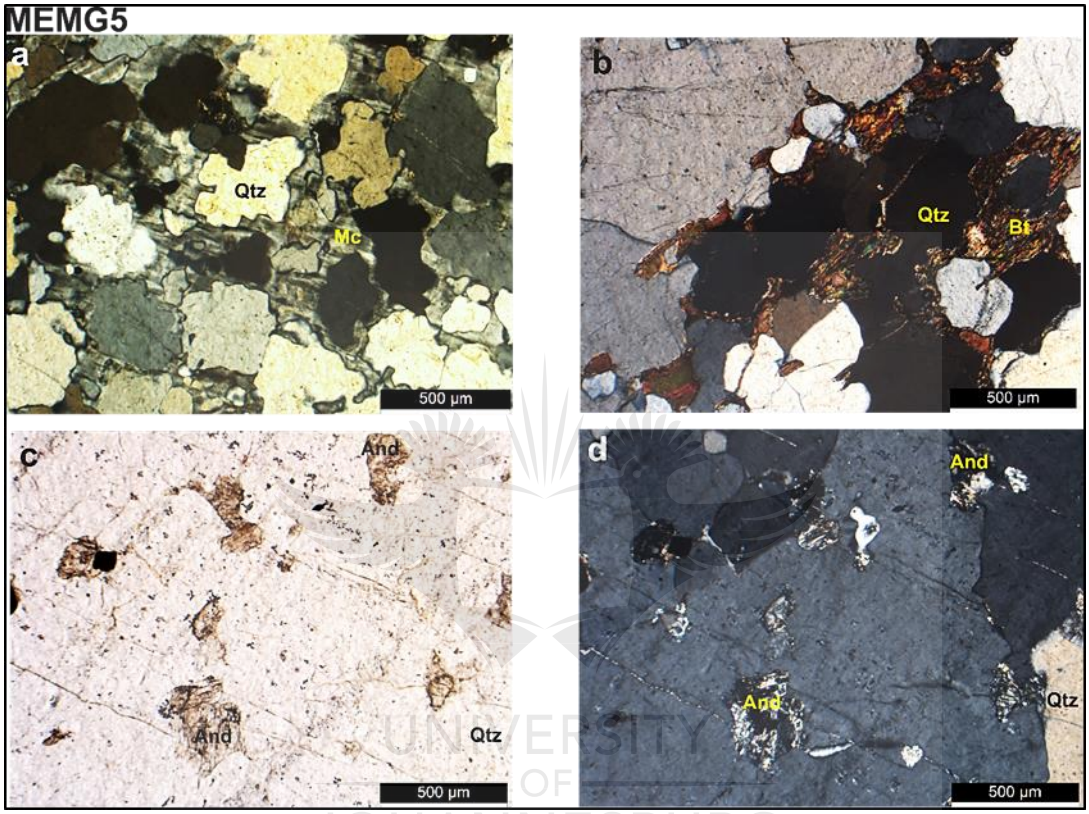

Figure 5.30: (a) Interstitial occurrence of microcline (XPL) (b) interstitial occurrence of biotite (XPL) (c) occurrence of andalusite (PPL) (d) occurrence of andalusite (XPL).

5.6.2. Zircon characteristics

These detrital zircons are commonly sub-rounded to elongate in shape. They range in length from 200 to 50 µm. The dominant texture is oscillatory zoning typical for magmatic zircons. The oscillatory zoning is superimposed by CL bright areas (e.g. Figure 5.31 f, g, h, i, m). Most of the grains contain fluid inclusions and fractures cutting across the inclusions.

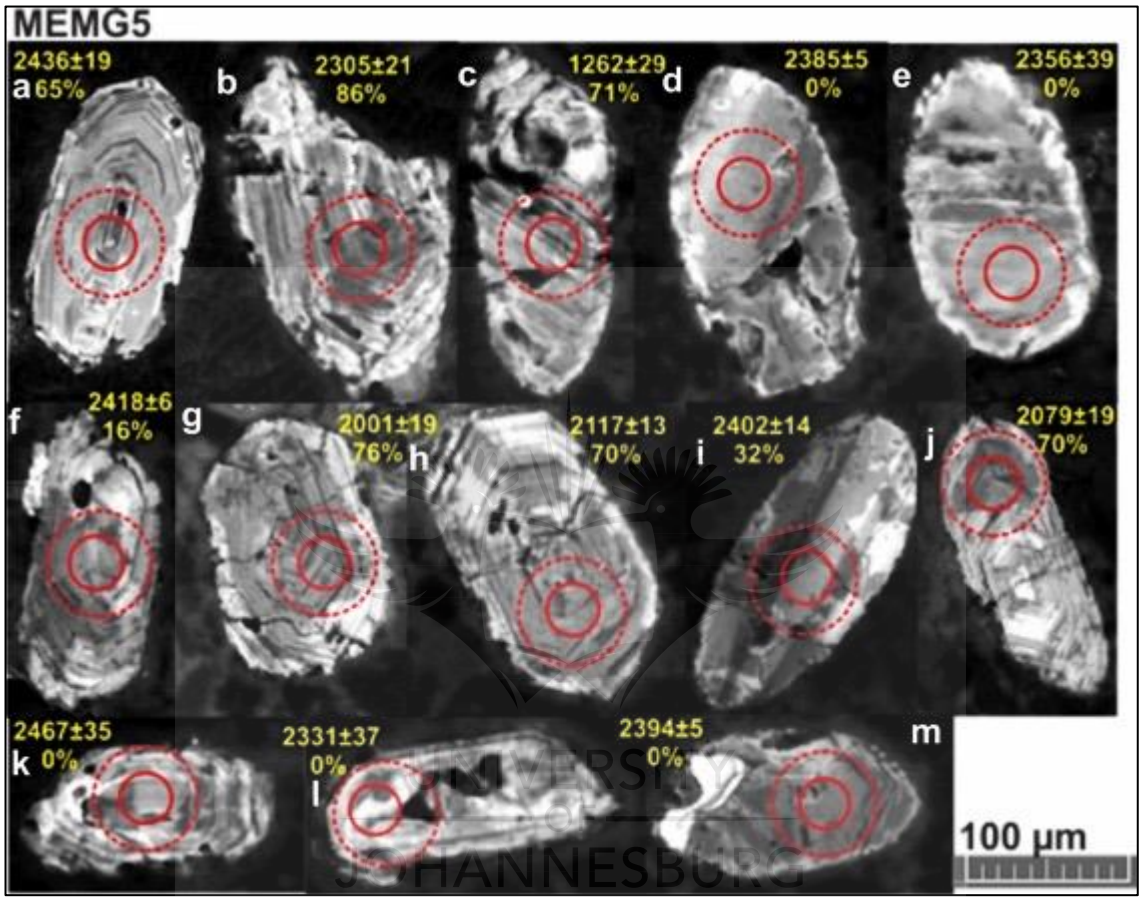

Figure 5.31: Cathodoluminescence images of selected zircon grains from MEMG5 with the solid and dashed circles representing U-Pb and Lu-Hf ablation sites, respectively. The numbers displayed are $^{207}Pb/^{206}Pb$ ages with 2 sigma errors and discordance percentage below the age.

5.6.3. U-Pb results

U-Pb results for one hundred and thirty analysed zircon grains for sample MEMG5 are given in Appendix A, Table 10. A concordia diagram for the analysed zircons is shown in Figure 5.32. Of the concordant zircon analyses, three have Archean $^{207}Pb/^{206}Pb$ ages between 2901±4 and 2754±6 Ma, and ca. 70% of the analyses have $^{207}Pb/^{206}Pb$ ages between 2467±35 and 2154±4 Ma. About 67% zircon grains are discordant and most of these discordant analyses have been corrected for common Pb. There is also one near-concordant (3.2%) zircon that plots at ca. 1855±31 Ma, with the highest uranium content of all grains, and a

$^{206}Pb/^{204}Pb$ ratio of 27068. Diagrams of uranium content versus discordance and $^{206}Pb/^{204}Pb$ versus $^{207}Pb/^{206}Pb$ age show a scattered correlation between the variables (Figure 5.33).

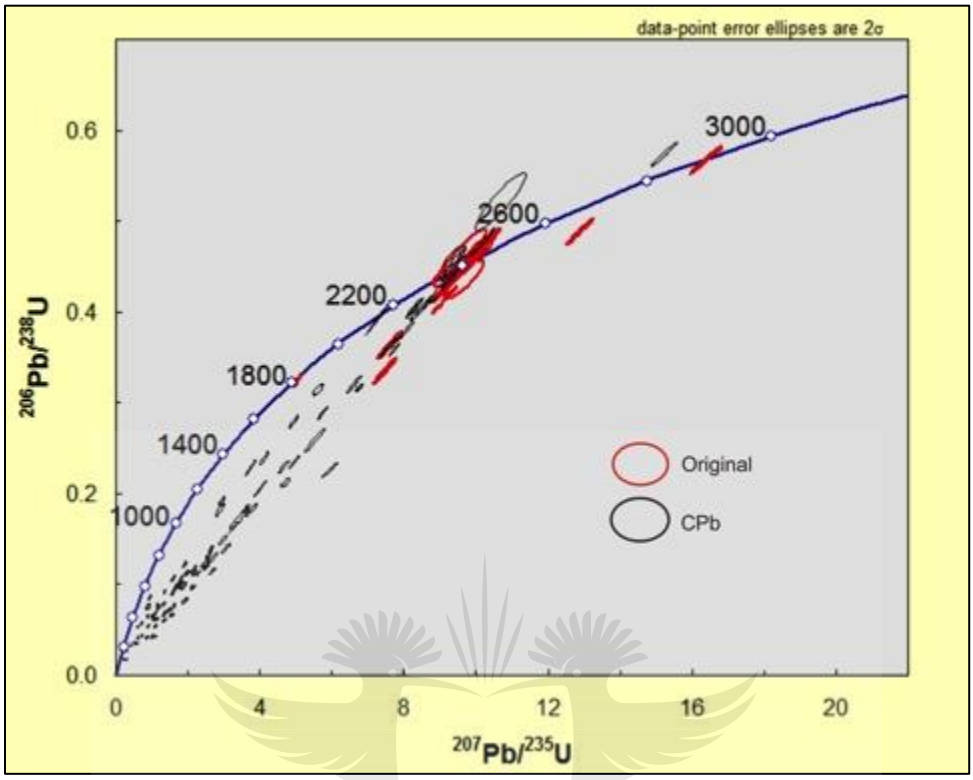

Figure 5.32: Wetherill concordia diagram for sample MEMG5.

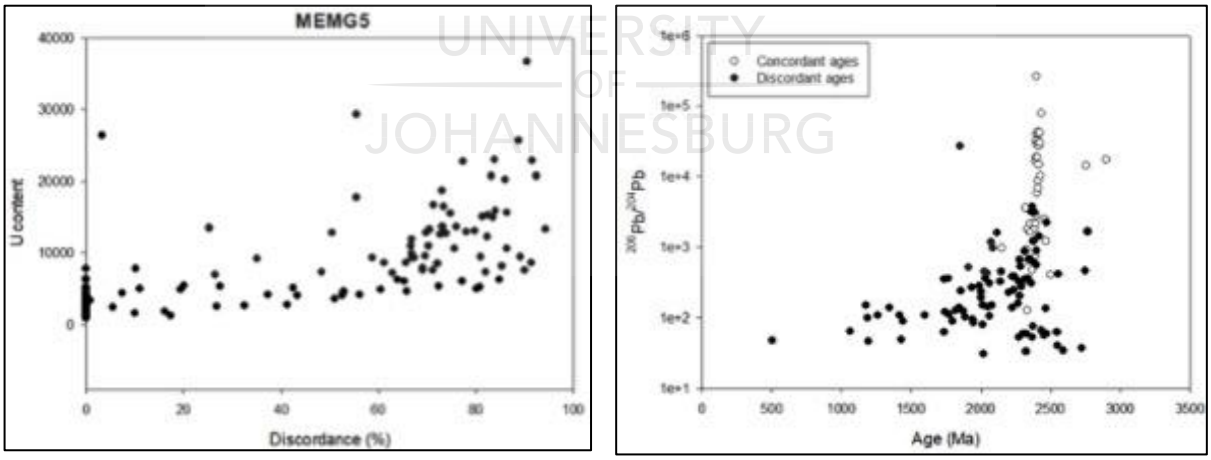

Figure 5.33: (a) Uranium content versus discordance (b) $^{206}Pb/^{204}Pb$ ratio versus $^{207}Pb/^{206}Pb$ age**.**

5.6.4. Lu-Hf results

Lu-Hf results for sample MEMG5 are given in Appendix B, Table 5. All concordant analyses plot near the CHUR; discordant analyses that have also been corrected for CPb form a sub-horizontal array of points towards younger ages (Figure 5.34). There are three grains with Archean ages, of which two have sub-chondritic $^{167}Hf/^{177}Hf$ isotopic ratios and one plots near the DM. There is a big variation in epsilon Hf values at the zircons' $^{207}Pb/^{206}Pb$ age for this sample, they range from 5.8 to -26.6; for the concordant, CPb-free analyses, the range is 0.8 to 4.3.

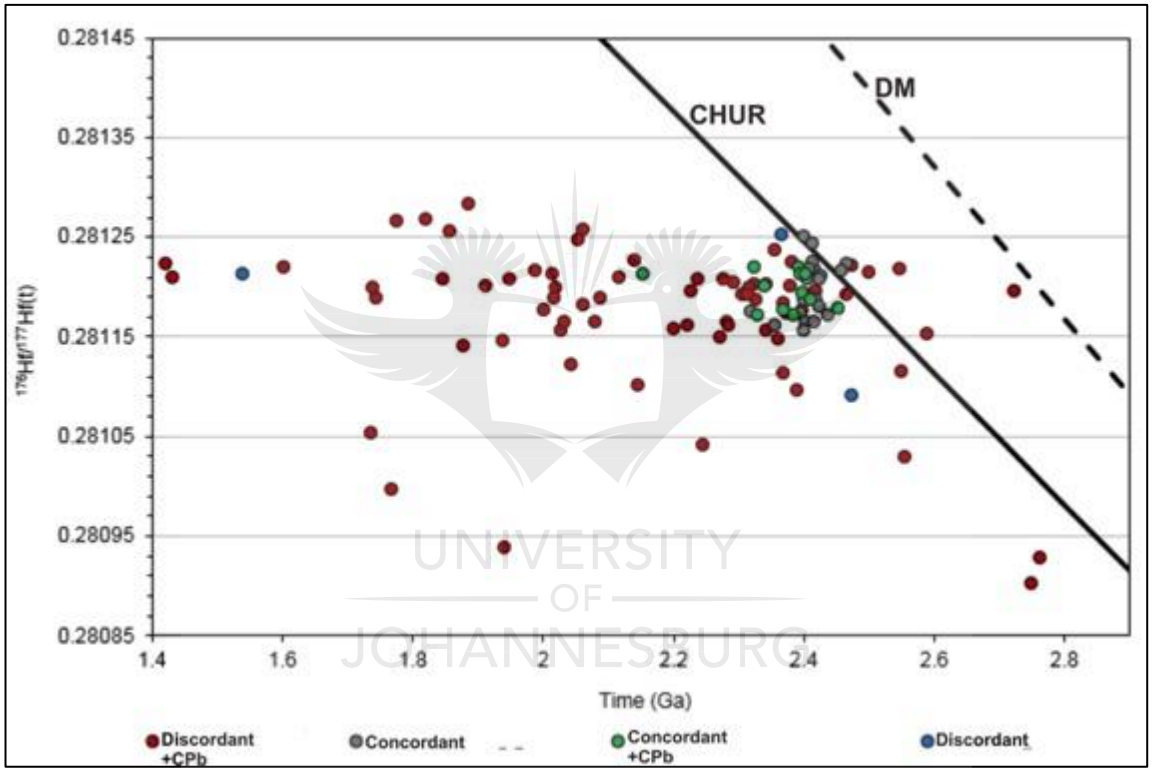

Figure 5.34: Initial Hf ratios versus age diagram for sample MEMG5 showing a near horizontal array of points, especially for grains corrected for common Pb.

Results: influence of Goudini Complex

5.7. Sample GOUD2

This sample is a loose block of silicate material potentially affected by the thermal and chemical effects of the carbonatitic Goudini complex, which is hosted by the Magaliesberg Formation – also the host to the Bushveld Complex, of which the nearest surface outcrop is Vlakfontein Subsuite and Kolobeng Norite of the Rustburg Layered Suite (Figure 5.1).

5.7.1. Petrographic characteristics

This material is characterized by a coarse-grained texture with quartz and alkali feldspar as dominant mineral phases. Like most samples from Magaliesberg formation investigated in this study, this sample contains cordierite as a minor mineral phase and it occurs interstitial to quartz and feldspar (Figure 5.35 a, b). Pseudomorphs probably after cordierite are also observed forming part of minor mineral phases (Figure 5.35 c). Zircon occurs within quartz grains as an accessory phase.

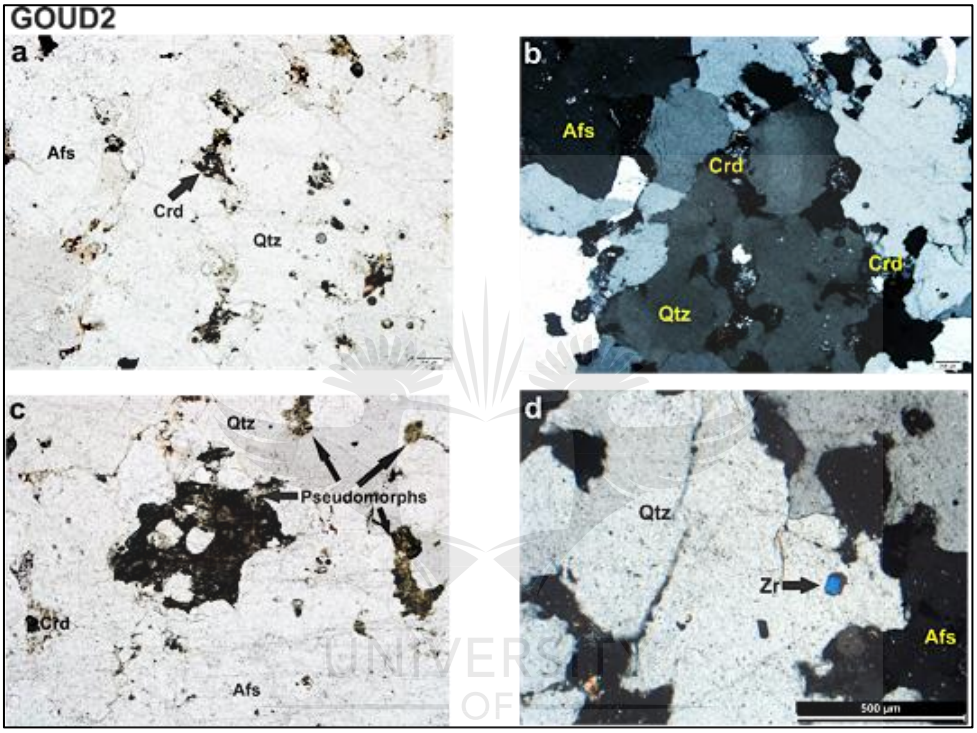

Figure 5.35: (a, b) Cordierite occurring interstitial to quartz and feldspar (PPL and XPL, respectively) (c) Pseudomorph material also forming part of minor mineral phase (PPL) (d) zircon grain occurring as an inclusion in quartz (XPL).

5.7.2. Zircon characteristics

Zircons in sample GOUD2 are elongated prismatic. They range in length from 300 to 50 µm. The two dominant textures are oscillatory zoning (Figure 5.36 e, f, g, j) and complex zoning patterns (Figure 5.36 b, c, d, h). These grains are also characterized by mineral and melt inclusions.

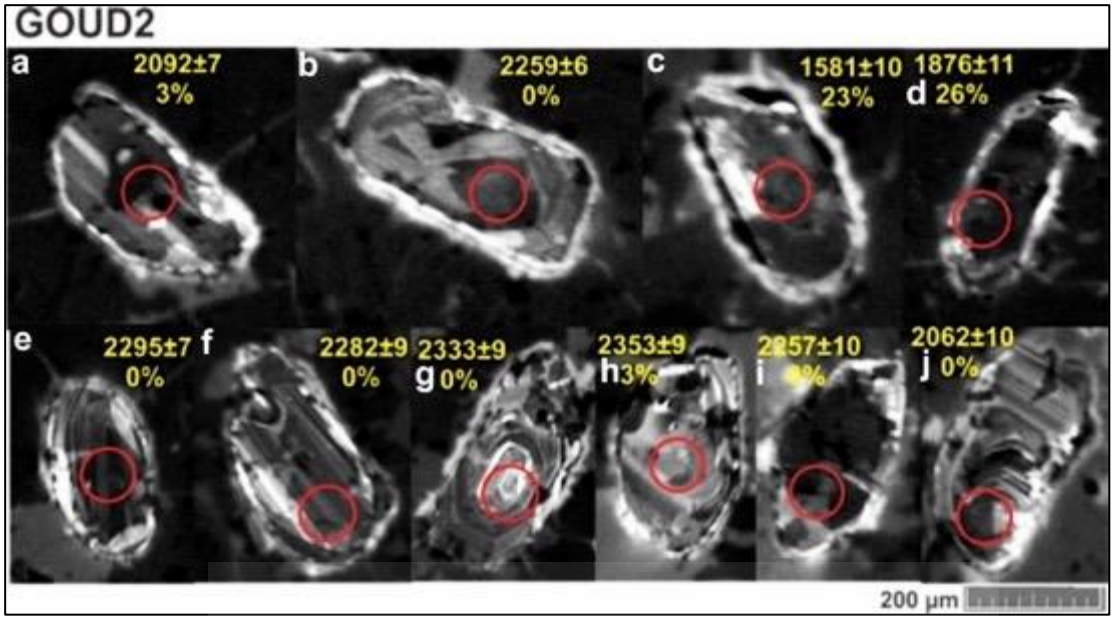

Figure 5.36 Cathodoluminescence images of selected detrital zircon grains from GOUD2 with the solid circles representing U-Pb ablation spots. The numbers displayed are $^{207}Pb/^{206}Pb$ ages with 2 sigma errors and discordance percentage below the age.

5.7.3. U-Pb results

U-Pb results for seventy analysed detrital zircon grains for GOUD2 are given in Appendix A, Table 11. About 65% of these analyses are concordant, and they can be grouped according to their $^{207}Pb/^{206}Pb$ ages into two groups (Figure 5.37). A minor percentage (15%) has Archean ages ranging between 2838±7 and 2505±8 Ma, and the majority has ages between 2483±9 and 2062±10 Ma. There are two grains that are concordant around 2055 and they have $^{207}Pb/^{206}Pb$ ages of 2064±10 and 2062±10 Ma, and there is also one grain that is just 2% discordant at 2052±7 Ma; these grains have $^{206}Pb/^{204}Pb$ ratios of >10,000. Discordant zircon grains have $^{207}Pb/^{206}Pb$ between 2364±13 and 1654±11 Ma. Diagrams of uranium content versus discordance and $^{206}Pb/^{204}Pb$ ratio versus $^{207}Pb/^{206}Pb$ age shows no correlation between the variables (Figure 5.38 a, b).

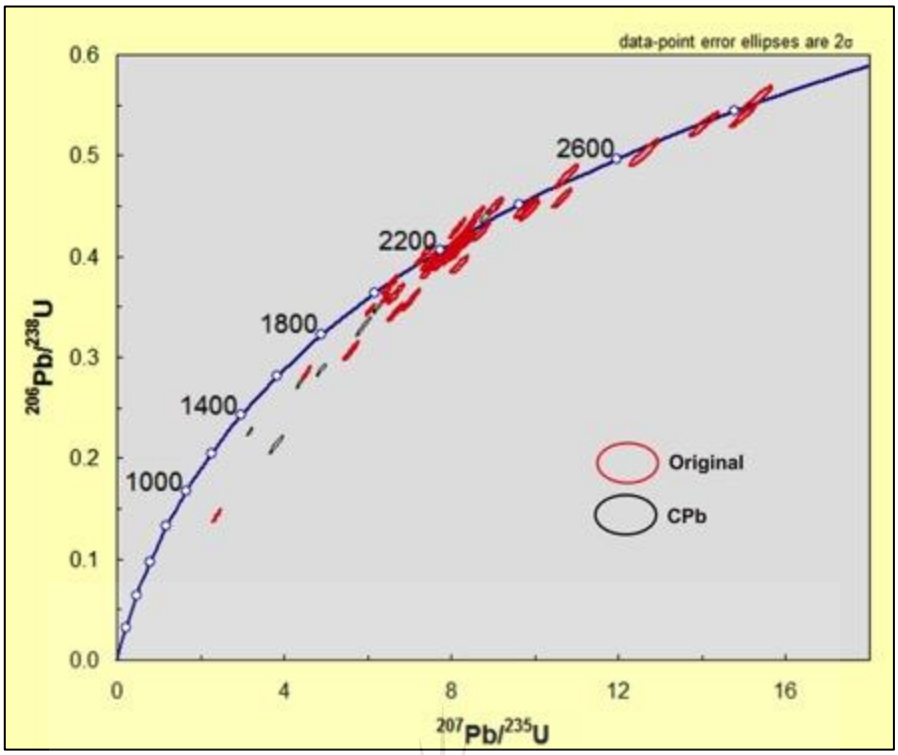

Figure 5.37: Wetherill concordia diagrams for sample GOUD2.

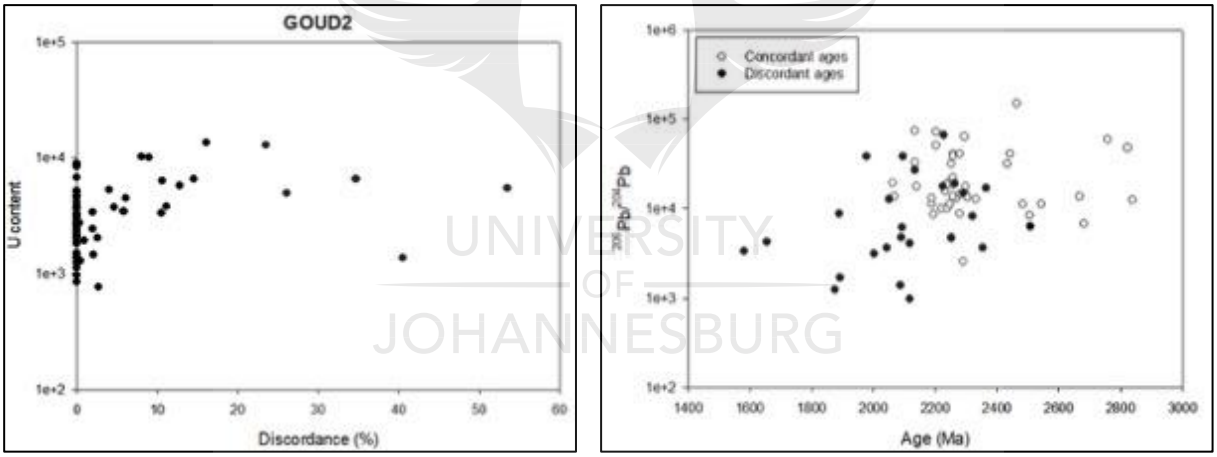

Figure 5.38: (a) Uranium content versus discordance (b) $^{206}Pb/^{204}Pb$ ratio versus age. These diagrams showing are not showing any correlation between variables.

5.8. Discussion

5.8.1. Comparison with previous work

Zeh et al. (2016) analyzed Magaliesberg quartzites for their age and Hf isotope signatures using LA-ICPMS with the aim to determine the age and sources for these quartzites. Among samples analyzed by Zeh et al. (2016) is quartzite sample Mag-R1 which was obtained in the western limb of the Bushveld Complex, 20.5 km from MEMG1 and 2 from this study (Figure 5.39). Samples BQz1 and 3 (Zeh et al. 2016) were collected in the eastern Bushveld Complex, less than a kilometer from MEMG 4 and about 2.5 km from MEMG3 from the current study (Figure 5.40). For the purpose of this study MEMG1 and 2 will be compared with Mag-R1, and MEMG4 will be both compared to BQz1 and 3. Some comparison will be done using the "Detzircr" program described by Andersen et al. (2017).

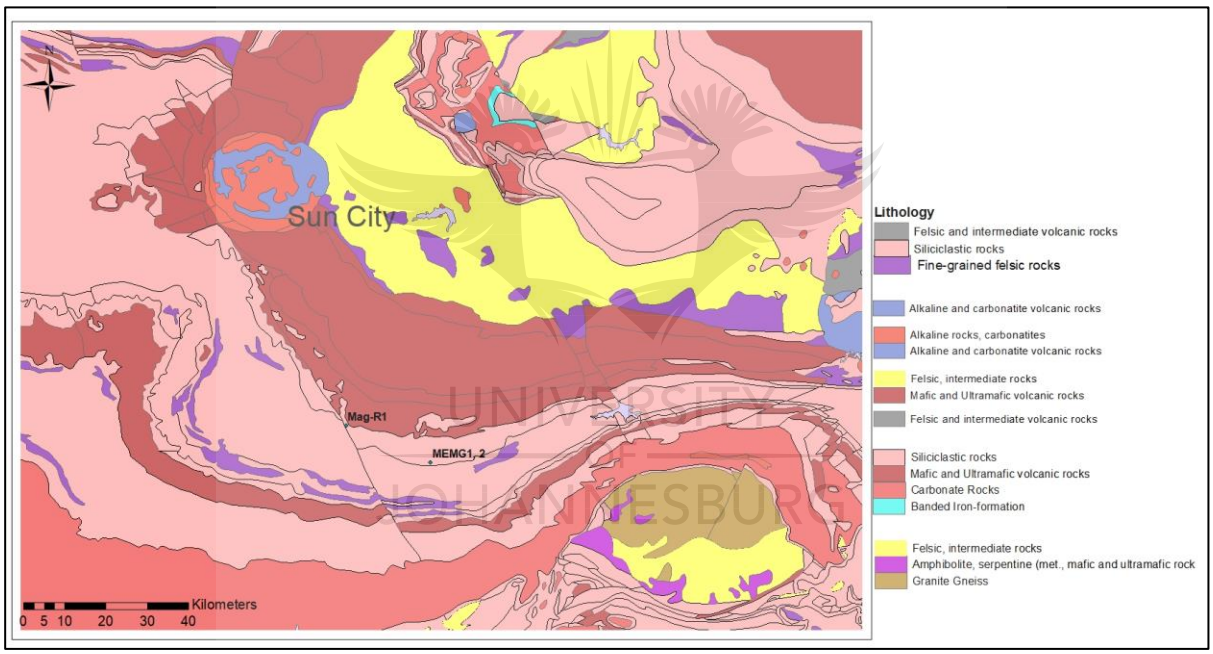

Figure 5.39: A close-up diagram showing sample locations for MEMG1 and 2 as well as Mag-R1.

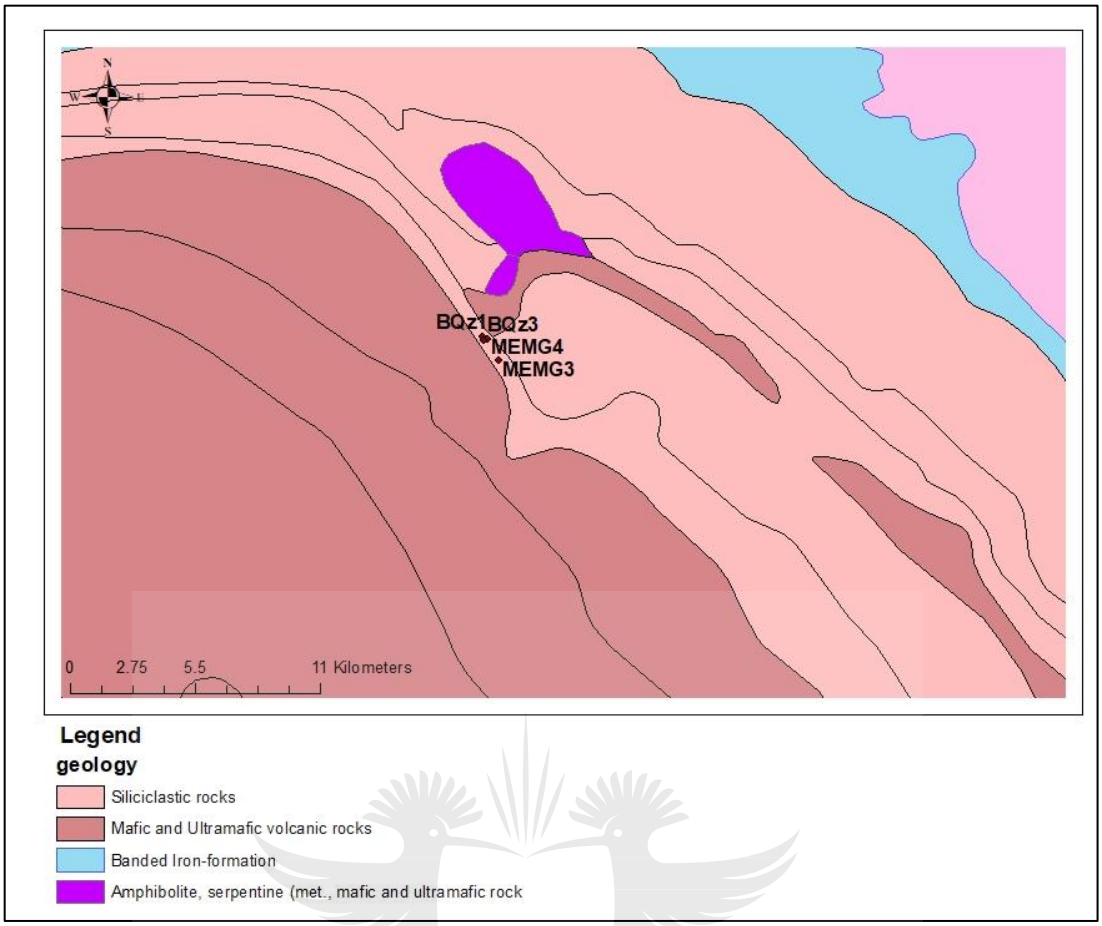

Figure 5.40: A close-up diagram showing sample locations for MEMG 3 and 4 as well as BQz1 and 3.

The concordia diagram for sample MEMG 4 for CPb-free and CPb-corrected zircons (Figure 5.41 a) show that zircon CPb correction actually shifts the data to the left of the concordia diagram, i.e. it shifts CPb-corrected analyses to the younger $^{207}Pb/^{206}Pb$ ages. Sample MEMG4 has a lot of analyses concordant around 2100 Ma, but when you look at analyses younger than 2100 Ma, about 60% of these are CPb corrected and only 40% are CPb free. This is also the case with BQz3 from Zeh et al. (2016): Figure 5.41 b shows a close-up of the concordia diagram for BQz3. These example show that the CPb correction indeed shifts the data more to the left of the diagram, and that the percentage of CPb correction does in fact play a role in the magnitude of the shift.

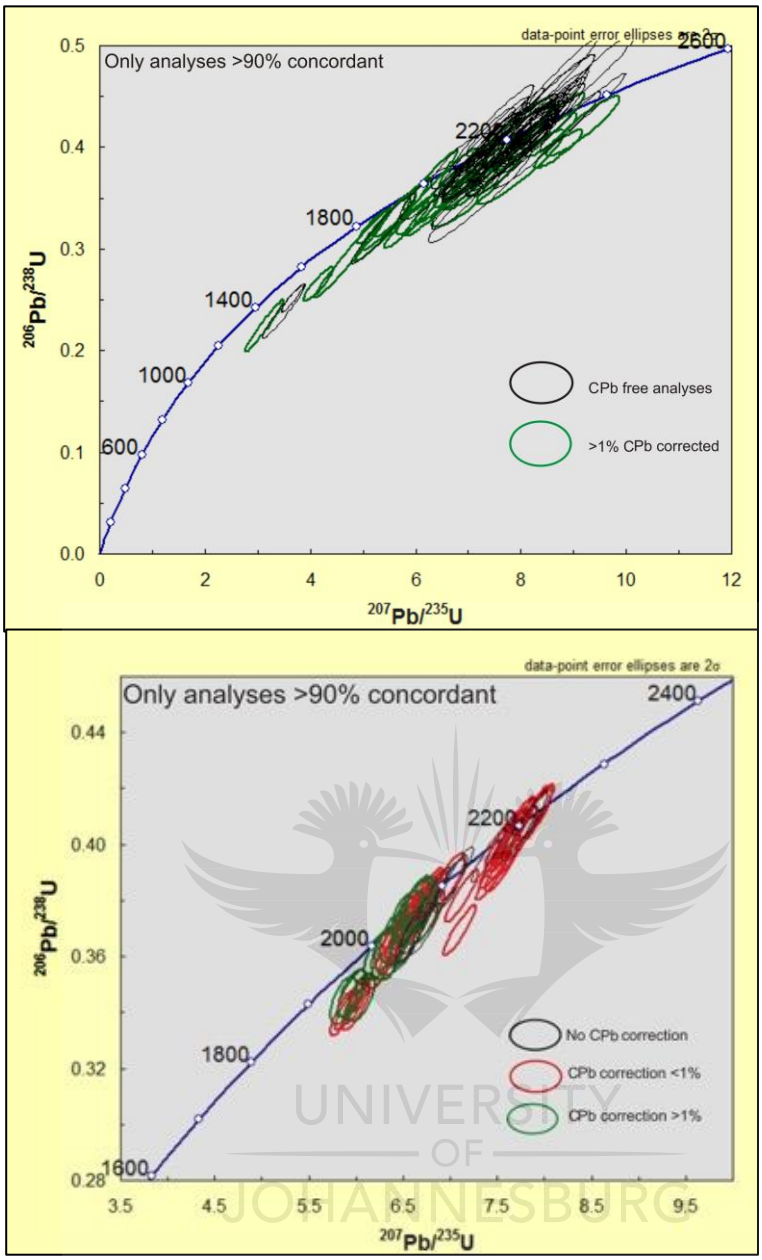

Figure 5.41: Concordia diagrams showing the shift in data caused by CPb correction (a) MEMG4, note that there are no analyses that are CPb corrected <1% (b) BQz3 (data from Zeh et al., 2016).

5.8.1.1. MEMG1 and 2 versus MagR1

MEMG1 and 2 fall within the same stratigraphic unit as Mag-R1. Note that the comparison in this section is only done on CPb-free analyses. Besides the similarity in locations where these three samples were collected, their probability density plots show a similar trend for their age distribution with age peaks around 2200 Ma as well as ca. 2800 Ma (Figure 5.42 a). Their empirical cumulative distribution curves for U-Pb ages are shown in Figure 5.42 b, and the confidence bands show that there is near-complete overlap between the samples, taking the statistical uncertainty into account.

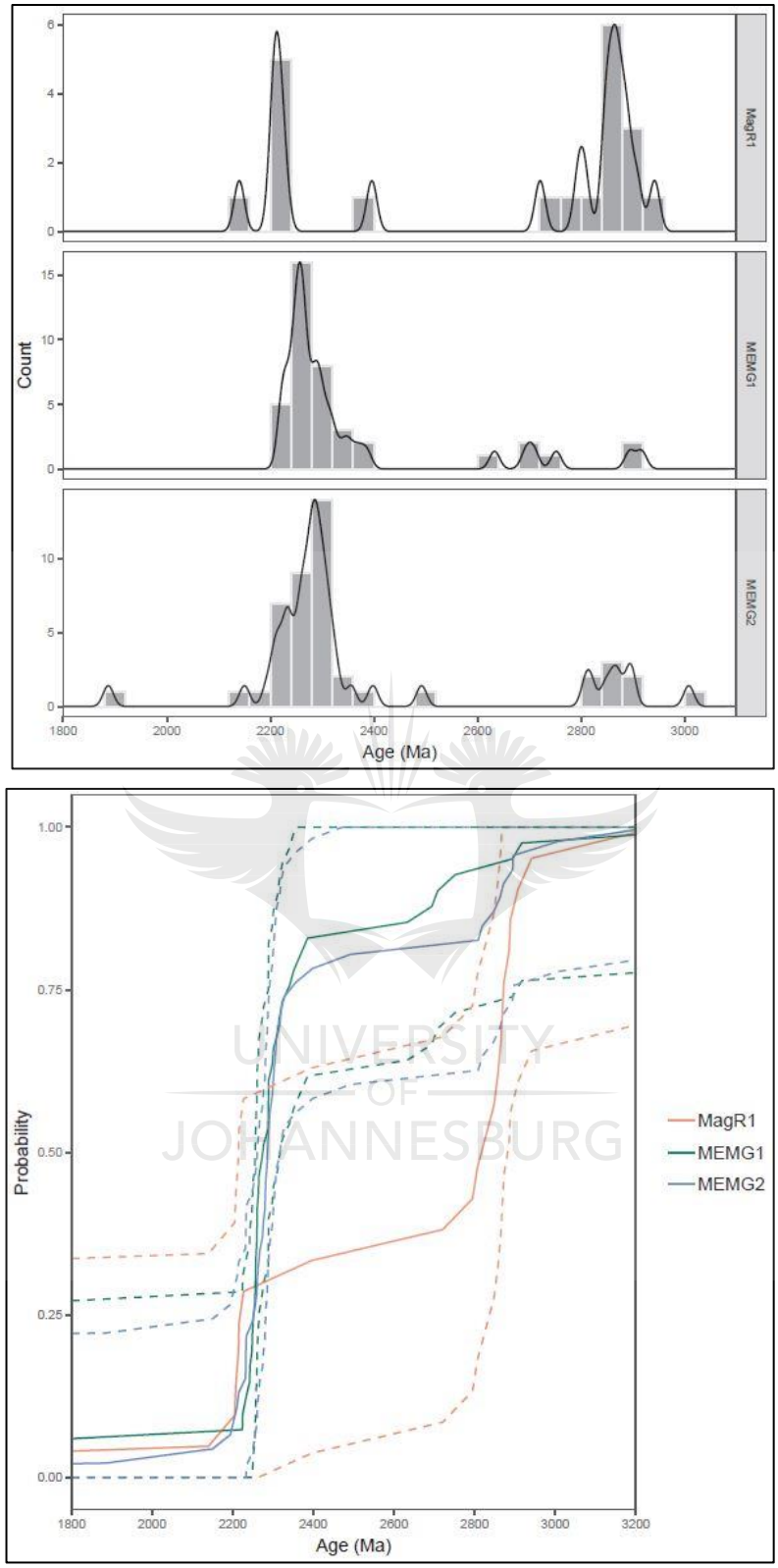

Figure 5.42: (a) Probability density plot for MEMG1, 2 and MagR1 (b) empirical cumulative distribution curve for U-Pb ages for sample MEMG1, 2 and MagR1.

5.8.1.2. MEMG4 versus BQz1 and 3

MEMG4 can be compared to samples BQz1 and 3 from Zeh et al. (2016) because of its proximity to these two samples. Again, the comparison in this section is only done on CPb-free analyses. Zircons from MEMG4 this study and from BQZ1 and 3 from Zeh et al. (2016) have several analyses with ages less than 2.080 Ga, BQz1 has a number of zircon analyses with Archean ages (Figure 5.43). Therefore, in terms of density plots, MEMG4 is more similar to BQz3 of Zeh et al. (2016). The empirical cumulative distribution curve indicates similarities for these samples (Figure 5.44). The upper quartile versus lower quartile diagram shows that MEMG4 overlaps within uncertainty with both BQz1 and 3 (Figure 5.45). An overlap is also observed in the initial epsilon Hf versus age diagram (Figure 5.46), there is one BQz3 analysis that has initial epilon Hf value higher than others, and there are no analyses from MEMG4 with high initial Hf ratios around this age. However, there are analyses with similar initial Hf ratios around 2200 Ma. The results from the "Detzircr" program show that MEMG4 is statistically similar to both BQz1 and3.

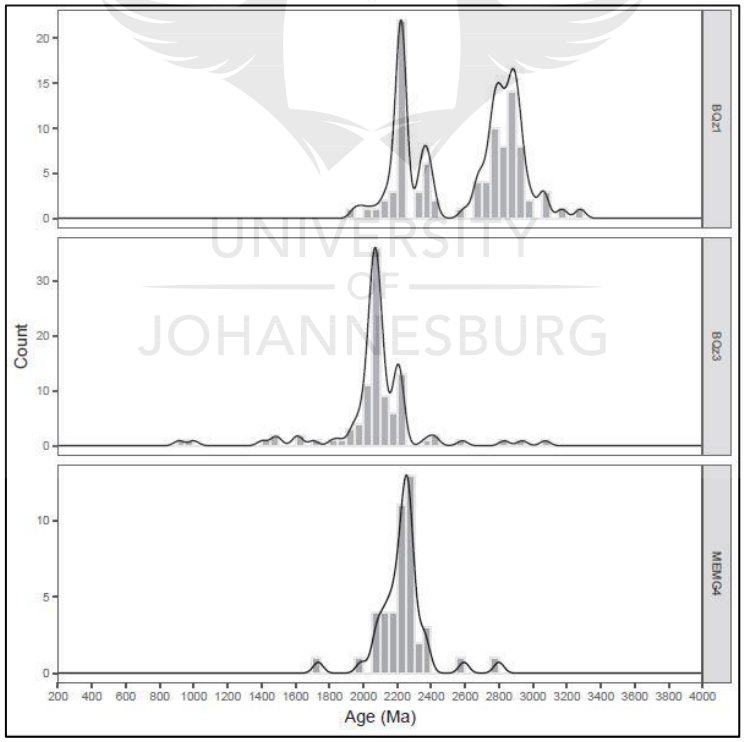

Figure 5.43: Probability density plot for MEMG4, BQz1 and 3.

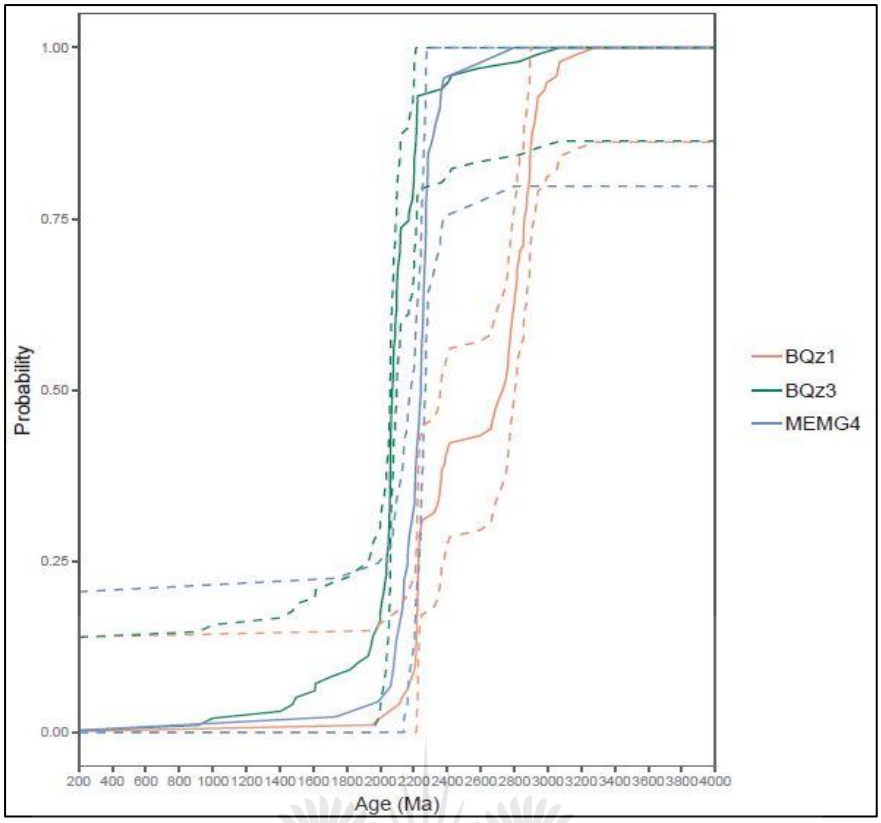

Figure 5.44: Empirical cumulative distribution curve for U-Pb ages for sample MEMG4, BQz1 and 3.

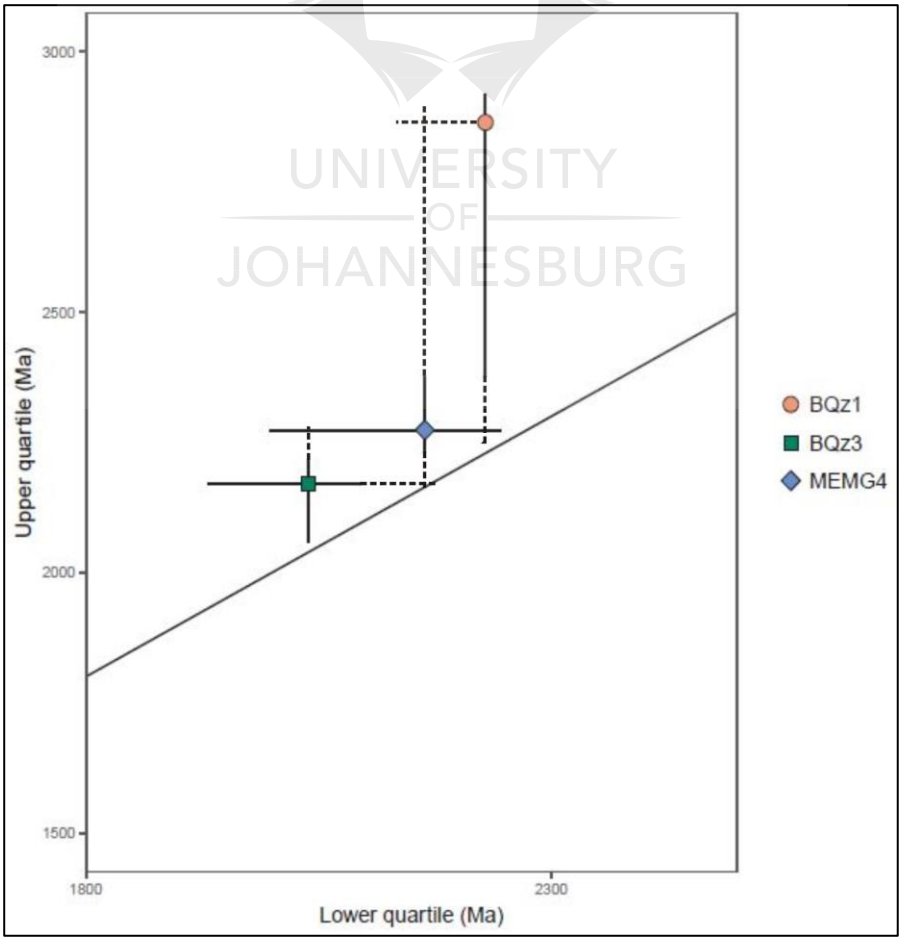

Figure 5.45: Lower versus upper quartile zircon age.

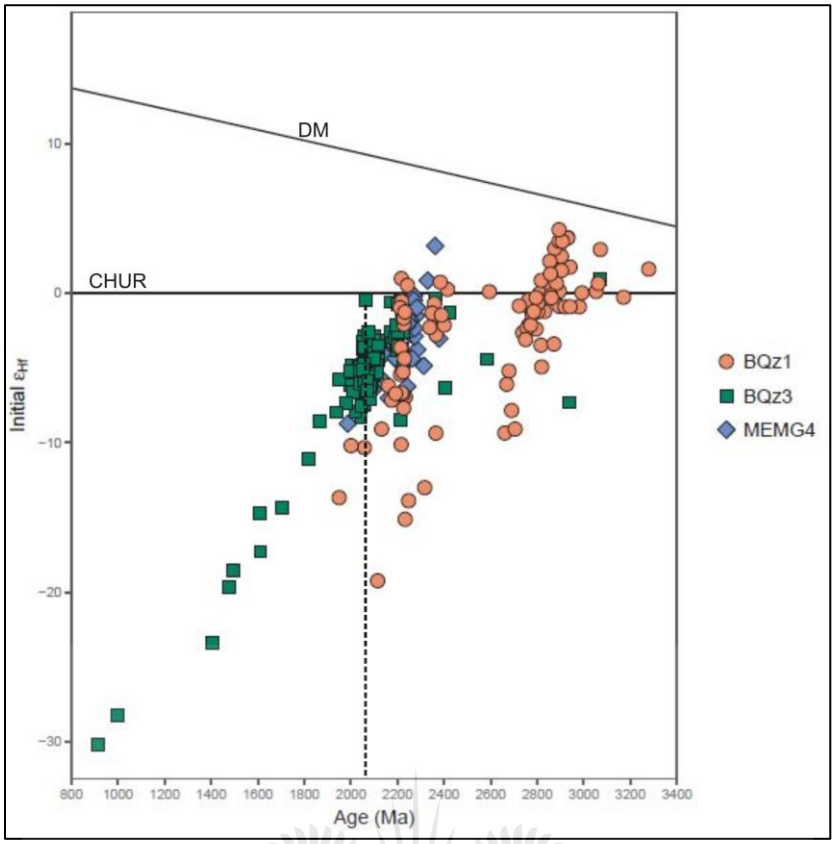

Figure 5.46: Initial epsilon Hf versus age for MEMG4, BQz1 and 3. The vertical dashed line represents the age of the Bushveld magmatism.

5.8.2. Petrographic Characteristics

Petrographic observations indicate that these rocks have undergone grain boundary migration, likely a result of elevated temperatures and/or directional stress. Samples MEMG1, 2 and 25 have undergone static recrystallization. Quartz grains in samples MEMG5 and Goud 2 have also undergone recrystallization. The presence of serrated boundaries which seem to have migrated in quartz grains in sample MEMG3 and 4 indicate that they have undergone dynamic recrystallization by bulging mechanism (e.g. Stipp et al., 2002). Appearance of andalusite and (pseudomorphs after) cordierite in several samples indicate that these sandstones were affected by metamorphism at low-pressure conditions (e.g. Vernon, 1988), which is most likely induced by the Bushveld Complex intrusion.

5.8.3. Zircon characteristics

The dominant zircon texture in these sandstones is oscillatory zoning, which is typical for magmatic zircons (Pidgeon, 1992). Some zircon grains also show different zoning patterns like sector zoning, convoluted zoning, as well as patchy complex zoning patterns. Zircon grains with complex zoning or "fading" of primary textures are characterized by high degrees of discordance. Zircon grains that show alteration of primary textures are usually light grey in CL with homogeneous areas (e.g. Puga et al., 2005), and most often contain fractures and

inclusions. These types of zircon grains are abundant in sample MEMG4 (e.g. Fig. 5.16 j) where this "altered" zircon grain has an age of 2056±20 Ma which is equivalent to Bushveld age. Sample MEMG 4 shows similarities with samples are also similarities in their initial Hf ratios. This suggests that, similar to the previous chapter, it cannot be excluded that there is, to some extent, influence of Bushveld event on partial Pb loss in zircon grains from the Magaliesberg sandstones, especially the ones closest to the contact with the Marginal Zone i.e. MEMG3 and 4. The zircons also continued to lose Pb after the Bushveld intrusion. Zircon grains characterized by CL dark areas are uranium rich when compared with other grains in the same sample and they also have higher discordance percentages, which is well demonstrated in sample MEMG1 (e.g. Fig. 5.3 c, h, r). High-U zircons are more likely to be metamict leading to CL dark areas in crystals. Therefore, for zircon grains that partially lost Pb during metamorphism, it can be argued that this loss was most likely influenced by radiation damage in zircons.

5.8.4. U-Pb data

All five analysed samples from the Magaliesberg Formation are dominated by zircons with ages around 2200 Ma. For MEMG3 and MEMG4, concordant analyses show peaks around 2055 Ma and even at younger ages (ca. 1800 Ma). Ages younger than ca. 2055 Ma can be attributed to CPb correction because over 90% of these ages are from CPb-corrected zircons. This CPb correction might be the cause of the shift of data towards younger ages. The majority zircon grains from these sandstones appear to have suffered partial Pb loss around 200 Ma for both Archean and Proterozoic zircons (Fig. 5.41 a, b), but the fact that all these highly discordant analyses have been corrected for, sometimes significant, common Pb content, makes this interpretation somewhat tenuous. Zeh et al. (2016) suggest depositional ages as young as of 2080±13 Ma which are much younger than depositional ages determined by studies prior to Zeh et al. (2016); for instance, Dorland, (2004) proposed a depositional age of <2205±13 Ma, based on the age of the youngest zircon out of the forty-nine grains he analysed by SHRIMP. CL images and age information from this study do not show evidence for new zircon growth.

There is a recent study by Wabo et al. (2019), in which dykes cross-cutting the Silverton Formation, which directly underlies the Magaliesberg Formation, were dated and yielded $^{39}Ar/^{40}Ar$ ages of 2253±45 and 2202±74 Ma, which means that Silverton Formation must be older. Since there is no sedimentological evidence for a major break between two formations,

a difference in depositional age of more than 150 million years between the Silverton and Magaliesberg formations is unlikely.

From a concordia diagram (Fig. 5.37) there is no evidence for any influence of the Goudini Complex at an age of ca. 1193 Ma for sample GOUD2. However, zircon grains from this sample yield $^{207}Pb/^{206}Pb$ ages as young as ca. 2062±10 Ma, so this block contained within the Goudini carbonatite might have been brought up from deeper levels of the Bushveld Complex.

5.8.5. Lu-Hf data

What is important to note from zircons with Proterozoic ages is that ca. 2200 Ma zircons have similar $^{176}Hf/^{177}Hf$ ratios as ca 2055 Ma zircons. This permits that the ca. 2055 Ma zircons reflect resetting of the U-Pb system, rather than them being a separate age group. So, this sheds more doubt on the interpretation of a <2.08 Ga depositional age. The fact that there is not much variation in initial Hf ratio versus age suggests that isotopic resetting affected only the U-Pb system, leaving $^{176}Hf/^{177}Hf$ ratios undisturbed. Therefore, Hf isotopes provide an invaluable indicator in this type of study as these systems have not been affected. They thereby make it possible to explain the complex history of the zircon populations and help to identify episodes of Pb loss.

5.8.6. Trace element data

Trace element analyses were done in MEMG4. Most of the variations in REE patterns are observed in LREE. The analyses that are the most discordant have high LREE concentrations (Fig. 5.20) although a few (<3%) near-concordant analyses also have high LREE concentrations. The same applies for Ce and Eu anomalies: the majority of analyses have positive Ce and negative Eu anomalies. There is no correlation observed between discordance and cerium anomalies in sample MEMG4. The correlation between discordance and LREE concentrations observed from this sample agrees with the observations from previous studies that LREE abundances may be useful indicators of modified/disturbance in zircon isotopic signatures (e.g. Bell et al., 2016; Kielman et al., 2018). However, similar to the problems noted by Kielman et al. (2018), the ablation spots for REE and U-Pb were done in different areas within a single grain, so the results from REE and U-Pb cannot be directly linked.

5.9. Conclusions

From the petrographic characteristics of these rocks, it is obvious that these sandstones have been metamorphosed. For MEMG3 and MEMG4, which are closer to the contact with the

Marginal Zone, the mineral assemblages indicate low pressure metamorphism, which may be linked to the intrusion of the Bushveld Complex intrusion.

From the concordia diagrams for MEMG3 and 4, it can be concluded that there are indeed contributions from the Bushveld-related thermal overprint to partial Pb loss. The Pb loss was also most likely influenced by radiation damage in zircons and access of metamorphic fluids to the metamict zircon grains; this is evidenced by zircon grains with high uranium contents having high discordance percentages, and this is also shown in the diagrams of U content versus discordance for samples from the Magaliesberg and Timeball Hill formations.

There are only small differences in initial Hf isotope ratios between zircon grains with ages ~ 2200 and ~ 2055 Ma, indicating that zircons with ages younger than ca. 2055 Ma might reflect resetting of the U-Pb system.

Lastly, it can also be concluded that resetting of the U-Pb system is not always accompanied by modifications of the typical compositional signature of the detrital zircons.

Chapter 6

6. Results: Bushveld Complex Granite

6.1. Sample MEPB44

This sample is derived from an outcrop of veined granite close to the Bakgatla gate of the Pilanesberg Complex. The granite interpreted to belong to the Bushveld Complex, and the veining appears to be related to the emplacement of the Pilanesberg Complex at ca. 1395 Ma (Elburg and Cawthorn, 2017). The sample was collected to assess whether the metasomatic effects from the Pilanesberg fluids have affected the zircons.

6.1.1. Petrographic Characteristics

This granite is coarse-grained, showing an inequigranular texture. It consists mainly of plagioclase, alkali feldspar and quartz (Figure 6.1 a). Hornblende, epidote and bluish-green amphibole, interpreted to be a sodic amphibole, constitute minor mineral phases (Figure 6.1 b, c). Zircon and titanite occur as accessory phases. The sodic amphibole and epidote occur in association with hornblende, which has pleochroism varying from light yellow to medium green, and they are probably a product of a reaction between hornblende and the fluids. The minerals in this granite are more altered that the ones from a more pristine Bushveld granite MEMG20 shown in Figure 6.1 d.

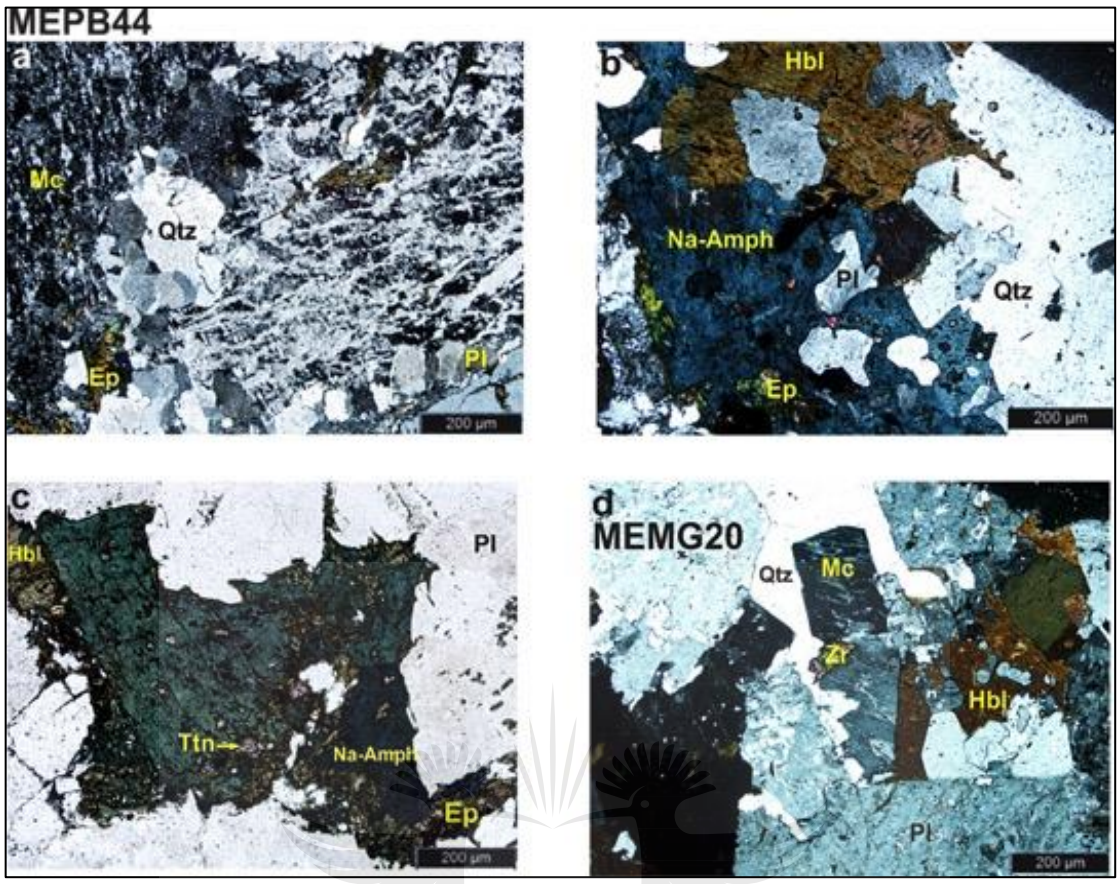

Figure 6.1(a) Alkali feldspar shows perthitic exsolution and interstitial epidote (XPL) (b, c) alteration of hornblende to sodic amphibole and epidote (XPL) (d) a more pristine Bushveld granite, hornblende is not altered (XPL).

6.1.2. Zircon characteristics

Zircon crystals in this sample are typically sub- to euhedral, prismatic elongate in shape (Figure 6.2). They range in length between 150 and 50 µm. They exhibit oscillatory zoning (e.g. Figure 6.2 e, f, g), although zones are not clearly defined in most crystals, and some crystals show patchy complex patterns (e.g. Figure 6.2 a, b, c, h, i). The latter contain inclusions of apatite crystals (enhanced signal intensity on CL images). Some of these zircon grains appear fractured (e.g. Figure 6.2 c, h, k, n).

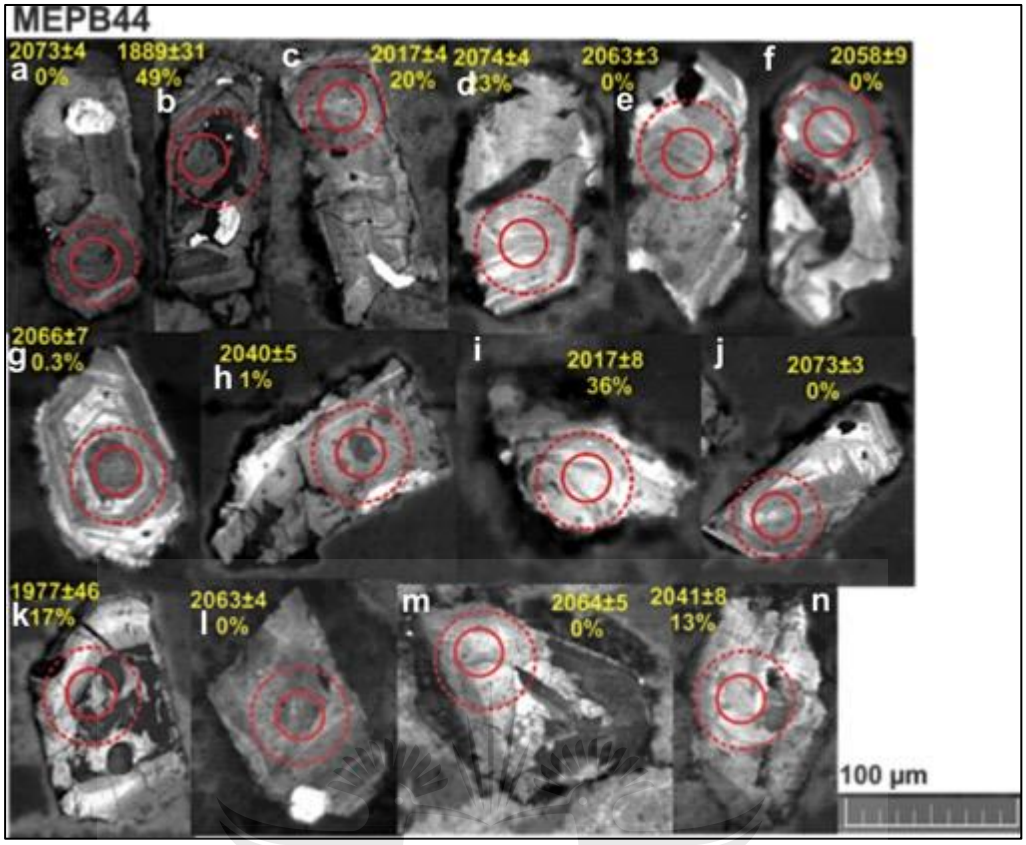

Figure 6.2: Cathodoluminescence images of selected zircon grains from MEPB44 with solid and dashed circles representing U-Pb and Lu-Hf ablation sites, respectively. The numbers displayed are $^{207}Pb/^{206}Pb$ ages with 2 sigma error; discordance percentages are shown below the ages.

6.1.3. U-Pb results

U-Pb results for analysed zircon grains for sample MEPB44 are given in Appendix A, Table 12. The concordia diagram for seventy-two CPb-free analyses is shown in Figure 6.3 a. Within these analyses, sixty-two are concordant at $^{207}Pb/^{206}Pb$ ages between 2016 ±12 and 2094±8 Ma, with the main population lying between 2057 and 2073 Ma (see Figure 6.4). The weighted average $^{207}Pb/^{206}Pb$ for these concordant points is 2068±2 Ma (MSWD=15). Isoplot calculated upper and lower intercept ages at 2076±12 Ma and 130±280 Ma, respectively. Thirty-two percent of the analyses are discordant and within these are two analyses with older $^{207}Pb/^{206}Pb$ ages of 2437±10 and 2478±15 Ma. The discordant CPb-free analyses show a linear trend of partial Pb loss towards the origin of the diagram. The concordia diagram for all ninety-nine zircon analyses is shown in Figure 6.3 b. For the combined population of CPb-free and CPb-corrected, the lower intercept age is 408±97 Ma. There are also two analyses that are concordant around 1200 Ma; these have higher U contents than other analyses in the same sample and they are also corrected for common Pb. A correlation between uranium

content versus age (negative correlation) and discordance (positive correlation) is observed (Figure 6.5 a, b).

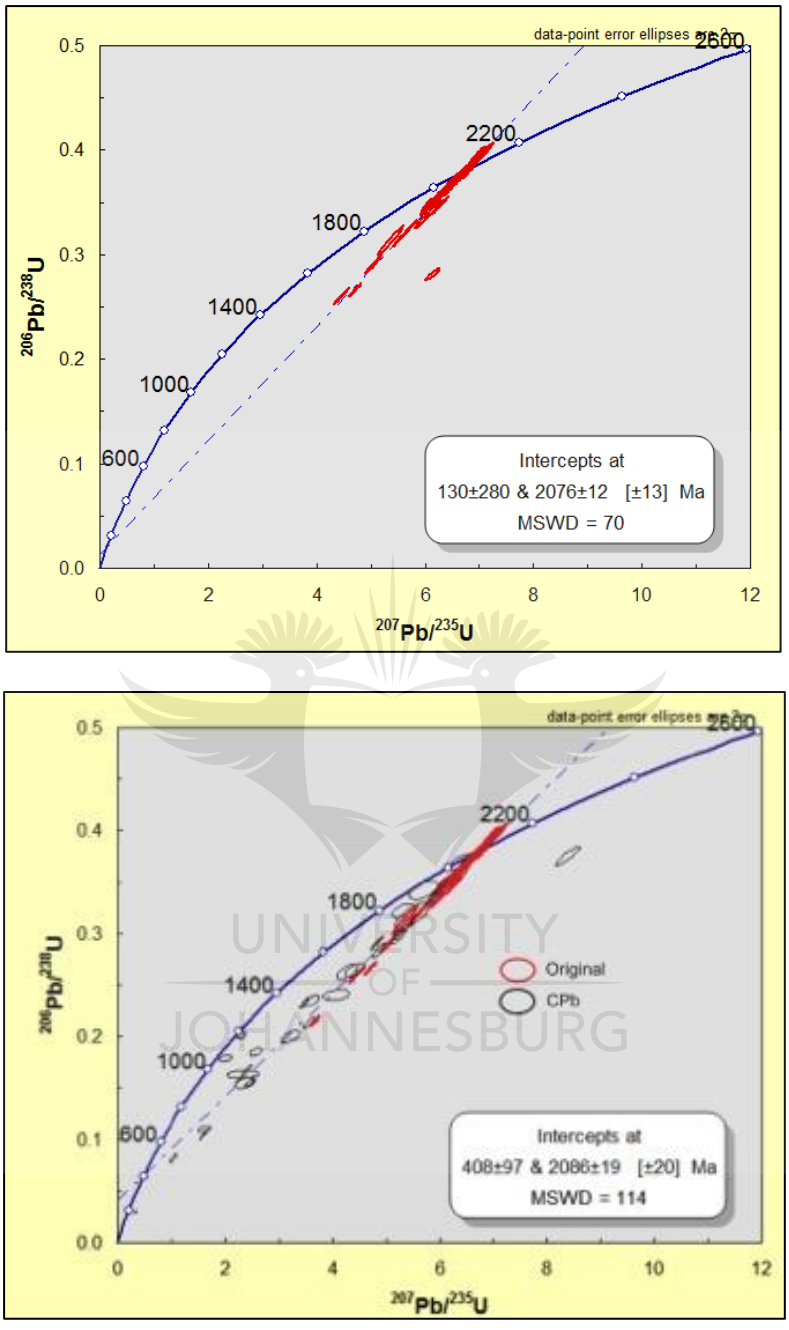

Figure 6.3: Wetherill concordia diagram for sample MEPB44 (a) Analyses that are CPb-free are mostly concordant, and the few discordant analyses show partial Pb loss towards the origin of the diagram (b) diagram including CPb-corrected analyses showing scattered age data, with a lower intercept around 400 Ma.

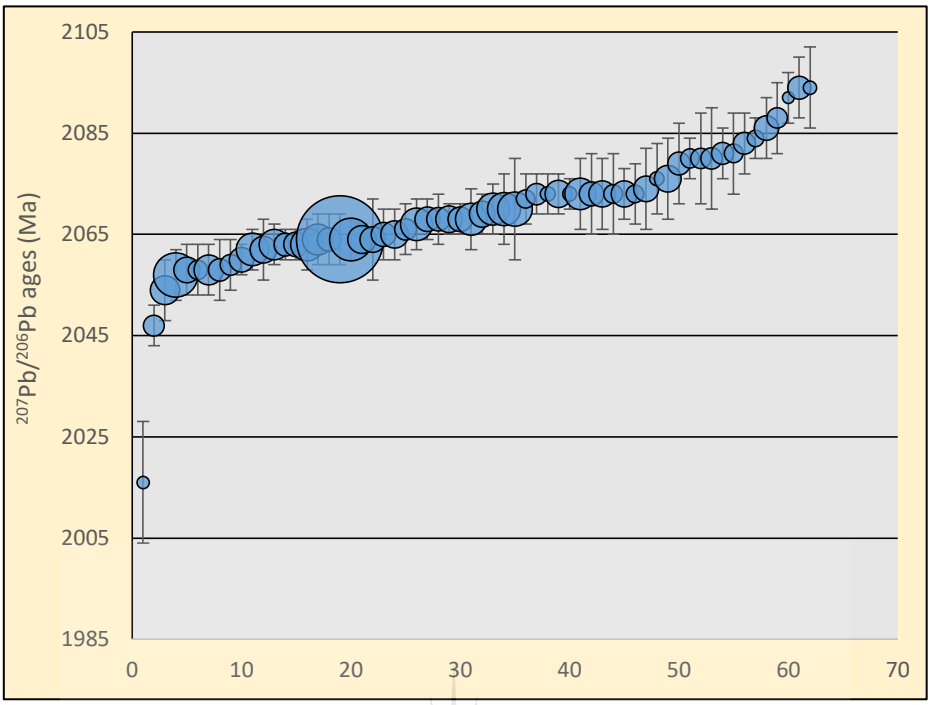

Figure 6.4 A diagram showing concordant $^{207}Pb/^{206}U$ ages in ascending order, with bubble size proportional to the $^{206}Pb/^{204}Pb$ ratio.

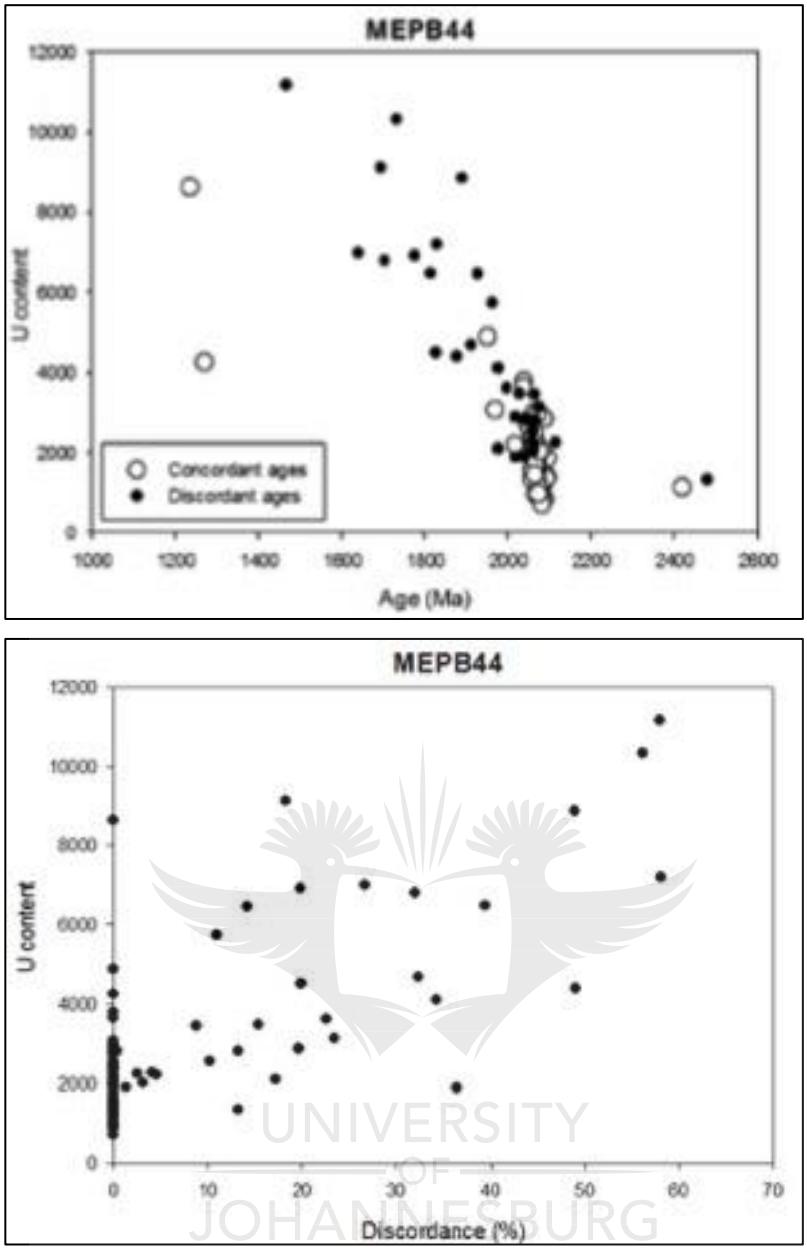

Figure 6.5: (a) Negative correlation for uranium content and age for MEPB44 (b) positive correlation between uranium content and discordance for MEPB44.

6.1.4. Lu-Hf results

Lu-Hf results for sample MEPB44 are given in Appendix B, Table 7. The initial Hf isotopic ratio versus age diagram is shown in Figure 6.6, with all analyses plotting significantly below CHUR. The initial Hf ratios range between 0.2811 and 0.2813. The concordant analyses form a vertical array of points at ca. 2068 Ma. A few discordant grains that have been corrected for common Pb show a sub-horizontal array of points towards younger ages, showing that they have suffered partial Pb loss. This sample is dominated by negative epsilon Hf values at the zircons' $^{207}Pb/^{206}Pb$ age, yielding an average epsilon Hf of -7.8 (± 1.2). The $^{176}Yb/^{177}Hf$ ratios range from ca. 0.15 to 0.017; they give an average value of 0.05.

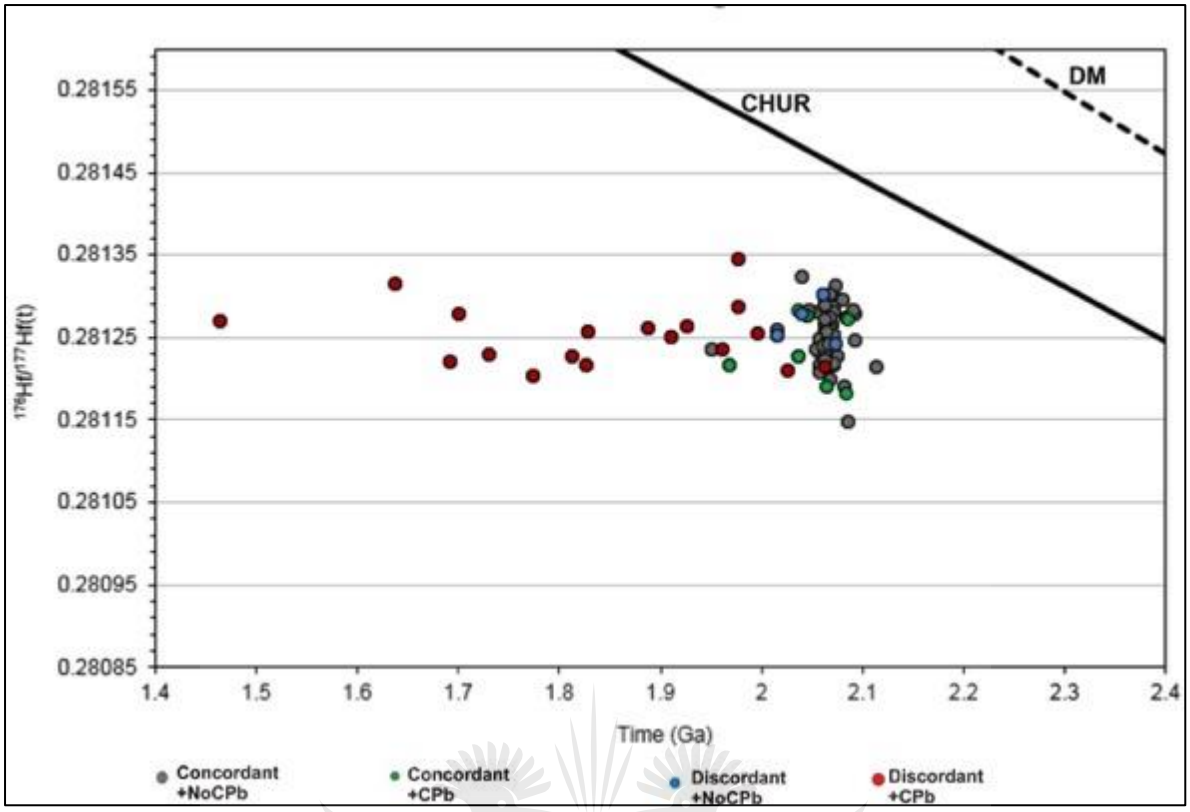

Figure 6.6: Initial Hf ratios vs age diagram for sample MEPB44 showing a horizontal array of points from ca. 2068 Ma.

6.1.5. Trace element chemistry

Representative trace-element compositions for MEPB44 are shown in Appendix C, Table 3. Most zircons from this sample are characterized by flat light rare earth element (LREE) patterns. There is no consistency in Ce and Eu anomalies (Figure 6.7). Interestingly, two zircon grains that are both <10% discordant and CPb-free stand out: one has a completely flat REE pattern and one with a very pronounced negative Eu anomaly. In general, concordant zircon grains (black) have lower LREE content whereas discordant grains (blue) have high LREE content. The diagrams of cerium anomalies against discordance (Figure 6.8 a) and La/Sm ratios against age (Figure 6.8 b) show no obvious correlations between these parameters.

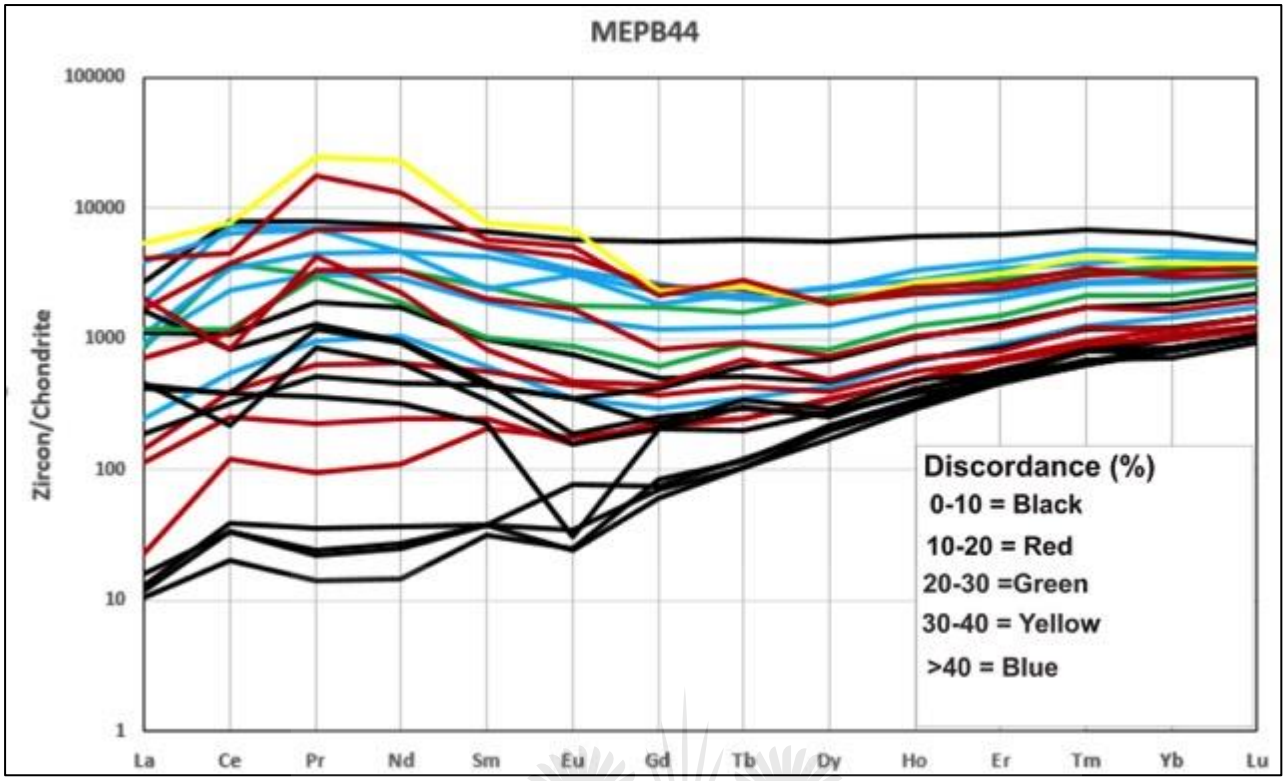

Figure 6.7: Chondrite-normalized REE patterns for zircons Bushveld Granite sample MEPB44 (normalisation after Sun and McDonough, 1989).

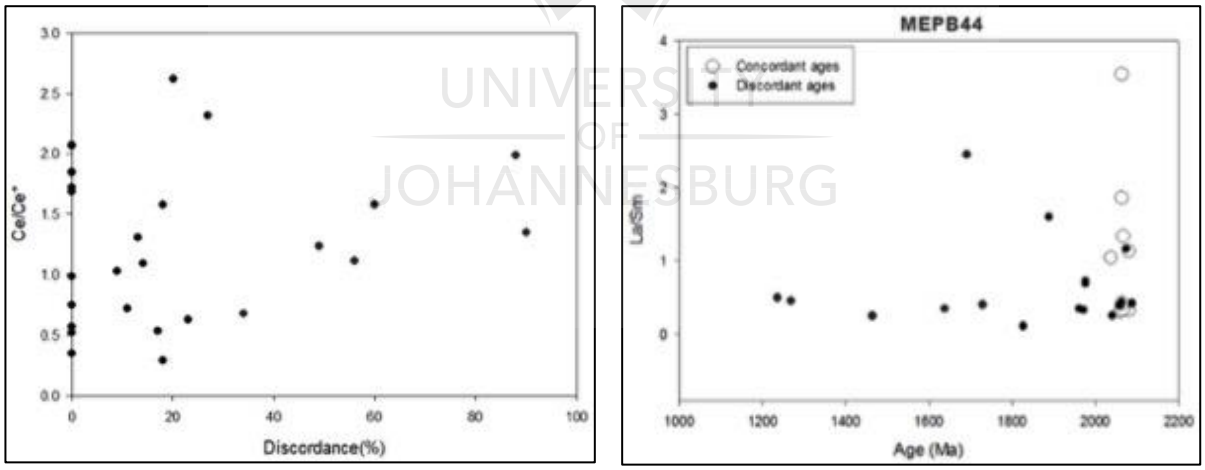

Figure 6.8: (a) Ce/Ce* vs discordance (b) La/Sm ratio vs age. Diagrams do not show any correlation between variables.

6.2. Sample MEMG12

This granite sample was collected to assess if the dolerite dyke that intruded into this granite has any effects on zircon signature.

6.2.1. Petrographic characteristics

This granite is coarse-grained and inequigranular. It consists mainly of plagioclase, microcline and quartz. Hornblende often shows incipient alteration to epidote and opaque minerals (Figure 6.9 a, b). Zircon occurs as an accessory phase within quartz and feldspar.

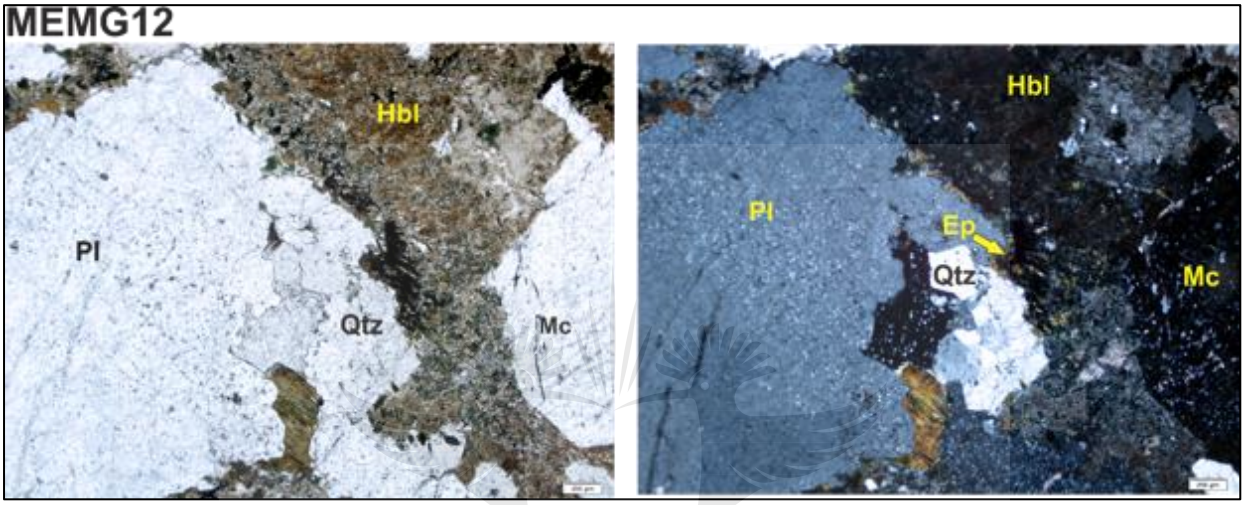

Figure 6.9: Hornblende alters to epidote and opaque minerals at the edges (a) PPL (b) XPL. The scale is 200 µm.

6.2.2. Zircon characteristics

Zircon crystals are euhedral and mostly elongated, and range in length from 250 to 30 µm (Figure 6.10). The dominant texture is oscillatory zoning, which is still preserved in most grains (e.g. Figure 6.10 b, c, e, i), but complex patchy zoning is also observed in cases (e.g. Figure 6.10 a, g, j). These zircon crystals also contain inclusions (e.g. Figure 6.10 c, d, h, i, j) and fractures (e.g. Figure 6.10 g).

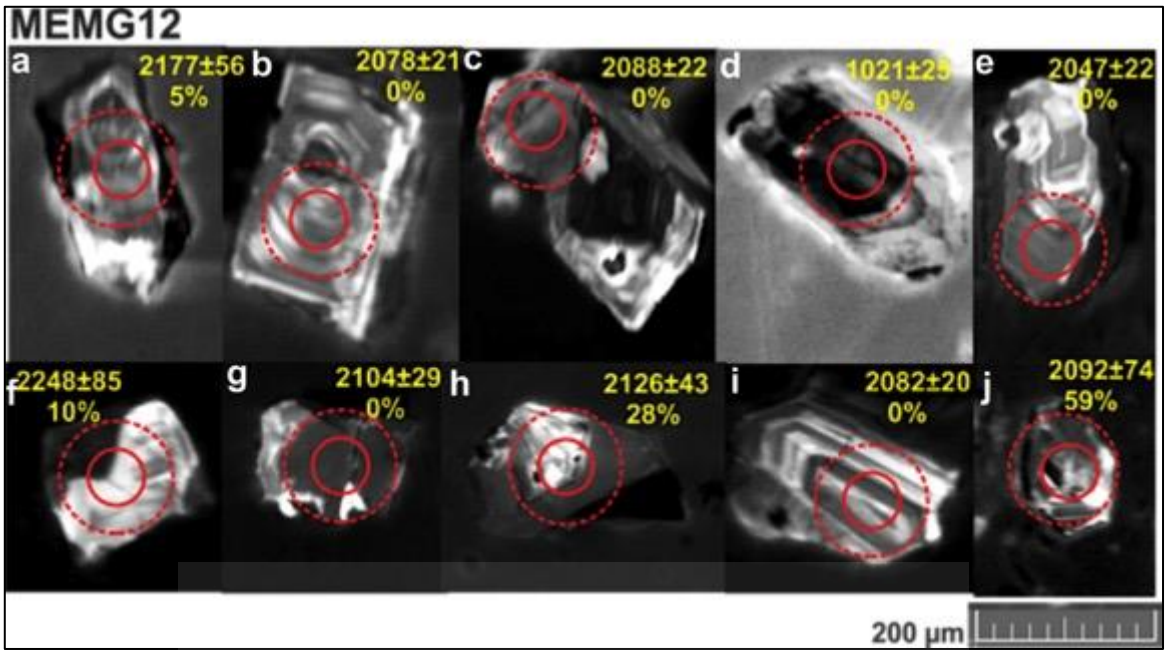

Figure 6.10: Cathodoluminescence images of randomly selected zircon grains of MEMG12 with solid circles and dashed circles representing U-Pb and Lu-Hf ablation sites, respectively. The numbers displayed are $^{207}Pb/^{206}Pb$ ages with 2 sigma error and discordance percentages below ages.

6.2.3. U-Pb results

U-Pb results for analysed zircon grains from sample MEMG12 are given in Appendix A, Table 13. The close-up concordia diagram for twenty-nine analyses that were CPb-free is shown in Figure 6.11 a, showing that all analyses are concordant at $^{207}Pb/^{206}Pb$ ages between 2051±11 and 2099±20 Ma, whereby the two youngest and three oldest analyses appear to be outliers (Figure 6.11). The concordant analyses have a weighted average $^{207}Pb/^{206}Pb$ age of 2056±5 Ma (MSWD=0.45). For CPb-free analyses, Isoplot calculated upper and lower intercept ages at 2055±9 and 9±420 Ma, respectively. The concordia diagram for all analyses is shown in Figure 6.11 b. Within the twenty-eight analyses corrected for common Pb (black ellipses), nine are concordant at $^{207}Pb/^{206}Pb$ ages between 1286±381 and 2183±35 Ma, but most of these have a very large uncertainty. The rest show partial Pb loss towards a lower intercept age of 248±100 Ma, but this discordia is very poorly defined, with an MSWD of 19. The diagrams of uranium content versus age and discordance show a clear correlation between variables: analyses that are discordant have higher uranium concentrations than concordant analyses (Figure 6.12 a, b).

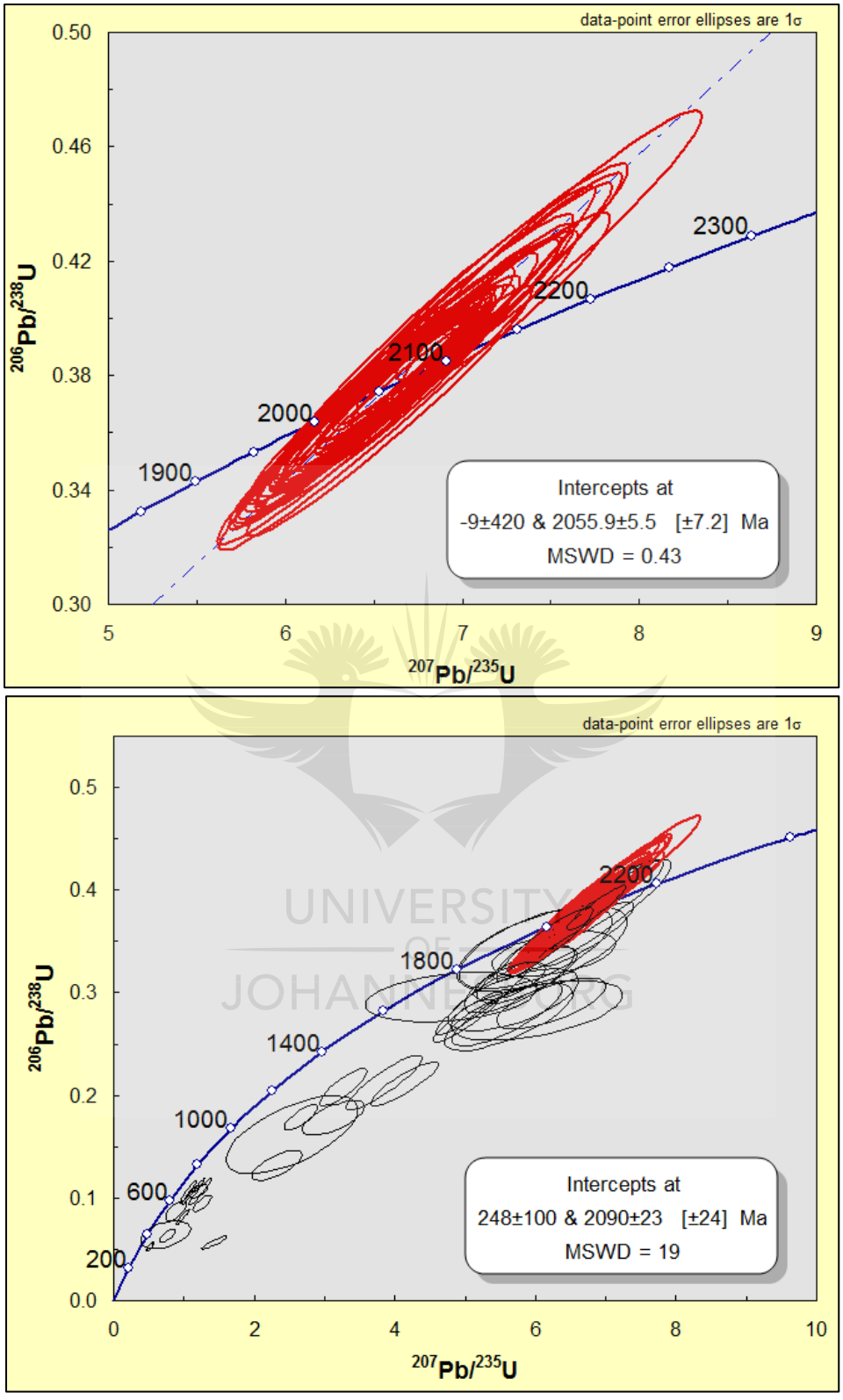

Figure 6.11: Wetherill concordia diagrams for sample MEMG12. (a) CPb-free analyses. (b) All Analysed zircon grains.

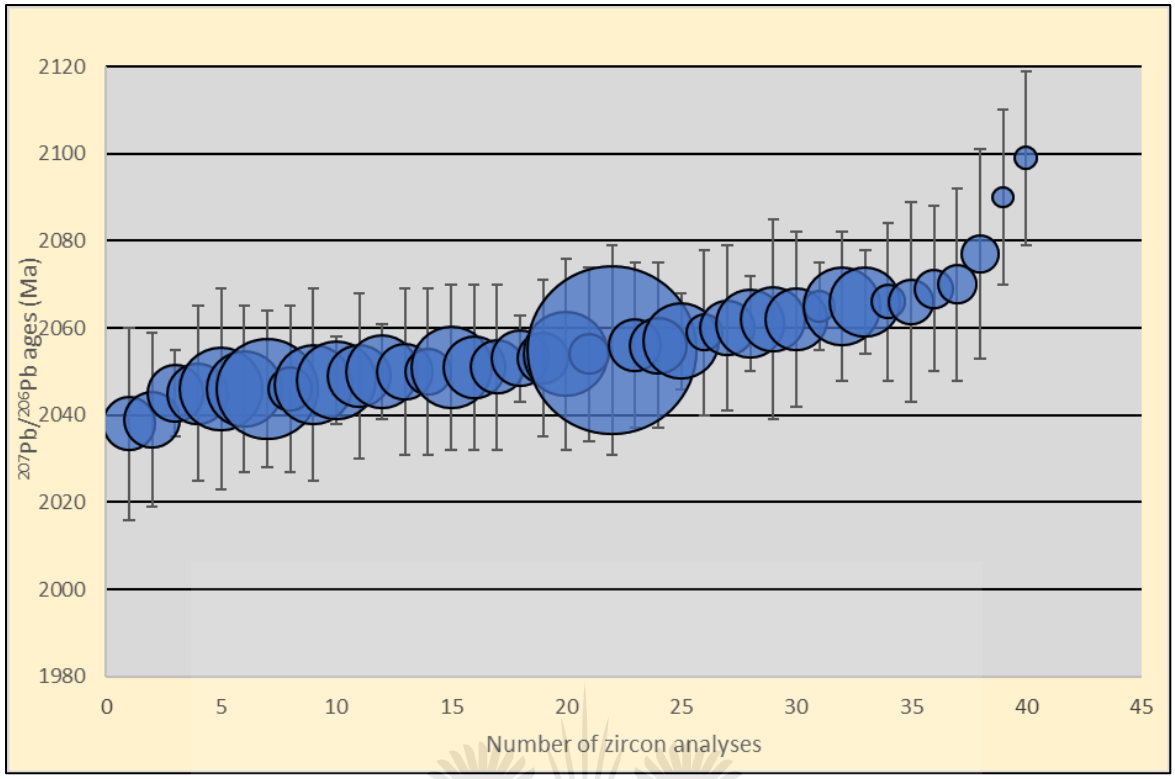

Figure 6.13: A diagram showing concordant $^{207}Pb/^{206}U$ ages in ascending order, with bubble size proportional to the $^{206}Pb/^{204}Pb$ ratio.

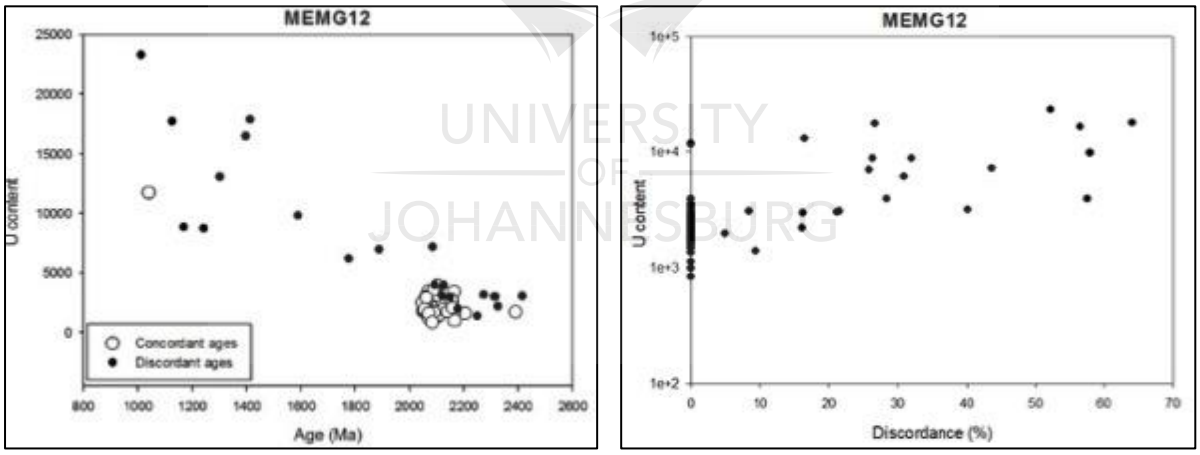

Figure 6.12: (a) Negative correlation between uranium content and age (b) positive correlation between uranium content and discordance for sample MEMG12.

6.2.4. Lu-Hf results

Lu-Hf results for sample MEMG12 are given in Appendix B, Table 8. The initial Hf ratio versus age diagram (Figure 6.14) shows a cluster of points between ~2100 and 2051 Ma, with initial $^{176}Hf/^{177}Hf$ ratios ranging between 0.2812 and 0.2813. The average epsilon Hf value is

-8.4±1.1. Only five discordant CPb grains form a horizontal array of points towards younger ages. The $^{176}Yb/^{177}Hf$ ratios range from ca. 0.18 to 0.018, giving an average of 0.06.

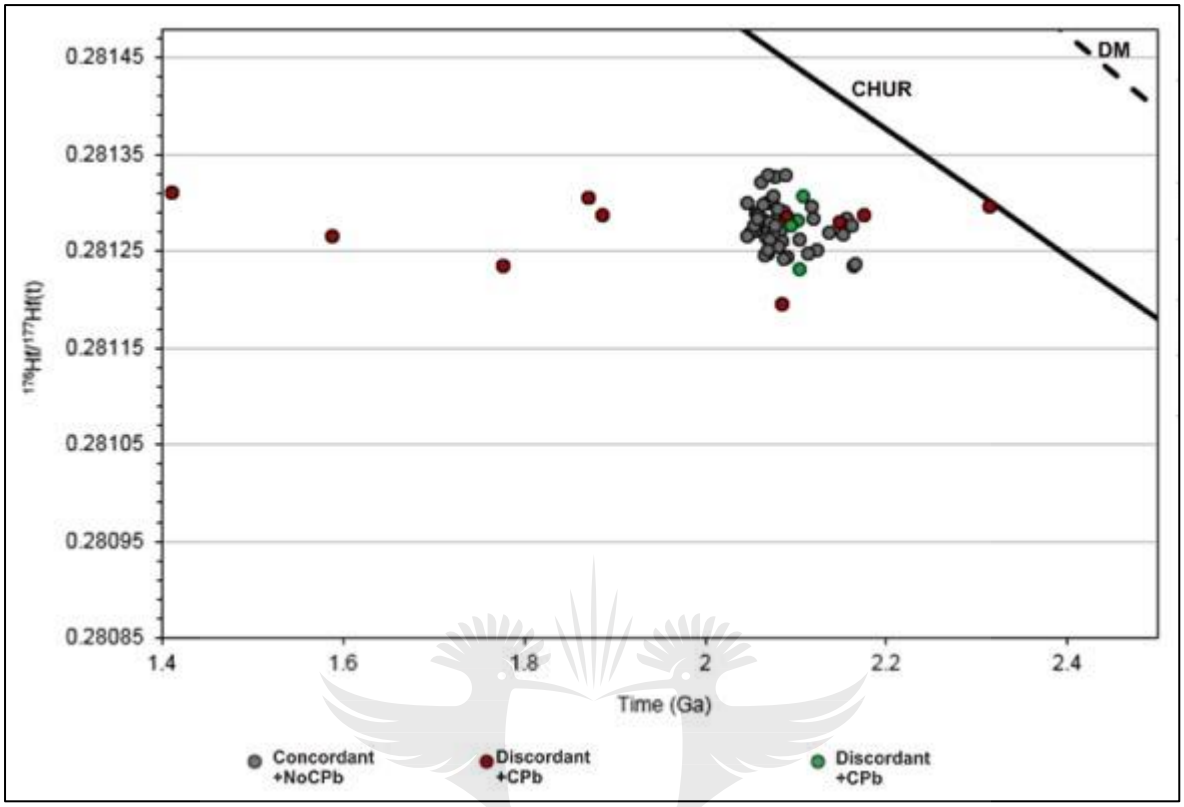

Figure 6.14: Initial Hf ratios vs age diagram for sample MEMG12.

Results: Influence Spitskop Complex

6.3. Sample 52.2

This fenite sample whose protolith is a granitic rock was collected within the Spitkop Complex, eastern Bushveld Complex to assess if there are any effects of the intrusion of cabonatite and concomitant fenitization on zircon signature.

6.3.1. Petrographic characteristics

This fenitized granite is medium-grained. The mineralogy consists mainly of carbonate minerals occurring together with plagioclase, alkali feldspar, aegirine and epidote (Figure 6.16 a, b). Alkali feldspar shows perthitic exsolution (Figure 6.16 c). Zircons occur as inclusions within epidote and feldspar (Figure 6.16 d).

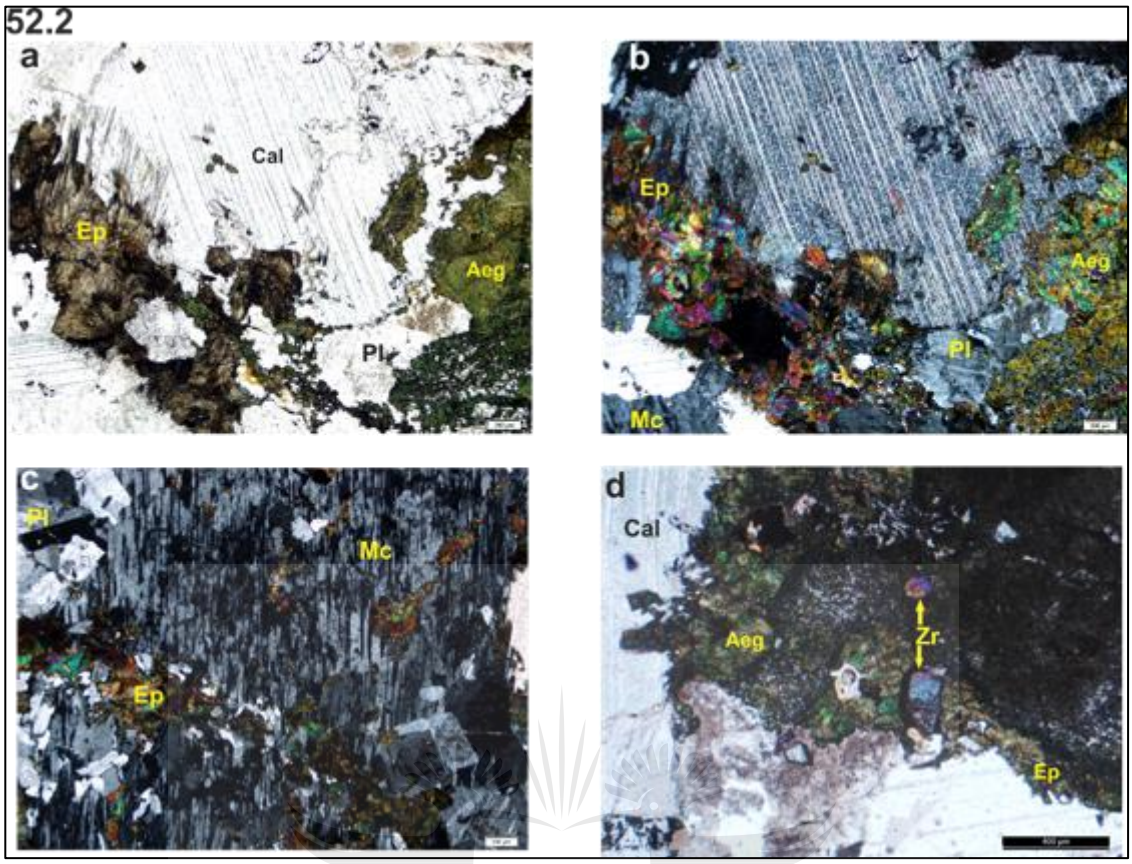

Figure 6.15 (a, b) Carbonate minerals occurring together with feldspar, epidote and aegirine (PPL and XPL, respectively) (c) perthitic exsolution in alkali feldspar (XPL) (d) zircon occurs as inclusion within epidote and feldspar (XPL).

6.3.2. Zircon characteristics

Zircon grains from this sample are mostly elongate, but there are few sub-rounded crystals. Their length ranges from 200 to 50 µm. Most crystals display oscillatory zoning although it is fading out in some grains (e.g.Figure 6.16 d, e, g, h). Some of these grains are highly fractured (e.g. Figure 6.16 b, c, f) and they also contain inclusions.

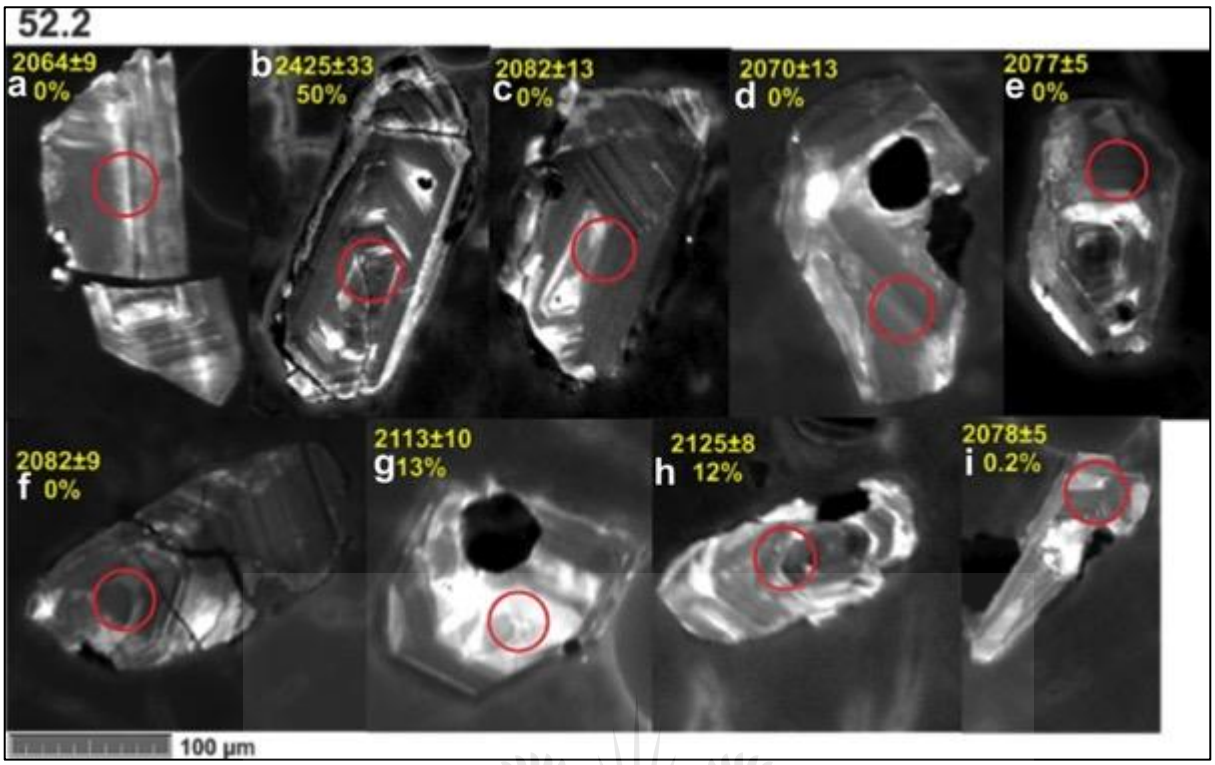

Figure 6.16: Cathodoluminescence images of selected zircon grains of sample 52.2. The circles represent U-Pb ablation sites and the numbers displayed are $^{207}Pb/^{206}Pb$ ages with 2 sigma error. Please note that the big black spots in figure 6.16 d, g are polishing artefacts.

6.3.3. U-Pb results

U-Pb results for eighty-seven analysed zircon grains for sample 52.2 are given in Appendix A, Table 14. About 84% of these zircon analyses are concordant (Figure 6.17), they yield a weighted average $^{207}Pb/^{206}Pb$ age of 2065±2 Ma (MSWD = 2.7). An upper intercept age is defined at 2064±2 Ma and a lower intercept age poorly defined at 342±160 Ma. The main population gives $^{207}Pb/^{206}Pb$ ages between 2055 and 2075 Ma (Figure 6.19). In the remaining 21% discordant analyses, most zircon crystals are CPb corrected, and Isoplot calculated upper and lower intercept ages at 2066±4 and 151±88 Ma, respectively. There is no evidence of influence from the Spitskop Complex. There is also no clear correlation between discordance and uranium content (Figure 6.20 a, b).

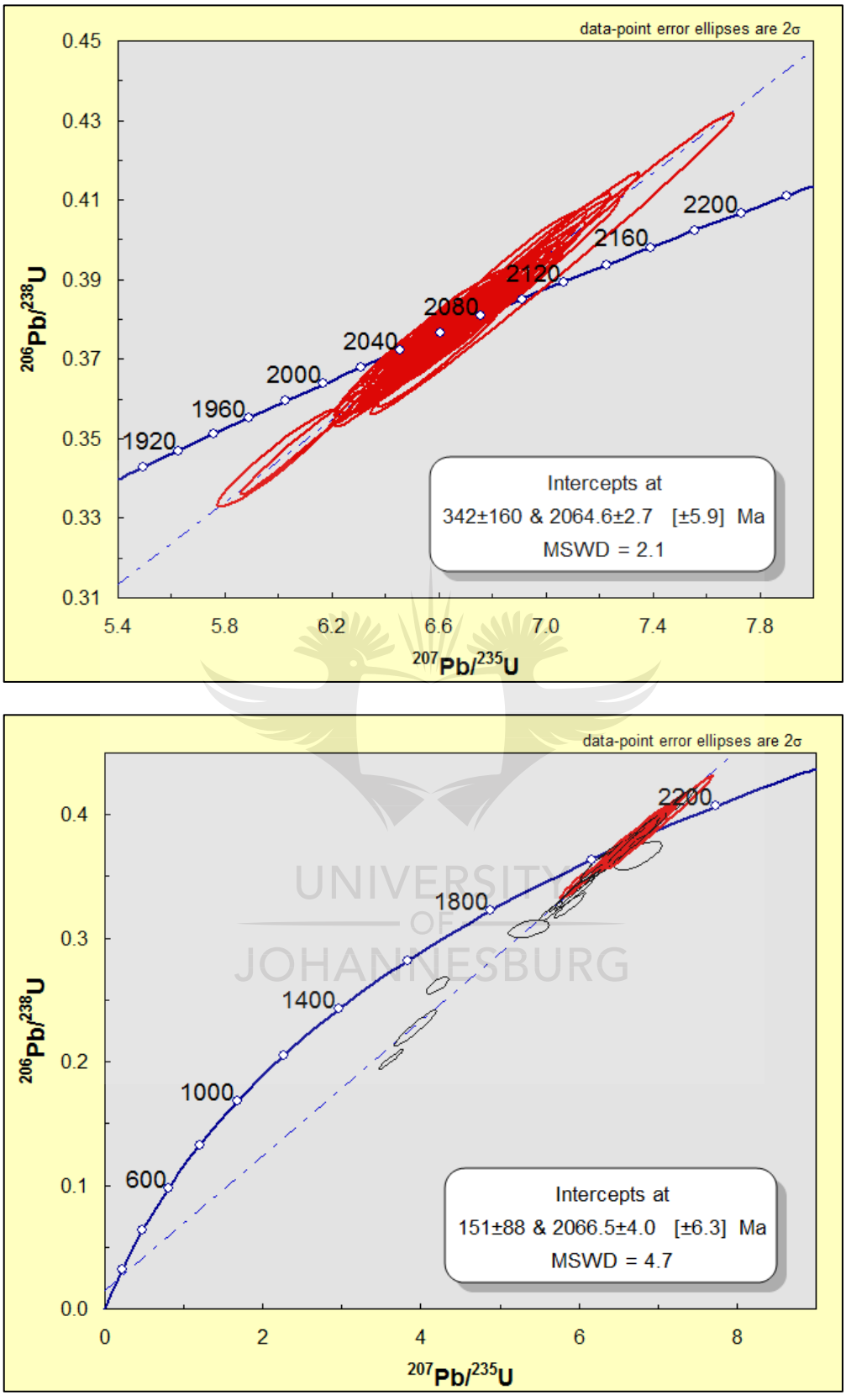

Figure 6.17: (a) Wetherill concordia diagram CPb-free analyses (b) concordia diagram for all analysed zircon crystals.

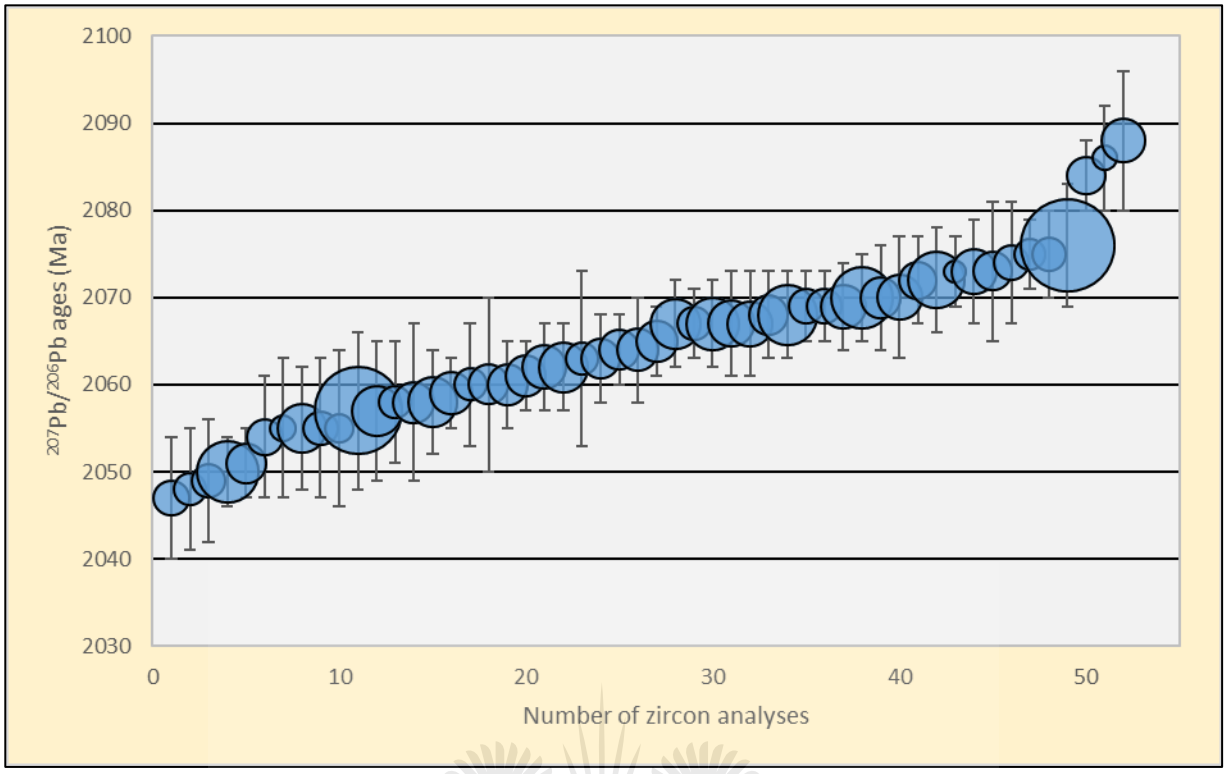

Figure 6.19: A diagram showing concordant $^{207}Pb/^{206}U$ ages in ascending order, with bubble size proportional to the $^{206}Pb/^{204}Pb$ ratio.

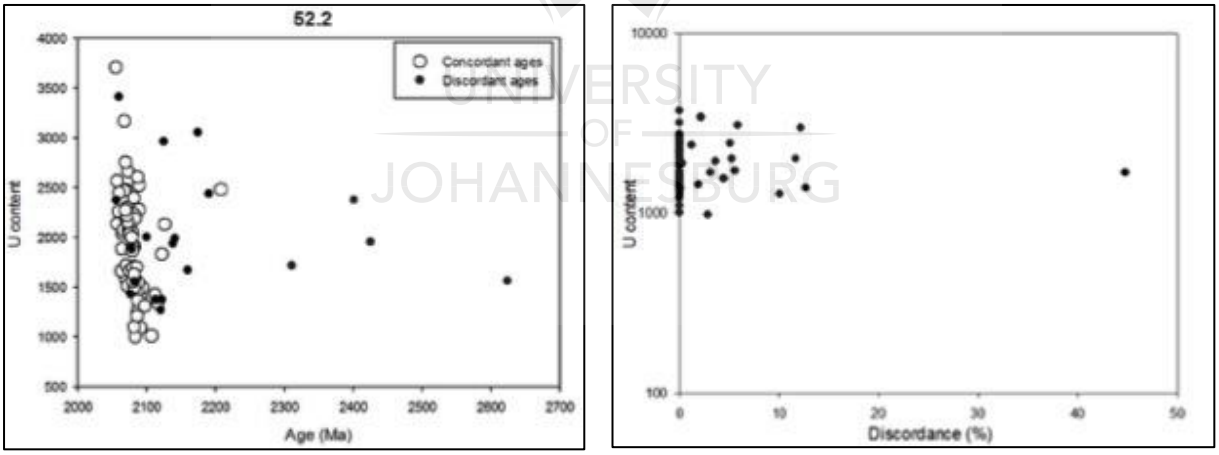

Figure 6.20: (a) Uranium content versus age (b) uranium content versus discordance. These diagrams show no clear correlation between uranium content and discordance.

6.4. Discussion

6.4.1. All Bushveld Complex granites

6.4.1.1. U-Pb results

The concordia diagram of all CPb-free analyses from Bushveld granites samples are displayed in Figure 6.21 a. These analyses indicate that MEPB44 has a higher number of discordant analyses. From both concordia diagrams and weighted average $^{207}Pb/^{206}Pb$ ages for individual samples in sections 6.3, 6.11 and 6.17, it can be deduced that the crystallization age for these Bushveld granites is around 2055 Ma. This is based on the results of sample MEMG12 which gave the statistically superior age at ca. 2055±5 with a MSWD of 0.45. According to Ludwig (2003) and Schoene et al. (2013), an MSWD close to 1 means that the scatter in the analyses is wholly explained by the analytical uncertainty. The other two analysed Bushveld granite samples MEPB44 and 52.2 have ages 2068±2 (MSWD=15) and 2065±2 (MSWD=2.7), which, as a result of their higher MSWD values, are less reliable. Figure 6.17b shows a concordia diagram for both CPb-free and CPb-corrected analyses, and the upper intercept ages calculated by Isoplot are even higher. When compared to MSWD shown in figure 6.17a, the MSWD in Figure 6.21 b is high and this is probably due to the addition of CPb-corrected analyses because according to Ludwig (2003), MSWD values of the regression can be used to correctly reflect CPb uncertainty.

In the previous studies of Bushveld granites, the Nebo granites from the northern lobe of Bushveld Complex and its variants e.g. Makhutso granites found in the central and eastern parts of Bushveld Complex indicated ages around 2055 Ma (e.g. Faurie, 1977; Walraven, 1988; Walraven and Hattingh, 1993). The granites they analyzed are at different locations from where samples from current studies, but they give an idea of the existing age information for these intrusive. Ages younger than 2055 Ma were also obtained in previous studies and they were interpreted to reflect isotopic disturbances (Coetzer et al., 1978; Walraven, 1988). The oldest zircon has an age of 2094±8 (sample MEPB44) and 2088±8 (sample 52.2) for these granites obtained from the current study can be attributed mainly to the presence of common Pb in these granite samples. These ages are comparable to the previously determined ages for Bushveld granites, such as the one determined by Walraven and Hattingh (1993), of 2065±70 Ma for the Klipkloof Granite, eastern Bushveld Complex using the Rb-Sr isotopic system on biotite. Here the explanation was that the initial ratio was too high to be meaningful, however the ages determined by Walraven (1987) are still within

uncertainty of accepted age for Bushveld granites. An age of 2074±9 Ma was determined by Gulson and Jones (1992) using U-Pb on cassiterite.

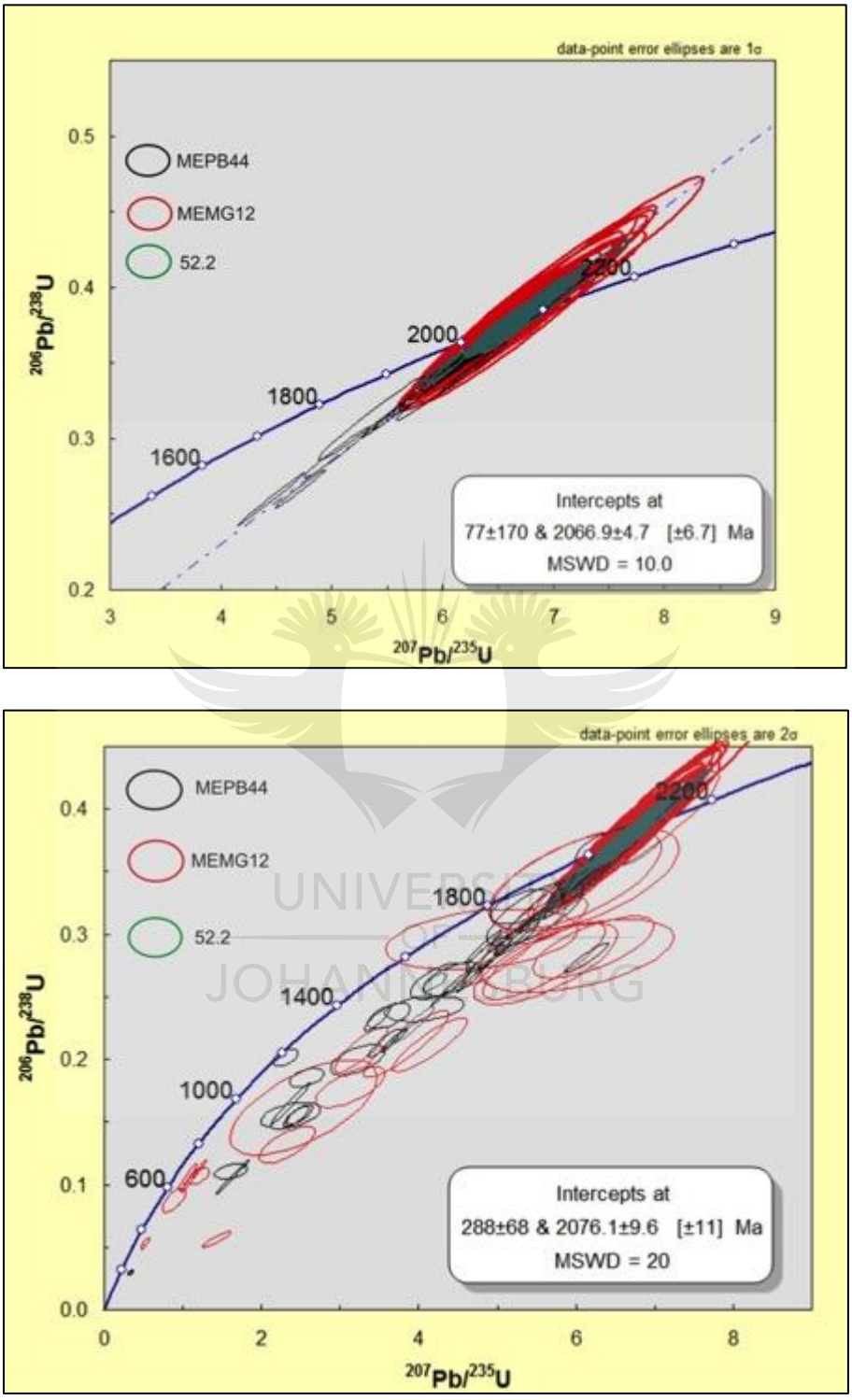

Figure 6.21 Concordia diagrams for analyzed Bushveld Complex granite samples (a) CPb-free analyses (b) both CPb-free and CPb-corrected analyses.

6.4.1.2. Lu-Hf Results

The Lu-Hf results have for the individual samples show initial Hf ratios ranging from 0.2811 to 0.2813 and from 0.2812 to 0.2813 for samples MEPB44 and MEMG12, respectively (refer to figures 6.6 and 6.14). These ratios are consistent with the ratios obtained by Zirakparvar et al. (2014) who analyzed two Bushveld granophyre samples B10-54 and B10-56 although these are found in the eastern limb whereas MEPB44 and MEMG12 are found in western and northern limbs, respectively (Fig. 6.22). The initial Hf ratios for two samples analyzed by Zirakparvar et al. (2014) range between 0.2811 and 0.2812. The average epsilon Hf value for Bushveld granites is -8.3±1.1 and these are comparable to average epsilon Hf value of -8.5±1.8 obtained by Zirakparvar et al. (2014). Figure 6.23 shows initial Hf ratio versus age diagram and the samples show an overlap, and again it is observed from the diagram that the zircon crystals with reset ages, forming a sub-horizontal array are also CPb-corrected.

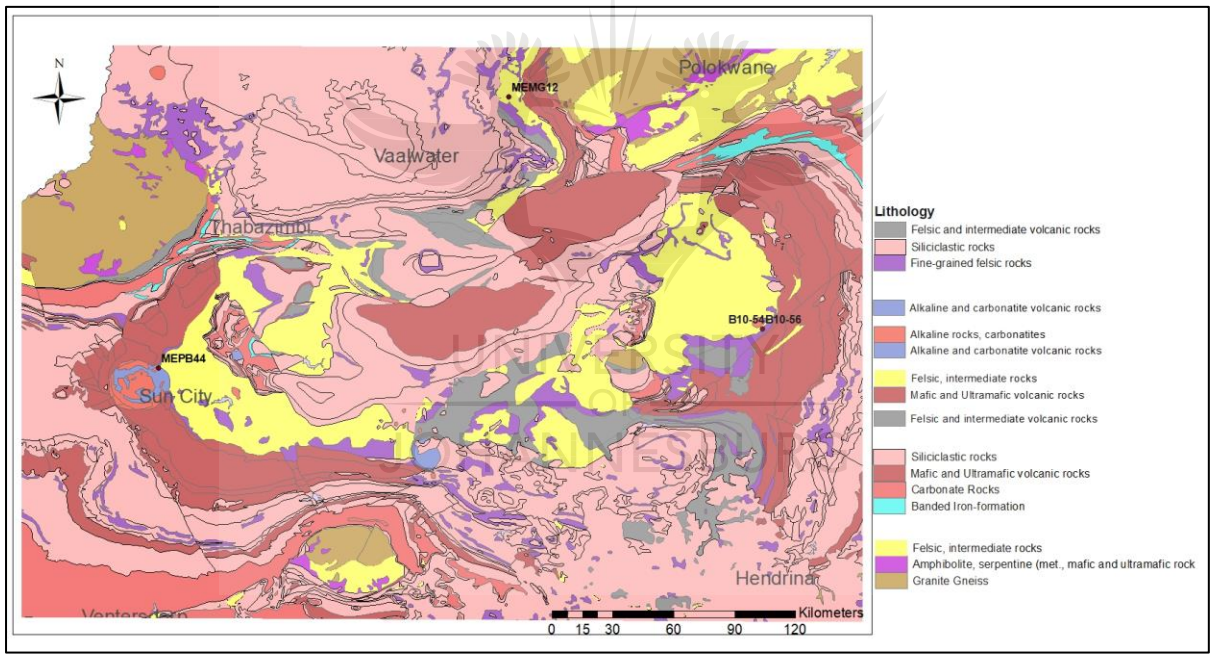

Figure 6.22: Map showing sample locations for MEPB44 and MEMG12 from current study, as well as B10-54 and B10-56.

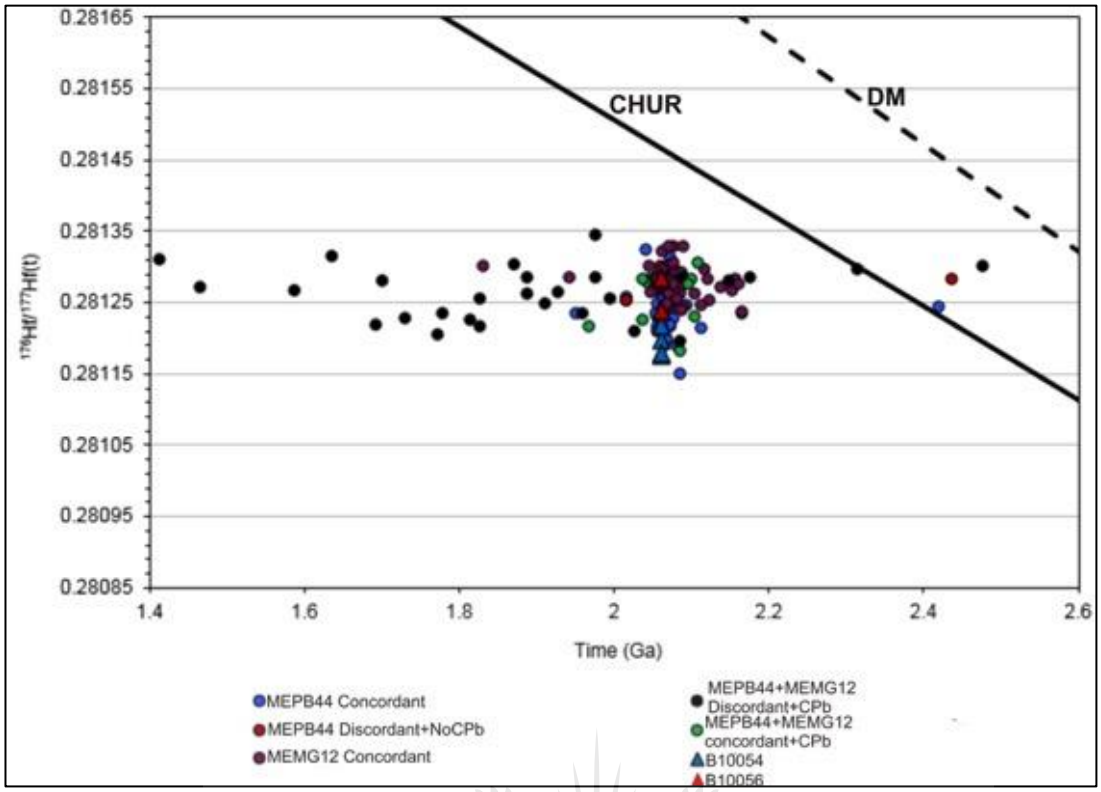

Figure 6.23: $^{176}Hf/^{177}Hf$ ratio versus age diagram showing an overlap in samples MEPB44, MEMG12, B10-54 and B10-56.

6.4.2. Petrographic characteristics

The results from transmitted light microscopy indicate that the Bushveld Complex Granite (MEPB44) north of Pilanesberg complex is highly metasomatized when compared to a more pristine Bushveld granite (MEMG20; see figure 6.1). Sample MEPB44 shows sodic amphibole and epidote occurring in association with hornblende, and they are probably the product of a reaction between hornblende and the fluids, probably from Pilanesberg Complex. Alteration of hornblende to epidote is also observed in the granite intruded by a dolerite dyke (MEMG12). Fenitized Bushveld granite found within Spitskop Complex contains carbonate minerals which occur in close association with silicate minerals.

6.4.3. Zircon characteristics

Zircons from the Bushveld granites are mostly characterized by complex patchy zoning patterns. Zircon grains with patchy zoning have higher discordance percentages than the ones that still maintain their oscillatory zoning (e.g. Fig. 6.2 b, c, I, k, n; Fig. 6.10 a, f, j; Fig. 6.16 g, h). So, the zircon textures observed in CL images can be correlated with the discordance observed in concordia diagrams.

6.4.4. U-Pb data

U-Pb isotopic analyses of the zircons from these Bushveld granites provide both concordant and discordant analyses. These zircons that give discordant ages often contain a high common lead content, but if we focus on analyses of which the CPb content was at background levels, it is clear that these zircons suffered partial lead loss at ca. 0 Ga. The information from U-Pb concordia diagrams, CL and petrography suggests that the zircon signatures in these granites have been affected. Spurious lower intercept ages, the correlation between uranium content and discordance for MEPB44 and MEMG12 as well as abundant fracturing in the zircons support the idea that the amount of lead loss in these samples is influenced by the fluids getting access to metamict zircon grains causing further disturbances in zircon U-Pb isotopic systems. However, there is no clear correlation between uranium content and discordance in the fenitized sample (52-2). Zircon grains that were corrected for common Pb do not follow linear arrays, as would be expected from a single Pb-loss event. Therefore, ages younger than ca. 2055 Ma can be attributed to the common Pb correction, causing further discordance to U-Pb systems. There is no evidence for any influence of the dolerite dyke, assumed to be of Karoo age, on the U-Pb isotope system in MEMG12; like MEPB44, the partial Pb loss occurred at ca. 0 Ga. Most of the zircons in the fenitized granite sample 52.2 are concordant, however a smaller percentage is partially reset at 0 Ga, and there is no evidence for effects from Spitskop complex, which intruded around 1341 Ma (Harmer, 1999). The older ages obtained from the current study can be attributed to the presence of common Pb, and for the ones that seem to be within the common Pb limit; it can also happen that there are some problems with undetected CPb.

6.4.5. Lu-Hf data

The Lu-Hf isotopic results for MEPB44 and MEMG12 indicate that the few discordant analyses observed in the U-Pb concordia diagrams are due to age resetting of grains that have been corrected for common lead, otherwise most of the grains are concordant and form a cluster of points at ages between ca. 2094 and ca. 2055 Ma which is the time for crystallization for these granitoid rocks. There are only small variations in initial Hf ratio versus age suggesting that isotopic resetting affected only the U-Pb system, leaving $^{176}Hf/^{177}Hf$ ratios undisturbed, this is also the case with Bushveld granites analysed by Zirakparvar et al. (2014).

6.4.6. Trace element analyses

Trace element analysis results of zircons in sample MEPB44 indicate that discordant crystals have higher LREE concentrations than concordant analyses, but the correlation is imperfect. Cerium anomalies versus discordance as well as La/Sm ratio vs age diagrams do not show any correlation between these parameters. Based on these observations, there is not enough proof to support that disturbances in U-Pb signatures of zircons are accompanied by modifications in REE concentrations.

Chapter 7

7. Overall discussions and conclusions

The results from this study have clearly indicated the possibility of zircon age resetting on zircons from Archean granites and Transvaal metasediments. Different processes that resulted in partial resetting of zircon ages include metamorphism that is accompanied by recrystallization of metamict zircons; the recrystallization is a result of radiation damage in the zircon lattice. The extent at which the strong thermal metamorphism in the Bushveld Complex influenced zircon age resetting is still in question.

There is however a number of theories that can explain why the influence of the Bushveld thermal overprint is not pronounced even for samples closest to the contact with metamorphic aureole:

- It is observed from U-Pb results from both Archean zircons and detrital zircons from Transvaal metasediments that there are multiple events that resulted in Pb loss. In concordia diagrams for Archean granites, it is even indicated that zircon analyses fall within a triangle between crystallization age, 2.05 and 0 Ga. So, although Bushveld metamorphic event might have been the first to cause zircon age resetting, perhaps the influence of zero-age Pb loss was more conspicuous to see earlier stages of age resetting.
- In terms of the duration of thermal pulse of the Bushveld Complex, there is still a gap in knowledge of how long it actually was, because another explanation could be that maybe the thermal pulse was too short to have an influence on resetting ages. However, through analysing the cooling history of the Bushveld Complex using a computer modelling, Cawthorn and Walraven (1998) suggested that the injection of sequential pulses of magma occurred thoughout 75 000 years. And Cawthorn and Walraven (1998) also postulated that the original temperatures of the pulses were around 1300ºC and they only cooled to 900ºC.
- Another important point is that different parts of zircon (e.g. rims and cores or different zones within zircon) should have been targeted to see the influence of resetting because perhaps only certain domains were affected while some were not.

However, another challenge was small sizes of most zircons, which required ablation of the whole grain.

The younger alkaline intrusions and dolerite intrusions did not have appreciable effects on zircon resetting. Although the petrographic characteristics of the Bushveld Granite sample MEPB44 show evidence for metasomatic effects from the Pilanesberg Complex. Concordia diagrams do not show evidence for partial Pb loss at Pilanesberg age.

It can be concluded that the zircon ages in the current study only show partial resetting because U-Pb isotopic system was partially affected, but none of the analysed samples showed complete age resetting in zircons. Considering that there is not much information that have reported a case of complete zircon resetting, it can be concluded from this study that complete zircon resetting is a rare case. Although the correlation is not perfect, the CL images can provide very useful information regarding the discordance and age resetting observed in U-Pb isotope systems, and again perhaps if multiple ablation sites were chosen in each zircon grain, there would even be clear correlations between zircon textures and discordance observed in U-Pb results.

The Hf isotope system and trace element signatures were not affected by the processes that resulted in zircon age resetting.

Reference List

- Ahrens, L. H. (1955). The convergent lead ages of the oldest monazites and uraninites (Rhodesia, Manitoba, Madagascar, Transvaal). *Geochimica et Cosmochimica Acta* **7**, pp 294-300.

- Albarède, F., Télouk, P., Blichert-Toft J., Boyet, M., Agranier, A., Nelson, B. (2004). Precise and accurate isotopic measurements using multiple-collector ICPMS. *Geochimica et Cosmochimica Acta* **68**, pp 2725-2744.

- Amelin, Y., Lee, D-C., Halliday, A.N., Pidgeon, R.T. (1999). Nature of the Earth's earliest crust from Hafnium isotopes in single detrital zircons. *Nature* **399**, pp 252-255.
- Andersen, T. (2002). Correction of common lead in U–Pb analyses that do not report ^{204}Pb. *Chemical Geology* **192**, pp 59–79.

- Andersen, T., Griffin W.L., Jackson, S.E., Knudsen, T.L., Pearson, N.J. (2004). Mid-Proterozoic magmatic arc evolution at the southwest margin of the basaltic shield. *Lithos* **73**, pp 289-318.

- Andersen, T., Sayeed, A., Gabrielsen, R. H., Olaussen, S. (2011). Provenance characteristics of the Brumunddal sandstone in the Oslo Rift derived from U-Pb, Lu-Hf and trace element analyses of detrital zircons by laser ablation ICMPS. *Norwegian Journal of Geology* **91**, pp 1–19.

- Andersen, T. (2012). Age, Hf isotope and trace element signatures of detrital zircons in the Mesoproterozoic Eriksfjord sandstone, southern Greenland: are detrital zircons reliable guides to sedimentary provenance and timing of deposition? *Geological Magazine* **150(3)**, pp 426-440.

- Andersen, T., Kristoffersen, M. Elburg, M.A. (2017). Visualizing, interpreting and comparing detrital zircon age and Hf isotope data in basin analysis-a graphical approach. *Basin Research* **30**, pp 132-147.

- Andersen, T., Elburg, M.A., Van Niekerk, H.S. (2019). Detrital zircon in sandstones from the Paleoproterozoic Waterberg and Nylstroom basins, South Africa: Provenance and Recycling. *South African Journal of Geology* **122**, pp 1-18.

- Bell, E.A., Boehnke, P., Harrison, T.M. (2016). Recovering the primary geochemistry of Jack Hills zircons through quantitative estimates of chemical alteration. *Geochimica et Cosmochimica Acta* **191**, pp 187–202.

- Belousova, E.A., Griffin, W., O'Reilly, S.Y., Fisher, N. (2002). Igneous zircon: Trace element composition as an indicator of source rock type. *Contributions to Mineralogy and Petrology* **143(5)**, pp 602-622.

- Belousova, E.A., Griffin, W.L., O'Reilly, S.Y. (2006). Zircon crystal morphology, trace element signatures on Hf isotope composition as a tool for petrogenetic modelling: examples from eastern Australian granitoids. *Journal of Petrology* **47**, pp 328-353.

- Benninghoven, A., Rudenauer, F. G. and Werner, H.W. (1987). *Secondary Ion Mass Spectrometry: Basic Concepts, Instrumental Aspects, Applications, and Trends*. Wiley, New York, 1227 pp.

- Bindeman, I.N., Simakin, A.G. (2014). Rhyolites—hard to produce but easy to recycle and sequester: integrating micro-geochemical observations and numerical models. *Geosphere* **10 (5)**, pp 930–957.

- Bindeman, I.N. and Melnik, O.E. (2016). Zircon survival, rebirth and recycling during crustal melting, magma crystallization, and mixing based on numerical modelling. *Journal of Petrology* 57(3), pp 437–460.

- Bingen, B., Austrheim, H., Whitehouse, M. (2001). Ilmenite as a source of zirconium during high grade metamorphism? Textural evidence from the Caledonides of Western Norway and implications of zircon geochronology. *Journal of Petrology* **42**, pp 355-375.

- Black, L.P. (1987). Recent Pb loss in zircon: a natural or laboratory induced phenomenon. *Chemical Geology* **65**, pp 25–33.

- Black, L.P., Kamo, S.L., Williams, I.S., Mundil, R., Davis, D.W., Korsch, R.J., Foudoulis, C. (2003). The application of SHRIMP to Phanerozoic geochronology: a critical appraisal of four zircon standards. *Chemical Geology* **200**, pp 171-188.

- Bleeker, W., Parrish, R.R., Kinsman, A. (1999). High-precision U-Pb geochronology of the Late Archean Kidd Creek deposit and surrounding Kidd volcanic complex. *Society of Economic Geologists* **10**, pp 43-70.

- Boehnke, P., Watson, E.B., Trail, D., Harrison, T.M., Schmitt, A.K. (2013). Zircon saturation re-revisited. *Chemical Geology* **351**, pp 324–334.

- Boggs, S Jr., and Krinsely, D. (2006). Cathodoluminescence features of zircon. *Applications of cathodoluminescence imaging to the study of sedimentary rocks***,** pp 79-81.

- Bomparola, R.M., Ghezzo, C., Belousova, E., Griffin, W.L., O'reilly, S.Y. (2006). Resetting of the U-Pb Zircon System in Cambro-Ordovician Intrusives of the Deep Freeze Range, NorthernVictoria Land, Antarctica. *Journal of Petrology* **48(2)**, pp 327-364.

- Brandl, G. (1986). *The geology of the Pietersburg area*. Explanation of the geological map of South Africa, scale 1:250000, sheet 2328. Ed. by the Geological Survey of South Africa.

- Brögger, W.G. (1921). Die eruptivegestein des kristianiagebietes, IV. *Das fengebiet in telemark. Norvegen. Naturv. Klasse* **9**, pp 150–167.

- Bruguier, O., Lancelot, J.R., Malavieille, J. (1997). U-Pb dating on single detrital zircon grains from the Triassic Songpan-Ganze flysch (Central China): provenance and tectonic correlations. *Earth and Planetary Science Letters* **152**, pp 217-231.

- Bühn, B., Pimentel, M.M., Matteini, M. Dantas, E.L. (2008). High spatial resolution analysis of Pb and U isotopes for geochronology by laser ablation multi-collector inductively coupled plasma mass spectrometry (LA-MC-ICP-MS). *Annals of the Brazilian Academy of Sciences* **81(1)**, pp 99-114.

- Button A. (1976). Stratigraphy and relations of the Bushveld floor in the eastern Transvaal. *Transactions of the Geological Society of South Africa* **79**, pp 3-12.

- Catuneanu, O., and Eriksson P.G. (2002). Sequence stratigraphy of the Precambrian Rooihoogte–Timeball Hill rift succession, Transvaal Basin, South Africa. *Sedimentary Geology* **147,** pp 71-88.

- Cawthorn, G.R. and Walraven, F. (1998). Emplacement and crystallization time for the Bushveld Complex. *Journal of Petrology* **39(9)**, pp 1669-1687.

- Cawthorn, R., Eales, H., Walraven, F., Uken, K., Watkeys, M. (2006). The Bushveld Complex. *The Geology of South Africa* **691**, pp 261-281.

- Cawthorn, G.R., Knight, J., McCarthy T.S. (2015). Geomorphological Evolution of the Pilanesberg. *Landscapes and Landforms of South Africa,* pp 39-46.

- Chen Y-X., Peng, G., Zheng Y.-F. (2015). The anatectic effect on the zircon Hf isotope composition of migmatites and associated granites. *Lithos* **238**, pp 174-184.

- Chew, D.M., Petrus J.A., Kenny, G.G., McEvoy N. (2017). Rapid high-resolution U–Pb LA-Q-ICPMS age mapping of zircon. *Journal of Analytical Atomic Spectrometry* **32(2)**, pp 262-276.

- Clement, S., Compston, W., Newstead, G. (1977). *Design of a large, high resolution ion microprobe*. Research School of Earth Sciences: The Australian National University Canberra ACT 0200 Australia, pp 1-6.

- Coertze, F.J., Burger, A.J., Walraven, F., Marlow, A.L., MacCaski, D.R. (1978). Field relationships and age determinations in the Bushveld Complex. *Transitions of the Geological Society of South Africa* **6**, pp 1-11.

- Compston, W. and Kröner, A. (1988). Multiple zircon growth within early Archean tonalitic gneiss from the Ancient Gneiss Complex, Swaziland. *Earth Planetary Science Letters* **87**, pp 13-28.

- Craw, D., Koons, P.O., Horton, T., Chamberlin, C.P. (2002). Tectonically driven fluid flow and gold mineralization in active collisional orogenic belts: Comparison between New Zealand and western Himalaya. *Tectonophysics* **348**, pp135–153.

- Cui, X., Nabelek, P.I., Liu, M. (2001). Heat and fluid flow in contact metamorphic aureoles with layered and transient permeability, with application to the Notch Peak aureole, Utah. *Journal of Geophysical Research* **106**, pp 6477-6491.

- Daly, S.J., Fanning, C.M., Fairclough, M.C. (1998). Tectonic evolution and exploration potential of the Gawler Craton, South Australia. *AGSO Journal of Australian Geology and Geophysics* **17**, pp 145–168.

- Davis, D.W., Williams, I.S., Krogh, E.T. (2003). Historical Development of Zircon Geochronology. *Reviews in Mineralogy and Geochemistry* **53**, pp 145-181.

- De Wit, M. J., Roering, C., Hart, R.J. (1992). Formation of an Archaean continent. *Nature***, 357(6379)**, 553-562.

- Dickin, A.P. (2005). *Radiogenic Isotope Geology*, *2nd edition*. Cambridge, UK: Cambridge University Press.

- Dickson, J.E. and Hess, P.C. (1982). Zircon saturation in lunar basalts and granites. *Earth Planetary Science Letters* **57**, pp 366-344.

- Dietrich, R.V. (1968). Behaviour of zirconium in certain artificial magmas under diverse P-T conditions. *Lithos* **1**, pp 20–29.

- Dorland, H.C. (2004). *Provenance Ages and Timing of Sedimentation of Selected Neoarchean and Paleoproterozoic Successions on the Kaapvaal craton* (PhD thesis (unpublished)). Rand Afrikaans University, 326 p.

- Dorland, H.C., Beukes, N.J., Gutzmer, J., Evans, D.A.D., Armstrong, R.A. (2004). Trends in detrital zircon provenance from Neoarchaean-Palaeoproterozoic sedimentary successions on the Kaapvaal craton: *Abstract volume, Geoscience Africa 2004 Congress, Geological Society of South Africa, Johannesburg*, pp 176-177.

- Dowman, E., Wall, F., Treloar, P.J., Rankin, A.H. (2017). Rare earth mobility as a result of multiple phases of fluid activity in fenite around the Chilwa Island Carbonatite, Malawi. *Mineralogical Magazine* **81**, pp 1367-1395.

- Duncan, R.A., Hooper, P.R., Rehacek, J., Marsh, J.S., Duncan, A.R. (1997). The timing and duration of the Karoo igneous event, southern Gondwana. *Journal of Geophysical Research* **102**, pp 127-138.

- Eglington, B.M. and Harmer, R.E. (1993). A review of the statistical principles of geochronometry: Additional concepts pertinent to radiogenic U-Pb studies. *South African Journal of Geology* **96**, pp 9-21.

- Eglington, B.M. and Armstrong R.A. (2004). The Kaapvaal Craton and adjacent orogens, southern Africa: a geochronological database and overview of the geological development of the craton. *South African Journal of Geology* **107(1-2),** pp 13-32.

- Elburg, M. and Goldberg, A. (2000). Age and geochemistry of Karoo dolerite dykes from northeast Botswana. *Journal of African Earth Sciences* **31**, pp 539–554.

- Elburg, M.A. and Cawthorn, G. (2017). Source and evolution of the alkaline Pilanesberg Complex, South Africa. *Chemical Geology* **455**, pp 148–165.

- Eriksson, P.G., Altermann, W. & Hartzer, F.J. (2006). The Transvaal Supergroup and Precursors. In: Johnson, MR., Annhaeusser, CR. Thomas, RJ. (Editors): *The Geology of South Africa. Geol. Society of South Africa*, pp 237-260.

- Faure, G. (1977). *Principles of Isotope Geology. 3rd ed*ition, John Wiley & Sons, Inc., New York.

- Feng, R., Machado, N., Ludden, J. (1993). Lead geochronology of zircon by laser-inductively coupled plasma mass spectrometry (ICP-MS). *Geochimica et Cosmochimica Acta* **57**, pp 3479-3486.

- Finch R.J., Hanchar, J.M. (2003). Structure and chemistry of zircon and zircon-group minerals. In: Hanchar JM, Hoskin PWO (eds) Zircon. *Mineralogical Society of America Reviews in Mineralogy & Geochemistry* **53**, pp 1-25.

- Fisher, C.M., Vervoort, J.D., Hanchar, J.M. (2014). Guidelines for reporting zircon Hf isotopic data by LA-MC-ICPMS and potential pitfalls in the interpretation of these data. *Chemical Geology* **363**, pp 125-133.

- Fraser, G., Ellis, D., Eggins, S. (1997). Zirconium abundance in granulite-facies minerals, with implications for zircon geochronology in high-grade rocks. *Geology* **25**, pp 607–610.

- Friend, C.R.L. and Nutman, A.P. (1992). Response of zircon U−Pb isotopes and whole-rock geochemistry to CO_2 fluid-induced granulite-facies metamorphism, Kabbaldurga, Karnataka, South India. *Contributions to Mineralogy and Petrology 111***(3)**, pp 299–310.

- Friese, A.E.W., Charlesworth, E.G., McCarthy, T.S. (1995). Tectonic processes within the Kaapvaal Craton during Kibaran orogeny: structural, geophysical and isotopic constraints from the Witwatersrand basin and environments. *University of the Witwatersrand, Economic Geology Research* Unit **292**, 79 pp.

- Frith, R.A. (1993). Precambrian geology of Indin Lake map area. *Geological survey of Canada* **1243**, pp 1-81.

- Frondel, C., and Collette, R.L. (1957). Hydrothermal synthesis of zircon, thorite and huttonite. *American Mineralogist*, **42**, pp 759 -765.

- Fryer, B. J., Jackson, S. E., Longerich, H. (1993). The application of laser ablation microprobe-inductively coupled plasma-mass spectrometry (LAM-ICP-MS) to *in situ* U-Pb geochronology. *Chemical Geology* **109**, 1-8.

- Garven, G. (1985). The role of regional fluid flow in the genesis of the Pine Point deposit, Western Canada sedimentary basin. *Economic Geology and the Bulletin of the Society of Economic Geologists* **80**, p. 307–324.

- Gebauer, D. Griffiths, B.J., Grünenfelder, M. (1981). U-Pb zircon and monazite dating of a mafic-ultramafic complex and its country rocks. *Contributions to Mineralogy and Petrology* **76**, pp 292-300.

- Geisler, T., Ulonska, M., Schleicher, H., Pidgeon, R. T., van Bronswijk, W. (2001). Leaching and differential recrystallization of metamict zircon under experimental hydrothermal conditions. *Contributions to Mineralogy and Petrology* **141**, pp 53-65.

- Geisler, T., Schaltegger, U., Tomaschek, F. (2007). Re-equilibration of zircon in aqueous fluids and melts. *Elements* **3**, pp 43–50.

- Gentry, R.V., Soworksi, T.S., McKown, H.S., Smith, D.H., Eby, R.E., Christie, W.H. (1982). Differential lead retention in zircons: implications for nuclear waste containment. *Science* **216**, pp 296-298.

- Gerdes, A. and Zeh, A. (2009). Zircon formation versus zircon alteration: new insights from combined U–Pb and Lu–Hf in-situ LA-ICP-MS analyses, and consequences for the interpretation of Archean zircon from the Central Zone of the Limpopo Belt. *Chemical Geology* **261**, pp 230-243.

- Gervasoni, F., Klemme, S., Roch-Junior, E.R.V., Berndt, J. (2016). Zircon saturation in silicate melts: a new and improved model for aluminous and alkaline melts. *Contributions to Mineralogy and Petrology* **171**, pp 1-12.

- Goldich, S. S. and Mudrey, M. G. Jr. (1975). Dilatancy model for discordant U-Pb zircon ages. In: *Recent contributions to geochemistry and analytical chemistry (*ed.: A. I. Tugarinov), New York, John Wiley & Sons, pp 466-470.

- Gose, W.A., Hanson, R.E., Harmer, R.E., Seidel, E.K. (2013). Reconnaissance paleo-magnetic studies of Mesoproterozoic alkaline igneous complexes in the Kaapvaal craton, South Africa. *Journal of African Earth Sciences* **85**. pp 22–30.

- Grauert, B., Hall, L.M. (1974). Rb-Sr isotopic study on small whole rock slabs and their minerals from the Manhattan Schist,New York. *Carnegie Institution of Washington Publication* **73**, pp 1007-1010.

- Guitreau, M., Blichert-Toft, J., Martin, H., Mojzsis, S.J., Albarède, F. (2012). Hafnium isotope evidence from Archean granitic rocks for deep-mantle origin of continental crust. *Earth Planetary Science Letters* **338**, pp 211–223.

- Guitreau, M., Blichert-Toft, J., Mukasa, S.B., Fahnestock, M.F. (2016). Pikes Peak batholith (Colorado, USA) revisited: A SIMS and LA-ICP-MS study of zircon U-Pb ages combined with solution. *Precambrian Research* **280**, pp 179-194.

- Gulson, B.L. and Krogh, T.E. (1975). Evidence of multiple intrusion, possible resetting of U-Pb ages, and new crystallization of zircons in the post-tectonic intrusions (`Rapakivi granites') and gneisses from South Greenland. *Geochimica et Cosmochimica Acta* **39**, pp 65-72.

- Gumsley, A.P., Chamberlain, K.R., Bleeker, W., Soderlund, U., de Kock, M.O., Larsson, E.R., Bekker, A. (2017). Timing and tempo of the Great Oxidation Event. *Proceedings of the National Academy of Sciences of the United States of America* **114**, pp 1811-1816.

- Hanson, R.B. (1995). The hydrodynamics of contact metamorphism, *Geological Society of America Bulletin* **107**, pp 595-611.

- Harley, S.L. and Kelly, N.M. (2007). Zircon tiny but timely. *Elements* **3**, pp 13–18.

- Harley, SL., Kelly, N.M., Moller A. (2007). Zircon behaviour and thermal histories of mountain chains. *Elements* **3**, pp 25–40.

- Harlov, D.E. and Dunkley, D. (2010). Experimental high-grade alteration of zircon using alkali and Ca-Bearing Solutions: Resetting geochronometer during metasomatism. *AGU Fall Meeting, San Francisco* **Abstract V41D-2301,** pp 68-90.

- Harlov, D. and Austrheim, H. (2013): Metasomatism and the chemical transformation of rock: Rock-mineral-fluid interaction in terrestrial and extraterrestrial environments. - In: Harlov, D., Austrheim, H. (Eds.), *Metasomatism and the chemical transformation of rock: The role of fluids in terrestrial and extraterrestrial processes*, (Lecture Notes in Earth System Sciences), Springer, pp. 1—16.

- Harmer, R.E. (1992). *The geochemistry of Spitskop and related alkaline complexes*. Ph.D. Thesis, University of Cape Town, 287 pp.

- Harmer, R.E. and Gittins, J. (1997). The origin of dolomitic carbonatites: field and experimental constraints. *Journal of African Earth Sciences* **25**, pp 5-28.

- Harmer, R.E. (1999). The Petrogenetic Association of Carbonatite and Alkaline Magmatism: Constraints from the Spitskop Complex, South Africa. *Journal of Petrology* **40(4),** pp 525-548.

- Harmer, R. E. and Armstrong, R.A. (2000). Duration of Bushveld Complex magmatism: constraints from new SHRIMP zircon chronology. *Workshop on the Bushveld Complex*. Gethane Lodge, Burgersfort, University of the Witswatersrand, Johannesburg.

- Harris, N., McMillan, A., Holness, M., Uken, R., Watkeys, M., Rogers, N., Fallick, A. (2003). Melt Generation and Fluid Flow in the Thermal Aureole of the Bushveld Complex. *Journal of Petrology* **44**, pp 1031–1054.

- Hay, D.C. and Dempster, T.J. (2009). Zircon behaviour during low-temperature metamorphism. *Journal of Petrology* **50**, pp 571-589.

- Heinonen, A.P., Andersen, T., Rämö, O.T. (2010). Source constraints from the Hf isotope composition of zircon in the rapakivi granites and associated mafic rocks of southern Finland. *Journal of Petrology* **51**, pp 1687–1709.

- Henderson, D. R., Long, L. E., Barton, J. M. (2000). Isotopic ages and chemical and isotopic compositions of the Archean Turfloop batholith, Pietersburg granite-greenstone terrane, Kaapvaal Craton, South Africa. *South African Journal of Geology* **103**, pp 38-46.

- Hofmann, A.W. (2014). Sampling Mantle Heterogeneity through Oceanic Basalts: Isotopes and Trace Elements. *Treatise on Geochemistry* **3**, pp 67-101.

- Högdahl, K., Gromet, L.P., Broman, C. (2001) Low P-T Caledonian resetting of U-rich Paleoproterozoic zircons, central Sweden. *American Mineralogist*, **86**, 534–546.

- Holmes, A. (1954). The oldest dated minerals of the Rhodesia Shield. *Nature* **173**, pp 612–617.

- Horstwood, M.S.A., Foster, G.L., Parrish, R.R., Noble, S.R., Nowell, G.M. (2003). Common-Pb corrected in situ U-Pb accessory mineral geochronology by LA-ICP-MS. *Journal of Analytical Atomic Spectrometry* **18(8)**, pp 837-846.

- Hoskin, P.W.O. and Black, L.P. (2000). Metamorphic zircon formation by solid state recrystallization of protolith igneous zircons. *Journal of Metamorphic Geology* **18**, 423-439.

- Hoskin, P.W.O. and Schaltegger, U. (2003). The composition of zircon and igneous and metamorphic petrogenesis. In: Hanchar JM, Hoskin PWO (eds) Zircon. *Mineralogical Society of America Reviews in Mineralogy & Geochemistry* **53**, pp 27-62.

- Huhma, H., Mänttäri, I., Peltonen, P., Kontinen, A., Halkoaho, T., Hanski, E., Hokkanen, T., Hölttä, P., Juopperi, H., Konnunaho, J., Layahe, Y., Luukkonen, E., Pietikäinen, K., Pulkkinen, A., Sorjonen-Ward, P., Vaasjoki, M., Whitehouse, M. (2012). The age of the Archaean greenstone belts in Finland. *Geological Survey of Finland, Special Paper* **54**, pp 74–175.

- Hunter, D. R. (1976). Some enigmas of the Bushveld Complex. *Economic Geology* **71**, pp 229-248.

- Ireland, T.R. and Williams, I.S. (2003) Considerations in zircon geochronology by SIMS. *Reviews in Mineralogy and Geochemistry* **53**, pp 215-241.

- Jackson, S.E., Pearson, N.J., Griffin, W.I., Belousova, E.A. (2004). The application of laser ablation inductively coupled plasma mass spectrometry to *in situ* U-Pb zircon geochronology. *Chemical Geology* **211**, pp 44-69.

- James, D.E., Niu, F., Rokosky, J. (2003). Crustal structure of the Kaapvaal craton and its significance for early crustal evolution. *Lithos* **71**, pp 413 – 429.

- Jago, B.C. and Gittins, J. (1991). The role of fluorine in carbonatite magma evolution. *Nature* **349**, 56-58.

- Janardhan, A. S., Newton, R. C., Hansen, E. C. (1982). The transformation of amphibolite facies gneiss to charnockite in southern Karnataka and northern Tamil Nadu, India. *Contributions to Mineralogy and Petrology* **79**, pp 130-149.

- Johnston, S., Gehrels, G., Valencia, V., Ruiz, J. (2008). Small volume U-Pb zircon geochronology by laser ablation multicollector ICP-MS. *Chemical Geology*, pp 1-12.

- Kamo, S.L., Czamanske, G.K., Krogh, T.E. (1996). A minimum U-Pb age for Siberian flood-basalt volcanism. *Geochimica et Cosmochimica Acta* **60**, pp 3505-3511.

- Kempe, U., Grunder, T., Nasdala, L., Wolf, D. (2000). Relevance of cathodoluminescence for the interpretation of U–Pb zircon ages, with an example of an application to a study of zircons from the Saxonian Granulite Complex, Germany. In Pagel, M., V. Barbin, P. Blanc, and D. Ohnenstetter (eds.), *Cathodoluminescence in Geosciences*, Berlin, *Springer-Verlag*, pp 415–455.

- Kielman, R. B., Nemchin, A. A., Whitehouse, M. J., Pidgeon, R. T., Bellucci, J. J. (2018). U-Pb age distribution recorded in zircons from Archean quartzites in the Mt. Alfred area, Yilgarn Craton, Western Australia. *Precambrian Research* **310**, pp 278-290.

- Kilic, A.D. (2016). Investigation of zircon by cathodoluminescence and Raman Spectroscopy. *Earth and Environmental Science* **44**, pp 1-6.

- Kinny, P.D., Compston, W., Williams, I.S. (1991). A reconnaissance ion-probe study of hafnium isotopes in zircons. *Geochimica et Cosmochimica Acta* **55**, pp 849–859.

- Kinny, D.P. and Maas, R. (2003). Lu–Hf and Sm–Nd isotope systems in zircon. *Reviews in Mineralogy and Geochemistry* **53(1)**, pp 327-341.

- Kita, N.T., Ushikubo, T., Fu, B., Valley, J.W. High precision SIMS oxygen isotope analysis and the effect of sample topography. *Chemical Geology* **264**, pp 43–57.

- Kober, B. (1986). Whole-grain evaporation for $^{207}Pb/^{206}Pb$ age investigations on single zircons using a double-filament thermal ion source. *Contributions to Mineralogy and Petrology* **93**, pp 482-490.

- Kohn, M.J., Corrie, S.L., Markely, C. (2015). The fall and rise of metamorphic zircon. *American Mineralogist* **100**, pp 897–908.

- Kooijman, E., Upadhyay, D., Mezger, K., Reith, M.M., Berndt, J., Srikantappa, C. (2011). Response of the U–Pb chronometer and trace elements in zircon to ultrahigh-temperature metamorphism: The Kadavur anorthosite complex, southern India. *Chemical Geology* **290**, pp 177-188.

- Kramers, J., Frei, R., Newville, M., Kober, B., Villa, I. (2009). The valency state of radiogenic lead in zircon and its consequences. *Chemical Geology* **261**, pp 4-11.

- Kramers, J.D., Henzen, M., Steidle, L. (2014). Greenstone belts at the northernmost edge of the Kaapvaal Craton: Timing of tectonic events and a possible crustal fluid source. *Precambrian Research* **253**, pp 96-113.

- Kretz, R. (1983). Symbols for rock forming minerals. *American Mineralogist* **68**, pp 277-279.

- Krogh, T.E. (1982). Improved accuracy of U-Pb zircon ages by creation of more concordant systems using an air abrasion technique. *Geochimica et Cosmochimica Acta* **46**, pp 637-649.

- Kröner, A., Jaeckel, P., Brandl, G. (2000). Single zircon ages for felsic to intermediate rocks from the Pietersburg and Giyani Greenstone belts and bordering

granitoid orthogneisses, northern Kaapvaal Craton, South Africa. *Journal of African Earth Sciences* **30**, pp 773-793.

- Kylander-Clark, A.R.C. (2017). Petrochronology by Laser-Ablation Inductively Coupled Plasma Mass Spectrometry. *Reviews in Mineralogy and Geochemistry* **83(1)**, pp183-198.

- Laurent, O., Paquette, J-L., Martin, H., Doucelance, R., Moyen, J-F. (2013). LA-ICP-MS dating of zircons from Meso- and Neoarchean granitoids of the Pietersburg block (South Africa): Crustal evolution at the northern margin of the Kaapvaal craton. *Precambrian Research* **230**, pp 209-226.

- Laurent, O., and Zeh, A. (2015). A linear Hf isotope-age array despite different granitoid sources and complex Archean geodynamics: Example from the Pietersburg block (South Africa). *Earth and Planetary Letters* **430**, pp 426-338.

- Lin, J., Liu, Y., Yang, Y., Hu, Z. (2016). Calibration and correction of LA-ICP-MS and LA-MC-ICP-MS analyses for element contents and isotopic ratios. *Solid Earth Sciences* **1**, pp 5-27.

- Liermann, H-P., Isachsen, C., Altenberger, U., Oberhänsli, R. (2002). Behavior of zircon during high-pressure, low-temperature metamorphism: Case study from the Internal Unit of the Sesia Zone. *European Journal of Mineralogy* **14**, pp 61–71.

- Lovering, J.F., Travis, G.A., Comaford, D.J, Kelly, P.R. (1981). Evolution of the Gondwana Archean shield: zircon dating by ion microprobe, and relationships between Australia and Wilkes Land, in Glover, J.E. and Groves, D.I. (Eds.). Archean Geology. *Geological Society of Australia, Special Publication* **7**, pp 193-203.

- Ludwig, K.R. (2003). Isoplot 3.0-a geochronological toolkit for Microsoft excel. *Berkeley Geochron Center, Berkeley*, special publication **4,** 70 p.

- Lurie, J. (1986). Mineralization of the Pilanesberg Alkaline Complex. In: Anhaeusser, C.R., and Maske, S. (Eds). Mineral Deposits of Southern Africa II. *Geological Society of South Africa,* 2376 p.

- Mapeo, R.B.M., Armstrong, R.A., Kampunzu, A.B., Modisi, M.P., Ramokate, L.V., Modie, B.N.J. (2006). A ca. 200 Ma hiatus between the Lower and Upper Transvaal Groups of southern Africa: SHRIMP U-Pb detrital zircon evidence from the Segwagwa Group, Botswana: Implications for Paleoproterozoic glaciations: *Earth and Planetary Science Letters* **244**, pp 113-132.

- Mark, D.F., Parnell, J., Kelley, S.P., Sherlock, S.C. (2007). Resolution of regional fluid flow related to successive orogenic events on the Laurentian margin. *Geology* **35**, pp 547–550.

- Mattinson, J.M. (2005). Zircon U–Pb chemical abrasion ("CA-TIMS") method: Combined annealing and multi-step partial dissolution analysis for improved precision and accuracy of zircon ages. *Chemical Geology* **220**, pp 47-66.

- McDonough, W.F., Sun, S., Kingwood, A.E., Jagoutz, E., Hofmann, A.W. (1991). K, Rb and Cs in the earth and moon, and evolution of the Earth's mantle. *Geochemica et Cosmochimica Acta*, Ross Taylor symposium volume, pp 183.

- Mezger, K. & Krogstad, E.J. (1997). Interpretation of discordant U-Pb zircon ages: An evaluation. *Journal of Metamorphic Geology* **15**, pp 127-140.

- Möller, A., O'Brien, P. J., Kennedy, A., Kroner, A. (2003). Linking growth episodes of zircon and metamorphic textures to zircon chemistry: an example from the ultrahigh-temperature granulites of Rogaland (SW Norway). In Geochronology: Linking the Isotopic Record with Petrology and Textures (eds). *Geological Society of London, Special Publication* **220**, pp 65–81.

- Morgan, A.J. (1985). X-ray microanalysis in electron microscopy for biologists. *Royal Microscopical Society* **5**, pp 79.

- Morris, G.A., Kirkland, C.L., Pease, V. (2015). Orogenic palaeofluid flow recorded by discordant detrital zircons in in the Caledonian foreland basin of northern Greenland. *Lithosphere* **7(2)**, pp 138-143.

- Mukasa, S.B., Choi, S.H., Andronikov, A.V., Osanai, Y. Harley, S.L., Kelly, N.M. (2007). Lu-Hf systematics of ultra-high temperature Napier Complex. East Antarctica: Evidence for early Archean differentiation of Earth's mantle. *U.S. Geological Survey and National Academics: 10th International Symposium on Antarctica Earth Sciences,* pp 1-4.

- Mundil, R., Ludwig, K.R., Metcalfe, I., Renne, P.R. (2004). Age and timing of the Permian mass extinctions: U/Pb dating of closed system zircons. *Science* **305**, pp 1760 – 1763.

- Murakami, T., Chakoumakos, B.C., Ewing, R.C., Lumpkin, G.R., Weber, W.J. (1991). Alpha-decay event damage in zircon. *American Mineralogist* **76**, pp 1510-1532.

- Nardi, L.V.S., Formoso, M.L.L., Muller, I.F., Fontana, E., Jarvis, K., Lamarao, C. (2013). Zircon/rock partition coefficients of REEs, Y, Th, U, Nb, and Ta in granitic

rocks: Uses for provenance and mineral exploration purposes. *Chemical Geology* **335**, pp 1-7.

- Nasdala, L., Irmer, G., Wolf, D. (1995). The degree of metamictization in zircon: A Raman spectroscopic study. *European Journal of Mineralogy* **7**, pp 471-478.

- Nasdala, L., Wenzel, M, Vavra, G., Irmer, G., Wenzel, T., Kober, B. (2001). Metamictization of natural zircons: Accumulation versus thermal annealing of thermal radioactivity radiation damage. *Contributions to Mineralogy and Petrology* **141**, pp 125-144.

- Nasdala, L., Lengauer, C.L., Hanchar, J., Kronz, A., Wirth, R., Blanc, P., Kennedy, A.K., Seydoux-Guillaume, A-M. (2002). Annealing radiation damage and the recovery of cathodoluminescence. *Chemical Geology* **191**, pp 121-140.

- Nagasawa, H. (1970). Rare earth concentrations in zircons and apatites and their host dacites and granites. *Earth Planetary Science Letters* **9**, pp 359-364.

- Nell, J. (1985). The Bushveld metamorphic aureole in the Potgietersrus area; evidence for a two-stage metamorphic event. *Chemical Geology* **80**, pp 1129-1152.

- Nelson, D.R., Chivas, A.R., Chappell, B.W., McCulloch, M.T. (1988): Geochemical and isotopic systematics of carbonatites and implications for the evolution of ocean island sources. *Geochimicca et Cosmochimica* Acta **52**, pp 1-17.

- Nesbitt, B.E. and Muehlenbachs, K. (1994). Paleohydrogeology of the Canadian Rockies and the origins of brines, Pb-Zn deposits and dolomitization in the Western Canadian sedimentary basin. *Geology* **22**, pp 243–246.

- Oliver, J. (1986). Fluids expelled tectonically from orogenic belts: Their role in hydrocarbon migration and other geologic phenomena. *Geology* **14**, pp 99–102.

- Olsson, J.R., Hamilton, M.A., Klausen, M.B., Soderlund, U., Helffrich, G.R. (2011). A late Archean radiating dyke swarm as possible due to the origin of the Bushveld Complex. *Nature Geoscience* **4**, pp 865-869.

- Öztürk, A., Nex, P., Kinnaird, J. (2017). Fenites from the Upper Zone and Nebo granites of the Bushveld Complex in the aureole of the Spitskop Complex. *The 9th Igneous and Metamorphic Studies Group Meeting* **9**, pp 63.

- Pagel, M., Barbin, V., Blanc, P., Ohnenstetter, D. (2000). *Cathodoluminescence in geoscience.* Springer-Verlag, Berlin, Germany, 523 p.

- Pan, Y. (1997). Zircon- and monazite- forming metamorphic reactions at Manitouwadge, Ontario. *The Canadian Mineralogist* **35**, pp 105-l18.

- Parrish, R.R. (1989). U-Pb geochronology of the Cape Smith Belt and Sugluk block, northern Quebec. *Geoscience Canada* **16**, pp 126-130.

- Parrish, R.R., and Noble, S.R. (2003). Zircon U-Th-Pb Geochronology by Isotope Dilution – Thermal Ionization Mass Spectrometry (ID-TIMS). In: Hanchar J.M., and Hoskin, P.W.O (Eds), Zircon. *Reviews in Mineralogy and Geochemistry* **53**, pp 183–213.

- Patchett, P. J. and Tastumoto, M. (1980). Hafnium isotope variations in oceanic basalts. *Geophysical Research Letters* **7**, pp 1077–1080.

- Patchett, P.J., Kouvo, O., Hedge, C. E., Tatsumoto, M. (1981). Evolution of Continental crust and mantle heterogeneity: Evidence from Hf isotopes. *Contributions to Mineralogy and Petrology* **778**, pp 279–297.

- Patchett, P. J. (1983). Importance of the Lu-Hf isotope system in studies of planetary chronology and chemical evolution. *Geochimica et Cosmochimica Acta* **47**, pp 81–91.

- Piazolo, S., Belousova, E., La Fontaine, A., Corcoran, C., Cairney, J.M. (2017). Trace element homogeneity from micron- to atomic scale: Implication for the suitability of the zircon GJ-1 as a trace element reference material. *Chemical Geology* **456**, pp 10-18.

- Pidgeon, T.T. (1992). Recrystallisation of oscillatory zoned zircon: some geochronological and petrological implications. *Contributions to Mineralogy and Petrology* **110(4)**, pp 463–472.

- Pidgeon R.T., O'Neil, J.R., Silver, L.T. (1966). Uranium and lead isotopic stability in metamict zircon under experimental hydrothermal conditions. *Science* **154**, pp 1538-1542.

- Pidgeon, R.T., Nemchin, A.A., Cliff, J. (2013). Interaction of weathering solutions with oxygen and U–Pb isotopic systems of radiation-damaged zircon from an Archean granite, Darling Range Batholith, Western Australia. *Contributions to Mineralogy and Petrology* **166**, pp 511–523.

- Pidgeon, R.T. Chapman, P.G., Denisik, M, Nemchin, A. (2017). Dry annealing of metamict zircon: A differential scanning calorimetry study. *American Mineralogist* **102**, pp 1066-1072.

- Poitrasson, F., Hanchar, J.M., Schaltegger, U. (2002). The current state and future of accessory mineral research. *Chemical Geology* **191**, pp 3–24.

- Poller, U. (2000). A combination of single zircon dating by TIMS and cathodoluminescence investigations of the same grain: the CLC method – U–Pb geochronology for metamorphic rocks. In Pagel, M., V. Barbin, P. Blanc, and D. Ohnenstetter (eds.), *Cathodoluminescence in Geosciences, Berlin, Springer-Verlag*, pp 401–14.

- Poujol, M., Robb, L.J., Anhaeusser, C.R, Gericke, B. (2002). Geochronological constrains on the evolution of the Kaapvaal Craton, South Africa. *Economic Geology Research Institute* **360**, pp 1-21.

- Press. W.H., Flannery, B.P., Teukolsky, S.A., Venerling, **VI/.T., 1992, Numerical Recipes,** Cambridge. UK, Cambridge University Press. 994 pp.

- Prieto, M. (2009). Thermodynamics of solid solution-aqueous solution systems. *Reviews in Mineralogy and Geochemistry* **70**, pp 47-85.

- Puga, E., Fanning, C.M., Nieto, J.M., De Federico, A.D. (2005). Recrystallization textures in zircon generated by ocean-floor and eclogite-facies metamorphism: a cathodoluminescence and U–Pb SHRIMP study, with constraints from REE elements. *The Canadian Mineralogist* **43(1)**, pp 183-202.

- Putnis, A. (2002). Mineral replacement reactions: from macroscopic observations to microscopic mechanisms. *Mineralogical Magazine* **66(5)**, pp 689-708.

- R Core Team (2014). *R: A Language and Environment for Statistical Computing*. R Foundation for Statistical Computing, Vienna, http://www.R-project.org.

- Rasmussen, B., Fletcher, I.R., Muhling, J.R., Mueller, A.G., Hall, G.C. (2007). Bushveld-aged fluid flow, peak metamorphism, and gold mobilization in the Witwatersrand basin, South Africa: Constraints from in situ SHRIMP U-Pb dating of monazite and xenotime. *Geology* **35**: pp 931–934.

- Reddy, S.M., Timms, N.E., Pantleon, W., Trimby, T. (2007). Quantitative characterization of plastic deformation of zircon and geological implications. *Contributions to Mineralogy and Petrology* **153**, pp 625–645.

- Reddy, S.M., Timms, N.E. (2010). Deformation of zircon and implications for geochemistry and geochronology, source abstracts with programs. *Geological Society of America* **42(5)**, pp 634.

- Reimink, J., Davies, J., Waldron, J.W. F., Rojas, X. (2016). Dealing with discordance: A novel approach for analysing U–Pb detrital zircon datasets. *Journal of the Geological Society, London* **173(4)**, pp 2015-114.

- Retief, E.A. (1963). Petrological and mineralogical studies in the southern part of the Pilanesberg Alkaline Complex, Transvaal, South Africa. *Ph.D. thesis, Oxford University (unpublished)*.

- Riley, T.R., and Knight, K.B. (2001). Review age of pre-break up Gondwana magmatism. *Antarctic Science* **13(2),** pp 99-110.

- Robb, L.J., Freeman, L.A., Armstrong, R.A. (2000). The nature and longevity of hydrothermal fluid flow and mineralization in granites of the Bushveld Complex. *Transactions of the Royal Society of Edinburgh: Earth Sciences* **91**, 269-281.

- Robb, L.J., Brandl, G., Anhaeusser, C.R., Poujol M. (2006). Archaean granitoid intrusions. In: Johnson, M., Anhaeusser, C.R., and Thomas R.J., (Eds). The Geology of South Africa. *Geological Society of South Africa/ Council for Geoscience*, 57-94.

- Roberts, N.M.W., and Spencer, C.J. (2014). *The zircon archive of continent formation through time*. In: Roberts, N. M. W., Van Kranendonk, M., Parman, S., Shirey, S. & Clift, P. D. (eds) Continent Formation Through Time. Geological Society, London, Special Publications **389**, pp 1-30.

- Rosa, D.R.N., Finch, A.A., Andersen, T., Inverno, C.N. (2009). U-Pb geochronology and Hf isotope ratios for magmatic zircons from the Iberian pyrite belt. *Mineralogy and Petrology* **95**, pp 47-69.

- Rubatto, D. and Gebauer, D. (2000). Use of cathodoluminescence for U–Pb zircon dating by ion microprobe: some examples from the western Alps. In Pagel, M., V. Barbin, P. Blanc, and D. Ohnenstetter (eds.). *Cathodoluminescence in Geosciences, Berlin, Springer-Verlag,* pp 373–400.

- Rubatto, D. (2002). Zircon trace element geochemistry: partitioning with garnet and the link between U-Pb ages and metamorphism. *Chemical Geology* **184**, pp 123-138.

- Rubatto, D. and Hermann, J. (2007). Zircon behaviour in deeply subducted rocks. *Elements* **3**, pp 31–35.

- Russell, R. D. and Ahrens, L.H. (1957). Additional regularities among discordant lead-uranium ages. *Geochimica et Cosmochimica Acta* **11**, pp 213-218.

- Scherer, E.E., Munker, C., Mezger, K. (2001). Calibration of the lutetium –hafnium clock. *Science* **293**, pp 383-688.

- Schersten, A. and Garde, A.A. (2012). Complete impact induced hydrothermal resetting of magmatic zircon, Maniitsoq Structure, West Greenland. *76th annual meteoritical Society meeting (2013)*.

- Schmitz, M.D. and Bowring, S.A. (2001). U-Pb zircon and titanite systematics of the Fish Canyon Tuff: An assessment of high-precision U-Pb geochronology and its application to young volcanic rocks. *Geochimica et Cosmochimica Acta* **65**, pp 2571-2587.

- Schoene, B., Latkoczy, C., Schaltegger, U., Gunther, D. (2010). A new method integrating high-precision U–Pb geochronology with zircon trace element analysis (U–Pb TIMS-TEA). *Geochimica et Cosmochimica Acta* **74**, pp 7144–7159.

- Schoene, B., Condon, D.J., Morgan, L., McLean., N. (2013). Precision and Accuracy in Geochronology. *Elements* **9**, pp 19–24.

- Schoene, B. and Baxter, E.F. (2017). Petrochronology and TIMS. *Reviews in Mineralogy and Geochemistry* **83**, pp 231–260.

- Schouwstra, R.P. and Kinloch, E.D. (2000). A Short Geological Review of the Bushveld Complex. *Platinum Metals Review* **44(1)**, pp 1-39.

- Shand, S.J. (1932). The geology of Pilanesberg in the Western Transvaal: A study of Alkaline Rocks and Ring intrusions. *Transaction Geological Society South Africa* **31**, pp 97-156.

- Silver, L.T. (1963). The relation between radioactivity and discordance in zircon. *National Academy of Sciences* **1075**, pp 34-39.

- Slama, J., Kosler, J., Condon, D.J., Crowley, J.L., Gerdes, A., Hanchar, J.M., Horstwood, M.S.A., Morris, G.A., Nasdala, L., Norberg, N., Schaltegger, U., Schoene, B., Tubrett, M.N., Whitehouse, M.J. (2008). Plesovice zircon - A new natural reference material for U-Pb and Hf isotopic microanalysis. *Chemical Geology* **249**, 1-35.

- Smet, I., De Muynck, D., Vanhaecke, F., Elburg, M. (2010). From volcanic rock powder to Sr and Pb isotope ratios: a fit-for-purpose procedure for multi-collector-ICP-mass spectrometric analysis. *Journal of Analytical Atomic Spectrometry* **25**, pp 1025-1032.

- Smith, P.E., Tatsumoto, M., Farquhar, R.M. (1987). Zircon Lu-Hf systematics and the evolution of the Archean crust in the southern Superior Province, Canada. *Contributions to Mineralogy and Petrology* **97**, pp 93–104.

- Speer, J.A. (1980). The actinide orthosilicates. In: *Reviews in Mineralogy and Geochemistry* **5**, pp 113-135.

- Stacey, J.S. and Kramers, J.D. (1975). Approximation of terrestrial lead isotope evolution by a two-stage model. *Earth and Planetary Science Letters* **26**, pp 207–221.

- Stahle, H.J., Raith, M., Hoernes, S., Delfs, A. (1987). Element mobility during incipient granulite formation at Kabbaldurga, southern India. *Journal of Petrology* **28**, pp 803-834.

- Stern, R.A. (1997). The GSC Sensitive High-Resolution Ion Microprobe (SHRIMP): analytical techniques of zircon V-Th-Pb age determinations and performance evaluation. *Radiogenic Age and Isotopic Studies Report* **10,** pp 1-31.

- Stern, R.A., Bodorkos, S., Kamo, S.L., Hickman, A.H., Corfu, F. (2009). Measurement of SIMS instrumental mass fractionation of Pb isotopes during zircon dating. *Geostandards and Geoanalytical Research* **33(2)**, pp145 – 168.

- Steyrer, H.P. and Sturm, R. (2002). Stability of zircon in a low-grade ultra-mylonite and its utility for chemical mass balancing: the shear zone at Miéville, Switzerland. *Chemical Geology* **187**, pp 1–19.

- Stipp, M., Stunitz, H., Heilbronner, R., Schmid, S.M. (2002). The eastern Tonale fault zone: a `natural laboratory' for crystal plastic deformation of quartz over a temperature range from 250 to 700 ºC. *Journal of Structural Geology* **24**, pp 1861-1884.

- Storey, B.C. and Kyle, P.R. (1997). An active mantle mechanism for Gondwana breakup. *South African Journal of Geology* **100(4),** pp 283–290.

- Sumner, D.Y., and Beukes, N.J. (2006). Sequence Stratigraphic Development of the Neoarchean Transvaal carbonate platform, Kaapvaal Craton, South Africa. *South African Journal of Geology* **109**, pp 11-22.

- Sun, S. and McDonough, W. (1989). Chemical and isotopic systematics of oceanic basalts: implications for mantle composition and processes. *Geological Society of London Special Publication* **42**, pp 313–345.

- Svensen, H., Corfu, F., Polteau, S., Hammer, Hammer, O., Planke, S. (2012). Rapid magma emplacement in the Karoo Large Igneous Province. *Earth and Planetary Science Letters* **325**, pp 1–9.

- Tatsumoto, M., Unruh, D.M., Patchett, P.J. (1981). U-Pb and Lu-Hf systematics of Antarctic meteorites. *Proc. 6th Symp. Antarctic meteorites*. 237-249. National Institute of Polar Research.

- Tessalina, S., Jourdan, F., Nunes, L., Kennedy, A., Denyszyn, S., Puchtel. I., Toubol, M., Creaser, R., Boyet, M., Belousova, E., Trinquier, A. (2015). Application of radiogenic isotopes in geosciences In: Kliti, G. *Principles and practise of analytical techniques in geosciences* **4**, Royal Society of Chemistry, Cambridge, *United Kingdom*, pp 69-86.

- Tilton, G.R., Patterson, C., Brown, H., Inghram, M., Hayden, R., Hess, D., Larsen, E. (1955). Isotopic composition and distribution of lead, uranium, and thorium in a Precambrian granite. *GSA Bulletin* **66**, pp 1131-1148.

- Tilton, G.R. (1960). Volume diffusion as a mechanism for discordant lead ages. *Journal of Geophysical Research* **65**, pp 2933-2945.

- Tole, M.P. (1985). The kinetics of dissolution of zircon. *Geochimica et Cosmochimica Acta* **49,** pp 453-458.

- Tomaschek, F., Kennedy, A.K., Villa, I.M., Lagos, M., Ballhaus, C. (2003) Zircons from Syros, Cyclades, Greece—Recrystallization and mobilization of zircon during high-pressure metamorphism. *Journal of Petrology* **44**, 1977–2002.

- Van Achterbergh, E., Ryan, C.G., Jackson, S.E., Griffin, W.L. (2001). Appendix 3, data reduction software for LA-ICP-MS, in: Sylvester, P.J. (Ed.), LA-ICP-MS in the Earth Sciences. *Mineralogical Association of Canada*, pp. 239-243.

- Vavra, G., Gebauer, D., Schmid, R., Compston, W. (1996). Multiple zircon growth and recrystallization during polyphase late Carboniferous to Triassic metamorphism in granulites of the Iverea Zone (Southern Alps): an ion microprobe (SHRIMP) study. *Contributions to Mineralogy and Petrology* **122**, pp 337–358.

- Vavra, G., Schmid, R., Gebauer, D. (1999). Internal morphology, habit and U–Th–Pb microanalysis of amphibolite-to-granulite facies zircons: geochronology of the Ivrea Zone (Southern Alps). *Contributions to Mineralogy and Petrology* **134**, pp 380–404.

- Vernon, R.H. (1988). Sequential growth of cordierite and andalusite porphyroblasts, Cooma Complex, Australia: microstructural evidence of a prograde reaction. *Journal of Metamorphic Geology* **6**, pp 255–269.

- Verwoerd, W.J. (1967). *The carbonatites of South Africa and South West Africa*. Handbook of Geological Survey of South Africa **6**, 452 pp.

- Verwoerd, W.J. (1986). Mineral deposits associated with carbonatites and alkaline rocks. In: Anhaeusser, C.R., and Maske, S. (Eds). *Mineral Deposits of southern Africa* **2**, pp 2173-2199.

- Verwoerd W.J. (2008). The Goudini carbonatite complex, South Africa: A re-appraisal. *The Canadian Mineralogist* **46**, pp 825-830.

- Wabo, H., Humbert, F., de Kock, M.O., Belyanin, G., Soderlund, U., Mare, L.P., Beukes, N.J. (2019). Constraining the chronology of the Mashishing Kaapvaal Craton in South Africa. In: Rajesh, K.S., Richard, E.E., Peng, P.E. (2019). Dyke Swarms of the World: A Modern Perspective. Chapter 5, pp 215-261.

- Wagner, G. and Van den haute, P. (1992). *Fission-Track Dating*. Kluwer Academic Press, the Netherlands, 285 pp.

- Walraven, F. (1988). Notes on the age and genetic relationships of the Makhutso Granite, Bushveld Complex, South Africa. *Chemical Geology* **72**, pp 17-28

- Walraven, F. and Hattingh, E. (1993). Geochronology of the Nebo Granite, Bushveld Complex. *South African Journal of Geology* **96**, pp 31-41.

- Watson, E.B. (1979). Zircon saturation in felsic liquids: experimental results and applications to trace element geochemistry. *Contributions to Mineralogy and Petrology* **70**, pp 407–419.

- Watson, E.B. and Harrison, T.M. (1983). Zircon saturation revisited: temperature and composition effects in a variety of crustal magma types. *Earth Planetary Science Letters* **64**, pp 295–304.

- Watt, G.R. and Harley, S.L. (1993). Accessory phase controls on the geochemistry of crustal melts and restites produced during water-undersaturated partial melting. *Contributions to Mineralogy and Petrology* **114**, pp 550-566.

- Wayne, D.M. and Sinha, K. (1988). Physical and chemical response of zircons to deformation. *Contributions to Mineralogy and Petrology* **98**, pp 109–121.

- Weber, W.J. (1990). Radiation induced effects and amorphization in zircon. *Journal of Material Research* **5**, pp 2687-2697.

- Westhues, A., Hanchar, J.M., LeMessurier, M.J., Whitehouse, M.J. (2017). Evidence for hydrothermal alteration and source regions for the Kiruna iron oxide–apatite ore (northern Sweden) from zircon Hf and O isotopes. *Geology* **45**, pp 571-574.

- Wetherill, G.W. (1956). Discordant uranium-lead ages. *Transactions American Geophysical Union* **37**, pp 320-326.

- Wiedenbeck, M., Alle, P., Corfu, F., Griffin W.L., Meier, M., Oberli, F., Von Quadt, A., Roddick, J.C., Spiegel, W. (1995). Three natural zircon standards for U-Th-Pb, Lu-Hf, trace element and REE analyses. *Geostand News* **19**, pp 1–23.

- Williams, I.S. (1992). Some observations on the use of zircon U-Pb geochemistry in the study of granitic rocks. *Transactions of the Royal Society of Edinburgh: Earth Sciences* **83**, pp 447-458.

- Williams, I.S. (1998). U-Th-Pb geochronology by ion microprobe. In McKibben, M.A., Shanks III, W.C., and Ridley, W.I. (eds): Applications of microanalytical techniques to understanding mineralizing processes. *Reviews in Economic Geology* **7**, pp 1-35.

- Wilson, A.H.A. (2012). A chill sequence to the Bushveld Complex: insight into the first stage of emplacement and implications for the parental magmas. *Journal of Petrology* **53**, pp 1123–1168.

- Woodhead, J. D. and Hergt, J.M. (2005). A preliminary appraisal of seven natural zircon reference materials for in situ Hf isotope determination, *Geostandards and Geoanalytical Research* **29**, pp 183–195.

- Zeh, A., Gerdes, A., Jackson N.B Jr. (2009). Archean accretion and crustal evolution of the Kalahari Craton, the zircon age and Hf isotope record of granitic rocks from Barberton/Swaziland to the Francistown Arc. *Journal of Petrology* **50(5)**, pp 933-966.

- Zeh, A., Gerdes, A., Will, T.M., Frimmel, H.E. (2010). Hafnium isotope homogenization during metamorphic zircon growth in amphibolite-facies rocks: Examples from the Shackleton Range, Antarctica. *Geochimica et Cosmochimica Acta* **74,** pp 4740–4758.

- Zeh, A., Schaltegger, U, Ovtiharova, M. (2015). The Bushveld Complex was emplaced and cooled in less than one million years- results of zirconology, and geotectonic implications. *Earth and Planetary Science Letters* **418**, pp 103-114.

- Zeh, A., Wilson, A.H. Ovtihavora, M. (2016). Source and age of upper Transvaal Supergroup, South Africa: Age-Hf isotope record of zircons in Magaliesberg quartzite. *Precambrian Research* **278**, pp 1–21

- Zheng, Y.-F., Wu, Y.-B., Zhao, Z.-F., Zhang, S.-B., Xu, P., Wu, F.-Y. (2005). Metamorphic effect on zircon Lu–Hf and U–Pb isotope systems in ultrahigh-pressure eclogite-facies metagranite and metabasite. *Earth and Planetary Science Letters* **240**, pp 378–400.

- Zirakparvar, N.A., Mathez, E.A., Scoates, J., Wall, C.J. (2014). Zircon Hf isotope evidence for an enriched mantle source for the Bushveld Igneous Complex. *Contributions to Mineralogy and Petrology* **168(3)**, pp 1-18.

Appendices

Appendix A: U-Pb supplementary data

Table 1: MEMG6

	ppm			*Ratios*							*U-Pb discordance*		*Ages (Ma)*					
Name	**U**	**^{206}Pb**	**^{206}Pb$_c$(%)**	**^{207}Pb*/^{206}Pb**	**1SE**	**^{207}Pb*/^{235}U***	**1SE**	**^{206}Pb*/^{238}U***	**1SE**	**Rho**	**Central (%)**	**Min. rim (%)**	**207/206**	**1s**	**207/235**	**1s**	**206/238**	**1s**
MEMG6-1	1817	296.6	.	0.18698	0.00165	12.89007	0.24861	0.49998	0.00857	0.889	-4.57	.	2716	14	2672	18	2614	37
MEMG6-2	819	123.9	.	0.19187	0.00166	12.2885	0.23697	0.4645	0.00801	0.894	-13.02	-7.11	2758	13	2627	18	2459	35
MEMG6-3	329	49.6	.	0.19672	0.00178	12.52061	0.24884	0.4616	0.00816	0.89	-15.11	-9.24	2799	15	2644	19	2447	36
MEMG6-4	273	43	.	0.19479	0.00184	12.72802	0.2607	0.47391	0.00862	0.888	-12.22	-5.96	2783	15	2660	19	2501	38
MEMG6-5	331	52.7	.	0.19433	0.00214	12.77125	0.3108	0.47665	0.01034	0.891	-11.56	-3.99	2779	18	2663	23	2513	45
MEMG6-6	3710	534	.	0.16894	0.00195	10.21428	0.30448	0.43851	0.01206	0.922	-9.51	.	2547	19	2454	28	2344	54
MEMG6-7	427	65.3	.	0.19336	0.00216	12.45767	0.30022	0.46728	0.00998	0.886	-12.99	-5.63	2771	18	2640	23	2472	44
MEMG6-8	809	126.1	.	0.19063	0.00226	12.5702	0.29267	0.47824	0.00958	0.861	-10.01	-2.81	2748	20	2648	22	2520	42
MEMG6-9	337	52	.	0.19322	0.00225	12.5708	0.31071	0.47187	0.01029	0.883	-12.08	-4.48	2770	19	2648	23	2492	45
MEMG6-10	493	77.3	.	0.19366	0.00229	12.70743	0.31846	0.4759	0.01052	0.882	-11.48	-3.72	2773	20	2658	24	2509	46
MEMG6-11	334	52.1	.	0.19449	0.00253	12.67945	0.3477	0.47283	0.01141	0.88	-12.32	-3.91	2780	21	2656	26	2496	50
MEMG6-12	382	58	.	0.19369	0.00256	12.43318	0.34773	0.46556	0.01147	0.881	-13.41	-4.92	2774	21	2638	26	2464	50
MEMG6-13	544	68	.	0.1889	0.00263	9.98148	0.27498	0.38323	0.00911	0.863	-27.41	-20.44	2733	23	2433	25	2091	42
MEMG6-14	506	78.6	.	0.19301	0.00265	12.67645	0.37078	0.47634	0.01231	0.883	-11.18	-2.02	2768	22	2656	28	2511	54
MEMG6-15	672	84.4	.	0.17974	0.00286	9.44046	0.27604	0.38092	0.00935	0.839	-25.1	-17.47	2651	25	2382	27	2081	44
MEMG6-16_CPb	6279	712.8	10.96	0.1441	0.00183	4.86874	0.18136	0.24505	0.00858	0.94	-42.16	-32.87	2277	21	1797	31	1413	44
MEMG6-17	1123	216.1	.	0.18627	0.00144	12.49948	0.24076	0.48669	0.00858	0.916	-6.84	-0.33	2709	12	2643	18	2556	37
MEMG6-18_CPb	3176	584.7	4.7	0.17835	0.00151	11.46265	0.28088	0.46612	0.01072	0.939	-7.8	.	2638	14	2562	23	2467	47
MEMG6-19_CPb	2716	321.4	9.39	0.19114	0.00161	7.30493	0.20106	0.27718	0.00726	0.952	-47.95	-42.56	2752	13	2149	25	1577	37
MEMG6-21	422	74.8	.	0.19071	0.00152	11.75084	0.20078	0.44688	0.00676	0.885	-15.94	-10.93	2748	13	2585	16	2381	30

Name	U	^{206}Pb	$^{206}Pb_c$(%)	$^{207}Pb^*/^{206}Pb$	1SE	$^{207}Pb/^{235}U^*$	1SE	$^{206}Pb/^{238}U^*$	1SE	Rho	Central (%)	Min. rim (%)	207/206	1s	207/235	1s	206/238	1s
MEMG6-22_CPb	7267	575.5	17.61	0.13618	0.00169	3.02795	0.13168	0.16126	0.00672	0.958	-59.91	-51.89	2179	21	1415	33	964	37
MEMG6-23_CPb	3684	581.2	1.68	0.17198	0.00149	9.628	0.20824	0.40603	0.00804	0.916	-17.39	-10.67	2577	14	2400	20	2197	37
MEMG6-24	394	75.5	.	0.19891	0.0018	13.57873	0.28947	0.49511	0.00956	0.906	-9.67	-2.89	2817	14	2721	20	2593	41
MEMG6-25_CPb	1571	298.2	3.02	0.19238	0.00168	12.5667	0.25379	0.47376	0.00863	0.902	-11.45	-5.11	2763	15	2648	19	2500	38
MEMG6-26	375	67.5	.	0.1931	0.00173	12.30493	0.23922	0.46217	0.00797	0.887	-13.85	-8.01	2769	14	2628	18	2449	35
MEMG6-27	282	50.1	.	0.19627	0.00198	12.49764	0.26009	0.46182	0.0084	0.874	-14.93	-8.85	2795	17	2643	20	2448	37
MEMG6-28_CPb	657	113.1	68.84	0.35072	0.01162	6.77847	0.49064	0.14018	0.00902	0.889	-81.98	-77.85	3710	49	2083	64	846	51
MEMG6-29	555	102.1	.	0.19312	0.00177	12.62361	0.25277	0.47408	0.00844	0.889	-11.64	-5.45	2769	15	2652	19	2501	37
MEMG6-30	373	74.4	.	0.19396	0.0018	13.9513	0.30812	0.52168	0.01045	0.907	-3.08	.	2776	15	2746	21	2706	44
MEMG6-31_CPb	1740	327.9	55.96	0.28813	0.005	9.32956	0.62784	0.23484	0.01527	0.966	-66.28	-58.23	3408	26	2371	62	1360	80
MEMG6-32	427	78.4	.	0.19169	0.00182	12.48306	0.25998	0.47231	0.00875	0.89	-11.49	-5.01	2757	15	2641	20	2494	38
MEMG6-33	343	57.2	.	0.193	0.00185	11.39031	0.24882	0.42802	0.0084	0.899	-20.19	-14.02	2768	16	2556	20	2297	38
MEMG6-34_CPb	1408	240.8	4.52	0.18266	0.00182	11.01234	0.31855	0.43725	0.01188	0.939	-15.07	-5.76	2677	16	2524	27	2338	53
MEMG6-35	577	106.9	.	0.19035	0.00187	12.62905	0.27554	0.4812	0.00938	0.893	-9.36	-2.36	2745	15	2652	21	2532	41
MEMG6-36	293	53.3	.	0.19393	0.0021	12.72324	0.29636	0.47583	0.00981	0.885	-11.58	-4.38	2776	17	2659	22	2509	43
MEMG6-37	318	57.5	.	0.19547	0.00214	12.71907	0.30088	0.47193	0.0099	0.887	-12.81	-5.6	2789	17	2659	22	2492	43
MEMG6-38_CPb	615	126.3	59.04	25.20558	0.31372	-0.64025	-27.88539	-0.00018	0.00802	-1	-99.99	.	9514	15	-1038	-78706	-1	52
MEMG6-39	259	47.6	.	0.19313	0.0022	12.90215	0.32767	0.48451	0.011	0.894	-9.7	-1.58	2769	18	2673	24	2547	48
MEMG6-40_CPb	1707	307.6	1.31	0.18447	0.00211	12.11222	0.32246	0.47621	0.01144	0.903	-8.18	.	2693	19	2613	25	2511	50
MEMG6-41_CPb	3117	253.8	14.85	0.15151	0.00209	3.77568	0.10139	0.18074	0.00416	0.857	-59.18	-54.99	2363	22	1588	22	1071	23
MEMG6-42_CPb	323	51.1	0.39	0.19088	0.00227	11.14039	0.32012	0.4233	0.01107	0.91	-20.43	-12.13	2750	19	2535	27	2275	50
MEMG6-43_CPb	6186	580.7	13.09	0.1506	0.00251	4.38538	0.14623	0.21119	0.0061	0.866	-52.06	-45.8	2353	28	1710	28	1235	32
MEMG6-44	612	100.1	.	0.18444	0.0027	11.15613	0.32928	0.4387	0.01124	0.868	-15.4	-6.56	2693	23	2536	28	2345	50

Name	U	^{206}Pb	$^{206}Pb_c(\%)$	$^{207}Pb^*/^{206}Pb$	1SE	$^{207}Pb^*/^{235}U$	1SE	$^{206}Pb/^{238}U^*$	1SE	Rho	Central (%)	Min. rim (%)	207/206	1s	207/235	1s	206/238	1s
MEMG6-45_CPb	2427	477.1	8.08	0.18697	0.00237	12.10595	0.34822	0.4696	0.01213	0.898	-10.36	-1.04	2716	21	2613	27	2482	53
MEMG6-46_CPb	5558	566.2	4.9	0.12633	0.00214	4.32006	0.15372	0.24802	0.00776	0.879	-33.66	-23.22	2047	29	1697	29	1428	40
MEMG6-47_CPb	3078	235.6	10.82	0.18287	0.00277	4.44052	0.14163	0.17611	0.00495	0.88	-65.82	-61.88	2679	24	1720	26	1046	27
MEMG6-48	555	110.2	.	0.19043	0.00244	13.71666	0.39637	0.5224	0.01354	0.897	-1.63	.	2746	21	2730	27	2709	57
MEMG6-49_CPb	718	70.6	6.75	0.20262	0.00338	6.53111	0.23416	0.23378	0.00742	0.885	-57.91	-52.6	2847	27	2050	32	1354	39
MEMG6-50_CPb	3593	418.7	11.15	0.18682	0.00281	7.04748	0.28195	0.2736	0.01014	0.927	-47.75	-39.83	2714	23	2117	36	1559	51
MEMG6-51	2420	400	.	0.1761	0.00236	10.54176	0.32355	0.43416	0.01199	0.9	-13.28	-3.37	2616	21	2484	28	2324	54
MEMG6-52	343	58.9	.	0.18262	0.0024	11.29431	0.38729	0.44856	0.0142	0.923	-12.86	-1.6	2677	22	2548	32	2389	63
MEMG6-53	308	55.7	.	0.19175	0.00274	12.94981	0.39237	0.48981	0.01308	0.882	-8.23	.	2757	23	2676	29	2570	57
MEMG6-54_CPb	3916	458.7	1.36	0.17587	0.00254	8.29735	0.31665	0.34218	0.01208	0.925	-31.58	-21.49	2614	24	2264	35	1897	58
MEMG6-55	971	170.5	.	0.19074	0.00239	11.64053	0.30189	0.44263	0.01005	0.876	-16.75	-9.19	2749	20	2576	24	2362	45
MEMG6-56	2711	461.7	.	0.1852	0.00216	10.74553	0.21225	0.42081	0.0067	0.806	-19.11	-13.86	2700	19	2501	18	2264	30
MEMG6-57	1049	197.7	.	0.19115	0.00253	12.54313	0.34801	0.47591	0.01161	0.879	-10.63	-1.91	2752	21	2646	26	2509	51
MEMG6-58	269	47.9	.	0.19912	0.00277	12.36465	0.34378	0.45037	0.01085	0.866	-17.89	-10.07	2819	22	2632	26	2397	48
MEMG6-59_CPb	865	124.1	1.9	0.19534	0.00278	10.23498	0.36879	0.38	0.01258	0.919	-29.76	-20.48	2788	22	2456	33	2076	59
MEMG6-60_CPb	1980	343.1	2.9	0.18644	0.00273	10.94345	0.32345	0.42571	0.01093	0.869	-18.57	-10.07	2711	24	2518	27	2286	49
MEMG6-61_CPb	4717	703.7	2.02	0.16575	0.00277	8.71862	0.33652	0.38151	0.01328	0.902	-20.06	-8.08	2515	26	2309	35	2083	62
MEMG6-62	1497	287.6	.	0.18862	0.0031	12.95954	0.53672	0.49831	0.01894	0.918	-5.5	.	2730	27	2677	39	2607	81
MEMG6-64	2441	476.1	.	0.18372	0.00287	12.57521	0.3981	0.49644	0.01367	0.87	-3.99	.	2687	25	2648	30	2598	59
MEMG6-65	1199	223.9	.	0.18969	0.00311	12.54413	0.41834	0.47963	0.01393	0.871	-9.42	.	2739	26	2646	31	2526	61
MEMG6-66	781	137.2	.	0.19115	0.0036	12.18566	0.47205	0.46235	0.01565	0.874	-13.18	-1.2	2752	30	2619	36	2450	69
MEMG6-67_CPb	4401	748	1.6	0.16895	0.00328	10.40139	0.4627	0.44651	0.01787	0.9	-7.86	.	2547	31	2471	41	2380	80

Name	U	^{206}Pb	$^{206}Pb_c$(%)	$^{207}Pb^*/^{206}Pb$	1SE	$^{207}Pb^*/^{235}U$	1SE	$^{206}Pb^*/^{238}U$	1SE	Rho	Central (%)	Min. rim (%)	207/206	1s	207/235	1s	206/238	1s
MEMG6-68_CPb	2289	371	2.7	0.18245	0.00366	9.9317	0.40973	0.39481	0.01424	0.874	-23.24	-11.7	2675	33	2428	38	2145	66
MEMG6-69_CPb	3096	371.2	13.2	0.16847	0.00439	6.10688	0.21953	0.2629	0.00652	0.689	-45.63	-39.5	2543	44	1991	31	1505	33
MEMG6-70_CPb	2771	396.5	8.34	0.18499	0.00393	8.37536	0.36719	0.32836	0.01259	0.875	-36.83	-26.73	2698	34	2273	40	1830	61
MEMG6-71_CPb	3126	355.2	12.2	0.17387	0.00393	6.12123	0.28047	0.25533	0.01017	0.87	-48.49	-39.65	2595	37	1993	40	1466	52
MEMG6-72	457	71.2	.	0.19824	0.00431	11.1749	0.51728	0.40884	0.0167	0.883	-25.23	-12.83	2812	33	2538	43	2210	76
MEMG6-73_CPb	3284	461.6	50.87	0.22308	0.00625	5.44176	0.30826	0.17692	0.00871	0.869	-70.18	-64.34	3003	42	1891	49	1050	48
MEMG6-74	499	86	.	0.19838	0.00452	12.33749	0.5615	0.45105	0.01777	0.866	-17.55	-4.35	2813	37	2630	43	2400	79
MEMG6-75	535	94	.	0.19653	0.00443	12.25445	0.52424	0.45224	0.01645	0.85	-16.77	-4.44	2798	37	2624	40	2405	73
MEMG6-76	420	86.1	.	0.19506	0.00196	13.12732	0.30747	0.48809	0.01033	0.904	-9.69	-2.18	2785	15	2689	22	2562	45
MEMG6-77	4947	837.4	.	0.1742	0.00243	11.16735	0.28768	0.46495	0.01007	0.841	-6.34	.	2598	22	2537	24	2461	44
MEMG6-78	468	73.1	.	0.19193	0.00195	10.07375	0.21521	0.38067	0.00716	0.88	-28.73	-23.42	2759	16	2442	20	2079	33
MEMG6-79	453	79.6	.	0.19795	0.00206	12.38443	0.27453	0.45375	0.00888	0.883	-16.93	-10.55	2809	17	2634	21	2412	39
MEMG6-80_CPb	5541	857.9	14.32	0.16469	0.00182	8.85329	0.35751	0.38988	0.01514	0.962	-17.88	-4.22	2504	19	2323	37	2122	70
MEMG6-81	491	95.2	.	0.19705	0.00207	13.01342	0.30118	0.47896	0.00988	0.891	-12.02	-4.91	2802	17	2681	22	2523	43
MEMG6-82	404	76.4	.	0.19694	0.00208	12.76179	0.27667	0.46997	0.00889	0.873	-13.64	-7.22	2801	17	2662	20	2483	39
MEMG6-83	459	84.2	.	0.19877	0.00213	12.34673	0.27523	0.45051	0.00881	0.877	-17.76	-11.47	2816	17	2631	21	2398	39
MEMG6-84_CPb	538	52.9	49.27	0.30657	0.00343	5.18279	0.1232	0.12261	0.00257	0.882	-83.02	-81.78	3504	17	1850	20	746	15
MEMG6-85	451	82.2	.	0.19868	0.00214	12.34904	0.2868	0.4508	0.00927	0.886	-17.68	-11.05	2815	17	2631	22	2399	41
MEMG6-86	529	96.4	.	0.19498	0.00222	12.22138	0.30921	0.4546	0.01027	0.893	-15.86	-8.35	2785	18	2622	24	2416	46
MEMG6-87_CPb	3265	597.3	0.22	0.18366	0.00218	12.10513	0.33438	0.47802	0.01192	0.903	-7.53	.	2686	20	2613	26	2519	52
MEMG6-88	360	69.6	.	0.19498	0.00246	12.42983	0.33764	0.46236	0.01112	0.885	-14.42	-6.26	2785	21	2637	26	2450	49
MEMG6-89	1102	212	.	0.19051	0.00238	12.01167	0.30427	0.45729	0.01007	0.869	-13.91	-6.33	2747	20	2605	24	2428	45
MEMG6-90_CPb	5591	567.1	1.12	0.14894	0.00214	5.58643	0.19169	0.27204	0.00847	0.908	-37.64	-28.89	2334	24	1914	30	1551	43
MEMG6-91_CPb	6365	508.9	37.83	0.16431	0.00373	3.01885	0.13322	0.13325	0.00504	0.858	-71.88	-67.16	2500	36	1412	34	806	29

Name	U	^{206}Pb	$^{206}Pb_c(\%)$	$^{207}Pb^*/^{206}Pb$	1SE	$^{207}Pb^*/^{235}U$	1SE	$^{206}Pb/^{238}U^*$	1SE	Rho	Central (%)	Min. rim (%)	207/206	1s	207/235	1s	206/238	1s
MEMG6-92_CPb	1673	129.4	21.25	0.2108	0.00288	4.79905	0.26237	0.16511	0.00874	0.968	-71.08	-64.98	2912	22	1785	46	985	48
MEMG6-93	3111	619.4	.	0.18239	0.00233	12.3147	0.34958	0.48968	0.01242	0.893	-4.78	.	2675	20	2629	27	2569	54
MEMG6-94	625	111.4	.	0.19299	0.00249	11.90153	0.31503	0.44727	0.01034	0.873	-16.6	-8.91	2768	21	2597	25	2383	46
MEMG6-95	222	39.9	.	0.19853	0.00262	12.28416	0.332	0.44876	0.01059	0.873	-18.01	-10.37	2814	20	2626	25	2390	47
MEMG6-96	480	89.1	.	0.19186	0.00288	12.09883	0.36065	0.45736	0.01178	0.864	-14.35	-5.48	2758	24	2612	28	2428	52
MEMG6-97	413	76.5	.	0.19066	0.00292	11.9402	0.36049	0.45419	0.01182	0.862	-14.55	-5.57	2748	25	2600	28	2414	52
MEMG6-98	305	55.7	.	0.19347	0.00299	12.14016	0.37558	0.45509	0.0122	0.867	-15.29	-6.18	2772	25	2615	29	2418	54
MEMG6-99	538	100.6	.	0.19208	0.003	12.22477	0.3911	0.46158	0.01288	0.872	-13.63	-3.93	2760	25	2622	30	2447	57

Table 2: MEMG7

	ppm			*Ratios*									*U-Pb discordance*		*Ages (Ma)*					
Name	**U**	**^{206}Pb**	**^{206}Pb$_c$(%)**	**^{207}Pb*/^{206}Pb**	**1SE**	**^{207}Pb*/^{235}U**	**1SE**	**^{206}Pb*/^{238}U**	**1SE**	**Rho**	**^{232}Th/^{238}U**	**1SE**	**Central (%)**	**Minimum rim (%)**	**207/206**	**1s**	**207/235**	**1s**	**206/238**	**1s**
MEMG7-1CPb	3911	388.8	1.16	0.14913	0.00097	5.35039	0.09836	0.26021	0.00447	0.935	0.07122	0.01824	-40.42	-35.98	2336	11	1877	16	1491	23
MEMG7-2	970	203.8	.	0.20573	0.00126	15.15437	0.26912	0.53425	0.00891	0.939	0.12334	0.03194	-4.83	.	2872	9	2825	17	2759	37
MEMG7-3	2484	518.9	.	0.20261	0.00105	15.21864	0.31067	0.54477	0.01076	0.967	0.06476	0.01592	-1.9	.	2847	8	2829	19	2803	45
MEMG7-4	1896	314.5	.	0.20291	0.00187	11.61298	0.28626	0.41508	0.00949	0.927	0.03504	0.00896	-25.34	-18.73	2850	15	2574	23	2238	43
MEMG7-6_CPb	1932	229.5	1.27	0.16465	0.0014	6.56256	0.14777	0.28908	0.00602	0.926	0.04403	0.01068	-39.1	-33.79	2504	13	2054	20	1637	30
MEMG7-7_CPb	3318	466.3	2.48	0.16158	0.00144	7.42285	0.18762	0.33318	0.00788	0.935	0.02394	0.00587	-28.72	-21.6	2472	15	2164	23	1854	38
MEMG7-8	2707	546.4	.	0.19834	0.00118	14.28085	0.34325	0.5222	0.01216	0.969	0.11343	0.02872	-4.53	.	2813	10	2769	23	2709	52
MEMG7-9_CPb	2146	416.3	0.45	0.20031	0.00136	13.70422	0.46575	0.49619	0.01652	0.98	0.01401	0.00367	-9.92	.	2829	11	2729	32	2597	71
MEMG7-10	1920	332	.	0.19721	0.00171	11.82226	0.41528	0.43478	0.0148	0.969	0.08196	0.02016	-20.19	-9.49	2803	14	2590	33	2327	67
MEMG7-11_CPb	3134	457	1.04	0.16323	0.00126	7.62163	0.17069	0.33865	0.00712	0.939	0.07082	0.01699	-28.15	-21.83	2489	13	2187	20	1880	34
MEMG7-13_CPb	3039	368.8	0.75	0.16179	0.00165	6.28697	0.12934	0.28183	0.00504	0.869	0.08908	0.02163	-39.77	-35.19	2474	16	2017	18	1601	25
MEMG5-14	1594	367.4	.	0.20337	0.00135	15.53274	0.47274	0.55394	0.01645	0.976	0.09767	0.02394	-0.52	.	2853	10	2848	29	2842	68
MEMG7-15_CPb	2370	401.3	1.05	0.17677	0.00157	9.46134	0.21099	0.38819	0.00795	0.918	0.01664	0.00401	-22.69	-16.26	2623	14	2384	20	2114	37
MEMG5-16	1217	279.6	.	0.20119	0.00149	15.45082	0.33741	0.557	0.01144	0.941	0.0485	0.01243	0.8	.	2836	12	2843	21	2854	47
MEMG7-17	1325	260.6	.	0.20155	0.00138	13.25799	0.38652	0.47708	0.01352	0.972	0.01761	0.00446	-13.77	-4.31	2839	11	2698	28	2515	59
MEMG7-18_CPb	2487	463.9	1.33	0.19822	0.00101	13.79675	0.26838	0.5048	0.00948	0.965	0.04228	0.01383	-7.67	-1.01	2812	8	2736	18	2634	41
MEMG7-19	2179	474.2	.	0.20297	0.0005	16.22938	0.24371	0.57992	0.00859	0.987	0.05894	0.0189	4.3	.	2850	4	2890	14	2948	35

Name	U	^{206}Pb	$^{206}Pb_c$(%)	$^{207}Pb^*/^{206}Pb$	1SE	$^{207}Pb^*/^{235}U$	1SE	$^{206}Pb^*/^{238}U$	1SE	Rho	Central (%)	Min. rim (%)	207/206	1s	207/235	1s	206/238	1s	Name	U
MEMG7-20_CPb	4411	508.4	1.02	0.16332	0.00127	7.52895	0.30103	0.33434	0.01311	0.981	0.04656	0.01568	-29.1	-17.18	2490	12	2176	36	1859	63
MEMG7-22_CPb	3022	616.2	0.37	0.1994	0.00055	15.27788	0.24744	0.55571	0.00887	0.985	0.04729	0.01536	1.21	.	2821	4	2833	15	2849	37
MEMG7-23	1748	347.3	.	0.20231	0.00065	15.44967	0.28223	0.55386	0.00996	0.984	0.05083	0.01674	-0.16	.	2845	5	2843	17	2841	41
MEMG7-24	2884	577.7	.	0.20118	0.00084	15.54909	0.26219	0.56056	0.00916	0.969	0.03461	0.01152	1.45	.	2836	7	2850	16	2869	38
MEMG7-25	1070	201.8	.	0.20378	0.0007	14.76749	0.28224	0.52559	0.00988	0.984	0.13537	0.04511	-5.74	.	2857	5	2800	18	2723	42
MEMG5-28	639	40.9	.	0.13636	0.001	3.28142	0.08849	0.17453	0.00453	0.962	0.02617	0.00957	-56.66	-51.48	2181	12	1477	21	1037	25
MEMG7-29	1198	229.5	.	0.20263	0.00056	14.36164	0.21571	0.51405	0.00759	0.983	0.0521	0.0167	-7.44	-2.27	2847	4	2774	14	2674	32
MEMG7-31	4887	580.6	.	0.18574	0.00115	8.20631	0.20355	0.32044	0.0077	0.968	0.04664	0.01478	-38.53	-32.67	2705	10	2254	22	1792	38
MEMG7-34_CPb	10885	649.8	1.9	0.11005	0.00049	2.41927	0.03954	0.15944	0.00251	0.963	0.00445	0.00146	-50.51	-46.48	1800	8	1248	12	954	14
MEMG7-35_CPb	3572	496.9	0.3	0.17706	0.00047	9.0371	0.12412	0.37017	0.00499	0.981	0.04006	0.01265	-26.37	-22.44	2626	4	2342	13	2030	23
MEMG7-36_CPb	6539	615.7	2.73	0.11685	0.00049	3.99706	0.05975	0.24809	0.00356	0.96	0.0214	0.00709	-28	-22.9	1909	8	1634	12	1429	18
MEMG7-37_CPb	4999	494.3	0.74	0.14521	0.00105	5.44925	0.10532	0.27217	0.00487	0.927	0.04554	0.01505	-36.2	-31.16	2290	12	1893	17	1552	25
MEMG7-41_CPb	4507	561.4	1	0.19477	0.00164	9.1583	0.1871	0.34103	0.00635	0.911	0.03958	0.01304	-36.83	-32.23	2783	14	2354	19	1892	31
MEMG7-43	3132	549.9	.	0.19718	0.00067	12.80562	0.27835	0.47102	0.01011	0.988	0.10023	0.0317	-13.52	-6.37	2803	5	2665	20	2488	44
MEMG7-49	1626	156.8	.	0.18655	0.00162	6.79311	0.24246	0.2641	0.00914	0.97	0.02049	0.00654	-49.5	-42.45	2712	14	2085	32	1511	47
MEMG7-53_CPb	7817	730.5	1.23	0.18323	0.0008	6.61642	0.15376	0.2619	0.00598	0.982	0.04479	0.01479	-49.25	-44.65	2682	7	2062	20	1500	31
MEMG7-58	877	153.1	.	0.20276	0.00082	13.63581	0.40278	0.48776	0.01427	0.991	0.05946	0.01966	-12.21	-2.32	2849	6	2725	28	2561	62

Table 3: MEMG8

	ppm			Ratios							U-Pb discordance		Ages (Ma)					
Name	U	206Pb	206Pbc(%)	207Pb/206Pb*	1SE	207Pb/235U*	1SE	206Pb/238U*	1SE	Rho	Central (%)	Minimum rim (%)	207/206	1s	207/235	1s	206/238	1s
MEMG8-1_CPb	4479	530.1	3.94	0.15527	0.00124	6.12683	0.13729	0.28618	0.00599	0.934	-36.71	-31.03	2405	13	1994	20	1622	30
MEMG8-2_CPb	5288	474.6	2.61	0.16521	0.00137	5.16859	0.13369	0.2269	0.00556	0.947	-52.33	-47.44	2510	14	1847	22	1318	29
MEMG8-3_CPb	3350	497.8	7.06	0.16353	0.00167	7.85023	0.2203	0.34816	0.0091	0.931	-26.24	-18.09	2493	17	2214	25	1926	43
MEMG8-5_CPb	3442	367.9	3.25	0.14998	0.00155	5.48176	0.13504	0.26508	0.00593	0.908	-39.6	-33.66	2346	16	1898	21	1516	30
MEMG8-6_CPb	6264	558.8	6.73	0.13977	0.00172	4.22695	0.13786	0.21934	0.00663	0.926	-46.77	-39.32	2224	20	1679	27	1278	35
MEMG4-8_CPb	4705	439.6	8.58	0.13572	0.0016	3.87736	0.11803	0.2072	0.00582	0.922	-48.32	-41.51	2173	20	1609	25	1214	31
MEMG8-10_CPb	2754	456.4	2.78	0.17652	0.00184	9.81897	0.2658	0.40343	0.01008	0.923	-19.56	-11.34	2620	17	2418	25	2185	46
MEMG8-11_CPb	4907	380.1	5.5	0.14713	0.00185	3.70689	0.09924	0.18273	0.00432	0.883	-57.66	-53.16	2313	21	1573	21	1082	24
MEMG8-16_CPb	4331	626.4	2.25	0.15697	0.00162	7.40965	0.19765	0.34237	0.00842	0.922	-24.97	-17.02	2423	17	2162	24	1898	40
MEMG8-18_CPb	1397	177.2	2.62	0.18957	0.0017	8.2196	0.22695	0.31448	0.00821	0.946	-40.58	-34.42	2738	14	2256	25	1763	40
MEMG8-19_CPb	5497	451.1	2.49	0.15293	0.00209	4.46196	0.17292	0.2116	0.00768	0.936	-52.59	-44.92	2379	23	1724	32	1237	41
MEMG8-21_CPb	3202	404.2	4.95	0.17303	0.00197	6.70839	0.23457	0.28119	0.0093	0.946	-43.06	-35.21	2587	19	2074	31	1597	47
MEMG8-22_CPb	7342	462	4.6	0.15128	0.00158	3.16249	0.10595	0.15161	0.00483	0.95	-65.71	-60.88	2360	17	1448	26	910	27
MEMG8-23_CPb	1435	170.7	4.94	0.19962	0.00216	7.99636	0.32126	0.29053	0.01124	0.963	-47.13	-39.02	2823	18	2231	36	1644	56
MEMG8-25_CPb	2663	247.1	.	0.16251	0.00169	5.37324	0.18139	0.2398	0.0077	0.951	-48.94	-41.93	2482	17	1881	29	1386	40
MEMG8-26_CPb	4480	501.7	1.36	0.15232	0.00191	5.90952	0.21519	0.28138	0.00962	0.939	-36.74	-27.13	2372	20	1963	32	1598	48

Name	U	^{206}Pb	$^{206}Pb_c$(%)	$^{207}Pb/^{206}Pb^*$	1SE	$^{207}Pb/^{235}U^*$	1SE	$^{206}Pb/^{238}U^*$	1SE	Rho	Central (%)	Min. rim (%)	207/206	1s	207/235	1s	206/238	1s
MEMG8-27_CPb	3043	389.2	3.77	0.16958	0.0023	7.33598	0.23465	0.31374	0.00909	0.906	-35.45	-27.57	2554	22	2153	29	1759	45
MEMG8-28_CPb	3308	390.2	3.4	0.16028	0.00182	6.3704	0.2147	0.28827	0.00914	0.941	-37.92	-29.43	2459	18	2028	30	1633	46
MEMG8-29_CPb	5350	519.6	4.77	0.14091	0.00196	4.21646	0.15362	0.21702	0.00731	0.924	-47.72	-39.53	2238	24	1677	30	1266	39
MEMG8-30_CPb	2403	330.5	2.15	0.16458	0.00214	7.31004	0.25254	0.32215	0.01031	0.927	-32.11	-22.82	2503	22	2150	31	1800	50
MEMG8-31_CPb	2340	381.8	1.6	0.17543	0.00246	9.05324	0.38479	0.37429	0.01501	0.944	-25.01	-12.4	2610	22	2343	39	2050	70
MEMG8-32_CPb	3127	515	3.15	0.16331	0.00215	8.6239	0.32214	0.38298	0.01338	0.936	-18.78	-6.58	2490	22	2299	34	2090	62
MEMG8-33_CPb	3558	521.3	2.12	0.15709	0.00225	7.20598	0.2792	0.33269	0.01198	0.929	-27.14	-15.6	2425	24	2137	35	1851	58
MEMG8-35_CPb	3004	419.7	3.27	0.17132	0.00221	7.93423	0.28859	0.33589	0.01142	0.935	-31.45	-21.65	2571	21	2224	33	1867	55
MEMG8-37_CPb	3154	472.5	1.83	0.17046	0.0024	8.27858	0.4303	0.35223	0.01762	0.963	-27.83	-12.27	2562	23	2262	47	1945	84
MEMG8-40_CPb	3920	554.5	3.27	0.16581	0.00261	7.23381	0.27808	0.31642	0.0111	0.913	-33.72	-23.72	2516	27	2141	34	1772	54
MEMG8-41_CPb	2130	341.9	3.8	0.16747	0.00259	8.27768	0.32545	0.35848	0.01296	0.919	-25.51	-13.99	2533	25	2262	36	1975	61
MEMG8-43	3686	408.2	.	0.16045	0.00122	6.17843	0.07483	0.27928	0.00264	0.779	-39.91	-37.46	2460	12	2001	11	1588	13
MEMG8-44_CPb	3807	477.5	2.8	0.17525	0.00157	7.45995	0.16074	0.30872	0.00605	0.91	-38.1	-33.15	2608	14	2168	19	1734	30
MEMG8-46	841	180.7	.	0.19987	0.00233	14.93611	0.23267	0.54199	0.00559	0.662	-1.45	.	2825	18	2811	15	2792	23
MEMG8-47	1906	347.9	.	0.19518	0.00174	12.61274	0.20913	0.46867	0.00656	0.844	-13.32	-8.54	2786	14	2651	16	2478	29
MEMG8-48_CPb	7681	1068.6	1.99	0.15009	0.00127	7.0954	0.10138	0.34286	0.00394	0.805	-21.93	-17.96	2347	14	2123	13	1900	19
MEMG8-50_CPb	2249	398.7	2.74	0.18373	0.0015	10.79303	0.17841	0.42606	0.00613	0.87	-17.6	-12.86	2687	12	2505	15	2288	28
MEMG8-51	2781	543.1	.	0.19041	0.00149	12.78051	0.20865	0.4868	0.00698	0.878	-8.33	-3.15	2746	13	2664	15	2557	30

Name	U	^{206}Pb	$^{206}Pb_c$(%)	$^{207}Pb/^{206}Pb^*$	1SE	$^{207}Pb/^{235}U^*$	1SE	$^{206}Pb/^{238}U^*$	1SE	Rho	Central (%)	Min. rim (%)	207/206	1s	207/235	1s	206/238	1s
MEMG8-52	2162	443.4	.	0.19548	0.00164	13.87058	0.39841	0.51463	0.01414	0.956	-4.92	.	2789	13	2741	27	2676	60
MEMG8-53	2042	432	.	0.20156	0.00187	15.11883	0.23646	0.54402	0.00684	0.804	-1.68	.	2839	15	2823	15	2800	29
MEMG8-54_CPb	3638	458.4	2.84	0.16341	0.00153	6.90143	0.11307	0.30631	0.00412	0.82	-35.07	-31.36	2491	15	2099	15	1723	20
MEMG8-55	4200	784.6	.	0.18298	0.00152	11.83383	0.25562	0.46905	0.00936	0.924	-9.01	-1.76	2680	13	2591	20	2479	41
MEMG8-56_CPb	3821	539.1	1.62	0.16749	0.00149	7.99868	0.1555	0.34637	0.00599	0.89	-28.03	-22.85	2533	14	2231	18	1917	29
MEMG8-57_CPb	2930	462.4	3.49	0.17918	0.0021	9.75444	0.19467	0.39483	0.00638	0.81	-22.18	-16.99	2645	18	2412	18	2145	29
MEMG8-58_CPb	5165	457.3	5.17	0.13988	0.00147	4.03421	0.09345	0.20917	0.00432	0.891	-49.28	-44.48	2226	17	1641	19	1224	23
MEMG8-59	2209	493.6	.	0.20167	0.00191	15.14794	0.29452	0.54477	0.00925	0.873	-1.58	.	2840	15	2825	19	2803	39
MEMG8-60_CPb	3262	465.7	1.43	0.16787	0.00172	7.96347	0.15849	0.34405	0.00588	0.858	-28.64	-23.54	2537	16	2227	18	1906	28
MEMG8-61	2831	411.1	.	0.187	0.00193	9.15571	0.21796	0.3551	0.00762	0.901	-32.23	-26.42	2716	17	2354	22	1959	36
MEMG8-62	2124	393.8	.	0.19179	0.00194	11.98576	0.29593	0.45324	0.01021	0.912	-15.1	-7.54	2758	15	2603	23	2410	45
MEMG8-63_CPb	2208	316.3	2.23	0.17027	0.00265	7.9639	0.22696	0.33923	0.0081	0.837	-30.43	-23.38	2560	25	2227	26	1883	39
MEMG8-64_CPb	4078	423.6	3.37	0.14568	0.0017	4.87657	0.09185	0.24278	0.00359	0.785	-43.25	-39.42	2296	20	1798	16	1401	19
MEMG8-65_CPb	3785	421.3	4.64	0.14091	0.00194	5.07488	0.09431	0.2612	0.00327	0.673	-37.09	-33.25	2238	23	1832	16	1496	17
MEMG8-66_CPb	4898	397.7	2.98	0.13793	0.00257	3.69814	0.12354	0.19445	0.00539	0.83	-52.23	-45.88	2201	30	1571	27	1145	29
MEMG8-67_CPb	3389	493.8	17.73	0.15323	0.00477	6.13627	0.27449	0.29045	0.00933	0.718	-35.03	-25.02	2382	51	1995	39	1644	47
MEMG8-68_CPb	2648	339.9	3.35	0.17446	0.00201	7.31667	0.23097	0.30417	0.00894	0.931	-38.8	-31.35	2601	19	2151	28	1712	44
MEMG8-69_CPb	5854	510.6	24.08	0.1402	0.00694	3.1811	0.17926	0.16456	0.00443	0.478	-60.18	-52.89	2230	86	1453	44	982	25

Name	U	^{206}Pb	$^{206}Pb_c$(%)	$^{207}Pb/^{206}Pb^*$	1SE	$^{207}Pb/^{235}U^*$	1SE	$^{206}Pb/^{238}U^*$	1SE	Rho	Central (%)	Min. rim (%)	207/206	1s	207/235	1s	206/238	1s
MEMG8-70_CPb	3541	444.2	5.14	0.1403	0.00247	5.54486	0.15243	0.28664	0.00605	0.768	-30.68	-23.68	2231	30	1908	24	1625	30
MEMG8-71	2682	593.9	.	0.19564	0.00242	14.55995	0.26004	0.53975	0.00695	0.721	-0.34	.	2790	20	2787	17	2782	29
MEMG8-72_CPb	2296	326.1	1.09	0.21255	0.00231	9.89577	0.28328	0.33767	0.00895	0.925	-41.19	-35.22	2925	16	2425	26	1875	43
MEMG8-73_CPb	2355	425.5	2.74	0.17103	0.00197	9.91311	0.22845	0.42037	0.00839	0.866	-14.09	-6.95	2568	19	2427	21	2262	38

Table 4: MEMG9

				Ratios							U-Pb discordance		Ages					
Name	U	^{206}Pb	$^{206}Pb_c$(%)	$^{207}Pb^*/^{206}Pb$	1SE	$^{207}Pb^*/^{235}U$	1SE	$^{206}Pb^*/^{238}U$	1SE	Rho	Central (%)	Minimum rim (%)	207/206	1s	207/235	1s	206/238	1s
MEMG9-1	2577	399.7	.	0.19218	0.00092	11.43082	0.17129	0.43139	0.00612	0.947	-19.31	-14.87	2761	8	2559	14	2312	28
MEMG9-2	4473	537.1	.	0.18729	0.00137	8.36776	0.24909	0.32404	0.00935	0.97	-38.23	-31.12	2718	12	2272	27	1809	46
MEMG9-3	7210	506.8	.	0.13984	0.00075	3.71644	0.0459	0.19275	0.00214	0.9	-53.24	-50.92	2225	9	1575	10	1136	12
MEMG9-4	2453	410.3	.	0.19802	0.00123	12.63678	0.1832	0.46283	0.00606	0.903	-15.29	-11	2810	10	2653	14	2452	27
MEMG9-6	4562	572.1	.	0.19349	0.00377	9.13713	0.27278	0.34249	0.00775	0.758	-36.25	-30.3	2772	31	2352	27	1899	37
MEMG9-7	14554	1723.3	.	0.17568	0.0008	8.06485	0.10526	0.33294	0.00408	0.938	-33.37	-30.11	2613	7	2238	12	1853	20
MEMG9-8	5373	513	.	0.15481	0.00092	5.54992	0.09662	0.26	0.00425	0.939	-42.35	-38.35	2400	10	1908	15	1490	22
MEMG9-9	3071	356.5	.	0.18306	0.00169	8.18704	0.18638	0.32437	0.00675	0.914	-37.1	-31.84	2681	14	2252	21	1811	33
MEMG9-11	3467	360.2	.	0.17719	0.00096	6.91989	0.08966	0.28324	0.00333	0.909	-43.69	-41.03	2627	8	2101	11	1608	17
MEMG9-13	3252	336.6	.	0.20131	0.00131	8.88001	0.25359	0.31993	0.0089	0.974	-42.13	-35.89	2837	10	2326	26	1789	43
MEMG9-14	6872	463	.	0.18367	0.00151	4.73652	0.08565	0.18704	0.00301	0.891	-63.82	-61.49	2686	13	1774	15	1105	16
MEMG9-15	3006	444.9	.	0.18066	0.0011	9.76865	0.2157	0.39217	0.00832	0.961	-23.18	-16.67	2659	10	2413	20	2133	39
MEMG9-16	8153	439	.	0.15173	0.00099	3.13354	0.04717	0.14978	0.00203	0.9	-66.22	-64.24	2366	11	1441	12	900	11
MEMG9-17	3287	390.2	.	0.17157	0.00097	7.74585	0.13669	0.32744	0.00547	0.947	-33.25	-28.72	2573	9	2202	16	1826	27
MEMG9-18	2575	326.6	.	0.17507	0.00101	8.36139	0.20346	0.34639	0.00819	0.971	-30.49	-23.83	2607	9	2271	22	1917	39
MEMG9-19	2933	562.7	.	0.20127	0.00112	14.52389	0.30653	0.52336	0.01065	0.965	-5.31	.	2837	9	2785	20	2713	45
MEMG9-20	5343	456.3	.	0.14355	0.00106	4.64269	0.07302	0.23456	0.00326	0.884	-44.44	-41.01	2271	12	1757	13	1358	17
MEMG9-21	1763	241.9	.	0.19643	0.0013	10.52356	0.23271	0.38855	0.0082	0.954	-28.47	-22.61	2797	11	2482	21	2116	38
MEMG9-22	3391	349.9	.	0.16447	0.00124	6.67434	0.12745	0.29432	0.00517	0.919	-37.94	-33.4	2502	12	2069	17	1663	26
MEMG9-24	3393	392.8	.	0.17439	0.00182	7.13587	0.22197	0.29678	0.0087	0.942	-40.27	-33.04	2600	17	2129	28	1675	43
MEMG9-23	4080	537.9	.	0.17425	0.00112	8.89343	0.15161	0.37016	0.00585	0.927	-25.45	-20.69	2599	10	2327	16	2030	28
MEMG9-25	2784	373.7	.	0.17175	0.00134	8.49907	0.18977	0.3589	0.00751	0.937	-26.89	-20.63	2575	12	2286	20	1977	36
MEMG9-26	6111	279.8	.	0.1874	0.00141	3.27502	0.07767	0.12675	0.00285	0.949	-75.85	-73.69	2719	12	1475	18	769	16
MEMG9-28	2811	342.4	.	0.16274	0.00114	7.4968	0.11916	0.33411	0.00477	0.898	-28.94	-24.7	2484	12	2173	14	1858	23
MEMG9-29	3855	525.3	.	0.18056	0.00162	9.46601	0.1718	0.38023	0.006	0.87	-25.49	-20.74	2658	15	2384	17	2077	28
MEMG9-30	2783	371.8	.	0.19291	0.0014	9.33689	0.21341	0.35102	0.00761	0.948	-34.52	-28.97	2767	12	2372	21	1939	36
MEMG9-31	2083	322.7	.	0.18696	0.00122	11.00715	0.19075	0.42699	0.00685	0.926	-18.5	-13.34	2716	10	2524	16	2292	31

Name	U	^{206}Pb	$^{206}Pb_c$(%)	$^{207}Pb^*/^{206}Pb$	1SE	$^{207}Pb^*/^{235}U$	1SE	$^{206}Pb^*/^{238}U$	1SE	Rho	Central (%)	Min. rim (%)	207/206	1s	207/235	1s	206/238	1s
MEMG9-32	3268	474.9	.	0.19196	0.00131	10.55382	0.1882	0.39874	0.00657	0.924	-25.36	-20.55	2759	11	2485	17	2163	30
MEMG9-33	3106	509.6	.	0.20507	0.00154	12.50475	0.38307	0.44225	0.01314	0.97	-21.04	-11.99	2867	12	2643	29	2361	59
MEMG9-35	2701	413.4	.	0.17429	0.00163	9.64827	0.2748	0.40149	0.0108	0.945	-19.16	-10.23	2599	15	2402	26	2176	50
MEMG9-36	3588	427.9	.	0.16895	0.00139	7.84224	0.14646	0.33666	0.00564	0.897	-30.53	-25.72	2547	13	2213	17	1871	27
MEMG9-37	2565	459.5	.	0.19852	0.00134	13.2835	0.29104	0.48531	0.01012	0.951	-11.33	-4.19	2814	11	2700	21	2550	44
MEMG9-38	2718	263.1	.	0.15653	0.00123	5.77406	0.12668	0.26754	0.00548	0.934	-41.23	-36.09	2418	12	1943	19	1528	28
MEMG9-39	4987	357	.	0.15271	0.00154	3.97209	0.10259	0.18865	0.00449	0.921	-57.68	-53.29	2376	16	1629	21	1114	24
MEMG9-40	4602	362	.	0.16359	0.0013	4.69783	0.11171	0.20827	0.00467	0.942	-55.89	-51.75	2493	12	1767	20	1220	25
MEMG9-41	4086	313.8	.	0.15921	0.00157	4.63663	0.09229	0.21122	0.00365	0.869	-54.26	-50.87	2447	16	1756	17	1235	19
MEMG9-43	3127	421	.	0.17826	0.00139	9.41884	0.20643	0.38321	0.00785	0.935	-24.17	-17.91	2637	12	2380	20	2091	37
MEMG9-44	10395	591.5	.	0.16542	0.00148	3.44568	0.11555	0.15107	0.00488	0.964	-68.29	-63.95	2512	15	1515	26	907	27
MEMG9-45	4855	440.3	.	0.15638	0.00118	5.17059	0.11465	0.23981	0.005	0.941	-47.28	-42.59	2417	12	1848	19	1386	26
MEMG9-46	1759	298.2	.	0.19617	0.0015	12.2818	0.3264	0.45407	0.01156	0.958	-16.33	-8.02	2795	12	2626	25	2413	51
MEMG9-47	3605	363.6	.	0.16031	0.00154	6.12908	0.13705	0.27729	0.0056	0.903	-40.29	-35.16	2459	16	1994	20	1578	28
MEMG9-48	3451	327.4	.	0.17113	0.00136	5.85306	0.16369	0.24806	0.00665	0.959	-49.33	-43.72	2569	13	1954	24	1428	34
MEMG9-50	4739	516.6	.	0.15422	0.00155	6.39108	0.14879	0.30056	0.00631	0.902	-33.14	-27.06	2393	17	2031	20	1694	31
MEMG9-52	1707	281.8	.	0.18997	0.00163	11.87441	0.23877	0.45333	0.00825	0.905	-14.48	-8.34	2742	14	2595	19	2410	37
MEMG9-53	3894	360.1	.	0.19993	0.00196	6.74752	0.16393	0.24477	0.00544	0.915	-55.51	-51.65	2826	15	2079	21	1411	28
MEMG9-54	3210	372.1	.	0.16894	0.00138	7.81021	0.232	0.33529	0.00958	0.961	-30.81	-22.59	2547	13	2209	27	1864	46

Table 5: MEMG 1

	ppm			*Ratios*							*U-Pb discordance*		*Ages (Ma)*					
Name	**U**	**^{206}Pb**	**^{206}Pb$_c$(%)**	**^{207}Pb*/^{206}Pb**	**1SE**	**^{207}Pb*/^{235}U**	**1SE**	**^{206}Pb*/^{238}U**	**1SE**	**Rho**	**Central (%)**	**Minimum rim (%)**	**207/206**	**1s**	**207/235**	**1s**	**206/238**	**1s**
MEMG1-1 CPb	5698	256.4	11.29	0.15464	0.00142	2.42446	0.14839	0.11371	0.00688	0.989	-74.76	-67.7	2398	15	1250	44	694	40
MEMG1-2	1941	253.1	.	0.14174	0.00126	7.50833	0.47919	0.38419	0.02428	0.99	-7.95	.	2249	14	2174	57	2096	113
MEMG1-3 CPb	4180	198.6	9.13	0.13332	0.00144	2.28824	0.14925	0.12448	0.00801	0.986	-68.42	-58	2142	18	1209	46	756	46
MEMG1-4	2178	297.1	.	0.14117	0.00128	7.68807	0.50101	0.39499	0.02549	0.99	-5.02	.	2242	15	2195	59	2146	118
MEMG1-5 CPb	3634	176.2	9.3	0.14804	0.00144	2.55375	0.17136	0.12512	0.00831	0.989	-71.17	-61.97	2323	16	1288	49	760	48
MEMG1-6 CPb	3875	134.5	23.44	0.15951	0.00182	1.68896	0.11541	0.0768	0.00517	0.986	-83.39	-78.22	2450	19	1004	44	477	31
MEMG1-7	2921	159.3	.	0.14589	0.00137	3.1587	0.22495	0.15703	0.01109	0.991	-63.34	-50.68	2298	16	1447	55	940	62
MEMG1-8 CPb	6793	166.9	19.13	0.1516	0.00174	1.1722	0.08162	0.05608	0.00385	0.986	-87.34	-83.18	2364	19	788	38	352	24
MEMG1-9 CPb	5652	154.8	26.75	0.15831	0.00215	1.20016	0.08683	0.05498	0.00391	0.982	-88.04	-84.04	2438	22	801	40	345	24
MEMG1-10	5486	177.4	.	0.13982	0.00138	1.75649	0.12378	0.09111	0.00636	0.99	-77.9	-70.13	2225	16	1030	46	562	38
MEMG1-11 CPb	2791	371.8	2.33	0.14427	0.00074	7.13374	0.14247	0.35862	0.00692	0.967	-15.44	-8.28	2279	8	2128	18	1976	33
MEMG1-12	2306	351.1	.	0.14268	0.0006	8.32307	0.15503	0.42308	0.00768	0.974	0.76	.	2260	7	2267	17	2274	35
MEMG1-13 CPb	7617	141.5	25.77	0.16286	0.00077	0.83652	0.01741	0.03725	0.00076	0.974	-92.08	-91.41	2486	8	617	10	236	5
MEMG1-14	2732	414.6	.	0.14694	0.00062	8.5961	0.16062	0.42428	0.00772	0.974	-1.58	.	2311	7	2296	17	2280	35
MEMG1-15	1888	291	.	0.14614	0.0007	8.5834	0.15577	0.42599	0.00745	0.964	-0.7	.	2301	8	2295	17	2288	34
MEMG1-16	1925	278.5	.	0.14512	0.00062	8.06164	0.15203	0.4029	0.0074	0.974	-5.5	.	2289	7	2238	17	2182	34
MEMG1-17 CPb	3112	277.1	7.68	0.1418	0.00068	4.33896	0.08489	0.22192	0.00421	0.969	-46.85	-42.39	2249	8	1701	16	1292	22
MEMG1-18	1566	284.4	.	0.18625	0.00079	12.96269	0.24339	0.50476	0.00923	0.974	-3.38	.	2709	7	2677	18	2634	40
MEMG1-19 CPb	4027	349.3	4.42	0.14283	0.00084	4.60515	0.10274	0.23384	0.00503	0.965	-44.36	-39.04	2262	9	1750	19	1355	26
MEMG1-20	1635	308.4	.	0.29888	0.00129	21.5173	0.58826	0.52214	0.0141	0.988	-26.62	-19.77	3464	6	3162	27	2708	60
MEMG1-21 CPb	10975	234.6	22.81	0.10761	0.0011	0.65854	0.01533	0.04438	0.00093	0.899	-85.86	-84.24	1759	18	514	9	280	6

Name	U	^{206}Pb	$^{206}Pb_c$(%)	$^{207}Pb^*/^{206}Pb$	1SE	$^{207}Pb^*/^{235}U$	1SE	$^{206}Pb^*/^{238}U$	1SE	Rho	Central (%)	Min. rim (%)	207/206	1s	207/235	1s	206/238	1s
MEMG1-22 CPb	13584	288.1	18.72	0.12447	0.00108	0.84532	0.02346	0.04926	0.0013	0.95	-86.63	-84.9	2021	15	622	13	310	8
MEMG1-23	990	142.4	.	0.14513	0.00063	7.98179	0.154	0.39887	0.0075	0.974	-6.45	.	2289	7	2229	17	2164	35
MEMG1-23B	3006	567.1	.	0.17788	0.00083	12.88395	0.25099	0.52532	0.00994	0.971	4.12	.	2633	8	2671	18	2722	42
MEMG1-24 CPb	6976	249.5	24.81	0.14284	0.00634	1.49198	0.08778	0.07575	0.00293	0.656	-81.98	-78.2	2262	75	927	36	471	18
MEMG1-25	3794	521.2	.	0.14278	0.00085	7.69949	0.17599	0.3911	0.00863	0.966	-6.92	.	2261	10	2197	21	2128	40
MEMG1-26	4464	218.7	.	0.1431	0.00069	2.6698	0.05629	0.13531	0.00278	0.974	-67.86	-64.94	2265	8	1320	16	818	16
MEMG1-27 CPb	3182	275.4	4.83	0.14769	0.00097	4.57621	0.11091	0.22473	0.00524	0.962	-48.1	-42.79	2319	11	1745	20	1307	28
MEMG1-28	3716	600	.	0.14223	0.00066	8.9343	0.18884	0.45558	0.00939	0.975	8.81	0.67	2255	8	2331	19	2420	42
MEMG1-29	761	122.3	.	0.18449	0.0009	11.6475	0.31419	0.4579	0.01215	0.983	-11.72	-2.41	2694	8	2576	25	2430	54
MEMG1-30 CPb	4797	262.6	7.25	0.14027	0.00096	2.67182	0.06731	0.13815	0.00335	0.962	-66.58	-62.92	2231	11	1321	19	834	19
MEMG1-31 CPb	4800	248	8.93	0.14421	0.0009	2.58809	0.06133	0.13016	0.00297	0.964	-69.3	-66.18	2278	11	1297	17	789	17
MEMG1-33	1206	174.6	.	0.1505	0.00072	8.44789	0.19596	0.40712	0.00924	0.978	-7.52	.	2352	8	2280	21	2202	42
MEMG1-34	3102	433.4	.	0.15202	0.00078	8.04454	0.16622	0.38379	0.00768	0.969	-13.57	-6.17	2369	8	2236	19	2094	36
MEMG1-35 CPb	3180	310.1	3.62	0.14376	0.00107	5.04204	0.13331	0.25437	0.00645	0.96	-39.83	-33.01	2273	13	1826	22	1461	33
MEMG1-36 CPb	7500	187.1	20.85	0.15231	0.0012	1.12098	0.02988	0.05338	0.00136	0.955	-88	-86.67	2372	13	763	14	335	8
MEMG1-37 CPb	6228	216.5	14.45	0.1473	0.00104	1.64396	0.03971	0.08094	0.00187	0.956	-81.26	-79.36	2315	12	987	15	502	11
MEMG1-38	2530	350	.	0.1441	0.00075	7.60672	0.16375	0.38285	0.008	0.97	-9.63	-1.32	2277	9	2186	19	2090	37
MEMG1-40	3022	475.4	.	0.20847	0.00104	12.34691	0.27888	0.42956	0.00946	0.975	-24.18	-17.85	2894	8	2631	21	2304	43
MEMG1-42	2383	379.7	.	0.14043	0.00073	8.50477	0.18439	0.43923	0.00924	0.971	6.13	.	2233	9	2286	20	2347	41
MEMG1-43 CPb	3872	231.2	23.07	0.15289	0.00186	2.65999	0.07359	0.12618	0.00313	0.898	-71.72	-68.63	2378	20	1317	20	766	18
MEMG1-44	2519	378	.	0.1474	0.00078	8.46888	0.19106	0.4167	0.00914	0.972	-3.61	.	2316	9	2283	20	2245	42
MEMG1-46 CPb	6274	240.6	14.49	0.14387	0.00104	1.76509	0.04316	0.08898	0.00208	0.955	-78.97	-76.78	2274	12	1033	16	549	12

Name	U	^{206}Pb	$^{206}Pb_c$(%)	$^{207}Pb^*/^{206}Pb$	1SE	$^{207}Pb^*/^{235}U$	1SE	$^{206}Pb^*/^{238}U$	1SE	Rho	Central (%)	Min. rim (%)	207/206	1s	207/235	1s	206/238	1s
MEMG1-47 CPb	5644	299.6	7.52	0.13535	0.00086	2.49371	0.06566	0.13363	0.00341	0.97	-66.58	-62.64	2168	11	1270	19	809	19
MEMG1-48 CPb	2928	274.3	2.59	0.14468	0.00085	4.95499	0.12282	0.24839	0.00598	0.971	-41.58	-35.35	2284	10	1812	21	1430	31
MEMG1-49	3910	623.8	.	0.14167	0.00079	8.51689	0.20437	0.43601	0.01018	0.973	4.51	.	2248	10	2288	22	2333	46
MEMG1-50	2435	361.5	.	0.14513	0.00082	8.23063	0.19747	0.41132	0.00959	0.972	-3.53	.	2289	9	2257	22	2221	44
MEMG1-51	804	116	.	0.14959	0.00085	8.22774	0.19935	0.39892	0.0094	0.972	-8.9	.	2341	9	2256	22	2164	43
MEMG1-52	2772	231.2	.	0.14196	0.00081	4.45132	0.10733	0.22741	0.00533	0.972	-45.59	-39.9	2251	10	1722	20	1321	28
MEMG1-53 CPb	3909	327.6	7.41	0.14288	0.00094	4.19021	0.10895	0.2127	0.00535	0.967	-49.41	-43.71	2262	11	1672	21	1243	28
MEMG1-54 CPb	2311	304.5	2.4	0.14963	0.002	7.29962	0.24084	0.35381	0.01067	0.914	-19.22	-8.34	2342	23	2149	29	1953	51
MEMG1-56	2701	391.7	.	0.15354	0.0009	8.40432	0.20726	0.397	0.00951	0.971	-11.36	-2.24	2386	9	2276	22	2155	44
MEMG1-55 CPb	8594	234	22.23	0.13399	0.00099	1.07041	0.02855	0.05794	0.00148	0.961	-85.37	-83.62	2151	12	739	14	363	9
MEMG1-57	1522	230	.	0.14802	0.00093	8.55869	0.23193	0.41935	0.01106	0.973	-3.35	.	2323	10	2292	25	2258	50
MEMG1-59	2648	282.3	.	0.14254	0.0009	5.76585	0.15772	0.29337	0.00781	0.973	-30.07	-21.73	2258	11	1941	24	1658	39
MEMG1-60 CPb	3706	219.2	10.24	0.14564	0.0012	2.91629	0.08382	0.14523	0.004	0.958	-66.05	-61.87	2295	14	1386	22	874	23
MEMG1-62	4520	751.7	.	0.14239	0.00092	8.87408	0.24709	0.45199	0.01224	0.973	7.84	.	2257	10	2325	25	2404	54
MEMG1-63 CPb	6498	228.9	13.12	0.13657	0.00112	1.59273	0.04818	0.08458	0.00246	0.962	-79.03	-76.19	2184	14	967	19	523	15
MEMG1-64 CPb	3232	260.3	13.97	0.14497	0.00476	3.84503	0.17604	0.19237	0.00614	0.697	-54.84	-47.6	2287	55	1602	37	1134	33
MEMG1-65	3617	454.9	.	0.21151	0.00142	10.04145	0.32587	0.34432	0.01093	0.978	-39.83	-32.52	2917	11	2439	30	1907	52
MEMG1-66 CPb	3564	186.5	12.41	0.14664	0.00117	2.49614	0.07797	0.12345	0.00373	0.967	-71.31	-67.44	2307	13	1271	23	750	21
MEMG1-67	2436	374	.	0.14364	0.00097	8.22911	0.23127	0.41551	0.01134	0.971	-1.64	.	2272	11	2257	25	2240	52
MEMG1-68	3618	590	.	0.14246	0.00097	8.8198	0.24949	0.44901	0.01233	0.971	7.08	.	2257	11	2320	26	2391	55
MEMG1-69	2213	335.2	.	0.14298	0.00097	8.33549	0.25623	0.42282	0.01268	0.975	0.5	.	2264	11	2268	28	2273	57
MEMG1-70	2111	288	.	0.145	0.001	7.31272	0.21692	0.36578	0.01055	0.972	-14.14	-3.09	2288	11	2150	26	2009	50
MEMG1-71	1860	347.7	.	0.19109	0.00132	13.62016	0.40902	0.51696	0.01511	0.973	-2.9	.	2752	10	2724	28	2686	64
MEMG1-72 CPb	7024	277.3	14.29	0.13566	0.00115	1.70528	0.0531	0.09117	0.00273	0.962	-77.25	-74.07	2173	15	1011	20	562	16

Name	U	^{206}Pb	$^{206}Pb_c$(%)	$^{207}Pb^*/^{206}Pb$	1SE	$^{207}Pb^*/^{235}U$	1SE	$^{206}Pb^*/^{238}U$	1SE	Rho	Central (%)	Min. rim (%)	207/206	1s	207/235	1s	206/238	1s
MEMG1-73 CPb	2706	254.4	8.38	0.20316	0.00224	6.67974	0.235	0.23846	0.00797	0.95	-57.14	-51.53	2852	18	2070	31	1379	41
MEMG1-74	3538	576.2	.	0.14131	0.00103	8.81787	0.27398	0.45257	0.01367	0.972	8.73	.	2243	12	2319	28	2407	61
MEMG1-75	2327	349.2	.	0.14277	0.00104	8.1811	0.2611	0.41561	0.01291	0.973	-1.08	.	2261	12	2251	29	2241	59
MEMG1-76 CPb	5472	256.5	11.51	0.14598	0.00124	2.23156	0.07741	0.11087	0.00373	0.97	-74.13	-70.21	2299	14	1191	24	678	22
MEMG1-77	3412	523	.	0.13974	0.00108	7.96664	0.26095	0.41348	0.01316	0.972	0.36	.	2224	13	2227	30	2231	60
MEMG1-78	3412	523	.	0.13974	0.00108	7.96664	0.26095	0.41348	0.01316	0.972	0.36	.	2224	13	2227	30	2231	60
MEMG1-79	3412	523	.	0.13974	0.00108	7.96664	0.26095	0.41348	0.01316	0.972	0.36	.	2224	13	2227	30	2231	60

Table 6: MEMG2

	ppm			Ratios							U-Pb discordance		Ages (Ma)					
Name	U	206Pb	206Pbc(%)	207Pb/206Pb*	1SE	207Pb/235U*	1SE	206Pb/238U*	1SE	Rho	Central (%)	Minimum rim (%)	207/206	1s	207/235	1s	206/238	1s
MEMG2-1	1112	179.6	.	0.15466	0.0006	8.42839	0.41544	0.39525	0.01942	0.997	-12.29	.	2398	6	2278	45	2147	90
MEMG2-2	4543	960.6	.	0.19789	0.00073	16.07487	0.60175	0.58913	0.02195	0.995	7.88	.	2809	6	2881	36	2986	89
MEMG2-3_CPb	4115	159	4.66	0.12636	0.00079	1.64431	0.08793	0.09438	0.00501	0.993	-74.76	-67.84	2048	11	987	34	581	30
MEMG2-4	1496	246.1	.	0.20571	0.00069	12.09427	0.48335	0.42641	0.01698	0.996	-24.03	-12.26	2872	6	2612	37	2290	77
MEMG2-5_CPb	4803	126.2	10.29	0.14028	0.00123	1.27887	0.05409	0.06612	0.00274	0.978	-84.01	-80.9	2231	14	836	24	413	17
MEMG2-6_CPb	4564	517.4	0.36	0.12864	0.00061	5.33494	0.2571	0.30079	0.01443	0.995	-20.99	-2.07	2079	8	1874	41	1695	71
MEMG2-7_CPb	5630	192.1	11.11	0.12714	0.00066	1.39758	0.06562	0.07973	0.00372	0.994	-78.81	-73.82	2059	9	888	28	494	22
MEMG2-8	2073	293.4	.	0.14275	0.00063	7.60572	0.35208	0.38642	0.01781	0.995	-8.01	.	2261	7	2186	42	2106	83
MEMG2-9	1811	177.5	.	0.15089	0.00055	5.54644	0.23274	0.26659	0.01114	0.996	-39.58	-28.29	2356	6	1908	36	1523	57
MEMG2-10	2052	335	.	0.14674	0.00067	8.96904	0.43121	0.4433	0.02122	0.995	2.96	.	2308	8	2335	44	2365	95
MEMG2-11_CPb	3327	258.3	2.64	0.1453	0.00085	4.15181	0.10955	0.20724	0.00533	0.975	-51.45	-45.91	2291	10	1665	22	1214	28
MEMG2-12_CPb	3986	292.4	2.9	0.1454	0.00084	3.71364	0.10629	0.18525	0.00519	0.98	-56.62	-51.21	2292	9	1574	23	1096	28
MEMG2-13_CPb	5933	142.8	11.19	0.15279	0.00073	1.19609	0.0314	0.05678	0.00147	0.983	-87.27	-85.85	2377	8	799	15	356	9
MEMG2-14_CPb	4102	183.9	6.42	0.14012	0.00092	2.1468	0.05481	0.11112	0.00274	0.966	-73.1	-70.09	2229	11	1164	18	679	16
MEMG2-15	1591	314.3	.	0.20862	0.00115	15.3708	0.38458	0.53437	0.01304	0.975	-5.73	.	2895	9	2839	24	2760	55
MEMG2-16_CPb	3839	208.9	8.7	0.13871	0.00086	2.50045	0.06934	0.13074	0.00353	0.975	-68.05	-64.11	2211	10	1272	20	792	20
MEMG2-17_CPb	6944	177.4	11.37	0.12568	0.0007	1.02933	0.0300	0.0594	0.0016	0.978	-84.03	-81.81	2038	11	719	15	372	10

					6		1		9									
MEMG2-18	2590	400.3	.	0.14039	0.00065	7.92182	0.1881	0.40926	0.00953	0.981	-1.08	.	2232	8	2222	21	2212	44
MEMG2-19_CPb	7418	297.1	5.54	0.12487	0.0008	1.71695	0.04949	0.09972	0.0028	0.975	-73.01	-69.31	2027	11	1015	18	613	16
MEMG2-20	2074	306.5	.	0.14386	0.00087	7.86997	0.21867	0.39675	0.01076	0.976	-6.21	.	2274	10	2216	25	2154	50
MEMG2-22	3903	460.8	.	0.14432	0.00082	6.14233	0.1749	0.30869	0.00861	0.98	-27.24	-18.18	2280	9	1996	25	1734	42
MEMG2-23	2879	474	.	0.14631	0.00106	8.64897	0.29826	0.42874	0.01445	0.978	-0.17	.	2303	12	2302	31	2300	65
MEMG2-24_CPb	3862	231.9	3.74	0.19018	0.00112	3.93695	0.13364	0.15014	0.00502	0.985	-71.7	-67.93	2744	9	1621	27	902	28
MEMG2-25_CPb	3158	226.6	3.04	0.14181	0.0011	3.63253	0.13103	0.18578	0.00654	0.976	-55.51	-48.32	2249	13	1557	29	1098	36
Name	**U**	**^{206}Pb**	**$^{206}Pb_c$(%)**	**$^{207}Pb/^{206}Pb^*$**	**1SE**	**$^{207}Pb/^{235}U^*$**	**1SE**	**$^{206}Pb/^{238}U^*$**	**1SE**	**Rho**	**Central (%)**	**Min. rim (%)**	**207/206**	**1s**	**207/235**	**1s**	**206/238**	**1s**
MEMG2-26	936	192.1	.	0.22377	0.00153	16.13085	0.53705	0.52281	0.01704	0.979	-12.07	-1.31	3008	11	2885	32	2711	72
MEMG2-27_CPb	5652	162.5	11.77	0.1352	0.0012	1.22186	0.04272	0.06555	0.00222	0.967	-83.59	-80.97	2167	15	811	20	409	13
MEMG2-28	2032	263.7	.	0.14453	0.00054	7.11596	0.13979	0.35708	0.00689	0.982	-15.94	-8.85	2282	6	2126	17	1968	33
MEMG2-29	1075	168.2	.	0.14776	0.00062	8.66244	0.1506	0.42518	0.00718	0.971	-1.85	.	2320	7	2303	16	2284	32
MEMG2-30	4097	598.2	.	0.14224	0.00058	7.87631	0.12611	0.40161	0.00622	0.967	-4.09	.	2255	7	2217	14	2176	29
MEMG2-31_CPb	2542	247.8	0.85	0.14391	0.00074	5.41108	0.18335	0.2727	0.00913	0.989	-35.56	-25.82	2275	8	1887	29	1554	46
MEMG2-33_CPb	3979	364.9	2.6	0.18238	0.00072	6.03678	0.10276	0.24007	0.00397	0.972	-53.31	-50.26	2675	6	1981	15	1387	21
MEMG2-34_CPb	6844	475.5	4.63	0.13707	0.00057	3.30019	0.06174	0.17463	0.00319	0.975	-56.85	-53.3	2190	7	1481	15	1038	17
MEMG2-35	2980	461.3	.	0.14657	0.00057	8.79853	0.1772	0.43537	0.0086	0.981	1.22	.	2306	7	2317	18	2330	39
MEMG2-37_CPb	5129	283.6	3.15	0.135	0.00065	2.75515	0.04894	0.14802	0.00253	0.962	-62.89	-60.01	2164	8	1343	13	890	14

MEMG2-38_CPb	4743	207.6	4.82	0.13786	0.00077	2.22376	0.06298	0.11699	0.00325	0.98	-71.25	-67.59	2201	10	1189	20	713	19
MEMG2-39_CPb	1857	274.2	0.79	0.14446	0.00073	8.11134	0.16813	0.40725	0.00818	0.97	-4.09	.	2281	8	2244	19	2202	37
MEMG2-40_CPb	5534	224	2.15	0.14309	0.00084	2.20313	0.07936	0.11167	0.00397	0.987	-73.47	-69.17	2265	10	1182	25	682	23
MEMG2-42	1451	218.1	.	0.14749	0.00061	8.42949	0.15479	0.41452	0.00742	0.975	-4.16	.	2317	7	2278	17	2236	34
MEMG2-43	1716	261.8	.	0.14056	0.00058	8.00932	0.13259	0.41326	0.00662	0.968	-0.23	.	2234	7	2232	15	2230	30
MEMG2-44_CPb	3960	487.5	0.6	0.15352	0.00112	7.1146	0.14002	0.33612	0.00614	0.929	-24.94	-19.06	2385	12	2126	18	1868	30
MEMG2-45_CPb	3752	298.2	2.36	0.14129	0.00067	3.93543	0.10406	0.20201	0.00525	0.984	-51.46	-45.79	2243	8	1621	21	1186	28
MEMG2-46	3484	573.9	.	0.14181	0.00061	8.69963	0.15554	0.44494	0.00772	0.97	6.56	.	2249	7	2307	16	2373	34
MEMG2-47	2832	456.4	.	0.13866	0.0006	8.53318	0.24302	0.44633	0.01256	0.988	9.11	.	2211	7	2289	26	2379	56
MEMG2-48	4264	563.9	.	0.1405	0.00066	7.01686	0.12769	0.36222	0.00637	0.966	-12.52	-5.69	2233	8	2114	16	1993	30
MEMG2-49_CPb	2584	248.4	3.17	0.14709	0.00136	5.23707	0.15085	0.25824	0.00704	0.947	-40.15	-32.89	2312	15	1859	25	1481	36
MEMG2-52_CPb	7850	267.2	7.62	0.12688	0.00062	1.44871	0.0304	0.08281	0.00169	0.973	-77.95	-75.81	2055	8	909	13	513	10
MEMG2-53_CPb	2925	242.9	2.54	0.14341	0.0007	4.22872	0.08131	0.21387	0.00398	0.967	-49.3	-45.15	2269	8	1680	16	1249	21
MEMG2-54_CPb	2843	373.7	0.25	0.12681	0.0006	6.11213	0.14565	0.34957	0.00816	0.98	-6.85	.	2054	8	1992	21	1933	39
MEMG2-55	2421	265.6	.	0.20262	0.00104	8.38915	0.17896	0.30028	0.00622	0.971	-45.93	-41.65	2847	8	2274	19	1693	31
Name	**U**	**^{206}Pb**	**$^{206}Pb_c$(%)**	**$^{207}Pb/^{206}Pb^*$**	**1SE**	**$^{207}Pb/^{235}U^*$**	**1SE**	**$^{206}Pb/^{238}U^*$**	**1SE**	**Rho**	**Central (%)**	**Min. rim (%)**	**207/206**	**1s**	**207/235**	**1s**	**206/238**	**1s**
MEMG2-56_CPb2ndHalf	1587	240.2	2.69	0.15084	0.00245	8.47463	0.28807	0.40746	0.01217	0.878	-7.62	.	2356	26	2283	31	2203	56
MEMG2-60	5312	851.8	.	0.14541	0.00071	8.37827	0.17427	0.41788	0.00845	0.972	-2.16	.	2293	8	2273	19	2251	38
MEMG2-61_CPb	9138	192	9.26	0.09962	0.00065	0.6904	0.0148	0.05026	0.00103	0.953	-82.37	-80.3	1617	11	533	9	316	6

MEMG2-62	3787	593.6	.	0.14498	0.0007	8.61231	0.2095	0.43084	0.0102	0.98	1.14	.	2288	8	2298	22	2310	46
							9		8									
MEMG2-63	5088	877	.	0.16353	0.0008	10.19867	0.2756	0.45232	0.0119	0.98	-4.18	.	2492	9	2453	25	2406	53
					8				8									
MEMG2-64	2604	405.8	.	0.1463	0.0007	8.68076	0.1960	0.43035	0.0094	0.974	0.22	.	2303	9	2305	21	2307	43
					5		3		6									
MEMG2-65	3341	682.9	.	0.19909	0.0011	15.23303	0.3634	0.55492	0.0128	0.97	1.18	.	2819	9	2830	23	2846	53
					5		5		5									
MEMG2-66	3259	406.1	.	0.13734	0.0007	6.40907	0.1464	0.33846	0.0074	0.968	-16.51	-8.14	2194	9	2034	20	1879	36
					9		6		9									
MEMG2-68_CPb	5928	252.1	7.33	0.13665	0.0008	1.8962	0.0524	0.10064	0.0027	0.978	-75.06	-71.95	2185	10	1080	18	618	16
							8		2									
MEMG2-69	1633	337.7	.	0.25964	0.0015	19.80254	0.4678	0.55316	0.0126	0.97	-15.44	-8.53	3245	9	3082	23	2838	53
							8		7									
MEMG2-70_CPb	4442	186	2.96	0.1474	0.0009	2.2599	0.0690	0.11119	0.0033	0.98	-74.28	-70.86	2316	10	1200	22	680	19
							5		3									
MEMG2-71	1905	304.6	.	0.14397	0.0007	8.55826	0.2070	0.43112	0.0101	0.974	1.84	.	2276	9	2292	22	2311	46
					9		7		6									
MEMG2-72	2603	218.7	.	0.14504	0.0008	4.55863	0.1117	0.22796	0.0054	0.968	-46.51	-40.89	2288	10	1742	20	1324	28
					9		6		1									
MEMG2-74_CPb	3938	168.5	6.55	0.14426	0.0009	2.12621	0.0522	0.1069	0.0025	0.967	-74.79	-72.13	2279	10	1157	17	655	15
							4		4									
MEMG2-75_CPb	6721	206.6	11.23	0.12729	0.0007	1.24766	0.0283	0.07109	0.0015	0.962	-81.13	-79.17	2061	10	822	13	443	9
					9		1		5									
MEMG2-76	7523	469.2	.	0.11546	0.0009	2.69805	0.0759	0.16948	0.0045	0.958	-50.17	-43.22	1887	14	1328	21	1009	25
					3		9		7									
MEMG2-77_CPb	1637	296.2	0.36	0.18485	0.0011	11.98331	0.2939	0.47017	0.0111	0.97	-9.49	-0.94	2697	9	2603	23	2484	49
							6		9									
MEMG2-78_CPb	4577	348.7	3.02	0.13628	0.0009	3.60694	0.0996	0.19196	0.0051	0.966	-52.3	-46.43	2180	12	1551	22	1132	28
					7		1		2									
MEMG2-79_CPb	6453	231.5	12.69	0.14207	0.0013	1.59932	0.0412	0.08165	0.0019	0.934	-80.48	-78.35	2253	16	970	16	506	12
					1		1		6									
MEMG2-80_CPb	5134	187.6	8.16	0.14345	0.0011	1.66199	0.0611	0.08403	0.0030	0.977	-80.09	-76.81	2269	13	994	23	520	18
					2		7		2									
MEMG2-81	4140	478.4	.	0.1339	0.0009	5.74103	0.1538	0.31097	0.0080	0.966	-21.44	-11.99	2150	11	1938	23	1745	40
					3		1		5									
MEMG2-82_CPb	6368	147.2	11.86	0.12524	0.0008	0.90413	0.0239	0.05236	0.0013	0.965	-85.87	-84.12	2032	12	654	13	329	8
					7		7		4									

MEMG2-83	3634	217.6	.	0.13905	0.00098	3.08613	0.10056	0.16097	0.00512	0.976	-60.75	-55	2215	11	1429	25	962	28
MEMG2-84	1956	300.9	.	0.14326	0.00091	8.16474	0.20506	0.41334	0.01004	0.967	-1.92	.	2267	11	2249	23	2230	46
MEMG2-85	1865	264.8	.	0.14583	0.00109	7.55799	0.27114	0.37589	0.01319	0.978	-12.22	.	2298	12	2180	32	2057	62
MEMG2-86	1201	149.3	.	0.14522	0.00099	6.63472	0.1857	0.33136	0.009	0.97	-22.32	-12.95	2290	11	2064	25	1845	44
Name	**U**	**^{206}Pb**	**^{206}Pb$_c$(%)**	**^{207}Pb/^{206}Pb***	**1SE**	**^{207}Pb/^{235}U***	**1SE**	**^{206}Pb/^{238}U***	**1SE**	**Rho**	**Central (%)**	**Min. rim (%)**	**207/206**	**1s**	**207/235**	**1s**	**206/238**	**1s**
MEMG2-87	3538	506.3	.	0.14272	0.00096	7.37374	0.21275	0.37473	0.01052	0.973	-10.78	.	2260	11	2158	26	2052	49
MEMG2-88	2611	392.4	.	0.143	0.00093	7.96139	0.25319	0.40379	0.01257	0.979	-4.03	.	2264	11	2227	29	2186	58
MEMG2-89_CPb	5351	116.7	12.59	0.14151	0.0017	0.99467	0.0366	0.05098	0.00177	0.945	-87.77	-85.79	2246	20	701	19	321	11
MEMG2-90	2500	544.2	.	0.20875	0.00133	17.05432	0.64741	0.59252	0.02218	0.986	4.48	.	2896	10	2938	36	3000	90
MEMG2-91	1771	265.2	.	0.14048	0.00095	7.48345	0.21178	0.38636	0.01062	0.971	-6.67	.	2233	11	2171	25	2106	49
MEMG2-92_CPb	2663	220.8	2.75	0.14218	0.00105	4.05982	0.12202	0.2071	0.00603	0.969	-50.52	-44	2254	13	1646	24	1213	32
MEMG2-93	3225	474.2	.	0.13872	0.00096	7.26255	0.21336	0.37969	0.01084	0.972	-7.22	.	2211	11	2144	26	2075	51
MEMG2-95	1370	203.2	.	0.1445	0.00098	7.85898	0.25604	0.39447	0.01257	0.978	-7.12	.	2282	11	2215	29	2144	58
MEMG2-96_CPb	8012	159.1	10.64	0.12202	0.00124	0.78349	0.02533	0.04657	0.00143	0.949	-87.09	-85.1	1986	17	587	14	293	9
MEMG2-97_CPb	2710	244.7	1.71	0.1429	0.00108	4.62204	0.15866	0.23458	0.00785	0.975	-44.21	-35.72	2263	13	1753	29	1358	41
MEMG2-98	1364	219.4	.	0.14842	0.00112	8.73804	0.26221	0.42699	0.0124	0.968	-1.82	.	2328	13	2311	27	2292	56

Table 7: MEMG3

	ppm			*Ratios*							*U-Pb discordance*		*Ages (Ma)*					
Name	**U**	**^{206}Pb**	**^{206}Pb$_c$(%)**	**^{207}Pb*/^{206}Pb**	**1SE**	**^{207}Pb*/^{235}U**	**1SE**	**^{206}Pb*/^{238}U**	**1SE**	**Rho**	**Central (%)**	**Minimum rim (%)**	**207/206**	**1s**	**207/235**	**1s**	**206/238**	**1s**
MEMG3-1	7380	289.3	.	0.16124	0.00201	2.22697	0.0945	0.10017	0.00406	0.956	-78.53	-74.73	2469	20	1190	30	615	24
MEMG3-3	751	160.9	.	0.19829	0.00271	15.07575	0.71392	0.55142	0.025	0.957	0.83	.	2812	21	2820	45	2831	104
MEMG3-4_CPb	5061	394.7	11.31	0.13364	0.002	3.24691	0.16629	0.17621	0.00863	0.956	-55.4	-44.58	2146	25	1468	40	1046	47
MEMG3-5	4261	657.1	.	0.12769	0.00174	6.83097	0.32484	0.388	0.01768	0.958	2.68	.	2066	24	2090	42	2114	82
MEMG3-7	2555	197.9	.	0.14955	0.00217	4.34712	0.25752	0.21081	0.01211	0.97	-51.85	-38.87	2341	24	1702	49	1233	64
MEMG3-8	3233	129	.	0.20422	0.00268	2.6598	0.10931	0.09446	0.00368	0.947	-83.09	-80.48	2860	21	1317	30	582	22
MEMG3-10	720	124.2	.	0.14639	0.00219	8.59989	0.45104	0.42606	0.02142	0.958	-0.84	.	2304	25	2297	48	2288	97
MEMG3-11	371	79.9	.	0.22892	0.00378	16.05786	0.93311	0.50876	0.02835	0.959	-15.72	.	3044	25	2880	56	2651	121
MEMG3-12_CPb	14167	723.7	6.48	0.10713	0.00179	1.67018	0.10056	0.11307	0.00654	0.961	-63.77	-50.92	1751	28	997	38	691	38
MEMG3-13_CPb	5803	347.3	6.78	0.11601	0.00182	2.00711	0.11594	0.12548	0.00697	0.962	-63.3	-51.81	1896	27	1118	39	762	40
MEMG3-14_CPb	6118	164.9	5.51	0.17958	0.00316	1.46086	0.09155	0.059	0.00355	0.96	-88.39	-85.37	2649	27	914	38	370	22
MEMG3-17	1209	195.4	.	0.14369	0.00259	7.37708	0.4875	0.37236	0.02367	0.962	-11.88	.	2272	29	2158	59	2041	111
MEMG3-18	3788	739.1	.	0.1363	0.00249	8.45894	0.57529	0.45011	0.02949	0.963	11.82	.	2181	31	2282	62	2396	131
MEMG3-21	6636	275	.	0.13179	0.00225	1.57308	0.08293	0.08657	0.00432	0.946	-77.79	-72.2	2122	29	960	33	535	26
MEMG3-22	3012	340.1	.	0.12842	0.00271	4.5704	0.38376	0.25812	0.02098	0.968	-32.08	-1.37	2076	35	1744	70	1480	107
MEMG3-25	956	237.4	.	0.22127	0.00429	16.26011	1.22391	0.53297	0.03877	0.966	-9.69	.	2990	29	2892	72	2754	163
MEMG3-26	1321	247.2	.	0.14048	0.00284	7.67494	0.59241	0.39625	0.02952	0.965	-4.29	.	2233	33	2194	69	2152	136
MEMG3-27	709	120.3	.	0.14211	0.00069	3.836	0.0872	0.19577	0.00435	0.977	-53.21	-48.59	2253	8	1600	18	1153	23
MEMG3-28	1007	278	.	0.12091	0.00061	5.66343	0.09036	0.3397	0.00515	0.949	-4.95	.	1970	9	1926	14	1885	25
MEMG3-30	421	154.5	.	0.15261	0.0007	9.34533	0.14831	0.44414	0.00675	0.958	-0.31	.	2375	7	2372	15	2369	30
MEMG3-32	423	145.6	.	0.13143	0.00059	7.46176	0.13013	0.41175	0.00694	0.966	5.91	.	2117	8	2168	16	2223	32
MEMG3-33	304	81	.	0.20586	0.00112	9.23734	0.29202	0.32543	0.01013	0.985	-42.05	-35.1	2873	8	2362	29	1816	49
MEMG3-35	1332	113	.	0.19831	0.00096	2.74294	0.11046	0.10032	0.00401	0.993	-81.66	-78.75	2812	8	1340	30	616	23
MEMG3-37	431	201.9	.	0.2002	0.00093	15.37512	0.25438	0.55701	0.00885	0.96	1.16	.	2828	7	2839	16	2854	37
MEMG3-38	1175	359.4	.	0.12324	0.00058	6.08107	0.08914	0.35786	0.00496	0.946	-1.84	.	2004	8	1988	13	1972	24
MEMG3-39	149	50.8	.	0.14294	0.00068	8.06483	0.13336	0.40921	0.00648	0.957	-2.71	.	2263	8	2238	15	2211	30

Name	U	^{206}Pb	$^{206}Pb_c$(%)	$^{207}Pb^*/^{206}Pb$	1SE	$^{207}Pb^*/^{235}U$	1SE	$^{206}Pb^*/^{238}U$	1SE	Rho	Central (%)	Min. rim (%)	207/206	1s	207/235	1s	206/238	1s
MEMG3-40_CPb	1895	69.6	7.98	0.12819	0.00088	0.73697	0.02454	0.0417	0.00136	0.978	-89.01	-87.27	2073	12	561	14	263	8
MEMG3-41	355	128.9	.	0.1395	0.00069	8.16836	0.11729	0.42467	0.00573	0.94	3.24	.	2221	8	2250	13	2282	26
MEMG3-43	441	201.6	.	0.19592	0.00102	14.51924	0.23164	0.53748	0.00811	0.945	-0.87	.	2793	8	2784	15	2773	34
MEMG3-44_CPb	4181	89.4	16.41	0.17075	0.001	0.60398	0.01402	0.02565	0.00058	0.967	-94.75	-94.27	2565	9	480	9	163	4
MEMG3-46	688	211.7	.	0.1362	0.00072	6.82719	0.12207	0.36355	0.00621	0.955	-9.62	-2.65	2179	9	2089	16	1999	29
MEMG3-47_CPb	900	109.2	10.43	0.152	0.00087	2.83212	0.08758	0.13513	0.00411	0.983	-69.57	-65.52	2369	9	1364	23	817	23
MEMG3-49	145	53.1	.	0.14483	0.00074	8.12673	0.10532	0.40698	0.00485	0.919	-4.37	.	2286	8	2245	12	2201	22
MEMG3-52	148	58.5	.	0.23947	0.00138	15.48514	0.37017	0.46899	0.01088	0.97	-24.56	-18.17	3116	9	2846	23	2479	48
MEMG3-53	2929	98.9	.	0.14856	0.00122	0.81714	0.01887	0.03989	0.00086	0.935	-90.83	-89.97	2329	13	606	11	252	5
MEMG3-55	7022	160.2	.	0.07808	0.00064	0.27661	0.00748	0.02569	0.00066	0.954	-86.83	-84.08	1149	15	248	6	164	4
MEMG3-57_CPb	6471	101.9	73.22	0.20669	0.00203	0.1284	0.00701	0.00451	0.00024	0.984	-99.2	-99.03	2880	15	123	6	29	2
MEMG3-58_CPb	3534	107.2	12.69	0.19317	0.00195	0.75053	0.02283	0.02818	0.00081	0.943	-94.75	-94.15	2769	16	569	13	179	5
MEMG3-59	1545	496.4	.	0.12693	0.00083	6.27781	0.15693	0.35871	0.00866	0.965	-4.51	.	2056	11	2015	22	1976	41
MEMG3-61_CPb	8310	103.2	36.32	0.11128	0.00225	0.1352	0.00522	0.00881	0.00029	0.852	-97.3	-96.8	1820	37	129	5	57	2
MEMG3-62	687	223.6	.	0.13618	0.00134	6.77118	0.14598	0.36062	0.00691	0.889	-10.34	-2.39	2179	17	2082	19	1985	33
MEMG3-63	309	116.7	.	0.13955	0.00084	7.88281	0.15082	0.40967	0.00744	0.949	-0.44	.	2222	10	2218	17	2213	34
MEMG3-64_CPb	2499	198.8	8.68	0.11901	0.00087	1.31469	0.03487	0.08012	0.00204	0.962	-77.2	-74.28	1941	13	852	15	497	12
MEMG3-65	734	80	.	0.22964	0.00172	3.82583	0.11362	0.12083	0.00347	0.968	-80.02	-77.88	3050	12	1598	24	735	20
MEMG3-66	202	75.1	.	0.2378	0.00149	13.06551	0.23418	0.39849	0.00669	0.937	-35.61	-31.66	3105	10	2684	17	2162	31
MEMG3-67_CPb	548	86.7	6.24	0.15592	0.00109	3.50001	0.0896	0.16281	0.00401	0.962	-64.12	-60.33	2412	12	1527	20	972	22
MEMG3-68	1713	131	.	0.18995	0.00135	2.18329	0.04837	0.08336	0.00175	0.947	-84.27	-82.97	2742	11	1176	15	516	10
MEMG3-69	451	184.4	.	0.13765	0.00095	8.3164	0.17914	0.43819	0.00894	0.947	7.85	.	2198	11	2266	20	2343	40
MEMG3-70	295	119.1	.	0.14079	0.00093	8.31547	0.16617	0.42837	0.00808	0.944	3.26	.	2237	11	2266	18	2298	36
MEMG3-71	108	56.3	.	0.21231	0.00142	16.214	0.37799	0.55387	0.01237	0.958	-3.47	.	2923	10	2889	22	2841	51
MEMG3-72_CPb	2334	105	23.38	0.15148	0.00105	0.77172	0.01786	0.03695	0.00082	0.954	-91.65	-90.85	2363	11	581	10	234	5
MEMG3-74	116	20.8	.	0.2106	0.00145	5.50869	0.11984	0.18971	0.00392	0.949	-66.75	-64.14	2910	11	1902	19	1120	21
MEMG3-75_CPb	5970	85.3	20.71	0.09685	0.00151	0.16179	0.00448	0.01212	0.00028	0.826	-95.59	-94.95	1564	29	152	4	78	2
MEMG3-76_CPb	1545	74.9	5.74	0.13469	0.00105	0.93395	0.03128	0.05029	0.00164	0.973	-87.36	-85.42	2160	14	670	16	316	10
MEMG3-77_CPb	1114	323.6	4.6	0.17831	0.00135	7.30529	0.16578	0.29714	0.00636	0.943	-41.22	-36.14	2637	12	2149	20	1677	32
MEMG3-78	95	37.7	.	0.14707	0.00106	8.41093	0.22478	0.41478	0.01068	0.963	-3.86	.	2312	11	2276	24	2237	49

Name	U	^{206}Pb	$^{206}Pb_c$(%)	$^{207}Pb^*/^{206}Pb$	1SE	$^{207}Pb^*/^{235}U$	1SE	$^{206}Pb^*/^{238}U$	1SE	Rho	Central (%)	Min. rim (%)	207/206	1s	207/235	1s	206/238	1s
MEMG3-79	97	52.8	.	0.23749	0.00172	18.33932	0.37972	0.56005	0.01086	0.937	-9.42	-3	3103	12	3008	20	2867	45
MEMG3-80	1270	98	.	0.12542	0.00104	1.4294	0.04178	0.08266	0.00232	0.959	-77.73	-74.68	2035	14	901	17	512	14
MEMG3-81	142	81.8	.	0.22928	0.00193	18.74646	0.36298	0.59299	0.01034	0.9	-1.87	.	3047	13	3029	19	3002	42
MEMG3-82_CPb	409	148.4	3.75	0.2003	0.00335	10.1467	0.33739	0.36741	0.01055	0.864	-33.3	-25.67	2829	25	2448	31	2017	50
MEMG3-83	3195	74.4	.	0.11836	0.00102	0.39948	0.01278	0.02448	0.00075	0.963	-92.99	-91.89	1932	16	341	9	156	5
MEMG3-84_CPb	1278	72.8	7.29	0.12987	0.00117	0.99492	0.04023	0.05556	0.00219	0.975	-85.54	-82.75	2096	15	701	20	349	13
MEMG3-86	484	261.8	.	0.18993	0.00151	13.20573	0.22185	0.50429	0.00746	0.881	-4.85	.	2742	13	2694	16	2632	32
MEMG3-87_CPb	426	52.4	20.34	0.23658	0.00517	3.58567	0.25916	0.10992	0.00757	0.953	-82.18	-77.33	3097	34	1546	57	672	44
MEMG3-88	394	85.9	.	0.22344	0.00187	6.70706	0.14218	0.2177	0.00424	0.919	-63.35	-60.68	3006	13	2074	19	1270	22
MEMG3-89	373	139.9	.	0.13903	0.00118	7.40761	0.24236	0.38642	0.01221	0.966	-5.76	.	2215	14	2162	29	2106	57
MEMG3-90_CPb	2834	84.2	10.53	0.10105	0.00097	0.38224	0.01368	0.02743	0.00095	0.963	-90.55	-88.61	1644	17	329	10	174	6
MEMG3-92	392	69	.	0.14483	0.00118	3.44359	0.11142	0.17245	0.0054	0.968	-59.48	-53.76	2286	14	1514	25	1026	30
MEMG3-93	1050	67.6	.	0.2217	0.00295	2.02643	0.0754	0.06629	0.0023	0.934	-88.78	-87.29	2993	20	1124	25	414	14

Table 8: MEMG4

	ppm			*Ratios*							*U-Pb discordance*		*Ages (Ma)*					
Name	**U**	**^{206}Pb**	**^{206}Pb$_c$(%)**	**^{207}Pb/^{206}Pb***	**1SE**	**^{207}Pb/^{235}U***	**1SE**	**^{206}Pb/^{238}U***	**1SE**	**Rho**	**Central (%)**	**Minimum rim (%)**	**207/206**	**1s**	**207/235**	**1s**	**206/238**	**1s**
MEMG4-1	2590	402.2	.	0.13951	0.00224	7.59225	0.25086	0.3947	0.01139	0.874	-4.05	.	2221	27	2184	30	2145	53
MEMG4-2	4397	749.8	.	0.14056	0.00232	8.22321	0.26758	0.42432	0.0119	0.862	2.44	.	2234	27	2256	29	2280	54
MEMG4-3	3913	608.3	.	0.12839	0.00212	6.84387	0.22717	0.38661	0.01113	0.867	1.75	.	2076	27	2091	29	2107	52
MEMG4-4	3103	505.3	.	0.14014	0.00233	7.91531	0.26261	0.40963	0.01175	0.865	-0.84	.	2229	28	2221	30	2213	54
MEMG4-5	3915	636.4	.	0.14124	0.00239	7.98528	0.27022	0.41005	0.01201	0.866	-1.44	.	2242	28	2229	31	2215	55
MEMG4-6	1482	223.7	.	0.14474	0.00246	7.55645	0.25271	0.37864	0.0109	0.861	-10.98	.	2285	28	2180	30	2070	51
MEMG4-7	8172	1166.9	.	0.12733	0.00223	6.23883	0.21968	0.35537	0.01086	0.868	-5.69	.	2061	30	2010	31	1960	52
MEMG4-8	11514	823.3	.	0.1509	0.00188	3.65073	0.14729	0.17547	0.00673	0.951	-60.23	-53.37	2356	20	1561	32	1042	37
MEMG4-9	4559	834.9	.	0.12912	0.00148	7.47587	0.31256	0.41992	0.01688	0.961	9.9	.	2086	19	2170	37	2260	77
MEMG4-10	4859	902.5	.	0.13811	0.00163	8.52698	0.35267	0.44778	0.01775	0.958	9.88	.	2204	19	2289	38	2385	79
MEMG4-11	7680	1087.7	.	0.12206	0.00151	5.38046	0.24548	0.3197	0.01404	0.962	-11.42	.	1987	21	1882	39	1788	69
MEMG4-12	1579	260.8	.	0.14863	0.0024	7.22447	0.4019	0.35252	0.01877	0.957	-19.05	.	2330	27	2140	50	1947	89
MEMG4-13	10896	1175.2	.	0.10613	0.00137	3.49608	0.16559	0.23891	0.01089	0.962	-22.59	-1.82	1734	23	1526	37	1381	57
MEMG4-14	4563	688.4	.	0.1736	0.00269	7.9943	0.3922	0.33399	0.01555	0.949	-32.54	-19.16	2593	25	2230	44	1858	75
MEMG4-15	2647	449.4	.	0.13584	0.00193	7.37792	0.363	0.39391	0.01856	0.957	-1.83	.	2175	24	2158	44	2141	86
MEMG4-16	9558	756.4	.	0.14258	0.00207	3.63463	0.18498	0.18488	0.00902	0.959	-55.94	-45.74	2259	24	1557	41	1094	49
MEMG4-17	2136	383	.	0.14366	0.00203	8.1997	0.41081	0.41397	0.0199	0.959	-2.02	.	2272	24	2253	45	2233	91
ME-MG-4-18	2400	344.8	.	0.1426	0.00136	8.12712	0.1937	0.41336	0.00903	0.917	-1.51	.	2259	15	2245	22	2230	41
MEMG4-19	2968	441.3	.	0.14294	0.00136	8.36245	0.19435	0.42431	0.00899	0.912	0.89	.	2263	15	2271	21	2280	41
MEMG4-20	3638	540.5	.	0.14227	0.00138	8.26187	0.19055	0.42119	0.00882	0.908	0.57	.	2255	16	2260	21	2266	40
MEMG4-21	3745	748.9	.	0.19667	0.00197	15.41194	0.3843	0.56835	0.01297	0.915	4.54	.	2799	16	2841	24	2901	53
MEMG4-22	6578	993.5	.	0.13858	0.00142	8.20448	0.19965	0.42939	0.00948	0.907	5.03	.	2210	17	2254	22	2303	43
MEMG4-23	1808	260.1	.	0.14442	0.00154	8.14431	0.21185	0.409	0.0097	0.912	-3.65	.	2281	17	2247	24	2210	44
MEMG4-24_CPb	3800	485	6.47	0.13116	0.00164	6.03324	0.16151	0.33363	0.00789	0.884	-14.01	-4.27	2114	21	1981	23	1856	38
MEMG4-25	7481	1003.7	.	0.1331	0.0013	6.85864	0.17671	0.37372	0.00891	0.926	-5.04	.	2139	17	2093	23	2047	42
MEMG4-26_CPb	12409	1211.1	4.16	0.11359	0.00133	4.15947	0.11702	0.26558	0.0068	0.91	-20.48	-9.72	1858	21	1666	23	1518	35

Name	U	^{206}Pb	$^{206}Pb_c$(%)	$^{207}Pb/^{206}Pb^*$	1SE	$^{207}Pb/^{235}U^*$	1SE	$^{206}Pb/^{238}U^*$	1SE	Rho	Central (%)	Min. rim (%)	207/206	1s	207/235	1s	206/238	1s
MEMG4-27_CPb	8669	1074.4	3.19	0.12169	0.00142	5.60732	0.16827	0.33421	0.00924	0.921	-7.11	.	1981	20	1917	26	1859	45
MEMG4-28	3940	589.9	.	0.14321	0.00176	8.40373	0.23952	0.42561	0.01094	0.902	1.02	.	2266	21	2276	26	2286	49
MEMG4-29	3456	425.8	.	0.14388	0.00154	6.78027	0.1971	0.34177	0.00923	0.929	-19.22	-9.37	2274	18	2083	26	1895	44
MEMG4-30	2262	345.6	.	0.1325	0.00096	7.41217	0.22205	0.40572	0.01179	0.97	3.54	.	2131	12	2162	27	2195	54
MEMG4-31	2630	475.7	.	0.1349	0.00092	8.74408	0.29623	0.47012	0.0156	0.979	17.94	3.68	2163	11	2312	31	2484	68
MEMG4-32	2024	336	.	0.14147	0.00107	8.49374	0.26962	0.43543	0.01343	0.971	4.5	.	2245	13	2285	29	2330	60
MEMG4-33	4688	870	.	0.14358	0.00129	9.43594	0.31291	0.47664	0.01521	0.962	12.87	0.02	2271	15	2381	30	2513	66
MEMG4-34_CPb	5144	757.8	3.31	0.12379	0.00099	6.28551	0.21278	0.36825	0.01211	0.972	0.55	.	2012	13	2016	30	2021	57
MEMG4-35	5348	923.1	.	0.15294	0.00109	9.16819	0.33466	0.43478	0.01556	0.981	-2.59	.	2379	12	2355	33	2327	70
MEMG4-36	2021	320.7	.	0.13505	0.00112	7.60849	0.26189	0.40859	0.01365	0.97	2.39	.	2165	14	2186	31	2208	62
MEMG4-37	2054	324	.	0.13899	0.00142	7.80018	0.27346	0.40703	0.01365	0.957	-0.71	.	2215	18	2208	32	2201	63
MEMG4-38	2982	502.5	.	0.13334	0.00099	7.71633	0.29704	0.41971	0.01585	0.981	6.47	.	2142	13	2199	35	2259	72
MEMG4-39	1790	305.2	.	0.14227	0.00122	8.46117	0.30896	0.43135	0.01531	0.972	3	.	2255	14	2282	33	2312	69
MEMG4-40	2471	412.8	.	0.14383	0.00144	7.88538	0.33743	0.39761	0.01655	0.972	-5.99	.	2274	17	2218	39	2158	76
MEMG4-41	1625	273.8	.	0.14465	0.00147	8.07541	0.36017	0.4049	0.01758	0.974	-4.75	.	2284	17	2239	40	2192	81
MEMG4-42_CPb	1012	171.6	10.25	0.14404	0.0027	7.18377	0.35375	0.36171	0.01647	0.925	-14.59	.	2276	30	2134	44	1990	78
MEMG4-43	4228	733.1	.	0.13111	0.00126	7.2482	0.36757	0.40094	0.01996	0.982	3.37	.	2113	15	2142	45	2173	92
MEMG4-44_CPb	8377	829.4	4.18	0.1011	0.00114	3.12523	0.14937	0.22419	0.01041	0.972	-22.85	-0.66	1644	20	1439	37	1304	55
MEMG4-45	1118	194.6	.	0.15137	0.0017	8.49136	0.41605	0.40684	0.0194	0.973	-8.04	.	2362	19	2285	45	2200	89
MEMG4-46_CPb	5019	749.7	6.06	0.12257	0.00152	5.56482	0.2928	0.32929	0.01684	0.972	-9.16	.	1994	21	1911	45	1835	82
MEMG4-47	4452	842.3	.	0.1384	0.00165	8.33295	0.43962	0.43668	0.02244	0.974	6.94	.	2207	20	2268	48	2336	101
MEMG4-48	3229	601.6	.	0.14112	0.00171	8.18022	0.45106	0.42043	0.02262	0.976	1.14	.	2241	20	2251	50	2262	103
MEMG4-49_CPb	7377	999.5	1.19	0.11768	0.0013	4.81393	0.29801	0.29668	0.01807	0.984	-14.56	.	1921	19	1787	52	1675	90
MEMG4-52CPbreal	12606	1084.3	6.89	0.12536	0.00189	4.13598	0.12144	0.23928	0.00602	0.857	-35.5	-27.37	2034	26	1661	24	1383	31
MEMG4-57_CPb	8765	591.3	20.51	0.16154	0.00217	4.12122	0.11649	0.18503	0.0046	0.88	-60.41	-56.16	2472	22	1659	23	1094	25

Name	U	^{206}Pb	$^{206}Pb_c$(%)	$^{207}Pb/^{206}Pb^*$	1SE	$^{207}Pb/^{235}U^*$	1SE	$^{206}Pb/^{238}U^*$	1SE	Rho	Central (%)	Min. rim (%)	207/206	1s	207/235	1s	206/238	1s
MEMG4-59_CPb	15436	1323.5	2.93	0.10946	0.00105	3.52068	0.09685	0.23328	0.00601	0.937	-27.13	-16.99	1790	17	1532	22	1352	31
MEMG4-60_CPb	5745	667.1	7.75	0.14888	0.00147	6.52247	0.20492	0.31774	0.00948	0.949	-27.14	-17.49	2333	17	2049	28	1779	46
MEMG4-63_CPb	5111	601.5	2.91	0.13083	0.00134	5.84016	0.17532	0.32377	0.00914	0.94	-16.35	-5.08	2109	17	1952	26	1808	45
MEMG4-64_CPb	1467	220.7	6.91	0.15819	0.00183	9.1817	0.28286	0.42096	0.01202	0.927	-8.35	.	2436	18	2356	28	2265	55
MEMG4-65_CPb	2250	268.8	1.28	0.13504	0.00147	6.33557	0.22027	0.34027	0.01123	0.949	-14.72	-1.44	2165	19	2023	30	1888	54
MEMG4-71_CPb	6759	629.1	13.15	0.15786	0.00188	5.73764	0.19708	0.2636	0.00849	0.938	-42.51	-34.45	2433	20	1937	30	1508	43
MEMG4-72_CPb	2479	369.5	1.08	0.14666	0.00163	8.52211	0.28058	0.42142	0.01306	0.941	-2.08	.	2307	18	2288	30	2267	59
MEMG4-73_CPb	2453	321.2	1.65	0.13944	0.00171	7.09565	0.2515	0.36906	0.01227	0.938	-10.24	.	2220	21	2123	32	2025	58
MEMG4-75_CPb	7078	822.4	1.5	0.12145	0.00145	5.43849	0.19022	0.32478	0.01067	0.94	-9.54	.	1978	20	1891	30	1813	52
MEMG4-76_CPb	4863	332.6	32.73	0.21139	0.00401	5.67521	0.23195	0.19472	0.00705	0.886	-65.96	-61.1	2916	29	1928	35	1147	38
MEMG4-77_CPb	2622	368.1	1.79	0.14033	0.00182	7.92105	0.29629	0.40938	0.01436	0.938	-1.02	.	2231	22	2222	34	2212	66
MEMG4-78-2_CPb	13062	558.8	11.99	0.13003	0.00188	2.17586	0.09723	0.12136	0.00513	0.946	-68.46	-61.82	2098	25	1173	31	738	29
MEMG4-81	1183	169.5	.	0.14716	0.00157	8.03786	0.20595	0.39615	0.00922	0.909	-8.22	.	2313	17	2235	23	2151	43
MEMG4-82_CPb	1589	234.3	8.13	0.21132	0.00302	12.3197	0.53856	0.42282	0.01747	0.945	-26.07	-14.14	2916	22	2629	41	2273	79
MEMG4-86_CPb	1746	234.2	6.19	0.15241	0.00242	7.99883	0.33846	0.38064	0.01493	0.927	-14.47	.	2373	25	2231	38	2079	70
MEMG4-87_CPb	4304	538.2	1.15	0.13427	0.00197	6.70177	0.28789	0.36201	0.01462	0.94	-8.78	.	2155	25	2073	38	1992	69
MEMG4-89_CPb	3412	452.7	1.81	0.13638	0.00214	7.11026	0.30668	0.37813	0.01519	0.932	-6.11	.	2182	26	2125	38	2068	71
MEMG4-91_CPb	5809	814.3	2.98	0.13798	0.00224	7.76983	0.33169	0.40842	0.01612	0.925	0.31	.	2202	27	2205	38	2208	74

Name	U	^{206}Pb	$^{206}Pb_c$(%)	$^{207}Pb/^{206}Pb^*$	1SE	$^{207}Pb/^{235}U^*$	1SE	$^{206}Pb/^{238}U^*$	1SE	Rho	Central (%)	Min. rim (%)	207/206	1s	207/235	1s	206/238	1s
MEMG4-94_CPb	15391	1119.9	17.15	0.15667	0.00135	4.50024	0.09221	0.20833	0.00387	0.907	-54.27	-50.64	2420	14	1731	17	1220	21
MEMG4-95_CPb	5985	780.2	2.25	0.12988	0.00113	6.80987	0.14569	0.38028	0.00743	0.913	-1.05	.	2096	15	2087	19	2078	35
MEMG4-96	1612	202	.	0.13702	0.00104	6.80459	0.12243	0.36018	0.00588	0.907	-10.96	-4.35	2190	12	2086	16	1983	28
MEMG4-97_CPb	15129	1176.3	3.35	0.11207	0.00092	3.42665	0.06618	0.22176	0.00388	0.905	-32.59	-26.44	1833	14	1511	15	1291	20
MEMG4-98_CPb	7302	1015.7	12.32	0.15859	0.00144	8.71077	0.18645	0.39837	0.00772	0.906	-13.44	-6.3	2441	15	2308	19	2162	36
MEMG4-99	5901	837.3	.	0.12978	0.00122	7.42634	0.18826	0.415	0.00977	0.929	8.07	.	2095	16	2164	23	2238	45
MEMG4-100	2867	431.2	.	0.14157	0.00122	8.42436	0.1801	0.43159	0.00844	0.915	3.52	.	2246	14	2278	19	2313	38
MEMG4-101_CPb	4206	527.7	5.88	0.14605	0.00162	7.5527	0.21285	0.37507	0.00972	0.919	-12.52	-2.38	2300	18	2179	25	2053	46
MEMG4-102	3010	439.5	.	0.14268	0.00134	8.26748	0.18919	0.42024	0.00878	0.913	0.08	.	2260	16	2261	21	2262	40
MEMG4-103_CPb	10229	1201.8	16.82	0.16187	0.00151	7.42685	0.1625	0.33276	0.00659	0.904	-28.91	-22.97	2475	15	2164	20	1852	32
MEMG4-104_CPb	8555	1267.4	8.38	0.15073	0.00152	8.56982	0.20246	0.41235	0.00881	0.904	-6.46	.	2354	16	2293	21	2226	40
MEMG4-105_CPb	8739	1015.9	1.91	0.11687	0.00114	5.1754	0.11846	0.32118	0.00666	0.905	-6.8	.	1909	16	1849	19	1795	32
MEMG4-106	1172	170.2	.	0.14551	0.0015	8.14519	0.20134	0.40598	0.00912	0.908	-5.01	.	2294	17	2247	22	2196	42
MEMG4-109_CPb	7823	1089.7	1.81	0.13405	0.00144	7.06369	0.1818	0.38216	0.00894	0.909	-3.56	.	2152	19	2119	23	2086	42
MEMG4-110_CPb	6279	870.1	4.72	0.14129	0.00193	7.09426	0.22901	0.36415	0.01065	0.906	-12.5	-0.7	2243	23	2123	29	2002	50
MEMG4-111	1992	273.3	.	0.13461	0.00149	6.96221	0.1855	0.37511	0.00909	0.909	-5.71	.	2159	18	2107	24	2053	43
MEMG4-115	2430	361.8	.	0.14511	0.00165	8.12357	0.22018	0.40601	0.00999	0.908	-4.77	.	2289	19	2245	25	2197	46
MEMG4-118	4877	699.1	.	0.1366	0.00178	7.0885	0.23261	0.37635	0.01134	0.918	-6.7	.	2185	22	2123	29	2059	53
MEMG4-117	4201	624.8	.	0.13563	0.00163	7.21217	0.20921	0.38566	0.01018	0.91	-3.75	.	2172	20	2138	26	2103	47
MEMG4-118_CPb	4877	699.1	1.98	0.1366	0.00178	7.0885	0.23261	0.37635	0.01134	0.918	-6.7	.	2185	22	2123	29	2059	53
MEMG4-112	3132	452	.	0.14417	0.00134	7.38004	0.16445	0.37126	0.00752	0.909	-12.41	-4.48	2278	16	2159	20	2035	35
MEMG4-119	4768	703.3	.	0.1372	0.002	6.93315	0.16536	0.36649	0.00692	0.792	-9.52	-1.38	2192	25	2103	21	2013	33

Name	U	^{206}Pb	$^{206}Pb_c$(%)	$^{207}Pb/^{206}Pb^*$	1SE	$^{207}Pb/^{235}U^*$	1SE	$^{206}Pb/^{238}U^*$	1SE	Rho	Central (%)	Min. rim (%)	207/206	1s	207/235	1s	206/238	1s
MEMG4-120	8480	1431.7	.	0.13289	0.00111	7.73368	0.17362	0.42208	0.0088	0.929	7.41	.	2136	14	2201	20	2270	40
MEMG4-121	3439	560.7	.	0.13239	0.00104	7.54899	0.15645	0.41354	0.00793	0.925	5.62	.	2130	13	2179	19	2231	36
MEMG4-122	2528	394	.	0.13339	0.00108	7.43775	0.19469	0.40441	0.01007	0.951	2.54	.	2143	14	2166	23	2189	46
MEMG4-123	1854	304.5	.	0.14438	0.00112	8.29921	0.17653	0.4169	0.00826	0.931	-1.77	.	2280	13	2264	19	2246	38
MEMG4-125	943	151.5	.	0.14548	0.00161	8.01036	0.21817	0.39935	0.00994	0.913	-6.54	.	2293	18	2232	25	2166	46
MEMG4-126	13562	1327.2	.	0.10559	0.00086	3.66246	0.08622	0.25157	0.00556	0.938	-17.98	-8.02	1725	14	1563	19	1447	29
MEMG4-127	3334	533.2	.	0.14042	0.00111	7.82912	0.1639	0.40436	0.00784	0.926	-2.29	.	2232	13	2212	19	2189	36

Table 9: MEMG25

	ppm			*Ratios*							*U-Pb discordance*		*Ages (Ma)*					
Name	**U**	**^{206}Pb**	**^{206}Pb$_c$(%)**	**^{207}Pb*/^{206}Pb**	**1SE**	**^{207}Pb*/^{235}U**	**1SE**	**^{206}Pb*/^{238}U**	**1SE**	**Rho**	**Central (%)**	**Minimum rim (%)**	**207/206**	**1s**	**207/235**	**1s**	**206/238**	**1s**
MEMG25-1	4361	616.9	.	0.14154	0.00056	7.87661	0.13973	0.40361	0.00698	0.975	-3.17	.	2246	7	2217	16	2186	32
MEMG25-2 CPb	6273	569.9	3.4	0.13381	0.00093	4.62292	0.08305	0.25056	0.00415	0.922	-36.66	-31.83	2149	12	1753	15	1441	21
MEMG25-3 CPb	3611	455.4	1.03	0.14034	0.00058	6.84456	0.1355	0.35372	0.00685	0.978	-14.48	-7.12	2231	7	2092	18	1952	33
MEMG25-04 CPb	4579	509.8	5.78	0.14217	0.00274	5.88859	0.1643	0.3004	0.00607	0.724	-28.22	-21.23	2254	32	1960	24	1693	30
MEMG25-5 CPb	2964	392.5	0.26	0.14264	0.00059	7.35637	0.11401	0.37404	0.00559	0.964	-10.9	-5.07	2260	7	2156	14	2048	26
MEMG25-7 CPb	2807	417	0.56	0.15914	0.00071	9.10545	0.16262	0.41497	0.00718	0.968	-10.1	-3.61	2447	7	2349	16	2238	33
MEMG25-8 CPb	11570	894.3	5.31	0.15307	0.0013	4.12689	0.0975	0.19554	0.00431	0.933	-56.23	-52.05	2381	14	1660	19	1151	23
MEMG25-11 CPb	3455	464.5	0.86	0.1472	0.00101	7.36262	0.15234	0.36277	0.00708	0.943	-15.98	-8.8	2314	12	2156	18	1995	34
MEMG25-12	1756	247.7	.	0.14803	0.0008	7.97383	0.15395	0.39067	0.00724	0.96	-9.97	-2.74	2323	9	2228	17	2126	34
MEMG25-13 CPb	9841	764	3.27	0.11901	0.00093	3.42725	0.07242	0.20885	0.0041	0.929	-40.57	-34.75	1941	14	1511	17	1223	22
MEMG25-16 CPb	2997	355	1.76	0.15861	0.00093	7.01309	0.14733	0.32067	0.00647	0.96	-30.34	-24.42	2441	9	2113	19	1793	32
MEMG25-18	2800	400.6	.	0.1405	0.00082	7.67867	0.16545	0.39637	0.00822	0.962	-4.27	.	2233	10	2194	19	2152	38
MEMG25-19 CPb	5268	418	3.78	0.13399	0.00126	4.014	0.11053	0.21727	0.00563	0.94	-45.14	-38.49	2151	16	1637	22	1267	30
MEMG25-20 CPb	7104	828.5	1.71	0.17698	0.00131	7.9362	0.20831	0.32522	0.00819	0.959	-35.29	-28.67	2625	12	2224	24	1815	40
MEMG25-21 CPb	2061	272	1.04	0.14134	0.00092	6.98694	0.15978	0.35854	0.00786	0.959	-13.87	-5.43	2244	11	2110	20	1975	37
MEMG25-22	2940	465.6	.	0.15536	0.00097	9.36468	0.21277	0.43719	0.00955	0.962	-3.35	.	2406	10	2374	21	2338	43
MEMG25-23 CPb	5678	434	3.39	0.12329	0.0014	3.62725	0.11464	0.21338	0.00629	0.933	-41.49	-32.87	2004	19	1556	25	1247	33
MEMG25-26	1535	243.6	.	0.16569	0.00049	9.18872	0.1471	0.40221	0.00633	0.983	-15.7	-10.29	2515	5	2357	15	2179	29
MEMG25-27 CPb	3617	350.8	4.91	0.14178	0.00073	4.51278	0.08403	0.23085	0.00413	0.961	-44.71	-40.32	2249	8	1733	15	1339	22
MEMG25-28 CPb	4467	670.3	0.37	0.1449	0.00042	7.52643	0.15782	0.37673	0.00782	0.99	-11.51	-3.48	2287	5	2176	19	2061	37
MEMG25-29 CPb	1328	202.9	3.64	0.14581	0.0008	7.61932	0.122	0.37899	0.0057	0.94	-11.48	-5.68	2297	9	2187	14	2072	27

Name	U	^{206}Pb	$^{206}Pb_c$(%)	$^{207}Pb^*/^{206}Pb$	1SE	$^{207}Pb^*/^{235}U$	1SE	$^{206}Pb^*/^{238}U$	1SE	Rho	Central (%)	Min. rim (%)	207/206	1s	207/235	1s	206/238	1s
MEMG25-31 CPb	3893	489	2.47	0.14007	0.00056	5.96644	0.0856	0.30895	0.00426	0.961	-25.17	-20.62	2228	7	1971	12	1736	21
MEMG25-32 CPb	10782	940.1	2.52	0.10233	0.00229	3.00112	0.09092	0.21271	0.00435	0.675	-27.91	-18.21	1667	40	1408	23	1243	23
MEMG25-35	3407	532.7	.	0.14371	0.00043	7.88761	0.12701	0.39806	0.0063	0.983	-5.82	.	2272	5	2218	15	2160	29
MEMG25-36	1192	158.8	.	0.14879	0.00052	6.81597	0.08296	0.33223	0.00388	0.958	-23.78	-19.98	2332	6	2088	11	1849	19
MEMG25-37 CPb	2954	506.7	0.18	0.16614	0.00053	10.03937	0.13188	0.43825	0.00559	0.97	-8.34	-3.6	2519	5	2438	12	2343	25
MEMG25-39 CPb	3974	436.4	5.31	0.14107	0.00108	5.16258	0.09233	0.26542	0.00429	0.903	-36.13	-31.5	2240	13	1846	15	1518	22
MEMG25-42 CPb	6026	589.7	2.42	0.13586	0.0007	4.52177	0.05839	0.24139	0.00286	0.916	-39.85	-36.63	2175	9	1735	11	1394	15
MEMG25-43 CPb	6362	582.3	3.53	0.13493	0.00054	4.19786	0.05768	0.22564	0.00297	0.957	-43.41	-40.06	2163	7	1674	11	1312	16
MEMG25-44	2716	449.3	.	0.14723	0.0005	8.5283	0.11394	0.4201	0.00543	0.967	-2.72	.	2314	5	2289	12	2261	25
MEMG25-45 CPb	2801	401.5	0.54	0.13927	0.00049	6.9037	0.09377	0.35951	0.00472	0.966	-12.47	-7.4	2218	6	2099	12	1980	22
MEMG25-46	2312	422.8	.	0.17034	0.00059	10.85036	0.1592	0.46198	0.00659	0.972	-5.29	.	2561	6	2510	14	2448	29

Table 10: MEMG5

	ppm			*Ratios*							*U-Pb discordance*		*Ages (Ma)*					
Name	**U**	**^{206}Pb**	**^{206}Pb$_c$(%)**	**^{207}Pb/^{206}Pb***	**1SE**	**^{207}Pb/^{235}U***	**1SE**	**^{206}Pb/^{238}U***	**1SE**	**Rho**	**Central (%)**	**Minimum rim (%)**	**207/206**	**1s**	**207/235**	**1s**	**206/238**	**1s**
MEMG5-1_CPb	6045	395.1	25.64	0.15815	0.00184	3.0522	0.10257	0.13997	0.00441	0.938	-69.52	-65.34	2436	19	1421	26	844	25
MEMG5-2_CPb	8607	244.7	47.1	0.18789	0.00217	1.09371	0.02417	0.04222	0.0008	0.853	-91.97	-91.36	2724	18	750	12	267	5
MEMG5-3_CPb	9406	350.9	33.56	0.14359	0.00252	1.34917	0.05672	0.06814	0.0026	0.908	-83.86	-80.97	2271	29	867	25	425	16
MEMG5-4_CPb	7257	263.6	28.22	0.14826	0.00176	1.46721	0.03559	0.07177	0.00152	0.871	-83.48	-81.92	2326	19	917	15	447	9
MEMG5-5_CPb	9297	450.8	15.41	0.12745	0.00157	1.97484	0.04533	0.11238	0.00218	0.844	-70.2	-67.38	2063	22	1107	15	687	13
MEMG5-6_CPb	10603	290.4	29.23	0.14643	0.00194	1.08956	0.0233	0.05397	0.00091	0.785	-87.44	-86.48	2305	21	748	11	339	6
MEMG5-7-CPb	4949	565.2	1.03	0.12918	0.00167	5.60568	0.11811	0.31472	0.00523	0.789	-17.67	-10.94	2087	22	1917	18	1764	26
MEMG5-8	1337	221.2	.	0.15543	0.0021	9.99613	0.2551	0.46644	0.0101	0.849	3.07	.	2407	21	2434	24	2468	44
MEMG5-9_CPb	5004	188.5	31.45	0.15211	0.00233	1.57758	0.06707	0.07522	0.00298	0.933	-83.07	-80.03	2370	25	961	26	468	18
MEMG5-10_CPb	7525	418.6	21.98	0.15249	0.00197	2.50274	0.05554	0.11904	0.00215	0.813	-73.26	-71.11	2374	21	1273	16	725	12
MEMG5-11	1680	265.7	.	0.15697	0.00254	9.69818	0.34935	0.4481	0.01443	0.894	-1.8	.	2423	26	2407	33	2387	64
MEMG5-13_CPb	6027	314.1	30.53	0.15961	0.00227	2.1414	0.05353	0.0973	0.002	0.823	-78.97	-77.08	2452	23	1162	17	599	12
MEMG5-14_CPb	7506	243.9	50.95	0.17331	0.0038	1.01448	0.04342	0.04245	0.00156	0.859	-91.41	-90.05	2590	37	711	22	268	10
MEMG5-15_CPb	8186	270	29.19	0.16163	0.00253	1.34706	0.04382	0.06045	0.00172	0.877	-87.07	-85.47	2473	25	866	19	378	10
MEMG5-16_CPb	13289	217.4	59.06	0.12436	0.00207	0.30336	0.0121	0.01769	0.00064	0.909	-95.19	-94.3	2020	29	269	9	113	4
MEMG5-17	1552	218.1	.	0.15533	0.00244	7.96261	0.21167	0.3718	0.00797	0.806	-17.8	-9.95	2405	26	2227	24	2038	37
MEMG5-18_CPb	5217	218.2	28.14	0.16888	0.00303	1.9113	0.07067	0.08208	0.00265	0.874	-83.06	-80.7	2547	29	1085	25	509	16
MEMG5-19_CPb	6256	280.9	42.55	0.16932	0.00302	1.56206	0.04523	0.06691	0.00152	0.787	-86.22	-84.86	2551	29	955	18	418	9
MEMG521_CPb	3158	565.7	4.24	0.14805	0.00238	9.40553	0.24894	0.46077	0.00968	0.794	6.18	.	2323	26	2378	24	2443	43
MEMG5-22	5105	775.9	.	0.14689	0.00222	7.46634	0.2984	0.36864	0.01364	0.926	-14.46	-0.01	2310	25	2169	36	2023	64
MEMG5-23_CPb	9470	335.4	53.52	0.14821	0.00264	0.85454	0.02687	0.04182	0.00108	0.824	-90.37	-89.23	2325	30	627	15	264	7
MEMG5-24	26359	3889.7	.	0.11342	0.00205	5.8754	0.16341	0.37569	0.00795	0.761	12.67	3.22	1855	31	1958	24	2056	37

Name	U	^{206}Pb	$^{206}Pb_c$(%)	$^{207}Pb/^{206}Pb^*$	1SE	$^{207}Pb/^{235}U^*$	1SE	$^{206}Pb/^{238}U^*$	1SE	Rho	Central (%)	Min. rim (%)	207/206	1s	207/235	1s	206/238	1s
MEMG5-25	871	143.2	.	0.16111	0.00337	9.69204	0.43501	0.43631	0.01733	0.885	-6.43	.	2467	35	2406	41	2334	78
MEMG5-26	2685	501.5	.	0.15637	0.00287	10.12544	0.27912	0.46963	0.00965	0.745	3.25	.	2417	31	2446	25	2482	42
MEMG5-27_CPb	2019	442.2	10.78	0.14867	0.00325	10.68355	0.57805	0.52119	0.02579	0.914	19.66	.	2331	37	2496	50	2704	109
MEMG5-28	1979	374.9	.	0.1644	0.00263	10.14017	0.43628	0.44735	0.01787	0.929	-5.64	.	2501	27	2448	40	2383	80
MEMG5-29	3090	550.4	.	0.15492	0.00303	9.62317	0.3056	0.45052	0.01127	0.788	-0.17	.	2401	33	2399	29	2398	50
MEMG5-30	14968	229.4	.	0.09559	0.00192	0.50071	0.01639	0.03799	0.00098	0.789	-85.92	-83.52	1540	37	412	11	240	6
MEMG5-31	3414	595	.	0.15092	0.00352	9.56715	0.5872	0.45976	0.0261	0.925	4.19	.	2356	39	2394	56	2439	115
MEMG5-32_CPb	11871	420.3	4.68	0.1062	0.00034	1.34923	0.02876	0.09215	0.00194	0.988	-70.17	-66.79	1735	6	867	12	568	11
MEMG5-33_CPb	16716	409.2	16.5	0.0827	0.00124	0.60985	0.0157	0.05348	0.00112	0.812	-75.27	-71.28	1262	29	483	10	336	7
MEMG5-34_CPb	9334	445.5	6.86	0.11353	0.0008	1.91546	0.04826	0.12236	0.00296	0.96	-63.34	-58.74	1857	13	1086	17	744	17
MEMG5-35	4842	801.5	.	0.15433	0.00042	9.34696	0.13884	0.43926	0.00641	0.983	-2.35	.	2394	5	2373	14	2347	29
MEMG5-36	1963	337.7	.	0.15731	0.00063	10.38931	0.24241	0.47899	0.01101	0.985	4.78	.	2427	7	2470	22	2523	48
MEMG5-37_CPb	4779	804	0.62	0.15351	0.00048	9.62679	0.19947	0.45482	0.00932	0.989	1.57	.	2385	5	2400	19	2417	41
MEMG5-38	3697	587.4	.	0.15528	0.00056	9.38322	0.21697	0.43827	0.01001	0.988	-3.07	.	2405	6	2376	21	2343	45
MEMG5-39_CPb	22996	374.1	39.2	0.07995	0.00189	0.29348	0.00999	0.02662	0.00065	0.719	-86.94	-83.93	1196	45	261	8	169	4
MEMG5-40	1027	168.3	.	0.1546	0.00043	9.28301	0.1466	0.43549	0.00677	0.984	-3.33	.	2397	5	2366	14	2330	30
MEMG5-42_CPb	5242	896.3	2.07	0.1494	0.00054	9.41247	0.24372	0.45693	0.01172	0.99	4.46	.	2339	6	2379	24	2426	52
MEMG5-43_CPb	3510	536.3	1.01	0.15298	0.00058	8.56586	0.1908	0.40611	0.00891	0.985	-9.04	-0.51	2379	6	2293	20	2197	41
MEMG5-44_CPb	4559	355.4	10.13	0.14314	0.00084	3.61837	0.06878	0.18333	0.00332	0.951	-56.47	-52.99	2266	10	1554	15	1085	18
MEMG5-45	1633	282.2	.	0.15539	0.00049	9.85524	0.18692	0.45998	0.0086	0.986	1.67	.	2406	5	2421	17	2439	38
MEMG5-47_CPb	3321	723.6	0.66	0.19251	0.00059	15.23752	0.28085	0.57407	0.01044	0.986	7.24	0.76	2764	5	2830	18	2925	43
MEMG5-48_CPb	9912	450.4	3.79	0.12599	0.00066	1.96738	0.03911	0.11326	0.00217	0.964	-69.62	-66.85	2043	9	1104	13	692	13

Name	U	^{206}Pb	$^{206}Pb_c$(%)	$^{207}Pb/^{206}Pb^*$	1SE	$^{207}Pb/^{235}U^*$	1SE	$^{206}Pb/^{238}U^*$	1SE	Rho	Central (%)	Min. rim (%)	207/206	1s	207/235	1s	206/238	1s
MEMG5-49_CPb	5069	785.3	0.69	0.14906	0.00053	8.28989	0.16427	0.40336	0.00786	0.984	-7.6	.	2335	6	2263	18	2184	36
MEMG5-50_CPb	1865	255.6	0.72	0.15644	0.00055	7.73091	0.12447	0.3584	0.00563	0.976	-21.24	-16.06	2418	6	2200	14	1975	27
MEMG5-51_CPb	13614	444.2	9.1	0.12302	0.00144	1.33532	0.03388	0.07872	0.00177	0.887	-78.37	-75.94	2001	19	861	15	488	11
MEMG5-52_CPb	13237	487.3	0.78	0.1314	0.001	1.80488	0.05941	0.09962	0.00319	0.973	-74.37	-70.45	2117	13	1047	22	612	19
MEMG5-53_CPb	5378	510.6	3.61	0.12484	0.00089	4.11552	0.10605	0.23909	0.00592	0.961	-35.28	-27.5	2027	12	1657	21	1382	31
MEMG5-54	7770	1359.9	.	0.15813	0.00058	9.98711	0.22248	0.45808	0.01007	0.986	-0.23	.	2436	6	2434	21	2431	45
MEMG5-55	3402	605	.	0.15708	0.00058	10.04043	0.2217	0.4636	0.01009	0.986	1.54	.	2424	6	2439	20	2455	44
MEMG5-56	20719	336.4	.	0.25356	0.00126	1.50245	0.0511	0.04297	0.00145	0.989	-93.33	-92.52	3207	8	931	21	271	9
MEMG5-56_CPb	20719	336.4	20.19	0.09078	0.00067	0.4292	0.01516	0.03429	0.00118	0.978	-86.32	-83.16	1442	14	363	11	217	7
MEMG5-57_CPb	13464	1241.4	5.95	0.11871	0.00055	3.73223	0.11147	0.22803	0.00673	0.988	-34.94	-25.25	1937	8	1578	24	1324	35
MEMG5-58_CPb	8568	446.7	5.96	0.15129	0.00228	2.69231	0.11191	0.12907	0.005	0.932	-70.81	-65.7	2361	25	1326	31	783	29
MEMG-59_CPb	2527	309.4	1.45	0.15477	0.00074	6.75528	0.07435	0.31655	0.00314	0.901	-29.8	-26.85	2399	8	2080	10	1773	15
MEMG5-60_CPb	15276	382.3	5.38	0.13315	0.00078	1.13461	0.02821	0.0618	0.00149	0.972	-84.3	-82.54	2140	10	770	13	387	9
MEMG5-61	3454	591.7	.	0.15503	0.00064	9.60644	0.24316	0.44942	0.01122	0.987	-0.47	.	2402	7	2398	23	2393	50
MEMG5-62_CPb	2641	262.5	2.39	0.15506	0.00132	5.53003	0.22862	0.25866	0.01047	0.979	-42.73	-32.49	2402	14	1905	36	1483	54
MEMG5-63_CPb	3457	545.9	3.07	0.15216	0.00103	8.48298	0.23885	0.40433	0.01105	0.971	-9.02	.	2370	11	2284	26	2189	51
MEMG564	2249	369.8	.	0.15648	0.00047	9.91686	0.16329	0.45964	0.00744	0.983	0.99	.	2418	5	2427	15	2438	33
MEMG5-65_CPb	15042	423	22.67	0.12404	0.0022	1.05926	0.02923	0.06194	0.00131	0.767	-83.12	-81.27	2015	30	733	14	387	8
MEMG5-66	4133	662	.	0.14766	0.00043	8.98736	0.16515	0.44143	0.00801	0.987	1.96	.	2319	5	2337	17	2357	36
MEMG5-67_CPb	12908	363.3	17.17	0.11547	0.00183	1.04508	0.03245	0.06564	0.00175	0.859	-80.7	-77.94	1887	28	726	16	410	11

Name	U	^{206}Pb	$^{206}Pb_c$(%)	$^{207}Pb/^{206}Pb^*$	1SE	$^{207}Pb/^{235}U^*$	1SE	$^{206}Pb/^{238}U^*$	1SE	Rho	Central (%)	Min. rim (%)	207/206	1s	207/235	1s	206/238	1s
MEMG5-68_CPb	22931	232.7	37.63	0.0903	0.00239	0.22035	0.00787	0.0177	0.00043	0.673	-92.88	-91.51	1432	46	202	7	113	3
MEMG5-69_CPb	5479	557	1.19	0.12834	0.00053	4.94657	0.09357	0.27953	0.00516	0.976	-26.4	-20.05	2075	7	1810	16	1589	26
MEMG5-70_CPb	8486	355.9	1.62	0.14753	0.00068	2.28059	0.0421	0.11212	0.002	0.968	-74.08	-72.08	2317	7	1206	13	685	12
MEMG5-71_CPb	13631	451.8	16.03	0.10861	0.00126	1.15405	0.0261	0.07706	0.0015	0.859	-75.71	-73.12	1776	20	779	12	479	9
MEMG5-72_CPb	7204	400.4	7.37	0.13786	0.00076	2.64803	0.05074	0.13931	0.00256	0.958	-65.76	-62.93	2200	9	1314	14	841	14
MEMG5-73_CPb	15547	480	13.17	0.11288	0.00123	1.16875	0.02814	0.0751	0.00161	0.892	-77.35	-74.78	1846	19	786	13	467	10
MEMG5-75_CPb	15619	314.6	18.42	0.11894	0.00054	0.70817	0.01497	0.04318	0.00089	0.977	-87.7	-86.45	1940	8	544	9	273	6
MEMG5-76_CPb	4475	377.6	3.52	0.19077	0.00094	5.94045	0.17182	0.22585	0.00644	0.985	-57.53	-52.75	2749	8	1967	25	1313	34
MEMG5-77_CPb	2705	246.8	4.39	0.1472	0.00107	4.65427	0.11615	0.22932	0.00548	0.957	-46.89	-41.3	2314	12	1759	21	1331	29
MEMG5-78_CPb	4888	308.2	8.04	0.1444	0.00188	2.96324	0.09097	0.14883	0.00414	0.905	-64.94	-60.49	2281	21	1398	23	894	23
MEMG579	4094	744.4	.	0.15696	0.00062	10.34937	0.2347	0.47822	0.01068	0.985	4.8	.	2423	6	2467	21	2519	47
MEMG5-80_CPb	4059	296.9	4.57	0.14969	0.00142	3.76056	0.12274	0.18221	0.00569	0.957	-58.41	-52.65	2342	15	1584	26	1079	31
MEMG5-81_CPb	4818	623.2	2.12	0.14978	0.00087	6.61396	0.16131	0.32027	0.00759	0.971	-26.94	-19.42	2343	10	2061	22	1791	37
MEMG5-82	925	153.1	.	0.15605	0.00071	9.29586	0.26858	0.43204	0.01233	0.987	-4.85	.	2413	8	2368	26	2315	55
MEMG5-83_CPb	10954	440.1	5.84	0.1253	0.00232	1.69629	0.05102	0.09819	0.00233	0.789	-73.52	-70.29	2033	31	1007	19	604	14
MEMG5-84_CPb	8547	381.1	4.64	0.10814	0.00055	1.59659	0.04285	0.10708	0.00282	0.982	-66.07	-61.25	1768	9	969	17	656	16
MEMG5-85	980	170.8	.	0.15486	0.00071	9.32292	0.23841	0.43664	0.01099	0.984	-3.21	.	2400	7	2370	23	2336	49
MEMG5-86_CPb	9268	427.3	7.47	0.123	0.00098	1.81668	0.04928	0.10712	0.00278	0.955	-70.55	-66.79	2000	14	1051	18	656	16
MEMG5-87_CPb	6232	354.9	7.06	0.14079	0.001	2.58374	0.0724	0.1331	0.00361	0.967	-67.92	-63.97	2237	12	1296	21	805	21
MEMG5-88	1238	173	.	0.16168	0.00094	7.46455	0.2719	0.33485	0.01204	0.987	-28.4	-17.4	2473	9	2169	33	1862	58

Name	U	^{206}Pb	$^{206}Pb_c$(%)	$^{207}Pb/^{206}Pb^*$	1SE	$^{207}Pb/^{235}U^*$	1SE	$^{206}Pb/^{238}U^*$	1SE	Rho	Central (%)	Min. rim (%)	207/206	1s	207/235	1s	206/238	1s
MEMG5-89_CPb	9490	438.8	11.23	0.12861	0.00147	1.78455	0.05825	0.10064	0.00308	0.937	-73.56	-69.62	2079	19	1040	21	618	18
MEMG5-90	2365	348.9	.	0.15178	0.00107	7.61393	0.26779	0.36382	0.01254	0.98	-17.96	-5.52	2366	12	2187	32	2000	59
MEMG5-91_CPb	12270	347.4	21.07	0.11957	0.0008	0.89558	0.02635	0.05432	0.00156	0.974	-84.62	-82.4	1950	11	649	14	341	10
MEMG5-92	2370	413.2	.	0.15552	0.00077	9.09966	0.25198	0.42437	0.01156	0.984	-6.27	.	2407	8	2348	25	2280	52
MEMG5-93_CPb	3995	329.7	4.19	0.14152	0.00061	4.00834	0.13347	0.20542	0.00678	0.992	-50.71	-43.31	2246	7	1636	27	1204	36
MEMG5-94_CPb	4204	349.3	13.11	0.11497	0.00187	2.88519	0.10138	0.18201	0.00567	0.887	-46.23	-37.21	1879	30	1378	26	1078	31
MEMG5-95_CPb	2726	417.9	1.45	0.13423	0.00033	7.23695	0.2372	0.39103	0.01278	0.997	-1.44	.	2154	4	2141	29	2128	59
MEMG5-96_CPb	7488	329.8	11.67	0.12419	0.00089	1.68187	0.05425	0.09822	0.00309	0.975	-73.27	-69.11	2017	12	1002	21	604	18
MEMG5-97_CPb	15888	303.8	15.61	0.1067	0.00194	0.6121	0.02286	0.04161	0.00136	0.873	-86.61	-84.06	1744	32	485	14	263	8
MEMG5-98_CPb	4568	232.1	3.32	0.14485	0.00125	2.48223	0.09451	0.12428	0.00461	0.974	-70.8	-65.86	2286	14	1267	28	755	26
MEMG5-99_CPb	4195	281.9	5.95	0.14552	0.00056	3.25769	0.11129	0.16236	0.00551	0.994	-62.01	-56.22	2294	7	1471	27	970	31
MEMG5-100	1064	172.1	.	0.16025	0.00038	9.1337	0.28978	0.41337	0.01308	0.997	-10.96	.	2458	4	2351	29	2230	60
MEMG5-102_CPb	2722	483.7	0.13	0.15579	0.0003	9.89585	0.32951	0.46068	0.01531	0.998	1.6	.	2411	3	2425	31	2443	68
MEMG5-103_CPb	13107	190.1	11.47	0.07916	0.00084	0.33908	0.01289	0.03107	0.00113	0.96	-84.48	-79.72	1176	20	296	10	197	7
MEMG5-104_CPb	7872	327.3	5.78	0.12732	0.00061	1.76429	0.05763	0.1005	0.00325	0.989	-73.33	-69.14	2061	8	1032	21	617	19
MEMG5-105_CPb	1549	266.6	2.26	0.15408	0.00126	9.04618	0.29227	0.42581	0.01331	0.967	-5.21	.	2392	14	2343	30	2287	60
MEMG5-106_CPb	10604	297.8	3.22	0.11705	0.00041	1.14702	0.04055	0.07107	0.0025	0.995	-79.41	-75.66	1912	6	776	19	443	15
MEMG5-107_CPb	5372	238.8	12.41	0.13967	0.00135	1.89072	0.06649	0.09818	0.00332	0.962	-76.16	-72.42	2223	16	1078	23	604	19
MEMG5-107-1_CPb	7254	386.4	7.31	0.14389	0.00259	3.43438	0.19989	0.1731	0.00958	0.951	-59.09	-48.19	2275	29	1512	46	1029	53

Name	U	^{206}Pb	$^{206}Pb_c$(%)	$^{207}Pb/^{206}Pb^*$	1SE	$^{207}Pb/^{235}U^*$	1SE	$^{206}Pb/^{238}U^*$	1SE	Rho	Central (%)	Min. rim (%)	207/206	1s	207/235	1s	206/238	1s
MEMG5-108_CPb	5142	434.5	2.53	0.1531	0.00055	4.95279	0.11152	0.23463	0.00522	0.987	-47.48	-42.49	2381	6	1811	19	1359	27
MEMG5-109_CPb	17716	511	15.14	0.08633	0.00398	0.89529	0.05171	0.07522	0.00262	0.603	-67.59	-55.42	1346	85	649	28	468	16
MEMG5-110_CPb	12833	484.2	17.25	0.07964	0.0006	0.93972	0.02195	0.08558	0.00189	0.947	-57.71	-50.53	1188	14	673	11	529	11
MEMG5-111_CPb	29344	404.8	38.52	0.05738	0.00087	0.18951	0.00487	0.02396	0.0005	0.805	-70.67	-55.47	506	34	176	4	153	3
MEMG5-112_CPb	2880	438.2	0.55	0.15451	0.00051	9.28042	0.20135	0.43563	0.00934	0.988	-3.25	.	2396	6	2366	20	2331	42
MEMG5-113_CPb	6931	723.8	2.3	0.14422	0.00048	5.74515	0.10626	0.28892	0.00526	0.984	-31.85	-26.44	2278	6	1938	16	1636	26
MEMG5-114_CPb	9220	726.4	13.48	0.11127	0.00119	2.94673	0.06551	0.19208	0.00374	0.877	-41.13	-35	1820	19	1394	17	1133	20
MEMG5-115	1333	224.6	.	0.19132	0.00068	12.88044	0.30596	0.48828	0.01147	0.989	-8.37	.	2754	6	2671	22	2563	50
MEMG5-116_CPb	16420	442.8	16.91	0.09875	0.00148	0.88174	0.02599	0.06476	0.00165	0.862	-77.02	-73.44	1601	28	642	14	405	10
MEMG5-117_CPb	22789	658.7	20.41	0.10999	0.00139	0.99041	0.02515	0.06531	0.00144	0.867	-79.72	-77.28	1799	22	699	13	408	9
MEMG5-118_CPb	4385	572.7	0.44	0.15395	0.00057	8.02527	0.19165	0.37809	0.00892	0.988	-15.77	-7.29	2390	6	2234	22	2067	42
MEMG5-119_CPb	12788	508.6	.	0.14002	0.00088	2.18319	0.05217	0.11309	0.00261	0.964	-72.6	-69.75	2227	11	1176	17	691	15
MEMG5-12_CPb	3528	317.5	10.88	0.16103	0.00222	4.6994	0.10689	0.21166	0.00383	0.795	-54.59	-51	2466	23	1767	19	1238	20
MEMG5-120_CPb	18710	449.6	16.98	0.08973	0.0014	0.70744	0.02019	0.05718	0.00137	0.837	-76.79	-72.97	1420	29	543	12	358	8
MEMG5-121	1877	373.4	.	0.20948	0.00056	16.39239	0.37123	0.56755	0.01276	0.993	-0.16	.	2901	4	2900	22	2898	52
MEMG5-122_CPb	12712	543.4	3.97	0.16971	0.0007	2.68063	0.07233	0.11456	0.00305	0.988	-76.44	-73.85	2555	6	1323	20	699	18
MEMG5-123_CPb	3271	474.4	1.5	0.14849	0.0007	8.28688	0.18916	0.40475	0.00904	0.979	-6.97	.	2329	8	2263	21	2191	41
MEMG5-124_CPb	7735	998.5	0.33	0.15198	0.00041	7.5613	0.18812	0.36084	0.00892	0.994	-18.72	-10.08	2368	4	2180	22	1986	42

Name	U	^{206}Pb	$^{206}Pb_c$(%)	$^{207}Pb/^{206}Pb^*$	1SE	$^{207}Pb/^{235}U^*$	1SE	$^{206}Pb/^{238}U^*$	1SE	Rho	Central (%)	Min. rim (%)	207/206	1s	207/235	1s	206/238	1s
MEMG5-125_CPb	36629	227.8	29.02	0.07489	0.00215	0.12862	0.00547	0.01246	0.00039	0.739	-93.07	-90.57	1066	55	123	5	80	2
MEMG5-126_CPb	12602	468.7	12.26	0.1267	0.00105	1.58776	0.0436	0.09089	0.00238	0.954	-75.76	-72.69	2053	14	965	17	561	14
MEMG5-127_CPb	10903	473.3	3.76	0.1335	0.00047	2.14306	0.05923	0.11643	0.00319	0.992	-70.5	-66.74	2145	6	1163	19	710	18
MEMG5-128_CPb	25703	341.7	6.19	0.12217	0.00064	0.58808	0.01901	0.03491	0.00111	0.987	-90.34	-88.8	1988	9	470	12	221	7
MEMG5-129	4312	655.9	.	0.15601	0.00048	9.3011	0.24252	0.4324	0.01119	0.993	-4.75	.	2413	5	2368	24	2317	50
MEMG5-130_CPb	6316	1009.4	0.62	0.1508	0.0005	9.32985	0.24586	0.44871	0.01173	0.992	1.75	.	2355	6	2371	24	2390	52
MEMG5-131	1901	304.5	.	0.15492	0.00046	9.74146	0.24469	0.45604	0.01137	0.993	1.05	.	2401	5	2411	23	2422	50
MEMG5-132_CPb	4770	803.9	0.5	0.15497	0.00053	10.19136	0.26872	0.47696	0.01247	0.992	5.66	.	2402	6	2452	24	2514	54
MEMG5-133_CPb	20226	367.4	28.85	0.10644	0.00215	0.52821	0.02033	0.03599	0.00118	0.851	-88.38	-86.14	1739	36	431	14	228	7
MEMG5-134	3094	505.7	.	0.15619	0.00051	10.03377	0.26746	0.4659	0.01232	0.992	2.53	.	2415	5	2438	25	2466	54

Table 11: GOUD2

	ppm			*Ratios*							*U-Pb discordance*		*Ages (Ma)*					
Name	**U**	**^{206}Pb**	**^{206}Pb$_c$(%)**	**^{207}Pb/^{206}Pb***	**1SE**	**^{207}Pb/^{235}U***	**1SE**	**^{206}Pb/^{238}U***	**1SE**	**Rho**	**Central (%)**	**Minimum rim (%)**	**207/206**	**1s**	**207/235**	**1s**	**206/238**	**1s**
GOUD2-1	2039	282	.	0.12958	0.00051	6.25349	0.09461	0.35001	0.00511	0.966	-8.72	-2.57	2092	7	2012	13	1935	24
GOUD2-2	2488	407.3	.	0.14558	0.00057	8.34153	0.1284	0.41556	0.00619	0.967	-2.81	.	2295	7	2269	14	2240	28
GOUD2-3	4675	824.8	.	0.15882	0.00063	9.89099	0.14951	0.45167	0.00659	0.965	-1.99	.	2443	6	2425	14	2403	29
GOUD2-4	2870	468.8	.	0.14262	0.00056	8.14625	0.12407	0.41426	0.0061	0.966	-1.3	.	2259	6	2247	14	2234	28
GOUD2-5	1452	221	.	0.13945	0.00056	7.51051	0.11722	0.39063	0.00589	0.967	-5	.	2220	7	2174	14	2126	27
GOUD2-6	5195	900.5	.	0.14158	0.00059	8.60842	0.14375	0.44099	0.00713	0.968	5.77	.	2247	7	2297	15	2355	32
GOUD2-7	1493	237.2	.	0.14594	0.00059	8.1695	0.11976	0.406	0.00572	0.962	-5.25	.	2299	7	2250	13	2197	26
GOUD2-8	12890	1008.5	.	0.09773	0.00056	2.65331	0.03988	0.19691	0.00274	0.926	-29.16	-23.48	1581	10	1316	11	1159	15
GOUUD2-9	2106	323.6	.	0.137	0.00069	7.46883	0.13758	0.39541	0.00701	0.962	-2.24	.	2190	8	2169	16	2148	32
GOUUD2-10	2555	413	.	0.14096	0.00061	7.89113	0.14651	0.406	0.00733	0.973	-2.24	.	2239	7	2219	17	2197	34
GOUUD2-11	2209	341.9	.	0.14051	0.00061	7.76826	0.13446	0.40098	0.00672	0.968	-3.16	.	2233	7	2205	16	2174	31
GOUUD2-12	1123	175	.	0.14436	0.00062	7.94976	0.12609	0.39941	0.0061	0.962	-5.87	.	2280	7	2225	14	2166	28
GOUUD2-13	2579	404.3	.	0.14261	0.00065	7.89445	0.12319	0.4015	0.00599	0.956	-4.34	.	2259	8	2219	14	2176	28
GOUUD2-14	6743	1125.4	.	0.13804	0.0006	8.14124	0.15947	0.42774	0.00817	0.975	5.01	.	2203	7	2247	18	2296	37
GOUUD2-15	1355	240.6	.	0.16877	0.00085	10.65732	0.18659	0.45798	0.00768	0.958	-5.41	.	2545	8	2494	16	2431	34
GOUUD2-16	1834	383.2	.	0.20143	0.0009	14.95903	0.25383	0.53862	0.00881	0.964	-2.61	.	2838	7	2813	16	2778	37
GOUUD2-17	3022	490.8	.	0.14353	0.00064	8.20783	0.1435	0.41474	0.00701	0.967	-1.76	.	2270	7	2254	16	2237	32
GOUUD2-19	2591	415.2	.	0.14242	0.00065	8.15092	0.15043	0.41507	0.00743	0.969	-0.99	.	2257	7	2248	17	2238	34
GOUUD2-20	769	119.7	.	0.15064	0.00081	8.34637	0.1388	0.40184	0.00632	0.946	-8.79	-2.64	2353	9	2269	15	2178	29
GOUUD2-21	3922	644.1	.	0.14191	0.00065	8.27919	0.15654	0.42314	0.00776	0.97	1.27	.	2251	8	2262	17	2275	35
GOUUD2-23	1814	293.3	.	0.14637	0.00067	8.40313	0.14644	0.41639	0.007	0.964	-3.07	.	2304	8	2276	16	2244	32
GOUD2-24	1378	213	.	0.14242	0.00072	7.73887	0.13389	0.39409	0.00652	0.956	-5.99	.	2257	8	2201	16	2142	30
GOUD-26	3207	659.2	.	0.19188	0.00104	14.06369	0.27691	0.53158	0.01006	0.962	-0.46	.	2758	8	2754	19	2748	42
GOUD-27	4554	673.6	.	0.13696	0.00072	7.52576	0.16868	0.39853	0.00868	0.972	-1.44	.	2189	8	2176	20	2162	40
GOUD-28 CPb	3345	365.3	0.73	0.1158	0.00067	4.40917	0.09602	0.27614	0.0058	0.965	-19.06	-10.48	1892	10	1714	18	1572	29
GOUD-29	964	158.9	.	0.14883	0.00076	8.7224	0.17281	0.42504	0.00814	0.966	-2.51	.	2333	9	2309	18	2283	37
GOUD-30	1262	196.1	.	0.14448	0.00074	7.98482	0.14533	0.40082	0.007	0.96	-5.62	.	2282	9	2229	16	2173	32
GOUD-32 CPb	5282	702.4	0.2	0.12933	0.00069	5.89962	0.14183	0.33083	0.00775	0.975	-13.56	-4.03	2089	9	1961	21	1842	38

Name	U	^{206}Pb	$^{206}Pb_c$(%)	$^{207}Pb/^{206}Pb^*$	1SE	$^{207}Pb/^{235}U^*$	1SE	$^{206}Pb/^{238}U^*$	1SE	Rho	Central (%)	Min. rim (%)	207/206	1s	207/235	1s	206/238	1s
GOUD-34 CPb	3300	568.6	0.82	0.14534	0.00107	8.90567	0.1817	0.44439	0.00845	0.932	4.09	.	2292	12	2328	19	2370	38
GOUD-35	2122	366.1	.	0.16066	0.00089	9.87706	0.18945	0.44587	0.00819	0.957	-4.16	.	2463	9	2423	18	2377	37
GOUD-36	2464	392.7	.	0.14155	0.00074	8.06891	0.15008	0.41342	0.00738	0.96	-0.83	.	2246	9	2239	17	2231	34
GOUD-38	3611	691.4	.	0.18178	0.00124	12.60021	0.2871	0.50272	0.01093	0.954	-1.99	.	2669	11	2650	21	2625	47
GOUD-39	845	153.7	.	0.16262	0.00088	10.7584	0.22559	0.47981	0.00972	0.966	2.11	.	2483	9	2502	19	2526	42
GOUD-40	1374	113.4	.	0.13146	0.00158	3.81993	0.09105	0.21075	0.00434	0.863	-45.8	-40.47	2118	21	1597	19	1233	23
GOUD2-41	2796	449.1	.	0.14428	0.00079	8.19813	0.16036	0.41211	0.00774	0.96	-2.84	.	2279	9	2253	18	2225	35
GOUD2-42	3813	455.9	.	0.12598	0.0007	5.22426	0.11528	0.30077	0.00642	0.968	-19.32	-11.11	2043	9	1857	19	1695	32
GOUD2-43	3733	802.3	.	0.19963	0.0011	15.30086	0.30539	0.55588	0.01066	0.961	1.16	.	2823	8	2834	19	2850	44
GOUD2-46	10155	1270.3	.	0.14006	0.00073	6.65651	0.15422	0.34469	0.00778	0.974	-16.51	-8.06	2228	9	2067	20	1909	37
GOUD2-47	8355	1214.8	.	0.13274	0.00074	7.41725	0.10756	0.40526	0.00542	0.923	3.24	.	2135	10	2163	13	2193	25
GOUD2-48	5732	626.4	.	0.1326	0.00079	5.59832	0.14515	0.30622	0.00773	0.973	-21.91	-12.73	2133	10	1916	22	1722	38
GOUD2-49 CPb	13510	1093	0.33	0.10163	0.00061	3.17405	0.05118	0.22652	0.00339	0.929	-22.56	-16.09	1654	11	1451	12	1316	18
GOUD2-50 CPb	6583	694.7	0.46	0.12321	0.00084	4.88835	0.08964	0.28776	0.0049	0.928	-21.04	-14.54	2003	12	1800	15	1630	25
GOUD2-51	3115	468.8	.	0.14245	0.00084	8.44179	0.12159	0.4298	0.00565	0.913	2.51	.	2257	10	2280	13	2305	25
GOUD2-52	3214	484.7	.	0.14263	0.00086	8.36792	0.10766	0.4255	0.00484	0.885	1.37	.	2259	9	2272	12	2285	22
GOUD2-53	2693	358.9	.	0.12751	0.00078	6.47363	0.08937	0.36821	0.00456	0.897	-2.43	.	2064	10	2042	12	2021	21
GOUD2-54	2325	304.2	.	0.12736	0.00079	6.46435	0.08433	0.36812	0.00423	0.88	-2.33	.	2062	10	2041	11	2021	20
GOUD2-55	2041	273.7	.	0.12771	0.0008	6.62642	0.08398	0.37633	0.00414	0.869	-0.43	.	2067	10	2063	11	2059	19
GOUD2-56	1924	274.5	.	0.14099	0.00097	7.81231	0.11464	0.40188	0.00522	0.884	-3.24	.	2239	11	2210	13	2178	24
GOUD2-58	2338	369.3	.	0.15804	0.0011	9.73225	0.15954	0.44664	0.00663	0.905	-2.68	.	2435	11	2410	15	2380	30
GOUD2-60	2721	375.2	.	0.13975	0.001	7.42298	0.1223	0.38525	0.00571	0.9	-6.49	-0.26	2224	12	2164	15	2101	27
GOUD2-61	1917	248.3	.	0.13151	0.00097	6.59238	0.09805	0.36355	0.0047	0.868	-6.55	-0.9	2118	13	2058	13	1999	22
GOUD2-62	1286	183.1	.	0.14521	0.00107	8.05395	0.11778	0.40227	0.00509	0.865	-5.7	-0.41	2290	13	2237	13	2180	23
GOUD2-64	3756	534.1	.	0.15163	0.00118	8.20306	0.15994	0.39237	0.00702	0.918	-11.44	-4.6	2364	13	2254	18	2134	32
GOUD2-66	4986	664.5	.	0.13316	0.00105	6.67682	0.15875	0.36366	0.00815	0.943	-7.63	.	2140	14	2070	21	2000	39
GOUD2-65	2171	345.1	.	0.14586	0.00112	9.05886	0.1491	0.45043	0.00656	0.885	5.17	.	2298	13	2344	15	2397	29
GOUD2-67	4471	564.6	.	0.1419	0.00123	7.07934	0.14611	0.36184	0.00678	0.908	-13.4	-6.11	2251	14	2121	18	1991	32
GOUD2-68 CPb	6503	515	1.04	0.12928	0.00107	3.80914	0.13648	0.2137	0.00745	0.973	-44.14	-34.69	2088	14	1595	29	1249	40
GOUD2-69	9984	1068.5	.	0.11565	0.0005	4.55144	0.08171	0.28544	0.00497	0.971	-16.22	-8.92	1890	7	1740	15	1619	25

Name	U	^{206}Pb	$^{206}Pb_c$(%)	$^{207}Pb/^{206}Pb^*$	1SE	$^{207}Pb/^{235}U^*$	1SE	$^{206}Pb/^{238}U^*$	1SE	Rho	Central (%)	Min. rim (%)	207/206	1s	207/235	1s	206/238	1s
GOUD2-70	3452	454	.	0.14288	0.00077	7.02991	0.17728	0.35685	0.00879	0.977	-15.12	-5.81	2262	9	2115	22	1967	42
GOUD2-72	4984	421.9	.	0.11477	0.00072	3.65829	0.0629	0.23118	0.0037	0.931	-31.57	-26.03	1876	11	1562	14	1341	19
GOUD2-74	4210	616.3	.	0.13745	0.00057	7.58889	0.09822	0.40043	0.00491	0.948	-1.31	.	2195	7	2184	12	2171	23
GOUD2-75	1225	200.3	.	0.16472	0.00083	10.38533	0.13071	0.45727	0.00527	0.916	-3.7	.	2505	8	2470	12	2427	23
GOUD2-76	2435	314.7	.	0.12985	0.00054	6.42107	0.07576	0.35865	0.00396	0.936	-6.65	-1.91	2096	7	2035	10	1976	19
GOUD2-77	8639	1265.4	.	0.13804	0.00063	7.59099	0.10363	0.39884	0.00513	0.943	-2.09	.	2203	7	2184	12	2164	24
GOUD2-78	3392	426.4	.	0.12667	0.00053	6.05991	0.08158	0.34696	0.00444	0.951	-7.45	-1.91	2052	7	1984	12	1920	21
GOUD2-79	6335	932.6	.	0.16513	0.00095	9.15426	0.13936	0.40206	0.00566	0.925	-15.5	-10.59	2509	9	2354	14	2179	26
GOUD2-80	8993	1296.5	.	0.13275	0.00057	7.26676	0.08555	0.39702	0.00435	0.931	1.14	.	2135	7	2145	11	2155	20
GOUD2-81	2010	350.9	.	0.18324	0.00091	12.54163	0.2255	0.4964	0.00858	0.961	-3.81	.	2682	8	2646	17	2598	37
GOUD2-82	1457	213.5	.	0.14778	0.00064	8.25712	0.09687	0.40525	0.00442	0.93	-6.46	-2.07	2320	7	2260	11	2193	20
GOUD2-83	5443	290	.	0.12148	0.00058	2.3938	0.08072	0.14292	0.00477	0.99	-60.2	-53.53	1978	8	1241	24	861	27

Table 12: MEPB44

	ppm			*Ratios*							*U-Pb discordance*		*Ages (Ma)*					
Name	**U**	**^{206}Pb**	**^{206}Pb$_c$(%)**	**^{207}Pb/^{206}Pb***	**1SE**	**^{207}Pb/^{235}U***	**1SE**	**^{206}Pb/^{238}U***	**1SE**	**Rho**	**Central (%)**	**Minimum rim (%)**	**207/206**	**1s**	**207/235**	**1s**	**206/238**	**1s**
MEPB44-1-CPb	4503	441.6	15.64	0.11169	0.0028	3.61512	0.11103	0.23475	0.00417	0.579	-28.36	-19.89	1827	43	1553	24	1359	22
MEPB44-2	1521	193.7	.	0.12713	0.00036	6.40135	0.08612	0.3652	0.0048	0.978	-2.93	.	2059	5	2032	12	2007	23
MEPB44-3	1902	235.1	.	0.1258	0.00039	6.04725	0.07165	0.34864	0.00399	0.966	-6.35	-1.36	2040	5	1983	10	1928	19
MEPB44-4_CPb	6480	499.5	31.99	0.11083	0.00646	2.36926	0.15281	0.15505	0.00428	0.428	-52.26	-39.41	1813	103	1233	46	929	24
MEPB44-5	1933	252.9	.	0.12703	0.00038	6.50768	0.08127	0.37154	0.00451	0.971	-1.17	.	2057	5	2047	11	2037	21
MEPB44-7	1343	175.8	.	0.12711	0.00039	6.49376	0.09316	0.37052	0.0052	0.977	-1.51	.	2058	5	2045	13	2032	24
MEPB44-8_CPb	2827	359.2	0.57	0.12766	0.00055	6.11154	0.11349	0.34721	0.00627	0.973	-8.1	-0.32	2066	7	1992	16	1921	30
MEPB44-10	1226	171.6	.	0.12912	0.00043	6.91268	0.0897	0.38829	0.00487	0.966	1.63	.	2086	6	2100	12	2115	23
MEPB44-11	1701	228.6	.	0.12817	0.00042	6.64877	0.09644	0.37623	0.00532	0.974	-0.81	.	2073	5	2066	13	2059	25
MEPB44-12	1663	226.3	.	0.12889	0.00046	6.66447	0.09021	0.37501	0.0049	0.965	-1.68	.	2083	6	2068	12	2053	23
MEPB44-16	999	133.8	.	0.1278	0.00047	6.46749	0.0956	0.36704	0.00526	0.969	-2.95	.	2068	6	2041	13	2015	25
MEPB44-17_CPb	6994	577	17.39	0.10077	0.00307	2.57376	0.08904	0.18523	0.00305	0.475	-35.99	-26.71	1638	56	1293	25	1096	17
MEPB44-18	1855	259.6	.	0.12972	0.0005	6.78115	0.09221	0.37913	0.00494	0.959	-1.23	.	2094	6	2083	12	2072	23
MEPB44-19_CPd	1331	178.9	3.91	0.16214	0.00147	8.38909	0.18283	0.37524	0.00744	0.91	-19.95	-13.26	2478	15	2274	20	2054	35
MEPB44-20	1560	225.2	.	0.12817	0.00054	6.8613	0.1343	0.38824	0.00742	0.976	2.35	.	2073	7	2094	17	2115	34
MEPB44-21	1889	151.3	.	0.12417	0.00054	3.68678	0.0674	0.21534	0.00382	0.971	-41.38	-36.42	2017	8	1569	15	1257	20
MEPB44-22_CPb	2105	232.9	10.23	0.12139	0.00327	4.42607	0.14994	0.26444	0.00543	0.606	-26.31	-17.24	1977	46	1717	28	1513	28
MEPB44-24	2024	264.3	.	0.12732	0.00055	6.01881	0.08678	0.34286	0.00471	0.954	-9	-3.17	2061	7	1979	13	1900	23
MEPB44-25	1723	247.5	.	0.12796	0.00056	6.67692	0.10869	0.37843	0.00593	0.963	-0.07	.	2070	7	2070	14	2069	28
MEPB44-26	1012	144.8	.	0.1282	0.00058	6.69335	0.10478	0.37865	0.00568	0.958	-0.2	.	2073	8	2072	14	2070	27
MEPB44-27	1164	167.7	.	0.12816	0.00055	6.66091	0.12117	0.37694	0.00666	0.972	-0.62	.	2073	7	2067	16	2062	31
MEPB44-28	1049	151.5	.	0.12827	0.00056	6.72415	0.14566	0.38021	0.00806	0.979	0.16	.	2074	8	2076	19	2077	38
MEPB44-29	969	134.9	.	0.12753	0.00061	6.40128	0.10032	0.36404	0.00544	0.953	-3.55	.	2064	8	2032	14	2001	26
MEPB44-30_CPb	4688	403.5	7.81	0.11703	0.00422	3.22269	0.14117	0.19972	0.00497	0.569	-42.14	-32.38	1911	63	1463	34	1174	27

Name	U	^{206}Pb	$^{206}Pb_c$(%)	$^{207}Pb/^{206}Pb^*$	1SE	$^{207}Pb/^{235}U^*$	1SE	$^{206}Pb/^{238}U^*$	1SE	Rho	Central (%)	Min. rim (%)	207/206	1s	207/235	1s	206/238	1s
MEPB44-32_CPb	6796	433.4	3.28	0.10427	0.00079	2.36691	0.10103	0.16464	0.00692	0.984	-45.49	-32.03	1701	14	1233	30	983	38
MEPB44-33	2255	285	.	0.13119	0.00031	6.2756	0.12376	0.34695	0.00679	0.993	-10.6	-2.54	2114	4	2015	17	1920	33
MEPB44-34	1461	202.4	.	0.12814	0.00024	6.47814	0.0955	0.36667	0.00536	0.992	-3.31	.	2073	3	2043	13	2014	25
MEPB44-35	2784	390.2	.	0.12749	0.00024	6.47295	0.09733	0.36823	0.00549	0.992	-2.41	.	2064	3	2042	13	2021	26
MEPB44-36	2484	351.6	.	0.12748	0.00024	6.53891	0.09957	0.37202	0.00562	0.993	-1.39	.	2063	3	2051	13	2039	26
MEPB44-37	2558	295	.	0.12731	0.00026	5.50438	0.09357	0.31358	0.00529	0.993	-16.77	-10.23	2061	3	1901	15	1758	26
MEPB44-38	2215	304.9	.	0.12721	0.00023	6.44122	0.0981	0.36723	0.00555	0.993	-2.46	.	2060	3	2038	13	2016	26
MEPB44-39_CPb	3617	379.6	13.54	0.12276	0.00584	4.07069	0.20565	0.2405	0.0041	0.338	-33.76	-22.66	1997	82	1648	41	1389	21
MEPB44-40_CPb	2253	327	1.77	0.12699	0.00072	6.54746	0.10292	0.37395	0.00548	0.933	-0.5	.	2057	9	2052	14	2048	26
MEPB44-41	2063	286.2	.	0.12782	0.00024	6.46033	0.09338	0.36657	0.00525	0.991	-3.09	.	2068	3	2041	13	2013	25
MEPB44-42_CPb	4110	364	9.15	0.12144	0.00125	3.57086	0.08498	0.21326	0.00458	0.902	-40.6	-34.24	1977	18	1543	19	1246	24
MEPB44-43_CPb	6913	636.9	2.88	0.10847	0.00104	3.47695	0.06785	0.23247	0.00396	0.872	-26.61	-19.85	1774	17	1522	15	1347	21
MEPB44-44	2550	363.5	.	0.12741	0.00025	6.54024	0.0972	0.37228	0.00548	0.991	-1.27	.	2063	3	2051	13	2040	26
MEPB44-45	3134	306.8	.	0.12825	0.00031	4.71436	0.092	0.2666	0.00516	0.992	-29.76	-23.42	2074	4	1770	16	1523	26
MEPB44-46_CPb	5740	614.1	0.27	0.12042	0.00042	4.83004	0.09034	0.29091	0.00535	0.983	-18.25	-10.95	1962	6	1790	16	1646	27
MEPB44-47_CPb	3651	525.3	1.9	0.12555	0.00253	6.40711	0.16822	0.37013	0.00623	0.641	-0.37	.	2037	33	2033	23	2030	29
MEPB44-49	2884	399.3	.	0.12896	0.0003	6.44726	0.09915	0.3626	0.00551	0.989	-4.98	.	2084	4	2039	14	1994	26
MEPB444-94	2529	347.8	.	0.12752	0.00036	6.32097	0.13495	0.35951	0.00761	0.991	-4.73	.	2064	5	2021	19	1980	36
MEPB44-50	2790	393.6	.	0.12778	0.00026	6.48518	0.09805	0.36809	0.00551	0.991	-2.66	.	2068	3	2044	13	2020	26
MEPB44-53	1178	172	.	0.12865	0.00027	6.765	0.11506	0.38139	0.00644	0.993	0.18	.	2080	4	2081	15	2083	30
MEPB44-54	4177	452.3	.	0.15828	0.00097	6.13663	0.11166	0.28119	0.00482	0.941	-38.81	-34.4	2437	10	1995	16	1597	24
MEPB44-59	2205	314.7	.	0.1279	0.00028	6.64095	0.10488	0.37658	0.00589	0.991	-0.51	.	2069	4	2065	14	2060	28
MEPB44-61	2025	283.2	.	0.12816	0.00027	6.43111	0.10454	0.36394	0.00586	0.991	-4.04	.	2073	4	2037	14	2001	28
MEPB44-63_CPb	10330	601	28.36	0.1059	0.00513	1.61099	0.08573	0.11033	0.00244	0.415	-64.16	-56.22	1730	89	974	33	675	14

Name	U	^{206}Pb	$^{206}Pb_c$(%)	$^{207}Pb/^{206}Pb^*$	1SE	$^{207}Pb/^{235}U^*$	1SE	$^{206}Pb/^{238}U^*$	1SE	Rho	Central (%)	Min. rim (%)	207/206	1s	207/235	1s	206/238	1s
MEPB44-64	2989	438	.	0.12738	0.00031	6.5554	0.11228	0.37326	0.00633	0.99	-0.98	.	2062	4	2053	15	2045	30
MEPB44-65_CPb	4886	694.1	12.48	0.1197	0.00311	5.3171	0.16575	0.32216	0.00555	0.553	-8.89	.	1952	46	1872	27	1800	27
MEPB44-66	1363	195.6	.	0.12953	0.00039	6.93699	0.13953	0.38843	0.00772	0.989	1.35	.	2092	5	2103	18	2116	36
MEPB44-67	1271	179.9	.	0.12815	0.00029	6.6478	0.11563	0.37622	0.00649	0.992	-0.8	.	2073	4	2066	15	2059	30
MEPB44-69	2888	275	.	0.12414	0.0003	4.45686	0.12291	0.26038	0.00715	0.996	-29.11	-19.65	2017	4	1723	23	1492	37
MEPB44-70	2942	426.2	.	0.12796	0.00035	6.5438	0.12064	0.3709	0.00676	0.989	-2.06	.	2070	5	2052	16	2034	32
MEPB44-71	1555	227.2	.	0.12782	0.00035	6.61091	0.13329	0.37512	0.00749	0.991	-0.83	.	2068	5	2061	18	2053	35
MEPB44-72	1947	281.8	.	0.12756	0.00035	6.46766	0.11995	0.36772	0.00675	0.989	-2.59	.	2065	5	2042	16	2019	32
MEPB44-73	2064	303.8	.	0.12872	0.00037	6.77738	0.12962	0.38187	0.00722	0.989	0.25	.	2081	5	2083	17	2085	34
MEPB44-74	2716	362.7	.	0.12632	0.00031	6.11028	0.13433	0.35083	0.00766	0.994	-6.15	.	2047	4	1992	19	1939	37
MEPB44-75_CPb	36235	541.4	23.32	0.08161	0.00205	0.33315	0.01183	0.02961	0.00074	0.708	-85.99	-82.74	1236	46	292	9	188	5
MEPB44-76_CPb	8854	753.5	31.79	0.11561	0.00213	2.48427	0.06936	0.15584	0.00327	0.752	-54.24	-48.96	1889	31	1267	20	934	18
MEPB44-78	1147	164.7	.	0.1282	0.00033	6.59643	0.11795	0.37318	0.0066	0.99	-1.64	.	2073	4	2059	16	2044	31
MEPB44-79_CPb	6470	720.7	6.85	0.11805	0.00335	4.27504	0.15562	0.26265	0.00597	0.625	-24.61	-14.17	1927	50	1689	30	1503	31
MEPB44-80	1703	233.7	.	0.12781	0.00032	6.28494	0.11216	0.35665	0.0063	0.99	-5.71	.	2068	4	2016	16	1966	30
MEPB44-81	2200	303.7	.	0.12742	0.00031	6.39854	0.11893	0.36419	0.00671	0.991	-3.42	.	2063	4	2032	16	2002	32
MEPB44-82	2415	340.8	.	0.12755	0.00031	6.43981	0.11734	0.36618	0.00661	0.991	-2.99	.	2064	4	2038	16	2011	31
MEPB44-83_CPb	7203	274.9	1.24	0.11178	0.00063	1.63142	0.08617	0.10585	0.00556	0.994	-67.73	-58.08	1829	10	982	33	649	32
MEPB44-84	1846	258	.	0.12755	0.00035	6.32618	0.12254	0.35971	0.0069	0.99	-4.71	.	2064	5	2022	17	1981	33
MEPB44-85	1581	222	.	0.12711	0.00036	6.35106	0.13009	0.36238	0.00735	0.991	-3.66	.	2058	5	2026	18	1993	35
MEPB44-86	2562	354	.	0.12676	0.00043	6.13065	0.11509	0.35077	0.00648	0.984	-6.5	.	2054	6	1995	16	1938	31
MEPB44-87	2378	328.6	.	0.12711	0.00035	6.3518	0.13074	0.36243	0.00739	0.991	-3.65	.	2058	5	2026	18	1994	35
MEPB44-88	1731	245.4	.	0.12766	0.00036	6.47484	0.13199	0.36785	0.00743	0.99	-2.64	.	2066	5	2042	18	2019	35
MEPB44-89	2207	273.6	.	0.12746	0.00035	5.69611	0.13404	0.32412	0.00757	0.993	-14.07	-4.59	2063	5	1931	20	1810	37
MEPB44-90	2324	335.8	.	0.12753	0.00036	6.58745	0.13706	0.37465	0.00772	0.991	-0.73	.	2064	5	2058	18	2051	36
MEPB44-91	2024	295.1	.	0.12841	0.00049	6.52093	0.12773	0.36831	0.00708	0.981	-3.08	.	2076	7	2049	17	2021	33

Name	U	^{206}Pb	$^{206}Pb_c$(%)	$^{207}Pb/^{206}Pb^*$	1SE	$^{207}Pb/^{235}U^*$	1SE	$^{206}Pb/^{238}U^*$	1SE	Rho	Central (%)	Min. rim (%)	207/206	1s	207/235	1s	206/238	1s
MEPB44-92	973	137.1	.	0.12807	0.00038	6.46898	0.13175	0.36634	0.00738	0.989	-3.34	.	2072	5	2042	18	2012	35
MEPB44-96	2825	330.9	.	0.12587	0.00055	5.0467	0.12073	0.29079	0.00684	0.983	-21.94	-13.17	2041	8	1827	20	1645	34
MEPB44-98_CPb	3488	427.8	9.37	0.1249	0.00154	4.89016	0.11635	0.28396	0.00578	0.856	-23.16	-15.42	2027	21	1801	20	1611	29
MEPB44-99	1448	202.2	.	0.12762	0.0004	6.39341	0.13898	0.36335	0.00781	0.989	-3.79	.	2065	5	2031	19	1998	37
MEPB44-100	2323	330.1	.	0.12708	0.00045	6.33026	0.13453	0.36127	0.00757	0.986	-3.94	.	2058	6	2023	19	1988	36
MEPB44-106	1398	175	.	0.12972	0.00064	6.05558	0.19333	0.33856	0.01068	0.988	-11.8	.	2094	8	1984	28	1880	51
MEPB44-107	1504	201.1	.	0.12819	0.00047	6.39252	0.20876	0.36167	0.01174	0.994	-4.67	.	2073	6	2031	29	1990	56
MEPB44-108	2022	289.1	.	0.1274	0.00048	6.36634	0.13583	0.36242	0.00761	0.985	-3.88	.	2062	6	2028	19	1994	36
MEPB44-110_CPb	3783	610.1	21.78	0.12562	0.00387	5.4853	0.25159	0.3167	0.01076	0.741	-14.8	.	2038	51	1898	39	1774	53
MEPB44-111	2193	262.6	.	0.12407	0.00087	5.36203	0.19775	0.31344	0.01135	0.982	-14.61	.	2016	12	1879	32	1758	56
MEPB44-112_CPb	3448	420.6	5.12	0.12747	0.00078	5.34346	0.15076	0.30404	0.00837	0.976	-19.4	-8.76	2063	10	1876	24	1711	41
MEPB44-113	2134	307.8	.	0.12747	0.0004	6.57644	0.1715	0.37419	0.00969	0.993	-0.81	.	2063	5	2056	23	2049	45
MEPB44-114-CPb	2792	377.4	2.26	0.12623	0.0007	6.01037	0.15104	0.34533	0.00846	0.975	-7.56	.	2046	10	1977	22	1912	41
MEPB44-115_CPb	4254	411.8	22.49	0.08298	0.00193	2.30616	0.06244	0.20156	0.00281	0.515	-7.34	.	1269	45	1214	19	1184	15
MEPB44-116	1753	255.4	.	0.12796	0.00078	6.99113	0.10438	0.39627	0.0054	0.913	4.65	.	2070	10	2110	13	2152	25
MEPB44-117	998	146.8	.	0.12867	0.00072	7.03769	0.10089	0.39668	0.00523	0.92	4.17	.	2080	10	2116	13	2154	24
MEPB44-118_CPb	4407	395.2	41.77	0.11478	0.00185	2.44043	0.06515	0.15421	0.00328	0.798	-54.36	-49.1	1876	28	1255	19	924	18
MEPB44-119	847	117.7	.	0.12924	0.00057	7.05538	0.16658	0.39592	0.00919	0.983	3.52	.	2088	7	2118	21	2150	42
MEPB44-109	2000	278.6	.	0.12776	0.00042	6.3007	0.1392	0.35769	0.00782	0.989	-5.39	.	2067	5	2019	19	1971	37
MEPB44-120	911	120.1	.	0.1286	0.0006	6.48359	0.08459	0.36566	0.00446	0.934	-3.92	.	2079	8	2044	11	2009	21
MEPB44-121_CPb	2754	363.4	0.51	0.12691	0.00059	6.41021	0.12397	0.36633	0.00688	0.971	-2.46	.	2056	8	2034	17	2012	32
MEPB44-122	1181	162.7	.	0.1282	0.00056	6.77521	0.14122	0.38331	0.00781	0.978	1.04	.	2073	8	2082	18	2092	36
MEPB44-123	1148	151.2	.	0.12841	0.0006	6.55502	0.14171	0.37022	0.00782	0.976	-2.58	.	2076	8	2053	19	2030	37
MEPB44-124	705	96.2	.	0.12876	0.00063	6.59527	0.09205	0.37148	0.00485	0.936	-2.51	.	2081	8	2059	12	2036	23
MEPB44-127	1299	191.8	.	0.12871	0.00072	6.8005	0.08817	0.38321	0.00448	0.901	0.61	.	2080	9	2086	11	2091	21

Table 13: MEMG12

	ppm			*Ratios*							*U-Pb discordance*		*Ages (Ma)*					
Name	**U**	**^{206}Pb**	**^{206}Pb$_c$(%)**	**^{207}Pb*/^{206}Pb**	**1SE**	**^{207}Pb*/^{235}U**	**1SE**	**^{206}Pb*/^{238}U**	**1SE**	**Rho**	**Central (%)**	**Minimum rim (%)**	**207/206**	**1s**	**207/235**	**1s**	**206/238**	**1s**
MEMG12-1 CPb	122	44.7	28.14	0.14074	0.00722	5.68552	0.37689	0.29298	0.01231	0.634	-29.35	-12.32	2236	85	1929	57	1656	61
MEMG12-2 CPb	234	89.3	6.24	0.13063	0.00268	7.01383	0.32929	0.3894	0.01645	0.9	0.76	.	2106	35	2113	42	2120	76
MEMG12-3	183	62.2	.	0.12795	0.0017	6.56262	0.2988	0.372	0.0162	0.957	-1.76	.	2070	22	2054	40	2039	76
MEMG12-4 CPb	210	64.9	7.96	0.13359	0.00474	5.7673	0.3198	0.31311	0.01334	0.768	-20.72	-2.97	2146	61	1942	48	1756	65
MEMG12-5 CPb	343	84.4	22.29	0.13123	0.00338	3.84095	0.21968	0.21228	0.01084	0.893	-45.32	-30.9	2114	43	1601	46	1241	58
MEMG12-7 CPb	267	74.2	4.2	0.12959	0.00232	5.24901	0.2702	0.29377	0.01417	0.937	-23.39	-4.66	2092	30	1861	44	1660	71
MEMG12-8	122	41.5	.	0.13465	0.00195	6.68524	0.32762	0.36008	0.01685	0.955	-9.51	.	2160	24	2071	43	1983	80
MEMG12-9	160	65.1	.	0.12769	0.0017	7.49029	0.35368	0.42543	0.01927	0.959	12.58	.	2066	23	2172	42	2285	87
MEMG12-10 CPb	311	118.3	1.74	0.12843	0.00182	6.86768	0.32048	0.38783	0.01724	0.953	2.04	.	2077	25	2094	41	2113	80
MEMG12-11 CPb	872	93.4	7.29	0.07275	0.00099	1.06311	0.04646	0.10599	0.0044	0.95	-37.31	-9.6	1007	27	735	23	649	26
MEMG12-12	159	61.2	.	0.13132	0.00165	7.08643	0.37145	0.39137	0.01992	0.971	0.75	.	2116	22	2122	47	2129	92
MEMG12-13 CPb	193	89.1	38.95	0.14734	0.00678	5.61487	0.37378	0.27639	0.01329	0.722	-36.04	-20.2	2315	76	1918	57	1573	67
MEMG12-14	146	58.9	.	0.12624	0.00168	7.06687	0.35482	0.40602	0.01965	0.964	8.68	.	2046	23	2120	45	2197	90
MEMG12-15 CPb	155	65.4	17.11	0.12643	0.00716	5.99715	0.44353	0.34403	0.01636	0.643	-8.05	.	2049	92	1975	64	1906	78
MEMG12-16	219	84.5	.	0.12626	0.00166	6.76717	0.35205	0.38873	0.01957	0.968	4.04	.	2047	22	2081	46	2117	91
MEMG12-17	213	84.9	.	0.12565	0.00163	6.85375	0.36788	0.39562	0.02061	0.97	6.4	.	2038	22	2093	48	2149	95
MEMG12-18	162	65.1	.	0.12677	0.00161	6.94296	0.39374	0.3972	0.02195	0.975	5.87	.	2054	22	2104	50	2156	101
MEMG12-19 CPb	147	64.6	20.84	0.12871	0.00828	6.09551	0.49337	0.34347	0.01688	0.607	-9.82	.	2080	108	1990	71	1903	81
MEMG12-21 CPb	1033	128.3	26.21	0.07343	0.00373	0.88494	0.06002	0.08741	0.00393	0.662	-49.33	-11.13	1026	101	644	32	540	23

Name	U	^{206}Pb	$^{206}Pb_c$(%)	$^{207}Pb^*/^{206}Pb$	1SE	$^{207}Pb^*/^{235}U$	1SE	$^{206}Pb^*/^{238}U$	1SE	Rho	Central (%)	Min. rim (%)	207/206	1s	207/235	1s	206/238	1s
MEMG12-22	86	35.2	.	0.13444	0.00185	7.14014	0.38273	0.38518	0.01995	0.966	-3.06	.	2157	22	2129	48	2100	93
MEMG12-24	239	107.6	.	0.13361	0.00191	7.56029	0.44416	0.41038	0.02338	0.97	3.89	.	2146	24	2180	53	2217	107
MEMG12-25 CPb	1013	156	56.27	0.08373	0.01492	0.74147	0.14643	0.06423	0.00547	0.431	-70.91	.	1286	381	563	85	401	33
MEMG12-28 CPb	1149	162.5	16.63	0.0839	0.00132	1.23034	0.06382	0.10635	0.00526	0.953	-52.01	-32.49	1290	30	814	29	652	31
MEMG12-29 CPb	151	72.7	12.98	0.13246	0.00334	6.86247	0.43367	0.37575	0.02178	0.917	-4.08	.	2131	42	2094	56	2056	102
MEMG12-30	178	66.6	.	0.1341	0.00187	6.18733	0.36867	0.33463	0.01939	0.972	-15.58	.	2152	23	2003	52	1861	94
MEMG12-32	137	58.2	.	0.1274	0.00173	6.62156	0.41215	0.37695	0.0229	0.976	-0.02	.	2062	23	2062	55	2062	107
MEMG12-33	72	30.6	.	0.12849	0.00175	6.63896	0.41518	0.37475	0.02287	0.976	-1.44	.	2077	24	2065	55	2052	107
MEMG12-34	254	112	.	0.12685	0.00172	6.78334	0.43519	0.38784	0.02432	0.977	3.31	.	2055	24	2084	57	2113	113
MEMG12-35	139	43.6	.	0.12758	0.00138	6.74626	0.23762	0.3835	0.01285	0.951	1.57	.	2065	17	2079	31	2093	60
MEMG12-37	175	52.6	.	0.12695	0.00137	6.45876	0.22314	0.36899	0.01211	0.95	-1.78	.	2056	19	2040	30	2025	57
MEMG12-39	1362	166.3	.	0.15799	0.00197	3.19285	0.1032	0.14657	0.00437	0.923	-68.05	-63.91	2434	21	1455	25	882	25
MEMG12-41 CPb	332	104.9	3.01	0.12882	0.00183	6.63862	0.24445	0.37376	0.0127	0.923	-1.95	.	2082	24	2064	32	2047	60
MEMG12-42	258	79.7	.	0.12624	0.00137	6.46755	0.22849	0.37158	0.01249	0.952	-0.54	.	2046	19	2041	31	2037	59
MEMG12-44	214	66.2	.	0.12649	0.00137	6.50154	0.23015	0.37278	0.01256	0.952	-0.42	.	2050	19	2046	31	2042	59
MEMG12-45	234	70.6	.	0.12673	0.00134	6.39041	0.26619	0.36573	0.01473	0.967	-2.48	.	2053	18	2031	37	2009	70
MEMG12-46	290	90.3	.	0.12645	0.00139	6.54358	0.2403	0.37532	0.01315	0.954	0.3	.	2049	19	2052	32	2054	62
MEMG12-47	274	84.5	.	0.1262	0.00137	6.46143	0.22665	0.37132	0.01239	0.951	-0.58	.	2046	18	2041	31	2036	58
MEMG12-51 CPb	269	86.9	23.97	0.11772	0.01153	4.8021	0.49721	0.29586	0.00991	0.323	-14.82	.	1922	180	1785	87	1671	49
MEMG12-53 CPb	1388	155.1	38.46	0.08728	0.00105	0.97845	0.03947	0.08131	0.00313	0.954	-65.57	-55.94	1367	22	693	20	504	19
MEMG12-54	203	62.9	.	0.12659	0.0014	6.48808	0.23667	0.37173	0.01292	0.953	-0.77	.	2051	19	2044	32	2038	61
MEMG12-55	222	68.4	.	0.12789	0.00146	6.56115	0.24417	0.37207	0.01318	0.952	-1.7	.	2069	19	2054	33	2039	62
MEMG12-58 CPb	165	47.3	8.45	0.13441	0.00455	5.88038	0.28769	0.3173	0.01122	0.723	-20.13	-5.31	2156	59	1958	42	1777	55
MEMG12-60	200	61.4	.	0.12724	0.00141	6.4037	0.23448	0.36502	0.01274	0.953	-3.06	.	2060	19	2033	32	2006	60

Name	U	^{206}Pb	$^{206}Pb_c$(%)	$^{207}Pb^*/^{206}Pb$	1SE	$^{207}Pb^*/^{235}U$	1SE	$^{206}Pb^*/^{238}U$	1SE	Rho	Central (%)	Min. rim (%)	207/206	1s	207/235	1s	206/238	1s
MEMG12-61 CPb	826	98.1	32.44	0.09665	0.00269	1.26121	0.05574	0.09464	0.00325	0.778	-65.44	-57.22	1560	51	828	25	583	19
MEMG12-62 CPb	1493	161.3	20.19	0.07591	0.00083	1.06885	0.03645	0.10212	0.0033	0.948	-44.71	-28.79	1093	21	738	18	627	19
MEMG12-63	169	52.6	.	0.12652	0.0014	6.43957	0.2373	0.36913	0.01297	0.954	-1.42	.	2050	19	2038	32	2025	61
MEMG12-66 CPb	134	44.6	9.33	0.13645	0.00276	6.72126	0.27525	0.35726	0.01272	0.869	-11.34	.	2183	35	2075	36	1969	60
MEMG12-68 CPb	323	135	40.94	0.15576	0.00577	6.21868	0.31547	0.28957	0.01003	0.683	-36.13	-25.31	2410	60	2007	44	1639	50
MEMG12-69 CPb	254	91.3	34.54	0.1455	0.00502	5.59445	0.31647	0.27886	0.0125	0.792	-34.75	-20.3	2294	58	1915	49	1586	63
MEMG12-70 CPb	586	118.1	11.54	0.11392	0.0025	3.26443	0.13731	0.20783	0.00746	0.853	-37.97	-25.54	1863	38	1473	33	1217	40
MEMG12-72 CPb	605	157.8	41.86	0.12742	0.00551	3.12795	0.1797	0.17804	0.00673	0.658	-52.79	-42.17	2063	75	1440	44	1056	37
MEMG12-74	144	48.2	.	0.15221	0.00202	8.2253	0.32047	0.39192	0.01436	0.94	-11.84	.	2371	21	2256	35	2132	67
MEMG12-75	225	70.8	.	0.12622	0.00141	6.41169	0.2428	0.36843	0.01333	0.955	-1.36	.	2046	19	2034	33	2022	63
MEMG12-77	196	62.6	.	0.12614	0.00141	6.64679	0.26442	0.38218	0.01459	0.959	2.38	.	2045	20	2066	35	2086	68
MEMG12-78 CPb	249	68	14.56	0.13211	0.00207	5.03963	0.19959	0.27667	0.01006	0.918	-29.19	-16.63	2126	27	1826	34	1575	51
MEMG12-79	180	62.4	.	0.1294	0.00151	7.25206	0.23788	0.40645	0.01245	0.934	6.15	.	2090	20	2143	29	2199	57
MEMG12-81	246	77.8	.	0.12714	0.0014	6.4731	0.31105	0.36926	0.01727	0.973	-1.86	.	2059	19	2042	42	2026	81
MEMG12-83	249	82.3	.	0.12766	0.00142	6.75438	0.33095	0.38374	0.01831	0.974	1.58	.	2066	18	2080	43	2094	85
MEMG12-84 CPb	1505	149.8	46.33	0.08795	0.00368	0.76554	0.04508	0.06313	0.00261	0.703	-73.58	-63.24	1381	79	577	26	395	16
MEMG12-85	195	61.7	.	0.1266	0.00143	6.39045	0.25161	0.36609	0.01381	0.958	-2.29	.	2051	19	2031	35	2011	65
MEMG12-86	142	48.4	.	0.12739	0.00149	6.97349	0.23466	0.39702	0.01253	0.938	5.31	.	2062	20	2108	30	2155	58
MEMG12-87	188	60.8	.	0.12654	0.00144	6.51426	0.26663	0.37336	0.01468	0.96	-0.3	.	2051	19	2048	36	2045	69
MEMG12-88 CPb	333	53.6	33.82	0.12784	0.00561	2.32474	0.14671	0.13189	0.00598	0.718	-65.14	-56.07	2068	73	1220	45	799	34
MEMG12-89 CPb	266	78.2	35.59	0.14195	0.00316	4.13806	0.19573	0.21142	0.00882	0.882	-49.42	-39.3	2251	37	1662	39	1236	47
MEMG12-90 CPb	1960	107.3	16.72	0.07166	0.0014	0.52046	0.02126	0.05268	0.00189	0.878	-67.78	-54.67	976	39	425	14	331	12
MEMG12-91	150	48.5	.	0.1301	0.00155	6.58981	0.32967	0.36736	0.01785	0.971	-4.57	.	2099	20	2058	44	2017	84

Name	U	^{206}Pb	$^{206}Pb_c$(%)	$^{207}Pb^*/^{206}Pb$	1SE	$^{207}Pb^*/^{235}U$	1SE	$^{206}Pb^*/^{238}U$	1SE	Rho	Central (%)	Min. rim (%)	207/206	1s	207/235	1s	206/238	1s
MEMG12-92 CPb	259	94.8	31.61	0.15429	0.01101	6.01725	0.49841	0.28285	0.0119	0.508	-37.11	-19.67	2394	122	1978	72	1606	60
MEMG12-93	160	50.8	.	0.12681	0.00146	6.29944	0.25409	0.3603	0.01393	0.958	-3.99	.	2054	20	2018	35	1984	66
MEMG12-94	126	42.5	.	0.12692	0.00146	6.74358	0.2787	0.38536	0.01529	0.96	2.6	.	2056	19	2078	37	2101	71
MEMG12-95	253	82.8	.	0.12575	0.00145	6.42378	0.26327	0.37048	0.01457	0.96	-0.44	.	2039	20	2036	36	2032	69
MEMG12-97 CPb	270	81.3	1.93	0.12807	0.0023	6.13249	0.2811	0.34729	0.01465	0.92	-8.37	.	2072	30	1995	40	1922	70
MEMG12-98 CPb	313	83.8	7.55	0.13125	0.00365	5.63336	0.20832	0.31129	0.0076	0.66	-19.82	-9.36	2115	47	1921	32	1747	37
MEMG12-99 CPb	137	42.5	2.38	0.13013	0.00114	6.872	0.17043	0.38301	0.00888	0.935	-0.52	.	2100	15	2095	22	2090	41
MEMG12-100 CPb	901	104.6	24.72	0.08158	0.00305	1.2004	0.0538	0.10671	0.00263	0.551	-49.49	-34.83	1236	73	801	25	654	15
MEMG12-101 CPb	687	71.2	57.17	0.18379	0.00387	1.42889	0.07264	0.05639	0.00261	0.91	-89.1	-86.97	2687	34	901	30	354	16
MEMG12-102	268	83.5	.	0.12613	0.00073	6.70279	0.16443	0.38543	0.00919	0.972	3.27	.	2045	10	2073	22	2102	43
MEMG12-103	116	35.9	.	0.12762	0.00075	6.77705	0.16982	0.38513	0.00938	0.972	1.97	.	2065	10	2083	22	2100	44
MEMG12-104 CPb	910	98.2	14.18	0.0786	0.0005	1.22189	0.03148	0.11275	0.00281	0.969	-42.92	-31.67	1162	12	811	14	689	16
MEMG12-105	160	48.5	.	0.12674	0.00075	6.58953	0.16755	0.37709	0.00932	0.973	0.54	.	2053	10	2058	22	2063	44
MEMG12-106 CPb	351	144.7	31.81	0.13444	0.00685	6.26232	0.36027	0.33783	0.00901	0.464	-14.98	.	2157	86	2013	50	1876	43
MEMG12-107 CPb	182	55	5.54	0.12581	0.00167	5.8306	0.17827	0.33612	0.00926	0.901	-9.72	.	2040	23	1951	27	1868	45
MEMG12-108 CPb	633	108.8	12.13	0.10815	0.00242	2.66535	0.09652	0.17874	0.00509	0.786	-43.37	-33.89	1768	39	1319	27	1060	28
MEMG12-109	227	73.9	.	0.12653	0.00084	6.70288	0.2002	0.38422	0.01119	0.975	2.61	.	2050	11	2073	26	2096	52
MEMG12-111	248	79.7	.	0.12703	0.00086	6.66689	0.20367	0.38063	0.01134	0.975	1.24	.	2057	11	2068	27	2079	53
MEMG12-112 CPb	146	50	1.25	0.13013	0.00098	6.87448	0.21668	0.38315	0.01173	0.971	-0.49	.	2100	12	2095	28	2091	55
MEMG12-113	219	70.2	.	0.12729	0.00088	6.54932	0.19719	0.37318	0.01094	0.973	-0.93	.	2061	11	2053	27	2044	51
MEMG12-115 CPb	730	158.3	41.22	0.11386	0.0132	2.53551	0.38195	0.16151	0.01553	0.638	-51.77	.	1862	208	1282	110	965	86
MEMG12-118	185	59.6	.	0.12764	0.00093	6.49896	0.22451	0.36929	0.01247	0.978	-2.23	.	2066	12	2046	30	2026	59

Table 14: Sample 52.2

	ppm			*Ratios*							*U-Pb discordance*		*Ages (Ma)*					
Name	**U**	**^{206}Pb**	**^{206}Pb$_c$(%)**	**^{207}Pb/^{206}Pb***	**1SE**	**^{207}Pb/^{235}U***	**1SE**	**^{206}Pb/^{238}U***	**1SE**	**Rho**	**Central (%)**	**Minimum rim (%)**	**207/206**	**1s**	**207/235**	**1s**	**206/238**	**1s**
52.1-01	152	62.2	.	0.12725	0.0005	6.54115	0.06822	0.37281	0.0036	0.927	-1	.	2060	7	2051	9	2043	17
52.1-02	180	75.1	.	0.12677	0.0005	6.53424	0.06885	0.37382	0.00365	0.927	-0.36	.	2054	7	2051	9	2047	17
52.1-03	249	102.5	.	0.12636	0.0005	6.60811	0.08672	0.37929	0.00474	0.953	1.43	.	2048	7	2060	12	2073	22
52.1-04	207	84	.	0.12632	0.00051	6.49225	0.08552	0.37275	0.00467	0.952	-0.29	.	2047	7	2045	12	2042	22
52.2-05	179	72.6	.	0.12708	0.00054	6.36548	0.06261	0.3633	0.00322	0.902	-3.4	.	2058	7	2028	9	1998	15
52.2-06	155	65.3	.	0.12684	0.00058	6.48738	0.0493	0.37094	0.00225	0.797	-1.18	.	2055	8	2044	7	2034	11
52.2-08	218	89.5	.	0.12642	0.00055	6.51731	0.08252	0.37388	0.00444	0.938	-0.07	.	2049	7	2048	11	2048	21
52.2-09	214	82.7	.	0.12603	0.00059	5.99604	0.0909	0.34505	0.00497	0.951	-7.48	-1.21	2043	8	1975	13	1911	24
52.2-10	197	80.8	.	0.1269	0.00056	6.57495	0.09451	0.37579	0.00514	0.951	0.07	.	2055	7	2056	13	2057	24
52.2-11	150	63.2	.	0.12685	0.00064	6.67581	0.08839	0.38169	0.00467	0.924	1.67	.	2055	8	2069	12	2084	22
52.2-12	204	88.1	.	0.12708	0.0007	6.64889	0.06302	0.37946	0.00293	0.815	0.9	.	2058	9	2066	8	2074	14
52.2-13	170	67.8	.	0.12684	0.00064	6.44156	0.07265	0.36833	0.00371	0.894	-1.88	.	2055	9	2038	10	2022	17
52.2-14_CPb	145	54.8	7.09	0.12653	0.00218	5.3641	0.10561	0.30748	0.00291	0.481	-17.88	-12.85	2050	30	1879	17	1728	14
52.2-15_CPb	230	90.7	0.8	0.12711	0.0007	6.21504	0.11503	0.35462	0.00627	0.955	-5.73	.	2058	9	2007	16	1957	30
52.2-16	200	82.7	.	0.12698	0.0007	6.45833	0.09525	0.36888	0.00505	0.928	-1.84	.	2057	9	2040	13	2024	24
52.2-17_CPb	148	45.3	1.31	0.11658	0.00103	4.21099	0.05815	0.26199	0.00277	0.766	-23.77	-19.55	1904	16	1676	11	1500	14
52.2-18	150	63.4	.	0.12722	0.00076	6.50988	0.07182	0.37111	0.00344	0.84	-1.43	.	2060	10	2047	10	2035	16
52.2-19	145	61.3	.	0.12743	0.00075	6.65341	0.10024	0.37868	0.00525	0.921	0.41	.	2063	10	2066	13	2070	25
52.2-21_CPb	123	44.6	0.06	0.12878	0.00031	6.72698	0.13185	0.37886	0.00737	0.993	-0.58	.	2081	4	2076	17	2071	34
52.2-22	190	63.8	.	0.12784	0.00027	6.4033	0.04502	0.36328	0.00244	0.955	-3.98	-1.03	2068	3	2033	6	1998	12
52.2-23_CPb	353	118.5	0.11	0.12733	0.00034	6.66769	0.08882	0.37978	0.00496	0.98	0.78	.	2061	4	2068	12	2075	23
52.2-24	211	73.1	.	0.12759	0.00027	6.62058	0.07381	0.37633	0.00412	0.982	-0.34	.	2065	4	2062	10	2059	19
52.2-25	119	41	.	0.12895	0.00031	6.88609	0.07257	0.3873	0.00398	0.974	1.49	.	2084	4	2097	9	2110	18
52.2-26	229	77	.	0.12786	0.00027	6.53172	0.08849	0.37051	0.00496	0.988	-2.08	.	2069	4	2050	12	2032	23
52.2-27 CPb	213	65.4	0.66	0.13062	0.00056	5.88769	0.07914	0.32691	0.00416	0.947	-15.41	-10.46	2106	7	1959	12	1823	20
52.2-28	195	67	.	0.12774	0.00033	6.42297	0.08599	0.36468	0.00479	0.981	-3.53	.	2067	5	2035	12	2004	23
52.2-29_CPb	143	48.2	0.09	0.12835	0.00029	6.68099	0.06449	0.37752	0.00354	0.972	-0.61	.	2076	4	2070	9	2065	17
52.2-30	107	36	.	0.12831	0.00029	6.6011	0.08884	0.37311	0.00495	0.986	-1.74	.	2075	4	2059	12	2044	23

Name	U	^{206}Pb	$^{206}Pb_c$(%)	$^{207}Pb/^{206}Pb^*$	1SE	$^{207}Pb/^{235}U^*$	1SE	$^{206}Pb/^{238}U^*$	1SE	Rho	Central (%)	Min. rim (%)	207/206	1s	207/235	1s	206/238	1s
52.2-31	270	91.2	.	0.12717	0.00028	6.54536	0.0412	0.37328	0.0022	0.938	-0.82	.	2059	4	2052	6	2045	10
52.2-32	270	90.5	.	0.12728	0.00028	6.60142	0.06828	0.37615	0.0038	0.978	-0.14	.	2061	4	2060	9	2058	18
52.2-33	316	107.3	.	0.12652	0.00029	6.43624	0.03782	0.36896	0.002	0.923	-1.45	.	2050	4	2037	5	2025	9
52.2-34	118	39.3	.	0.12818	0.00032	6.54882	0.08926	0.37053	0.00497	0.983	-2.32	.	2073	4	2052	12	2032	23
52.2-35_CPb	262	89.3	0.04	0.1273	0.00029	6.69383	0.0332	0.38135	0.00168	0.888	1.22	.	2061	4	2072	4	2083	8
52.2-36 CPb	104	34.9	1.03	0.13352	0.00163	6.75202	0.12116	0.36675	0.00483	0.734	-7.09	-1.12	2145	21	2079	16	2014	23
52.2-37	181	59.8	.	0.12774	0.0003	6.54845	0.08506	0.3718	0.00475	0.983	-1.65	.	2067	4	2052	11	2038	22
52.2-38_CPb	158	54.2	0.05	0.12826	0.00031	6.7245	0.08375	0.38024	0.00464	0.981	0.18	.	2074	4	2076	11	2077	22
52.2-39_CPb	152	49.9	0.01	0.12783	0.00032	6.55149	0.06336	0.3717	0.00347	0.966	-1.75	.	2068	4	2053	9	2037	16
52.2-40_CPb	270	89.5	0.22	0.12734	0.00033	6.46691	0.08426	0.36834	0.0047	0.98	-2.26	.	2062	5	2041	11	2022	22
52.2-41	255	86	0.01	0.1266	0.00032	6.58392	0.06302	0.37719	0.00348	0.964	0.68	.	2051	4	2057	8	2063	16
52.2-42	362	111.9	.	0.12652	0.00031	6.0887	0.09437	0.34903	0.00534	0.988	-6.78	-0.13	2050	4	1989	14	1930	26
52.2-43	151	52.1	.	0.12832	0.00036	6.76385	0.0886	0.38229	0.00489	0.976	0.67	.	2075	5	2081	12	2087	23
52.2-44	159	52.6	.	0.12911	0.00042	6.60028	0.0949	0.37078	0.00519	0.974	-2.95	.	2086	6	2059	13	2033	24
52.2-45_CPb	117	40	0.18	0.12822	0.00038	6.56193	0.04783	0.37118	0.00247	0.913	-2.18	.	2074	5	2054	6	2035	12
52.2-46	200	63.3	.	0.12788	0.00032	6.47825	0.07053	0.36741	0.0039	0.974	-2.92	.	2069	4	2043	10	2017	18
52.2-47	279	93.6	.	0.12751	0.00032	6.87821	0.06725	0.39122	0.00369	0.966	3.67	.	2064	4	2096	9	2128	17
52.2-48_CPb	163	53.4	0.12	0.12788	0.00034	6.58925	0.08304	0.37372	0.0046	0.977	-1.25	.	2069	5	2058	11	2047	22
52.2-49	174	55.3	.	0.12796	0.00034	6.52098	0.06938	0.36959	0.00381	0.968	-2.4	.	2070	5	2049	9	2027	18
52.2-50_CPb	347	113.2	0.1	0.12653	0.00032	6.65506	0.0979	0.38148	0.00553	0.985	1.88	.	2050	4	2067	13	2083	26
52.2-52 CPb	178	32.5	1.91	0.1299	0.00061	3.62207	0.06148	0.20222	0.0033	0.961	-47.39	-43.41	2097	8	1554	14	1187	18
52.2-53	208	66	.	0.12788	0.00036	6.57904	0.08416	0.37313	0.00466	0.976	-1.41	.	2069	5	2057	11	2044	22
52.2-54	190	62.8	.	0.12809	0.00036	6.8652	0.07593	0.38873	0.00416	0.968	2.55	.	2072	5	2094	10	2117	19
52.2-55	225	73.4	.	0.12777	0.00037	6.75585	0.0857	0.38348	0.00473	0.973	1.42	.	2068	5	2080	11	2093	22
52.2-56	166	56.2	.	0.12776	0.00038	7.00445	0.14065	0.39764	0.0079	0.989	5.17	.	2067	5	2112	18	2158	36
52.2-57	244	81	.	0.12736	0.00036	6.60263	0.10065	0.376	0.00563	0.983	-0.24	.	2062	5	2060	13	2058	26
52.2-58_CPb	246	78.5	0.28	0.12645	0.00038	6.53774	0.09391	0.37499	0.00527	0.978	0.21	.	2049	5	2051	13	2053	25
52.2-59	226	75.1	.	0.12783	0.00037	6.69092	0.08198	0.37961	0.00452	0.972	0.34	.	2068	5	2071	11	2074	21
52.2-60_CPb	217	67.2	0.86	0.1268	0.00106	6.28768	0.1009	0.35963	0.00493	0.854	-4.17	.	2054	15	2017	14	1980	23
52.2-61_1	264	90.2	.	0.13775	0.00304	7.38128	0.19906	0.38864	0.00602	0.574	-4.4	.	2199	37	2159	24	2117	28

Name	U	^{206}Pb	$^{206}Pb_c$(%)	$^{207}Pb/^{206}Pb^*$	1SE	$^{207}Pb/^{235}U^*$	1SE	$^{206}Pb/^{238}U^*$	1SE	Rho	Central (%)	Min. rim (%)	207/206	1s	207/235	1s	206/238	1s
52.2-62	250	78.1	.	0.12722	0.00039	6.51858	0.12932	0.37162	0.00728	0.988	-1.29	.	2060	5	2048	17	2037	34
52.2-63	239	77.3	.	0.12745	0.0004	6.68471	0.08442	0.38039	0.00466	0.969	0.85	.	2063	5	2071	11	2078	22
52.2-64	212	71.8	.	0.12751	0.00046	6.96802	0.11239	0.39635	0.00623	0.974	5.04	.	2064	6	2107	14	2152	29
52.2-65_CPb	231	76.1	0.19	0.12788	0.00059	6.8549	0.10125	0.38878	0.00545	0.95	2.73	.	2069	8	2093	13	2117	25
52.2-66_CPb	163	54.8	0.16	0.12803	0.00053	6.95376	0.13873	0.39393	0.00769	0.978	3.97	.	2071	7	2106	18	2141	36
52.2-67	236	77.3	.	0.12737	0.0004	6.62849	0.11073	0.37745	0.00619	0.982	0.14	.	2062	5	2063	15	2064	29
52.2-68_CPb	209	60.2	0.4	0.12708	0.00048	5.9727	0.14075	0.34088	0.00793	0.987	-9.36	.	2058	6	1972	20	1891	38
52.2-70_CPb	187	57.4	1.22	0.12625	0.00082	6.30399	0.11615	0.36216	0.00624	0.935	-3.06	.	2046	11	2019	16	1992	30
52.2-71 CPb	325	96.9	1.28	0.12791	0.00064	5.96481	0.11314	0.33821	0.00619	0.965	-10.66	-2.99	2069	9	1971	16	1878	30
52.2-72	254	81.2	.	0.12712	0.00043	6.62185	0.07878	0.37781	0.00431	0.959	0.43	.	2058	6	2062	10	2066	20
52.2-73_CPb	113	36.2	0.1	0.12907	0.00048	6.68815	0.10861	0.37583	0.00594	0.974	-1.6	.	2085	6	2071	14	2057	28
52.2-74_CPb	283	89.5	0.06	0.12721	0.00044	6.6812	0.1306	0.38093	0.00733	0.984	1.19	.	2060	6	2070	17	2081	34
52.2-75_CPb	158	43.8	0.5	0.12732	0.00058	5.64697	0.05928	0.32167	0.00304	0.901	-14.63	-10.85	2061	8	1923	9	1798	15
52.2-76_CPb	154	46.3	.	0.12824	0.00048	6.2977	0.08154	0.35617	0.00441	0.957	-6.15	-0.77	2074	6	2018	11	1964	21
52.2-77	168	55.1	.	0.12814	0.00046	6.85645	0.0555	0.38808	0.00282	0.897	2.34	.	2073	6	2093	7	2114	13
52.2-78	232	74.6	.	0.12773	0.00047	6.68389	0.08922	0.37953	0.00487	0.961	0.4	.	2067	6	2070	12	2074	23
52.2-79	170	57.1	.	0.12811	0.00046	6.85304	0.1208	0.38798	0.0067	0.979	2.34	.	2072	6	2093	16	2113	31
52.2-80	232	74.4	.	0.12772	0.00049	6.64903	0.08597	0.37756	0.00466	0.955	-0.11	.	2067	6	2066	11	2065	22
52.2-81_1_CPb	130	44.3	0.07	0.12836	0.00051	7.22154	0.11193	0.40802	0.00612	0.967	7.41	1.29	2076	7	2139	14	2206	28
52.2-82	136	44.1	.	0.12839	0.0005	6.67102	0.10495	0.37684	0.00575	0.969	-0.82	.	2076	7	2069	14	2062	27
52.2-83	200	67.3	.	0.12821	0.00054	6.96527	0.12673	0.39402	0.00698	0.973	3.85	.	2074	7	2107	16	2141	32
52.2-84	328	108.8	.	0.12703	0.00055	6.90292	0.10173	0.39412	0.00555	0.956	4.84	.	2057	8	2099	13	2142	26
52.2-85	140	45.6	.	0.12816	0.00061	6.73247	0.13677	0.38101	0.00753	0.973	0.46	.	2073	8	2077	18	2081	35
52.2-86_CPb	212	68.7	0.16	0.12762	0.00052	6.7729	0.09938	0.38491	0.00542	0.96	1.91	.	2065	7	2082	13	2099	25
52.2-87	178	55	.	0.12797	0.00051	6.62602	0.13811	0.37554	0.00768	0.981	-0.83	.	2070	7	2063	18	2055	36
52.2-88_CPb	153	48	0.03	0.12827	0.00054	6.6875	0.12936	0.37813	0.00714	0.976	-0.38	.	2074	7	2071	17	2068	33
52.2-89_CPb	190	62.2	0.24	0.12803	0.00067	6.89278	0.08518	0.39046	0.00437	0.905	3.05	.	2071	9	2098	11	2125	20
52.2-90	134	41.8	.	0.12927	0.00059	7.02161	0.27813	0.39394	0.0155	0.993	2.98	.	2088	8	2114	35	2141	72
52.2-91_CPb	267	52.9	4.93	0.12534	0.0011	3.9299	0.1087	0.2274	0.00597	0.949	-38.69	-30.85	2034	15	1620	22	1321	31

Appendix B: Lu-Hf supplementary data

Table 1: MEMG8

Number	Sample	207Pb/206Pb age (Ma)	1s (Ma)	$^{176}Hf/^{177}Hf$	1s	$^{176}Lu/^{177}Hf$	1s	$^{176}Yb/^{177}Hf$	1s
1_CPb	MEMG8	2405	13	0.2810183	0.00000914	0.00108586	0.00000684	0.03718724	0.000236
2_CPb	MEMG8	2510	14	0.2810292	0.00000876	0.00113002	0.00000831	0.03840472	0.000243
3_CPb	MEMG8	2493	17	0.2810174	0.0000156	0.00143399	0.00000843	0.05346462	0.000308
4_CPb	MEMG8	2693	28	0.2809816	0.0000119	0.00122771	0.0000186	0.04539316	0.000714
5_CPb	MEMG8	2346	16	0.2809578	0.0000192	0.0010905	0.0000067	0.03800922	0.0002
6_CPb	MEMG8	2224	20	0.2809916	0.0000171	0.00126782	0.0000193	0.04523138	0.000538
7_CPb	MEMG8	2608	20	0.2810574	0.0000208	0.0010896	0.0000215	0.03674217	0.000821
8_CPb	MEMG8	2173	20	0.2811135	0.0000144	0.00267399	0.0000552	0.09252291	0.00196
9	MEMG8	2858	15	0.2810166	0.0000325	0.00145078	0.00000413	0.05339424	0.000293
10_CPb	MEMG8	2620	17	0.2810233	0.000031	0.0013915	0.0000146	0.04768173	0.000468
11_CPb	MEMG8	2313	21	0.2809218	0.0000131	0.00122452	0.0000167	0.04161477	0.000592
12_CPb	MEMG8	2881	14	0.2810173	0.0000131	0.0017111	0.00000839	0.05518206	0.000335
13_CPb	MEMG8	2761	13	0.2810312	0.0000209	0.00125628	0.00000491	0.04472243	0.00016
14_CPb	MEMG8	2698	13	0.2809982	0.0000141	0.000893	0.0000152	0.03148712	0.000641
15	MEMG8	2642	13	0.2809685	0.000016	0.00094473	0.00000853	0.03228039	0.000213
16_CPb	MEMG8	2423	17	0.2810286	0.0000116	0.0012642	0.00000603	0.04506685	0.000218
17	MEMG8	2637	21	0.2809902	0.0000195	0.00129238	0.0000187	0.04513588	0.000779
18_CPb	MEMG8	2738	14	0.2810256	0.0000117	0.00056177	0.00000732	0.01764191	0.000199
19_CPb	MEMG8	2379	23	0.2810325	0.0000158	0.00122559	0.00000818	0.04448517	0.00039
21_CPb	MEMG8	2587	19	0.2810301	0.0000263	0.00148316	0.00000999	0.0517674	0.000567
22_CPb	MEMG8	2360	17	0.2810701	0.0000328	0.00168391	0.0000273	0.0601526	0.00102
23_CPb	MEMG8	2823	18	0.2810105	0.0000138	0.0009859	0.0000091	0.03333539	0.000355
25_CPb	MEMG8	2482	17	0.2810217	0.0000256	0.00128752	0.0000262	0.04572281	0.000906
26_CPb	MEMG8	2372	20	0.2810506	0.0000144	0.00181217	0.0000107	0.05998824	0.000299
27_CPb	MEMG8	2554	22	0.2810251	0.0000125	0.00120708	0.0000151	0.04224223	0.000505
29_CPb	MEMG8	2238	24	0.2810218	0.0000132	0.0017354	0.00000694	0.06375209	0.000285
30_CPb	MEMG8	2503	22	0.2810496	0.0000156	0.00108291	0.00000663	0.03806429	0.000205
31_CPb	MEMG8	2610	22	0.2809973	0.0000226	0.00114425	0.00001	0.03949608	0.000248

Number	Sample	207Pb/206Pb age (Ma)	1s (Ma)	$^{176}Hf/^{177}Hf$	1s	$^{176}Lu/^{177}Hf$	1s	$^{176}Yb/^{177}Hf$	1s
32_CPb	MEMG8	2490	22	0.281024	0.0000194	0.00121358	0.00000686	0.0419286	0.000233
33_CPb	MEMG8	2425	24	0.2809763	0.0000368	0.00135896	0.00000902	0.04127977	0.000241
34	MEMG8	2655	21	0.2809982	0.0000106	0.00100724	0.00000135	0.03423642	0.0000994
35_CPb	MEMG8	2571	21	0.2810383	0.0000202	0.00105734	0.00000547	0.03686892	0.00019
36	MEMG8	2634	22	0.2810048	0.0000255	0.00131777	0.0000152	0.04512041	0.000566
37_CPb	MEMG8	2562	23	0.2810301	0.0000189	0.00092973	0.0000131	0.0304176	0.000471
38	MEMG8	2383	23	0.2810025	0.000023	0.0014122	0.0000053	0.04811957	0.000231
39	MEMG8	2311	23	0.2810593	0.0000212	0.00125234	0.0000114	0.04159545	0.000464
40_CPb	MEMG8	2516	27	0.2810258	0.0000108	0.00147562	0.0000151	0.05395273	0.000603
41_CPb	MEMG8	2533	25	0.2810077	0.0000101	0.00089149	0.00000689	0.03414725	0.000272
42	MEMG8	2649	22	0.2809997	0.0000125	0.00108796	0.00000408	0.04110282	0.000226
44_CPb	MEMG8	2608	14	0.2810333	0.0000169	0.00141119	0.00000985	0.05380623	0.000413
48_CPb	MEMG8	2347	14	0.2810126	0.00000822	0.00113757	0.00000585	0.04136658	0.000253
50_CPb	MEMG8	2687	12	0.2810144	0.0000128	0.00100677	0.00000466	0.03686468	0.00021
51	MEMG8	2746	13	0.2810182	0.0000109	0.00095044	0.00000498	0.03570513	0.000215
52	MEMG8	2789	13	0.2810386	0.00000974	0.00094185	0.0000126	0.03390183	0.000458
53	MEMG8	2839	53	0.2810247	0.0000107	0.00090688	0.0000107	0.03330887	0.000333
54_CPb	MEMG8	2491	15	0.2810073	0.0000192	0.00128889	0.0000135	0.05076852	0.000646
55	MEMG8	2680	13	0.2810418	0.0000135	0.00102259	0.0000037	0.03688332	0.000138
56_CPb	MEMG8	2533	14	0.281065	0.0000154	0.00200938	0.0000237	0.06539216	0.00062
57_CPb	MEMG8	2645	18	0.2810363	0.0000174	0.00118304	0.0000168	0.0425325	0.000405
59	MEMG8	2840	15	0.2810254	0.0000191	0.0012008	0.00000395	0.0437625	0.000152
60_CPb	MEMG8	2537	16	0.2810534	0.0000189	0.00133725	0.000013	0.0490783	0.000666
61	MEMG8	2716	17	0.2810123	0.0000186	0.00120622	0.00000946	0.04663606	0.000383
62	MEMG8	2758	15	0.2809883	0.0000112	0.00103098	0.0000189	0.03599646	0.000492
63_CPb	MEMG8	2560	25	0.2810192	0.0000142	0.00146592	0.0000162	0.05396346	0.000484
64_CPb	MEMG8	2296	20	0.2810233	0.0000101	0.0011489	0.00000384	0.04313694	0.000112
66_CPb	MEMG8	2201	30	0.2810199	0.0000117	0.00104364	0.00000634	0.03863931	0.000261
67_CPb	MEMG8	2382	51	0.2810734	0.0000177	0.00090252	0.00000584	0.03415546	0.000297
68_CPb	MEMG8	2601	19	0.2810004	0.00000992	0.00087873	0.00000524	0.03231266	0.000211
69_CPb	MEMG8	2230	86	0.2810134	0.0000197	0.00088424	0.0000125	0.03397321	0.00058

Number	Sample	207Pb/206Pb age (Ma)	1s (Ma)	$^{176}Hf/^{177}Hf$	1s	$^{176}Lu/^{177}Hf$	1s	$^{176}Yb/^{177}Hf$	1s
70_CPb	MEMG8	2231	30	0.2809893	0.0000151	0.00098399	0.0000117	0.03668497	0.000471
71	MEMG8	2790	20	0.2810808	0.000014	0.0024438	0.0000137	0.08544302	0.000379
72_CPb	MEMG8	2925	16	0.280863	0.0000132	0.00092196	0.00002	0.03126358	0.000781

Table 2: MEMG9

Number	Sample	207Pb/206Pb age (Ma)	1s (Ma)	$^{176}Hf/^{177}Hf$	1s	$^{176}Lu/^{177}Hf$	1s	$^{176}Yb/^{177}Hf$	1s
1	MEMG9	2761	8	0.2810633	0.0000313	0.00090897	0.00000346	0.03300281	0.000122
2	MEMG9	2718	12	0.2809962	0.0000292	0.00101017	0.00000878	0.03331355	0.00032
3_CPb	MEMG9	2225	9	0.2810744	0.0000261	0.00136731	0.00000466	0.04813177	0.000262
4	MEMG9	2810	10	0.2810164	0.0000481	0.00101817	0.00000197	0.0381847	0.00011
6_CPb	MEMG9	2772	31	0.281005	0.0000468	0.00132532	0.0000124	0.04777485	0.000438
8_CPb	MEMG9	2400	10	0.2810499	0.0000258	0.00131274	0.0000153	0.04779993	0.000368
11_CPb	MEMG9	2627	8	0.2810113	0.0000327	0.00103048	0.0000163	0.03469703	0.000429
13_CPb	MEMG9	2837	10	0.2809844	0.000041	0.0007143	0.00000937	0.02433125	0.000392
14_CPb	MEMG9	2686	13	0.2810387	0.0000232	0.00076037	0.0000118	0.02750215	0.000572
15_CPb	MEMG9	2659	10	0.2810004	0.0000344	0.00104556	0.00000717	0.03737246	0.000232
16_CPb	MEMG9	2366	11	0.2810266	0.0000305	0.000971	0.00000757	0.03202035	0.000268
17_CPb	MEMG9	2573	9	0.2809518	0.0000358	0.00117062	0.0000119	0.03724611	0.000572
19_CPb	MEMG9	2837	9	0.281071	0.0000443	0.00123115	0.0000123	0.04277562	0.000476
20	MEMG9	2271	12	0.281033	0.0000129	0.00111574	0.00000456	0.03625102	0.000189
21	MEMG9	2797	11	0.281024	0.0000164	0.00099225	0.00000315	0.03493601	0.000104
22_CPb	MEMG9	2502	12	0.28099	0.0000294	0.00114267	0.0000033	0.0388999	0.00031
23_CPb	MEMG9	2599	10	0.2809849	0.0000288	0.00144536	0.00000668	0.05172909	0.000262
24_CPb	MEMG9	2600	17	0.2809723	0.0000316	0.00136989	0.00000351	0.0444943	0.000152
25	MEMG9	2575	12	0.2809023	0.0000336	0.00110917	0.00000852	0.03706443	0.000252
26_CPb	MEMG9	2719	12	0.2810146	0.0000168	0.00090623	0.000015	0.03200037	0.000604
28_CPb	MEMG9	2484	12	0.2810228	0.0000206	0.00115652	0.00000765	0.04150179	0.000225
29_CPb	MEMG9	2658	15	0.2810374	0.000021	0.00102484	0.0000196	0.03509209	0.000709
30_CPb	MEMG9	2767	12	0.280994	0.0000331	0.00102933	0.00000825	0.03658541	0.000304
31_CPb	MEMG9	2716	10	0.2809607	0.0000513	0.00071819	0.0000129	0.02341356	0.000605
32	MEMG9	2759	11	0.2810132	0.0000367	0.00117083	0.00000564	0.03937596	0.0000803
33_CPb	MEMG9	2867	12	0.2809906	0.0000323	0.00121647	0.00000982	0.04092735	0.000421
35_CPb	MEMG9	2599	15	0.2811081	0.0000285	0.00143869	0.0000242	0.05120634	0.000932
37	MEMG9	2814	11	0.2810547	0.0000272	0.00128912	0.0000203	0.04563206	0.000705
38_CPb	MEMG9	2418	12	0.2810009	0.0000358	0.00142764	0.0000156	0.04561929	0.00033
39_CPb	MEMG9	2376	16	0.2810316	0.0000287	0.00166477	0.00000794	0.05712339	0.000496

Number	Sample	207Pb/206Pb age (Ma)	1s (Ma)	$^{176}Hf/^{177}Hf$	1s	$^{176}Lu/^{177}Hf$	1s	$^{176}Yb/^{177}Hf$	1s
40_CPb	MEMG9	2493	12	0.2809645	0.0000296	0.00104518	0.00000295	0.03652999	0.000166
41_CPb	MEMG9	2447	16	0.2809924	0.0000446	0.00171742	0.00000914	0.06111437	0.000526
43_CPb	MEMG9	2637	12	0.2809833	0.0000228	0.00102778	0.00000888	0.03488423	0.00015
44_CPb	MEMG9	2512	15	0.2809764	0.0000501	0.00105396	0.00000476	0.03984377	0.000274
45_CPb	MEMG9	2417	12	0.2809634	0.0000305	0.00100249	0.00000508	0.03470276	0.000202
46_CPb	MEMG9	2795	12	0.2810486	0.0000536	0.001272	0.00000954	0.04227552	0.000254
47_CPb	MEMG9	2459	16	0.2810243	0.0000299	0.00137107	0.00000457	0.04884868	0.000411
48_CPb	MEMG9	2569	13	0.2809563	0.0000137	0.00014708	2.18E-07	0.00541437	0.00000801
50_CPb	MEMG9	2393	17	0.281086	0.0000538	0.00126346	0.0000133	0.04224896	0.000732
52	MEMG9	2742	14	0.2810509	0.000038	0.00102258	0.0000148	0.03304989	0.000446
53_CPb	MEMG9	2826	15	0.2810075	0.0000326	0.00160411	0.0000102	0.05283967	0.000383
54	MEMG9	2547	13	0.2810021	0.0000334	0.00258874	0.00000839	0.09800712	0.000314

Table 3: MEMG3

Number	Sample	207Pb/206Pb age (Ma)	1s (Ma)	$^{176}Hf/^{177}Hf$	1s	$^{176}Lu/^{177}Hf$	1s	$^{176}Yb/^{177}Hf$	1s
1	MEMG3	2469	20	0.2810014	0.00000814	0.00037836	2.22E-07	0.00960737	0.0000129
2	MEMG3	3138	22	0.2811293	0.0000141	0.0027471	0.0000534	0.1040415	0.00236
3	MEMG3	2812	21	0.2810124	0.00000939	0.00082559	0.00000707	0.02927626	0.00035
4_CPb	MEMG3	2146	25	0.2813906	0.0000141	0.00314038	0.0000299	0.118632	0.00105
5	MEMG3	2066	24	0.2812171	0.00000799	0.00061696	0.00000309	0.01707682	0.0000863
6	MEMG3	3188	23	0.2807772	0.00000974	0.00140239	0.000033	0.03866856	0.000903
7	MEMG3	2341	24	0.2812986	0.0000106	0.00102512	0.00000699	0.03205041	0.00027
8	MEMG3	2860	21	0.281081	0.0000107	0.00186681	0.00000643	0.06799505	0.000408
9	MEMG3	2804	23	0.2811832	0.0000142	0.00326918	0.0000319	0.0987057	0.00114
10	MEMG3	2304	25	0.2812221	0.0000149	0.00056423	0.00000245	0.01718592	0.0000548
11	MEMG3	3044	25	0.2809235	0.00000931	0.00065068	0.00000839	0.01850343	0.000228
12_CPb	MEMG3	1751	28	0.2812173	0.0000473	0.00207839	0.00000971	0.07704623	0.000324
13_CPb	MEMG3	1896	27	0.2812668	0.000023	0.00307515	0.0000118	0.1043248	0.00082
14_CPb	MEMG3	2649	27	0.2810104	0.0000335	0.00158181	0.0000265	0.0521974	0.000903
18	MEMG3	2181	31	0.2812394	0.00000951	0.00098859	0.00000607	0.03377436	0.000134
21	MEMG3	2122	29	0.2812941	0.0000264	0.00187402	0.0000299	0.08303628	0.00164
22	MEMG3	2076	35	0.2813317	0.0000154	0.00154342	0.0000118	0.04970995	0.000538
25	MEMG3	2990	29	0.2808533	0.00000819	0.00093777	0.00000728	0.03187085	0.000152
26	MEMG3	2233	33	0.2813325	0.00000854	0.00067414	0.00000238	0.02234332	0.000101
27	MEMG3	1970	9	0.2812529	0.0000139	0.00160905	0.00000833	0.06682806	0.000661
30	MEMG3	2375	7	0.2812582	0.0000289	0.00140973	0.0000145	0.03886671	0.000305
31	MEMG3	2117	8	0.2812181	0.0000085	0.00085241	0.00000439	0.02769648	0.000184
33	MEMG3	2873	8	0.2809403	0.00000981	0.00159614	0.0000289	0.05599875	0.00129
35	MEMG3	2812	8	0.2809805	0.0000126	0.0027842	0.0000146	0.1207874	0.000578
36	MEMG3	2079	15	0.2815553	0.0000485	0.00818265	0.000131	0.3407175	0.00599
37	MEMG3	2828	7	0.2809979	0.0000088	0.00092961	0.00000829	0.02876812	0.000288
38	MEMG3	2004	8	0.2811964	0.00000907	0.0011102	0.00000913	0.03762509	0.000311
39	MEMG3	2263	8	0.2812392	0.00000923	0.00065258	0.00000535	0.02188793	0.000155
40_CPb	MEMG3	2073	12	0.281339	0.0000145	0.00183908	0.0000171	0.0721669	0.000609
41	MEMG3	2221	8	0.2812324	0.0000113	0.00091426	0.00000528	0.0308839	0.000224

Number	Sample	207Pb/206Pb age (Ma)	1s (Ma)	$^{176}Hf/^{177}Hf$	1s	$^{176}Lu/^{177}Hf$	1s	$^{176}Yb/^{177}Hf$	1s
43	MEMG3	2793	8	0.2809782	0.0000092	0.00065826	0.0000093	0.02412526	0.000502
44_CPb	MEMG3	2565	9	0.2810585	0.0000159	0.00179576	0.0000525	0.06701292	0.00169
46	MEMG3	2179	9	0.2813321	0.0000108	0.00101897	0.00000392	0.03223284	0.000169
49	MEMG3	2286	8	0.2812827	0.00000894	0.00110766	0.0000129	0.04459337	0.000582
55	MEMG3	1149	15	0.2815531	0.0000275	0.00504721	0.0000824	0.2120687	0.00407
58_CPb	MEMG3	2769	16	0.2812834	0.0000372	0.00501568	0.000227	0.2070107	0.0103
59	MEMG3	2056	11	0.2814017	0.0000095	0.00086671	0.0000174	0.02761465	0.000538
62	MEMG3	2179	17	0.2812141	0.0000107	0.00088308	0.00000475	0.0276096	0.000199
63	MEMG3	2222	10	0.2813136	0.00000992	0.00081516	0.0000147	0.02789444	0.000512
64_CPb	MEMG3	1941	13	0.2814987	0.0000168	0.00271104	0.000014	0.08555447	0.000559
65	MEMG3	3050	12	0.280947	0.0000199	0.00171619	0.00000733	0.06122191	0.000427
66	MEMG3	3105	10	0.2808843	0.0000161	0.00105431	0.00000379	0.03425399	0.000182
67_CPb	MEMG3	2412	12	0.2812537	0.0000093	0.00092476	0.000002	0.02772056	0.000156
68	MEMG3	2742	11	0.2811329	0.0000116	0.00243397	0.0000258	0.08728754	0.000935
69	MEMG3	2198	11	0.281322	0.00000963	0.00064603	9.09E-07	0.02236766	0.0000786
70	MEMG3	2237	11	0.281273	0.000013	0.001274	0.00000733	0.03873041	0.000205
71	MEMG3	2923	10	0.2813054	0.00000924	0.00076764	0.00000421	0.02240829	0.00016
72_CPb	MEMG3	2363	11	0.281259	0.0000128	0.0016383	0.0000161	0.05270757	0.000458
74	MEMG3	2910	11	0.2809041	0.0000107	0.00023709	0.00000153	0.00783207	0.0000471
76_CPb	MEMG3	2160	14	0.2812411	0.0000126	0.00161562	0.00000505	0.05514293	0.000268
77_CPb	MEMG3	2637	12	0.2809412	0.0000136	0.00189937	0.0000409	0.06639209	0.00172
78	MEMG3	2312	11	0.2811052	0.0000162	0.00049309	0.00000202	0.01371322	0.0000356
79	MEMG3	3103	12	0.2809046	0.0000194	0.00109084	0.000013	0.03156468	0.000405
80	MEMG3	2035	14	0.2811509	0.0000109	0.0014781	0.0000171	0.05699745	0.000911
81	MEMG3	3047	13	0.280849	0.00000814	0.00054706	0.0000022	0.01554172	0.0000769
82_CPb	MEMG3	2829	25	0.2809632	0.0000095	0.00097539	0.0000152	0.02680235	0.000554
83	MEMG3	1932	16	0.2813434	0.0000136	0.00396349	0.0000238	0.1655423	0.00129
84_CPb	MEMG3	2096	15	0.2812817	0.0000109	0.00200312	0.00000764	0.08120893	0.000431
85	MEMG3	2278	18	0.2812904	0.0000206	0.0029851	0.0000167	0.1145103	0.000501
86	MEMG3	2742	13	0.280856	0.00000919	0.0005887	0.00000331	0.01703672	0.000123
87	MEMG3	3097	34	0.2808281	0.00000925	0.00063739	0.0000064	0.01898113	0.000189

Number	Sample	207Pb/206Pb age (Ma)	1s (Ma)	$^{176}Hf/^{177}Hf$	1s	$^{176}Lu/^{177}Hf$	1s	$^{176}Yb/^{177}Hf$	1s
88	MEMG3	3006	13	0.2808874	0.0000169	0.00140868	0.0000123	0.04617782	0.000545
89	MEMG3	2215	14	0.2814062	0.000009	0.00103101	0.0000137	0.03312036	0.000499
90_CPb	MEMG3	1644	17	0.281326	0.0000291	0.00407766	0.0000253	0.1598802	0.00102
92	MEMG3	2286	14	0.2812117	0.0000139	0.0007961	0.00000168	0.02804411	0.0000915
93	MEMG3	2993	20	0.2806876	0.0000186	0.00121098	0.00000774	0.04491695	0.000295

Table 4: MEMG4

Number	Sample	207Pb/206Pb age (Ma)	1s (Ma)	$^{176}Hf/^{177}Hf$	1s	$^{176}Lu/^{177}Hf$	1s	$^{176}Yb/^{177}Hf$	1s
2	MEMG4	2234	27	0.2813561	0.0000128	0.00065333	0.00000107	0.02488904	0.000062
3	MEMG4	2034	64	0.2813508	0.0000119	0.00071152	6.87E-07	0.02364248	0.0000225
4	MEMG4	2195	68	0.2813556	0.0000145	0.00086757	0.00000403	0.03400651	0.00014
5	MEMG4	2209	66	0.2812243	0.0000162	0.00119715	0.0000105	0.04634852	0.000366
6	MEMG4	2254	65	0.2812412	0.0000152	0.00062516	0.00000429	0.02399084	0.000206
7	MEMG4	2061	30	0.2813544	0.0000177	0.00175309	0.00000635	0.06310881	0.000288
8	MEMG4	2356	20	0.2812547	0.0000145	0.00099118	0.00000232	0.03654792	0.0000726
9	MEMG4	2086	19	0.2813691	0.0000149	0.00073573	0.00000368	0.02614263	0.000172
10	MEMG4	2204	19	0.2813182	0.000018	0.0017617	0.00000983	0.06861197	0.000448
11	MEMG4	1987	21	0.2813361	0.0000175	0.00177371	0.00000878	0.06140182	0.000204
12	MEMG4	2330	27	0.2813555	0.0000154	0.00092185	0.00000923	0.03716524	0.000487
14	MEMG4	2593	25	0.2814152	0.0000142	0.00113354	0.00000357	0.04241186	0.000132
15	MEMG4	2175	24	0.2813201	0.0000132	0.00093325	0.000002	0.03252807	0.000085
16	MEMG4	2259	24	0.2813312	0.000015	0.00165985	0.00000879	0.06055686	0.000243
17	MEMG4	2272	24	0.2813729	0.0000259	0.00114147	0.0000021	0.04075285	0.000155
18	MEMG4	2259	15	0.2813246	0.0000143	0.00039019	2.46E-07	0.01450032	0.0000255
19	MEMG4	2263	15	0.2812331	0.0000133	0.00049896	0.00000443	0.01853404	0.000157
20	MEMG4	2255	16	0.2813302	0.0000131	0.00079548	0.00000306	0.03008027	0.000169
21	MEMG4	2799	16	0.2809837	0.0000133	0.00061031	9.33E-07	0.01986122	0.000032
22	MEMG4	2210	17	0.2813206	0.0000145	0.00060934	9.95E-07	0.02253292	0.0000509
23	MEMG4	2281	17	0.2813219	0.0000172	0.00095774	0.00000371	0.0369139	0.00019
24_CPb	MEMG4	2114	21	0.2812948	0.0000187	0.00074309	0.00000321	0.02926516	0.000157
25	MEMG4	2139	17	0.2812953	0.0000201	0.00108746	0.0000052	0.04116601	0.000293
26_CPb	MEMG4	1858	21	0.2813692	0.0000165	0.00155267	0.00000398	0.05505421	0.000113
27_CPb	MEMG4	1981	20	0.2813529	0.0000193	0.0008788	0.00000303	0.03204246	0.000123
28	MEMG4	2266	21	0.2813536	0.0000253	0.00118427	0.00000922	0.04658476	0.000432
29	MEMG4	2274	18	0.2812782	0.0000166	0.00073707	0.00000667	0.02766675	0.000306
31	MEMG4	2163	11	0.2812605	0.000017	0.00140581	0.00000803	0.05060512	0.000215
32	MEMG4	2245	13	0.2813013	0.0000168	0.00065761	0.00000263	0.0257565	0.0000813
33	MEMG4	2271	15	0.2813694	0.0000226	0.00123091	0.00000913	0.04302969	0.000314

Number	Sample	207Pb/206Pb age (Ma)	1s (Ma)	$^{176}Hf/^{177}Hf$	1s	$^{176}Lu/^{177}Hf$	1s	$^{176}Yb/^{177}Hf$	1s
34_CPb	MEMG4	2012	13	0.2813553	0.000015	0.00105522	0.00000253	0.04131883	0.0000837
35	MEMG4	2379	12	0.2812319	0.0000143	0.00128967	0.00000652	0.04445963	0.000221
36	MEMG4	2165	14	0.2813407	0.0000142	0.00071953	0.00000351	0.02542749	0.000151
37	MEMG4	2215	18	0.2813353	0.0000146	0.00107887	0.00000415	0.03914781	0.000149
38	MEMG4	2142	13	0.2813721	0.0000162	0.00181071	0.00000746	0.06175852	0.00029
39	MEMG4	2255	14	0.2813162	0.0000164	0.00064887	0.00000352	0.02547201	0.000177
40	MEMG4	2274	17	0.2812933	0.0000177	0.00073317	0.00000389	0.02486342	0.000143
41	MEMG4	2284	17	0.2813661	0.0000187	0.00165429	0.00000418	0.06075755	0.000108
42_CPb	MEMG4	2276	30	0.2813421	0.000017	0.00118454	0.000011	0.04557159	0.000439
43	MEMG4	2113	15	0.281402	0.000016	0.0013999	0.0000104	0.05178409	0.000398
44_CPb	MEMG4	1644	20	0.2814188	0.0000154	0.00222477	0.0000137	0.07763386	0.000476
45	MEMG4	2362	19	0.2814306	0.0000174	0.00159531	0.00000574	0.06160297	0.000201
46_CPb	MEMG4	1994	21	0.2812773	0.000019	0.00177842	0.00000407	0.0707741	0.000231
47	MEMG4	2207	20	0.2813265	0.0000163	0.00091543	0.0000051	0.03224571	0.000191
48	MEMG4	2241	20	0.2813185	0.0000149	0.00144784	0.00000393	0.05071578	0.00015
49_CPb	MEMG4	1921	19	0.2813669	0.0000389	0.00126486	0.00000515	0.0421258	0.000218
52_CPb	MEMG4	2034	26	0.281355	0.0000188	0.00078383	0.00000232	0.02803813	0.0000853
57_CPb	MEMG4	2472	22	0.2813954	0.0000201	0.00173022	0.0000122	0.06546416	0.000367
60_CPb	MEMG4	2333	17	0.2813809	0.0000189	0.00077853	0.00000224	0.02913178	0.0000845
64_CPb	MEMG4	2436	18	0.2813744	0.0000155	0.00140497	0.0000034	0.05088878	0.000102
65_CPb	MEMG4	2165	19	0.2813528	0.0000149	0.00049974	0.00000204	0.01681445	0.0000775
71_CPb	MEMG4	2433	20	0.2813579	0.0000187	0.00137039	0.00000384	0.04950644	0.00016
72_CPb	MEMG4	2307	18	0.2813793	0.0000218	0.00119903	0.00000605	0.04835617	0.000186
73_CPb	MEMG4	2220	21	0.2813547	0.0000217	0.00095018	0.00000875	0.03486661	0.000397
75_CPb	MEMG4	1978	20	0.2814255	0.0000174	0.0013217	0.0000069	0.05007201	0.000234
76_CPb	MEMG4	2916	29	0.2813702	0.0000196	0.00160255	0.00000372	0.05796903	0.000183
77_CPb	MEMG4	2231	22	0.2813152	0.0000203	0.00195782	0.000011	0.06798126	0.000321
78_CPb	MEMG4	2098	25	0.2814024	0.0000219	0.00252304	0.0000061	0.08690385	0.000134
81	MEMG4	2313	17	0.2812803	0.0000521	0.00260581	0.00000594	0.088982	0.000279
86	MEMG4	2373	25	0.2814223	0.0000204	0.00171367	0.0000471	0.06651624	0.00183
87_CPb	MEMG4	2155	25	0.281312	0.0000205	0.00083559	0.00000552	0.03312329	0.000308

Number	Sample	207Pb/206Pb age (Ma)	1s (Ma)	$^{176}Hf/^{177}Hf$	1s	$^{176}Lu/^{177}Hf$	1s	$^{176}Yb/^{177}Hf$	1s
89_CPb	MEMG4	2182	26	0.2813469	0.000017	0.00074356	0.00000496	0.02730978	0.00019
91_CPb	MEMG4	2202	27	0.2812927	0.0000509	0.0016003	0.0000153	0.06019686	0.000538
94_CPb	MEMG4	2420	14	0.2813103	0.0000123	0.0010872	0.00000403	0.04104765	0.000113
95_CPb	MEMG4	2096	15	0.2813814	0.0000193	0.00196079	0.0000169	0.07032231	0.000606
96_CPb	MEMG4	2190	12	0.2813305	0.0000354	0.0016769	0.0000102	0.05934912	0.000476
97_CPb	MEMG4	1833	14	0.2813783	0.0000186	0.00172199	0.0000109	0.0656992	0.000346
98_CPb	MEMG4	2441	15	0.2813706	0.000019	0.00190481	0.00000268	0.07591056	0.00009
99	MEMG4	2095	16	0.2813406	0.0000228	0.00197122	0.0000115	0.07527404	0.000392
100	MEMG4	2246	14	0.2813171	0.0000174	0.00065531	0.00000142	0.02627317	0.0000703

Table 5: MEMG5

Number	Sample	207Pb/206Pb age (Ma)	1s (Ma)	$^{176}Hf/^{177}Hf$	1s	$^{176}Lu/^{177}Hf$	1s	$^{176}Yb/^{177}Hf$	1s
1_CPb	MEMG5	2436	19	0.2812745	0.0000122	0.00096821	0.00000614	0.03456338	0.000354
2_CPb	MEMG5	2724	18	0.2812947	0.0000146	0.0018954	0.00000995	0.0733044	0.000591
3_CPb	MEMG5	2271	29	0.2812392	0.0000145	0.00208007	0.00000955	0.07713411	0.000445
4_CPb	MEMG5	2326	19	0.281286	0.0000155	0.00223619	0.0000102	0.09249915	0.000641
5_CPb	MEMG5	2063	22	0.2813532	0.0000121	0.00243633	0.00000987	0.07740606	0.000297
6_CPb	MEMG5	2305	21	0.2812953	0.0000139	0.00234701	0.00000897	0.09513808	0.000289
7_CPb	MEMG5	2087	22	0.2812239	0.0000165	0.00089652	0.000012	0.02873743	0.000355
8	MEMG5	2407	21	0.2812223	0.0000121	0.00064263	0.00000906	0.01952195	0.000284
9_CPb	MEMG5	2370	25	0.2812085	0.0000163	0.00209017	0.0000363	0.08436237	0.0016
10_CPb	MEMG5	2374	21	0.2812449	0.0000148	0.0015964	0.0000137	0.06593766	0.000592
11	MEMG5	2423	26	0.2812439	0.0000136	0.00076906	0.0000014	0.02418623	0.0000616
12_CPb	MEMG5	2466	23	0.2812259	0.0000119	0.00070415	0.00000309	0.02193664	0.0000947
13_CPb	MEMG5	2452	23	0.2812636	0.0000135	0.00183599	0.00000446	0.06874968	0.000204
14_CPb	MEMG5	2590	37	0.2812299	0.0000126	0.00155893	0.0000114	0.06344105	0.000552
15_CPb	MEMG5	2473	25	0.2813153	0.0000159	0.00198069	0.0000177	0.07420359	0.000738
16_CPb	MEMG5	2020	29	0.2812666	0.0000104	0.00177325	0.00000567	0.06330538	0.000241
17	MEMG5	2405	26	0.281204	0.0000145	0.00070405	0.00000249	0.02217438	0.0000753
18_CPb	MEMG5	2547	29	0.2812821	0.0000166	0.00131237	0.0000071	0.04534925	0.000188
19_CPb	MEMG5	2551	29	0.2812132	0.0000151	0.00202744	0.0000163	0.07566214	0.000805
21	MEMG5	2323	26	0.2812612	0.0000128	0.00094541	0.0000095	0.02935808	0.000426
22	MEMG5	2310	25	0.281128	0.0000219	0.00057471	0.00000105	0.01633482	0.0000668
23_CPb	MEMG5	2325	30	0.2813153	0.0000124	0.00253936	0.0000149	0.09377641	0.000675
25	MEMG5	2467	35	0.2812763	0.0000132	0.00114008	0.00000565	0.03897908	0.000233
26	MEMG5	2417	31	0.2812408	0.0000134	0.00051263	0.00000199	0.01556169	0.0000585
28	MEMG5	2501	27	0.2812479	0.0000133	0.00070787	0.00000181	0.02339715	0.0000808
29	MEMG5	2401	33	0.2812118	0.0000126	0.0005569	0.00000147	0.01847863	0.0000775
30	MEMG5	1540	37	0.2812599	0.0000203	0.00164044	0.00000553	0.05499935	0.000285
31	MEMG5	2356	39	0.2812208	0.0000139	0.00133583	0.00000749	0.04746046	0.000221
32_CPb	MEMG5	1735	6	0.2810893	0.0000117	0.0010995	0.0000164	0.05031477	0.000726
33_CPb	MEMG5	1262	29	0.2812876	0.0000174	0.00267483	0.000027	0.1099388	0.00111

Number	Sample	207Pb/206Pb age (Ma)	1s (Ma)	$^{176}Hf/^{177}Hf$	1s	$^{176}Lu/^{177}Hf$	1s	$^{176}Yb/^{177}Hf$	1s
34_CPb	MEMG5	1857	13	0.2813737	0.0000158	0.00335868	0.0000162	0.1302098	0.000684
35	MEMG5	2394	5	0.2812019	0.0000128	0.0006444	0.00000551	0.02051249	0.000163
36	MEMG5	2427	7	0.2812518	0.0000128	0.00088424	0.00000537	0.02757337	0.00018
37_CPb	MEMG5	2385	5	0.2811872	0.000012	0.00035324	7.39E-07	0.01129358	0.0000235
38	MEMG5	2405	6	0.2812415	0.0000134	0.00069445	0.00000306	0.02011228	0.0000673
39_CPb	MEMG5	1196	45	0.2813228	0.0000134	0.00264914	0.0000174	0.1039295	0.000855
40	MEMG5	2397	5	0.2812223	0.0000153	0.00061021	0.00000123	0.01919601	0.000122
42_CPb	MEMG5	2339	6	0.2812332	0.0000124	0.00074441	0.00000745	0.02519976	0.000286
43_CPb	MEMG5	2379	6	0.281271	0.0000168	0.00154378	0.0000403	0.05753686	0.00169
45	MEMG5	2406	5	0.2812413	0.0000127	0.00072143	0.00000913	0.02238249	0.00029
47_CPb	MEMG5	2764	5	0.280966	0.0000131	0.00071062	0.00000497	0.02071625	0.000146
48_CPb	MEMG5	2043	9	0.2812501	0.0000215	0.00330924	0.000019	0.1248538	0.00102
50_CPb	MEMG5	2418	6	0.2812516	0.000014	0.00120598	0.0000105	0.04593116	0.000461
51_CPb	MEMG5	2001	19	0.281271	0.0000171	0.00246885	0.00000387	0.1002463	0.000262
52_CPb	MEMG5	2117	13	0.2812444	0.0000133	0.0008908	0.0000125	0.03025205	0.000536
53_CPb	MEMG5	2027	12	0.281217	0.0000149	0.00156201	0.0000299	0.04918127	0.00113
54	MEMG5	2436	6	0.2811787	0.0000108	0.00016617	2.58E-07	0.00511459	0.0000205
55	MEMG5	2424	6	0.2812058	0.000013	0.00056765	0.00000379	0.01758122	0.0000952
56_CPb	MEMG5	1442	14	0.2812793	0.00000883	0.00228013	0.00000759	0.08674351	0.000332
57_CPb	MEMG5	1937	8	0.2811938	0.0000173	0.00132799	0.0000171	0.04388782	0.00076
58_CPb	MEMG5	2361	25	0.2812171	0.000015	0.00156172	0.0000212	0.05572563	0.000637
59_CPb	MEMG5	2399	8	0.2812565	0.0000136	0.0017372	0.0000152	0.06762447	0.000561
60_CPb	MEMG5	2140	10	0.2813065	0.0000142	0.00196549	0.00000824	0.08128635	0.0004
61	MEMG5	2402	7	0.2811977	0.0000126	0.00072174	0.00000195	0.02175513	0.0000448
62_CPb	MEMG5	2402	14	0.281255	0.0000136	0.00144023	0.0000113	0.04425356	0.000324
63_CPb	MEMG5	2370	11	0.2812387	0.0000159	0.00138707	0.00000452	0.05213533	0.000317
64	MEMG5	2418	5	0.2812187	0.0000143	0.00069503	0.00000321	0.02071064	0.000127
65_CPb	MEMG5	2015	30	0.2812651	0.0000167	0.0013746	0.00000866	0.05128078	0.00039
66	MEMG5	2319	5	0.2813911	0.0000213	0.00489234	0.0000293	0.1863129	0.00123
67_CPb	MEMG5	1887	28	0.2813136	0.0000143	0.00083371	0.00000393	0.0275726	0.000136
68_CPb	MEMG5	1432	46	0.281362	0.0000163	0.00561138	0.0000332	0.2506686	0.00154

Number	Sample	207Pb/206Pb age (Ma)	1s (Ma)	$^{176}Hf/^{177}Hf$	1s	$^{176}Lu/^{177}Hf$	1s	$^{176}Yb/^{177}Hf$	1s
70_CPb	MEMG5	2317	7	0.2812349	0.0000127	0.0008105	0.00000751	0.03534624	0.000448
71_CPb	MEMG5	1776	20	0.2813952	0.0000234	0.00384514	0.0000234	0.1765956	0.00102
72_CPb	MEMG5	2200	9	0.2812047	0.000013	0.00110151	0.00000978	0.04393874	0.000575
73_CPb	MEMG5	1846	19	0.2812649	0.0000123	0.0016492	0.00003	0.06600234	0.000949
75_CPb	MEMG5	1940	8	0.2811478	0.0000148	0.00567274	0.0000183	0.2541336	0.00083
76_CPb	MEMG5	2749	8	0.2809706	0.0000129	0.0012913	0.0000146	0.05439607	0.000597
77_CPb	MEMG5	2314	12	0.2812469	0.0000136	0.00122519	0.00000708	0.04604051	0.000277
78_CPb	MEMG5	2281	21	0.2812227	0.0000158	0.00135267	0.0000208	0.05044076	0.000753
79_CPb	MEMG5	2423	6	0.2812262	0.000012	0.00039193	0.00000059	0.01205578	0.0000452
80_CPb	MEMG5	2342	15	0.2812462	0.0000172	0.0020326	0.0000304	0.08804685	0.00128
81_CPb	MEMG5	2343	10	0.2812661	0.0000134	0.00140938	0.00000783	0.05673956	0.000355
82	MEMG5	2413	8	0.2812887	0.0000164	0.00138909	0.0000145	0.05705192	0.000522
83_CPb	MEMG5	2033	31	0.2812236	0.0000156	0.00151913	0.00000618	0.06094282	0.000273
84_CPb	MEMG5	1768	9	0.2810647	0.0000121	0.00205452	0.00000872	0.09515626	0.00051
85	MEMG5	2400	7	0.2812875	0.0000161	0.0008102	0.00000497	0.03065095	0.000183
87_CPB	MEMG5	2237	12	0.2812552	0.0000126	0.00113089	0.00000852	0.04774008	0.000405
88	MEMG5	2473	9	0.2811394	0.0000152	0.00101283	0.0000107	0.03935647	0.000542
89_CPb	MEMG5	2079	19	0.281229	0.0000137	0.00163608	0.00000445	0.06978061	0.000206
90	MEMG5	2366	12	0.2813185	0.0000149	0.00147644	0.00000835	0.05542855	0.000484
91_CPb	MEMG5	1950	11	0.2812399	0.0000114	0.00089138	0.00000669	0.03162999	0.00031
92	MEMG5	2407	8	0.2812505	0.0000122	0.0007004	0.0000026	0.02627813	0.000181
93_CPB	MEMG5	2246	7	0.2810856	0.0000136	0.00104703	0.0000117	0.04096181	0.000398
94_CPb	MEMG5	1879	30	0.2812259	0.0000144	0.00240385	0.0000168	0.1083265	0.00109
95_CPb	MEMG5	2154	4	0.2812809	0.0000141	0.00167579	0.0000109	0.06208136	0.000272
96_CPb	MEMG5	2017	12	0.2812553	0.0000132	0.00172303	0.00000564	0.07392406	0.00026
97_CPb	MEMG5	1744	32	0.2812308	0.0000154	0.00129565	0.00000667	0.04849629	0.000449
98_CPb	MEMG5	2286	14	0.2812396	0.0000224	0.00178954	0.0000164	0.0733047	0.00124
99_CPb	MEMG5	2294	7	0.2813061	0.000017	0.00231675	0.0000231	0.09438143	0.00106
100	MEMG5	2458	4	0.2812718	0.0000134	0.001186	0.0000194	0.04964424	0.000846
102_CPb	MEMG5	2411	3	0.2812148	0.0000119	0.00060396	0.00000344	0.02172991	0.000112
104_CPb	MEMG5	2061	8	0.2812537	0.0000133	0.00182253	0.0000214	0.0795631	0.00103

Number	Sample	207Pb/206Pb age (Ma)	1s (Ma)	$^{176}Hf/^{177}Hf$	1s	$^{176}Lu/^{177}Hf$	1s	$^{176}Yb/^{177}Hf$	1s
105_CPb	MEMG5	2392	14	0.281258	0.0000126	0.00085412	0.0000148	0.03395289	0.000633
106_CPb	MEMG5	1912	6	0.2813458	0.0000168	0.00398464	0.0000085	0.1729555	0.000615
107_CPb	MEMG5	2223	16	0.2812226	0.0000132	0.00146865	0.00000521	0.06293612	0.000334
108_CPb	MEMG5	2381	6	0.2813131	0.0000152	0.00195155	0.0000308	0.07444524	0.00127
109_CPb	MEMG5	1346	85	0.2812489	0.0000152	0.00272793	0.000011	0.1272521	0.000545
111_CPb	MEMG5	506	34	0.2813357	0.000014	0.00371569	0.00000388	0.1652695	0.000263
112_CPb	MEMG5	2396	6	0.2812979	0.0000272	0.00186593	0.0000339	0.06523731	0.00104
113_CPb	MEMG5	2278	6	0.2812447	0.0000132	0.00085476	0.0000031	0.03672304	0.000144
114_CPb	MEMG5	1820	19	0.2813309	0.0000203	0.001829	0.0000209	0.06903771	0.000807
115	MEMG5	2754	6	0.2807904	0.0000134	0.00083354	0.00000327	0.03131386	0.000119
116_CPb	MEMG5	1601	28	0.281276	0.0000158	0.00188217	0.00000722	0.08147034	0.000228
118_CPb	MEMG5	2390	6	0.2811289	0.0000117	0.00071174	0.0000045	0.02411076	0.000108
119_CPb	MEMG5	2227	11	0.2812476	0.0000227	0.00123645	0.0000122	0.04085568	0.000471
120_CPb	MEMG5	1420	29	0.2812959	0.000015	0.00269175	0.0000138	0.1164168	0.000744
121	MEMG5	2901	4	0.2810576	0.000013	0.00072441	0.00000082	0.02237419	0.0000431
122_CPb	MEMG5	2555	6	0.2811508	0.0000365	0.00248384	0.00000781	0.09673347	0.00049
123_CPb	MEMG5	2329	8	0.2812657	0.000017	0.0021024	0.0000318	0.08380454	0.00113
124_CPb	MEMG5	2368	4	0.2812093	0.0000111	0.00056169	0.00000107	0.01805466	0.0000731
126_CPb	MEMG5	2053	14	0.2813002	0.0000129	0.00136999	0.0000103	0.05780057	0.000438
127_CPb	MEMG5	2145	6	0.2811649	0.000013	0.00157612	0.00000677	0.0729251	0.000301
128_CPb	MEMG5	1988	9	0.2812299	0.0000143	0.00036075	8.61E-07	0.01305554	0.0000576
129	MEMG5	2413	5	0.2812895	0.0000149	0.00098754	0.0000269	0.04325314	0.00119
130_CPb	MEMG5	2355	6	0.281253	0.0000126	0.00036334	7.37E-07	0.01083307	0.0000464
131	MEMG5	2401	5	0.2811976	0.0000152	0.00090963	0.00000406	0.0326461	0.000131
132_CPb	MEMG5	2402	6	0.2812488	0.0000121	0.00079666	0.00000373	0.02567195	0.000143
133_CPb	MEMG5	1739	36	0.281315	0.000017	0.0035315	0.0000287	0.1677517	0.00157
134	MEMG5	2415	5	0.2812137	0.0000144	0.00105992	0.00000831	0.03912141	0.000244

Table 6: MEMG25

Number	Sample	207Pb/206Pb age (Ma)	1s (Ma)	$^{176}Hf/^{177}Hf$	1s	$^{176}Lu/^{177}Hf$	1s	$^{176}Yb/^{177}Hf$	1s
1	MEMG25	2246	7	0.2813555	0.0000154	0.00070363	0.00000388	0.02007606	0.000119
2_CPb	MEMG25	2149	12	0.2811246	0.0000252	0.00123721	0.00000662	0.03788588	0.000257
3_CPb	MEMG25	2231	7	0.2812692	0.0000183	0.00095291	0.00000414	0.03029898	0.000212
5_CPb	MEMG25	2260	7	0.2813761	0.000018	0.00100555	0.0000113	0.02890537	0.000294
7_CPb	MEMG25	2447	7	0.2811882	0.0000196	0.00055723	0.0000044	0.01622362	0.000149
11_CPb	MEMG25	8.8	12	0.281247	0.0000247	0.00177999	0.0000214	0.0545591	0.00048
12	MEMG25	2.74	9	0.2813504	0.0000265	0.00049438	0.00000385	0.01395516	0.000187
13_CPb	MEMG25	34.75	13	0.2813003	0.0000158	0.00140114	0.00000632	0.04410419	0.000269
16_CPb	MEMG25	2441	9	0.2812567	0.0000231	0.00063343	0.00000186	0.01792146	0.0000597
18	MEMG25	2233	10	0.2813942	0.0000307	0.0003866	0.00000343	0.01174364	0.0000894
19_CPb	MEMG25	2151	16	0.2813048	0.000038	0.00102429	0.0000139	0.03027993	0.000323
20_CPb	MEMG25	2625	12	0.2812889	0.0000275	0.00081803	0.00000252	0.02564264	0.0000551
21_CPb	MEMG25	2244	11	0.2809315	0.0000268	0.00085497	0.00000318	0.02427675	0.000233
22	MEMG25	2406	10	0.2812302	0.0000226	0.00061066	9.23E-07	0.01823426	0.0000519
23_CPb	MEMG25	2004	19	0.2814193	0.0000177	0.0021374	0.0000212	0.06776038	0.000852
26	MEMG25	2515	5	0.2812409	0.0000193	0.0010481	0.0000171	0.03087566	0.000542
27_CPb	MEMG25	2249	8	0.2814726	0.0000258	0.00079177	0.00000409	0.02269304	0.0000852
28_CPb	MEMG25	2287	5	0.2813889	0.0000194	0.00063027	0.00000228	0.01715217	0.0000425
29_CPb	MEMG25	2297	9	0.2813057	0.0000183	0.00040268	0.0000069	0.01290034	0.000292
32_CPb	MEMG25	1667	40	0.2812486	0.0000172	0.00084043	0.0000105	0.02573439	0.000309
35	MEMG25	2272	5	0.2813241	0.0000334	0.00086222	0.00000412	0.02953094	0.00012
36	MEMG25	2332	6	0.2814155	0.0000318	0.00047137	0.0000024	0.01304234	0.000104
37_CPb	MEMG25	2519	5	0.2811804	0.0000176	0.00023838	0.00000287	0.0072306	0.000078
39_CPb	MEMG25	2240	13	0.2813724	0.0000214	0.00052948	0.00000833	0.01474931	0.000198
42_CPb	MEMG25	2175	9	0.2812546	0.0000284	0.00122052	0.0000178	0.03871441	0.000395
43_CPb	MEMG25	2163	7	0.2812032	0.0000227	0.00177883	0.00000353	0.05115735	0.00012
45_CPb	MEMG25	2218	6	0.2812881	0.0000427	0.00100833	0.0000024	0.03177297	0.000134
46	MEMG25	2561	6	0.2812324	0.0000369	0.00096722	0.00000827	0.02764432	0.000123

Table 7: MEPB44

Number	Sample	207Pb/206Pb age (Ma)	1s (Ma)	$^{176}Hf/^{177}Hf$	1s	$^{176}Lu/^{177}Hf$	1s	$^{176}Yb/^{177}Hf$	1s
1_CPb	MEPB 44	1827	43	0.281265	0.0000263	0.00141607	0.00000915	0.04511128	0.000301
2	MEPB 44	2059	5	0.2812704	0.0000121	0.0006923	0.00000193	0.02061322	0.0000854
3	MEPB 44	2040	5	0.2813884	0.000014	0.00169111	0.0000207	0.06296345	0.00078
5	MEPB 44	2057	5	0.2813292	0.0000145	0.00124215	0.0000115	0.04234156	0.000459
7	MEPB 44	2058	5	0.2812389	0.0000138	0.00061654	0.00000389	0.01935395	0.000169
10	MEPB 44	2086	6	0.2811924	0.0000392	0.00112562	0.00000916	0.03341757	0.000227
11	MEPB 44	2073	5	0.2813461	0.0000224	0.00118181	0.0000146	0.03670933	0.000491
12	MEPB 44	2083	6	0.2812273	0.0000266	0.00095606	0.00000659	0.02942992	0.000325
16	MEPB 44	2068	6	0.2812268	0.0000138	0.00071616	0.00000519	0.02137462	0.000156
18	MEPB 44	2094	6	0.281329	0.0000361	0.0012992	0.0000105	0.04337359	0.000285
20	MEPB 44	2073	7	0.2812771	0.0000116	0.00123025	0.00000226	0.04154724	0.000129
25	MEPB 44	2070	7	0.2812613	0.000012	0.00091209	0.0000153	0.03142406	0.000427
26	MEPB 44	2073	8	0.2812726	0.000012	0.00143738	0.00000553	0.05222231	0.000226
27	MEPB 44	2073	7	0.2812929	0.0000172	0.00120176	0.00000826	0.03956309	0.00012
28	MEPB 44	2074	8	0.2813771	0.0000151	0.00165291	0.0000199	0.07149048	0.000584
29	MEPB 44	2064	8	0.2812945	0.0000107	0.00076454	0.00000627	0.02629337	0.000138
33	MEPB 44	2114	4	0.281262	0.0000184	0.00122756	0.0000147	0.04263977	0.000275
34	MEPB 44	2073	3	0.2813237	0.0000117	0.00095772	0.00000848	0.03384179	0.000359
36	MEPB 44	2063	3	0.2812993	0.0000298	0.00126538	0.00000384	0.04179481	0.000238
38	MEPB 44	2060	3	0.2812823	0.0000156	0.00107041	0.00000418	0.03568553	0.000199
41	MEPB 44	2068	3	0.281329	0.0000104	0.00072843	0.00000144	0.02531322	0.0000765
44	MEPB 44	2063	3	0.2813326	0.0000123	0.00117888	0.00000965	0.03682108	0.000196
49	MEPB 44	2084	4	0.2812925	0.0000109	0.0004937	0.00000349	0.01700716	0.000145
50	MEPB 44	2068	3	0.2812919	0.0000355	0.00086988	0.00000272	0.02754674	0.000174
59	MEPB 44	2069	4	0.2812825	0.0000193	0.00096782	0.00000742	0.0335046	0.000137
61	MEPB 44	2073	4	0.2812649	0.0000157	0.00078564	0.0000058	0.02669349	0.000184
64	MEPB 44	2062	4	0.281276	0.0000207	0.00096585	0.0000141	0.03239237	0.00029
65_CPb	MEPB 44	1952	46	0.2812769	0.0000121	0.0011343	0.000012	0.03967089	0.000342
66	MEPB 44	2092	5	0.2813202	0.0000106	0.00097785	0.0000109	0.03665685	0.000515
67	MEPB 44	2073	4	0.2813063	0.0000111	0.00069195	0.0000153	0.02575634	0.00067

Number	Sample	207Pb/206Pb age (Ma)	1s (Ma)	$^{176}Hf/^{177}Hf$	1s	$^{176}Lu/^{177}Hf$	1s	$^{176}Yb/^{177}Hf$	1s
70	MEPB 44	2070	5	0.2813056	0.0000121	0.00104505	0.00000309	0.03632202	0.000158
71	MEPB 44	2068	5	0.2813139	0.0000135	0.00133743	0.00000565	0.04448061	0.0000951
72	MEPB 44	2065	5	0.2813272	0.0000113	0.00150441	0.00000577	0.05214054	0.000185
73	MEPB 44	2081	5	0.2813482	0.0000201	0.0013539	0.0000137	0.04321551	0.000285
74	MEPB 44	2047	4	0.2813218	0.00001	0.00104697	0.0000021	0.037493	0.0000744
80	MEPB 44	2068	4	0.2813017	0.0000101	0.00075018	8.67E-07	0.02566394	0.000069
81	MEPB 44	2063	4	0.2812852	0.0000101	0.00071488	0.0000052	0.02412091	0.000105
82	MEPB 44	2064	4	0.2812715	0.0000173	0.00129041	0.0000227	0.04197965	0.000681
84	MEPB 44	2064	5	0.2813305	0.0000176	0.00104085	0.00000807	0.03659007	0.000208
85	MEPB 44	2058	5	0.2812712	0.00006	0.00102272	0.0000117	0.03665594	0.00035
86	MEPB 44	2054	6	0.2812815	0.000036	0.00122273	0.00000322	0.03900185	0.0000924
87	MEPB 44	2058	5	0.2812966	0.0000111	0.00122663	0.00000469	0.04382951	0.00017
88	MEPB 44	2066	5	0.2812763	0.0000121	0.00084031	0.00000388	0.02886845	0.000141
89	MEPB 44	2063	5	0.2812785	0.0000114	0.00118481	0.0000115	0.03962021	0.000242
90	MEPB 44	2064	5	0.2813266	0.0000215	0.00098996	0.0000186	0.03595522	0.000798
91	MEPB 44	2076	7	0.281275	0.0000288	0.00121828	0.0000126	0.03945612	0.000513
92	MEPB 44	2072	5	0.2812751	0.0000134	0.00060987	0.00000416	0.0194388	0.0000719
94	MEPB 44	2064	5	0.2812952	0.00000989	0.0005978	0.00000266	0.02332365	0.000153
99	MEPB 44	2065	5	0.2812982	0.000012	0.00108413	0.00000294	0.03673593	0.0000513
100	MEPB 44	2058	6	0.2812401	0.0000154	0.00082485	0.00000291	0.02652085	0.0000822
106	MEPB 44	2094	8	0.2813608	0.0000273	0.00288188	0.00008	0.1166351	0.00326
107	MEPB 44	2073	6	0.2812776	0.000019	0.001509	0.0000357	0.0592914	0.00135
108	MEPB 44	2062	6	0.2812722	0.0000159	0.00082703	0.00000548	0.02547978	0.00021
109	MEPB 44	2067	5	0.2812725	0.0000108	0.00078031	0.00000146	0.02602881	0.000103
111	MEPB 44	2016	12	0.2813136	0.0000152	0.00143605	0.00000357	0.04886056	0.000124
113	MEPB 44	2063	5	0.2812592	0.0000137	0.00095381	0.00000406	0.03362475	0.0000633
112_CPb	MEPB 44	2063	10	0.2812514	0.0000167	0.00099724	0.00000711	0.03350583	0.000206
46_CPb	MEPB 44	1962	6	0.2812779	0.0000102	0.00115372	0.00000373	0.04268369	0.000235
19_CPb	MEPB 44	2478	15	0.2813492	0.0000289	0.00102936	0.0000141	0.03070848	0.000437
79_CPb	MEPB 44	1927	50	0.2813212	0.0000104	0.00160859	0.0000103	0.06531302	0.000533
98_CPb	MEPB 44	2027	21	0.2812575	0.0000315	0.00126645	0.0000058	0.04103039	0.000178

Number	Sample	207Pb/206Pb age (Ma)	1s (Ma)	$^{176}Hf/^{177}Hf$	1s	$^{176}Lu/^{177}Hf$	1s	$^{176}Yb/^{177}Hf$	1s
22_CPb	MEPB 44	1977	46	0.2814689	0.0000186	0.00331469	0.0000433	0.1534002	0.00224
55_CPb	MEPB 44	1692	181	0.2812737	0.0000196	0.00170543	0.0000129	0.06676796	0.000518
43_CPb	MEPB 44	1774	17	0.2812473	0.0000213	0.00131132	0.00000883	0.04936522	0.000266
39_CPb	MEPB 44	1997	82	0.2813343	0.0000169	0.00210951	0.0000275	0.07748593	0.000706
17_CPb	MEPB 44	1638	56	0.2813878	0.0000158	0.00238259	0.0000441	0.08833456	0.00188
32_CPb	MEPB 44	1701	14	0.2813112	0.0000104	0.00104939	0.00000607	0.03727176	0.000193
30_CPb	MEPB 44	1911	63	0.2813857	0.000014	0.00376622	0.0000931	0.1516085	0.00401
42_CPb	MEPB 44	1977	18	0.2813224	0.0000146	0.00096985	0.00000477	0.03738999	0.00022
4_CPb	MEPB 44	1813	103	0.2812828	0.0000209	0.00165573	0.0000261	0.05361446	0.00103
76_CPb	MEPB 44	1889	31	0.2813176	0.0000105	0.00160681	0.0000229	0.06536384	0.000935
63_CPb	MEPB 44	1730	89	0.2812858	0.0000261	0.00177027	0.0000387	0.07056315	0.00185
102_CPb	MEPB 44	1465	45	0.281337	0.0000197	0.00247759	0.0000302	0.09923051	0.00155
83_CPb	MEPB 44	1829	10	0.2813279	0.0000159	0.00207136	0.0000391	0.08602722	0.00148
75_CPb	MEPB 44	1236	46	0.2813187	0.0000179	0.00233788	0.0000285	0.09263268	0.000804
21	MEPB 44	2017	8	0.2812756	0.0000109	0.00064715	0.00000613	0.02478442	0.0002
54	MEPB 44	2437	10	0.2813612	0.0000152	0.0017023	0.00000683	0.05881921	0.000433
45	MEPB 44	2074	4	0.2813234	0.0000131	0.00206428	0.00000901	0.07516358	0.000363
69	MEPB 44	2017	4	0.2812779	0.00000954	0.00066782	0.00000158	0.02280122	0.000077
96	MEPB 44	2041	8	0.2813082	0.0000115	0.00079943	0.00000595	0.02759457	0.000264
37	MEPB 44	2061	3	0.2813637	0.0000242	0.00159504	0.0000151	0.05574682	0.000389
8_CPb	MEPB 44	2066	7	0.2812335	0.0000209	0.00111729	0.00000367	0.03382268	0.000182
105_CPb	MEPB 44	1969	56	0.2812543	0.00003	0.0010369	0.0000101	0.03241828	0.000192
110_CPb	MEPB 44	2038	51	0.2812715	0.0000166	0.00117824	0.0000238	0.04426415	0.000733
114_CPb	MEPB 44	2046	10	0.2813423	0.0000153	0.00169386	0.0000119	0.05850151	0.000352
13_CPb	MEPB 44	1233	78	0.281354	0.0000252	0.00432489	0.000104	0.1481573	0.00329
47_CPb	MEPB 44	2037	33	0.2813155	0.0000334	0.00086921	0.0000047	0.03318547	0.000293
58	MEPB 44	2084	5	0.2812114	0.0000281	0.00073943	0.00000496	0.0266982	0.000161
56	MEPB 44	2087	18	0.2813034	0.0000131	0.0007869	0.0000117	0.02576727	0.000255

Table 8: MEMG12

Number	Sample	207Pb/206Pb age (Ma)	1s (Ma)	$^{176}Hf/^{177}Hf$	1s	$^{176}Lu/^{177}Hf$	1s	$^{176}Yb/^{177}Hf$	1s
1_CPb	MEMG12	2248	85	0.2813351	0.0000212	0.00112492	0.0000325	0.03313146	0.000991
2_CPb	MEMG12	2119	33	0.2813704	0.0000138	0.00184416	0.0000242	0.06021165	0.000915
3	MEMG12	2082	20	0.2813468	0.000012	0.00153393	0.000011	0.04666847	0.000329
4_CPb	MEMG12	2157	60	0.2813667	0.0000155	0.00205957	0.00000796	0.0669606	0.000361
7	MEMG12	2104	29	0.2812913	0.0000131	0.00077581	0.00000369	0.0229274	0.000151
8	MEMG12	2165	33	0.2812601	0.000013	0.0006369	0.00000578	0.01865205	0.00018
9	MEMG12	2078	21	0.2813857	0.0000143	0.00151459	0.0000177	0.04640243	0.000512
10_CPb	MEMG12	2088	22	0.2813437	0.0000152	0.00162896	0.0000101	0.0515562	0.000315
11_CPb	MEMG12	1831	22	0.2814091	0.0000138	0.00317389	0.0000169	0.1031315	0.000526
12	MEMG12	2125	18	0.2812893	0.0000153	0.00095901	0.0000048	0.02964837	0.000212
13_CPb	MEMG12	2324	77	0.2813435	0.0000172	0.00105238	0.00000909	0.03430852	0.000301
14	MEMG12	2057	21	0.2813214	0.0000132	0.00085486	0.00000186	0.02587838	0.000103
15_CPb	MEMG12	2059	94	0.2813303	0.0000148	0.00111371	0.00000741	0.03433218	0.000252
16	MEMG12	2056	21	0.2813274	0.0000165	0.0014469	0.0000131	0.04620037	0.000497
17	MEMG12	2047	22	0.2813266	0.0000124	0.00070498	0.00000208	0.02065782	0.0000978
18	MEMG12	2056	33	0.2813277	0.0000171	0.00132921	0.00000217	0.04091016	0.000118
19_CPb	MEMG12	2090	107	0.2813821	0.0000141	0.0013594	0.0000121	0.04338028	0.000429
21_CPb	MEMG12	1040	95	0.28148	0.0000144	0.00445722	0.0000443	0.1440125	0.00155
22	MEMG12	2166	20	0.281288	0.0000338	0.00125331	0.0000114	0.03874631	0.000254
24	MEMG12	2154	22	0.2813381	0.0000147	0.00174166	0.0000102	0.05665254	0.000423
29_CPb	MEMG12	2138	40	0.2813224	0.0000158	0.00131115	0.00000797	0.04040268	0.000239
32	MEMG12	2070	22	0.2813123	0.0000164	0.00106973	0.00000687	0.0322619	0.000137
33	MEMG12	2084	22	0.2812948	0.0000177	0.00060366	0.0000101	0.02001258	0.000356
34	MEMG12	2062	22	0.2814156	0.0000275	0.00240454	0.0000625	0.0783573	0.00246
35	MEMG12	2085	16	0.2812982	0.0000157	0.00095927	0.0000147	0.03105476	0.000596
37	MEMG12	2076	15	0.2813093	0.0000153	0.00106241	0.00000934	0.0313438	0.00023
42	MEMG12	2067	14	0.2813314	0.0000153	0.00127594	0.00000997	0.03819547	0.000288
44	MEMG12	2071	16	0.2812839	0.0000212	0.00092404	0.00000144	0.02780356	0.0000824
46	MEMG12	2071	15	0.2813803	0.00002	0.00132935	0.00000975	0.03901776	0.000213
51	MEMG12	1945	174	0.2813357	0.0000156	0.00136708	0.00000912	0.0422019	0.00029

Number	Sample	207Pb/206Pb age (Ma)	1s (Ma)	$^{176}Hf/^{177}Hf$	1s	$^{176}Lu/^{177}Hf$	1s	$^{176}Yb/^{177}Hf$	1s
53	MEMG12	1396	19	0.2814603	0.0000202	0.00489336	0.0000105	0.1625275	0.000187
55	MEMG12	2091	16	0.2812852	0.0000178	0.00103987	0.0000146	0.03005014	0.0004
60	MEMG12	2082	15	0.2812969	0.0000123	0.00109857	0.00000423	0.03839961	0.0000931
63	MEMG12	2073	15	0.2813321	0.0000124	0.00131984	0.0000115	0.04822897	0.000547
74	MEMG12	2390	19	0.2813733	0.0000145	0.00155975	0.0000175	0.05502778	0.00074
75	MEMG12	2069	15	0.2813292	0.0000122	0.00075198	0.0000031	0.0253396	0.000109
77	MEMG12	2068	15	0.2812957	0.0000124	0.0008556	0.0000173	0.02887151	0.00064
79	MEMG12	2114	17	0.2812884	0.000013	0.0010327	0.00000795	0.03650898	0.000342
81	MEMG12	2080	15	0.2813538	0.0000162	0.0015418	0.0000314	0.0612011	0.00136
83	MEMG12	2088	15	0.2813272	0.0000129	0.00093888	0.00000687	0.03258781	0.000245
86	MEMG12	2087	17	0.2813594	0.0000094	0.002989	0.000011	0.1054796	0.000304
87	MEMG12	2074	16	0.2813476	0.0000128	0.00113788	0.000018	0.04016576	0.000743
98_CPb	MEMG12	2120	47	0.2813877	0.0000212	0.00260913	0.000015	0.09474765	0.000779
100_CPb	MEMG12	1242	71	0.2813997	0.0000115	0.00311531	0.0000122	0.1201511	0.000511
102	MEMG12	2051	11	0.2813047	0.000012	0.00095474	0.000013	0.03195293	0.000334
103	MEMG12	2072	11	0.281298	0.0000132	0.00094338	0.0000386	0.03387146	0.0015
104_CPb	MEMG12	1169	13	0.2813739	0.0000125	0.00318108	0.0000444	0.120505	0.00166
105	MEMG12	2054	12	0.2813063	0.0000121	0.0008003	0.00000701	0.02702932	0.000293
106_CPb	MEMG12	2163	86	0.2813558	0.0000138	0.00192926	0.0000121	0.07217867	0.000442
107_CPb	MEMG12	2048	24	0.281301	0.0000127	0.00093158	0.0000127	0.03329349	0.000586
92_CPb	MEMG12	2414	120	0.2813154	0.0000192	0.00150761	0.00000738	0.05458112	0.00017
93	MEMG12	2078	16	0.2813149	0.0000113	0.00101419	0.0000162	0.03586232	0.000666
95	MEMG12	2064	16	0.281332	0.0000128	0.00086857	0.00000638	0.03012297	0.000271
109	MEMG12	2059	13	0.2813361	0.0000125	0.0013525	0.00000289	0.04649999	0.0000864
111	MEMG12	2066	14	0.281291	0.000013	0.00117367	0.00000548	0.04156195	0.000227
113	MEMG12	2070	13	0.2812872	0.000013	0.00095131	0.0000153	0.03246791	0.000433
118	MEMG12	2076	14	0.2813431	0.0000155	0.00091628	0.0000118	0.03288673	0.000513
58_CPb	MEMG12	2177	56	0.2813401	0.0000112	0.00131734	0.000023	0.04780986	0.000774
61_CPb	MEMG12	1588	49	0.2814232	0.0000325	0.00523735	0.0000148	0.1838518	0.000697
62_CPb	MEMG12	1125	17	0.2813916	0.0000148	0.00342865	0.0000208	0.1315158	0.000902
66_CPb	MEMG12	2204	33	0.2813553	0.0000261	0.00264493	0.000013	0.09181276	0.000234

Number	Sample	207Pb/206Pb age (Ma)	1s (Ma)	$^{176}Hf/^{177}Hf$	1s	$^{176}Lu/^{177}Hf$	1s	$^{176}Yb/^{177}Hf$	1s
69_CPb	MEMG12	2314	56	0.2814321	0.0000148	0.00308818	0.0000444	0.1115153	0.00168
70_CPb	MEMG12	1888	36	0.2813613	0.0000108	0.00210541	0.0000441	0.08547495	0.00204
72_CPb	MEMG12	2086	73	0.2814199	0.0000204	0.00569349	0.000114	0.2378704	0.00461
78_CPb	MEMG12	2149	25	0.2813459	0.0000156	0.00165216	0.00000756	0.05752718	0.000345
84_CPb	MEMG12	1412	75	0.2813409	0.0000147	0.00119207	0.0000122	0.04159969	0.000497
88_CPb	MEMG12	2092	74	0.2813877	0.0000212	0.00260913	0.000015	0.09474765	0.000779
108_CPb	MEMG12	1777	40	0.281288	0.0000171	0.00158456	0.0000527	0.0589022	0.00169
115_CPb	MEMG12	1871	213	0.2814355	0.0000133	0.00370833	0.0000224	0.1423682	0.000959
41_CPb	MEMG12	2103	22	0.2813534	0.0000167	0.00181402	0.0000106	0.05477031	0.000361
97_CPb	MEMG12	2096	28	0.2813307	0.0000154	0.00136343	0.00000859	0.04763802	0.000407
99_CPb	MEMG12	2105	16	0.2812767	0.0000214	0.00117123	0.00000567	0.04015445	0.000282
112_CPb	MEMG12	2109	14	0.2813568	0.0000128	0.0012539	0.00000511	0.04413235	0.00014

Appendix C: Trace element data

Table 1: MEMG8

Trace Element Concentrations in ppm.

Element	P	Ti	Y	Nb	La	Ce	Pr	Nd	Sm	Eu	Gd	Tb	Dy	Ho	Er	Tm	Yb	Lu	Hf	Ta	Th	U
MEMG8-1	BDL	31.22	1636	16.34	77.44	452	46.93	221	56.73	5.96	71.39	15.64	156	49.36	222	47.11	439	81.3	10590	1.515	111	577
MEMG8-6	BDL	334	2310	27.55	71.06	469	52.51	275	88.79	11.19	121.02	26.4	232	67.99	290	55.63	471	93.22	8920	2.88	432	949
MEMG8-2	BDL	426	1483	27.23	34.86	217	25.08	116.27	33.6	4.84	48	11.24	121	43.9	205	45.07	437	84.81	11690	4.3	85	647
MEMG8-64	BDL	205	991	11.6	18.56	63	8.58	35.73	10.55	1.83	27.58	7.49	85	30.51	141	29.31	263	50.88	8717	1.358	123	240
MEMG8-72	BDL	326	1711	28.65	40.69	241	24.94	128	44.32	12.72	59.46	14.67	153	45.5	227	48.14	494	92.62	10464	3.01	141	523
MEMG8-68	BDL	129	1201	23.94	48.83	241	23.94	110	33.82	4.44	44.09	11.02	112	36.33	168	37.04	353	67.57	11811	2.67	162	574
MEMG8-63	BDL	187	1384	20.74	24	171	16.19	85.05	30.56	4.81	58.46	13.35	130	40.36	181	33.78	330	61.25	12048	2.56	202	421
MEMG8-53	BDL	244	1553	25.25	37.48	250	26.62	133.55	39.12	5.32	56.47	14.06	157	48.68	211	44.82	401	75.81	10951	2.59	182	469
MEMG8-55	BDL	396	1461	20.79	73.28	253	26.14	108.2	32.15	3.89	51.69	12.72	130	43.06	188	40.9	362	69.57	10786	2.36	126	431
MEMG8-58	BDL	42.41	1341	12.75	9.91	58	3.82	16.69	5.8	1.51	27.26	9.67	114	41.23	201	42.22	386	76.2	10386	2.02	188	413
MEMG8-54	BDL	79.8	2008	21.33	30.82	211	21.51	101.53	38.12	6.16	67.92	19.82	201	63.13	268	54.35	457	88.42	9922	2.51	276	494
MEMG8-57	6986	194	2083	20.36	21.91	158	14.14	65.94	26.46	3.35	60.29	15.01	186	60.65	296	60.91	536	101.15	9697	2.43	192	452
MEMG8-7	1625	53.94	895	12.4	2.52	42	2.02	12.11	7.96	1.32	24.56	6.88	80	27.58	127	27.42	229	44.85	9587	1.35	96	168
MEMG8-59	1491	59.88	1643	13.47	26.33	184	20.09	105.03	39.33	5.12	60.3	15.4	161	50.3	220	43.93	399	72.76	9556	3.91	155	376
MEMG8-48	6907	203	1890	14.77	72.22	156	18.9	85.02	27.95	3.15	47.85	13.24	155	56.28	274	63.21	611	117.39	12815	3.21	102	898
MEMG8-42	2065	451	1603	34.77	61.97	398	48.4	227.08	60.3	4.8	76.68	15.23	141	45.28	184	40.16	364	68.84	10322	3.57	163	568

Element	P	Ti	Y	Nb	La	Ce	Pr	Nd	Sm	Eu	Gd	Tb	Dy	Ho	Er	Tm	Yb	Lu	Hf	Ta	Th	U
MEMG8-46	2444	817	1476	18.12	17.13	64	8.18	38.03	14	2.39	35.83	10.77	126	44.86	201	39.6	364	64.32	9041	3.03	413	563
MEMG8-62	5333	415	2088	24.83	35.13	230	20.12	102.69	37.42	7.71	63.47	15.74	158	55.51	268	62.47	589	110.34	11663	3.89	60	779
MEMG8-15	1565	387	1577	16.57	22.81	115	10.35	49	19.94	3.39	45.9	12.87	134	44.45	207	41.19	360	70.1	10313	2.03	198	367
MEMG8-10	1545	158	1767	16.35	34.85	196	17.38	84.1	26.35	3.37	52.73	14.56	160	53.44	253	54.08	499	97.62	9234	2.12	260	521
MEMG8-5	609	499	1954	29.91	52.51	202	20.17	100	36.21	37.64	64.13	16.81	160	52.72	235	53.42	494	93.6	13772	4.51	115	821
MEMG8-4	2339	167	1484	10.9	665.52	1486	153.72	560	122.61	6.14	109.4	20.38	153	44.8	181	36.31	323	63.7	9390	2.1	176	465
MEMG8-9	1205	313	2010	19.5	37.95	273	29.02	161	60.9	8.91	97.98	22.33	193	53.23	229	41.6	361	66.73	8111	1.79	167	509
MEMG8-21	BDL	303	2180	43.61	62.36	375	48.42	242	68.37	5.39	101.95	21.77	187	61.12	233	50.76	441	74.76	7835	4.21	383	597
MEMG8-26	1264	108	2050	18.92	33.86	237	19.76	100	30.03	6.16	68.66	17.31	190	63.28	280	59.2	533	106	9252	1.5	237	655
MEMG8-33	323	1241	1897	27.28	18.2	143	16.85	66.37	25.63	3.86	55.96	14.15	168	57.42	267	57.07	460	105	11802	2.47	264	517
MEMG8-44	283	84	1918	11.82	52.72	133	9.53	50	21.61	6.46	70.19	18.79	194	63.25	268	48.36	419	77.29	8255	1.32	207	243
MEMG8-18	353	629	1004	11.93	36.48	202	21.24	99.77	29.8	4.25	43.09	9.69	85	26.86	118	24.97	226	51.32	12033	3.32	149	777
MEMG8-32	1030	187	1710	18	15.42	104	7.8	53.09	18.22	2.35	54.55	12.86	157	50.38	242	45.76	447	87.65	9965	2.87	243	681

Table 2: MEMG4

Trace Element Concentrations in ppm.

Element	P	Ti	Y	Nb	La	Ce	Pr	Nd	Sm	Eu	Gd	Tb	Dy	Ho	Er	Tm	Yb	Lu	Hf	Ta	Th	U
MEMG4-8	445	45.03	1613	10.43	9.24	97	8.31	59	31.1	5.41	67.76	15.97	155	50.78	211	43.09	382	73.49	7654	1.101	482	953
MEMG4-16	458	1269	1560	14.14	34.21	362	31.68	168	37.2	8.7	52.9	12.2	127	44.99	225	48.27	490	96.35	10277	2.21	232	1437
MEMG4-14	500	909	1185	10.6	5.53	34	2.49	14	7.41	3.2	27.75	7.92	89	34.55	165	35.19	327	68.43	9678	1.146	137	492
MEMG4-59	819	326	2580	18.26	10.43	101	6.32	42	19.71	10.17	59.05	17.3	210	76.08	359	80.45	759	144.76	11344	7.41	572	2385
MEMG4-56	353	17.72	918	8.63	2.29	29	1.38	8	6.02	2.67	26.29	7.39	79	26.47	115	21.62	189	37.96	7938	0.585	104	181
MEMG4-57	452	64.05	1236	9.06	21.97	120	10.46	54	21.52	6.16	43.95	11.24	110	36.37	159	32.2	297	55.73	11025	1.295	384	1174
MEMG4-52	777	BDL	1221	10.76	7.1	59	3.83	18	9.08	1.85	27.41	8.61	96	37.4	178	38.07	375	74.34	8754	1.65	340	966
MEMG4-78	623	44.27	1841	8.85	65.2	300	35.2	175	62.55	10.38	105.31	22.39	193	59.65	245	46.34	405	72.74	8409	1.011	317	918
MEMG4-90	604	63.32	1629	10.91	11.23	78	6.86	38	20.6	10.48	53.42	14.26	152	50.85	224	45.92	411	79.79	9354	1.469	268	529
MEMG4-54	3041	BDL	841	8.69	28.09	95	10.69	49	16.8	1.04	34.53	8.43	80	28.22	120	22.81	196	38.87	8100	1.111	153	386
MEMG4-17	370	12.96	1148	9.42	2.65	19	1.87	15	13.02	2.14	46.11	11.51	114	38.54	159	29.14	253	49.54	6894	0.333	151	249
MEMG4-48	633	34.28	971	8.35	14.4	66	4.45	22	11.28	4.14	30.84	7.93	84	27.1	127	26.51	247	52.39	7365	0.831	171	332
MEMG4-45	2888	74.81	871	9.77	59.32	152	18.47	84	19.42	2.79	32.57	7.96	84	28.66	127	25.46	225	42.78	7652	0.883	82	196
MEMG4-13	1036	32.22	1587	11.16	7.02	58	2.78	13	7.16	5.33	28.11	9.29	116	46.07	229	50.93	508	102.77	10910	2.7	370	1335
MEMG4-35	1333	38.37	1521	17.4	10.47	62	5.36	30	14.91	9.49	33.51	10.6	119	44.05	212	47.6	484	103.24	10987	8.09	16	629
MEMG4-25	1381	BDL	855	10.56	18.93	73	6.66	30	9.96	1.59	24.89	6.91	74	25.7	122	24.4	217	41.58	8730	1.319	290	712
MEMG4-65	486	17.86	1075	8.19	2.25	32	1.45	8	6.98	2.48	29.45	7.93	93	34.9	156	32.14	302	60.81	8974	0.585	147	228

Element	P	Ti	Y	Nb	La	Ce	Pr	Nd	Sm	Eu	Gd	Tb	Dy	Ho	Er	Tm	Yb	Lu	Hf	Ta	Th	U
MEMG4-117	905	28.11	1484	7.27	2.98	66	2.73	20	22.62	7.55	64.68	15.38	146	45.01	190	37.3	366	68.42	6094	0.654	856	926
MEMG4-30	1537	BDL	860	8.41	11.96	61	3.25	16	8.07	2.85	25.92	6.9	72	24.82	115	23.26	213	41.25	8518	1.046	134	244
MEMG4-01	1024	133.99	1016	9.49	19.79	88	5.8	31	14.34	4.49	37.82	9.65	94	30.99	134	27.26	255	52.46	8293	0.864	308	487
MEMG4-15	992	119.52	1182	8.91	10.21	77	4.6	27	12.25	4.39	35.87	9.18	99	34.66	157	34.37	332	67.71	8958	1.104	220	427
MEMG4-88	714	10.83	785	7.94	0.284	12	0.695	7	8.58	0.796	30.79	7.99	81	26.21	109	20.89	178	34.54	6851	0.431	97	167
MEMG4-3	3105	221.33	1447	10.88	4.67	63	3.67	24	11.25	4.27	33.71	10.44	124	44.44	213	44.55	424	81.91	8994	1.69	341	768
MEMG4-91	1347	184.92	1583	15.49	140.86	139	30.68	123	36.61	7.57	76.61	18.55	182	56.11	216	38.13	327	56.18	7380	2.32	466	1199
MEMG4-51	4037	12.4	1209	9.83	8.75	53	3.01	16	8.13	2.41	26.62	7.74	97	36.65	183	37.65	358	70.69	7782	1	184	422
MEMG4-34	5137	141.25	2009	16.07	25.7	109	9.81	38	13.15	3.33	44.42	15.35	179	66.88	304	60.45	550	96.15	9142	3.12	428	1383
MEMG4-95	2362	13.52	1002	7.92	1.64	30	1.51	10	9.1	2.58	29.03	8.3	89	31.52	147	30.03	292	56.64	8020	0.921	106	143
MEMG4-07	2025	28.73	1576	10.67	9.36	83	3.47	17	8.28	2.06	31.03	10.37	125	49.05	233	49.34	480	92.34	8884	1.64	300	877
MEMG4-9	1944	16.82	757	10.19	2.79	47	2.29	14	7.36	2.33	20.17	5.79	60	21.83	105	23.25	244	48.97	9272	2.09	344	800
MEMG4-81	1878	11.84	1759	8.54	0.557	20	0.903	7	9.26	1.55	37.13	12.47	150	55.34	268	53	486	91.03	7769	0.592	320	471
MEMG4-33	3058	748.84	1187	10.57	42.19	170	10.46	42	16.46	3.79	39.52	10.51	109	35.61	157	31.56	304	57.27	6743	1.39	288	910

Table 3: MEPB44

Trace Element Concentrations in ppm.

Element	P	Ti	Y	Nb	La	Ce	Pr	Nd	Sm	Eu	Gd	Tb	Dy	Ho	Er	Tm	Yb	Lu	Hf	Ta	Th	U
MEPB44-6	411	1360	7545	1698	707	7054	977	5407	1134	294	815	120	959	240	863	135	1067	155	10625	13	2221	2300
MEPB44-2	286	15	801	26	4.32	32	3	17.5	8.68	2.97	21.44	5.98	75.9	26.38	119	22.43	208	39.82	8156	1.06	76.64	180
MEPB44-1	365	62	1165	30	8.24	116	13.07	79.23	47.14	15.34	64.51	14.11	131	40.54	169	30.57	270	48.72	9144	1.23	171	234
MEPB44-17	BDL	598	6347	1102	315	3593	418	2378	572	156	530	92	796	203	724	117	894	124	8830	11	3626	1382
MEPB44-117	BDL	17	857	13	3.8	20	1.96	10.36	7.32	2.17	25.53	6.88	84.14	28.76	131.4	24.26	213	41.18	7918	0.83	70.62	132
MEPB44-119	238	BDL	818	13	5.91	32	3.29	19.44	8.81	6.7	22.7	6.94	76.25	27.6	120	23.35	211	40.72	8284	1.06	69.32	166
MEPB44-115	1441	39	1238	50	41.32	242	31.01	177	57.59	13.77	69.95	14.26	131	41.87	180	33.86	291	55.08	9541	2.06	196	305
MEPB44-109	192	BDL	740	15	4.69	37	4.81	26.18	8.81	2.12	18.33	5.98	65.19	24.68	115	22.8	198	38.5	8200	1.26	87.42	167
MEPB44-113	2617	BDL	999	13	153	366	49.5	232	51.92	2.71	62.72	11.65	104	34.48	145	29.04	248	46.75	9869	1.69	105	208
MEPB44-102	BDL	957	5993	798	395	3324	614	3307	1000	280	699	119	731	192	568	99	726	116	7305	4.82	1096	1023
MEPB44-94	507	1518	17122	2230	1011	7660	1078	5296	1522	496	1684	334	2111	522	1559	245	1629	208	5542	17	3700	2538
MEPB44-75	373	855	4097	424	344	2228	432	2040	437	125	369	71	482	145	505	93	686	115.5	9201	9.5	815	1339
MEPB44-63	194	104	1594	93	91.18	520	131	747	143	30	89	20	164	57	226	45	359	66.65	9180	3.16	375	421
MEPB44-76	331	1212	8417	1197	1434	6121	942	3285	566	267	569	129	925	286	977	172	1147	165	6066	18.96	8195	1630
MEPB44-79	1217	1041	5255	1239	625	3574	941	4899	1185	375	769	140	733	187	603	110	802	135	8141	11.71	1295	1021
MEPB44-96	161	86	1318	127	52.49	376	86	463	129	38	113	25	149	47	171	34	249	45.8	8005	3.55	281	327
MEPB44-112	3389	101	2334	57	69.42	308	71	330	102	30	129	36	269	87	319	63	454	85.67	8774	2.82	385	354

Element	P	Ti	Y	Nb	La	Ce	Pr	Nd	Sm	Eu	Gd	Tb	Dy	Ho	Er	Tm	Yb	Lu	Hf	Ta	Th	U
MEPB44-124	7022	417	1574	252	407	1047	263	1249	228	67	155	30	183	59	214	42	299	55.59	7420	9.14	421	379
MEPB44-81	7748	43	878	41	614	799	178	677	109	16	78	17	102	33	118	25	180	35.49	8892	2.22	110.74	166
MEPB44-45	6105	579	2662	230	440	1134	411	1377	239	76	192	53	319	108	371	78	542	99.64	9152	8.63	408.21	820
MEPB44-46	159	279	2231	228	263	1065	458	2392	475	147	256	55	283	91	301	62	415	74.46	8824	4.08	527.79	638
MEPB44-42	290	1632	6483	1726	1963	7406	3379	16309	1799	602	728	147	717	235	781	151	943	146	7538	27.06	2668.84	2260
MEPB44-110	1534	93	983	98	164	365	164	659	99	30	69	20	113	42	135	30	210	39.62	8821	5.21	215.81	213
MEPB44-80	4471	38	849	29	169	211	118	471	79.84	13.57	62.28	17.79	97.16	35.31	129	28.4	200.37	41.68	8915	4.59	116.15	188
MEPB44-22	626	1012	5289	896	1516	4342	2422	9383	1315	438	663	164	714	213	654	123	738	117	7460	35.66	2627.63	1810
MEPB44-55	11058	197	1517	94	741	805	579	1623	190	41	138	40	186	61	203	43.83	293	56.1	9746	9.53	437.5	369